

**School of Science and Engineering
Department of Civil Engineering**

**Experimental modelling for flexible pavement materials applying
advanced laboratory tests to develop Mechanistic-Empirical design
procedure**

Hossein Asadi

**This thesis is presented for the Degree of
Doctor of Philosophy
of
Curtin University**

April 2015

Declaration

To the best of my knowledge and belief this thesis contains no material previously published by any other person except where due acknowledgment has been made.

This thesis contains no material which has been accepted for the award of any other degree or diploma in any university.

Signature:

A handwritten signature in black ink, appearing to be 'H. A.', written over the dotted line for the signature field.

Date:

2.10.4.2015

CONTENTS

1	INTRODUCTION	1
1.1	BACKGROUND.....	1
1.2	SIGNIFICANCE OF THE RESEARCH.....	2
1.3	OBJECTIVES OF THE RESEARCH.....	3
1.4	STRUCTURE OF THE THESIS.....	3
2	LITERATURE REVIEW	4
2.1	INTRODUCTION	4
2.2	MODES OF FAILURE OF FLEXIBLE PAVEMENTS.....	4
2.3	FATIGUE AND DYNAMIC MODULUS.....	7
2.3.1	<i>Fatigue</i>	7
2.3.2	<i>Numerical investigations on the fatigue life of flexible pavements.....</i>	8
2.3.3	<i>Experimental investigations carried out on laboratory fatigue life.....</i>	8
2.3.4	<i>Effect of healing on fatigue life.....</i>	14
2.3.5	<i>Fatigue endurance limit</i>	16
2.3.6	<i>Dynamic modulus of asphalt.....</i>	17
2.4	SUMMARY	21
2.4.1	<i>Study gaps.....</i>	22
2.5	OBJECTIVES OF THE RESEARCH.....	22
3	SAMPLE PREPARATION.....	24
3.1	DETAILS OF TESTING CONDUCTED ON THE MIXES	24
3.1.1	<i>PSD and binder content.....</i>	26
3.1.2	<i>Maximum density.....</i>	27
3.2	PREPARATION OF ASPHALT SAMPLES	28
3.2.1	<i>Preparation of beams from slabs for fatigue testing.....</i>	28
3.2.2	<i>Preparation of cylinders for AMPT testing</i>	29
3.3	VOLUMETRIC PROPERTIES OF PREPARED SAMPLES.....	30
4	RESULTS OF PRELIMINARY TESTING AND DEVELOPMENT OF REVISED PROTOCOLS.....	33
4.1	INTRODUCTION	33
4.2	DEFINITION OF 'VALIDITY' AND 'RELIABILITY'	34
4.3	TEST EQUIPMENT.....	35
4.3.1	<i>UTS15.....</i>	36
4.3.2	<i>UTS18.....</i>	37
4.3.3	<i>UTS19.....</i>	37
4.3.4	<i>UTS6.....</i>	38
4.4	ASSOCIATED ERRORS.....	39
4.4.1	<i>Errors associated with UTS 15 and suggested solutions.....</i>	39
4.4.2	<i>Errors associated with UTS6 and suggested solutions.....</i>	44
4.5	A NEW TESTING PROTOCOL FOR THE EN STANDARD TESTER AND THE AMPT	48
4.5.1	<i>EN Standard tester testing protocol steps while operating UTS15 software</i>	48
4.5.2	<i>AMPT testing protocol: steps while operating the UTS6 software</i>	49
4.6	SUMMARY	50
5	TEST RESULTS AND ANALYSIS	52
5.1	INTRODUCTION	52
5.1.1	<i>Fatigue behaviour of asphalt mixes under repeated loading</i>	52
5.1.2	<i>Linear viscoelastic behaviour of asphalt mix</i>	52
5.2	APPROACHES USED.....	53
5.3	APPROACH 1.....	53
5.4	APPROACH 2.....	54

5.5	APPROACH 3.....	57
5.5.1	<i>Haversine loading mode</i>	58
5.5.2	<i>Sinusoidal loading mode</i>	60
5.5.3	<i>Modelling the fatigue curve</i>	61
5.5.4	<i>Comparison of fatigue life predictions (scenario 1 and scenario 2)</i>	73
5.5.5	<i>Major findings (approach 3)</i>	79
5.6	APPROACH 4.....	80
5.6.1	<i>Major findings</i>	83
5.6.2	<i>Summary</i>	88
5.7	APPROACH 5.....	88
5.7.1	<i>Major findings</i>	93
5.8	APPROACH 6.....	93
5.8.1	<i>Shift factor when binder properties are available</i>	96
5.8.2	<i>Shift factor when binder properties are unavailable</i>	98
5.8.3	<i>Development of compressive and bending master curves for WA mix</i>	98
5.8.4	<i>Major findings</i>	104
6	CONCLUSIONS AND RECOMMENDATIONS	106
6.1	LITERATURE REVIEW	107
6.2	DEVELOPMENT OF TESTING PROTOCOLS.....	107
6.3	FATIGUE TESTING AND THE DEVELOPMENT OF MASTER CURVES	108
6.3.1	<i>Approach 1</i>	108
6.3.2	<i>Approach 2</i>	109
6.3.3	<i>Approach 3</i>	109
6.3.4	<i>Approach 4</i>	109
6.3.5	<i>Approach 5</i>	110
6.3.6	<i>Approach 6</i>	110
6.4	SUMMARY	110
6.5	RECOMMENDATIONS	111
	REFERENCES.....	113
	APPENDIX A UTS15 OUTPUT IN APPROACH 3 FOR HAVERSINE LOADING.....	118
	APPENDIX B UTS18 OUTPUT IN APPROACH 3 FOR SINUSOIDAL LOADING	130
	APPENDIX C CURVE FITTING IN APPROACH 3 FOR SCENARIO1 AND SCENARIO2	142
	APPENDIX D THREE STEPS IN APPROACH 4.....	151
	APPENDIX E UTS 6 OUTPUTS (AMPT – DYNAMIC MODULUS TEST).....	166

TABLES

TABLE 3.1: PROPERTIES OF AC14/75 ASPHALT MIX	24
TABLE 3.2: PARTICLE SIZE DISTRIBUTION (PSD) OF AGGREGATES (PROVIDED BY BGC HAZELMERE WA)	25
TABLE 3.3: STANDARDS USED FOR TESTING DURING SAMPLE PREPARATION	25
TABLE 3.4: PSD OF COMBINED AGGREGATES IN AC14/75 MIX	26
TABLE 3.5: LOWER AND UPPER LIMITS OF PSD (BGC HAZELMERE WA)	27
TABLE 3.6: GYRATORY COMPACTOR SETTINGS	29
TABLE 4.1: PROPOSED PID GAINS FOR 4°C	46
TABLE 4.2: PROPOSED PID GAINS FOR 20°C AND 40°C	46
TABLE 5.1: SUMMARY OF TESTING CONDITIONS (IN ACCORDANCE WITH AGPT/T233)	54
TABLE 5.2: TESTING CONDITIONS AND NUMBER OF SAMPLES TESTED (APPROACH 2)	55
TABLE 5.3: RESULTS OF TESTING (APPROACH 2)	55
TABLE 5.4: AVERAGED RESULTS FOR EACH STRAIN LEVEL AND ALL SAMPLES (APPROACH 2)	56
TABLE 5.5: COMPARISON OF THREE METHODS OF ANALYSIS	57
TABLE 5.6: RELIABILITY FACTORS FOR DESIRED PROJECT RELIABILITY (AUSTRROADS 2012)	58
TABLE 5.7: TESTING CONDITION (APPROACH 3)	58
TABLE 5.8: PROPERTIES OF SAMPLES AND TEST CONDITIONS (HAVERSINE LOADING)	59
TABLE 5.9: SUMMARY OF TEST RESULTS (HAVERSINE LOADING)	59
TABLE 5.10: PROPERTIES OF SAMPLES AND TESTING CONDITIONS (SINUSOIDAL LOADING)	60
TABLE 5.11: SUMMARY OF TEST RESULTS (SINUSOIDAL LOADING)	60
TABLE 5.12: FITTED CURVES FOR DIFFERENT TEMPERATURES (SCENARIO 1)	62
TABLE 5.13: PARAMETERS IN SCENARIO 1 UNDER DIFFERENT TESTING CONDITIONS (HAVERSINE LOAD)	63
TABLE 5.14: PARAMETERS IN SCENARIO 1 UNDER DIFFERENT TESTING CONDITIONS (SINUSOIDAL LOAD)	64
TABLE 5.15: PARAMETERS IN SCENARIO 2 UNDER DIFFERENT TESTING CONDITIONS (HAVERSINE LOAD)	65
TABLE 5.16: PARAMETERS IN SCENARIO 2 UNDER DIFFERENT TESTING CONDITIONS (SINUSOIDAL LOAD)	65
TABLE 5.17: EXTRAPOLATED FATIGUE LIFE FOR UNTERMINATED TESTS (HAVERSINE LOADING)	67
TABLE 5.18: EXTRAPOLATED FATIGUE LIFE FOR UNTERMINATED TESTS (SINUSOIDAL LOADING)	67
TABLE 5.19: COMPARISON OF ESTIMATED FATIGUE LIFE WITH LABORATORY RESULTS (SCENARIO 2)	68
TABLE 5.20: TEMPLATE ADJUSTMENT FACTORS FOR DIFFERENT STIFFNESS REDUCTION STATES	72
TABLE 5.21: PREDICTED FATIGUE LIFE (TERMINATED TESTS)	73
TABLE 5.22: ESTIMATED FATIGUE LIFE OF UNTERMINATED TESTS (HAVERSINE LOADING)	73
TABLE 5.23: ESTIMATED FATIGUE LIFE OF UNTERMINATED TESTS (SINUSOIDAL LOADING)	74
TABLE 5.24: FATIGUE LIFE OF THE BEAMS WHICH ARE RECORDED AS THE EVIDENCE FOR FEL	75
TABLE 5.25: COMPARISON OF AUSTRROADS AND LABORATORY FATIGUE LIFE PREDICTIONS	76
TABLE 5.26: TESTING CONDITIONS (APPROACH 4)	80
TABLE 5.27: PARAMETERS OF FITTED CURVES FOR DIFFERENT TESTING CONDITIONS (APPROACH 4)	83
TABLE 5.28: TESTING CONDITIONS USED IN APPROACH 5	89
TABLE 5.29: EXTRAPOLATED FATIGUE LIVES OF UNTERMINATED TESTS (APPROACH 5)	91
TABLE 5.30: ESTIMATED LABORATORY FATIGUE LIVES (APPROACH 5)	92
TABLE 5.31: VOLUMETRIC PROPERTIES OF CYLINDERS	99
TABLE 5.32: TESTING CONDITIONS (HAVERSINE LOADING MODE)	99
TABLE 5.33: TESTING CONDITIONS (SINUSOIDAL LOADING MODE)	100
TABLE 5.34: AVERAGE VOLUMETRIC PROPERTIES USED TO DEVELOP FLEXURAL MASTER CURVE	101
TABLE 5.35: MASTER CURVE FITTING PARAMETERS (UNCONFINED CYLINDERS)	101
TABLE 5.36: MASTER CURVE FITTING PARAMETERS (CONFINING PRESSURE OF 65 kPa)	102
TABLE 5.37: MASTER CURVE FITTING PARAMETERS FOR CONFINED CYLINDERS IN 135 kPa	102
TABLE 5.38: FLEXURAL MASTER CURVE FITTING PARAMETERS (HAVERSINE AND SINUSOIDAL LOADING)	103

FIGURES

FIGURE 2-1: LITERATURE REVIEW SCOPE OF WORK.....	5
FIGURE 2-2: SCHEMATIC STRAIN-STRESS HYSTERESIS LOOP.....	11
FIGURE 2-3: SCHEMATIC RDEC PLOT (SHEN AND CARPENTER 2007)	13
FIGURE 2-4: SCHEMATIC SINGLE EDGE NOTCHED BEAM [SE (B)] (A) AND DOUBLE EDGE NOTCHED TENSION (DENT) (B) (KIM AND MARASTEANU 2012)	14
FIGURE 2-5: TYPICAL DYNAMIC MODULUS MASTER CURVE (NCHRP 2008A).....	18
FIGURE 3-1: AGGREGATES PSD (PROVIDED BY BGC HAZELMERE WA).....	25
FIGURE 3-2: PSD OF COMBINED AGGREGATES IN AC14/75 MIX	26
FIGURE 3-3: LOWER AND UPPER LIMITS PROVIDED BY BGC HAZELMERE WA	27
FIGURE 3-4: SLAB COMPACTION.....	28
FIGURE 3-5: (A) PREPARED SLAB AND (B) TEMPERATURE CONTROL	28
FIGURE 3-6: CUTTING PROCESS AND BEAMS PREPARED FOR TESTING	29
FIGURE 3-7: PREPARATION OF CYLINDERS FOR AMPT TESTING	29
FIGURE 3-8: TEMPERATURE CONTROL OF AMPT CYLINDERS DURING COMPACTION.....	30
FIGURE 3-9: CUTTING OF PREPARED AMPT CYLINDERS	30
FIGURE 3-10: ASPHALT MIX PHASE DIAGRAM	31
FIGURE 3-11: EXAMPLES OF INCORRECT AND CORRECT STORAGE OF SAMPLES	32
FIGURE 4-1: SCHEMATIC EXPLANATION OF VALIDITY AND RELIABILITY	34
FIGURE 4-2: CURTIN UNIVERSITY GEOMECHANICAL LABORATORY EN STANDARD TESTER	35
FIGURE 4-3: CURTIN UNIVERSITY GEOMECHANICAL LABORATORY AMPT	36
FIGURE 4-4: UTS15 TEST LAYOUT AND DESCRIPTION (UTS15 HELP MENU).....	37
FIGURE 4-5: UTS18 TEST LAYOUT AND DESCRIPTION (UTS18 HELP MENU).....	38
FIGURE 4-6: UTS19 TEST LAYOUT AND DESCRIPTION (UTS19 HELP MENU).....	38
FIGURE 4-7: UTS6 TEST LAYOUT AND DESCRIPTION (UTS6 HELP MENU).....	39
FIGURE 4-8: PHASE LAG BETWEEN STRESS AND STRAIN.....	40
FIGURE 4-9: ORIGINAL POSITION OF NEUTRAL LINE BEFORE TESTING.....	40
FIGURE 4-10: CHANGE IN LOCATION OF NEUTRAL LINE AFTER TESTING	41
FIGURE 4-11: COMPARISON OF HAVERSINE AND SINUSOIDAL LOAD SHAPES	41
FIGURE 4-12: COMPARISON OF LOADING ADJUSTMENTS REQUIRED TO REACH 200 $\mu\epsilon$ (HAVERSINE AND SINUSOIDAL WAVE FORMS)	42
FIGURE 4-13: INCORRECT PHASE ANGLE OUTPUTS VARYING FROM -100° AND 270°	42
FIGURE 4-14: FLIPPING THE SAMPLE FROM THE NORMAL POSITION TO PROPOSED CONDITION TO OVERCOME THE PHASE ANGLE PROBLEM.....	43
FIGURE 4-15: PHASE ANGLES AFTER PROPOSED CORRECTION METHOD APPLIED	43
FIGURE 4-16: NOISE INTERFERENCE: CONTROLLED SINUSOIDAL STRESS AT 40°C AND A FREQUENCY OF 0.01 Hz.....	44
FIGURE 4-17: OUT OF RANGE STRAIN LEVEL AND LOAD STANDARD ERROR IN 40°C AND 0.01 Hz IN UTS6 OUTPUT	44
FIGURE 4-18: SCHEMATIC PID CONTROLLER FLOWCHART.....	46
FIGURE 4-19: ADOPTIVE LEVEL CONTROL (ALC) CHECK-BOX IN UTS6 TUNING INTERFACE	47
FIGURE 4-20: HOW TO APPLY 0.5% DITHER TO THE UTS6 SYSTEM SETUP	48
FIGURE 4-21: SINUSOIDAL STRESS SHAPE BEFORE AND AFTER REFINEMENT	49
FIGURE 4-22: STRAIN LEVEL AND LOAD STANDARD ERROR REFINEMENT FOLLOWING THE PROPOSED PROTOCOL.....	50
FIGURE 5-1: FATIGUE CURVES FOR BEAMS UNDER HAVERSINE LOADING (TESTING IN ACCORDANCE WITH AGPT/T233)	54
FIGURE 5-2: REGRESSION EQUATION: APPROACH 2, ALL BEAMS	56
FIGURE 5-3: REGRESSION EQUATION: APPROACH 2, WITHOUT FAILED BEAMS.....	56
FIGURE 5-4: REGRESSION EQUATION FOR AVERAGED RESULTS AT DIFFERENT STRAIN LEVELS (APPROACH 2).....	56
FIGURE 5-5: DIFFERENT PHASES IN THE LABORATORY FATIGUE BEHAVIOUR OF ASPHALT (SOURCE: DI BENEDETTO ET AL. 2004)	61
FIGURE 5-6: EXAMPLE OF CURVE FITTING FOR DEFINED SCENARIOS (HAVERSINE LOADING).....	66
FIGURE 5-7: EXAMPLE OF CURVE FITTING FOR DEFINED SCENARIOS (SINUSOIDAL LOADING).....	66
FIGURE 5-8: DIFFERENCE BETWEEN PROPOSED MODEL AND LABORATORY RESULTS.....	68
FIGURE 5-9: ADJUSTING THE TERMINATION STIFFNESS FOR MODELLED FATIGUE CURVE	69
FIGURE 5-10: ADJUSTING THE TERMINATION STIFFNESS FOR FITTED CURVE.....	69
FIGURE 5-11: ADJUSTING THE TERMINATION STIFFNESS FOR FITTED CURVE ON 43.5% STIFFNESS REDUCTION STATE....	70
FIGURE 5-12: ADJUSTMENT FACTORS FOR TERMINATED TESTS IN DIFFERENT STIFFNESS LOSS STATE.....	70
FIGURE 5-13: AVERAGE, MAXIMUM AND MINIMUM ADJUSTMENT FACTORS FOR FATIGUE LIFE PREDICTION	71

FIGURE 5-14: SCHEMATIC OF LOCATIONS OF INFLECTION POINTS FOR DIFFERENT TERMINATION CONDITIONS	74
FIGURE 5-15: COMPARISON BETWEEN AUSTROADS AND LABORATORY FATIGUE LIFE PREDICTIONS (100 $\mu\epsilon$).....	77
FIGURE 5-16: COMPARISON BETWEEN AUSTROADS AND LABORATORY FATIGUE LIFE PREDICTIONS (200 $\mu\epsilon$).....	77
FIGURE 5-17: COMPARISON BETWEEN AUSTROADS AND LABORATORY FATIGUE LIFE PREDICTIONS (300 $\mu\epsilon$).....	78
FIGURE 5-18: COMPARISON BETWEEN AUSTROADS AND LABORATORY FATIGUE LIFE PREDICTIONS (400 $\mu\epsilon$).....	78
FIGURE 5-19: COMPARISON OF AUSTROADS AND LABORATORY RESULTS IN TERMS OF LOG (N_f).....	79
FIGURE 5-20: COMPARISON OF SINUSOIDAL AND HAVERSINE RESULTS IN TERMS OF LOG (N_f)	79
FIGURE 5-21: RESULTS OF FOUR-POINT BENDING TESTING A FREQUENCY OF 5 HZ AND A TEMPERATURE OF 4°C WITH THE STRAIN LEVEL GRADUALLY INCREASING (BEAM 53)	81
FIGURE 5-22: RESULTS OF FOUR-POINT BENDING TESTING A FREQUENCY OF 5 HZ AND A TEMPERATURE OF 4°C WITH THE STRAIN LEVEL GRADUALLY INCREASING (BEAM 53)	81
FIGURE 5-23: LINE-OF-BEST-FIT TO (FREQUENCY OF 5 HZ AND A TEMPERATURE OF 4°C FOR BEAM 53).....	82
FIGURE 5-24: OBSERVED HEALING PHENOMENON AT DIFFERENT FREQUENCIES AND A TEMPERATURE OF 4°C.....	84
FIGURE 5-25: OBSERVED HEALING PHENOMENON AT DIFFERENT FREQUENCIES AND A TEMPERATURE OF 20°C	85
FIGURE 5-26: OBSERVED HEALING PHENOMENON AT DIFFERENT FREQUENCIES AND A TEMPERATURE OF 40°C	86
FIGURE 5-27: SIGMOIDAL-FITTED CURVES AT DIFFERENT FREQUENCIES AND A TEMPERATURE OF 4°C	87
FIGURE 5-28: SIGMOIDAL AND HOMOGRAPHIC FUNCTIONS FITTED TO DATA COLLECTED AT 20°C AT DIFFERENT FREQUENCIES	87
FIGURE 5-29: HOMOGRAPHIC FITTED CURVES IN DIFFERENT FREQUENCIES AT 40°C	88
FIGURE 5-30: FATIGUE CURVES (HAVERSINE LOADING AND 0.1 SECOND REST PERIOD)	89
FIGURE 5-31: FATIGUE CURVES (HAVERSINE LOADING AND 0.3 SECONDS REST PERIOD)	89
FIGURE 5-32: FATIGUE CURVES (HAVERSINE LOADING AND 0.9 SECOND REST PERIOD)	90
FIGURE 5-33: FATIGUE CURVES (SINUSOIDAL LOADING AND 0.1 SECOND REST PERIOD)	90
FIGURE 5-34: FATIGUE CURVES (SINUSOIDAL LOADING AND 0.3 SECOND REST PERIOD)	90
FIGURE 5-35: FATIGUE CURVES (SINUSOIDAL LOADING AND 0.1 SECOND REST PERIOD)	91
FIGURE 5-36: FITTED FATIGUE CURVES (UNTERMINATED TESTS, APPROACH 5).....	91
FIGURE 5-37: MAXIMUM FATIGUE LIVES WHEN TESTING WAS CONDUCTED WITH AND WITHOUT REST PERIODS	93
FIGURE 5-38: RELATIONSHIP BETWEEN DYNAMIC MODULUS AND FREQUENCY FOR A RANGE OF TEMPERATURES	94
FIGURE 5-39: TYPICAL MASTER CURVE DEVELOPED BY TIME-TEMPERATURE SUPERPOSITION THEORY.....	95
FIGURE 5-40: MASTER CURVES FOR CYLINDRICAL SAMPLES (UNCONFINED CONDITION).....	101
FIGURE 5-41: MASTER CURVES FOR CYLINDRICAL SAMPLES (65 kPa CONFINING PRESSURE)	102
FIGURE 5-42: MASTER CURVES FOR CYLINDRICAL SAMPLES (135 kPa CONFINING PRESSURE)	103
FIGURE 5-43: FLEXURAL MASTER CURVES (HAVERSINE AND SINUSOIDAL LOADING)	103
FIGURE 5-44: MASTER CURVES FOR DIFFERENT TESTING CONDITION (APPROACH 6).....	104
FIGURE 5-45: TIME-TEMPERATURE SHIFT FACTORS FOR DIFFERENT TESTING CONDITIONS	104
FIGURE 5-46: VARIATION IN PHASE ANGLE FOR DIFFERENT TEST CONDITIONS.....	105

ACKNOWLEDGMENT

First and foremost, I would like to express my sincere gratitude to my supervisor, Professor Hamid Nikraz, for his support, for his patience, motivation, enthusiasm and both technical and personal guidance.

As well as my supervisor, I would like to especially thank Mr Kieran Sharp from ARRB Group for his skills and knowledge and for the technical review and editing of my thesis. Without his help, the preparation of this thesis by the due deadline would have been impossible.

I would also like to thank Mr Jim Beesley from the Australian Asphalt Pavement Association for his help and support and the technical staff from Curtin University Geomechanical Laboratory, especially Mr Darren Isaac for his great support during the testing program.

I wish to express my gratitude to the Australian Research Council (ARC) for the financial support of this research, under the ARC Linkage Scheme (LP110100634), conducted at the Department of Civil Engineering, Curtin University.

Last but not least, a special thanks to my family. Words cannot express how grateful I am to my mother, brothers and wife for all of the sacrifices that you have made on my behalf. I also thank all of my friends who supported and motivated me to strive towards my goal.

SUMMARY

The fatigue performance of asphalt is addressed in the mechanistic-empirical pavement thickness design procedure used in Australia. In this procedure, the Shell laboratory model is adjusted to field conditions through the use of a reliability factor. However, the use of these procedures can result in the fatigue life being longer than predicted, which is an issue of concern to industry. The aim of the research presented in this thesis was to investigate the laboratory fatigue performance of a typical asphalt mix used in Western Australia as a structural (>40 mm thick) layer, including the development of new testing protocols, a new fatigue life prediction model, an accelerated testing approach, and master curves that can be input into the ME design procedures used in Australia. Testing was conducted using the EN Standard Tester (a four-point bending beam apparatus) and the Asphalt Mixture Performance Tester (AMPT). New testing protocols were developed to minimise errors associated with the use of the EN Standard Tester and the AMPT. An innovative technique has been proposed to refine the out-of-range phase angle problem with the current software used to control the bending beam tests. Enhanced control engineering techniques can be used to address issues associated with noisy stress-shapes, out-of-range strain levels and load standard errors. The results are more reliable and robust. Two scenarios are proposed to extrapolate fatigue life when the termination condition (50% of initial stiffness) is not met. A new accelerated testing approach, which involves increasing the strain level continuously at different temperatures and frequencies, is also proposed. Finally, flexural bending master curves for both haversine and sinusoidal loading were developed which can be compared with compressive master curves developed as a result of testing cylindrical specimens. Recommendations for further research are also provided.

1 INTRODUCTION

1.1 Background

Each year road agencies in Australia spend billions of dollars managing their road network. A major component of that budget is devoted to providing, and maintaining pavements whose structures are designed to provide a safe and smooth surface capable of performing under the increasing heavy vehicle axle loads being applied to them.

Traditionally, methods for the structural design of flexible pavements were empirical in nature. This approach did not allow designers to consider the properties of the pavement materials when determining likely fatigue and rutting performance. In order to take due consideration of the properties of the materials in the design process, mechanistic-empirical (ME) approaches were developed which allowed due account to be taken of the response of the pavement material to repeated loading. In the ME approach, shift factors are applied to laboratory-derived theoretical models to provide a closer fit with observed field performance.

The most common flexible pavement type used in Australia consists of one or more unbound granular layer(s) protected by a thin bituminous surfacing (sprayed seal). These surfacings provide a smooth ride and act as a water-proofing agent to prevent the ingress of moisture into the pavement structure (assuming that adequate drainage of the lower layers of the pavement is also provided). Sprayed seals are not considered to contribute any structural capacity to a pavement.

As the number of axles on heavy vehicles, and the associated axle loads, continues to increase, the use of asphalt¹ pavements – either full depth asphalt or a structural surfacing over a stabilised or granular base – is becoming more common, particularly on major freight routes serving urban areas.

The fatigue performance of asphalt is addressed in the ME pavement thickness design procedure used in Australia (Austroads 2012). In this procedure, the Shell (1978) laboratory model is adjusted to field conditions through the use of a reliability factor. However, the use of these procedures can result in the fatigue performance being longer than predicted, which is an issue of concern to industry.

¹ The term 'asphalt' is used in Australia to describe a structural layer composed of graded aggregate and bituminous binder, unlike usage in other countries (such as the USA) where the term 'asphalt' is used to describe the binder only.

As discussed in more detail in Section 1.3, the aim of the research presented in this thesis was to investigate the laboratory fatigue performance of a typical asphalt mix used in Western Australia as a structural (>40 mm thick) layer, including the development of new testing protocols, a new fatigue life prediction model, an accelerated testing approach, and master curves that can be input into the ME design procedures used in Australia.

Testing was conducted using the EN Standard Tester (a four-point bending beam apparatus) and the Asphalt Mixture Performance Tester (AMPT) developed by IPC Global. The EN Standard Tester was used to examine the fatigue behaviour of the asphalt and also to develop flexural master curves, whilst the AMPT was used to examine the viscoelastic behaviour of the same mix by developing compressive master curves. All testing was conducted at the Curtin University Geomechanical Laboratory.

1.2 Significance of the research

Fatigue cracking of asphalt has been investigated by many researchers, with the four-point bending beam apparatus being the most common test used in these investigations. Testing is generally conducted on beams, rectangular in cross-section, cut from slabs prepared in the laboratory.

There are two types of test modes: constant stress and constant strain. In the constant stress mode, which is also referred to as the constant force mode, the load is kept constant, with the deflection of the test beams changing (increasing) during testing. In the constant strain mode, which is sometimes referred to as the constant deflection mode, the deflection is kept constant, with the applied force changing during testing so as to induce a constant deflection.

As four-point bending testing can be very time-consuming, and therefore expensive, new accelerated testing methodologies – and new approaches to data analysis – are being developed in this study which make the testing and analysis process faster and more reliable.

A large number of studies have also addressed the viscoelastic behaviour of asphalt mixes. The majority of these studies involve the use of dynamic modulus testing and the development of master curves for different mix types. However, very few studies of the viscoelastic properties of asphalt have been conducted on Western Australian mixes. It was therefore considered crucial that a set of dynamic modulus

master curves be developed for a mix typically used in Western Australia. Master curves for other mixes could be developed in future studies.

1.3 Objectives of the research

The objectives of the research presented in this thesis were to:

1. Develop testing protocols for the evaluation of the fatigue and viscoelastic properties of a standard asphalt mix commonly used as a structural (> 40 mm thick) layer in pavements in WA.
2. Develop a new fatigue life prediction model based on the laboratory test data.
3. Develop a new accelerated laboratory testing approach that allows the fatigue behaviour of asphalt to be modelled at different test temperatures, loading frequencies and strain levels.
4. Develop master curves for the asphalt mix that can be input into the mechanistic-empirical design procedures used in Australia.

1.4 Structure of the thesis

This thesis is divided into six chapters as follows:

1. Introduction – the significance and objectives of the research.
2. Literature review – a review of previous work, including its relevance to practice in WA, and the identification of research gaps.
3. Sample preparation and the characterisation of the AC14/75 mix, e.g. particle size distribution (PSD), bulk density and maximum density.
4. Results of preliminary testing – including the resolution of errors associated with the use of the EN Standard tester and the AMPT and the presentation of a new testing protocol which aims to address these errors and minimise their impact on the results.
5. Presentation of test results and data analysis – including details of a new fatigue model and a new accelerated testing method as well as the development of master curves for the AC14/75 mix.
6. Summary, conclusions and recommendations.

Relevant data are also provided in five Appendices.

2 LITERATURE REVIEW

2.1 Introduction

This chapter summarises research conducted on the fatigue behaviour of asphalt mixes, including the determination of dynamic modulus and the development of master curves. The scope of work presented in this chapter is outlined in Figure 2-1.

The failure modes of flexible pavements are first discussed, followed by background on the fatigue failure and dynamic modulus of asphalt. The fatigue studies are divided into two parts: numerical analyses and experimental studies. As this research involves the modelling of asphalt, the majority of this chapter concentrates on experimental studies. Finally, a summary of the review is presented, including the identification of research gaps and how the research presented in this thesis addresses some of these gaps.

2.2 Modes of failure of flexible pavements

Austroroads (2010) defines a pavement as 'that portion of a road designed for the support of, and to form the running surface for, vehicular traffic'. It also defines the pavement structure as 'the portion of the road, excluding shoulders, placed above the design subgrade level for the support of, and to form a running surface for, vehicular traffic'.

Road pavements are divided into three major types: flexible, rigid (concrete pavements) and composite pavements (Huang 1993; Austroroads 2012). The focus of the research presented in this thesis is on flexible pavements, specifically pavements composed of one or more asphalt layers.

The thickness and strength of each layer of a flexible pavement varies depending on several parameters. In addition, each layer is affected by the ability of the upper layers to transfer the load to the next layer. The upper layers should be of higher quality and strength due to the fact that they are more exposed to traffic loads and environment conditions (Huang 1993).

The deterioration of flexible pavements is associated with many, often inter-associated, factors. Pavement failure/distress is associated with the magnitude of

the stresses and strains generated in the pavement under load and over time (Adlinge & Gupta 2013).

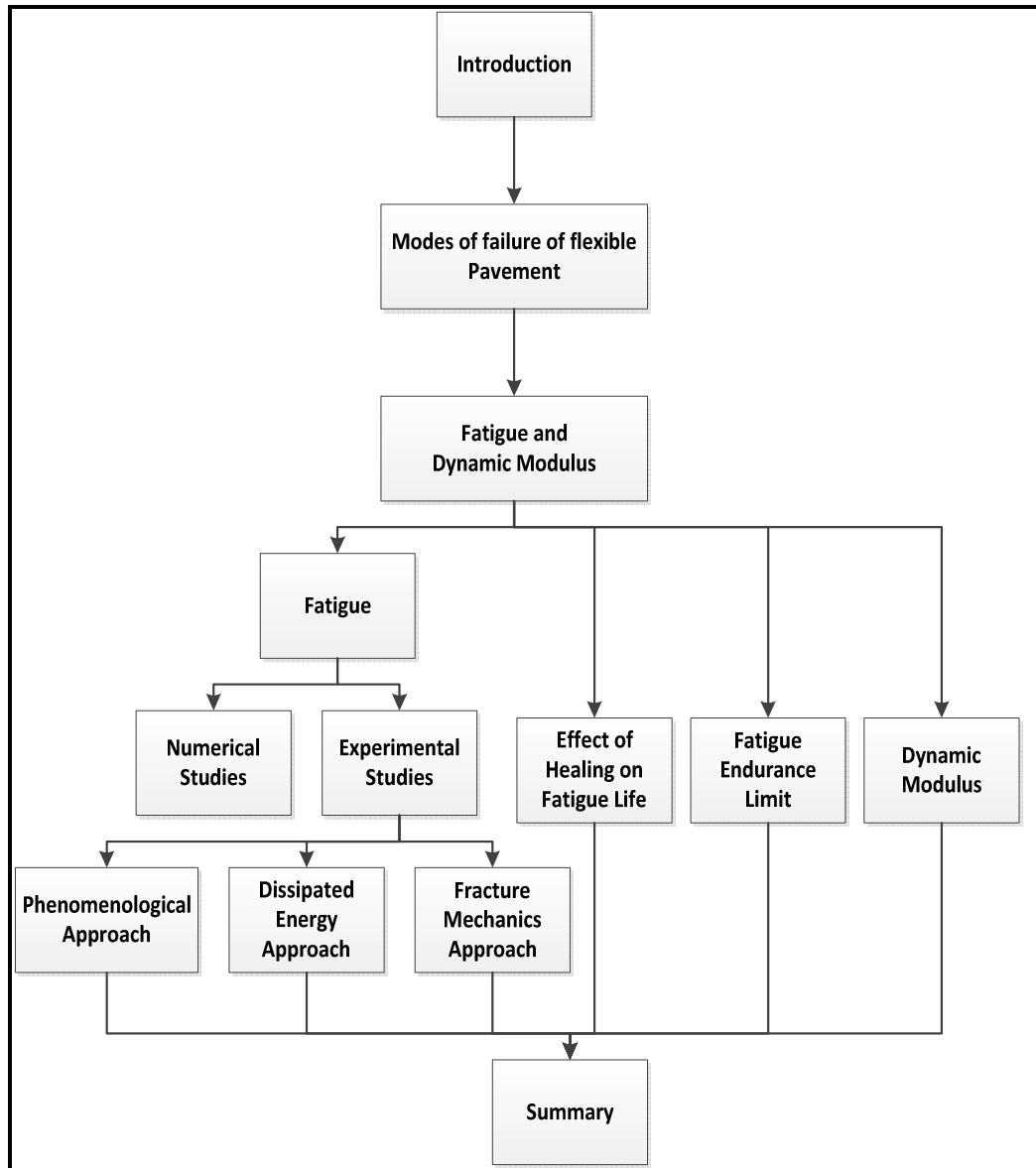


Figure 2-1: Literature review scope of work

Pavement distresses can be divided into four major types: cracking, surface deformation (rutting, shoving, etc.), disintegration (potholes, etc.) and surface defects (bleeding, raveling, etc.). The most common types of cracking in pavements are fatigue cracking, longitudinal cracking, transverse cracking, block cracking, slippage cracking, reflective cracking and edge cracking. The addition of some form of additive (polymer, latex, tyre rubber, etc.) can increase the workability of asphalt however it can mitigate cracking.

Fatigue cracking can be associated with an increase in traffic loading (number of vehicles, axle load, etc.), changes in temperature profiles, the (poor) condition of the

road shoulders, inadequate drainage, and poor temperature control of the asphalt during manufacture.

In many countries, rutting is the major mode of failure of flexible pavements because of the axle loads, tyre pressures and environmental conditions under which the pavement operates. Rutting can occur in all layers of the pavement. It can lead to ponding of water in the wheelpaths and the associated problems of spray and hydroplaning and a loss of ride quality. The control of permanent deformation in an asphalt pavement is a key design consideration (Choi and Kim 2013).

Rutting mostly occurs under heavy traffic loading in areas of high pavement temperature, though it can also be related to the action of slow-moving and braking traffic at intersections. As a result, rutting is confined to the top layers of the pavement (Long 2001). Shear deformation (no volume change) and densification (volume change) are related to permanent deformation/rutting (Miljković and Radenberg 2011).

Rutting can be categorised into three basic groups: one-dimensional (or vertical deformation), lateral flow (or plastic movement), and mechanical deformation (Miljković and Radenberg 2011).

Many studies have been undertaken on the role that asphalt mix design plays in controlling rutting (Garba 2002). For example, Miljković & Radenberg (2011) reported that, whilst the properties of the aggregate and bitumen are directly related to rutting, load magnitude, loading rates and temperature also have a strong influence on the rutting performance of asphalt mixes. They carried out dynamic modulus, repeated load permanent deformation (flow number) and static permanent deformation (flow time) testing, including a comparison of the effect of gyratory compaction on rutting performance compared to more traditional forms of compaction.

Choi and Kim (2013) developed a shift model to determine the rut depth of asphalt pavements. Rut depths were measured at sites located at the National Centre for Asphalt Technology (NCAT) test track and sections subjected to accelerated pavement testing using the Federal Highway Administration's Accelerated Load Facility (FHWA ALF). It was found that the model – and the associated Triaxial Stress Sweep (TSS) test protocol – could accurately determine rutting of asphalt under accelerated loading. They concluded, however, that the proposed model

needed further development if an accurate rut depth was to be predicted in cases where shear flow regulated permanent deformation.

As the emphasis in this thesis is on asphalt fatigue, the rest of this review will concentrate on that issue.

2.3 Fatigue and dynamic modulus

2.3.1 Fatigue

Fatigue cracking is one of the most common pavement failure modes of asphalt or other bound layers (e.g. cemented material). It is induced by the application of heavy repetitive traffic movements and associated high degree of flexing in the asphalt which generate the stresses and strains that eventually cause fatigue in the mix (Asadi, Leek and Nikraz 2013; Adeyinka Azeez 2013). The maximum tensile strain during traffic loading generally occurs at the bottom of asphalt layer and this is where it was generally believed where cracking was initiated. Over time, these cracks start to connect and propagate to the surface until the surface is similar to the skin of an alligator (alligator cracking) (Shahin 1994). This type of cracking also is known as bottom-up fatigue cracking.

More recent studies, however, have shown that fatigue cracking can be initiated at both the top and bottom layers of the asphalt layer(s). The fatigue cracking that originates at the top of asphalt layer is associated with stiffness and roughness whereas the fatigue cracking that originates at the bottom is associated with the cyclic tensile stresses and strains.

In thick asphalt pavements, such as full depth asphalt pavements, there is evidence of top-down cracking, i.e. cracking initiating at the top. Normally these cracks initiate in the longitudinal wheelpath of traffic. Although several causes have been suggested for this mode of failure, no robust conclusion has been reached in terms of the mechanisms for this cracking. Explanations of this top-down cracking phenomenon offered in the literature include the combination of shear and tensile strains associated with high tyre pressures, shear failure resulted from ageing of the asphalt – which makes the surface stiffer and more brittle – and higher temperature gradients (Abojaradeh 2003).

The design of asphalt pavements requires laboratory testing to be conducted at a range of loads, loading times, rest periods, and at a range of environmental conditions to take account of temperature, healing, aging, etc. (Baburamani 1999).

In summary, the fatigue performance of asphalt mixes is very complex and depends on many different parameters. Many investigations have been conducted aimed at developing a more precise procedure for predicting fatigue life.

2.3.2 Numerical investigations on the fatigue life of flexible pavements

Aure and Ioannides (2012) reported studies of the fatigue behaviour of pavement slabs using numerical finite element (FE) analysis. The FE program ABAQUS/STANDARD®, version 6.9-2, was used in the study. They also examined the influence of softening curve, cohesive zone width and mesh, loading mode, tensile strength, and fracture energy. The results indicated that the type of softening curve and cohesive zone width and mesh did not significantly influence the response and that fracture energy had a greater influence on the fracture process than tensile strength.

Ziaei-Rad et al. (2012) investigated the meso-structure of asphalt mixes using a new technique based on the fact that the aggregate particles can join together into a simulation area by defining the simulated interface forces between the particles. In addition, the generated isolated grains will try to fill the space using Voronoi tessellation method. It was concluded that the use of this model resulted in an enhanced understanding of the influence of loads moving at different speeds on the mechanical response of asphalt layers.

It was found that the calculated stresses in the mastic zone were in line with the computed strength values, and stated that the 2D models were very consistent in terms of their ability to determine stress states in the mastic of the asphalt mix. In addition, the results indicated the significant effect of the stiffness of the elastic foundation on the displacement of the asphalt surface. However, the elastic stiffness of the foundation did not have a significant effect on the Von Mises stress in the mastic area.

2.3.3 Experimental investigations carried out on laboratory fatigue life

Several methods have been suggested in the literature to investigate the laboratory fatigue behaviour of asphalt mixes. The main approaches can be categorised as follows (Baburamani 1999):

- strain-stress approach (sometimes known as phenomenological approach)
- dissipated energy approach
- fracture mechanics approach.

In addition, different testing protocols and devices are used to evaluate the fatigue performance of asphalt mixes in the laboratory, including the four-point bending beam test, the three-point bending beam test, and the trapezoidal cantilever test (which is also known as the two-point bending beam test).

2.3.3.1 Strain-stress approach

Over the past 50 years, a large number of asphalt fatigue life prediction models have been proposed by different researchers. Two of the most simple and well-known fatigue life prediction models were suggested by Monismith et al. (1961) and Pell (1962). These models relate tensile strain or tensile stress to the fatigue life using some experimental coefficients as shown in Equation 2-1 and Equation 2-2.

$$N_f = K_1 \left(\frac{1}{\epsilon_t} \right)^{K_2} \quad 2-1$$

$$N_f = K_1 \left(\frac{1}{\sigma_t} \right)^{K_2} \quad 2-2$$

where

N_f = fatigue life (cycles)

ϵ_t = horizontal tensile strain at bottom of specimen

σ_t = horizontal tensile stress at bottom of specimen

K_1 and K_2 = experimental coefficients obtained from laboratory testing

The Asphalt Institute (1982) and Shell (1978) modified Equation 2-1 by proposing a new fatigue model which considered the initial stiffness of the asphalt as a major parameter. As the stiffness varies with temperature and frequency of loading, they became a base for other fatigue life prediction models. The Asphalt Institute and Shell fatigue prediction models are shown in Equation 2-3 and Equation 2-4 respectively:

$$N_f = 0.0796(\epsilon_t)^{-3.291}(E_1)^{-0.854} \quad 2-3$$

$$N_f = 0.0685(\epsilon_t)^{-5.671}(E_1)^{-2.363} \quad 2-4$$

where

E_1 = flexural stiffness of asphalt layer (psi)

Other researchers (e.g. Pell et al. 1975; Harvey et al. 1995) concluded that the air void content of the mix played a significant role in the fatigue life of asphalt. Based on this, they added to the model one of the volumetric properties of asphalt, viz. voids filled with asphalt (VFA), to account for the effect of air voids content. This model is shown in Equation 2-5.

$$N_f = K_1 \left(\frac{1}{\epsilon_t} \right)^{K_2} \left(\frac{1}{E_1} \right)^{K_3} (VFA)^{K_4} \quad 2-5$$

where

$$\begin{aligned} VFA &= \text{voids filled with asphalt (\%)} \\ K_1, K_2, K_3 \text{ \& } K_4 &= \text{experimental coefficients obtained from laboratory testing} \end{aligned}$$

Several researchers have attempted to develop their own models by modifying Equation 2-1 to Equation 2-5. For example, Pais and Minhoto (2010) attempted to modify Equation 2-1 by performing fatigue tests on more than 50 asphalt mix specimens, composed of four different aggregates and binders. Four-point bending beam testing was conducted at a temperature of 20°C and a frequency of 10 Hz. They suggested that establishing an accurate relationship between k_1 and k_2 would result in more precise fatigue life prediction. They proposed the following relationship between K_1 and K_2 (Equation 2-6). By feeding Equation 2-6 into Equation 2-1, they proposed a new fatigue life prediction model (Equation 2-7).

$$K_1 = 2503.836 \times e^{6.968K_2} \quad 2-6$$

$$N_f = 2503.836 \times e^{6.968K_2} \left(\frac{1}{\epsilon_t} \right)^{K_2} \quad 2-7$$

Using Equation 2-5 as a base Witczak and Mirza (2000) added the thickness of the asphalt layer and the bitumen penetration index (PI) to the model. This model uses a sigmoidal function to predict the fatigue life of in-service flexible pavements as shown in Equation 2-8:

$$N_f = A_f \left(1 + \frac{13909S_m^{-0.4} - 1}{1 + e^{(1.354h_{ac} - 5.408)}} (0.0252PI - 0.00126PI \times V_b - 0.0167)^5 \epsilon_t^{-5} S_m^{-1.4} \right) \quad 2-8$$

where

$$\begin{aligned} A_f &= \text{adjustment factor to relate laboratory results to field observations} \\ S_m &= \text{stiffness of mix (psi)} \\ V_b &= \text{binder content of mix by volume (\%)} \\ h_{ac} &= \text{thickness of asphalt layer (inch)} \\ PI &= \text{Penetration Index} \end{aligned}$$

In another research study (El-Basyoun and Witczak 2005), the Asphalt Institute model was modified so it could be used to predict in-service asphalt pavement fatigue life (Equation 2-9 to Equation 2-12). This model is currently used in the

AASHTO Mechanistic-Empirical Pavement Design Guide (MEPDG) (AASHTO 2008)².

$$N_f = 0.00432 \times K \times C(\epsilon_t)^{-3.9492}(E_1)^{-1.281} \quad 2-9$$

$$C = 10^M \quad 2-10$$

$$M = 4.84\left(\frac{v_{be}}{v_{be} + v_a} - 0.69\right) \quad 2-11$$

$$K = \frac{1}{0.000398 + \frac{0.003602}{1 + e^{(11.02 - 3.49h_{ac})}}} \quad 2-12$$

where

v_{be} = effective binder content (%)

v_a = air void content (%)

2.3.3.2 Dissipated energy approach

Basically, the dissipated energy is the area of the hysteresis loop generated when the normalised stresses and strains, normally generated during four-point bending beam testing, are compared as shown in Figure 2-2.

The dissipated energy can be calculated using Equation 2-13:

$$W_i = \pi \sigma_i \epsilon_i \sin \phi_i \quad 2-13$$

where

W_i = dissipated energy at loading cycle i

σ_i = stress at loading cycle i

ϵ_i = strain at loading cycle i

ϕ_i = phase lag between stress and strain at loading cycle i

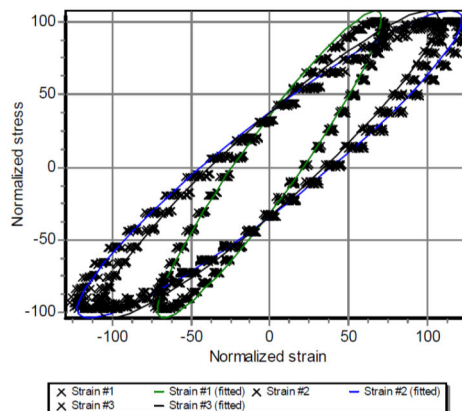


Figure 2-2: Schematic strain-stress hysteresis loop

² A presentation describing the AASHTO Guide can be accessed at:
http://vtcaonline.com/images/presentations/LB1012_MEPDG.pdf.

By summing all the recorded dissipated energy for each cycle, the cumulative dissipated energy can be calculated using Equation 2-14.

$$W_c = \sum_{i=1}^N W_i \quad 2-14$$

where

W_c = cumulative dissipated energy at cycle N

Van et al. (1972) suggested that the dissipated energy approach was a useful method for simulating the fatigue performance of asphalt mixes in the laboratory. They proposed a model (Equation 2-15) which relates the fatigue life of asphalt to the cumulative dissipated energy. In other research, Van and Visser (1977) concluded that the dissipated energy was independent of loading mode, temperature and frequency.

$$W_{fatigue} = AN_f^Z \quad 2-15$$

where

$W_{fatigue}$ = cumulative dissipated energy when fatigue failure occurs

N_f = number of cycles to fatigue failure

A & Z = experimental coefficient obtainable from laboratory test data

During SHRP2, Project A-404 (SHRP 1994) it was found, after extensive laboratory testing, that the dissipated energy was very sensitive to loading mode.

Hopman et al. (1989), Pronk and Hopman (1990), Rowe (1993), Rowe and Bouldin (2000) and Abojaradeh (2003) also used the energy ratio concept to predict the fatigue life of asphalt mixes.

Carpenter and Jansen (1997) proposed the *ratio of dissipated energy change (RDEC)* methodology to predict the fatigue life of asphalt mixes. Shen and Carpenter (2007) found that the energy dissipates in different ways (e.g. thermal) and that a percentage of the dissipated energy results in fatigue failure. The relationship between the dissipated energy ratio change from cycle a to b and the energy after cycles a and b is shown in Equation 2-16.

$$RDEC_a = \frac{DE_a - DE_b}{DE_a \times (b - a)} \quad 2-16$$

where

- $RDEC_a$ = dissipated energy ratio change from cycle a to b
 DE_a = dissipated energy at cycle a
 DE_b = dissipated energy at cycle b

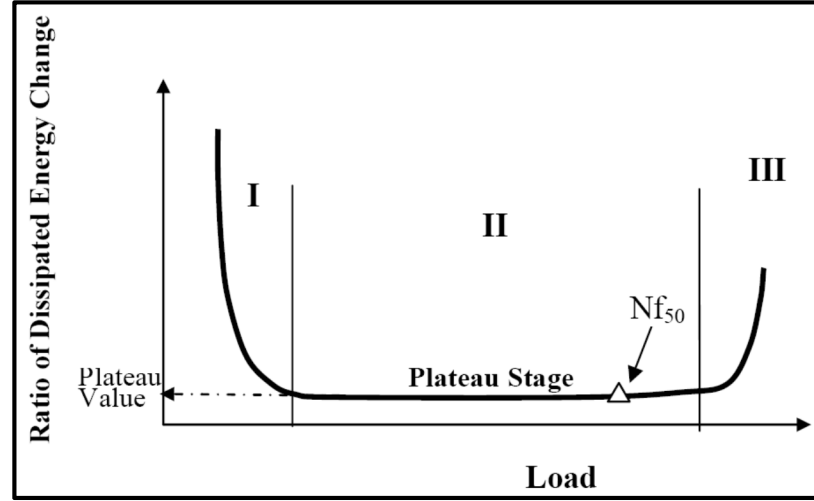


Figure 2-3: Schematic RDEC plot (Shen and Carpenter 2007)

Shen and Carpenter (2007) also presented a curve to better explain the RECD (see Figure 2-3). They also identified the Plateau Value (PV), which is the point in the RECD curve where fatigue failure occurs. Based on test results obtained on fine aggregate matrix (FAM), Bhasin et al. (2009) found that the RECD was highly correlated to the loading mode.

2.3.3.3 Fracture mechanics approach

Majidzadeh (1975) used fracture mechanics theory to establish a relationship between the rate of crack propagation and intensity factor using Paris' (1963) law (Equation 2-17):

$$N_f = \int_{C_0}^{C_f} \frac{1}{AK^n} dc \quad 2-17$$

where

- N_f = number of cycles to the failure
 C_0 = starting flaw
 C_f = final crack length
 A & n = experimental parameters
 K = stress intensity factor

Basically, two types of testing have been used: *single edge notched beam [SE (B)]* and *double edge notched tension (DENT)* which are illustrated in Figure 2-4 (Kim and Marasteanu 2012).

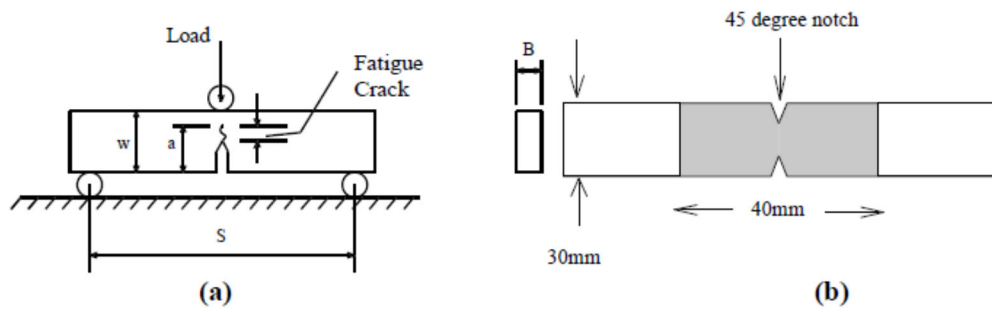


Figure 2-4: Schematic single edge notched beam [SE (B)] (a) and double edge notched tension (DENT) (b) (Kim and Marasteanu 2012)

Anderson et al. (2001) examined the fracture toughness of 14 binders (including 'standard' and modified binders) using the SE(B) apparatus. The aim of the study was to observe the effect of different gradings on low-temperature cracking resistance. Olard and Di Benedetto (2004) also studied the effect of temperature and frequency of loading using the SE(B) apparatus. They found that the temperature and frequency of loading did not affect the fracture toughness significantly.

Andriescu et al. (2004) also examined the fracture energy of five different notch lengths. They used the DENT test to estimate the fatigue life of a range of asphalt binders. Other researchers, including Roy and Hesp (2001), Zofka and Marasteanu (2007) and Gauthier and Anderson (2006) compared the DENT test results with results obtained using direct tension testing (DTT) on different binder types at different temperatures. They concluded that the DENT was more reliable than the DTT in terms of repeatability and fatigue cracking prediction.

2.3.4 Effect of healing on fatigue life

Self-healing of asphalt mixes during laboratory testing has been researched over last 40 years. The phenomenon is related to the fact that, directly after cracks connect together, molecular movement commences and, if there is no extra loading, the cracks heal.

Whether or not self-healing is observed is generally related to the length of the rest period, the test temperature and the size of the cracks when they first develop (Qiu et al. 2012). This has also been observed in several other studies, with the rate of healing increasing as the temperature increased.

On that basis, it would be reasonable to suggest that, in warmer environments such as those operating in Western Australia, micro-cracks in pavements could be observed to heal (Rickards 2012).

Philips (1998) identified the following three stages in micro-crack healing:

1. closure after cracks join together due to surface energy (termed as 'wetting')
2. closure due to consolidating stresses and binder flow
3. complete recovery of the material's mechanical properties.

Mamlouk et al. (2012), Castro and Sanchez (2006) and Bonnaure et al. (1982) attempted to investigate crack-healing by introducing rest periods to the loading regime during four-point bending beam testing. They observed significant increases in laboratory fatigue life after rest periods were added.

Qiu et al. (2012) investigated the self-healing behaviour of an asphalt beam on an elastic foundation (BOEF). It was observed that the micro-cracks of the BOEF healed. The authors reported that, at the commencement of the healing period, the delayed viscoelastic healing was the major purpose of the crack opening displacement (COD). They concluded that the healing was related to viscoelastic recovery and viscous flow. Qiu et al. (2012) attempted to observe the self-healing of a dense-graded asphalt mix (type DAC 0/8) again using the BOEF. A notched asphalt beam was placed on a low-modulus rubber foundation, with a constant load applied via loading-unloading-healing-reloading cycles. The elastic foundation was used to prevent permanent deformation, and to control the healing process. The results showed that, under different healing conditions, both the loading and reloading paths of all the specimens were almost the same.

Garcia, Schlangen and Van de Ven (2010) assessed two new methods to increase the healing rate of asphalt. The first method was passive self-healing, which involves encapsulated chemicals being added to the binder. When the micro-cracks start to initiate in the binder due to ageing and accumulated damage, the capsules break and the chemicals penetrate into the binder and repair the asphalt. In other words, by reducing the stiffness, the healing of bitumen rate increases. The second method involves an active self-healing mechanism which is directed at the cracks to close them and seal the asphalt pavement. In this case the binder is repaired by inside-healing of the material to improve its properties.

Shen, Chiu and Huang (2010) studied the influence of cohesive healing, without the interaction of aggregates. They attempted to quantify healing using the dissipated energy approach and the Dynamic Shear Rheometer test and a specifically tailored intermittent loading sequence. The healing rate was considered to be the rate of dissipated energy (DE) recovery per unit of rest time, and this was used to calculate the healing rate of the binder. The test results indicated the significant effect of binder type, strain level and temperature on binder healing.

The tests were conducted on two asphalt binder types (PG64-28 and PG70-28) in the constant stress mode at a frequency of 10 Hz with different rest periods and two temperatures (15°C and 25°C). Fatigue lives were also determined when testing was conducted without any rest periods. The strain-Nf50 followed a linear trend for each binder and tests condition. Shorter fatigue lives were observed at the lower temperatures at the same initial strain level. Healing rates for the PG64-28 binder were higher 15°C compared to 25°C.

2.3.5 Fatigue endurance limit

The magnitude of the tensile strain at the bottom of an asphalt layer is the major factor in terms of controlling the fatigue cracking of a pavement (Soltani, Solaimanian and Anderson 2006; Austroads 2012).

A great deal of research has been conducted examining the relationship between the tensile strain at the bottom of an asphalt layer and fatigue life. For example, Ning et al. (2010) found that, if the tensile strain at the bottom of an asphalt layer is preserved at the lower level of the fatigue endurance limit (FEL) of asphalt, then the fatigue life will be unlimited.

Ning et al. (2010) examined two primary parameters, tensile strain and flexural stiffness, under different strain levels and temperatures using both the four-point bending beam test and the monotonic uniaxial tensile test (MUTT). In addition, a new parameter, the initial stress ratio (R_{initial}), was investigated as a means of linking the two tests. This new parameter *was defined as the ratio of applied initial stress and tensile strength of the sample*. It was found that the FEL could be described as a function of the initial flexural stiffness, frequency and stiffness. The test results indicated that R_{initial} increased sharply, resulting in a shorter fatigue life.

Carpenter, Ghuzlan and Shen (2003) examined the FEL by carrying out testing on asphalt with different binder types over a wide range of load repetitions (5 to 48

million) and at tensile strain levels as low as $70 \mu\epsilon$. The test results confirmed that the fatigue endurance limit ranged between 70 and $90 \mu\epsilon$.

2.3.6 Dynamic modulus of asphalt

According to Ceylan et al. (2008) the dynamic modulus ($|E^*|$) is one of the most important properties of asphalt. It is input into all three hierarchical levels in the AASHTO (2008) Mechanistic Empirical Pavement Design Guide (MEPDG). There is a difference between *resilient modulus* and *dynamic modulus*. The *dynamic modulus* is the absolute value of complex modulus. The *resilient modulus* is derived from testing when the load is applied in any waveform with a certain rest period, whilst the *dynamic modulus* is derived from testing conducted using a sinusoidal or haversine waveform and without any rest period (Huang 1993).

Archila and Diaz (2011) studied the effect of material properties on the rutting behaviour of asphalt mixes by comparing two scenarios: (1) where only the dynamic modulus was used to model the permanent deformation, and (2) where the rutting prediction model was modified by adding the air void and binder contents to the MEPDG rutting prediction model based on relationships developed in the laboratory. The results showed the significant effect of air void and binder content and binder type on both the dynamic modulus and rutting behaviour of the mixes.

Currently in Australia, the pavement design methodology (Austroads 2012) only uses the resilient modulus of the pavement materials; the viscoelastic behaviour is not included in design and analysis. However, the dynamic modulus is used in the AASHTO MEPDG procedure.

Kumlai et al. (2014) examined the differences resulting if the dynamic modulus was converted to resilient modulus, compared with the resilient modulus. Three concrete mixes having different maximum aggregate sizes were selected. The resilient and dynamic moduli were determined using the universal testing machine (UTM-25P) tester and the asphalt mixture performance tester (AMPT) respectively. The dynamic and resilient modulus values were higher for the mixes having the greater maximum aggregate size. The results showed that, without a reliable method, it was not possible to compare the dynamic and resilient modulus values. They concluded that comparison would be possible only when testing conditions (e.g. temperature and frequency) for both tests were kept the same.

The AMPT is designed to evaluate the engineering properties of an asphalt mix. This system can evaluate the rutting resistance of asphalt mixes quickly using flow number tests. In addition, it can simplify the development of dynamic modulus master curves (FHWA 2013).

Diaz and Archila (2013) developed software (Hot Mix Asphalt Analysing Tool (HMA AT)) which is compatible with the AMPT. This software allows users to automatically generate master curves for a variety of mix types, temperatures and frequency levels.

As already discussed, two factors that have a large influence on the dynamic modulus of asphalt are temperature and loading rate. Typical dynamic modulus master curves developed at temperatures of 4°C, 20°C and 40°C and loading frequencies of 10, 1, 0.1 and 0.01 Hz are shown in Figure 2-5. Whilst the aggregate type, gradation, volumetric properties and binder type can influence the shape of the master curve, the overall range will not change extensively (NCHRP 2008a).

In terms of the influence of confining pressure on the test results, studies have suggested that the sensitivity of dynamic modulus measurements to confining pressure differs for dense-graded mixes compared to gap-graded and open-graded mixes (NCHRP 2008a).

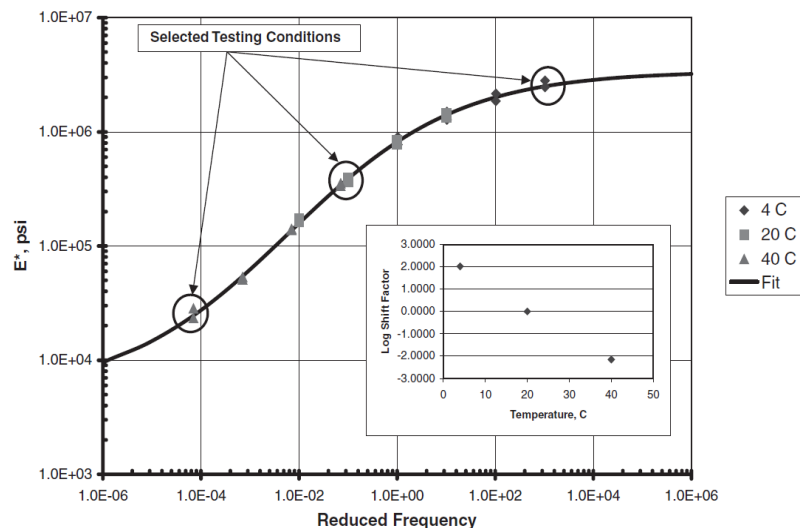


Figure 2-5: Typical dynamic modulus master curve (NCHRP 2008a)

Shahadan et al. (2013) carried out some investigation on the dynamic modulus and phase angle of asphalt mixtures including reclaimed asphalt pavement (RAP). In this research, the effect of three different temperatures (20°C, 40°C and 50°C) and

six different loading frequencies (0.1, 0.5, 1, 5, 10 and 25 HZ) were examined using the AMPT.

It was found that increasing the RAP content and loading frequency at a constant temperature resulted in an increase in dynamic modulus. However, when the RAP content and the temperature increased, the dynamic modulus values decreased.

Statistical analysis (ANOVA) showed that the temperature and load frequency had a major effect on the dynamic modulus and phase angle. The results confirmed that increasing the RAP content made the material more rut resistant, the addition of more than 20% RAP resulted in a decrease in fatigue life. Maintaining the loading frequency between 15 Hz and 20 Hz resulted in higher dynamic modulus values than at the other frequencies.

Nair and Priyadharshini (2013) investigated the dynamic modulus of modified and unmodified asphalt mixes in India, specifically the influence of temperature and loading frequency. The dynamic modulus results were then used to develop a master curve. It was found that the laboratory performance of the modified mixes was superior to the unmodified mixes at higher temperatures, the dynamic modulus of the modified mixes was lower at different frequencies and that the modified mix was more resistant to rutting than the unmodified mix.

Ceylan et al. (2008) attempted to improve the dynamic modulus prediction models using Artificial Neural Networks (ANN) followed by laboratory analysis and measurement. The ANN model was also compared with the Hirsch dynamic modulus prediction model utilising the same input variables. It was concluded that the ANN model was able to better predict the dynamic modulus than Hirsch model.

Ghaffarpour et al. (2009) developed stiffness master curves for some asphalt mixes. Their study revealed that loading time and temperature were the factors which had the most significant influence on the mechanical properties of viscoelastic materials. The experimental test results obtained at various temperatures were compared with the frequency. In this investigation, two different sigmoidal and polynomial models were used to represent the master curve function using a non-linear least square regression technique (Ghaffarpour et al. 2009). The polynomial and sigmoidal models were compared using Williams, Landel & Ferry (WLF) equation. A good consistency was achieved using the sigmoidal model at temperatures of 5°C, 25°C, and 45°C.

Zhu et al. (2011) investigated the influence of four polymer modifiers on the performance of asphalt mixes. In this study, the effect of temperature, frequency and confining pressure on the dynamic modulus of asphalt was investigated and the master curves developed. They used Witczak's (2002) model to predict the dynamic modulus and then adjusted the results to a reference temperature of 40°C. The results showed that the Witczak model could be used to predict the dynamic modulus of polymer-modified asphalt mixes. In addition, the dynamic modulus was higher at high frequencies, low temperatures and high confining pressures.

The AASHTO MEPDG uses dynamic modulus and Poisson's ratio to determine the characteristics of asphalt mixes. Cross and Sumesh (2007) conducted testing at various temperatures, stress levels and loading frequencies. A master curve was developed to explain the correlation between stiffness, mix temperature and frequency of loading. The master curve was also united with a binder aging model. The use of this master curve resulted in an increase in the predicted service life of the pavement.

Clyne et al. (2003) carried out complex modulus testing of four typical Minnesota asphalt mixes and generated master curves. The values estimated from these master curves for those mixes were compared, under the same conditions with values determined from two predictive equations proposed in the AASHTO (2002) Pavement Design Guide. The dynamic modulus of 20 specimens was used to develop the master curves. When testing was conducted on the same mixes, the dynamic modulus decreased when the temperature increased. The phase angle decreased when the temperature was increased from 40°C to 54°C.

Zou et al. (2010) carried out dynamic shear testing and used the time-temperature superposition principal to obtain the rheological functions for the asphalt mixes. The Christensen-Anderson-Marasteanu rheological model (Marasteanu and Anderson 1999) and morphology theory was used to determine the morphological properties of the rheological master curves. Four equations were used: complex modulus master curves, phase angle master curve, temperature shift factor and strain shift factor. In addition, two different types of asphalt and two mixture gradations were utilised.

Asgharzadeh and Tabatabaee (2013) carried out some tests to evaluate modified binder time-temperature properties and their performance in accordance with their rheological master curves. A PG58-22 base binder was modified with styrene

butadiene styrene (SBS), ethylene vinyl acetate, polyphosphoric acid and crumb rubber. 'G' master curves (Dynamic Shear Modulus master curves) and phase angles of these modified binders were generated based on the results obtained from the dynamic shear rheometer and bending beam rheometer at temperatures ranging from 30°C to about 88°C.

The 'G' master curves for both polymer modified binders (PMBs) indicated a significant increase in stiffness for the low frequency range at high temperature and some decrease at the lower temperatures. In addition, due to a reduction in the phase angle master curves over the entire frequency range, the behaviour of the SBS-modified binder was more elastic than the unmodified binder. The stiffness of the modified binders increased with temperature but softened at low temperatures.

Al-Khateeb et al. (2006) developed a new simple mechanistic empirical model to predict the dynamic modulus of asphalt at various loading frequencies and temperatures. In developing this model, the dynamic modulus of asphalt mixes having various performance grades covering highly modified and unmodified binders was determined based on the results of simple performance testing (SPT). A sigmoid function was used to determine the dynamic modulus and the reference temperature was 19°C. The Hirsch model was also used to predict the dynamic modulus of all the asphalt mixes.

2.4 Summary

A great deal of research directed at the modelling of the behaviour of asphalt has been conducted. Some of this research was directed at predicting the fatigue life of asphalt whilst some was directed to the development of new models to make the mechanistic-empirical design more accurate and reliable.

The different approaches can be summarised as follows:

- numerical approach
- experimental approach
- combination of numerical and experimental approaches.

In terms of the experimental approach, three methods to investigate the fatigue behaviour of asphalt were identified:

- strain-stress approach (sometimes known as phenomenological approach)

- dissipated energy approach
- fracture mechanics approach.

The majority of the approaches involved four-point bending beam testing and almost all the researchers described the test as very time-consuming.

A great deal of research was directed at modelling the viscoelastic behaviour of asphalt by measuring the dynamic modulus and developing master curves. However, few studies were identified which were relevant to typical mixes used in Western Australia.

2.4.1 Study gaps

The need to predict the fatigue life of asphalt relying on very time-consuming tests is challenging. Furthermore, the testing programs reported were conducted on different materials. This limits the ability to draw a base line for material testing and modelling.

As the work reported in this thesis involves extensive laboratory testings on a single material type (AC14/75 blows), the following areas were identified where further research was needed and could be addressed in the program reported in this thesis:

1. Develop testing protocols which will allow more reliable and valid test results.
2. Predict the fatigue life when the termination condition (i.e. when the stiffness is reduced to 50% of its initial value) is not met.
3. Model the behaviour of the asphalt at different temperatures, loading frequencies and strain levels.
4. Investigate the relevance and applicability of current models to the typical WA mix selected for this study.
5. Conduct further investigations on the fatigue endurance limit (FEL).
6. Conduct further investigations on the healing of viscoelastic material.

2.5 Objectives of the research

Owing to time constraints, it was not possible to address all the challenges and study gaps which have been identified in this chapter. However, it was possible to identify the following objectives which were both achievable in terms of available resources and also relevant to practice in Western Australia:

1. Develop testing protocols for the evaluation of the fatigue and viscoelastic properties of a standard asphalt mix commonly used as a structural (> 40 mm thick) layer in pavements in WA.
2. Develop a new fatigue life prediction model based on the laboratory test data.
3. Develop a new accelerated laboratory testing approach that allows the fatigue behaviour of asphalt to be modelled at different test temperatures, loading frequencies and strain levels.
4. Develop master curves for the asphalt mix that can be input into the mechanistic-empirical design procedures used in Australia.

3 SAMPLE PREPARATION

One of the most important tasks of every experimental study is the sample preparation. A high degree of confidence is needed that the sample manufacture has been carried out correctly; otherwise, the reliability and validity of the results can be compromised.

This study involved two methods of samples preparation:

1. the preparation of beams of asphalt for repeated loading using the four-point bending beam apparatus
2. the preparation of cylinders of asphalt for compressive cyclic loading using the AMPT.

The asphalt selected for testing was an AC14 with 75 Marshall blows (AC14/75) provided by BGC Hazelmere WA. This is a typical asphalt mix widely used in WA as structural and surfacing layer. The typical minimum thickness is 40 mm. The properties of the mix are presented in Table 3.1.

Table 3.1: Properties of AC14/75 asphalt mix

Bitumen class	320
Bitumen content (%)	4.7±0.3
Marshall voids (%)	4-6
Minimum stability (kN)	8
Flow (mm)	2 - 4
Minimum refusal void (350 cycles Gyropac)	2.5

The aggregates type used in the mix was a combination of 14 mm, 10/7 mm and 5 mm aggregate and dust. The particle size distribution (PSD) of each aggregate is shown in Table 3.2 and Figure 3-1.

3.1 Details of testing conducted on the mixes

A number of tests were conducted during the sample preparation stage in line with the standards shown in Table 3.3. The results of this testing are discussed in the following sub-sections.

Table 3.2: Particle size distribution (PSD) of aggregates (Provided by BGC Hazelmere WA)

Sieve Size (mm)	Aggregate category			
	14 mm	10/7 mm	5 mm	Dust
	% passing	% passing	% passing	% passing
19.00	100	100	100	100
13.20	87.3	100	100	100
9.50	22.8	89.6	100	100
6.70	5.4	49.3	100	100
4.75	2.2	13.5	93.6	99.9
2.36	1.3	2.8	38.4	91.5
1.18	1	1.9	24.4	69.89
0.600	0.4	0.7	15.4	48.97
0.300	0.4	0.7	9.7	31
0.150	0.4	0.7	5.5	17.04
0.075	0.35	0.67	3.02	9

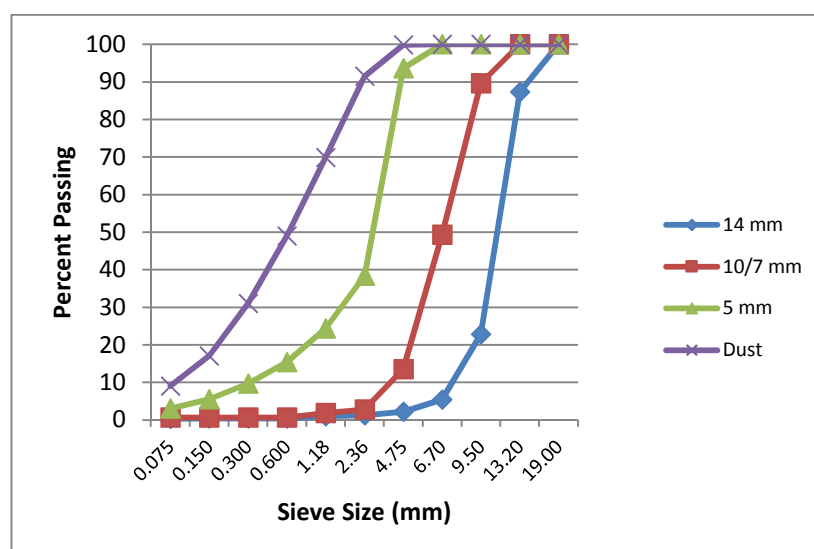


Figure 3-1: Aggregates PSD (provided by BGC Hazelmere WA)

Table 3.3: Standards used for testing during sample preparation

Standard	Title	Year
WA 730.1	Bitumen content and particle size distribution of asphalt and stabilised soil: Centrifuge method	2011
AS 2150	Hot mix asphalt a guide to good practice	2005
WA 732.2	Maximum density of asphalt – Rice method	2011
AS 2891.2.1	Sample preparation – Mixing, quartering and conditioning of asphalt in the laboratory	1995
AGPT/T220	Compaction of asphalt slabs suitable for characterisation	2005
AS 2891.2.2	Sample preparation – Compaction of asphalt test specimens using a Gyratory compactor	2014
AS 2891.9.2	Determination of bulk density of compacted asphalt – Pre-saturation method	2005

3.1.1 PSD and binder content

After the binder was extracted from the asphalt mix, the PSD of the aggregate was determined in accordance with WA 730.1-2011. The PSD of the combined aggregates is presented in Table 3.4 and Figure 3-2. The binder content of this mix (by mass) was 4.69%, which will be reported as 4.7% in the remainder of this thesis.

Table 3.4: PSD of combined aggregates in AC14/75 mix

Sieve size (mm)	Lower limit ¹	Upper limit ²	Mix PSD
19.0	100	100	100
13.2	90	100	90.4
9.5	72	83	78.3
6.7	54	71	69.1
4.75	43	61	56.7
2.36	28	45	42.6
1.18	19	35	33.3
0.600	13	27	22.4
0.300	9	20	17.3
0.150	6	13	11
0.075	4	7	4.3

¹&² In accordance with AS 2150-2005.

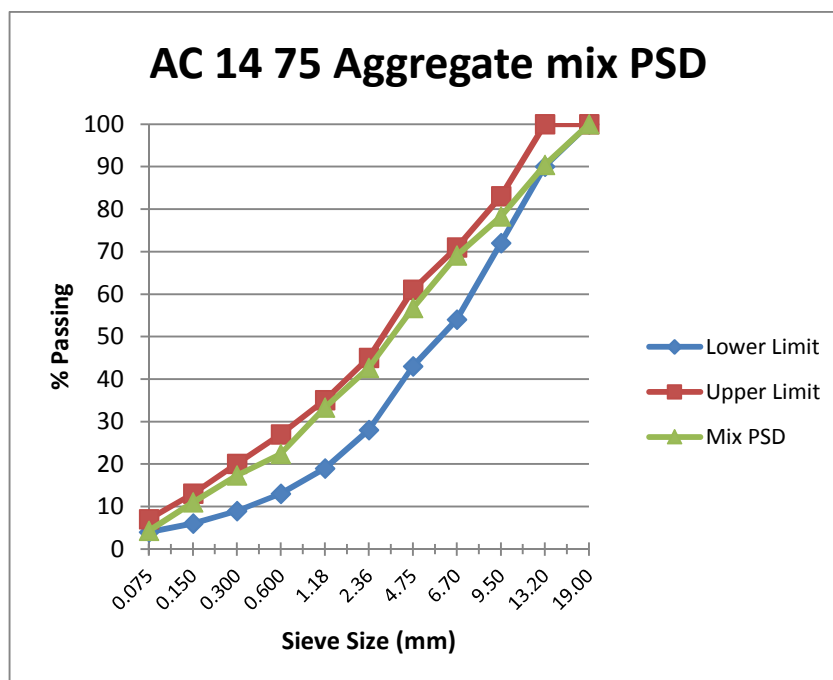


Figure 3-2: PSD of combined aggregates in AC14/75 mix

The lower and upper limits of the allowable PSD are shown in Table 3.5 and Figure 3-3. It is apparent that the PSD was close to the upper limit defined AS 2150-2005 (Table 3.4) and close to the lower limit defined by BGC Hazelmere WA (Table 3.5).

Table 3.5: Lower and upper limits of PSD (BGC Hazelmere WA)

Sieve size (mm)	Lower limit ¹	Upper limit ²	Mix PSD
19.0	100	100	100
13.2	100	100	90.4
9.5	85	100	78.3
6.7	70	85	69.1
4.75	62	75	56.7
2.36	53	70	42.6
1.18	35	52	33.3
0.600	24	40	22.4
0.300	15	30	17.3
0.150	10	24	11
0.075	7	16	4.3
^{1&2} Provided by BGC Hazelmere WA			

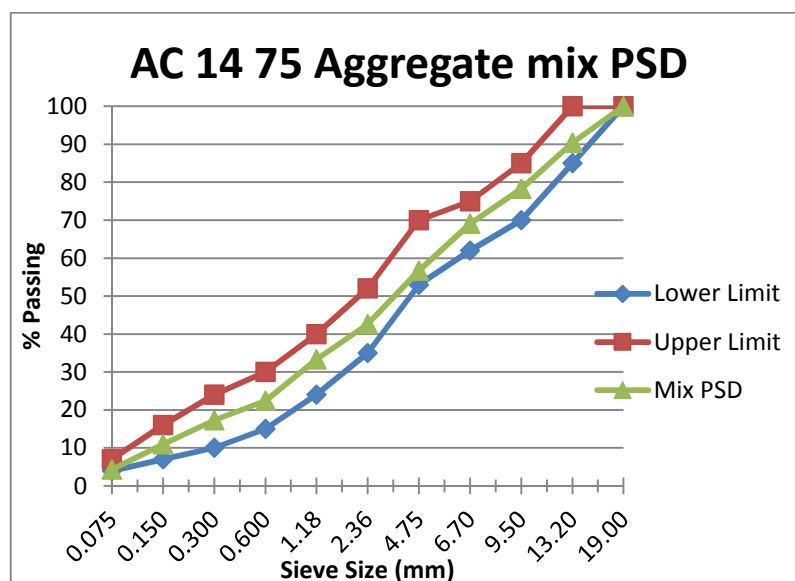


Figure 3-3: Lower and upper limits provided by BGC Hazelmere WA

3.1.2 Maximum density

The maximum density of a mix is used together with bulk density of the mix and the density of the binder to obtain volumetric quantities such as air voids, voids in the mineral aggregate, voids field with asphalt and effective asphalt content. The testing was conducted in accordance with WA 732.2-2011. The average maximum density was 2.449 t/m³ (2.45 t/m³.)

3.2 Preparation of asphalt samples

As the mix was provided by BGC Hazelmere WA in approximately 50 steel containers with the capacity of 25 kg it was necessary to reheat the mix prior to the manufacture of the samples. The sample preparation was carried out in accordance with AS 2891.2.1. As already stated, two sets of samples were prepared: beams cut from slabs for fatigue testing and cylindrical moulds for AMPT testing.

3.2.1 Preparation of beams from slabs for fatigue testing

The slabs were compacted in accordance with Austroads Test Method AGPT/T220 (Austroads 2005). A cooper roller-slab compactor (Figure 3-4) was used to compact the mix at the target air void content (Figure 3-5a). Temperature control during the compaction process is very important. For this reason, a digital thermometer was used to control the temperature of the mix during the conditioning and compacting stages (Figure 3-5b). After the cooling-down process, but within 48 hours, the slabs were cut into beams (Figure 3-6).



a) Compaction with roller compactor

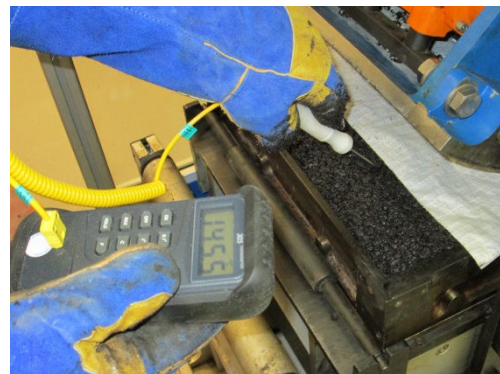


b) Pressure adjustment

Figure 3-4: Slab compaction



a) Compacted slab



b) Temperature control of slab during compaction

Figure 3-5: (a) Prepared slab and (b) temperature control

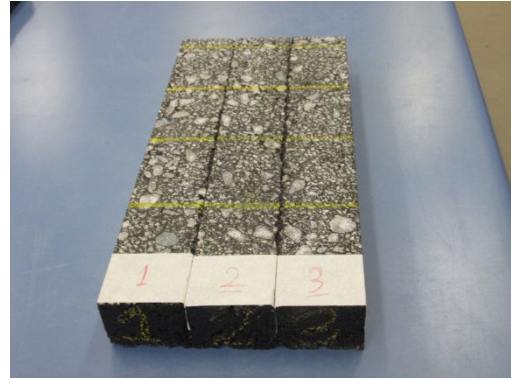


Figure 3-6: Cutting process and beams prepared for testing

3.2.2 Preparation of cylinders for AMPT testing

All the cylinders were compacted in accordance with AS 2891.2.2. A Gyratory compactor was used to compact the mixes (Figure 3-7). The set-up of the Gyratory compactor is shown in Table 3.6 which is commonly used in Australia for AC14/75 mixes. Once again, the temperature during conditioning and compaction was controlled using a digital thermometer illustrated in Figure 3-8. After compaction, the moulds were cooled for 48 hours and then cut into cylinders (Figure 3-9).

Table 3.6: Gyratory compactor settings

Target Height (mm)	171.3
Angle of Gyration (Degree)	3
Mould Diameter (mm)	150



Figure 3-7: Preparation of cylinders for AMPT testing



Figure 3-8: Temperature control of AMPT cylinders during compaction



Figure 3-9: Cutting of prepared AMPT cylinders

3.3 Volumetric properties of prepared samples

Apart from maximum density and binder content, there are other volumetric properties of asphalt that need to be identified prior to testing. A schematic asphalt mix phase diagram, which explains the volumetric properties of the mix, is presented in Figure 3-10.

The following volumetric properties were determined before testing commenced:

- maximum density of mix (G_{mm})
- bulk density of asphalt (G_{mb})
- bulk density of aggregates (G_{sb})
- binder density (G_b)
- air voids content (V_a)

- % binder content by mass (P_b)
- % aggregate content by mass (P_s)
- voids in mineral aggregates (VMA)
- voids filled with asphalt (VFA).

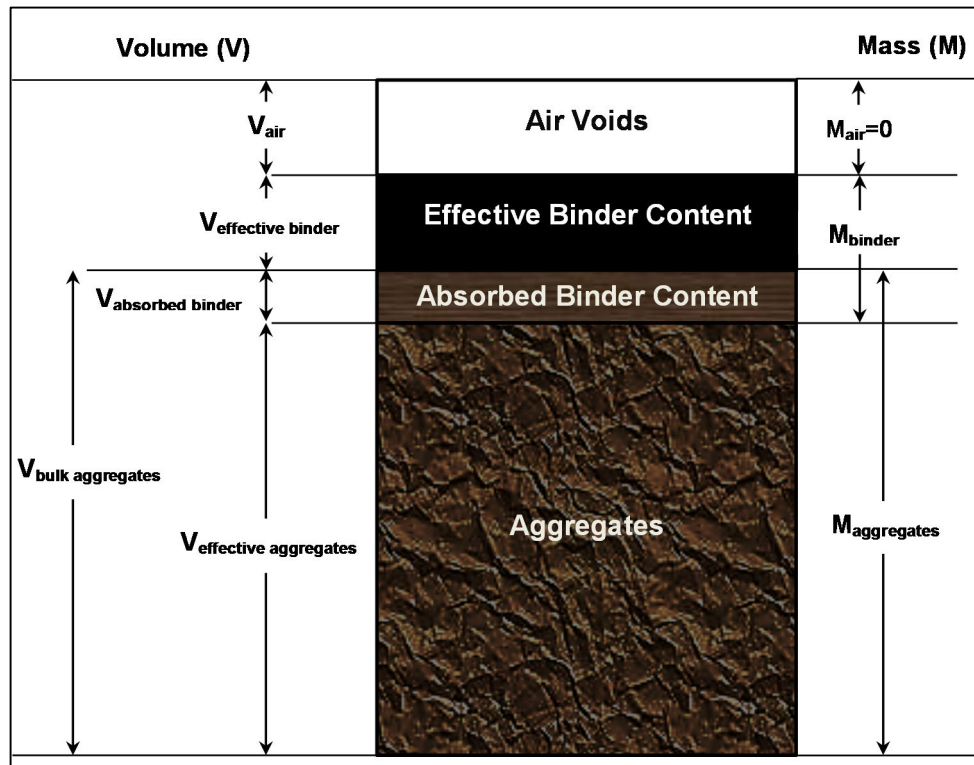


Figure 3-10: Asphalt mix phase diagram

The bulk density was determined in accordance with AS2891.9.2 (pre-saturation method). The following equations were used to calculate the other parameters:

$$V_a = 100 \times \frac{(G_{mm} - G_{mb})}{G_{mm}} \quad 3-1$$

where

$$\begin{aligned} V_a &= \% \text{ air voids} \\ G_{mm} &= \text{maximum density (2.449 t/m}^3\text{)} \\ G_{mb} &= \text{bulk density (t/m}^3\text{)} \end{aligned}$$

$$P_s = 100 - P_b = 100 - 4.7 = 95.3 \quad 3-2$$

where

$$\begin{aligned} P_b &= \% \text{ binder content by mass} \\ P_s &= \% \text{ aggregate content by mass} \end{aligned}$$

$$VMA = 100 - \left(\frac{G_{mb} \times P_s}{G_{sb}} \right) \quad 3-3$$

where

VMA = voids in mineral aggregates
 G_{sb} = bulk density of aggregates (t/m³)

$$VFA = 100 \times \left(\frac{VMA - V_a}{VMA} \right) \quad 3-4$$

where

VFA = voids filled with asphalt

As discussed earlier, sample preparation is the preliminary step in any experimental testing program and precise control of the asphalt mix in terms of temperature control, air voids content and compaction is required if reliable and consistent results are to be generated. It is acknowledged that it is impossible to address all the errors introduced during sample preparation, including operator error or repeatability. However, in order to minimise the errors introduced during the sample preparation stage the following guidelines are offered:

- Condition and compact the asphalt under controlled temperature conditions using a digital thermometer.
- Compact the material in a consistent way to achieve an air voids content as close as possible to the design value.
- Store the samples in a safe, temperature-controlled, location where the probability of damage is minimised. Examples of correct and incorrect storage are shown in Figure 3-11.



a) Incorrect sample storage



b) Correct sample storage

Figure 3-11: examples of incorrect and correct storage of samples

4 RESULTS OF PRELIMINARY TESTING AND DEVELOPMENT OF REVISED PROTOCOLS

4.1 Introduction

After performing more than ten trial dynamic modulus tests on cylindrical specimens using the AMPT machine, some problems were noted in terms of the standard error on the load, which was greater than 10%, and also the peak-to-peak strain level, which should have been between 85-115 $\mu\epsilon$ based on Project 9-29 (NCHRP 2008b).

In addition, after performing more than 20 trial tests on beams it was found that there were some issues with the outputs from the EN Standard Tester (the four-point bending beam apparatus), specifically the phase angle not being in the required range. This will be discussed in detail later in this chapter. There was also another problem related to the deformation of the beams when the haversine loading mode was applied.

In terms of the testing of the cylindrical samples using the AMPT, there were also some problems, especially at higher temperatures ($\geq 40^{\circ}\text{C}$) and at lower frequencies (0.01-0.1 Hz) where there were some problems achieving the correct load pulse shape (haversine or sinusoidal). The issues arose because of the need to stay within the defined strain level, the associated low levels of stress being applied to the samples and the introduction of errors associated with noise generated by the machine.

Clearly, if there are errors in any of the parameters (phase angle, load, deformation and applied level of strain) introduced during testing, then the results will not be valid. The main purpose of this chapter, therefore, is to propose some solutions aimed at overcoming the problems associated with the use of enhanced testing techniques such as those adopted in the study reported in this thesis. It will be explained how it is possible to obtain valid data at higher temperatures and low frequencies through the use of the dithering technique (the addition of an external signal to the operating system), Proportional, Integral and Derivative (PID) control and Adaptive Level of Control (ALC).

4.2 Definition of ‘validity’ and ‘reliability’

There are two significant terms which must be taken into account with any experimental program: ‘validity’ and ‘reliability’. An explanation of ‘validity’ and ‘reliability’ is presented in Figure 4-1.

In terms of reliability, when testing similar samples under the same conditions, the reliability of the test results can be defined as the level of consistency which is mostly explained by percentage³. Design reliability is discussed further in Section 5.2.3 and 5.5. In terms of ‘validation’, Austroads (2012) defines a ‘validation test’ as a standardised procedure to test the validity of test results from a measuring device.

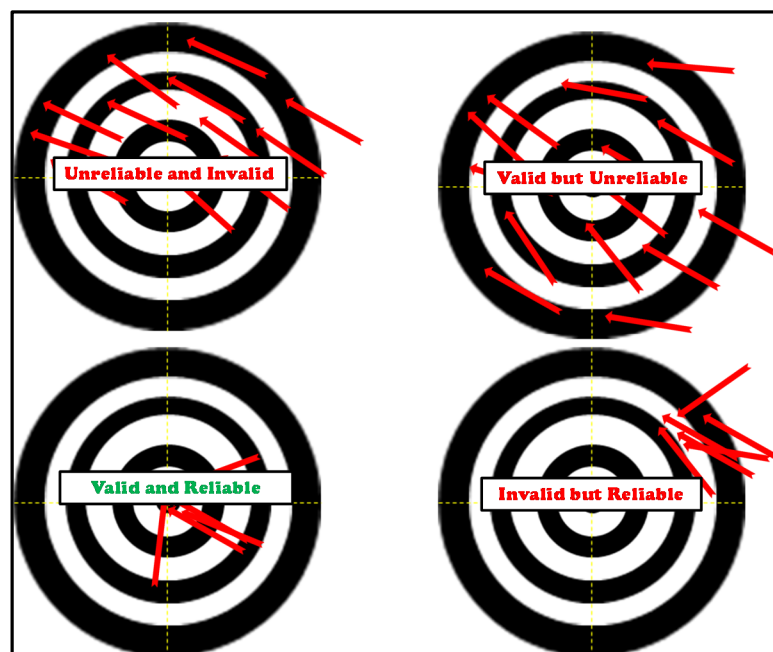


Figure 4-1: Schematic explanation of validity and reliability

Errors introduced during laboratory are related to either the method of sample preparation and/or the testing equipment. Some methods to minimise the errors in sample preparation were proposed in the previous chapter.

³ Reliability factors are incorporated into the pavement design procedures presented in Austroads (2012). Reliability factors are transfer functions that, in the case of asphalt, relate a mean laboratory fatigue life (Shell 1978) to the predicted in-service fatigue life at a desired level of project reliability. In effect they comprise two components:

- a shift factor relating mean laboratory fatigue life to a mean in-service fatigue life, taking account of the differences between the laboratory test conditions and the conditions applying to the in-service pavement
- a reliability factor relating mean in-service fatigue life to the in-service life predicted at a desired project reliability, taking into account factors such as construction variability, environment and traffic loading.

The focus in this chapter will be the identification of the possible errors associated with the operation of the EN standard tester and the AMPT and the development of solutions aimed at minimising these generated errors, so that the data generated during testing will be more reliable and valid.

4.3 Test equipment

As already discussed, the EN Standard Tester is a four-point bending beam apparatus which runs fatigue tests on beams cut from slabs (Figure 4-2). The hardware is compatible with series of software developed by the IPC Global Company (known as UTS15, UTS18 and UTS19). The main jig is placed in a temperature-controlled chamber; the temperature can be varied from 4°C to 60°C.

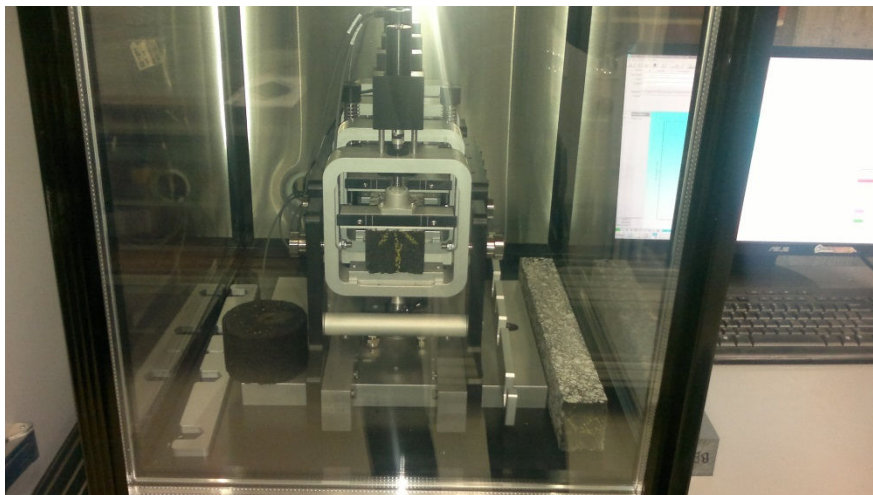


Figure 4-2: Curtin University Geomechanical Laboratory EN Standard Tester

In addition to EN Standard Tester, IPC Global provided an Asphalt Mixture Performance Tester (AMPT) to run dynamic modulus tests on cylindrical samples (Figure 4-3).

The US Federal Highway Administration (FHWA 2013) defines the AMPT as follows:

“The AMPT is a computer-controlled hydraulic testing machine capable of subjecting a compacted asphalt mixture specimen to cyclic loading over a range of temperatures and frequencies. The device evaluates asphalt mixture properties to assess potential performance. Transportation agencies can use the AMPT to develop inputs for the structural design of flexible pavements and to obtain information helpful in monitoring mixes and performing quality assurance. The AMPT builds upon past efforts to develop a testing device for determining fundamental asphalt mixture performance properties. The current equipment and test methods have

been developed to optimize both testing time and cost. The AMPT has also been known as the Simple Performance Tester (SPT) in earlier research work and references.”

The major components of this equipment are a triaxial cell, a temperature and air pressure control chamber and the data acquisition system. The compatible software with this equipment is the UTS6.

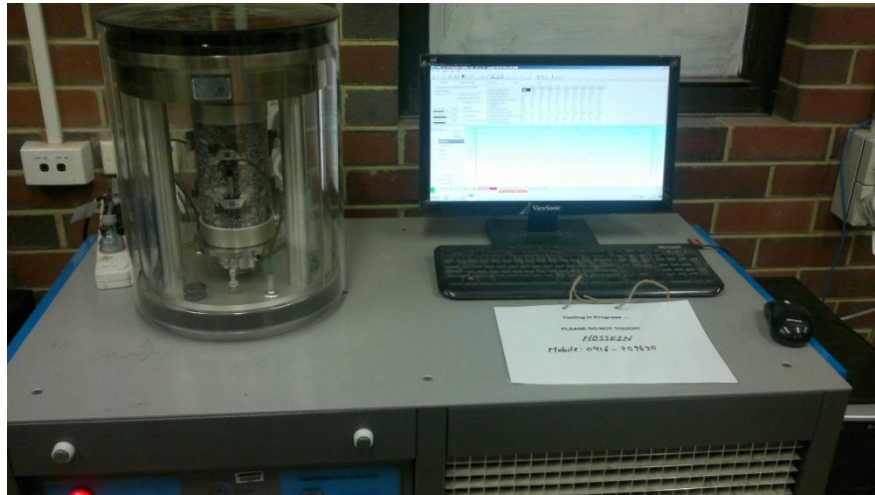


Figure 4-3: Curtin University Geomechanical Laboratory AMPT

4.3.1 UTS15

This software is compatible with Austroads Test Method AGPT/T233 (Austroads 2006). Although the loading mode template is defined as haversine, the user can change the shape to sinusoidal. Major outputs of this software are beam stiffness, phase lag between stress and strain, dissipated energy for each cycle and cumulative dissipated energy. The UTS15 user interface is shown in Figure 4-4.

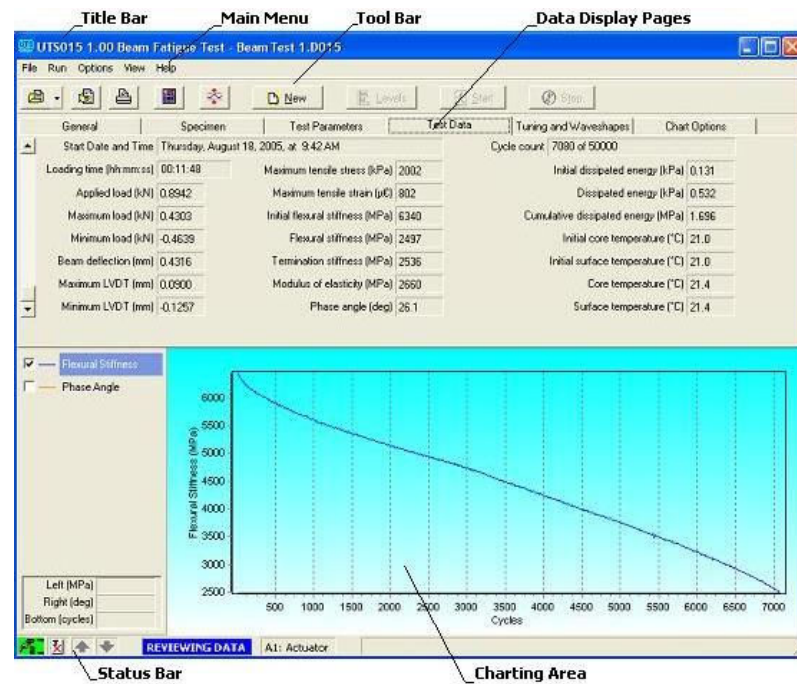


Figure 4-4: UTS15 test layout and description (UTS15 help menu)

4.3.2 UTS18

This software is compatible with the EN 12697 (2012). The loading shape is sinusoidal and there is no option to change the shape of the load. The major outputs are beam complex modulus, phase lag between stress and strain, dissipated energy for each cycle and cumulative dissipated energy. This software is also able to plot the hysteresis loop for each load cycle. The UTS18 user interface is shown in Figure 4-5.

4.3.3 UTS19

This software is known as user-programmable software; the user can program it to change the shape of the load and the rest periods and apply multiple load cycles. The software is suitable for researching the healing phenomenon by applying rest periods to the loads. Major output of this software is the material stiffness and it does not record the phase lag between stress and strain (It is important to mention that phase angle is not recordable while applying rest periods to the loads). The UTS19 user interface is shown in Figure 4-6.

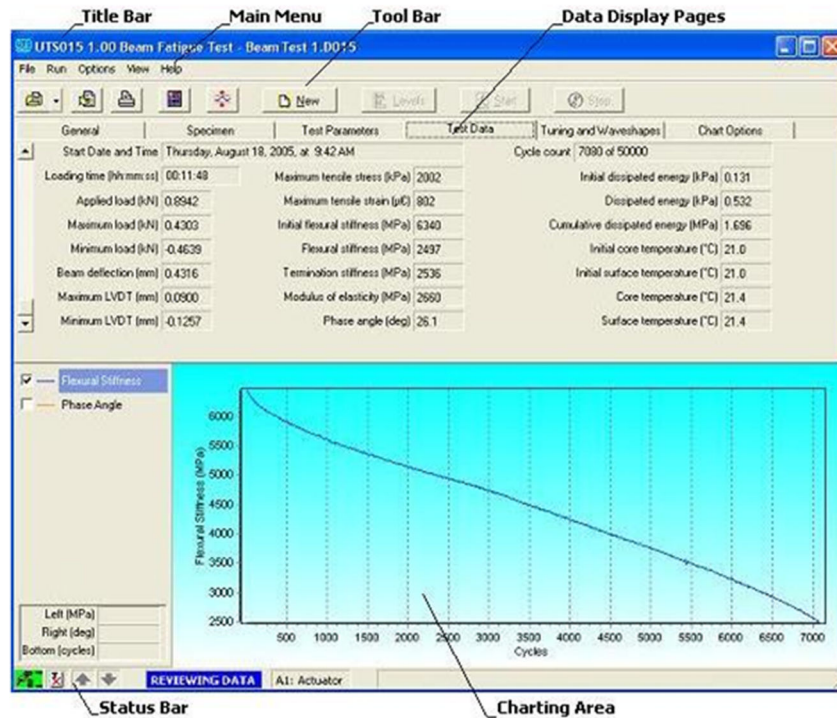


Figure 4-5: UTS18 test layout and description (UTS18 help menu)

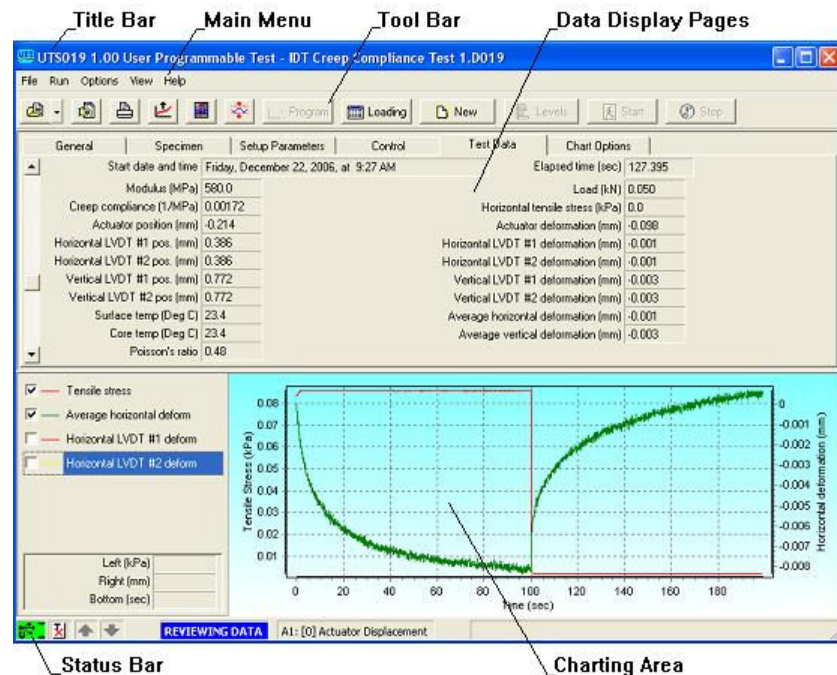


Figure 4-6: UTS19 test layout and description (UTS19 help menu)

4.3.4 UTS6

This software is compatible with NCHRP (2008b) for running the dynamic modulus test at different temperatures and frequencies to generate master curves. The major outputs are dynamic modulus, phase angle, hysteresis loop, cumulative dissipated energy, and strain and stress. The UTS6 user interface is shown in Figure 4-7.

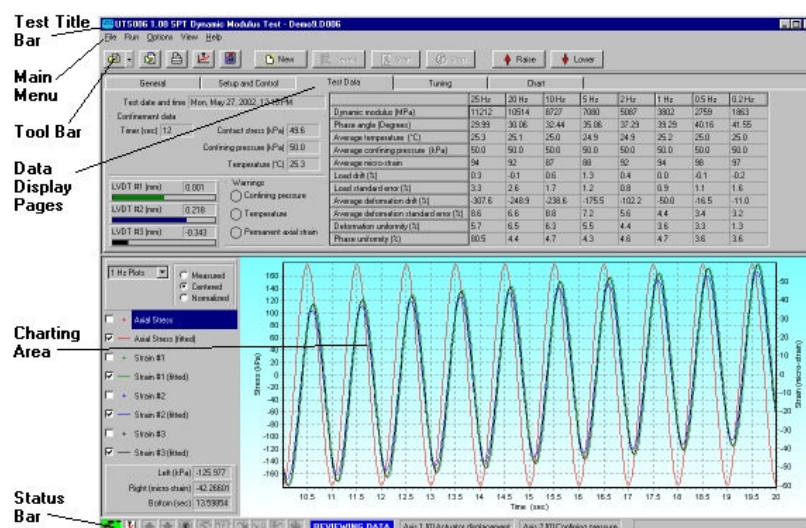


Figure 4-7: UTS6 test layout and description (UTS6 help menu)

4.4 Associated errors

After running several trial tests on the EN standard tester and the AMPT, it was observed that some errors were generated by the UTS15 and UTS6 programs. An explanation of these errors, and some techniques to overcome them, are now presented.

4.4.1 Errors associated with UTS 15 and suggested solutions

When a sinusoidal stress is applied to a viscoelastic material there is a time lag between the applied stress and resulting strain during which some energy dissipated. This time lag between the stress and strain sinusoids can be associated with an angular lag. The angular lag between the two sinusoids is defined as the phase angle. The relationship between stress and strain can be defined using the Kelvin Model for viscoelastic material which is represented in Equation 4-1:

$$E^* = \frac{\sigma_0}{\epsilon_0} (\cos \varphi + i \sin \varphi) \quad 4-1$$

where

- E^* = complex modulus of viscoelastic material (MPa)
- σ_0 = initial stress ($\mu\epsilon$)
- ϵ_0 = initial strain ($\mu\epsilon$)
- φ = phase lag between stress and strain (degrees)

Theoretically the maximum phase angle is 90° for a totally viscous material and 0° for a totally elastic material (see Figure 4-8). Values for asphalt mixes are always in between these two theoretical limits.

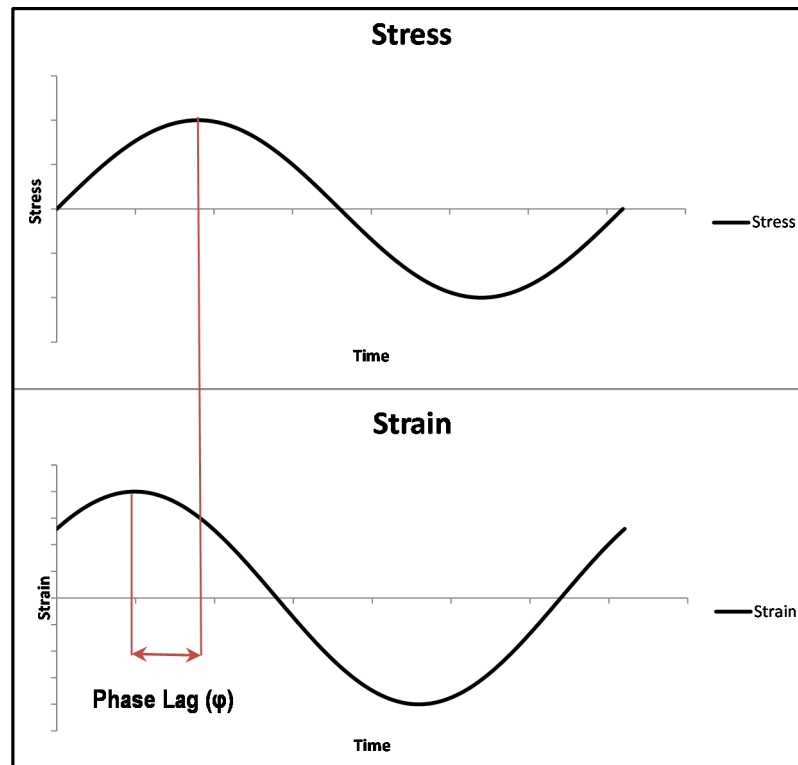


Figure 4-8: Phase lag between stress and strain

Problems generated by applying haversine loading in the UTS15 can be related to: (1) beam deformation, and (2) phase angle range.

4.4.1.1 *Beam deformation*

While applying the haversine loading, after a few cycles the neutral position of the beam changes and the stress trend becomes sinusoidal rather than haversine. The change in neutral line position is compared in Figure 4-9 and Figure 4-10.

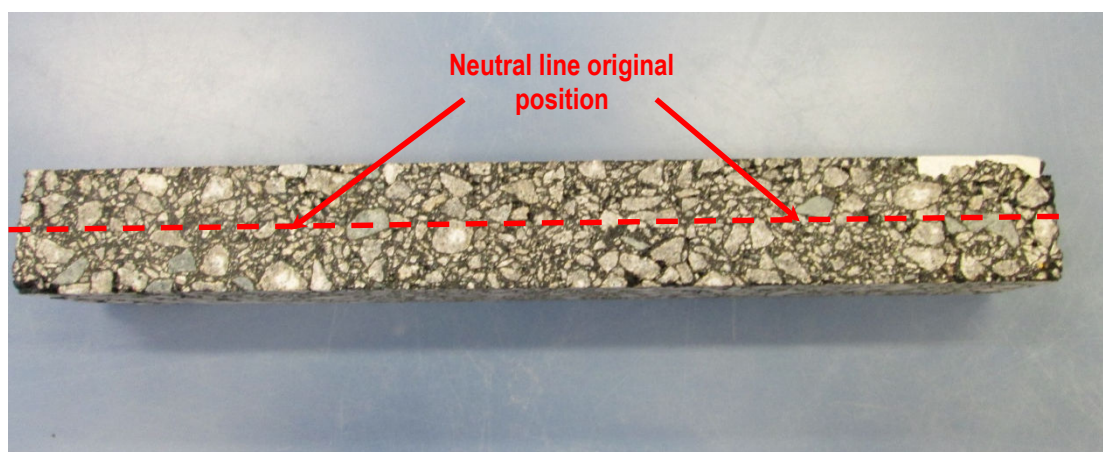


Figure 4-9: Original position of neutral line before testing

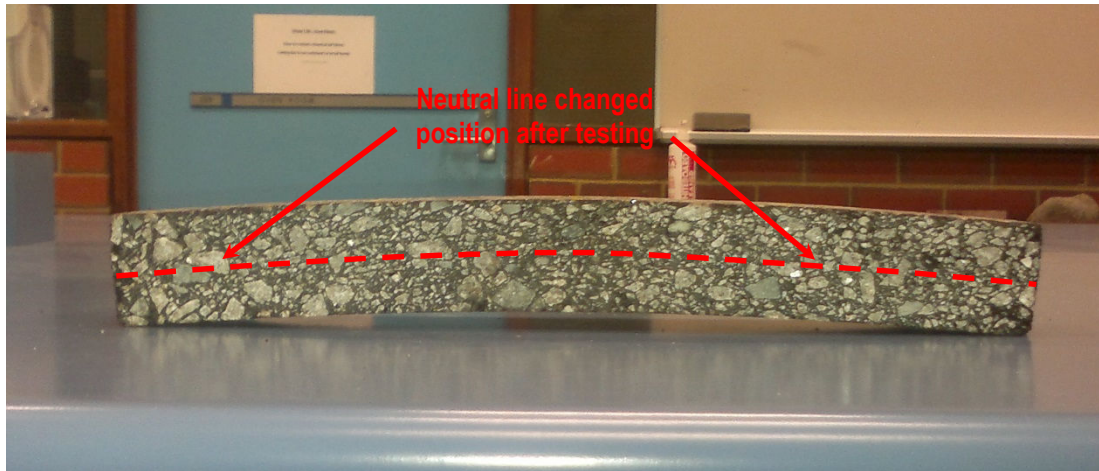


Figure 4-10: Change in location of neutral line after testing

Most recent studies of the fatigue behaviour of asphalt mixes have involved either sinusoidal (Equation 4-2) or haversine loading (Equation 4-3).

$$y = \sin \theta \quad 4-2$$

$$y = \sin^2\left(\frac{\theta + \pi}{2}\right) \quad 4-3$$

Figure 4-11 shows the shape of these load forms. It can be seen from this Figure that, for the same domain, the range of the sinusoidal loading is double that of the haversine loading. On that basis, and for the same specified deflection of the beam, the strain level for the sinusoidal loading should be set at one-half of the level for the haversine loading.

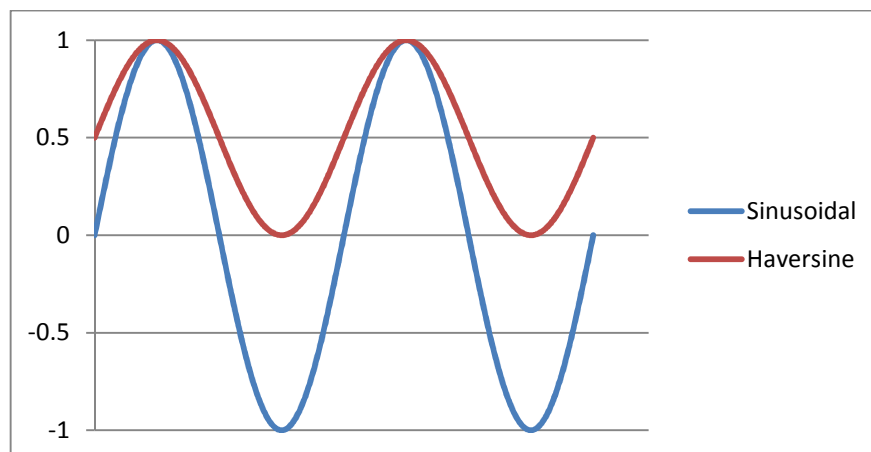


Figure 4-11: Comparison of haversine and sinusoidal load shapes

The loading adjustment required to reach a strain level of 200 $\mu\epsilon$ for both haversine and sinusoidal loading is shown in Figure 4-12.

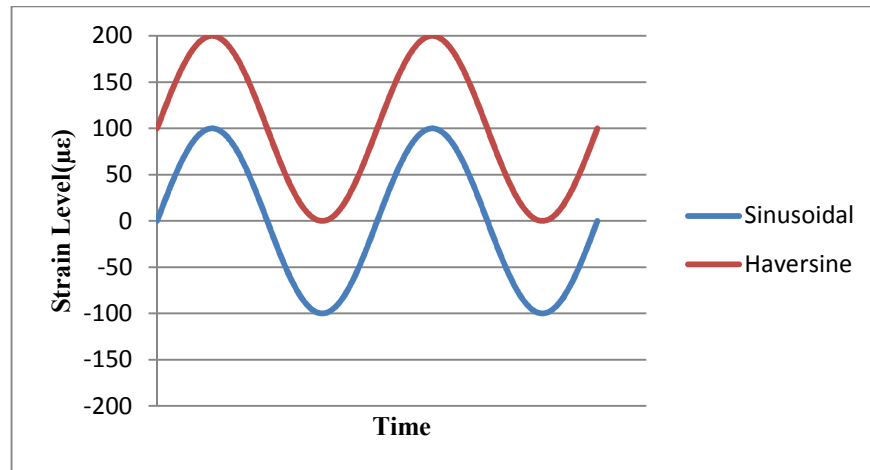


Figure 4-12: Comparison of loading adjustments required to reach 200 $\mu\epsilon$ (haversine and sinusoidal wave forms)

Although it is stated in Austroads (2006) that the cyclic loading shape should be haversine, most researches apply sinusoidal loading rather than haversine loading when trying to address shape loss problems. This keeps the neutral line position in the same location because the beam is pushed down and then pulled back to its original position.

4.4.1.2 Phase angle range

After running some trial tests on asphalt beams using the UTS15 software, it was noted that the recorded phase angle was out of range, ranging from -100° to 270° as illustrated in Figure 4-13. To overcome this issue, and after some trial-and-error, an innovative method was developed.

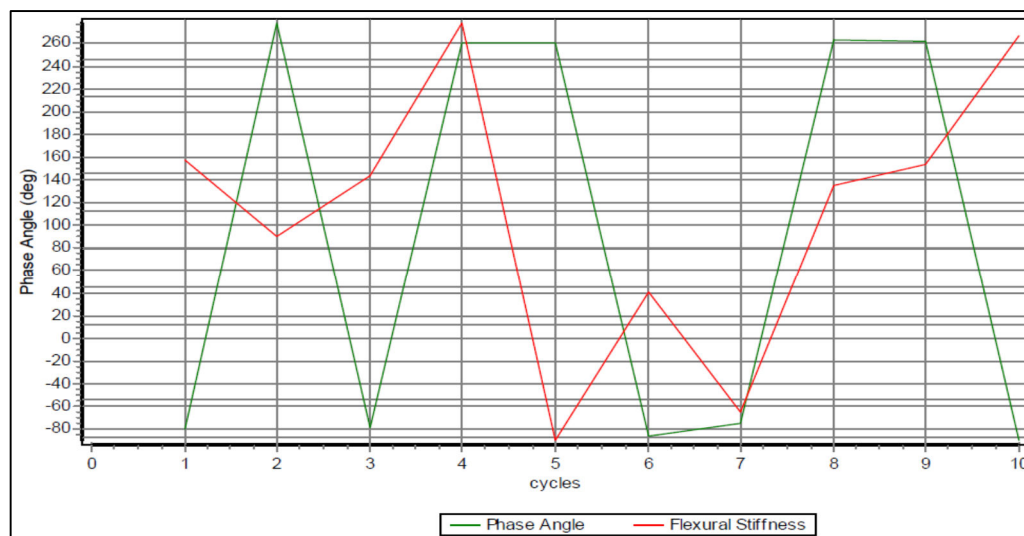


Figure 4-13: Incorrect phase angle outputs varying from -100° and 270°

It was suggested that, rather than placing the beam in the normal condition, it should be flipped in such a way that the top of the beam seats on the supports and the clamps seat on the bottom surface. The load setting should then be changed from positive to negative, making the load 'upside down'. The set-up is shown in Figure 4-14.

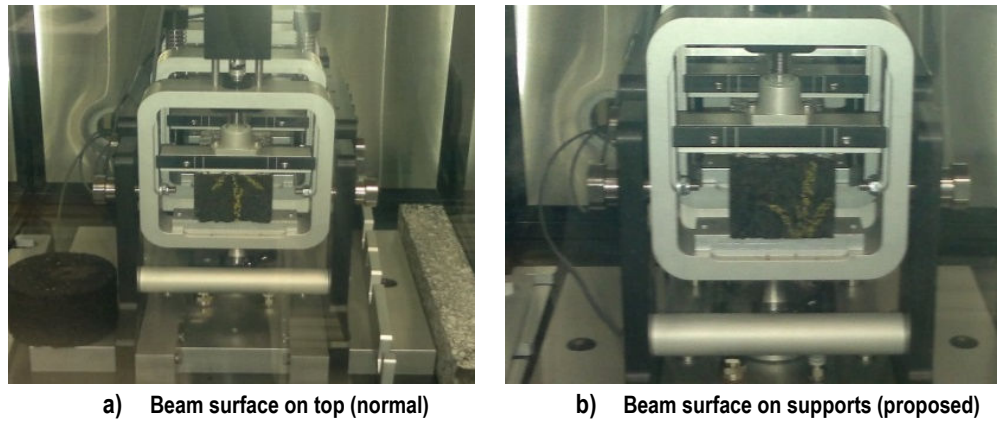


Figure 4-14: Flipping the sample from the normal position to proposed condition to overcome the phase angle problem

Using this arrangement, in some situations the output is negative, e.g. -130° should be $+50^\circ$. This can be corrected in the Excel spreadsheet by adding 180 to negative results. Using this technique resolves almost all the errors associated with the phase angle. The desired phase angle output after this revised set-up is applied is shown in Figure 4-15.

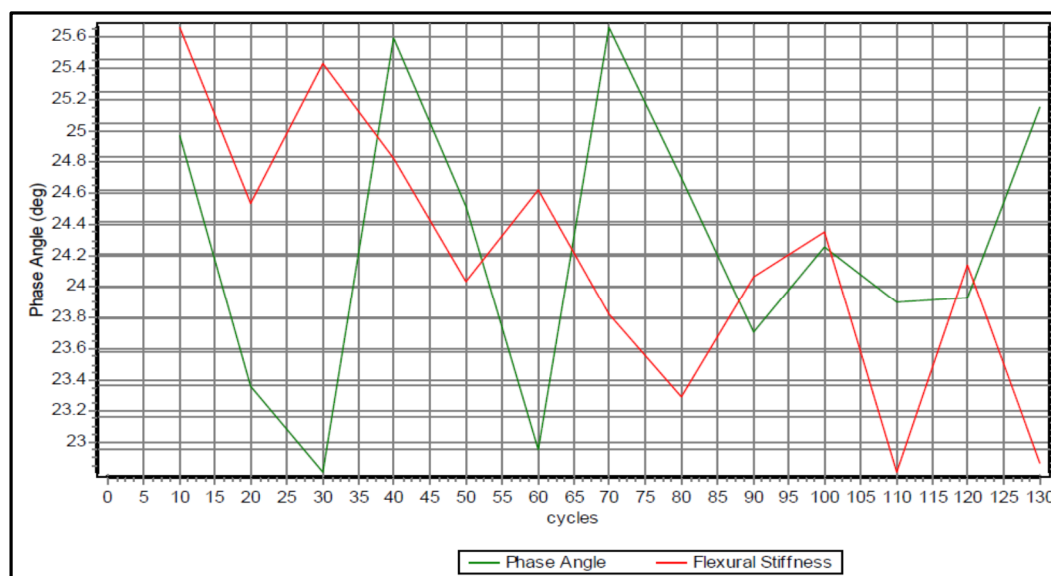


Figure 4-15: Phase angles after proposed correction method applied

4.4.2 Errors associated with UTS6 and suggested solutions

Based on the recommendations in NCHRP 9-29 (NCHRP 2008b), the standard error for the load in each test should not be more than 10% and the strain level should remain between 85 $\mu\epsilon$ and 115 $\mu\epsilon$. Staying at the mentioned threshold requires the application of very small load to the specimen. At such low load levels, the load measurement noise becomes so large relative to target load that the load standard error of 10% is easily exceeded and that the resulting strain is usually below the target range of the strain level of 85 $\mu\epsilon$ to 115 $\mu\epsilon$.

A typical noisy wave shape when testing was conducted at a temperature of 40°C and a frequency of 0.01 Hz is shown in Figure 4-16.

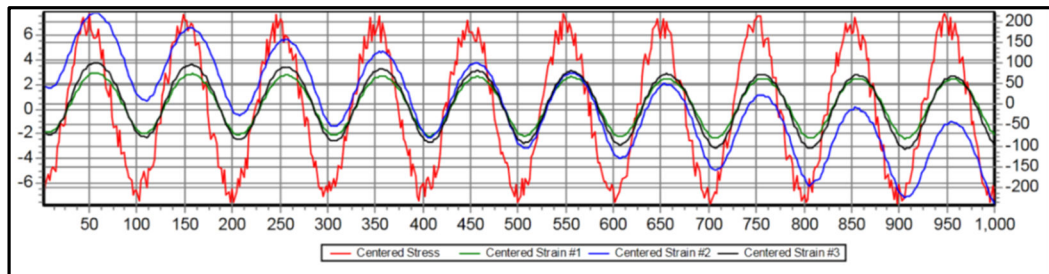


Figure 4-16: Noise interference: controlled sinusoidal stress at 40°C and a frequency of 0.01 Hz

It can be seen from Figure 4-17 that, at a high temperature (40°C) and a frequency of 0.01 Hz the load standard error and strain level are out of the range defined in NCHRP (2008b).

	25 Hz	20 Hz	10 Hz	5 Hz	2 Hz	1 Hz	0.5 Hz	0.2 Hz	0.1 Hz	0.01 Hz
Dynamic modulus (MPa)	2088	1980	1529	1149	772.4	561.9	395.2	251.5	180.5	75.7
Phase angle (Degrees)	35.18	34.66	35.18	35.64	35.71	35.39	35.10	34.42	32.78	26.07
Average temperature (°C)	40.1	40.1	40.1	40.1	40.1	40.1	40.1	40.0	40.1	40.1
Average confining pressure (kPa)	0.2	0.2	0.3	0.3	0.3	0.3	0.3	0.3	0.3	0.3
Average micro-strain	92	93	94	94	93	90	90	91	85	71
Load drift (%)	-0.7	-0.7	0.4	0.4	2.1	-2.2	0.1	1.0	-0.9	0.6
Load standard error (%)	7.3	6.4	5.3	4.6	3.8	3.3	5.9	8.2	10.1	30.7
Average deformation drift (%)	-448.1	-360.8	-296.4	-227.1	-169.0	-117.8	-68.5	-39.3	-10.5	97.3
Average deformation standard error (%)	11.1	8.7	7.3	5.5	4.6	5.1	5.6	5.7	4.2	5.2
Deformation uniformity (%)	3.6	4.4	4.8	5.1	5.5	5.7	6.6	8.0	9.1	9.1
Phase uniformity (Degrees)	0.5	0.4	0.6	0.6	0.8	1.0	1.2	1.4	1.6	2.1

Figure 4-17: Out of range strain level and load standard error in 40°C and 0.01 Hz in UTS6 output

To overcome these errors some control engineering techniques can be used as follows: 1) proportional, integral and derivative (PID) controls, 2) Adaptive level of control, and 3) dithering.

4.4.2.1 PID controls

Almost all system controllers use PID control, comprising a proportional controller, an integral controller and a derivative controller.

Proportional controller: As the name implies, while the system is in the proportional control mode, the controller measures the errors and calculates the number of actions needed to correct them by proportioning the output value to the error. This is achieved by multiplying the raised error to proportional gain. Equation 4-4 is used to calculate the output of the proportional controller.

$$P_{out} = K_p e(t) \quad 4-4$$

where

- P_{out} = output value of proportional controller
- K_p = proportional gain
- e = error (set point – present value)
- t = time (seconds)

Integral controller: In this control mode, the system tries to bring the output to a set-point as close as possible over a defined period of time. Equation 4-5 is used to calculate the output of the integral controller:

$$I_{out} = K_i \int_0^t e(\tau) d\tau \quad 4-5$$

where

- I_{out} = output value of integral controller
- K_i = integral gain
- τ = integration variable

Derivative controller: This control mode tries to minimise the system's overshoot and undershoot by estimating the error in the system's future operation. Equation 4-6 is used to calculate the output of the derivative controller:

$$D_{out} = K_d \frac{de(t)}{dt} \quad 4-6$$

where

- D_{out} = output value of derivative controller,
- K_d = derivative gain

By summing proportional, integral and derivative output values the PID controller output can be calculated using Equation 4-7.

$$u(t) = K_p e(t) + K_i \int_0^t e(\tau) d\tau + K_d \frac{de(t)}{dt} \quad 4-7$$

where

$u(t)$ = output value of PID controller,

A schematic flowchart for the PID controller is shown in Figure 4-18.

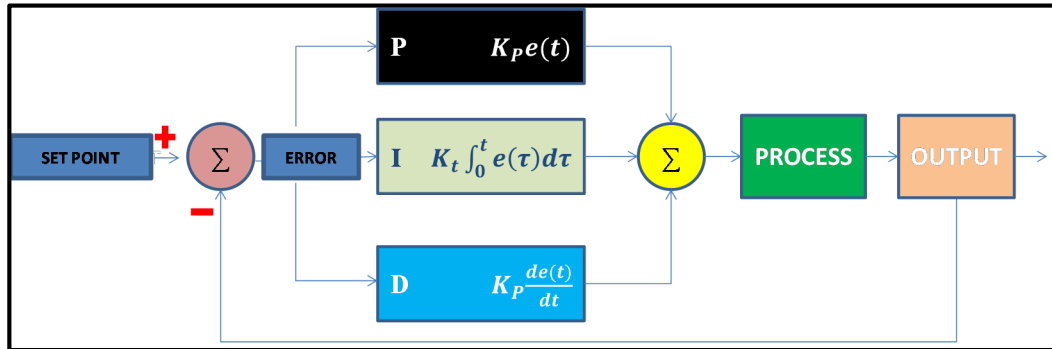


Figure 4-18: Schematic PID controller flowchart

After a large number of AMPT trials to reach the desired wave shape at each temperature and frequency, a default PID gain was established. The PID gains for different temperatures are shown in Table 4.1 and Table 4.2.

Table 4.1: Proposed PID gains for 4°C

PID Gains	Frequency (Hz)									
	25	20	10	5	2	1	0.5	0.2	0.1	0.01
P	1600	1600	1500	1500	1500	1500	1500	1500	1600	1600
I	12	12	12	12	12	12	12	12	12	12
D	1300	1300	1300	1300	1300	1300	1300	1300	1300	1300

Table 4.2: Proposed PID gains for 20°C and 40°C

PID Gains	Frequency (Hz)									
	25	20	10	5	2	1	0.5	0.2	0.1	0.01
P	1000	1000	1000	1000	1000	1000	1000	1000	1000	1000
I	15	15	15	15	15	15	15	15	15	15
D	2000	2000	2000	2000	2000	2000	2000	2000	2000	2000

4.4.2.2 Adaptive level control (ALC)

One of the most important requirements when testing materials is that the output in remains in the range set by user. For example, when testing using the AMPT machine, and as discussed earlier, the applied strain level should remain in the range of 85-115 $\mu\epsilon$. For this reason, in UTS6 software user interface, there is an option where the user can select ALC by ticking the related check box which is

shown in the Figure 4-19. This automatically adjusts the system controllers during testing.

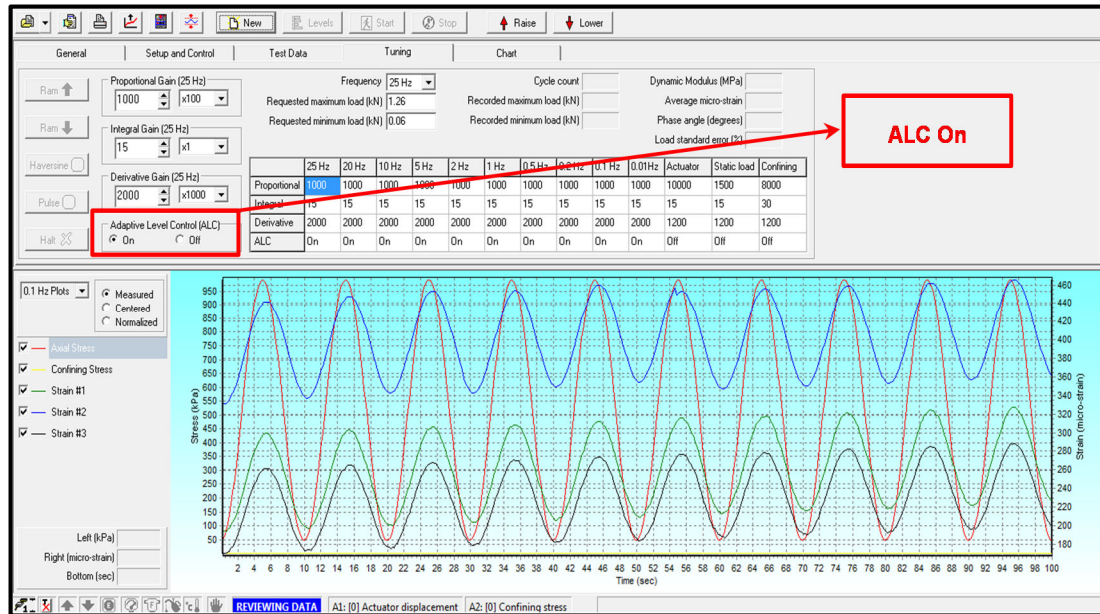


Figure 4-19: Adaptive Level Control (ALC) check-box in UTS6 Tuning interface

4.4.2.3 Dithering

Sometimes it is not possible to obtain the desirable load shape by just using the PID control and the ALC because of the presence of noise in the system. As a result, it is very desirable that the noise level be minimised as much as possible. This can be achieved by adding an external signal to the operating system called “dithering”.

As shown in Figure 4-16, while running the test at a low frequency level (e.g. 0.01 Hz) and at a high temperature (e.g. 40°C) the shape of sinusoidal curve is very noisy. Dithering is one of the best control engineering techniques used to remove this noise. For this reason it is recommended that a dither with a span altitude of 0.5% be added to the system. This can be done by modifying UTS6 software system setup (Figure 4-20).

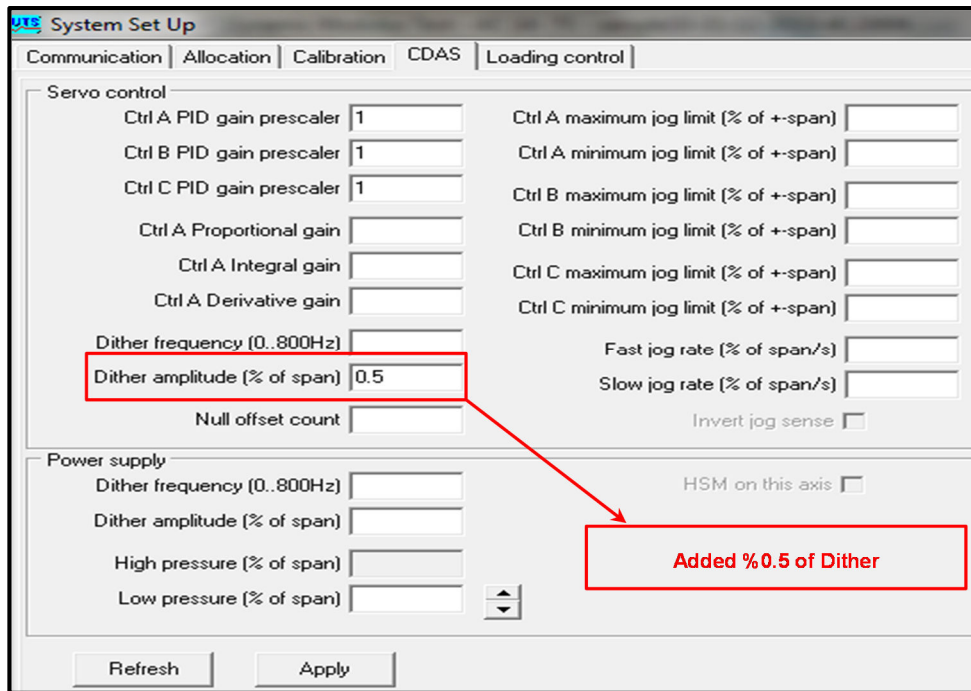


Figure 4-20: How to apply 0.5% dither to the UTS6 system setup

4.5 A new testing protocol for the EN Standard Tester and the AMPT

As discussed earlier in this chapter, there are some techniques that have been developed to minimise the errors associated with EN standard Tester and AMPT outputs. Following are testing protocols that have been developed for both testing apparatus.

4.5.1 EN Standard tester testing protocol steps while operating UTS15 software

The steps that should be taken to minimise the out-of-range phase angle problems discussed earlier are as follows:

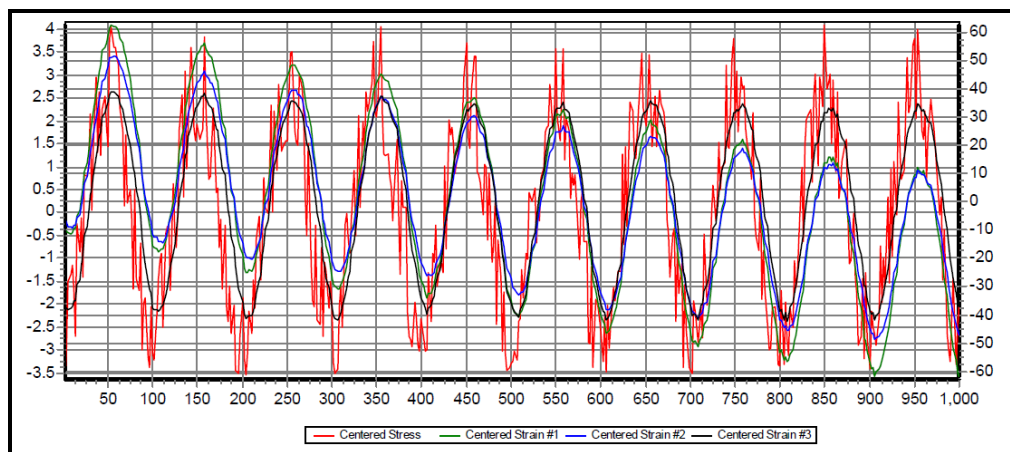
- Step 1. Flip the sample over in such a way that the beam's top surface seats on the support.
- Step 2. Apply the load in reverse order to reach the same condition as if the normal testing procedure was used.
- Step 3. Add 180° in the CSV output to the negative phase angles (e.g. -130) and save it as a new Excel spreadsheet.

4.5.2 AMPT testing protocol: steps while operating the UTS6 software

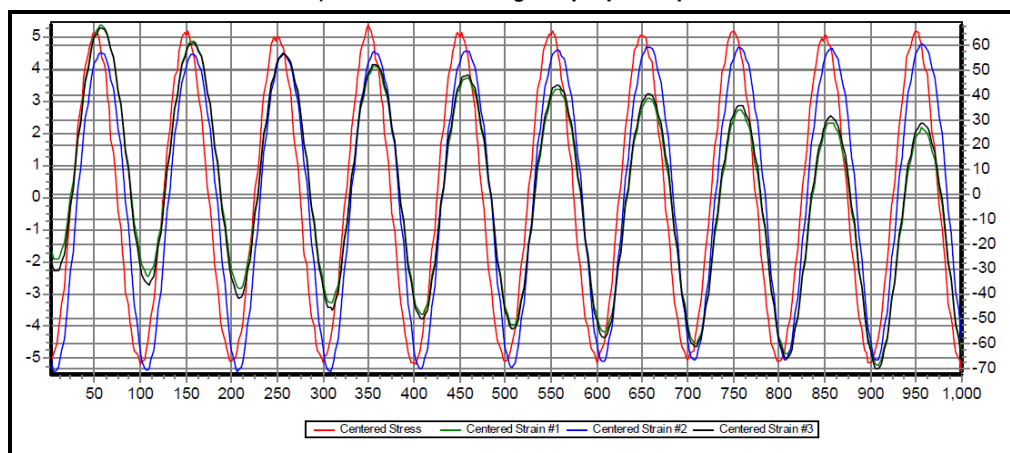
The steps that should be taken to minimise the errors associate with out-of-range strain levels and load standard errors are as follows:

- Step 1. Before testing, set the PID gains using the proposed template values illustrated in Table 4.1 and Table 4.2 for different temperatures.
- Step 2. If the testing is being conducted at higher temperatures (e.g. 40°C and above) choose the ALC option in the Adoptive Level Control check-box shown in Figure 4-19 (this should be done only for high temperatures).
- Step 3. If the testing is being conducted at a high temperature (e.g. 40°C and above) apply dither with 0.5% of span amplitude as illustrated in Figure 4-20 (this should be done only for high temperatures).

The UTS6 output before and after applying the proposed protocol is shown in Figure 4-21 and Figure 4-22.



a) Before following the proposed protocol



b) After following the proposed protocol

Figure 4-21: Sinusoidal stress shape before and after refinement

Tabulated Results Summary										
	25 Hz	20 Hz	10 Hz	5 Hz	2 Hz	1 Hz	0.5 Hz	0.2 Hz	0.1 Hz	0.01 Hz
Dynamic modulus (MPa)	2088	1980	1529	1149	772.4	561.9	395.2	251.5	180.5	75.7
Phase angle (Degrees)	35.18	34.66	35.18	35.64	35.71	35.39	35.10	34.42	32.78	26.07
Average temperature (°C)	40.1	40.1	40.1	40.1	40.1	40.1	40.1	40.0	40.1	40.1
Average confining pressure (kPa)	0.2	0.2	0.3	0.3	0.3	0.3	0.3	0.3	0.3	0.3
Average micro-strain	92	93	94	94	93	90	90	91	85	71
Load drift (%)	-0.7	-0.7	0.4	0.4	2.1	-2.2	0.1	1.0	-0.9	0.6
Load standard error (%)	7.3	6.4	5.3	4.6	3.8	3.3	5.9	8.2	10.1	30.7
Average deformation drift (%)	-448.1	-360.8	-296.4	-227.1	-169.0	-117.8	-68.5	-39.3	-10.5	97.3
Average deformation standard error (%)	11.1	8.7	7.3	5.5	4.6	5.1	5.6	5.7	4.2	5.2
Deformation uniformity (%)	3.6	4.4	4.8	5.1	5.5	5.7	6.6	8.0	9.1	9.1
Phase uniformity (Degrees)	0.5	0.4	0.6	0.6	0.8	1.0	1.2	1.4	1.6	2.1

a) Before following the proposed protocol

Tabulated Results Summary										
	25 Hz	20 Hz	10 Hz	5 Hz	2 Hz	1 Hz	0.5 Hz	0.2 Hz	0.1 Hz	0.01 Hz
Dynamic modulus (MPa)	2478	2348	1854	1429	979.1	722.0	521.5	337.5	241.6	94.6
Phase angle (Degrees)	32.57	32.16	32.93	33.57	34.17	34.17	33.98	33.50	32.98	27.37
Average temperature (°C)	40.1	40.1	40.1	40.1	40.1	40.1	40.1	40.0	40.1	40.1
Average confining pressure (kPa)	0.0	-0.1	0.0	0.0	0.0	0.0	0.0	0.0	0.0	0.0
Average micro-strain	94	96	95	95	96	96	100	101	99	108
Load drift (%)	-2.0	-1.1	0.3	0.4	0.2	0.3	-0.2	0.2	-0.2	0.8
Load standard error (%)	9.1	8.1	6.0	4.3	2.6	1.0	0.3	0.6	0.7	1.7
Average deformation drift (%)	-359.8	-284.1	-243.2	-189.9	-134.0	-98.8	-70.9	-40.6	-17.8	55.5
Average deformation standard error (%)	10.2	8.5	7.1	5.2	3.4	3.0	2.7	3.0	3.3	5.1
Deformation uniformity (%)	4.4	5.0	5.4	5.9	6.4	6.7	8.3	9.3	10.1	12.3
Phase uniformity (Degrees)	0.1	0.0	0.2	0.3	0.5	0.6	0.8	0.9	1.0	0.7

b) After following the proposed protocol

Figure 4-22: Strain level and load standard error refinement following the proposed protocol

4.6 Summary

During preliminary dynamic modulus testing on cylindrical specimens using the AMPT machine, some problems were noted in terms of the standard error on the load, which was greater than 10%, and also the peak-to-peak strain level, which should have been between 85-115 $\mu\epsilon$. In addition, after performing trial four-point bending fatigue testing on beams it was found that there were some issues with the outputs from the EN Standard Tester, specifically the phase angle not being in the required range. There was also a problem related to the deformation of the beams when the haversine loading mode was applied.

In terms of the testing of the cylindrical samples using the AMPT, there were also some problems, especially at higher temperatures ($\geq 40^\circ\text{Celsius}$) and at lower frequencies (0.01-0.1 Hz) where there were difficulties achieving the correct load pulse shape (haversine or sinusoidal). These issues were associated with the need to stay within the defined strain level, the low levels of stress being applied to the samples and the introduction of errors associated with noise generated by the machine during testing.

Clearly, if there are errors in any of the parameters (phase angle, load, deformation and applied level of strain) introduced during testing, then the results will not be valid.

One purpose of this chapter, therefore, was to describe in detail the problems encountered during this preliminary and the steps taken to overcome the problems associated with the use of enhanced testing techniques such as those adopted in the study reported in this thesis. It was demonstrated that it is possible to obtain valid data at higher temperatures and low frequencies through the introduction of proportional, integral and adoptive control and the addition of an external signal to the operating system. This is discussed in detail in this Chapter.

The other purpose of this chapter was to present revised testing protocols for the EN Standard Tester (four-point bending) and AMPT testing which were developed to minimise the errors introduced during testing, in particular out-of-range phase angle problems associated with the EN tester and out-of-range strain levels and load standard errors associated with the AMPT tester.

5 TEST RESULTS AND ANALYSIS

5.1 Introduction

The objective of this chapter is to present the test results carried out at the Curtin University Geomechanical Laboratory and an analysis of those results. The scope of the testing program can be divided into two major sections:

1. the fatigue behaviour of the asphalt mix using the four-point bending beam apparatus
2. the linear viscoelastic behaviour of the asphalt mix and the development of compressive and bending master curves under different testing conditions.

5.1.1 *Fatigue behaviour of asphalt mixes under repeated loading*

In order to gain a better understanding of the behaviour of the asphalt under repeated loading the following tests were conducted:

- eight tests in accordance with the Austroads (2006)
- 18 tests in accordance with EN Standard 12697-24 (2012) to determine the fatigue curve equation
- 24 tests at four strain levels, three temperatures and two loading modes (haversine and sinusoidal) to evaluate the influence of wave shape on behaviour
- 15 tests at five frequencies (0.1, 1, 5, 10 and 25 Hz) at three different temperatures (4°C, 20°C and 40°C) and different strain levels (100-1500 $\mu\epsilon$) to evaluate the influence of frequency and temperature on behaviour
- 26 tests to examine the healing properties of asphalt using three rest periods (0.1, 0.3 and 0.9 seconds) and two loading modes (haversine and sinusoidal). All results were compared with the results obtained without rest periods.

This testing was in addition to the testing conducted to develop the testing protocol presented in Chapter 4. During the abovementioned testing program, some beams failed due to unexpected reasons, e.g. power outage, hydraulic jack damages, etc.; these results were excluded from the analysis.

5.1.2 *Linear viscoelastic behaviour of asphalt mix*

In order to study the linear viscoelastic behaviour of the asphalt, testing of both beams and cylindrical samples was conducted to generate data which would enable

master curves for different testing conditions to be developed. The following testing was conducted:

- eight tests of cylindrical samples without confining pressure
- three tests of cylindrical samples with 65 kPa confining pressure
- three tests of cylindrical samples with 135 kPa confining pressure
- ten tests of beams using haversine loading (to develop one single master curve)
- 28 tests of beams using sinusoidal loading (to develop one single master curve).

5.2 Approaches used

In terms of both fatigue behaviour (Section 5.2.1) and the development of master curves (Section 5.2.2), six different approaches were adopted:

1. The determination of the fatigue life of asphalt beams according to Austroads (2006) using the four-point bending beam apparatus and the UTS15 software.
2. The development of a fatigue relationship in accordance with EN Standard 12697 using the four-point bending beam apparatus and the UTS18 software.
3. The determination of the effect of temperature on fatigue life using non-standard testing and the UTS15 and UTS18 software.
4. The examination of the fatigue behaviour of asphalt beams when tested at different frequencies, temperatures and strain levels and modelled using the non-standard form of tests using the UTS15 software.
5. Examination of the healing of asphalt by introducing rest periods to both the haversine and sinusoidal load shapes using the UTS19 user-programmable software and the four-point bending beam apparatus.
6. Development of master curves based on the testing of both asphalt cylinders and beams.

5.3 Approach 1

A total of eight asphalt beams were tested in accordance with Austroads (2006) at a temperature of 20°C, a strain level of 400 $\mu\epsilon$ and a frequency of 10 Hz. A summary of the testing conditions is presented in Table 5.1 whilst the results of the testing are presented in Figure 5-1.

Table 5.1: Summary of testing conditions (in accordance with AGPT/T233)

Sample no.	Frequency (Hz)	Strain level ($\mu\epsilon$)	Temperature ($^{\circ}\text{C}$)	Test status	Air voids (%)	Initial stiffness (MPa)	Total cycle count
1	10	400	20	failed	6.0	6021	34,900
2	10	400	20	completed	5.6	6696	61,170
3	10	400	20	failed	5.9	6979	37,270
4	10	400	20	completed	5.1	7799	112,450
5	10	400	20	completed	5.2	7600	131,570
6	10	400	20	completed	5.2	6801	98,610
7	10	400	20	completed	5.5	6948	127,020
8	10	400	20	completed	5.5	7038	68,600
Average for all samples					5.5	6991	83,949
Average without failed samples					5.32	7155	99,903

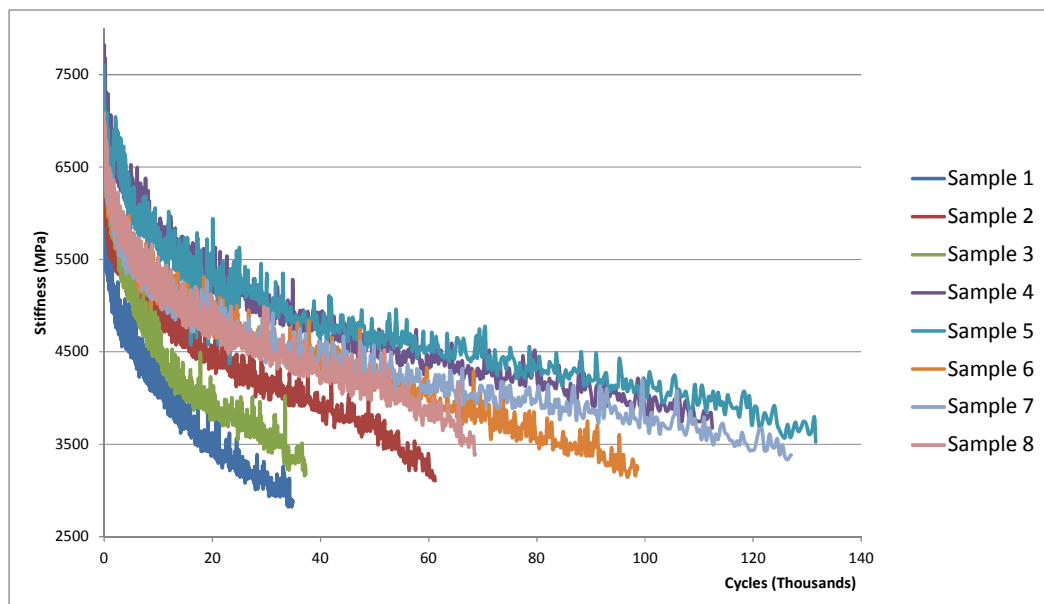


Figure 5-1: Fatigue curves for beams under haversine loading (testing in accordance with AGPT/T233)

It is apparent from Table 5.1 and Figure 5-1 that samples 1 and 3 failed during testing. Excluding those results, the average fatigue life was just under 100,000 cycles (99,903 cycles).

5.4 Approach 2

As stated in EN 12697-24 (2012) the predicted fatigue life should be derived using linear regression of the number of cycles required for the stiffness of the asphalt to reduce to 50% of its initial value (N_f) and the initial strain amplitude recorded after 100 cycles of load (Equation 5-1):

$$\ln(N_f) = A_0 + A_1 \times \ln(\epsilon_i) \quad 5-1$$

where

- N_f = number of cycles required for the stiffness of the asphalt to reduce to 50% of its initial value
 ϵ_i = initial strain level recorded after 100 load cycle
 A_0 and A_1 = experimental coefficients extracted by linear regression

To meet the standard requirements, a minimum of 18 beams should be tested before the regression analysis is attempted. The test conditions are presented in Table 5.2, whilst the results are summarised in Table 5.3.

Table 5.2: Testing conditions and number of samples tested (approach 2)

Number of samples	Loading shape	Frequency (Hz)	Strain level ($\mu\epsilon$) (Peak-to-Peak)	Temperature ($^{\circ}\text{C}$)
6	Sinusoidal	10	300	20
6	Sinusoidal	10	400	20
6	Sinusoidal	10	500	20

Table 5.3: Results of testing (approach 2)

Strain Level ($\mu\epsilon$)	Beam no	N_f	ϵ_i	$\ln N_f$	$\ln \epsilon_i$	Test status
500	9	65,445	494.974	11.089	6.205	completed
	10	140,894	495.6	11.856	6.206	completed
	11	27,732	497.164	10.230	6.209	failed
	12	27,538	497.96	10.223	6.210	failed
	13	78,137	496.572	11.266	6.208	completed
	14	88,441	496.658	11.390	6.208	completed
400	15	16,123	398.784	9.688	5.988	failed
	16	66,613	397.408	11.106	5.985	failed
	17	299,395	397.288	12.610	5.985	completed
	18	321,900	397.122	12.682	5.984	completed
	19	137,959	396.37	11.835	5.982	completed
	20	306,667	398.704	12.634	5.988	completed
300	21	827,519	297.906	13.626	5.697	completed
	22	836,031	299.02	13.636	5.701	completed
	23	2,000,000	299.242	14.509	5.701	failed
	24	810,014	299.262	13.605	5.701	completed
	25	284,339	299.512	12.558	5.702	failed
	26	189,559	298.402	12.152	5.698	failed

It can be seen from Table 5.3, that the fatigue life of some samples was very short. Although it is stated in EN 12697-24 that the number of samples tested, and used to develop the regression equation, should be 18, it was decided to remove the failed samples from the analysis and re-analyse the data. Three methods were used to develop the regression equation were based on:

1. the results for 18 samples (Figure 5-2)
2. the results without the failed samples (Figure 5-3)
3. the average for each testing condition (Table 5.4 and Figure 5-4).

Table 5.4: Averaged results for each strain level and all samples (approach 2)

Strain level ($\mu\epsilon$)	Average			
	N_f	ϵ_i	$\ln N_f$	$\ln \epsilon_i$
500	71364.5	496.488	11.010	6.208
400	191442.8	397.613	11.759	5.985
300	824577	298.891	13.348	5.700

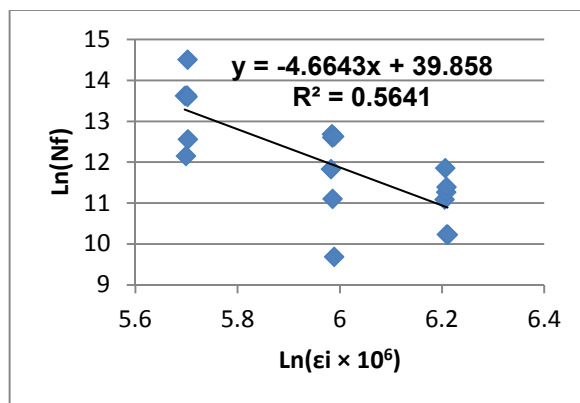


Figure 5-2: Regression equation: approach 2, all beams

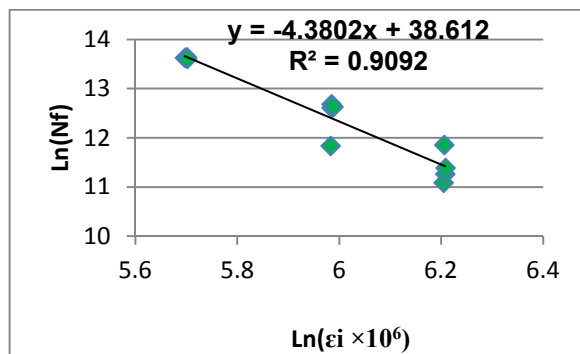


Figure 5-3: Regression equation: approach 2, without failed beams

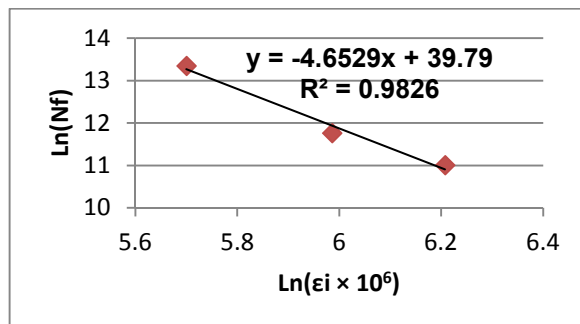


Figure 5-4: Regression equation for averaged results at different strain levels (approach 2)

The calculated experimental coefficients are presented in Table 5.5. It can be seen from this Table that the difference between Method 1 and Method 3 was almost negligible.

Table 5.5: Comparison of three methods of analysis

Method	Analysis method	A ₀	A ₁	R ²	ε(10 ⁶) (με)
1	all beams	39.858	-4.6643	0.5641	265.9651
2	without failed samples	38.612	-4.3802	0.9092	287.4476
3	average	39.79	-4.6529	0.9826	265.7166

Using the fatigue relationships developed for all three methods the predicted strain level after 1 million load repetitions was calculated and the results are also presented in Table 5.5. Once again, it can be seen that the calculated strains for Method 1 and Method 3 were almost identical and the difference between the results for these two methods, and Method 2, was 21 με which might not be negligible in practice.

5.5 Approach 3

The asphalt fatigue relationship published in Austroads (2012) (Equation 5-2) is the Shell (1978) laboratory fatigue prediction model refined to replicate field conditions by multiplying it by a reliability factor (RF):

$$N = RF \times \left[\frac{6918 (0.856V_b + 1.08)}{S_{mix}^{0.36} \mu\epsilon} \right] \quad 5-2$$

where

- N = allowable number of repetitions of load
- RF = reliability factor for asphalt fatigue (considered as 0.67)
- V_b = percentage, by volume, of binder in the asphalt (11.2%)
- S_{mix} = asphalt modulus (MPa)
- $\mu\epsilon$ = tensile strain (constant strain mode)

As discussed in Section 4.2, reliability factors are incorporated into the pavement design procedures. The reliability factors for a desired project reliability published in Austroads (2012) are shown in Table 5.6.

Table 5.6: Reliability factors for desired project reliability (Austroads 2012)

Desired project reliability				
80%	85%	90%	95%	97.5%
2.5	2	1.5	1.0	0.67

The aim of this approach was to compare the laboratory predicted fatigue life with the Austroads model assuming a reliability factor of 0.67 for a desired project reliability of 97.5%. An attempt was also made to assess the effect of temperature and loading mode on the fatigue life. For this reason the haversine wave form was initially applied at a range of strain levels and temperatures. Following this, the same testing protocol was adopted but this time the sinusoidal wave form was used. Twelve beams were tested for each wave form as shown in Table 5.7.

5.5.1 Haversine loading mode

The UTS15 software was used to control the fatigue testing, which was conducted, in constant strain mode, on 12 prepared beams at temperatures of 4°C, 20°C and 40°C and a frequency of 10 Hz. Testing was conducted at four strain levels: 100 $\mu\epsilon$, 200 $\mu\epsilon$, 300 $\mu\epsilon$ and 400 $\mu\epsilon$. The properties of the samples and test conditions are presented in Table 5.7.

Table 5.7: Testing condition (approach 3)

Loading Shape	Temperature (°C)	Beam no.	Strain level ($\mu\epsilon$)	Loading Shape	Temperature (°C)	Beam no.	Strain level ($\mu\epsilon$)
Haversine	4	27	100	Sinusoidal	4	39	100
		28	200			40	200
		29	300			41	300
		30	400			42	400
	20	31	100		20	43	100
		32	200			44	200
		33	300			45	300
		34	400			46	400
	40	35	100		40	47	100
		36	200			48	200
		37	300			49	300
		38	400			50	400

Table 5.8: Properties of samples and test conditions (haversine loading)

Beam no.	Dimensions (mm)	Air void content (%)	Compaction temperature (°C)	Strain level (µε)	Frequency (Hz)	Temperature (°C)
27	400×63×50	5.6	142	100	10	4
28	400×63×50	5.1	142	200	10	4
29	400×63×50	5.2	142	300	10	4
30	400×63×50	5.2	142	400	10	4
31	400×63×50	6	143	100	10	20
32	400×63×50	5.9	143	200	10	20
33	400×63×50	5.9	143	300	10	20
34	400×63×50	5.5	142	400	10	20
35	400×63×50	5.5	142	100	10	40
36	400×63×50	4.7	142	200	10	40
37	400×63×50	5.5	143	300	10	40
38	400×63×50	5.6	143	400	10	40

The results of the fatigue testing are presented in Table 5.9. It is apparent from the Table that, in some cases, and especially at lower strain levels, the termination condition (viz. stiffness to reduce to 50% of the initial stiffness) was never attained. For example, whilst over 3 million cycles of load were applied to beam 27, there was no evidence of any significant change (reduction) in stiffness.

Table 5.9: Summary of test results (haversine loading)

Beam no.	Strain level (µε) (Peak-to-Peak)	Temperature (°C)	Cycles	Initial stiffness (MPa)	Final Stiffness (MPa)
27	100	4	3,362,530	15545	16345
28	200	4	2,000,000	15728	9244
29	300	4	240,800	13617	6767
30	400	4	57,540	14705	7295
31	100	20	2,000,000	6885	5922
32	200	20	2,000,000	6750	4844
33	300	20	705,230	6629	3295
34	400	20	93,800	5987	2993
35	100	40	2,000,000	1238	970
36	200	40	1,693,900	1170	637
37	300	40	2,000,000	985	610
38	400	40	1,000,000	952	468

The UTS15 outputs for all the tested beams are presented in Appendix A.

5.5.2 Sinusoidal loading mode

The UTS18 software was again used to control the testing of 12 different beams. The testing conditions were identical apart from the wave form adopted. The properties of the samples and test conditions are presented in Table 5.10.

Table 5.10: Properties of samples and testing conditions (sinusoidal loading)

Beam no.	Dimensions (mm)	Air void content (%)	Compaction temperature (°C)	Strain level (µε)	Frequency (Hz)	Temperature (°C)
39	400×63×50	6.3	148	100	10	4
40	400×63×50	6.5	148	200	10	4
41	400×63×50	6.0	148	300	10	4
42	400×63×50	6.4	145	400	10	4
43	400×63×50	6.5	145	100	10	20
44	400×63×50	6.6	145	200	10	20
45	400×63×50	6.3	151	300	10	20
46	400×63×50	6.4	151	400	10	20
47	400×63×50	5.0	145	100	10	40
48	400×63×50	5.5	150	200	10	40
49	400×63×50	5.5	150	300	10	40
50	400×63×50	5.4	150	400	10	40

The results of the fatigue testing are presented in Table 5.11. Once again, it is apparent from the Table that, in some cases, and especially at lower strain levels, the termination condition (viz. 50% stiffness reduction) was never attained.

Table 5.11: Summary of test results (sinusoidal loading)

Beam no.	Strain level (µε) (Peak-to-Peak)	Temperature (°C)	Cycles	Initial stiffness (MPa)	Final Stiffness (MPa)
39	100	4	292,865	13080	13517
40	200	4	1,421,602	14897	12090
41	300	4	61,660	13653	6804
42	400	4	71,890	15023	7501
43	100	20	1,000,000	5822	5346
44	200	20	2,000,000	5628	4281
45	300	20	835,317	585	2940
46	400	20	305,102	4899	2449
47	100	40	2,000,000	1216	983
48	200	40	1,467,800	1177	818
49	300	40	1,394,584	1137	706
50	400	40	916,690	1021	509

The UTS18 outputs for all tested beams are presented in Appendix B.

5.5.3 Modelling the fatigue curve

Two scenarios were used to model the fatigue life data:

1. modelling based on the phase diagram
2. modelling by curve-fitting on the test results.

The fatigue data and the fitted curves for the different scenarios are presented in Appendix C.

5.5.3.1 Scenario 1

Normally three phases can be identified in a fatigue curve: the adjustment phase, the quasi-stationary phase, and the failure phase (Figure 5-5).

Using this scenario, the fatigue curves for both the haversine and sinusoidal loading mode were investigated for each of the three phases. At the lowest temperature level (4°C) the behaviour of the asphalt under repeated loading in Phase I was polynomial whereas, at the other temperatures (20°C & 40°C), the trend was logarithmic. For Phase II and Phase III, under all testing conditions, the polynomial trend better replicated behaviour.

As a result, Equation 5-3 was used to model the fatigue behaviour of the beams for temperatures of 20°C & 40°C in Phase I and Equation 5-4 was used to model the fatigue behaviour of the beams at a temperature of 4°C in Phase I and all temperatures in Phases II and III. The test temperatures and the fitted curves for each phase are shown in Figure 2-1.

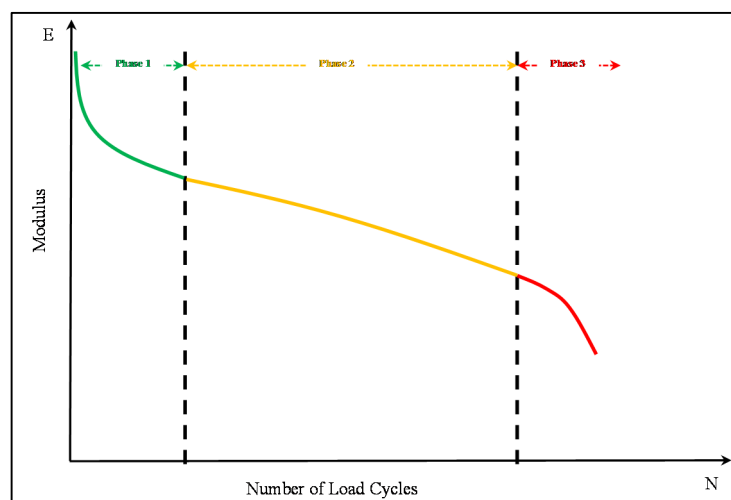


Figure 5-5: Different phases in the laboratory fatigue behaviour of asphalt
(Source: Di Benedetto et al. 2004)

Table 5.12: Fitted curves for different temperatures (scenario 1)

Temperature (°C)	Curve type		
	Phase I	Phase II	Phase III
4	polynomial Equation 5-4	polynomial Equation 5-4	polynomial Equation 5-4
20	logarithmic Equation 5-3	polynomial Equation 5-4	polynomial Equation 5-4
40	logarithmic Equation 5-3	polynomial Equation 5-4	polynomial Equation 5-4

$$E = a \ln N + b \quad 5-3$$

where

- E = material stiffness (MPa)
- N = number of load cycles during testing
- a, b = experimental coefficients extracted by regression analysis

$$E = cN^3 + dN^2 + fN + g \quad 5-4$$

where

- c, d, f & g = experimental coefficients extracted by regression analysis

The fitted parameters in scenario 1 for the haversine and sinusoidal loads under the different testing conditions (temperature, strain) are shown in Table 5.13 and Table 5.14 respectively.

Table 5.13: Parameters in scenario 1 under different testing conditions (haversine load)

Testing condition		Phase no	Parameters						
Temperature (°C)	Strain (µε)		a	b	c	d	f	g	R ²
4	100	I, II, III	Nil						
	200	I	—	—	0	1E-8	-0.011	15279	0.9602
		II	—	—	0	1E-10	-0.0025	13731	0.9938
		III	Nil						
	300	I	—	—	0	3E-8	-0.0202	13390	0.9612
		II	—	—	0	-1E-7	0.0144	11691	0.9988
		III	—	—	0	2E-7	-0.1594	31055	0.9922
	400	I	—	—	0	6E-6	-0.2296	14372	0.9835
		II	—	—	0	-8E-7	-0.0438	12889	0.9983
		III	—	—	0	2E-6	-0.4869	28161	0.9975
20	100	I	-99.05	7457.7	—	—	—	—	0.9409
		II, III	Nil						
	200	I	-162.9	7603	—	—	—	—	0.9872
		II	—	—	0	0	-0.0004	5542	0.954
		III	Nil						
	300	I	-228.5	7867.7	—	—	—	—	0.9631
		II	—	—	-1E-14	1E-8	-0.0067	5577	0.9967
		III	—	—	0	-3E-8	0.0384	8036.5	0.9966
	400	I	-266.4	7244.8	—	—	—	—	0.9638
		II	—	—	-7E-12	1E-6	-0.0679	5156.7	0.9953
		III	—	—	0	-3E-8	-0.0048	3723.8	0.9973
40	100	I	-30.86	1468.9	—	—	—	—	0.8496
		II	—	—	-2E-16	8E-10	-0.0011	1495.9	0.2088
		III	Nil						
	200	I	-28.25	1307.8	—	—	—	—	0.9281
		II	—	—	-2E-16	6E-10	-0.0006	1049.3	0.9465
		III	Nil						
	300	I	-25.93	1105.8	—	—	—	—	0.946
		II	—	—	-6E-17	2E-10	-0.0003	819.74	0.9659
		III	Nil						
	400	I	-33.59	1106.6	—	—	—	—	0.9591
		II	-52.5	1277.8	—	—	—	—	0.9706
		III	—	—	0	-5E-11	-7E-5	593.74	0.9809

Table 5.14: Parameters in scenario 1 under different testing conditions (sinusoidal load)

Testing condition		Phase no	Parameters						
Temperature (°C)	Strain (μϵ)		a	b	c	d	f	g	R²
4	100	I, II, III	Nil						
	200	I	—	—	-3E-15	9E-9	-0.0072	14783	0.9781
		II, III	Nil						
	300	I	—	—	0	4E-6	-0.1928	13555	0.9856
		II	—	—	0	5E-7	-0.1498	13881	0.999
		III	—	—	0	5E-7	-0.1453	13094	0.9993
	400	I	—	—	0	1E-5	-0.3797	14984	0.9936
		II	—	—	0	1E-7	-0.0906	13368	0.9993
		III	—	—	0	0	-0.0474	10885	0.9993
20	100	I	-51.39	6116.8	—	—	—	—	0.9244
		II, III	Nil						
	200	I	-103.3	6178.1	—	—	—	—	0.9384
		II	—	—	6E-18	3E-11	-0.0003	4788	0.9955
		III	Nil						
	300	I	-189.5	6799.2	—	—	—	—	0.9626
		II	—	—	-9E-15	1E-8	-0.0065	4821.4	0.989
		III	—	—	0	-3E-8	0.0384	8036.5	0.9966
	400	I	-165.6	5684.2	—	—	—	—	0.9801
II		—	—	-1E-13	7E-8	-0.0146	4156.8	0.9942	
III		—	—	0	-2E-8	-0.0043	2610.7	0.9998	
40	100	I	-20.75	1333.2	—	—	—	—	0.9014
		II	—	—	0	-6E-9	0.0239	22535	0.712
		III	Nil						
	200	I	-28.55	1307.8	—	—	—	—	0.9281
		II	—	—	-1E-16	3E-10	-0.0004	989.34	0.9844
		III	Nil						
	300	I	-25.93	1313.3	—	—	—	—	0.9895
		II	—	—	-4E-16	1E-9	-0.0008	953.65	0.9664
		III	Nil						
	400	I	-34.71	1183.5	—	—	—	—	0.998
		II	—	—	-2E-15	3E-9	0.0014	865.14	0.9664
		III	—	—	0	-5E-9	0.0085	-2837	0.988

5.5.3.2 Scenario 2

In this scenario the best fit of the fatigue life data was sought using the Microsoft Excel® Solver analysis tool. After fitting different curves to the fatigue test results it was found that the logarithmic equation explained the fatigue behaviour the best for different temperatures. The fatigue life model for different temperatures, for both haversine and sinusoidal loading conditions, is given in Equation 5-5.

$$E = \alpha [\ln(\beta N + \gamma)] + E_{max} \quad 5-5$$

where

- E = material stiffness (MPa)
 N = number of load cycle during testing
 α, β, γ = curve fitting parameters
 E_{max} = maximum theoretical stiffness (MPa)

The fitted parameters in scenario 2 for the haversine and sinusoidal loads under the different testing conditions (temperature, strain) are shown in Table 5.15 and Table 5.16 respectively.

Table 5.15: Parameters in scenario 2 under different testing conditions (haversine load)

Beam no	Strain ($\mu\epsilon$)	Temperature ($^{\circ}\text{C}$)	Parameters				
			α	β	γ	E_{max}	R^2
27	100	4	—	—	—	—	—
28	200	4	-2404.16	0.000930	204.9861	28058.88	0.9943
29	300	4	-47478.9	0.000131	273.0574	279808.5	0.9775
30	400	4	-66173.4	0.000442	261.5319	382310.6	0.9934
31	100	20	-118.623	0.000232	0.505345	6704.244	0.9797
32	200	20	-221.493	0.000701	1.140445	6612.877	0.9909
33	300	20	-510.053	0.00829	57.43464	8358.673	0.9865
34	400	20	-611.225	0.004149	5.836144	6877.806	0.9973
35	100	40	-34.4806	0.0028	1.879754	1307.761	0.9335
36	200	40	-68.2936	0.00143	24.98016	1318.393	0.9719
37	300	40	-49.3504	0.003519	15.44289	1068.225	0.9917
38	400	40	-63.9396	0.003708	13.62051	1053.156	0.9865

Table 5.16: Parameters in scenario 2 under different testing conditions (sinusoidal load)

Beam no	Strain ($\mu\epsilon$)	Temperature ($^{\circ}\text{C}$)	Parameters				
			α	β	γ	E_{max}	R^2
39	100	4	—	—	—	—	—
40	200	4	734.007	0.002149	95.95034	18192.93	0.9943
41	300	4	65920.7	0.000474	260.5978	380128.8	0.9973
42	400	4	3486.84	0.011442	134.0903	31957.35	0.9969
43	100	20	83.0708	0.000151	0.508049	5751.48	0.9974
44	200	20	197.861	0.000467	2.561016	5733.522	0.9939
45	300	20	379.508	0.00917	11.23672	6738.068	0.9956
46	400	20	382.912	0.008216	13.45101	5802.541	0.9938
47	100	40	39.1738	0.000494	4.635038	1259.937	0.9345
48	200	40	44.8581	0.0024	2.249163	1199.548	0.9964
49	300	40	48.2966	0.003097	1.040576	1132.366	0.9973
50	400	40	58.4286	0.002399	2.395716	1049.351	0.9947

Examples of curve fittings for both scenario 1 and scenario 2 are presented in Figure 5-6 and Figure 5-7.

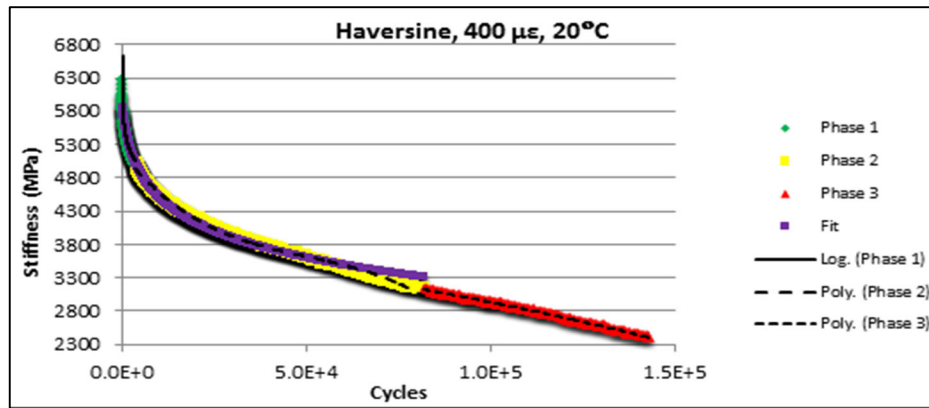


Figure 5-6: Example of curve fitting for defined scenarios (haversine loading)

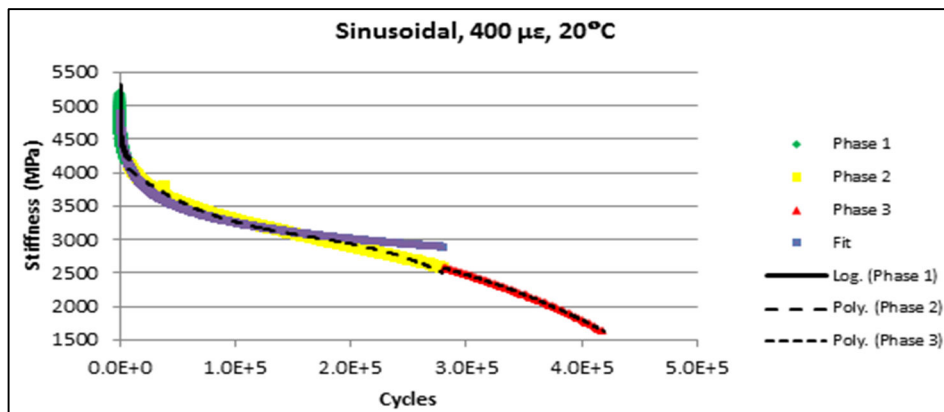


Figure 5-7: Example of curve fitting for defined scenarios (sinusoidal loading)

5.5.3.3 Applying extrapolation methodology to scenario 1 and scenario 2

As stated earlier, in some tests the termination condition was not met and fatigue life could not be determined. In these cases it was necessary to extrapolate the data to estimate after how many loading cycles the stiffness reached 50% of its initial value. This was done using the equations proposed for the aforementioned scenarios.

Extrapolation using scenario 1 model

It is obvious from the fatigue curve phase diagram (Figure 5-5) that the most important phase for extrapolation is phase II. By feeding the fitted parameters presented in Table 5.13 and Table 5.14 into Equation 5-4 the fatigue life for unterminated tests was determined. The results for scenario 1 are shown in Table 5.17 and Table 5.18 for haversine and sinusoidal loading respectively.

Table 5.17: Extrapolated fatigue life for unterminated tests (haversine loading)

Testing condition		Fitting Parameters for Phase II							Need for extrapolation?	Fatigue life
Temperature (°C)	Strain (µε)	a	b	c	d	f	g	R ²		
4	100	Nil							yes	unpredictable
	200	—	—	0	1E-10	0.0025	13731	0.9938	yes	2,495,000
	300	—	—	0	-1E-7	0.0144	11691	0.9988	no	240,800
	400	—	—	0	-8E-7	0.0438	12889	0.9983	no	57,540
20	100	Nil							yes	unpredictable
	200	—	—	0	0	0.0004	5542	0.954	yes	5,245,000
	300	—	—	-1E-14	1E-8	0.0067	5577	0.9967	no	705,230
	400	—	—	-7E-12	1E-6	0.0679	5156.7	0.9953	no	93,800
40	100	—	—	-2E-16	8E-10	0.0011	1495.9	0.2088	yes	unpredictable
	200	—	—	-2E-16	6E-10	0.0006	1049.3	0.9465	yes	2,070,000
	300	—	—	-6E-17	2E-10	0.0003	819.74	0.9659	yes	2,092,000
	400	52.5	1277.8	—	—	—	—	0.9706	no	1,000,000

Table 5.18: Extrapolated fatigue life for unterminated tests (sinusoidal loading)

Testing condition		Fitting Parameters for Phase II					Need for Extrapolation?	Fatigue life
Temperature (°C)	Strain (µε)	c	d	f	g	R ²		
4	100	Nil					yes	unpredictable
	200	-3E-15	9E-9	0.0072	14783	0.9781	yes	unpredictable
	300	0	5E-7	0.1498	13881	0.999	no	61,660
	400	0	1E-7	0.0906	13368	0.9993	no	71,890
20	100	Nil					yes	unpredictable
	200	6E-18	3E-11	0.0003	4788	0.9955	yes	569,000,000
	300	-9E-15	1E-8	0.0065	4821.4	0.989	no	835,317
	400	-1E-13	7E-8	0.0146	4156.8	0.9942	no	305,102
40	100	0	-6E-9	0.0239	22535	0.712	yes	5.3×10 ¹⁰
	200	-1E-16	3E-10	0.0004	989.34	0.9844	yes	286,883,192
	300	-4E-16	1E-9	0.0008	953.65	0.9664	yes	11,224,983
	400	-2E-15	3E-9	0.0014	865.14	0.9664	no	916,690

Extrapolation using scenario 2 model

In order to precisely determine fatigue life in the laboratory the most important step is to compare the laboratory fatigue life when the test is terminated with the fatigue life estimated by the model. For this reason, Equation 5-5 has been re-arranged into Equation 5-6 to predict the fatigue life.

$$N_f = \frac{e^{\left(\frac{E_i - 2E_{max}}{2\alpha}\right)} - \gamma}{\beta} \quad 5-6$$

where

- E_i = initial stiffness recorded at cycle number 100 (MPa)
- N_f = estimated fatigue life (cycles)
- α, β, γ = curve fitting parameters

$$E_{max} = \text{maximum theoretical stiffness (MPa)}$$

By feeding the fitting parameters presented in Table 5.15 and Table 5.16 into Equation 5-5, the fatigue life for scenario 2 was estimated and the results are presented in Table 5.19 for tests where the fatigue life was known and there was no need for extrapolation.

Table 5.19: Comparison of estimated fatigue life with laboratory results (scenario 2)

Loading Mode	Beam no	Strain ($\mu\epsilon$)	Temp. ($^{\circ}\text{C}$)	Parameters					Laboratory fatigue life	Model predicted fatigue life
				α	β	γ	E_{max}	E_i		
haversine	29	300	4	47478.9	0.000131	273.0574	279808.5	13617.8	240,800	314,000
haversine	30	400	4	66173.4	0.000442	261.5319	382310.6	14705.7	57,540	62,100
haversine	33	300	20	510.053	0.00829	57.43464	8358.673	6629.5	705,230	2,370,000
haversine	34	400	20	611.225	0.004149	5.836144	6877.806	5987.3	93,800	137,000
haversine	38	400	40	63.9396	0.003708	13.62051	1053.156	951.9	1,000,000	2,240,000
sinusoidal	41	300	4	65920.7	0.000474	260.5978	380128.8	13562.6	61,660	57,800
sinusoidal	42	400	4	3486.84	0.011442	134.0903	31957.35	15022.6	71,890	85,200
sinusoidal	45	300	20	379.508	0.00917	11.23672	6738.068	5885.1	835,317	2,400,000
sinusoidal	46	400	20	382.912	0.008216	13.45101	5802.541	4899.2	305,102	771,000
sinusoidal	50	400	40	58.4286	0.002399	2.395716	1049.351	1021.3	916,690	4,210,000

It is apparent from Table 5.19 that almost all the fatigue lives predicted by the models are much higher than the laboratory results. It is also apparent from Figure 5-8 that feeding the termination stiffness of 2,994 MPa into the proposed model resulted in a higher predicted fatigue life compared to the laboratory test results. The termination stiffness therefore should be adjusted using an adjustment factor (Φ). This adjustment is explained in Figure 5-9.

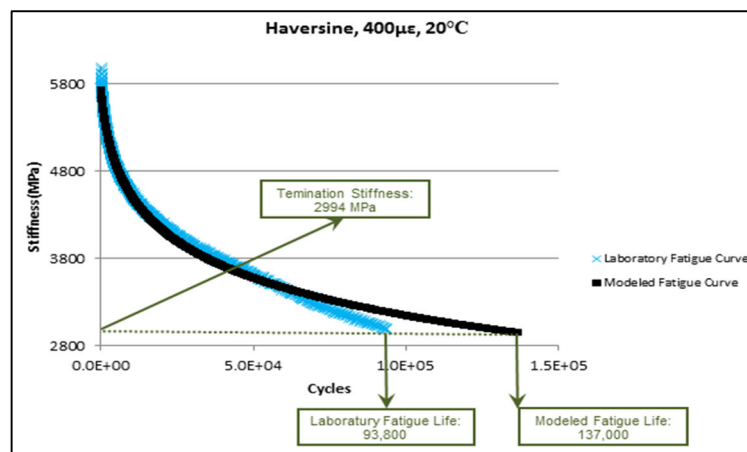


Figure 5-8: Difference between proposed model and laboratory results

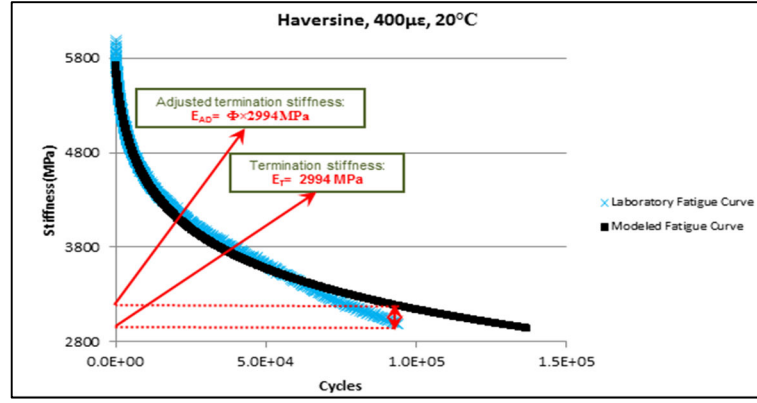


Figure 5-9: Adjusting the termination stiffness for modelled fatigue curve

By applying the adjustment factor to the termination stiffness and the model predicts the fatigue life more accurately. The modified fatigue life prediction model which uses the adjusted termination stiffness is shown in Equation 5-7.

$$N_f = \frac{e^{\left(\frac{\phi E_i - 2E_{max}}{2\alpha}\right) - \gamma}}{\beta} \quad 5-7$$

where

ϕ = adjustment Factor

In terms of how to determine the adjustment factor, the following step-by-step methodology is proposed:

1. A curve fitted on terminated (50% stiffness reduction) laboratory fatigue result and the adjusted stiffness was recorded (Figure 5-10).

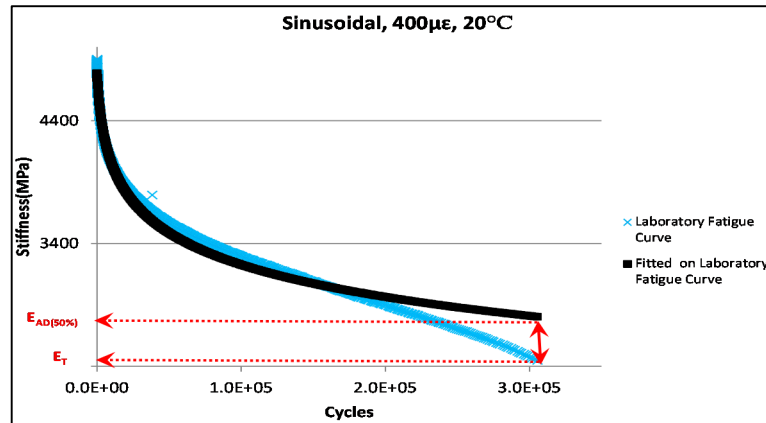


Figure 5-10: Adjusting the termination stiffness for fitted curve

2. It was assumed that the tested beam had lost only 43.5% of its original stiffness so a curve was fitted on 43.5% stiffness reduction. This fitted curve has extended to the termination stiffness (50% reduction in stiffness) and the adjusted stiffness was recorded (Figure 5-11).

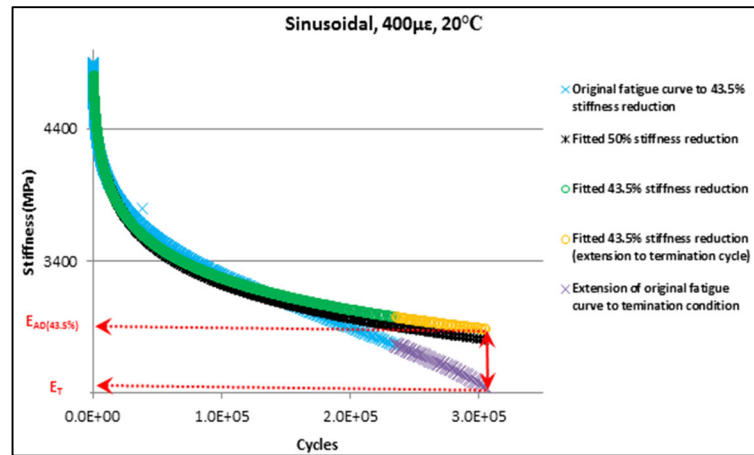


Figure 5-11: Adjusting the termination stiffness for fitted curve on 43.5% stiffness reduction state

3. Repeat Step 2 by decreasing the stiffness reduction in 0.5% intervals until a reduction of 6.5% is achieved
4. Repeat Steps 1 and 2 for all terminated tests and develop an adjustment factor template using Equation 5-8.

$$\phi_j = \frac{E_{ADj}}{E_T} \quad 5-8$$

where

- j = stiffness reduction (43.5%, 43%, 42.5%..., 6.5%)
- ϕ_j = adjustment factor for j
- E_{ADj} = adjusted stiffness for j
- E_T = termination stiffness

The adjustment factors for the terminated tests are plotted in Figure 5-12. It is apparent from this Figure that the maximum and minimum adjustment factors were 1.5 and 1.1 respectively. Note also that there are two zones in this plot: if a material loses more than 20% of its initial stiffness then the adjustment factor falls into the linear trend zone; otherwise, it falls into non-linear trend zone.

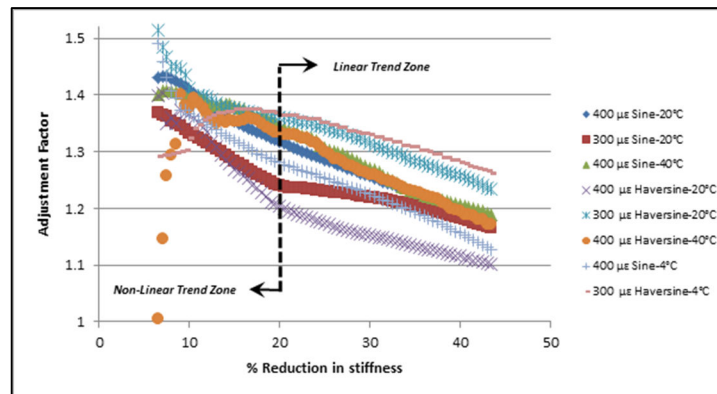


Figure 5-12: Adjustment factors for terminated tests in different stiffness loss state

In order to predict the fatigue life of the unterminated tests the adjustment factors were averaged and the maximum and minimum adjustment factors for each stiffness reduction state recorded. The plotted average adjustment factors are shown in Figure 5-13. It is apparent from this Figure that the fatigue life estimation for the unterminated tests is more precise in the linear trend zone where the minimum stiffness reduction is 10%.

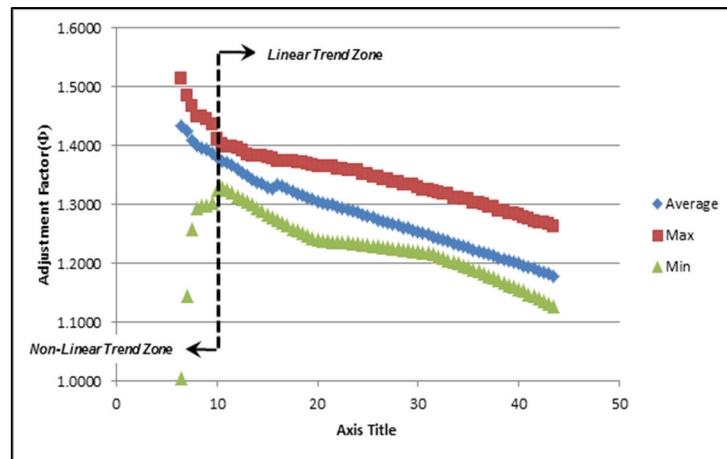


Figure 5-13: Average, maximum and minimum adjustment factors for fatigue life prediction

The average, maximum, minimum and standard deviation of the adjustment factors are shown in Table 5.20.

Table 5.20: Template adjustment factors for different stiffness reduction states

% Stiffness Loss	Adjustment factors (Φ_i)			STD	% Stiffness loss	Adjustment factors (Φ_i)			STD
	Average	Max	Min			Average	Max	Min	
43.5	1.1788	1.2625	1.1264	0.0489	25	1.2809	1.3523	1.2307	0.0556
43	1.1816	1.2661	1.1318	0.0490	24.5	1.2838	1.3523	1.2315	0.0559
42.5	1.1850	1.2693	1.1358	0.0491	24	1.2877	1.3574	1.2329	0.0567
42	1.1878	1.2694	1.1399	0.0490	23.5	1.2902	1.3575	1.2340	0.0564
41.5	1.1909	1.2727	1.1438	0.0494	23	1.2922	1.3575	1.2351	0.0564
41	1.1935	1.2758	1.1477	0.0492	22.5	1.2944	1.3598	1.2360	0.0567
40.5	1.1965	1.2790	1.1528	0.0494	22	1.2967	1.3599	1.2367	0.0564
40	1.1995	1.2821	1.1565	0.0493	21.5	1.2994	1.3649	1.2369	0.0566
39.5	1.2020	1.2851	1.1601	0.0494	21	1.3010	1.3649	1.2373	0.0564
39	1.2044	1.2852	1.1636	0.0490	20.5	1.3034	1.3650	1.2384	0.0561
38.5	1.2077	1.2900	1.1682	0.0493	20	1.3058	1.3650	1.2406	0.0551
38	1.2101	1.2901	1.1715	0.0488	19.5	1.3092	1.3683	1.2436	0.0550
37.5	1.2134	1.2957	1.1758	0.0497	19	1.3119	1.3705	1.2470	0.0547
37	1.2156	1.2957	1.1789	0.0494	18.5	1.3159	1.3706	1.2508	0.0522
36.5	1.2181	1.2994	1.1829	0.0495	18	1.3192	1.3706	1.2553	0.0508
36	1.2210	1.3034	1.1867	0.0500	17.5	1.3234	1.3748	1.2593	0.0493
35.5	1.2234	1.3036	1.1894	0.0495	17	1.3267	1.3747	1.2644	0.0482
35	1.2263	1.3086	1.1929	0.0502	16.5	1.3307	1.3747	1.2694	0.0453
34.5	1.2285	1.3087	1.1962	0.0501	16	1.3331	1.3749	1.2743	0.0438
34	1.2310	1.3115	1.1994	0.0500	15.5	1.3264	1.3775	1.2788	0.0419
33.5	1.2339	1.3115	1.2031	0.0498	15	1.3303	1.3797	1.2831	0.0406
33	1.2376	1.3178	1.2058	0.0511	14.5	1.3350	1.3834	1.2887	0.0378
32.5	1.2401	1.3179	1.2091	0.0505	14	1.3388	1.3839	1.2939	0.0358
32	1.2430	1.3216	1.2123	0.0513	13.5	1.3430	1.3835	1.2999	0.0329
31.5	1.2454	1.3217	1.2153	0.0510	13	1.3484	1.3851	1.3041	0.0294
31	1.2485	1.3257	1.2174	0.0519	12.5	1.3537	1.3924	1.3093	0.0285
30.5	1.2511	1.3259	1.2186	0.0519	12	1.3607	1.3969	1.3147	0.0263
30	1.2540	1.3305	1.2199	0.0528	11.5	1.3662	1.3982	1.3201	0.0264
29.5	1.2569	1.3335	1.2213	0.0532	11	1.3707	1.3988	1.3249	0.0264
29	1.2594	1.3335	1.2222	0.0536	10.5	1.3739	1.4036	1.3290	0.0271
28.5	1.2614	1.3336	1.2235	0.0535	10	1.3807	1.4118	1.3249	0.0304
28	1.2645	1.3375	1.2247	0.0542	9.5	1.3878	1.4351	1.3017	0.0394
27.5	1.2668	1.3377	1.2258	0.0544	9	1.3935	1.4458	1.2994	0.0430
27	1.2704	1.3428	1.2268	0.0551	8.5	1.3955	1.4500	1.2983	0.0505
26.5	1.2724	1.3430	1.2278	0.0548	8	1.4013	1.4500	1.2934	0.0548
26	1.2748	1.3474	1.2284	0.0552	7.5	1.4085	1.4677	1.2587	0.0678
25.5	1.2776	1.3475	1.2293	0.0548	7	1.4253	1.4840	1.1456	0.1021
					6.5	1.4338	1.5132	1.0054	0.1496

The fatigue lives of the terminated tests were calculated using the adjustment factors in Equation 5-5. The results are presented in Table 5.21.

Table 5.21: Predicted fatigue life (terminated tests)

Loading Mode	Beam no	Strain ($\mu\epsilon$)	Temp. ($^{\circ}\text{C}$)	Laboratory fatigue life	fatigue life without adjustment	Adjustment factor			Fatigue life with adjustment		
						Min	Ave	Max	Min	Ave	Max
haversine	29	300	4	240,800	314,000	1.084	1.147	1.237	234,000	264,000	285,000
haversine	30	400	4	57,540	62,100	1.084	1.147	1.237	45,100	51,500	56,000
haversine	33	300	20	705,230	2,370,000	1.084	1.147	1.237	503,000	908,000	1,370,000
haversine	34	400	20	93,800	137,000	1.084	1.147	1.237	42,000	66,100	90,500
haversine	38	400	40	1,000,000	2,240,000	1.084	1.147	1.237	381,000	748,000	1,200,000
sinusoidal	41	300	4	61,660	57,800	1.084	1.147	1.237	43,000	48,600	52,500
sinusoidal	42	400	4	71,890	85,200	1.084	1.147	1.237	46,400	58,900	69,100
sinusoidal	45	300	20	835,317	2,400,000	1.084	1.147	1.237	382,000	768,000	1,250,000
sinusoidal	46	400	20	305,102	771,000	1.084	1.147	1.237	168,000	300,000	450,000
sinusoidal	50	400	40	916,690	4,210,000	1.084	1.147	1.237	529,000	1,160,000	2,020,000

5.5.4 Comparison of fatigue life predictions (scenario 1 and scenario 2)

The fatigue life of those beams where the termination condition was not met was estimated using the aforementioned extrapolation methodology in scenario 1 and scenario 2. The results are presented in Table 5.22 and Table 5.23 for haversine and sinusoidal loading respectively.

Table 5.22: Estimated fatigue life of unterminated tests (haversine loading)

Beam no.	Strain ($\mu\epsilon$)	Temp. ($^{\circ}\text{C}$)	Total cycle count	Cycles to 50% reduction in stiffness			Best fatigue life prediction
				Test result	Predicted life (Scenario 1)	Predicted life (Scenario 2)	
27	100	4	3,362,530	NA	unpredictable	unpredictable	$>10^{12}$
28	200	4	2,000,000	NA	2,495,000	2,300,000	2,300,000
29	300	4	240,800	240,800	NA	264,000	240,800
30	400	4	57,540	57,540	NA	51,500	57,540
31	100	20	2,000,000	NA	2.9×10^{17}	2.01×10^{11}	2.01×10^{11}
32	200	20	2,000,000	NA	5,245,000	58,000,000	58,000,000
33	300	20	705,230	705,230	NA	908,000	705,230
34	400	20	93,800	93,800	NA	66,100	93,800
35	100	40	2,000,000	NA	2.8×10^{11}	809,000,000	809,000,000
36	200	40	1,693,900	NA	2,070,000	6,960,000	6,960,000
37	300	40	2,000,000	NA	2,092,000	4,060,000	4,060,000
38	400	40	1,000,000	1,000,000	NA	748,000	1,000,000

Table 5.23: Estimated fatigue life of unterminated tests (sinusoidal loading)

Beam No	Strain ($\mu\epsilon$)	Temp. ($^{\circ}\text{C}$)	Total Cycle count	Cycles to 50% reduction in stiffness			Best fatigue life prediction
				Test result	Predicted life (Scenario 1)	Predicted life (Scenario 2)	
39	100	4	292,865	NA	unpredictable	unpredictable	$> 10^{13}$
40	200	4	1,421,602	NA	unpredictable	43,700,000	43,700,000
41	300	4	61,660	61,660	NA	48,600	61,660
42	400	4	71,890	71,890	NA	58,900	71,890
43	100	20	1,000,000	NA	7.1×10^{17}	3.82×10^{12}	3.82×10^{12}
44	200	20	2,000,000	NA	569,000,000	91,300,000	91,300,000
45	300	20	835,317	835,317	NA	768,000	835,317
46	400	20	305,102	305,102	NA	300,000	305,102
47	100	40	2,000,000	NA	5.3×10^{10}	278,000,000	278,000,000
48	200	40	1,467,800	NA	286,883,192	12,700,000	12,700,000
49	300	40	1,394,584	NA	11,224,983	3,110,000	3,110,000
50	400	40	916,690	916,690	NA	1,160,000	916,690

As discussed earlier, scenario 1 uses a polynomial function to fit a curve to the data obtained during the quasi-stationary phase (Phase II). Almost all the fitted curves in scenario 2, Phase II, follow a third-degree polynomial trend. Third-degree polynomial curves include an inflection point (IP). An obvious drawback of scenario 1 is that this IP is unknown (see Figure 5-14).

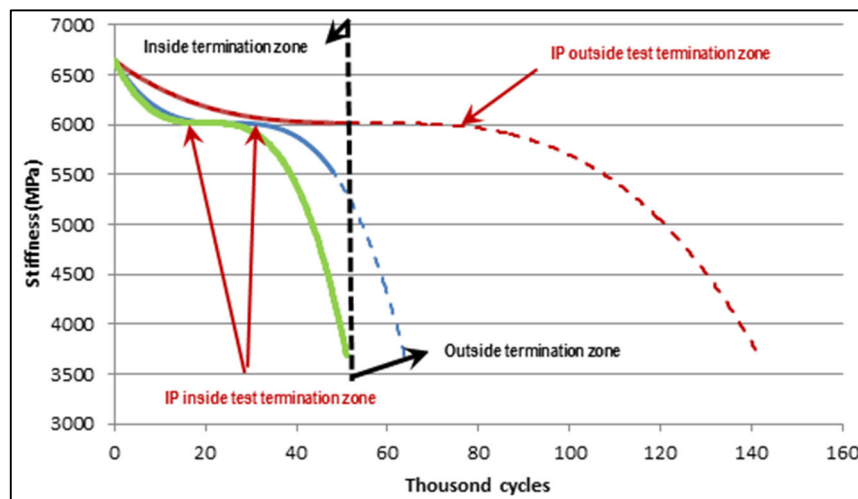


Figure 5-14: Schematic of locations of inflection points for different termination conditions

As can be seen from Figure 5-14, the scenario 1 extrapolation method is very sensitive to the location of the IP. If the loss of stiffness is minor and the IP falls outside the termination zone, then the predicted fatigue life would be much higher than reality. However, if the IP falls inside the termination zone then the estimated fatigue life would be close to or less than reality. In other words, the extrapolations

are not robust enough to enable an accurate predicted of fatigue life. This problem is addressed in scenario 2 by using the adjustment factors.

5.5.4.1 Fatigue Endurance Limit (FEL)

As discussed in the literature review, the Fatigue Endurance Limit (FEL) is defined as the strain level that, if a material experiences less than this strain level, then it will not fail due to fatigue associated from cumulative damage. Using this approach, and at a low level of strain (100 $\mu\epsilon$), there is evidence (see Table 5.24) that the beams will last more than 100 million cycles. The testing conditions under which extrapolation suggests that the beams will survive more than 100 million cycles of load are summarised in Table 5.24.

Table 5.24: Fatigue life of the beams which are recorded as the evidence for FEL

Beam no	Strain ($\mu\epsilon$)	Temperature ($^{\circ}\text{C}$)	Loading mode	Estimated fatigue life
27	100	4	haversine	$>10^{12}$
31	100	20	haversine	2.01×10^{11}
35	100	40	haversine	809,000,000
39	100	4	sinusoidal	$>10^{13}$
43	100	20	sinusoidal	3.82×10^{12}
47	100	40	sinusoidal	278,000,000

5.5.4.2 Austroads versus laboratory fatigue life predictions

As already discussed, Equation 5-2 (Austroads 2012a) is used to calculate the fatigue life of asphalt. These predicted lives are compared with the laboratory-determined lives, for both haversine and sinusoidal loading modes, Table 5.25. The Austroads and laboratory predicted fatigue lives for both the haversine and sinusoidal loading modes are also compared in Figure 5-15 to Figure 5-18. The fatigue life is plotted on these Figures in both logarithmic and real scale for different strain levels.

Table 5.25: Comparison of Austroads and laboratory fatigue life predictions

Beam no.	Loading mode	Strain ($\mu\epsilon$)	Temp. ($^{\circ}\text{C}$)	Binder content by volume (%)	Initial stiffness (MPa)	Austroads fatigue life prediction	Laboratory fatigue life prediction
27	haversine	100	4	11.2	15629	4.182E+06	$>10^{12}$
28	haversine	200	4	11.2	15827	1.279E+05	2.300E+06
29	haversine	300	4	11.2	13778	2.184E+04	2.408E+05
30	haversine	400	4	11.2	14827	4.513E+03	5.754E+04
31	haversine	100	20	11.2	6800	1.811E+07	2.010E+11
32	haversine	200	20	11.2	6740	5.867E+05	5.800E+07
33	haversine	300	20	11.2	6713	7.979E+04	7.052E+05
34	haversine	400	20	11.2	6025	2.275E+04	9.300E+04
35	haversine	100	40	11.2	1291	3.977E+08	8.090E+08
36	haversine	200	40	11.2	1183	1.376E+07	6.960E+06
37	haversine	300	40	11.2	998	2.468E+06	4.060E+06
38	haversine	400	40	11.2	968	6.229E+05	1.000E+06
39	sinusoidal	100	4	11.2	12766	5.706E+06	$>10^{13}$
40	sinusoidal	200	4	11.2	14850	1.411E+05	4.370E+07
41	sinusoidal	300	4	11.2	13740	2.174E+04	6.166E+04
42	sinusoidal	400	4	11.2	15340	4.343E+03	7.189E+04
43	sinusoidal	100	20	11.2	5848	2.449E+07	3.820E+12
44	sinusoidal	200	20	11.2	5716	8.137E+05	9.130E+07
45	sinusoidal	300	20	11.2	6097	9.887E+04	8.353E+05
46	sinusoidal	400	20	11.2	5159	3.264E+04	3.051E+05
47	sinusoidal	100	40	11.2	1233	4.106E+08	2.780E+08
48	sinusoidal	200	40	11.2	1223	1.359E+07	1.270E+07
49	sinusoidal	300	40	11.2	1226	1.908E+06	3.110E+06
50	sinusoidal	400	40	11.2	1119	5.489E+05	9.167E+05

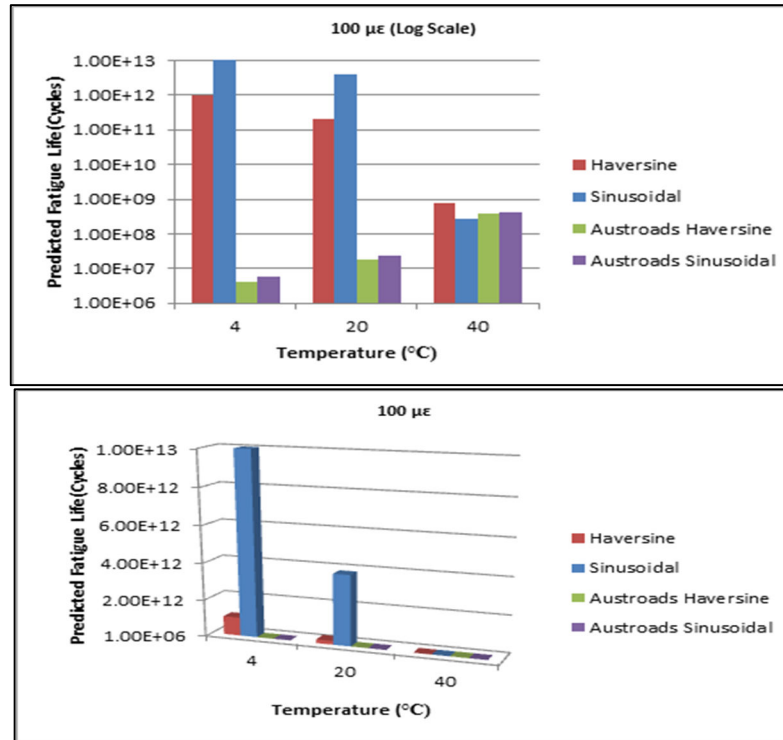


Figure 5-15: Comparison between Austroads and laboratory fatigue life predictions (100 µε)

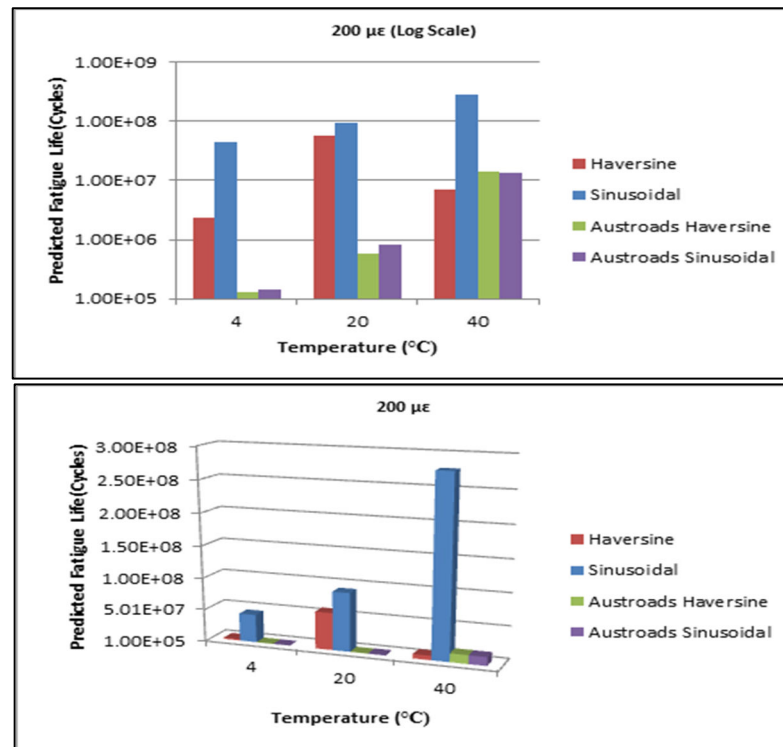


Figure 5-16: Comparison between Austroads and laboratory fatigue life predictions (200 µε)

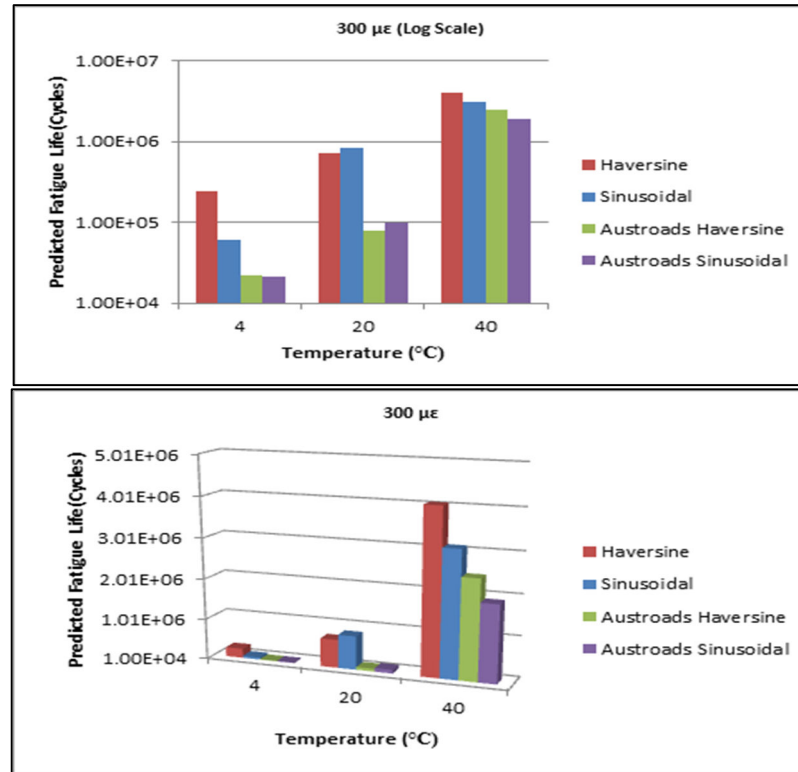


Figure 5-17: Comparison between Austroads and laboratory fatigue life predictions (300 µε)

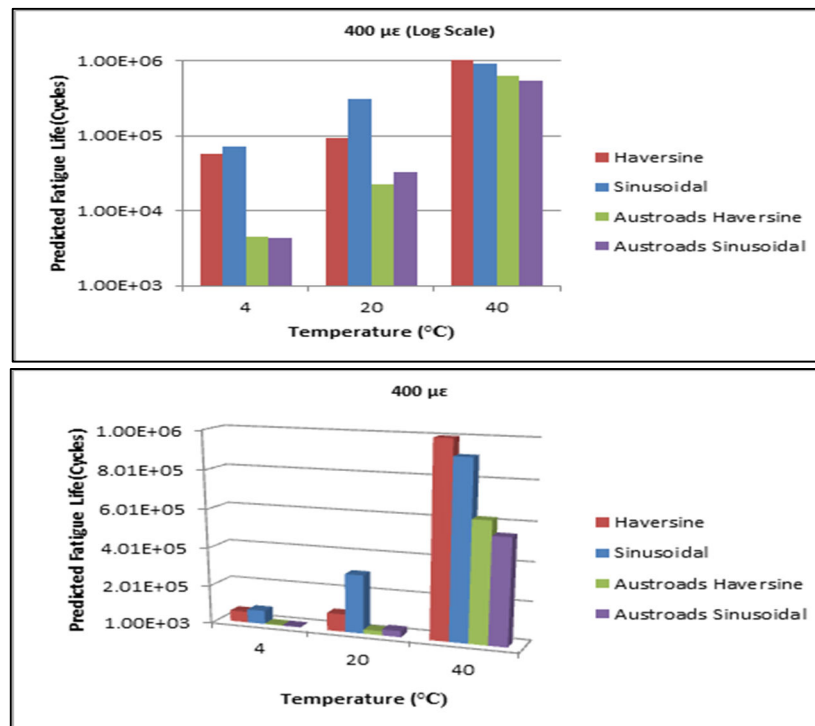


Figure 5-18: Comparison between Austroads and laboratory fatigue life predictions (400 µε)

It is apparent from these Figures that, in most cases the Austroads model underestimates the fatigue life compared to the laboratory-predicted lives. The difference between the Austroads and laboratory-predicted lives ($\log(N_f)$) is shown in Figure 5-19.

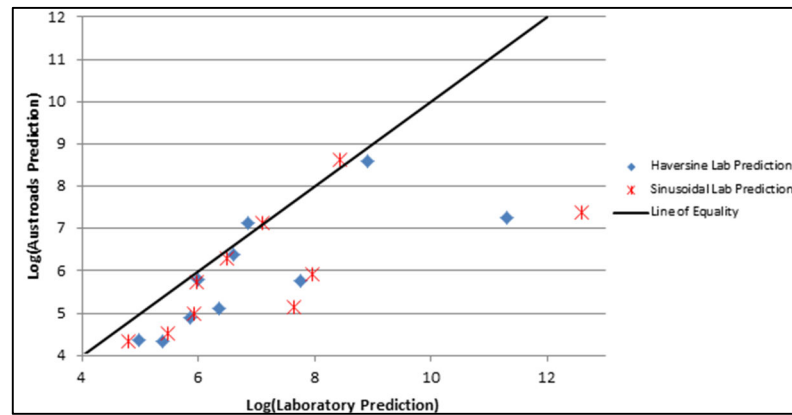


Figure 5-19: Comparison of Austroads and laboratory results in terms of $\log(N_f)$

A comparison of the predicted fatigue lives under haversine and sinusoidal loading is shown in Figure 5-20. It can be seen that sinusoidal loading mode resulted in longer fatigue lives under all testing conditions.

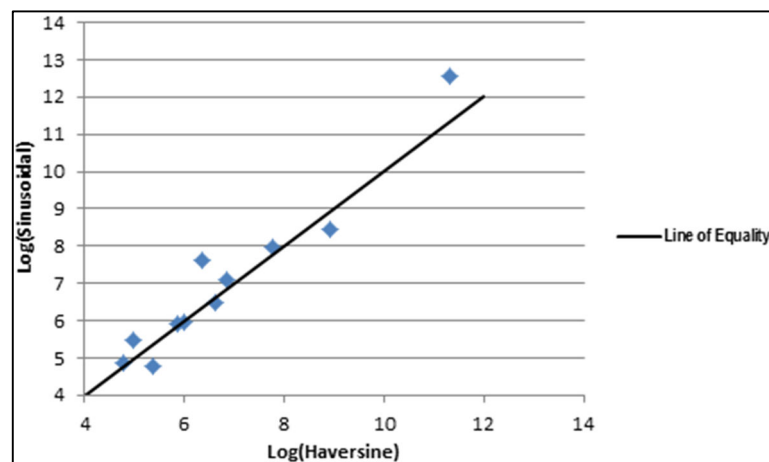


Figure 5-20: Comparison of sinusoidal and haversine results in terms of $\log(N_f)$

5.5.5 Major findings (approach 3)

The major findings as a result of using this approach are:

- after extrapolation there was evidence of the presence of a 'Fatigue Endurance Limit'
- the Austroads fatigue life prediction model generally under-predicted the fatigue life compared to the lives obtained using the 'approach 3' method.

5.6 Approach 4

Almost all previous studies to model the behaviour of asphalt mixes under dynamic loading, using the four-point bending beam apparatus, have focussed on determining the fatigue life of the samples in the laboratory and relating it to field conditions. As the fatigue testing of beams is very time-consuming, no study was identified in the literature review (Chapter 2) that investigated the influence of frequency, temperature and strain level together under repeated loading. As a result, it was decided to conduct four-point bending beam testing at each temperature and frequency previously used but this time with the strain level gradually increased. The testing conditions, which can be termed 'accelerated testing', are summarised in Table 5.26.

Table 5.26: Testing conditions (approach 4)

Beam no.	Frequency (Hz)	Temp. (°C)	Strain range ($\mu\epsilon$)	Strain interval ($\mu\epsilon$)	Loading Shape	Number of cycles in each testing interval
51	0.1	4	100–1000	100	Haversine	110
52	1	4	100–1300	100	Haversine	1000
53	5	4	100–1200	100	Haversine	1000
54	10	4	100–1300	100	Haversine	1000
55	25	4	100–400	100	Haversine	2500
56	0.1	20	100–1400	100	Haversine	110
57	1	20	100–1300	100	Haversine	1000
58	5	20	100–1200	100	Haversine	1000
59	10	20	100–900	100	Haversine	1000
60	25	20	100–1200	100	Haversine	2500
61	0.1	40	100–1200	100	Haversine	110
62	1	40	100–1200	100	Haversine	1000
63	5	40	100–1000	100	Haversine	1000
64	10	40	100–1300	100	Haversine	1000
65	25	40	100–1000	100	Haversine	2500

The main target of this approach is to find a best behaviour curve for aforementioned testing conditions. To determine the shape of the curves the following steps were followed:

1. Set up the temperature and frequency and strain level and run the test.
2. As soon as the test is completed at that strain level increase the strain level by 100 $\mu\epsilon$ and repeat the tests in line with the protocol shown in Table 5.26.

3. Report all the results for each test. For example, the results for beam 51 are shown in Figure 5-21. Generate plots for all beams. This step is named the 'unprocessed step'.
4. A single curve is plotted for each beam by adding the previous strain level's cycle number to the start of next one (Figure 5-22). This step is termed the 'processed step'.
5. The 'line of best fit' to the data is then established (Figure 5-23). This step is termed the 'curve fitting step'.

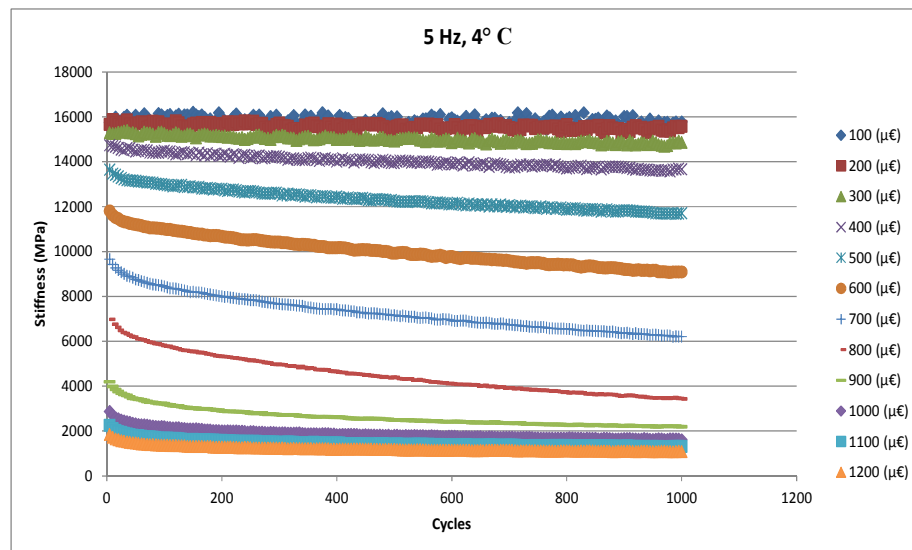


Figure 5-21: Results of four-point bending testing a frequency of 5 Hz and a temperature of 4°C with the strain level gradually increasing (beam 53)

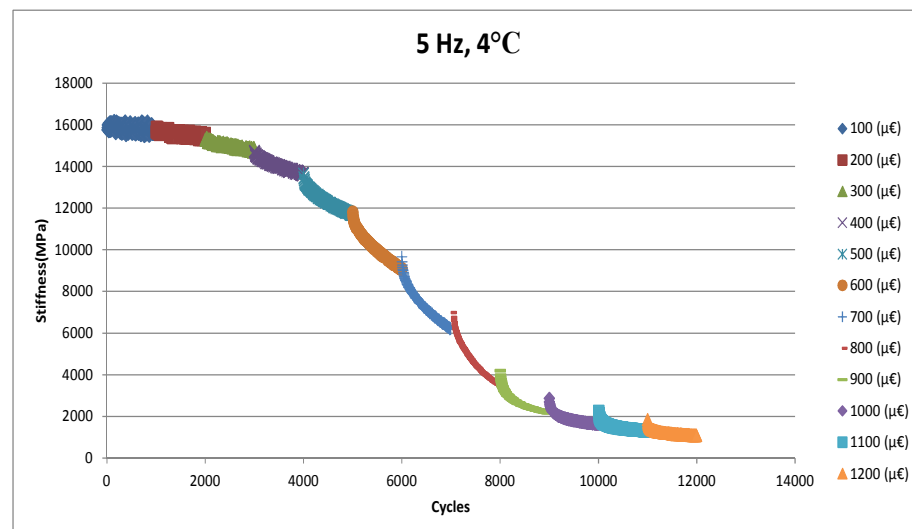


Figure 5-22: Results of four-point bending testing a frequency of 5 Hz and a temperature of 4°C with the strain level gradually increasing (beam 53)

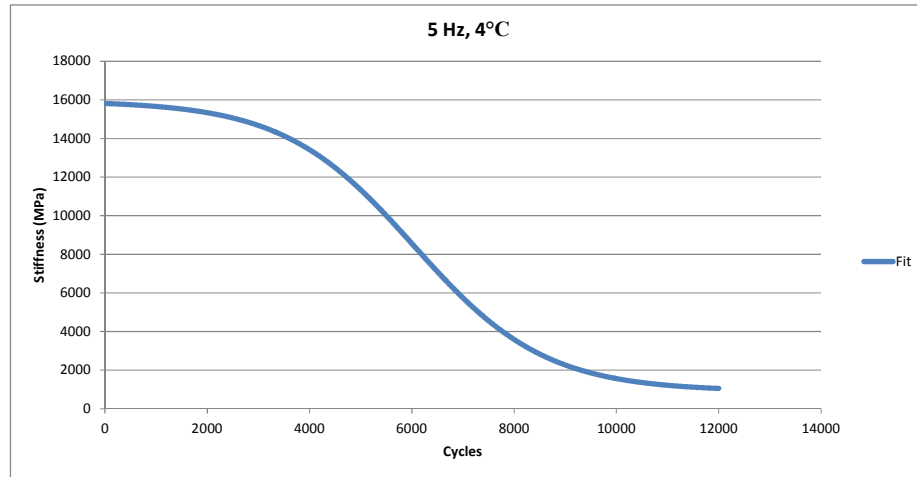


Figure 5-23: Line-of-best-fit to (frequency of 5 Hz and a temperature of 4°C for beam 53)

Microsoft Excel® Solver Tool was used to determine the best fit for each curve to represent the behaviour of the asphalt under repeated haversine loading under different testing conditions. It was found that the sigmoidal and homographic functions provided the closest fit to the data. The sigmoidal function is shown in Equation 5-9 whilst the homographic function is shown in Equation 5-10.

$$E = MAX - \left[\frac{(MAX - MIN)}{\left(1 + \alpha e^{\frac{IP-N}{\beta}} \right)} \right] \quad 5-9$$

$$E = \frac{MAX}{1 + \alpha N^{\beta}} \quad 5-10$$

where

- E = stiffness (MPa)
- MAX = maximum theoretical stiffness (MPa)
- MIN = minimum theoretical stiffness (MPa)
- IP = inflection point of fitted curve
- N = cycle number
- α, β = fitting parameters

The maximum and minimum theoretical stiffness were then calculated using curve fitting. The unprocessed, processed and curve fitting steps are presented in Appendix D, whilst the parameters for each fitted curve are summarised in Table 5.27.

Table 5.27: Parameters of fitted curves for different testing conditions (approach 4)

Beam no.	Testing condition		Fitted curve function	Fitted curve parameters					
	F ¹	T ²		MAX	MIN	IP	α	β	R ²
51	0.1	4	sigmoidal	10670.76	1167.626	2494.377	0.007738	351.2332	0.9995
52	1	4	sigmoidal	13749.51	357.2856	6465.978	1.10257	2173.2	0.9997
53	5	4	sigmoidal	15946.9	1157.125	6044.617	0.983616	1278.203	0.9995
54	10	4	sigmoidal	1278.203	362.5874	08493.618	0.358378	1405.574	0.9997
55	25	4	Nil	Nil	Nil	Nil	Nil	Nil	Nil
56	0.1	20	sigmoidal	23272.45	614.76	-1134.46	0.456761	583.7609	0.9939
			homographic	2063.532	-	-	0.001929	0.944535	0.9942
57	1	20	sigmoidal	25820.66	767.3429	-7343.99	0.553647	6293.939	0.9960
			homographic	4385.768	-	-	1.82E-5	1.241486	0.9959
58	5	20	sigmoidal	30894.75	-3734.77	-11006.4	0.957541	14602.09	0.9992
			homographic	6685.928	-	-	1.08E-7	1.787688	0.9967
59	10	20	sigmoidal	8883.501	-202.724	7628.745	0.690642	4490.217	0.9988
			homographic	6685.928	-	-	1.08E-7	1.787688	0.9976
60	25	20	sigmoidal	9195.598	-199.246	16486.01	0.782494	5508.42	0.9961
			homographic	NA	NA	NA	NA	NA	NA
61	0.1	40	homographic	360.074	-	-	0.14945	0.734744	0.9637
62	1	40	homographic	638.3448	-	-	0.001721	0.74129	0.9880
63	5	40	homographic	939.4524	-	-	0.000986	0.76916	0.9943
64	10	40	homographic	1399.687	-	-	0.000115	0.996548	0.9958
65	25	40	sigmoidal	1911.194	-100.598	19332.46	0.858879	17931.73	0.9774
			homographic	1498.637	-	-	0.000206	0.828356	0.9844

¹ Frequency (Hz)

² Temperature (° C)

5.6.1 Major findings

The major findings can be categorised in two parts: (1) the presence of healing and (2) the behaviour of the asphalt beams under different temperature and frequency conditions.

5.6.1.1 Presence of healing

As apparent from Figure 5-24, Figure 5-25 and Figure 5-26, on some occasions during testing (as indicated in the Figures) beams were able to recover their stiffness because of the viscoelastic nature of asphalt. This phenomenon was more apparent at higher frequencies (5, 10 and 25 Hz).

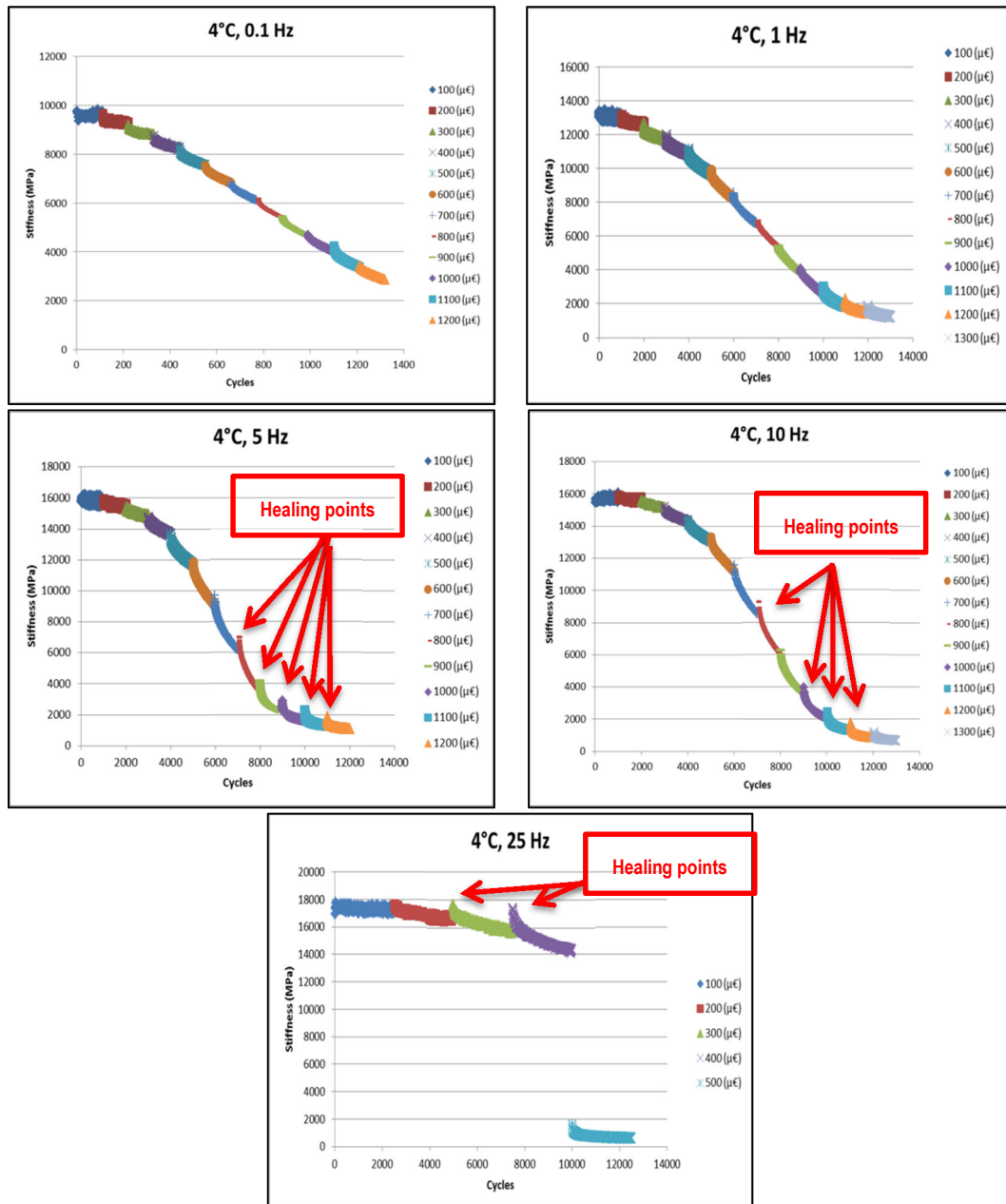


Figure 5-24: Observed healing phenomenon at different frequencies and a temperature of 4°C

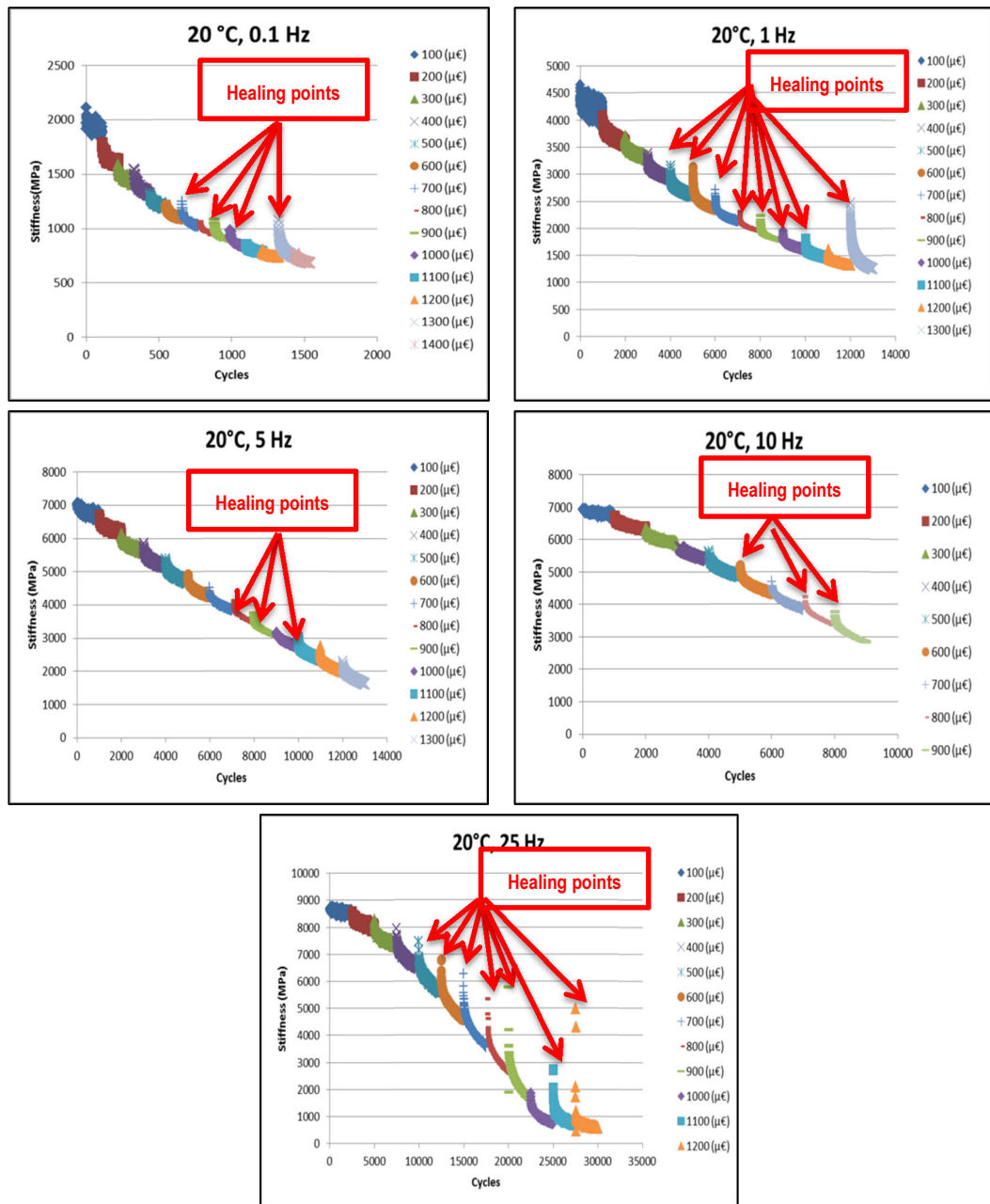


Figure 5-25: Observed healing phenomenon at different frequencies and a temperature of 20°C

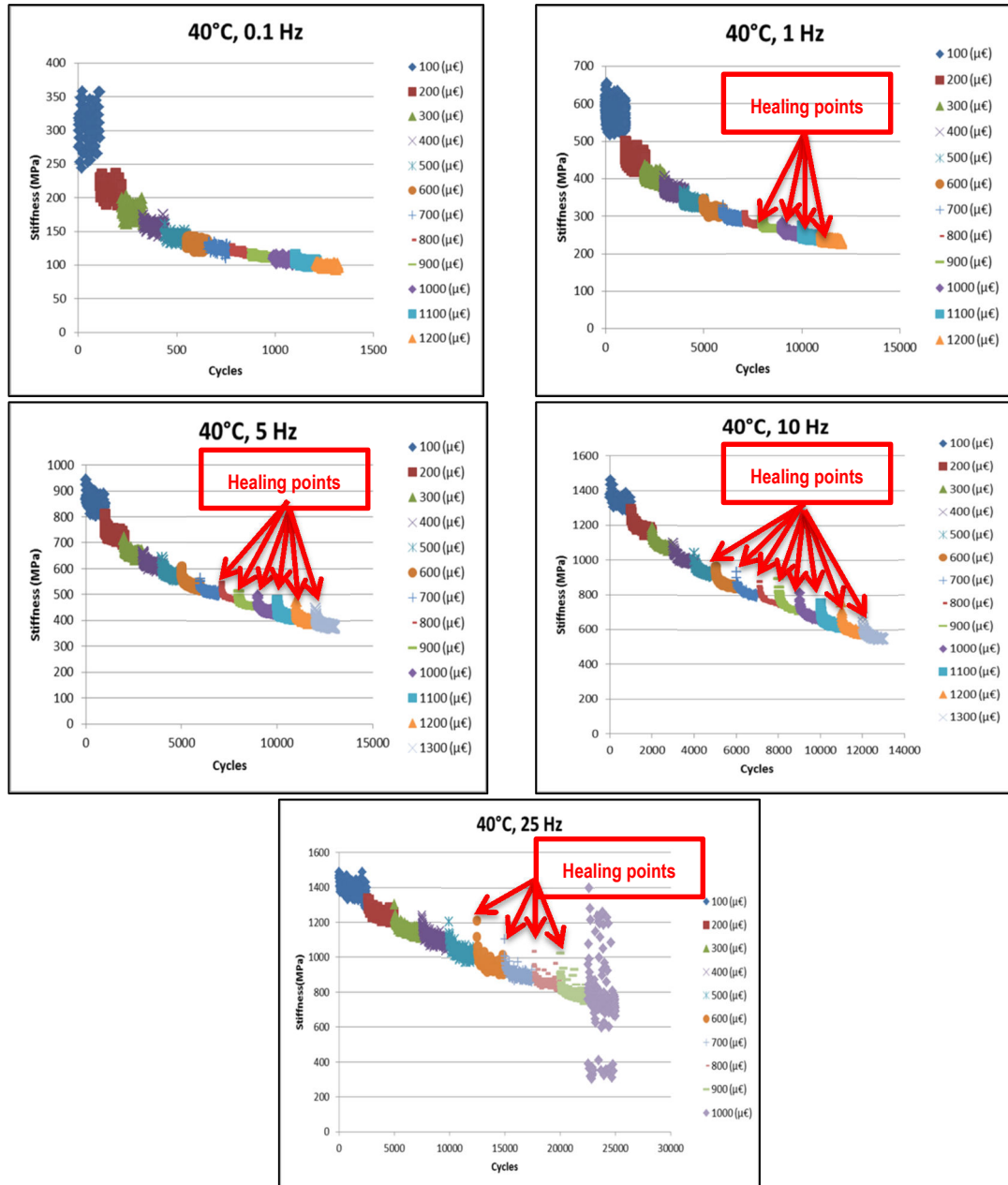


Figure 5-26: Observed healing phenomenon at different frequencies and a temperature of 40°C

5.6.1.2 Behaviour of asphaltic beams at different temperatures and frequencies

As stated previously sigmoidal and homographic functions were used to model the behaviour of the beams in the accelerated testing method proposed in Approach 4. The results showed that, when the temperature was low (e.g. 4°C) the behaviour of the material was non-linear elastic and the sigmoidal function better modelled this non-linear elastic behaviour (see Figure 5-27).

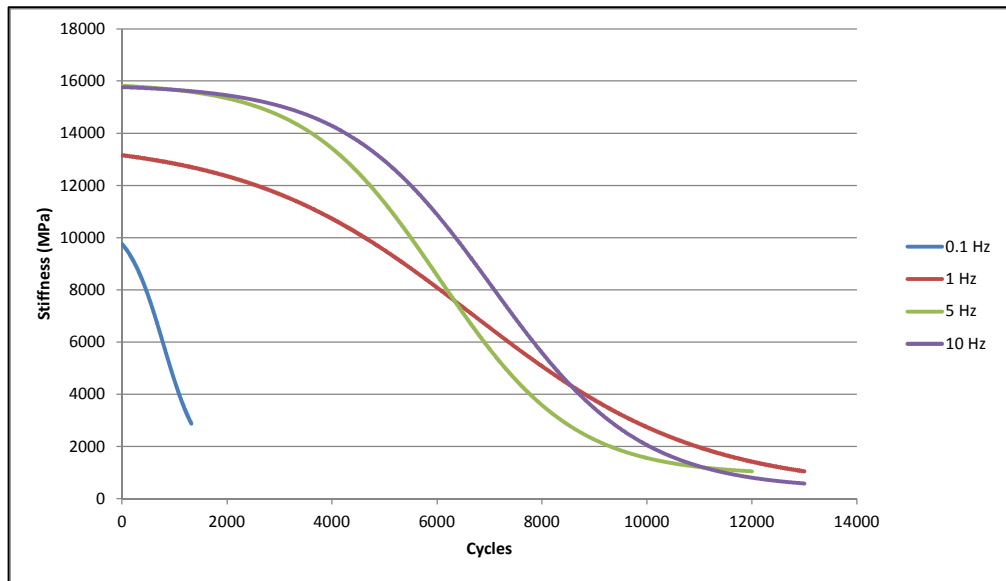


Figure 5-27: Sigmoidal-fitted curves at different frequencies and a temperature of 4°C

The most complex situation was observed when the temperature was set on 20°C. As is apparent from Figure 5-28, when the frequency was low (0.1 Hz and 1 Hz) the homographic function provided a better fit to the data; however, at the higher frequencies (5 Hz, 10 Hz and 25 Hz) the sigmoidal function provided a better fit. This is because when the frequency is low, the material behaviour is viscoelastic whereas, at the higher frequencies, the behaviour is non-linear elastic.

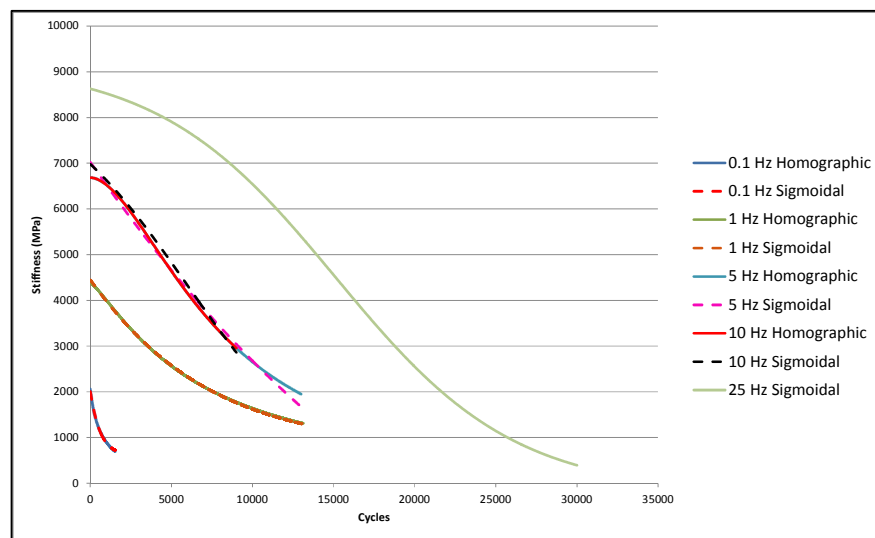


Figure 5-28: Sigmoidal and homographic functions fitted to data collected at 20°C at different frequencies

At the temperature level of 40°C, the homographic function was generally the most suitable for modelling the behaviour. However, at the highest frequency level of 25 Hz, both the sigmoidal and homographic functions could be used to model the

behaviour with very little difference in the goodness of fit (R^2) values (see Figure 5-29).

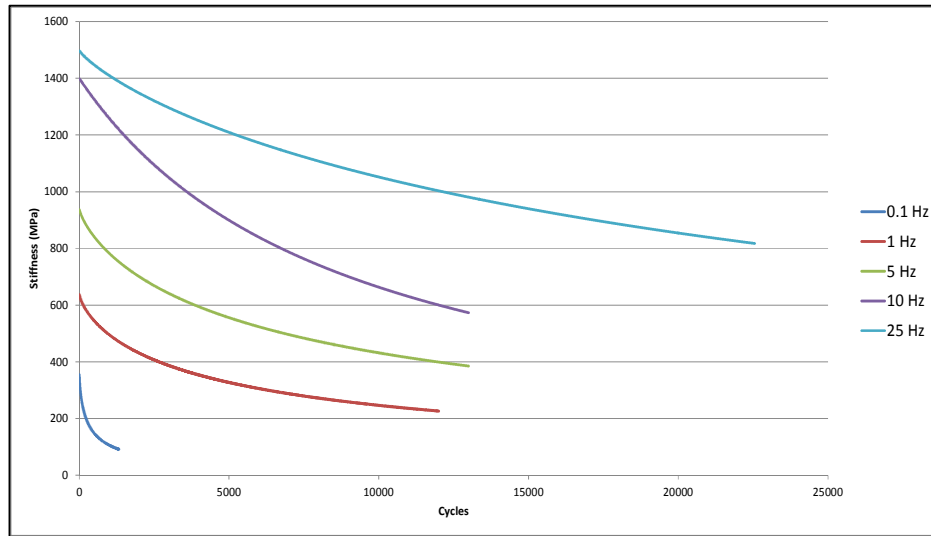


Figure 5-29: Homographic fitted curves in different frequencies at 40°C

5.6.2 Summary

It can be concluded from Approach 4, that increasing the temperature from 4°C to 40°C resulted in the line-of-best-fit changing from a sigmoidal function to a homographic function as the test frequency increased from 0.1 Hz to 25 Hz. Generally, however, the behaviour of the material was more in line with the sigmoidal function than the homographic function in lower temperatures and highest frequency.

5.7 Approach 5

Micro-cracks generated in asphalt can be ‘healed’ during the rest periods because asphalt is a viscoelastic material. As discussed in the literature review in Chapter 2, a large number of studies have been conducted examining the healing properties of asphalt during four-point bending beam testing. This is one of the reasons that a ‘rest period’ is applied during testing – the other reason being that, by applying a rest period, the wave pulse is more indicative of actual loading conditions in the field.

After observing the presence of healing during the Approach 4 testing, it was decided to conduct another series of tests (approach 5) where different rest periods and load shapes were introduced, at the same time keeping the temperature, frequency and strain level constant. The testing conditions adopted for this part of the program are presented in Table 5.28.

Table 5.28: Testing conditions used in approach 5

Beam no.	Number of beams	Strain ($\mu\epsilon$)	Frequency (Hz)	Temperature ($^{\circ}\text{C}$)	Load shape	Rest period (sec)
66–69	4	400	10	20	haversine	0.1
70–72	3	400	10	20	haversine	0.3
73–79	7	400	10	20	haversine	0.9
80–83	4	400	10	20	sinusoidal	0.1
84–87	4	400	10	20	sinusoidal	0.3
88–91	4	400	10	20	sinusoidal	0.9

The results of this testing are presented in Figure 5-30 to Figure 5-35.

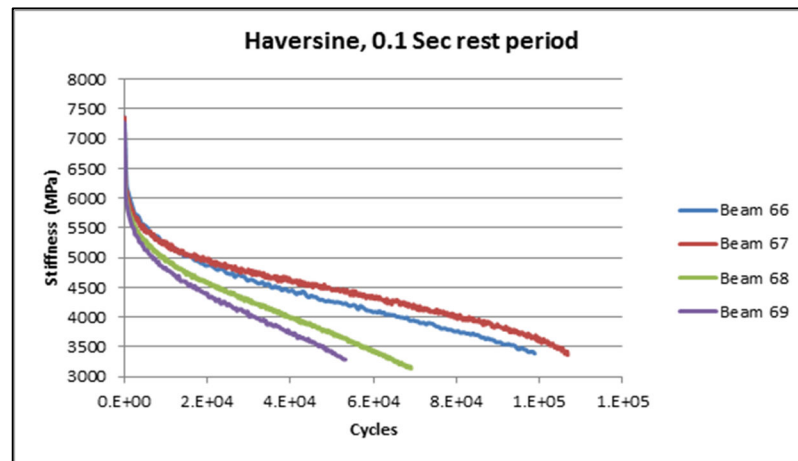


Figure 5-30: Fatigue curves (haversine loading and 0.1 second rest period)

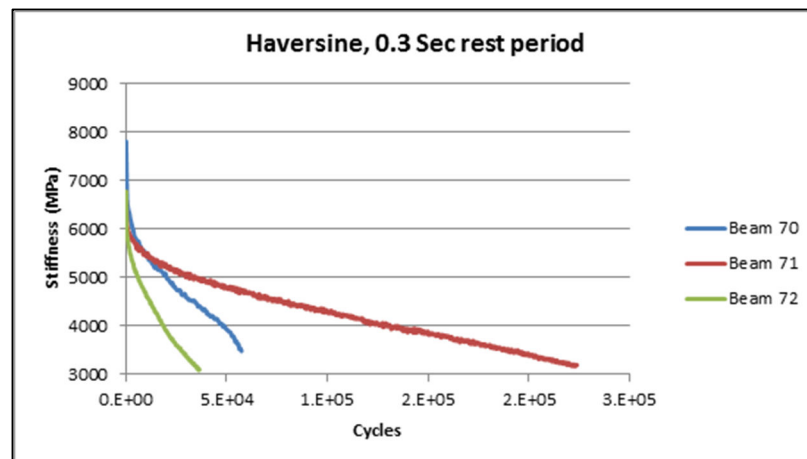


Figure 5-31: Fatigue curves (haversine loading and 0.3 seconds rest period)

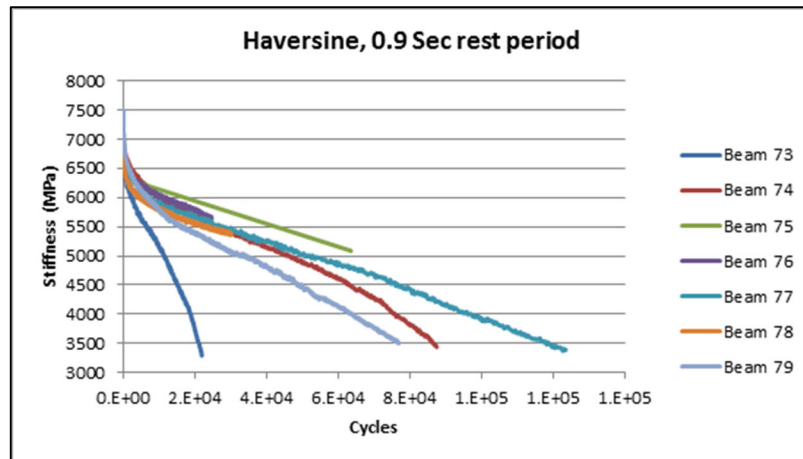


Figure 5-32: Fatigue curves (haversine loading and 0.9 second rest period)

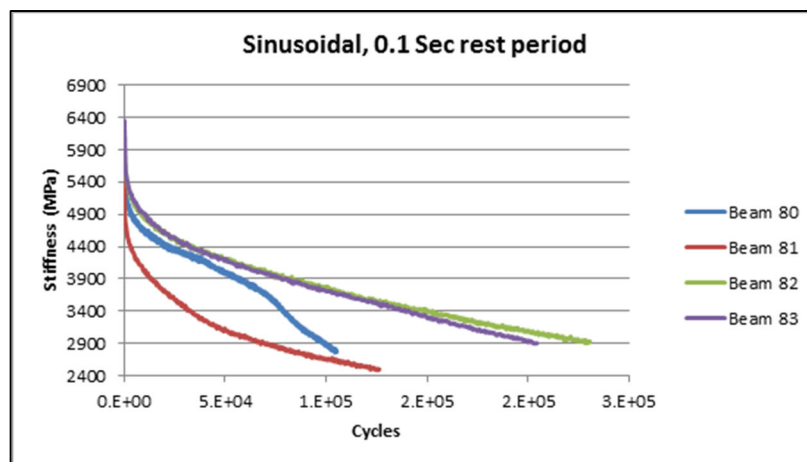


Figure 5-33: Fatigue curves (sinusoidal loading and 0.1 second rest period)

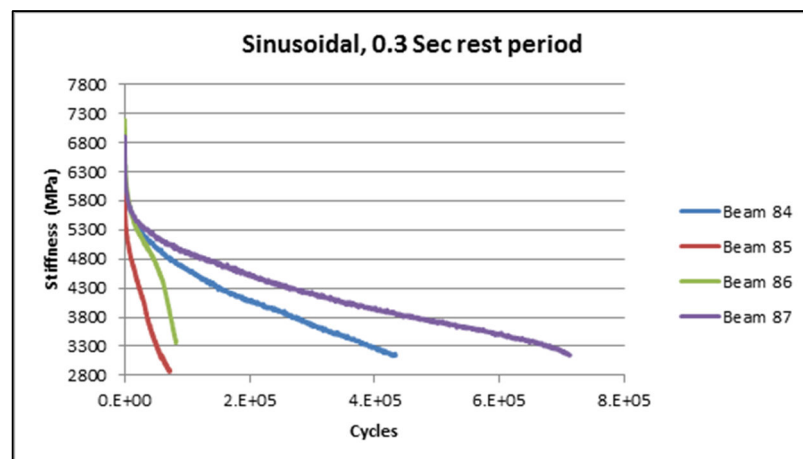


Figure 5-34: Fatigue curves (sinusoidal loading and 0.3 second rest period)

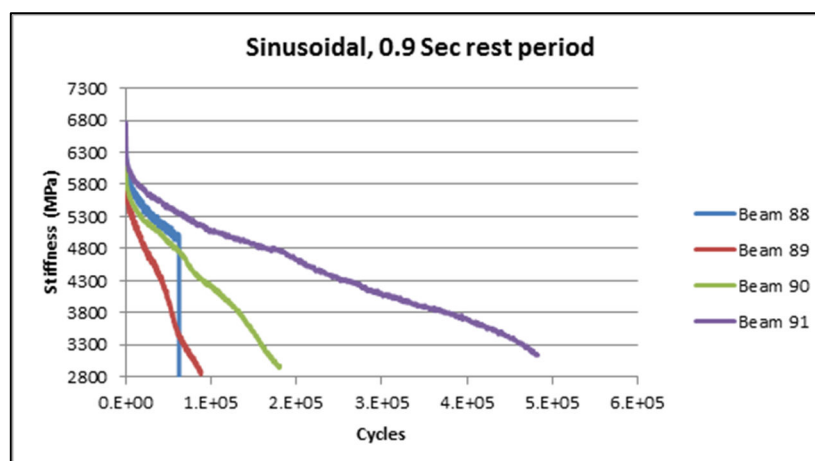


Figure 5-35: Fatigue curves (sinusoidal loading and 0.1 second rest period)

It is apparent from Figure 5-32 and Figure 5-35 that the fatigue testing on beam 75, 76, 78 and 88 were not terminated. As a result, the data needed to be extrapolated before the fatigue life could be determined using the extrapolation technique adopted for scenario 2 in approach 3. The extrapolated fatigue lives for these beams are presented in Table 5.29 whilst the curves fitted to this data are shown in Figure 5-36.

Table 5.29: Extrapolated fatigue lives of unterminated tests (approach 5)

Beam no.	Load shape	Rest period (sec)	Initial stiffness (MPa)	% reduction in stiffness	Adjusted stiffness (MPa)	Extrapolated fatigue life
75	haversine	0.9	6768	7.14	5120.7	1,207,509
76	haversine	0.9	6608.5	12.26	4480.6	242,000
78	haversine	0.9	6611.7	18.93	4333.9	475,379
88	sinusoidal	0.9	6409	22.47	4146.6	460,000

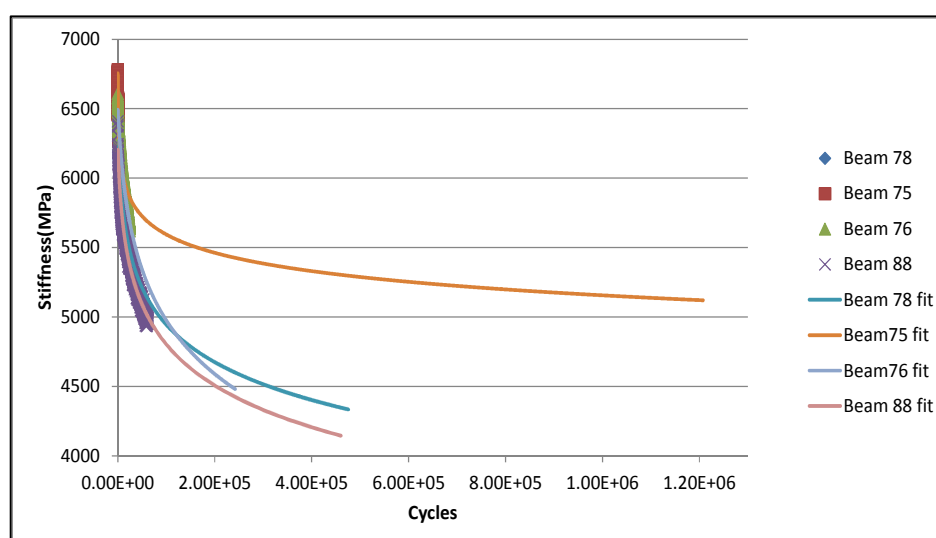


Figure 5-36: Fitted fatigue curves (unterminated tests, approach 5)

Following this extrapolation all the fatigue life were determined and the results are shown in Table 5.30. It can be seen from the Table that the fatigue life results were not consistent and there was a great deal of scatter in the data. The test results obtained using this approach were compared with the results obtained using the other approaches (i.e. without rest periods) and the results are also shown in the (right-hand column in Table 5.30. It should be noted that beams 72 and 73 failed during testing; the reasons for this could not be identified.

Table 5.30: Estimated laboratory fatigue lives (approach 5)

Beam no.	Load shape	Rest period (sec)	Testing status	Fatigue life	Maximum fatigue life (with rest period)	Maximum fatigue life in all approaches (without rest period)
66	haversine	0.1	terminated	98,817	106,753	131,570 (beam 5, approach 1)
67	haversine	0.1	terminated	106,753		
68	haversine	0.1	terminated	69,057		
69	haversine	0.1	terminated	53,249		
70	haversine	0.3	terminated	57,300	223,760	131,570 (beam 5, approach 1)
71	haversine	0.3	terminated	223,760		
72	haversine	0.3	failed	36,400		
73	haversine	0.9	failed	21,891	1,207,509	131,570 (beam 5, approach 1)
74	haversine	0.9	terminated	87,428		
75	haversine	0.9	unterminated	1,207,509		
76	haversine	0.9	unterminated	242,000		
77	haversine	0.9	terminated	123,397		
78	haversine	0.9	unterminated	475,000		
79	haversine	0.9	terminated	76,806		
80	sinusoidal	0.1	terminated	105,153	230,401	321,900 (beam 18, approach 2)
81	sinusoidal	0.1	terminated	126,209		
82	sinusoidal	0.1	terminated	230,401		
83	sinusoidal	0.1	terminated	204,289		
84	sinusoidal	0.3	terminated	433,721	712,736	321,900 (beam 18, approach 2)
85	sinusoidal	0.3	terminated	72,449		
86	sinusoidal	0.3	terminated	82,433		
87	sinusoidal	0.3	terminated	712,736		
88	sinusoidal	0.9	unterminated	460,000	482,819	321,900 (beam 18, approach 2)
89	sinusoidal	0.9	terminated	88,202		
90	sinusoidal	0.9	terminated	180,488		
91	sinusoidal	0.9	terminated	482,819		

The maximum fatigue lives obtained with the different loading modes are presented in Figure 5-37.

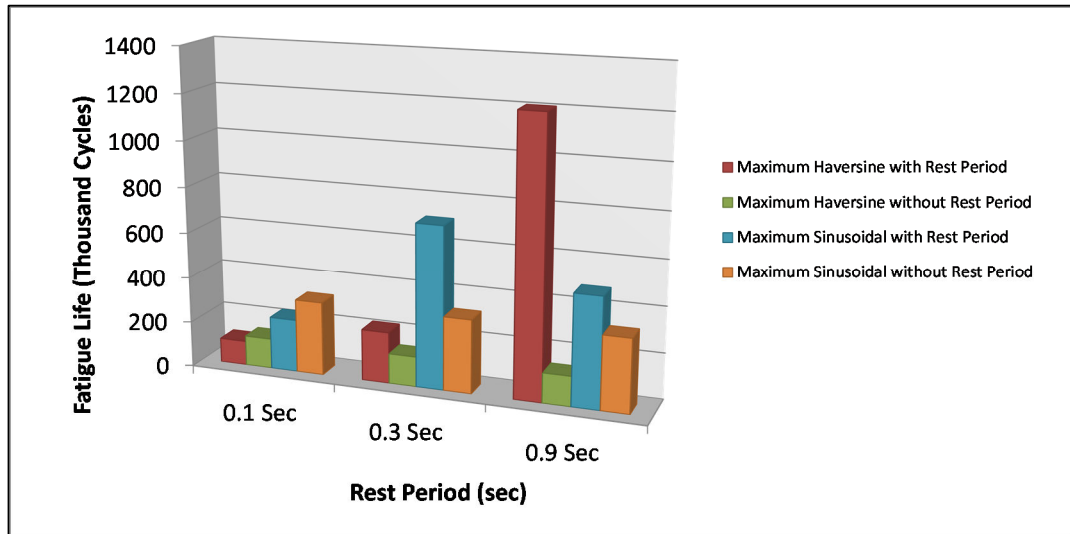


Figure 5-37: Maximum fatigue lives when testing was conducted with and without rest periods

5.7.1 Major findings

It can be concluded from the data presented in Table 5.30 and Figure 5-37 that the application of a rest period of 0.1 seconds with both the haversine and sinusoidal load functions did not have a significant effect on the laboratory fatigue life. However, the use of rest periods of 0.3 and 0.9 seconds resulted in an increase in the fatigue life of many of the beams and, in some cases, a dramatic increase.

However, based on the test results obtained using this approach, no clear relationship between the duration of the rest period and fatigue life could be established, although there was some indication that an increase in the rest period could be associated with an increase in laboratory fatigue life. Further work is required to investigate the effect of rest period duration on fatigue life.

5.8 Approach 6

It is generally accepted that the behaviour of an asphalt mix under repeated sinusoidal loading can be modelled using the theory of viscoelasticity. For this reason, the complex modulus (E^*) is used to relate the stress and strain of linear viscoelastic materials. The stress and strain relationship is shown in Equation 5-11:

$$E^* = \frac{\sigma}{\varepsilon} = \frac{\sigma_0 \sin \omega t}{\varepsilon_0 \sin(\omega t - \varphi)} = \frac{\sigma_0 e^{i\omega t}}{\varepsilon_0 e^{i(\omega t - \varphi)}}$$

where

- E^* = complex modulus
- σ_0 = peak (maximum) stress
- ε_0 = peak (maximum) strain
- φ = phase angle (degrees)
- ω = angular velocity
- t = time (seconds)

Normally, the absolute value of complex modulus (or 'dynamic modulus') is used for design purposes. As linear viscoelastic materials are very sensitive to temperature and loading, the dynamic modulus will vary according to temperature and frequency of loading. An example of this variation on a typical cylindrical sample is shown in Figure 5-38.

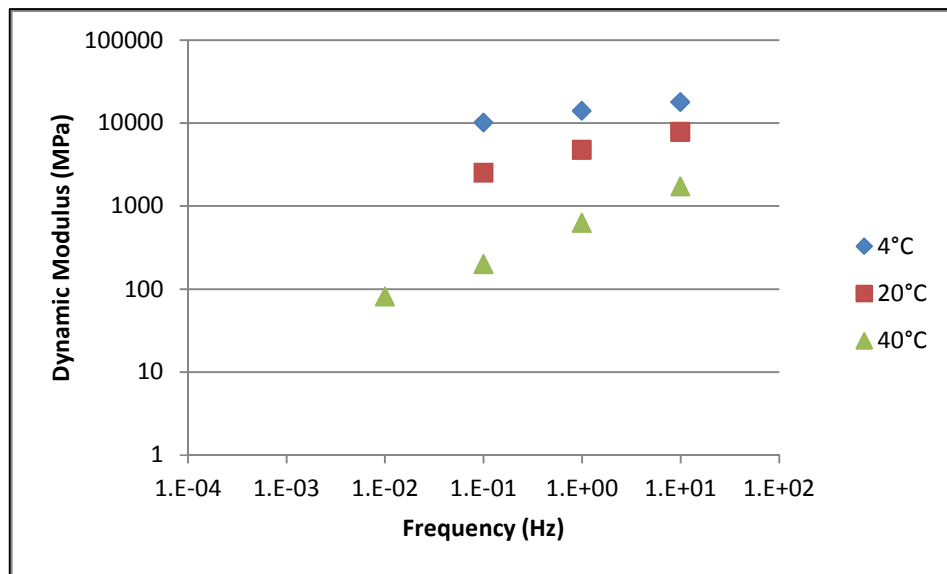


Figure 5-38: Relationship between dynamic modulus and frequency for a range of temperatures

Using time-temperature superposition concept, it is possible to generate a single sigmoidal curve at different temperatures and frequencies. This single sigmoidal curve is called the 'master curve'. An example of a typical master curve, where the time-temperature superposition theory was used to shift the results obtained at temperatures of 4°C and 40°C to a reference temperature of 20°C, is shown in Figure 5-39.

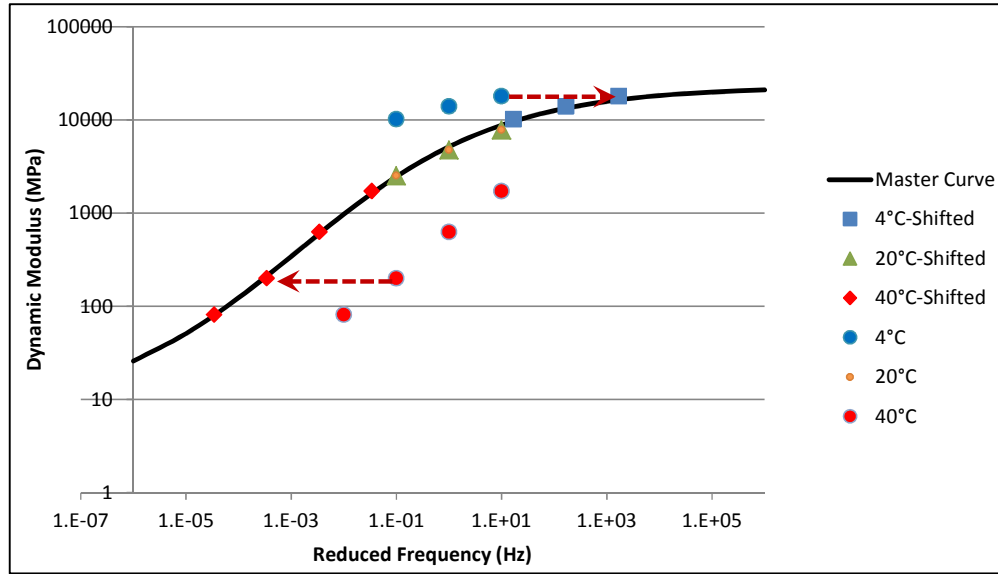


Figure 5-39: Typical master curve developed by time-temperature superposition theory

A commonly used expression of a 'master curve' relating dynamic modulus to reduced frequency (NCHRP 2008b) is shown in Equation (5-12):

$$\log|E^*| = \delta + \frac{\alpha}{1 + e^{\beta + \gamma(\log \omega_r)}} \quad 5-12$$

where

- $|E^*|$ = dynamic modulus
- ω_r = reduced frequency (Hz)
- δ = minimum value of the logarithm of dynamic modulus
- $\delta + \alpha$ = maximum value of the logarithm of dynamic modulus
- β, γ = sigmoidal curve shape parameters

The reduced frequency is determined by multiplying the test frequency by a time-temperature shift factor. The relationship between reduced frequency, shift factor and frequency is given in Equation (5-13)

$$\omega_r = a(T) \times \omega \quad 5-13$$

where

- ω_r = reduced frequency (Hz)
- $a(T)$ = temperature-frequency shift factor (see Equation 5-15)
- ω = Frequency (Hz)

Equation 5-14 shows the logarithmic shape of Equation 5-13:

$$\log \omega_r = \log \omega + \log a(T) \quad 5-14$$

As explained earlier, the time-temperature superposition theory is used to fit a master curve to the test results. This is done using a time-temperature shift factor (a_T). Several equations have been developed to calculate the time-temperature shift factor, including (Kwan 1998):

- Williams, Landel and Ferry (WFL) equation

$$\log a_T = -\frac{c_1(T - T_r)}{c_2 + (T - T_r)} \quad 5-15$$

where

- a_T = shift factor
- T = measured temperature (°K)
- T_r = reference temperature (°K)
- c_1 & c_2 = constants

- Kaelble (modified WFL) equation

$$\log a_T = -\frac{c_1(T - T_r)}{c_2 + |T - T_r|} \quad 5-16$$

- Arrhenius equation

$$\begin{aligned} \log a_T &= c \times \left(\frac{1}{T} - \frac{1}{T_r} \right) = \frac{0.4347 \Delta E_a}{R} \times \left(\frac{1}{T} - \frac{1}{T_r} \right) \\ &= \frac{\Delta E_a}{19.14714} \times \left(\frac{1}{T} - \frac{1}{T_r} \right) \end{aligned} \quad 5-17$$

where

- c = constant
- ΔE_a = activation energy
- R = ideal gas constant

According to NCHRP (2008b) there are two ways of determining the time-temperature shift factor: (1) when the properties of the binder (e.g. viscosity and dynamic shear modulus) are available, and (2) when the properties of the binder are not available.

5.8.1 Shift factor when binder properties are available

Mirza and Witczak (1995) generated a model based on WFL equation which relates the time-temperature shift factor to binder viscosity (the Global Aging Model):

$$\log a_T = c(\log \eta - \log \eta_{70 \text{ RTFOT}}) \quad 5-18$$

where

- c = constant
- η = viscosity for different ranges of temperature and age

$\eta_{70 \text{ RTFOT}}$ = viscosity at the reference temperature of 70°F (21°C)
based on AASHTO T240 (AASHTO 2013)

Based on this model a new shift factor was generated (Equation 5-19):

$$\log a_T = c[10^{A+VTS \log T_R} - \log \eta_{70 \text{ RTFOT}}] \quad 5-19$$

where

T_R = temperature (Rankine)⁴
A, VTS = viscosity-temperature parameters (AASHTO T240)

It was proposed in NCHRP (2008b) that master curves be generated using the model shown in Equation 5-20 when the binder and volumetric properties were available:

$$\log |E^*| = \delta + \frac{Max - \delta}{1 + e^{\beta + \gamma \{ \log \omega + c [10^{A+VTS \log T_R - \log \eta_{70 \text{ RTFOT}}}]\}} \quad 5-20$$

where

Max = specified limiting logarithm of maximum modulus
 δ = specified limiting logarithm of minimum modulus
 α, β, γ = fitting parameters
and c

To calculate the limiting maximum and minimum modulus, NCHRP (2008b) proposed that the Hirsch model be used (Equation 5-21 and Equation 5-22):

$$|E^*|_{mix} = P_c \left[4.2 \times 10^6 \left(1 - \frac{VMA}{100} \right) + 3|G^*|_{binder} \left(\frac{VFA \times VMA}{10^4} \right) \right] + \frac{\left[\frac{(1 - \frac{VMA}{100})}{4.2 \times 10^6} + \frac{VMA}{3VFA|G^*|_{binder}} \right]}{1 - P_c} \quad 5-21$$

where

$$P_c = \frac{(20 + \frac{3VFA|G^*|_{binder}}{VMA})^{0.58}}{650 + (\frac{3VFA|G^*|_{binder}}{VMA})^{0.58}} \quad 5-22$$

$|E^*|_{mix}$ = dynamic modulus of mix (psi⁵)
VMA = voids in mineral aggregates (%)
VFA = voids filled with asphalt (%)
 $|G^*|_{binder}$ = dynamic shear modulus of binder (psi)

⁴ The Rankine (R) degree is defined as equal to 1°F, rather than 1°C used by the Kelvin scale. A temperature of -459.67°F is exactly equal to 0°R ($T(^{\circ}R) = T(^{\circ}F) + 459.67$).

⁵ 1 psi = 6.89 kPa.

5.8.2 Shift factor when binder properties are unavailable

When the binder properties of the mix are not available there is an alternative method for developing the master curve: the use of the Arrhenius shift factor presented in Equation 5-23. Substituting the Arrhenius equation into the sigmoidal master curve equation (Equation 5-12) the master curve formula can be rewritten as follows:

$$\log|E^*| = \delta + \frac{Max - \delta}{1 + e^{\beta + \gamma \left[\log \omega + \frac{\Delta E_a}{19.14714} \times \left(\frac{1}{T} - \frac{1}{T_r} \right) \right]}} \quad 5-23$$

where

δ, β, γ and ΔE_a = fitting parameters

It has been proposed (NCHRP 2008b) that, for mixes with a VFA value between 55% and 85% and a VMA value between 10% and 20%, the maximum limiting modulus be determined using Equation 5-24 and Equation 5-25:

$$Max = P_c \left[4.2 \times 10^6 \left(1 - \frac{VMA}{100} \right) + 4.35 \times 10^5 \left(\frac{VFA \times VMA}{10^4} \right) \right] \quad 5-24$$

$$+ \frac{\left[\frac{(1 - \frac{VMA}{100})}{4.2 \times 10^6} + \frac{VMA}{4.35 \times 10^5} \right]}{1 - P_c}$$

where

$$P_c = \frac{(20 + \frac{4.35 \times 10^5 VFA}{VMA})^{0.58}}{650 + (\frac{4.35 \times 10^5 VFA}{VMA})^{0.58}} \quad 5-25$$

5.8.3 Development of compressive and bending master curves for WA mix

Due to the absence of the equipment required to run the dynamic shear test at the Curtin University Geomechanical laboratory, it was decided to generate the master curves for the AC14/75 mix based on the Arrhenius time-temperature shift factor.

In order to develop a single master curve for a cylindrical sample, testing should be conducted at temperatures of 4°C, 20°C and 40°C. The AMPT was used to conduct the dynamic modulus testing on the prepared specimens. A total of eight samples were tested without applying confining pressure. In order to study the effect of confining pressure on the shape of the master curve, testing was conducted at two levels of confining pressure (65 and 135 kPa). The volumetric properties of the test cylinders are presented in Table 5.31. All UTS6 outputs for different frequencies and temperatures are presented in Appendix E.

Table 5.31: Volumetric properties of cylinders

Cylinder number	Confining pressure (kPa)	Air voids (%)	%VFA	%VMA
1	0	5.5	69.1	16.2
2	0	5.4	67.3	16.6
3	0	5.6	66.5	16.8
4	0	4.8	69.8	16.0
5	0	3.9	74.1	15.1
6	0	5.2	68.1	16.4
7	0	5.3	67.8	16.5
8	0	4.6	70.7	15.8
9	65	4.5	71.4	15.6
10	65	4.9	69.7	16.0
11	65	5.0	69.2	16.2
12	135	4.6	71.5	15.6
13	135	4.5	70.8	15.8
14	135	4.7	70.6	15.8

Work was also conducted aimed at developing flexural master curves for the asphalt mix using the EN Standard tester. Beams are tested by applying two loading modes: haversine and sinusoidal. The testing conditions for haversine loading are shown in Table 5.32. The UTS15 software was used to control the tests. Each beam was tested at a single frequency and temperature because the UTS15 does not cater for frequency sweep on a single beam.

Table 5.32: Testing conditions (haversine loading mode)

Beam no.	Temp (°C)	Strain Level ($\mu\epsilon$) (Peak-to-Peak)	Frequency (Hz)	Air voids (%)	%VFA	%VMA
92	4	50	0.1	5.0	69.2	16.1
93	4	50	1	5.2	68.2	16.4
94	4	50	10	5.8	65.5	17.0
95	20	50	0.1	5.4	67.3	16.6
96	20	50	1	5.3	67.6	16.5
97	20	50	10	5.7	66.3	16.8
98	40	50	0.01	Nil	Nil	Nil
99	40	50	0.1	5.5	67.5	16.5
100	40	50	1	5.8	66.0	16.9
101	40	50	10	5.7	66.1	16.9

The UTS18 software was used to generate bending master curve for the sinusoidal loading mode. One of the advantages of this software is that it allows frequency sweep testing. The testing conditions for sinusoidal loading are shown in Table 5.33.

Table 5.33: Testing conditions (sinusoidal loading mode)

Beam no.	Temp. (°C)	Strain Level ($\mu\epsilon$) (Peak-to-Peak)	Frequency (Hz)	Air voids (%)	%VFA	%VMA
102	4	50	0.1, 1, 10	5	69.2	16.1
103	4	50	0.1, 1, 10	5.2	68.2	16.4
104	4	50	0.1, 1, 10	5.8	65.5	17
105	20	50	0.1, 1, 10	6.4	63.6	17.6
106	20	50	0.1, 1, 10	6.2	64.5	17.3
107	20	50	0.1, 1, 10	6.4	63.7	17.5
108	20	50	0.1, 1, 10	5.3	67.9	16.4
109	20	50	0.1, 1, 10	5	69.1	16.2
110	20	50	0.1, 1, 10	5.3	67.9	16.3
111	20	50	0.1, 1, 10	6.3	63.9	17.5
112	20	50	0.1, 1, 10	6.2	64.4	17.4
113	20	50	0.1, 1, 10	5.8	65.7	17
114	20	50	0.1, 1, 10	6.2	64.4	17.3
115	20	50	0.1, 1, 10	6.2	64.1	17.4
116	20	50	0.1, 1, 10	5.6	66.6	16.8
117	20	50	0.1, 1, 10	5.8	65.9	17
118	20	50	0.1, 1, 10	5.6	66.6	16.8
119	20	50	0.1, 1, 10	6.1	64.8	17.2
120	20	50	0.1, 1, 10	6.1	64.7	17.3
121	20	50	0.1, 1, 10	6.4	63.7	17.5
122	20	50	0.1, 1, 10	6.3	63.9	17.5
123	20	50	0.1, 1, 10	6.3	64.1	17.4
124	20	50	0.1, 1, 10	6.6	63	17.7
125	20	50	0.1, 1, 10	6.5	63.1	17.7
126	40	50	0.01, 0.1, 1, 10	5.4	67.4	16.6
127	40	50	0.01, 0.1, 1, 10	5.5	67.1	16.6
128	40	50	0.01, 0.1, 1, 10	5.5	66.9	16.7
129	40	50	0.01, 0.1, 1, 10	5	68.9	16.2

One of the disadvantages of flexural master curves compared to compressive master curves is that, in order to generate a single master curve, at least three beams need to be tested using sinusoidal loading. It is even worse for haversine loading, where at least ten samples need to be tested. This makes the testing process very time-consuming. Another drawback is associated with the volumetric properties. It can be seen in Table 5.32 and Table 5.33 that the volumetric parameters of the samples vary and this might affect the shape of the master curve. To overcome this problem more samples may need to be tested to make the results more statistically robust. This was partially addressed in this study, with 27 beams tested under sinusoidal loading. However, it was not possible to conduct any further testing using haversine loading due to time constraints and the need to conduct maintenance of the testing equipment. The average mix volumetric conditions needed as input into the development of the flexural master curve are shown in Table 5.34.

Table 5.34: Average volumetric properties used to develop flexural master curve

Master curve type	Air voids (%)	%VFA	%VMA
haversine	5.5	67.1	16.6
sinusoidal	5.9	65.7	17.0

To generate master curves for both cylindrical and beam specimens, the Arrhenius formula (Equation 5-23) was used.

5.8.3.1 Cylindrical master curves

The master curve-fitting parameters for the samples tested without confining pressure –and after running numerical optimisation using the Microsoft Excel® Solver Tool – are shown in Table 5.35 whilst the master curves shown in Figure 5-40.

Table 5.35: Master curve fitting parameters (unconfined cylinders)

Sample no.	Max (MPa)	δ (MPa)	β	γ	ΔE_a	R2
1	22618.284	6.946	-1.497	-0.523	216590.643	0.996
2	22414.480	4.675	-1.480	-0.490	220558.500	0.998
3	22315.442	7.216	-1.442	-0.521	213443.973	0.997
4	22694.534	2.740	-1.505	-0.466	216216.089	0.997
5	23144.581	7.519	-1.399	-0.554	207484.194	0.996
6	22506.497	4.998	-1.497	-0.510	213601.715	0.997
7	22468.687	4.741	-1.543	-0.486	213336.756	0.997
8	22791.418	6.344	-1.577	-0.510	209361.096	0.996
Average	22654.964	5.515	-1.490	-0.506	212145.645	0.997

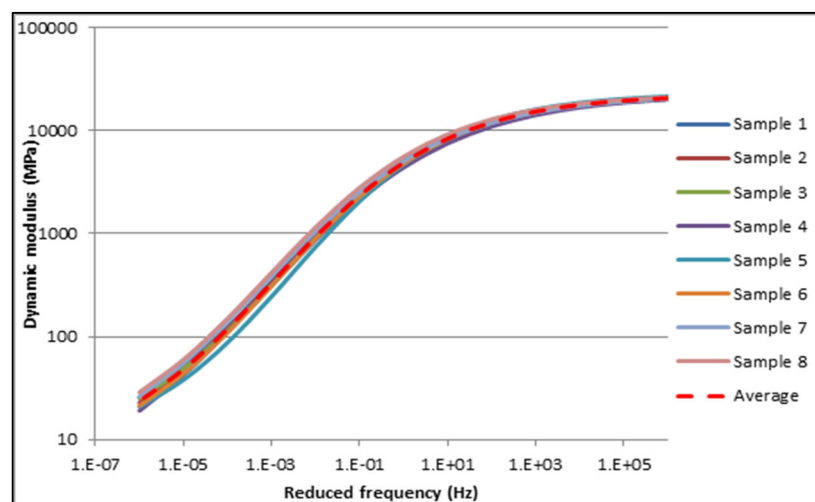


Figure 5-40: Master curves for cylindrical samples (unconfined condition)

The same method was used to develop master curves for samples confined with a pressure of 65 kPa and 135 kPa. The curve-fitting parameters are shown in Table 5.36 and Table 5.37 and the master curves are presented in Figure 5-41 and Figure 5-42.

Table 5.36: Master curve fitting parameters (confining pressure of 65 kPa)

Sample no.	Max (MPa)	δ (MPa)	β	γ	ΔE_a	R2
7	22873.457	36.979	-1.332	-0.569	199780.044	0.995
8	22684.785	2.232	-1.491	-0.378	212808.621	0.990
9	22623.019	7.339	-1.468	-0.446	203184.943	0.994
Average	22777.150	11.764	-1.391	-0.465	204975.626	0.995

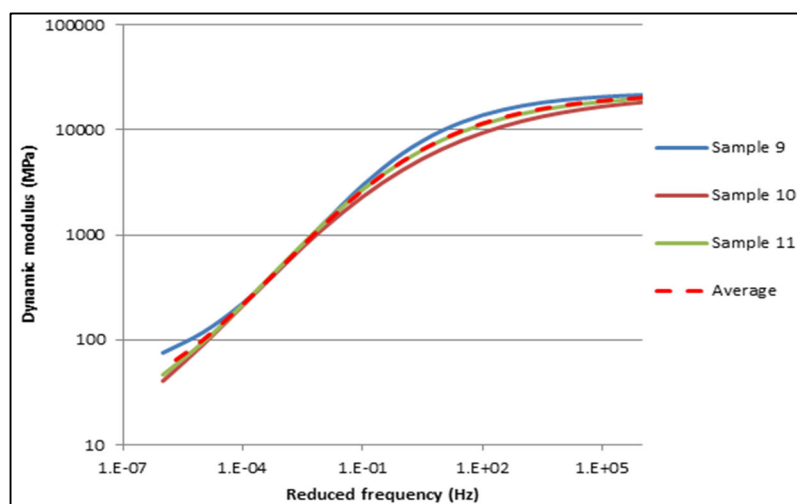


Figure 5-41: Master curves for cylindrical samples (65 kPa confining pressure)

Table 5.37: Master curve fitting parameters for confined cylinders in 135 KPa

Sample no.	Max (MPa)	δ (MPa)	β	γ	ΔE_a	R2
10	22889.762	29.931	-1.415	-0.568	203749.759	0.995
11	22801.715	32.747	-1.409	-0.562	215897.907	0.996
12	22782.028	28.211	-1.283	-0.539	203337.503	0.995
Average	22838.366	30.763	-1.373	-0.569	202114.831	0.995

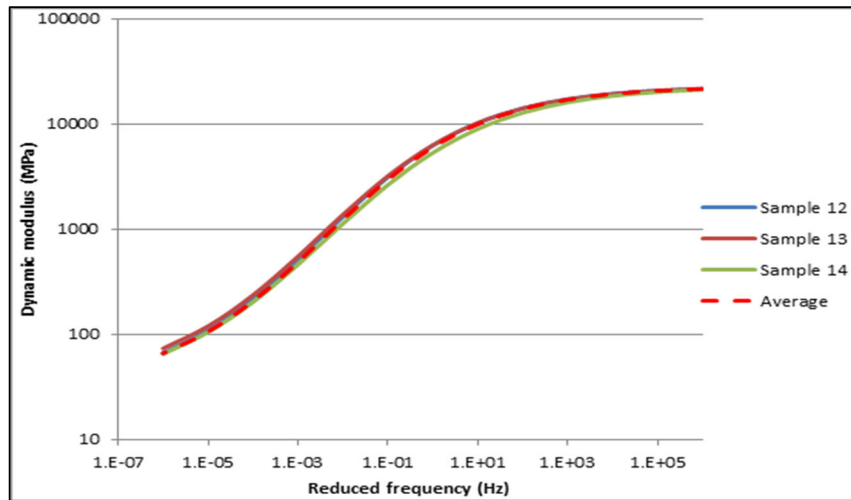


Figure 5-42: Master curves for cylindrical samples (135 kPa confining pressure)

5.8.3.2 Flexural master curves

Flexural master curves were generated for both the haversine and sinusoidal loading modes. As stated previously, ten beams were tested under haversine loading and 28 beams under sinusoidal loading.

The curve-fitting parameters are shown in Table 5.38 and the master curves are shown in Figure 5-43. It can be seen in the Figure that the dynamic modulus for haversine loading was higher than the modulus for sinusoidal loading, especially at lower frequency levels.

Table 5.38: Flexural master curve fitting parameters (haversine and sinusoidal loading)

Loading mode	Max (MPa)	δ (MPa)	β	γ	ΔE_a	R2
haversine	22392.678	47.957	-1.066	-0.551	225860.712	0.994
sinusoidal	22191.519	19.256	-1.092	-0.516	214609.241	0.998

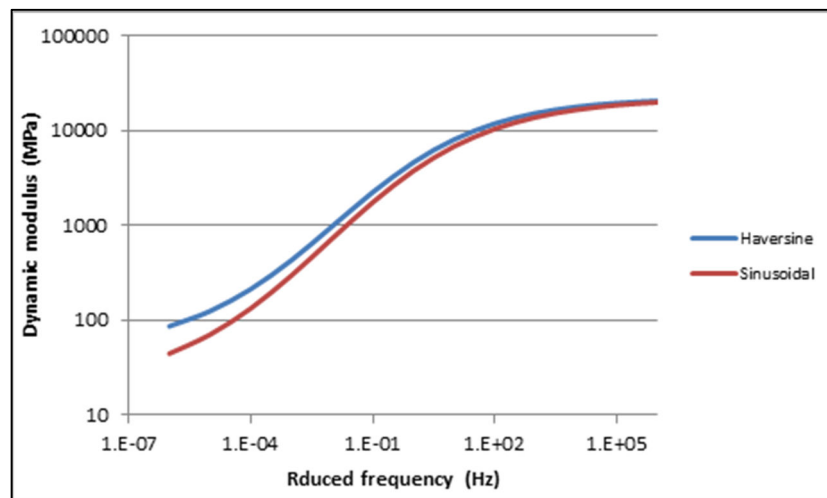


Figure 5-43: Flexural master curves (haversine and sinusoidal loading)

5.8.4 Major findings

All the master curves developed under different testing conditions for approach 6 are presented in Figure 5-44 whilst the time-temperature shift factors and phase angles for the same master curves are presented in Figure 5-45 and Figure 5-46.

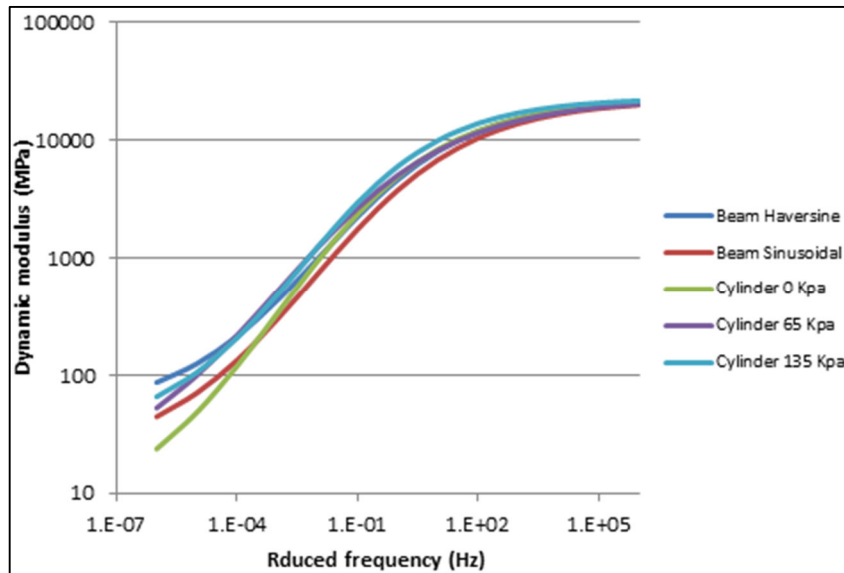


Figure 5-44: Master curves for different testing condition (approach 6)

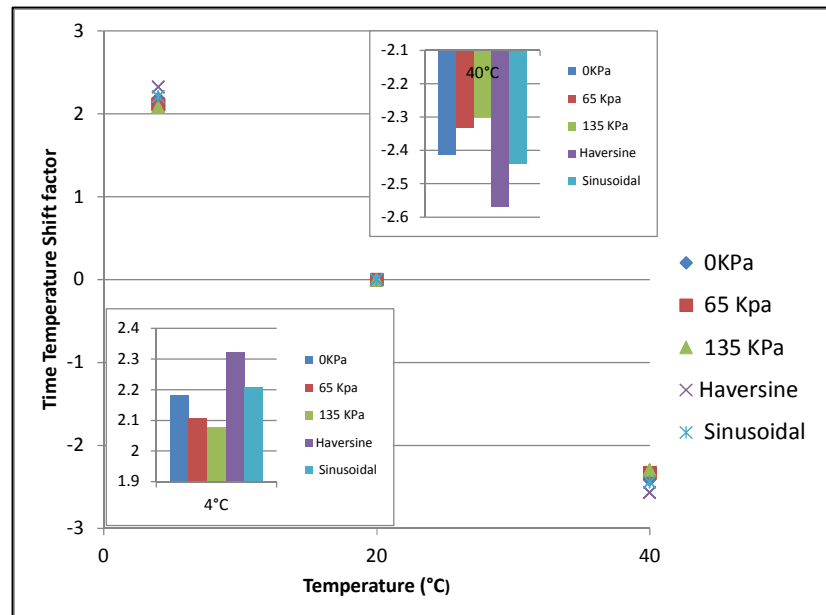


Figure 5-45: Time-temperature shift factors for different testing conditions

Major findings of this approach (approach 6) can be summarised as following:

- Applying a confining pressure resulted in an increase in the dynamic modulus at lower load frequencies (Figure 5-44).

- The values of the shift factor are smaller with higher confinement (Figure 5-45)

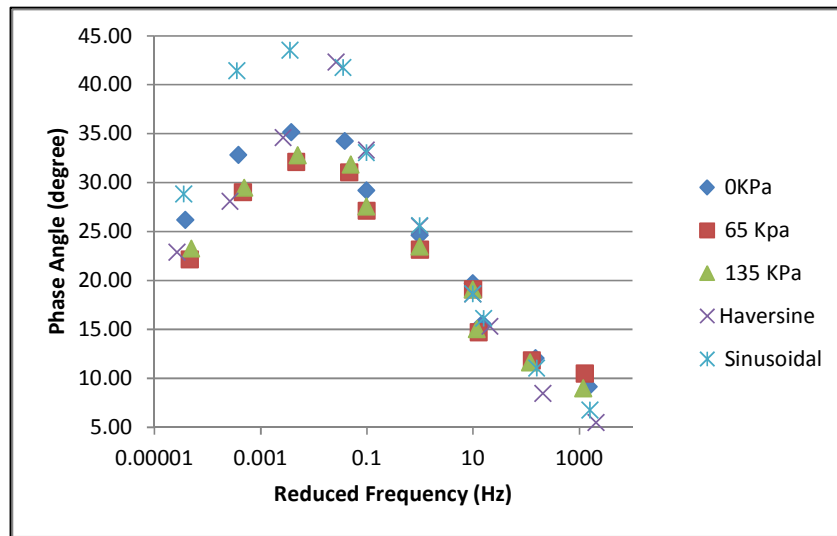


Figure 5-46: Variation in phase angle for different test conditions

- At lower frequency levels the phase angle without confinement was greater than the cases when a confining pressure was applied (Figure 5-44).
- The sinusoidal flexural master curve showed more viscous behaviour compared to the haversine curve at lower frequencies.
- The shift factors for the flexural master curves were greater than the compressive master curves, with the maximum shift being associated with the haversine master curve.

6 CONCLUSIONS AND RECOMMENDATIONS

The most common flexible pavement type used in Australia is the unbound granular pavement with a thin bituminous surfacing (sprayed seal). These surfacings provide a smooth riding surface and act as a water-proofing agent to prevent the ingress of moisture into the pavement structure (assuming that adequate drainage of the lower layers of the pavement is also provided).

However, as the number of axles on heavy vehicles, and the associated axle loads, continues to increase, the use of asphalt pavements – either full depth asphalt or a structural surfacing over a stabilised or granular base – is becoming more common, particularly on major freight routes serving urban areas.

The fatigue performance of asphalt is addressed in the Austroads (2012) mechanistic-empirical pavement thickness design procedure. In this procedure, the Shell (1978) laboratory model is adjusted to field conditions through the use of a reliability factor. However, the use of these procedures can result in the fatigue performance in the field being better than predicted, which is an issue of concern to industry.

The research presented in this thesis addresses these concerns through a program of work involving detailed laboratory testing and analysis, including the development of:

1. improved protocols to minimise errors introduced during testing
2. a new fatigue life prediction model based on the laboratory test data
3. a new accelerated laboratory testing approach that allows the fatigue behaviour of asphalt to be modelled at different test temperatures, loading frequencies and strain levels
4. master curves for the asphalt mix that can be input into the mechanistic-empirical design procedures used in Australia after validation process.

Following the literature review – including its relevance to practice in WA – and the identification of research gaps (Chapter 2), details of the sample preparation and the determination of the fundamental properties AC14/75 mix used in the testing program described in the subsequent chapters are presented in Chapter 3. The results of the preliminary testing and the development of improved protocols to minimise errors introduced during testing are presented in Chapter 4.

The test results and the analysis of the results – including details of a new fatigue model, a new accelerated testing method and master curves developed for the AC14/75 mix – are presented in Chapter 5.

6.1 Literature review

The main effort in this chapter has been placed on finding the study gaps regarding the experimental modelling of asphalt material. After a comprehensive literature review it was found that future study is essential on following areas:

- testing protocols in terms of validity and reliability
- fatigue life extrapolation for the tests when the termination condition is not reached
- new accelerated testing methods to analyse the asphalt material behaviour in different testing conditions in terms of frequency, temperature and strain level faster than previous testing protocols
- developing new base line for dynamic modulus of Western Australia's typical mixes
- fatigue endurance limit (FEL)
- More investigations on healing phenomenon in viscoelastic material

6.2 Development of testing protocols

During preliminary dynamic modulus testing on cylindrical specimens using the AMPT machine, some problems were noted in terms of the standard error on the load, which was greater than 10%, and also the peak-to-peak strain level, which should have been between 85-115 $\mu\epsilon$. In addition, after performing trial four-point bending fatigue testing on beams it was found that there were some issues with the outputs from the EN Standard Tester, specifically the phase angle not being in the required range. There was also a problem related to the deformation of the beams when the haversine loading mode was applied.

In terms of the testing of the cylindrical samples using the AMPT, there were also some problems, especially at higher temperatures ($\geq 40^{\circ}\text{C}$) and at lower frequencies (0.01-0.1 Hz) where there were difficulties achieving the correct load pulse shape (haversine or sinusoidal). These issues were associated with the need to stay

within the defined strain level, the low levels of stress being applied to the samples and the introduction of errors associated with noise generated by the machine during testing.

Clearly, if there are errors in any of the parameters (phase angle, load, deformation and applied level of strain) introduced during testing, then the results will not be valid.

One purpose of Chapter 4, therefore, was to describe in detail the problems encountered during this preliminary phase and the steps taken to overcome the problems associated with the use of enhanced testing techniques such as those adopted in the study reported in this thesis. It was demonstrated that it is possible to obtain valid data at higher temperatures and low frequencies through the introduction of proportional, integral and adoptive control and the addition of an external signal to the operating system. This is discussed in detail in this Chapter.

The other purpose of this chapter was to present revised testing protocols for the EN Standard Tester (four-point bending) and AMPT testing which were developed to minimise the errors introduced during testing, in particular out-of-range phase angle problems associated with the EN tester and out-of-range strain levels and load standard errors associated with the AMPT tester.

The use of this protocol resolved the issues associated with phase angle during four-point bending beam testing and also reduced the load standard errors and noise issues associated with the AMPT testing.

6.3 Fatigue testing and the development of master curves

The analysis of the fatigue behaviour of the asphalt mix and the development of the master curves involved the use of six approaches (Chapter 5). The findings were as follows.

6.3.1 Approach 1

This approach involved the determination of the fatigue life of the asphalt mix according to Austroads (2006), viz. four-point bending beam testing. When fatigue testing was conducted in accordance with this test method (i.e. haversine loading with frequency level of 10 Hz at 20°C), the average fatigue life was 99,903 cycles (100,000 cycles).

6.3.2 Approach 2

In this approach, the predicted fatigue life is derived using linear regression of the number of cycles required for the stiffness of the asphalt to reduce to 50% of its initial stiffness and the initial strain amplitude recorded after 100 cycles of load (EN 12697-24 2012). Three methods were used to develop the regression equation:

- the results for all samples
- the results without the failed samples
- the average for each testing condition.

It was found that there was no significant difference between the predicted strain levels after 1,000,000 cycles with all three methods if the results associated with beams which failed were omitted from the analysis.

6.3.3 Approach 3

In this approach, a new method for fatigue life prediction was proposed, as was a new model capable of predicting fatigue life when the termination condition of testing was not met (i.e. 50% loss in initial recorded stiffness). This was made possible by the development of a template for assigning adjustment factors during different stages of testing (i.e. stiffness loss). Using this approach, it was found that:

- the Austroads fatigue life prediction model under-predicted the fatigue life compared to the results obtained using the above method (under both haversine and sinusoidal loading)
- when testing was conducted at the lowest strain level ($100 \mu\epsilon$), the fatigue life at all temperatures was greater than 100 million cycles. This could be evidence of the Fatigue Endurance Limit (FEL), which is defined as the strain level that, if a material experiences less than this strain level, then it will not fail due to fatigue associated from cumulative damage.

6.3.4 Approach 4

In this approach, emphasis was placed on developing a new accelerated testing method which allows testing to be conducted under different frequency, strain level and temperature conditions. The major outcomes of this work were as follows:

- A curve fitting step carried out after numerical optimisation using Microsoft EXCEL® Solver Tool revealed that two sigmoidal and homographic functions provided the best model of the behaviour of the asphalt.

- The sigmoidal function was more appropriate when the material responded elastically to the loading at both lower temperatures and higher frequencies of loading.
- The homographic function provided a better fit to the data when the behaviour of the material was more viscoelastic than elastic at both higher temperatures and lower frequency levels.
- There was evidence of self-healing of the asphalt mix.

6.3.5 Approach 5

As self-healing was observed using the previous approach, effort in approach 5 was placed on investigating this phenomenon by introducing rest periods of 0.1, 0.3 and 0.9 seconds to continuous loading in both the haversine and sinusoidal modes. It was found that introducing rest periods 0.3 and 0.9 seconds resulted in a significant increase in laboratory fatigue life. Further investigation is needed to examine longer rest periods (e.g. 1, 3 and 9 seconds).

6.3.6 Approach 6

In this approach, emphasis was placed on the development of flexural master curves for beam specimens and compressive master curves for cylindrical samples. Master curves were developed for cylinders at different confining pressures (0, 65 and 135 kPa). However, there was significant scatter in the results at lower frequencies whilst, at higher frequencies, the difference was not significant.

6.4 Summary

New testing protocols were developed for both the EN Standard Tester (four-point bending beam testing) and the asphalt mix performance tester (AMPT) which can be considered for introduction into standards currently adopted in Western Australia and other Australian states. Although four-point bending beam test is very time-consuming and expensive, the suggested new approach (approach 4) is an innovative accelerated method which examines the fatigue behaviour of asphalt beams and considers all influential parameters (frequency, temperature, strain level). More research should be conducted to further develop accelerated asphalt fatigue testing protocols.

Major innovations can be categorised into four parts:

1. A new testing protocol developed to minimise the associated errors with EN Standard Tester and AMPT outputs. An innovative technique has been proposed to refine the out-of-range phase angle problem with the current software used to control bending beam tests. Enhanced control engineering techniques such as the PID controller, Adoptive Level Control (ALC) and dithering can be used to address issues associated with noisy stress-shapes, out-of-range strain levels and load standard errors. The result is more valid and reliable and an increased level of robustness has been reached.
2. Two scenarios are proposed in approach 3 on how to extrapolate fatigue life when the termination condition (50% of initial stiffness) is not met.
3. A new accelerated testing approach (approach 4) which involves increasing the strain level continuously at different temperatures and frequencies.
4. Flexural master curves for both haversine and sinusoidal loading which can be compared with compressive master curves for cylindrical samples.

6.5 Recommendations

Recommendations for further research include the following:

- Although this research has involved a great deal of testing, and new testing protocols have been developed, testing was only conducted on one asphalt mix. Testing should be conducted on other asphalt mixes in order that the experimental models developed in this study can be refined through the input of more data pertaining to a wider range of mixes.
- The new model and approach for fatigue life estimation should be calibrated against data obtained in the field. This will enable:
 - an evaluation of the proposed new method in terms of whether the increased fatigue lives suggested in some of the approaches are also observed in the field
 - a shift factor to be developed which relates laboratory and field performance.
- The observed healing of the asphalt samples when rest periods were applied should be examined in more detail, including the application of longer rest periods and to a wider range of asphalt mixes. The influence of temperature

and loading frequency on healing should also be examined for a wider range of mixes.

- The new method for fatigue life prediction, and the new model capable of predicting fatigue life when the termination condition of testing was not met (i.e. 50% loss in initial recorded stiffness) should also be examined for a wider range of mixes.
- The Fatigue Endurance Limit (FEL) should be examined in more detail by running the fatigue tests at lower strain ranges of 50-150 $\mu\epsilon$ and at different temperatures, and on a range of mixes.
- More work on the development of refined models used to generate master curves, and time-temperature shift factors, should be conducted. This could include an investigation of the correct reference temperature which takes account of the climatic conditions operation at the locations where the asphalt mix is to be applied.

REFERENCES

- Abojaradeh, M. (2003). *Predictive fatigue models for Arizona asphalt concrete mixtures*, Ph.D. Dissertation, Arizona State University, December.
- Adeyinka Azeez, A., (2013). *Fatigue failure and testing method*, Bachelor's thesis, HAMK University of Applied Science.
- Adlinge, S. and Gupta, K. (2013), *Pavement deterioration and its causes*, IOSR Journal of Mechanical & Civil Engineering, pp. 9–15.
- Al-Khateeb, G., Shenoy, A., Gibson, N., and Harman, T. (2006). *A new simplistic model for dynamic modulus predictions of asphalt paving mixtures*. Journal of the AAPT, Vol. 75E.
- American Association of State and Highway Transportation Officials AASHTO (2008). *Mechanistic-empirical pavement design guide, interim edition: a manual of practice*, Washington, DC.
- American Association of State Highway and Transportation Officials (AASHTO) (2013). *Standard method of test for effect of heat and air on a moving film of asphalt binder (rolling thin-film oven test)*, T240-13-UL, AASHTO, Washington D.C.
- Anderson, D.A., Champion-Lapalu, L., Marasteanu, M.O., LeHir, Y.M., Planche, J.P. and Martin, D. (2001). *Low-temperature thermal cracking of asphalt binders as ranked by strength and fracture properties*, Transportation Research Record: Journal of the Transportation Research Board, Vol. 1766, pp. 1–6.
- Andriescu, A., Hesp, S.A.M. and Youtcheff, J.S. (2004). *On the essential and plastic works of ductile fracture in asphalt binders*, 83rd Annual Meeting of the Transportation Research Board, Washington, D.C.
- Archilla, A.R. and Diaz, L.G. (2011). *Effects of asphalt mixture properties on permanent deformation response*, Transportation Research Record: Journal of the Transportation Research Board, Vol. 2210, pp. 1–8.
- AS2150 2005. *Hot mix asphalt – a guide to good practice*.
- AS2891.2.1 1995. *Methods of sampling and testing asphalt, method 2.1: sample preparation – mixing, quartering and conditioning of asphalt in the laboratory*.
- AS2891.2.2 2014. *Methods of sampling and testing asphalt, method 2.2: Compaction of asphalt test specimens using a Gyratory compactor*.
- AS2891.9.2 2005. *Methods of sampling and testing asphalt, method 2.2: Determination of bulk density of compacted asphalt – Pre-saturation method*.
- Asadi, H., Leek, C. and Nikraz, H. (2013). *Effect of temperature on fatigue life of asphalt mixtures*, Proceedings of the 15th AAPA International Flexible Pavements Conference, 22-25 September, Royal International Conference Centre, Brisbane.
- Asgharzadeh, S.M. and Tabatabaee, N. (2013). *Rheological master curves for modified asphalt binders*, Scientia Iranica, © Sharif University of Technology, Vol. 20, No.6, pp.1654-1661.
- Asphalt Institute (1982). *Research and development of Asphalt Institute's thickness design manual*, 9th Ed., Research Report 82-2, The Asphalt Institute.
- Aure, T.W. and Ioannides, A.M. (2012). *Numerical analysis of fracture process in pavement slabs*, Canadian Journal of Civil Engineering, Vol. 39, No. 5, pp. 506–514.
- Austroroads (2005). *Compaction of asphalt slabs suitable for characterisation*, test method AGPT/T220, August, Austroroads, Sydney, NSW.
- Austroroads (2006). *Fatigue life of compacted bituminous mixes subject to repeated flexural bending*, test method AGPT/T233, January, Austroroads, Sydney, NSW.
- Austroroads (2010). *Glossary of terms*, fourth edition, August, prepared by P Milne, K Sharp & B Ungers, Austroroads: Sydney.

- Austrroads (2012). *Austrroads guide to pavement technology, part 2: pavement structural design*, AGPT02-12, Austrroads, Sydney, NSW.
- Baburamani, P. (1999). *Asphalt fatigue life prediction models – a literature review*, ARRB research report, ARR no. 334.
- Bhasin, A., Castelo Branco, V.T.F., Masad, E. and Little, D.N. (2009). *Quantitative comparison of energy methods to characterize fatigue in asphalt materials*, Journal of Materials in Civil Engineering, Vol. 21, No. 2, pp. 461–470.
- Bonnaure, F., Huibers, A., and Boonders, A.A. (1982). *Laboratory investigation of the influence of rest periods on the fatigue characteristics of bituminous mixes*, Journal of the Association of Asphalt Paving Technologists, Kansas City, Missouri, Vol.51, pp.104–128.
- Carpenter, S.H., and Jansen, M. (1997). *Fatigue behavior under new aircraft loading conditions*, Proceedings of Aircraft Pavement Technology in the Midst of Change, pp. 259–271.
- Carpenter, S.H., Ghuzlan, K., and Shen, S. (2003). *A fatigue endurance limit for highway and airport pavements*, Annual Meeting of the Transportation Research Board (TRB), January.
- Castro, M. and Sanchez, J.A. (2006). *Fatigue and healing of asphalt mixtures: Discriminate analysis of fatigue curves*, Journal of Transportation Engineering, ASCE, Vol. 132, No. 2, pp.168–174.
- Ceylan, H., Gopalakrishnan, K. and Kim, S. (2008). *Advanced approaches to hot-mix asphalt dynamic modulus prediction*, Canadian Journal of Civil Engineering, Vol. 35, No. 7, pp. 699-707.
- Choi, Y. and Kim, Y. (2013). *Road materials and pavement design, Implementation and verification of a mechanistic permanent deformation model (shift model) to predict rut depths of asphalt pavements*, Department of Civil, Construction & Environmental Engineering, North Carolina State University, Raleigh, NC 27695-7908, USA.
- Clyne, T., Li, X., Marasteanu, M.O. and Skok, E.L. (2003). *Dynamic and resilient modulus of Mn/DOT asphalt mixtures*, Report No. MN/RC – 2003-09, February.
- Cross, S., and Sumesh, K.C. (2007). *Determination of dynamic modulus master curves for Oklahoma HMA mixtures*. College of Engineering Architecture and Technology, Oklahoma state University, Stillwater, Oklahoma, December.
- Diaz, L.G. and Archilla, A.R. (2013). *From testing to design: An easy way to use and interpret the results from the asphalt mixture performance tester (AMPT)*, International Journal of Pavement Research and Technology, Vol.6, No.5, September, pp.527–538.
- El-Basyouny, M.M., and Witczak, M.W. (2005). *Calibration of alligator fatigue cracking model for 2002 design guide*, Transportation Research Record, No. 1919, pp. 77–86.
- EN 12697-24 (2012), *Bituminous mixtures, test methods for hot mix asphalt, resistance to fatigue*.
- Garba, R. (2002). *Permanent deformation properties of asphalt concrete mixtures*, Department of Road and Railway Engineering, Norwegian University of Science and Technology.
- Garcia, A., Schlangen, E. and Van de Ven, M., (2010). *Two ways of closing cracks on asphalt concrete pavements: microcapsules and induction heating*. Key Engineering Materials, Trans Tech Publications, Switzerland, Vols 417-418, pp. 573–576.
- Gauthier, G.G. and Anderson, D.A. (2006). *Fracture mechanics and asphalt binders*. International Journal of Road Materials and Pavement Design, Vol. 7, pp. 9–35.
- Ghaffarpour Jahromi, S. and Khodaii, A. (2009). *Master curves for stiffness asphalt concrete*. International Journal of Pavement Research and Technology, Vol. 2, No. 4, July, pp. 148–153.

- Harvey, J.T., Deacon, J.A., Tsai, B.W. and Monismith, C.L. (1995). *Fatigue performance of asphalt concrete mixes and its relationship to asphalt concrete pavement performance in California*, Report No. RTA-65W485-2, Institute of Transportation Studies, University of California at Berkeley, USA.
- Hopman, P.C., Kunst, P.A.J.C. and Pronk, A.C. (1989). *A renewed interpretation method for fatigue measurements, verification of Miner's Rule*, 4th Eurobitume Symposium in Madrid, Vol. 1, pp. 557–61.
- Huang, Y.H. 1993, *Pavement Analysis and Design*, Prentice Hall, NJ USA.
- Kim, Y. and Marasteanu, M.O. (2012). *Use of fracture tests and models, applications of advanced models to understand behavior and performance of asphalt mixtures*, Transportation Research Circular Number E-C161, Transportation Research Board, Washington DC.
- Kumlai, S., Jitsangiam, P. & Nikraz, H. (2014). *Comparison between resilient modulus and dynamic modulus of Western Australian hot mix asphalt based on flexible pavement design perspectives*, Proceedings 26th ARRB conference – research driving efficiency, Sydney, New South Wales.
- Kwan, K.S. (1998). *The role of penetrant structure in the transport and mechanical properties of a thermoset adhesive*, PhD thesis, Faculty of the Virginia Polytechnic Institute, Blacksburg.
- Long, M. (2001). *Permanent deformation of asphalt concrete pavement: a nonlinear viscoelastic approach to mix analyses and design*, Ph.D. Dissertation. University of California, Berkeley, September.
- Main Roads Western Australia (2011). *Bitumen content and particle size distribution of asphalt and stabilised soil: centrifuge method*, test method WA 730.1.
- Main Roads Western Australia (2011). *Maximum density of asphalt – Rice method*, test method WA 732.2.
- Majidzadeh, K. et al. (1975). *Application of Fracture Mechanics for Improved Design of Bituminous Concrete*, Vol. 2, Ohio State University Research Foundation, Ohio.
- Mamlouk, M., Souliman, M. and Zeiada, W. (2012). *Optimum testing conditions to measure HMA fatigue and healing using flexural bending test*, 91st annual meeting of the Transportation Research Board (TRB).
- Marasteanu, M.O. and Anderson, D. (1999). *Improved model for bitumen rheological characterization*, Eurobitume Workshop on Performance Related Properties for Bituminous Binders, Eurobitume, Brussels.
- Miljković, M. and Radenberg, M. (2011). *Rutting mechanisms and advanced laboratory testing of asphalt mixtures resistance against permanent deformation*, Series: Architecture and Civil Engineering Vol. 9, No. 3, pp. 407–17.
- Mirza, M.W. and Witczak, M.W. (1995). *Development of a global aging system for short and long term aging of asphalt cements*, Journal of the Association of Asphalt Paving Technologists, Vol. 64, pp. 393–430.
- Monismith, C.L., Secor, K.E. and Blackmer, W. (1961). *Asphalt mixture behaviour in repeated flexure*, Proceedings of Association of Asphalt Paving Technologists, Vol. 30, pp. 188–222.
- Nair, R.K and Priyadarshini, R.Y. (2013). *Evaluation of dynamic modulus and unconfined asphalt mixtures*, International Journal of Innovative Research in Science, Engineering and Technology, Vol. 2, Special Issue 1, December, pp. 231–239.
- National Cooperative Highway Research Program (2008a). *Ruggedness testing of the dynamic modulus and flow number tests with the simple performance tester*, NCHRP Report 629, Transportation Research Board, Washington D.C.
- National Cooperative Highway Research Program (2008b). *Refining the simple performance tester for use in routine practice*, NCHRP Report 614, Transportation Research Board, Washington D.C.

- Ning, L., Molenaar, A., Van de Ven, M. and Shaopeng, W. (2010). *Estimation of the fatigue endurance limit of HMA for perpetual pavement*, Journal of Wuhan University of Technology, Vol. 25, No. 4, pp. 645–649.
- Olard, F. and Di-Benedetto, H. (2004). *Fracture toughness and fracture energy of bituminous binders at low temperatures*, Proceedings of 5th RILEM International Conference on Cracking in Pavements, Limoges, France.
- Pais, J.C. and Minhoto, M.J.C. (2010). *The prediction of fatigue life of asphalt mixtures using four point bending test*, Proceedings 24th ARRB Conference – Building on 50 years of road and transport research, Melbourne, Australia 2010.
- Paris, P.C. and Erdogan, E. (1963). *A critical analysis of crack propagation laws*, Journal of Basic Engineering, Series D, Vol. 85, pp. 528–534.
- Pell, P.S. (1962). *Fatigue characteristics of bitumen and bituminous mixes*, Ann Arbor, Michigan: International Conference on The Structural Design of Asphalt Pavements.
- Pell P.S. and Cooper, K.E. (1975). *The effect of testing and mix variables on the fatigue performance of bituminous materials*, Proceedings of Association of Asphalt Paving Technologists, Vol. 44, pp. 1–37.
- Philips, M.C. (1998). *Multi-step models for fatigue and healing, and binder properties involved in healing*, Proceedings of Eurobitume Workshop on Performance Related Properties for Bituminous Binders, No. 115, Luxembourg.
- Pronk, A.C. and Hopman P.C. (1990). *Energy dissipation: the leading factor of fatigue, highway research: sharing the benefits*, Proceedings of the Conference, the United States Strategic Highway Research Program, London, pp. 225–237.
- Qiu, J., Molenaar, A., Van de Ven, M., Wu, S. and Yu, J. (2012). *Investigation of self-healing behaviour of asphalt mixes using beam on elastic foundation setup*, Journal of Materials and Structures, Vol. 45, pp. 777–791.
- Rickards, I. (2012). *The perpetual pavement solution for urban arterials – a sustainable future*, IPWEA Conference, Perth, March.
- Rowe, G.M. (1993). *Performance of asphalt mixtures in the trapezoidal fatigue test*, Journal of Association of Asphalt Paving Technology, pp. 344–84.
- Rowe, G.M. and Bouldin, M.G. (2000). *Improved techniques to evaluate the fatigue resistance of asphaltic mixes*, Proceedings of the Second Eurasphalt and Eurobitume Congress, Spain, book 1, pp. 754–763
- Roy, S.D., and Hesp, S.A.M. (2001). *Low-temperature binder specification development: thermal stress restrained specimen testing of asphalt binders and mixtures*. Presented at 80th Annual Meeting of the Transportation Research Board, Washington, D.C.
- Shahadan, Z., Hamzah, M.O., Yahya, A.S. and Jamshidi, A. (2013). *Evaluation of the dynamic modulus of asphalt mixture incorporating reclaimed asphalt pavement*, Indian Journal of Engineering and material sciences. Vol. 20, October, pp. 376-384.
- Shahin, M.Y. (1994). *Pavement Management for Airports, Roads and Parking Lots*, Chapman and Hall, New York, NY.
- Shell (1978). *Asphalt pavements and overlays for road traffic*, Shell International Petroleum Company Limited, London.
- Shen, S., Chiu, H., and Huang, H. (2010). *Characterization of fatigue and healing in asphalt binders*, Journal of Materials in Civil Engineering © ASCE, September, Vol. 22, pp. 846–852.
- Shen, S. and Carpenter, S.H. (2007). *An energy approach for airport pavement low damage fatigue behaviour*, FAA Worldwide Airport Technology Transfer Conference, Atlantic City, New Jersey, USA.
- SHRP A-404 (1994). *Fatigue response of asphalt-aggregate mixes*, strategic highway research program, Berkeley: Institute of Transportation Studies, University of California.

- Soltani, A., Solaimanian, M. and Anderson, D. (2006). *An investigation of the endurance limit of hot-mix asphalt concrete using a new uniaxial fatigue test protocol*, University-Based Research, Education, and Technology Transfer Program, Pennsylvania Transportation Institute, May, Report no. FHWA-HIF-07-002.
- Van Dijk, W. and Visser, W. (1977). *The energy approach to fatigue for pavement design*, Journal of Association of Asphalt Paving Technology, Vol. 46, pp. 1–40.
- Witczak, M.W. and Mirza, M.W. (2000). *AC fatigue analysis for 2002 design guide*, Research Report for NCHRP 1-37A Project, Arizona State University, Tempe, Arizona, USA.
- Witczak, M.W., Kaloush, K., Pellinen, T., El-Basyouny, M. and von Quintus, H. et al. (2002). *Simple performance test for Superpave mix design*, NCHRP Report 465, Transportation Research Board, Washington, DC.
http://onlinepubs.trb.org/onlinepubs/nchrp/nchrp_rpt_465.pdf.
- Zhu, H., Sun, L., Yang, J., Chen, Z. and Gu, W. (2011). *Developing master curves and predicting dynamic modulus of polymer-modified asphalt mixtures*, Journal of Materials in Civil Engineering © ASCE, February, Vol. 23, pp. 131–137.
- Ziaei-Rad, V., Nouri, N., Ziaei-Rad, S. and Abtahi, M. (2012). *Numerical study on mechanical performance of asphalt mixture using a meso-scale finite element model*, Journal of finite element in analysis and design, Vol. 57, pp. 81–91.
- Zofka, A. and Marasteanu, M.O. (2007). *Development of double edge notched tension (DENT) test for asphalt binders*, Journal of Testing and Evaluation, Vol. 35, No. 3, pp. 259–265.
- Zou, G., Zhang, X., Xu, J. and Chi, F. (2010). *Morphology of asphalt mixture rheological master curves*, Journal of Materials in Civil Engineering © ASCE, August, Vol. 22, pp. 806–810.

"Every reasonable effort has been made to acknowledge the owners of copyright material. I would be pleased to hear from any copyright owner who has been omitted or incorrectly acknowledged."

Appendix A

UTS15 OUTPUT IN APPROACH 3
FOR HAVERSINE LOADING

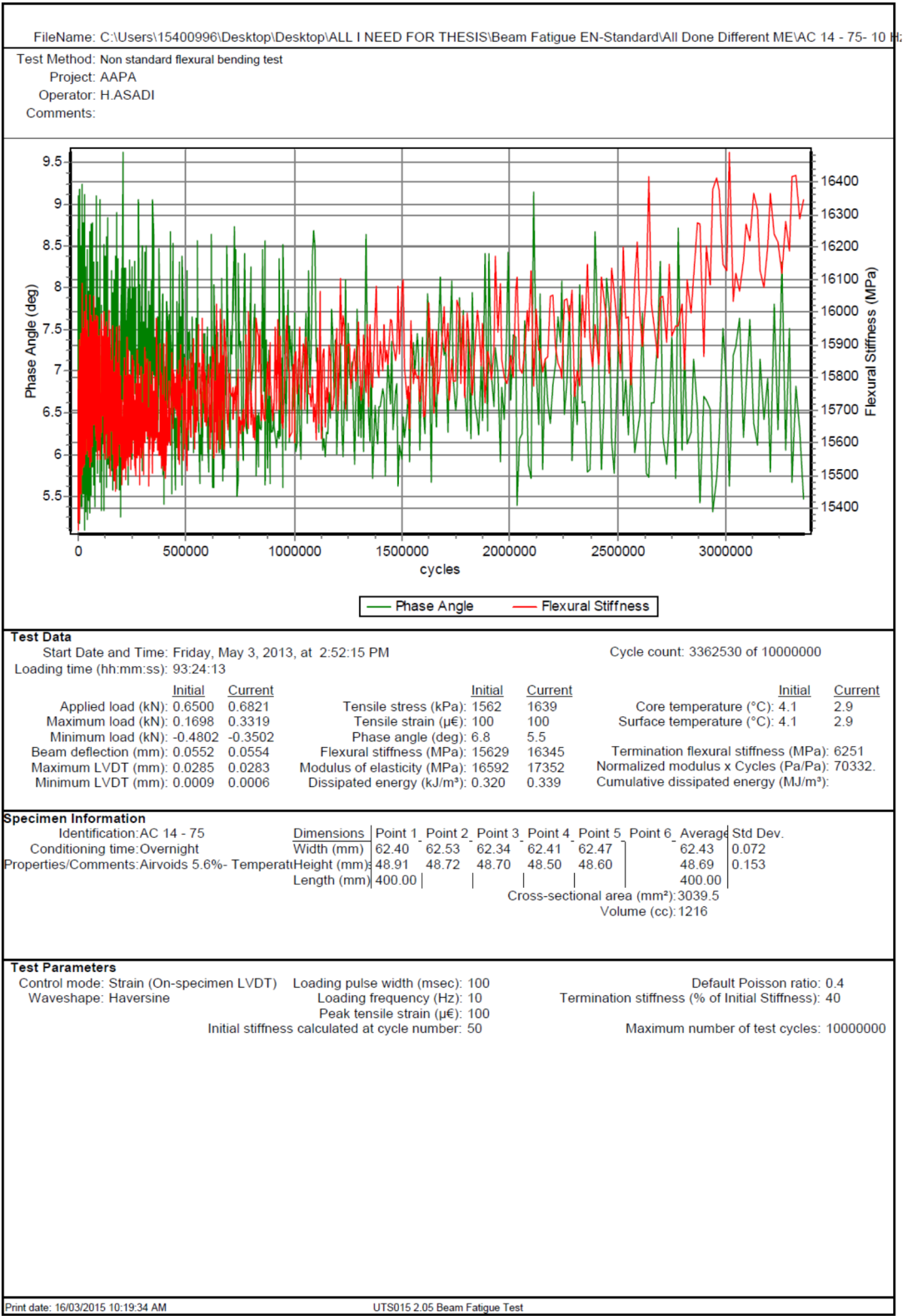


Figure A - 1. UTS 15 output for beam number 27

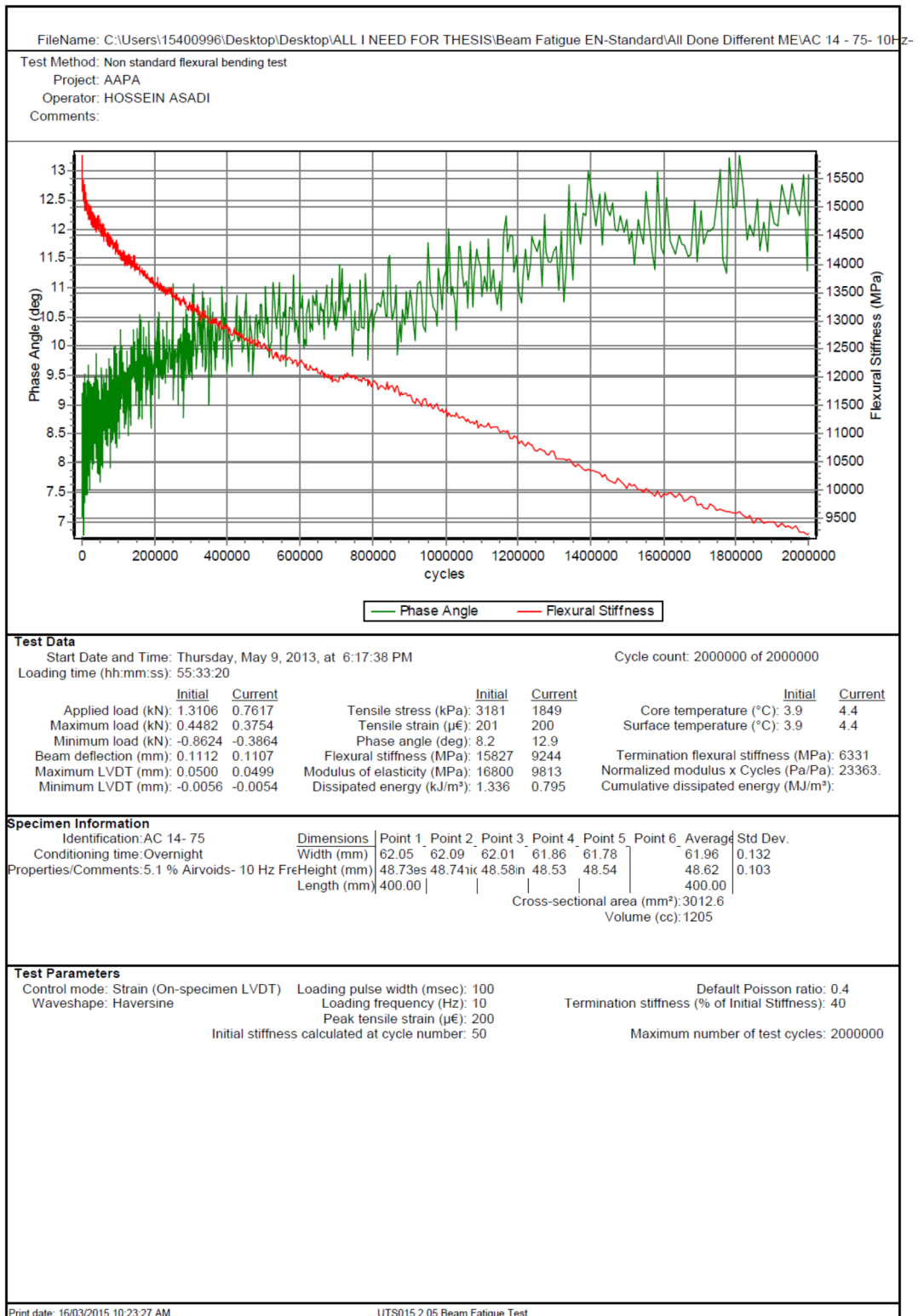


Figure A - 2. UTS 15 output for beam number 28

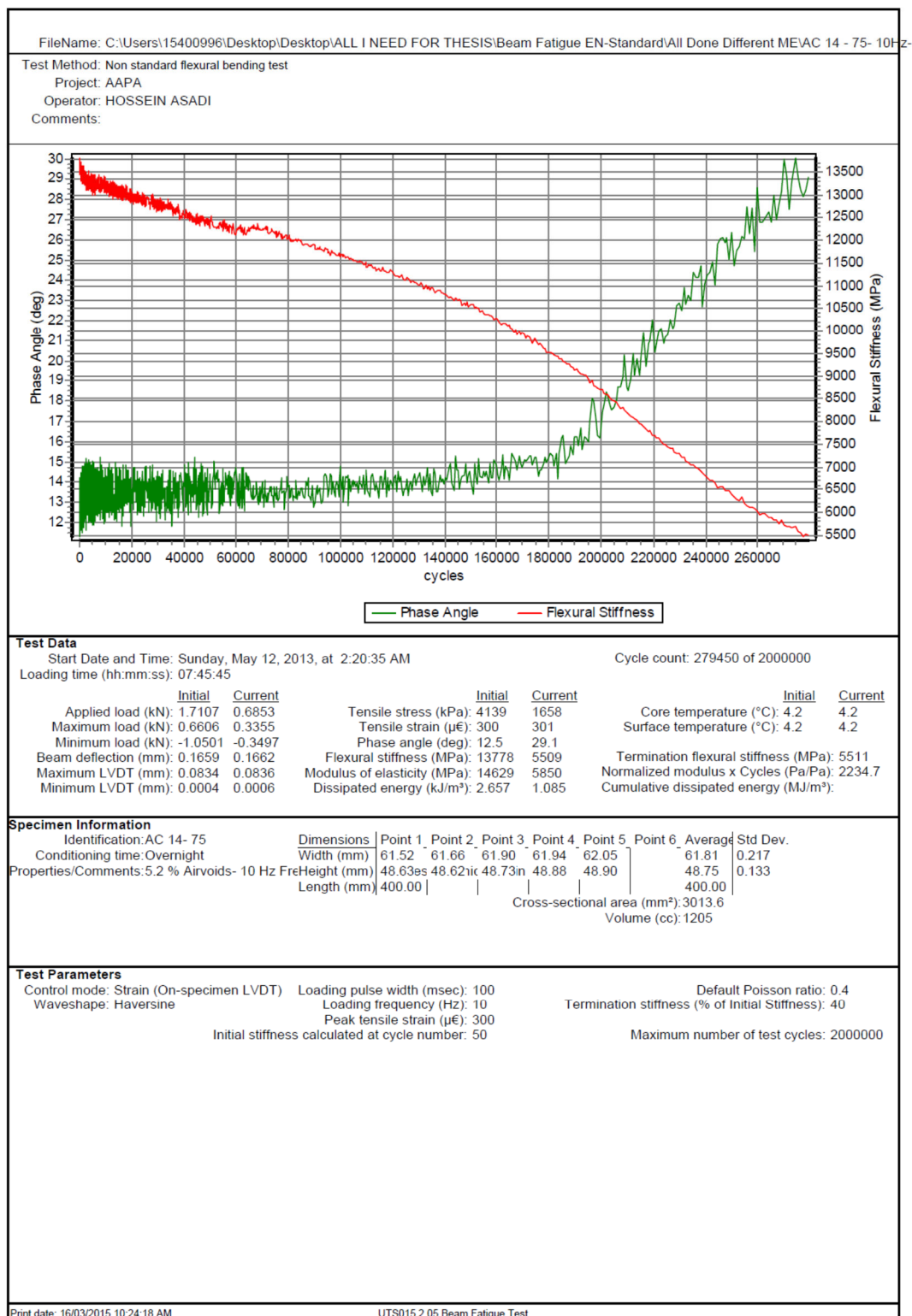


Figure A - 3. UTS 15 output for beam number 29

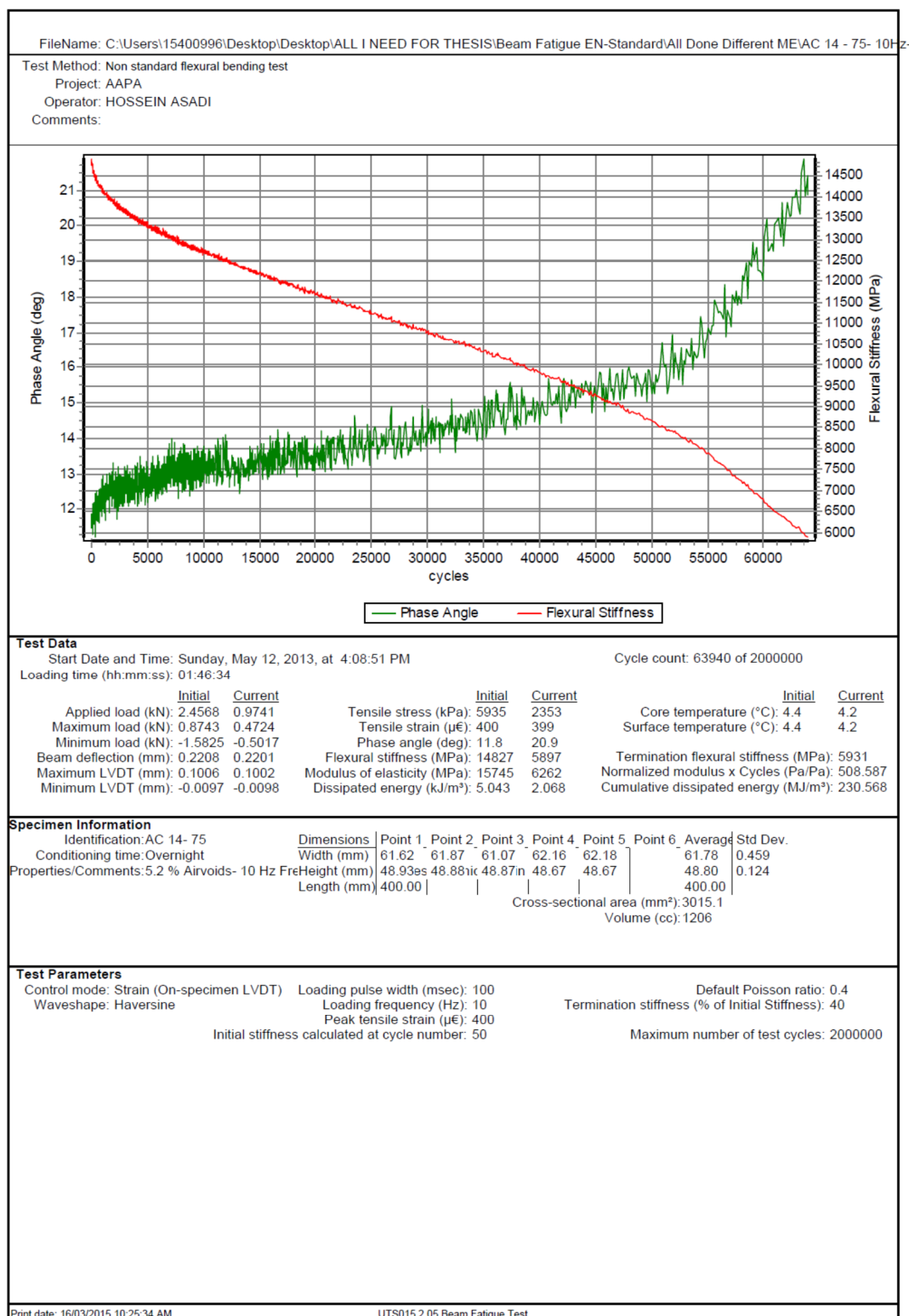


Figure A - 4. UTS 15 output for beam number 30

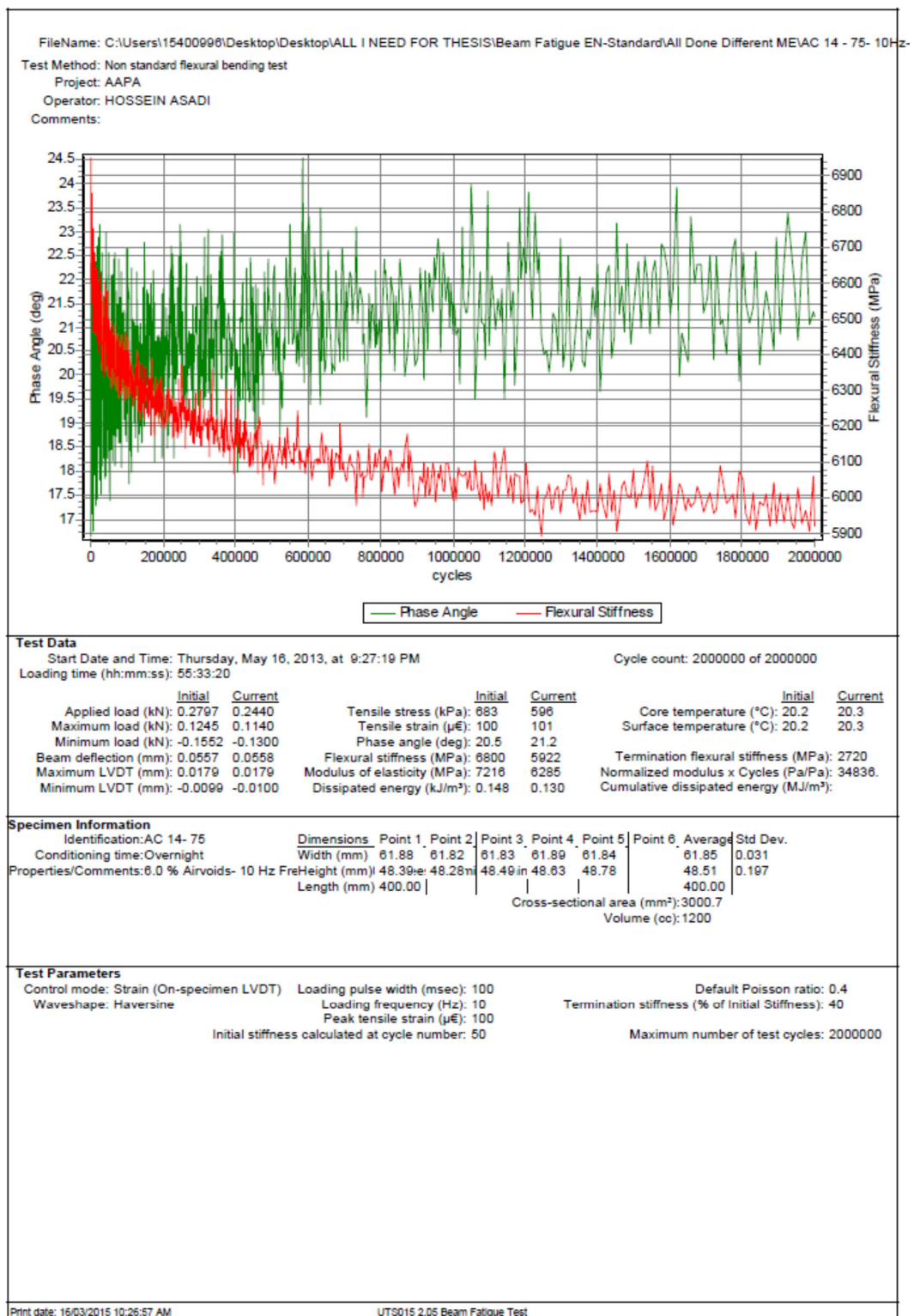


Figure A - 5. UTS 15 output for beam number 31

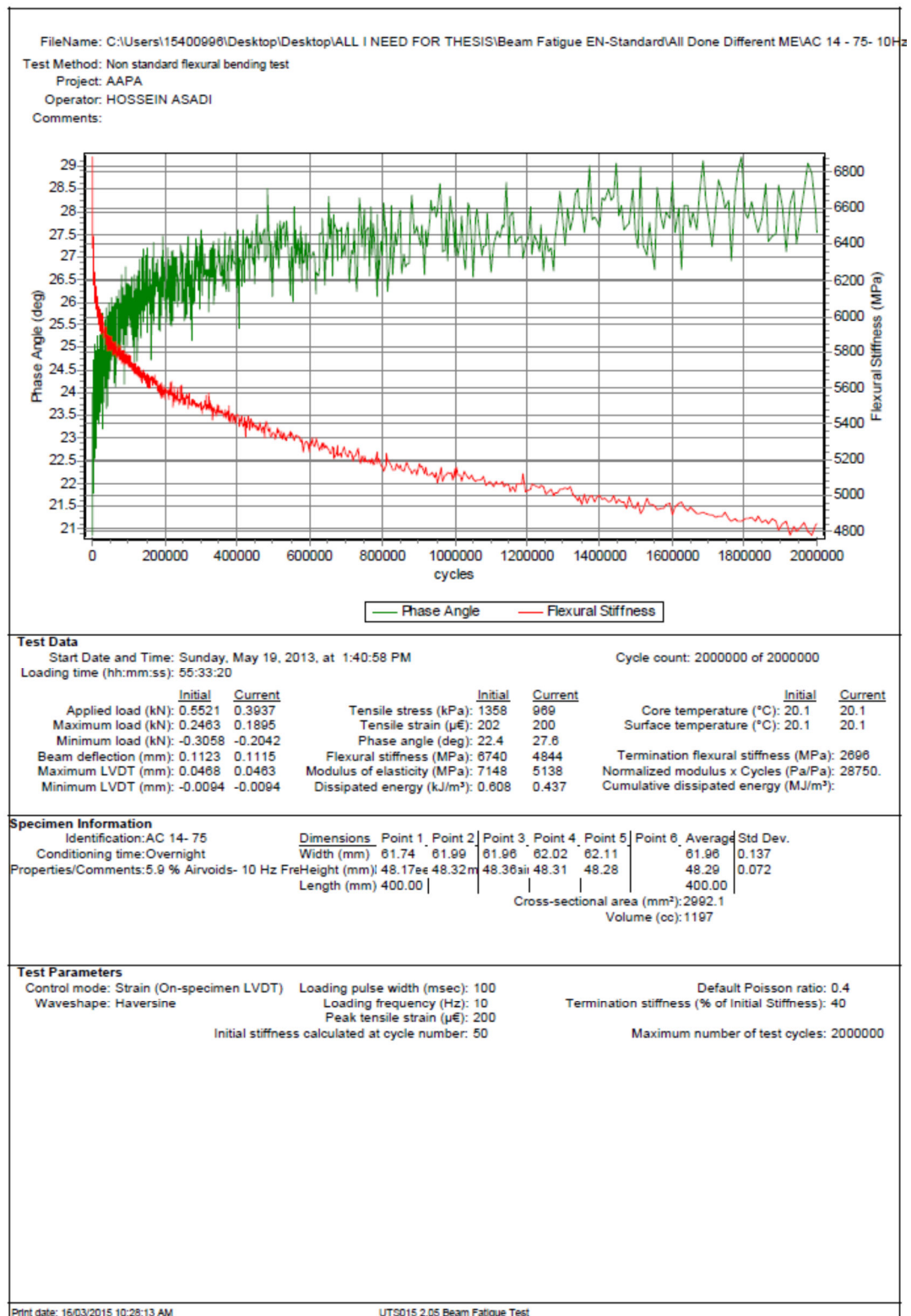


Figure A - 6. UTS 15 output for beam number 32

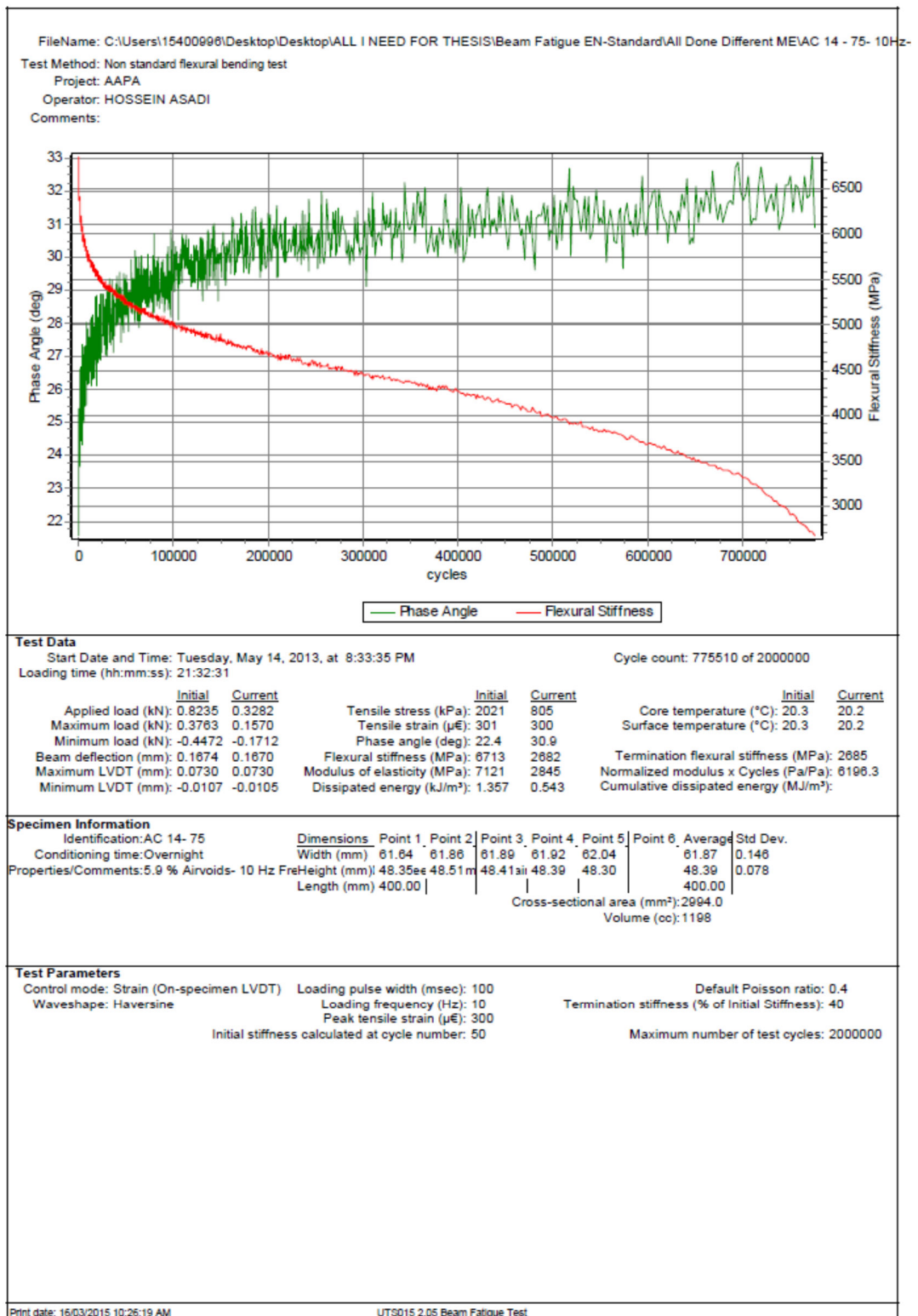


Figure A - 7. UTS 15 output for beam number 33

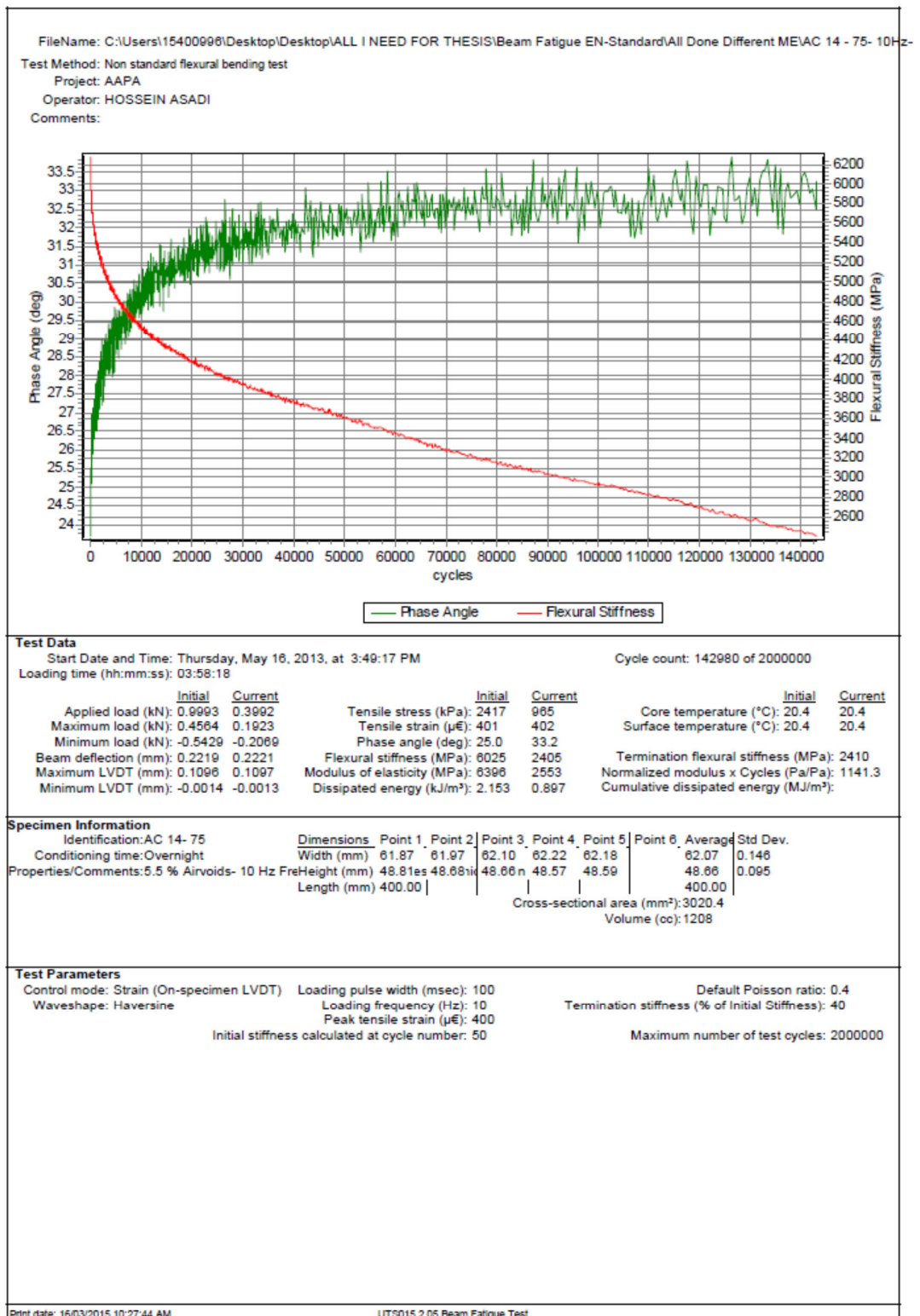


Figure A - 8. UTS 15 output for beam number 34

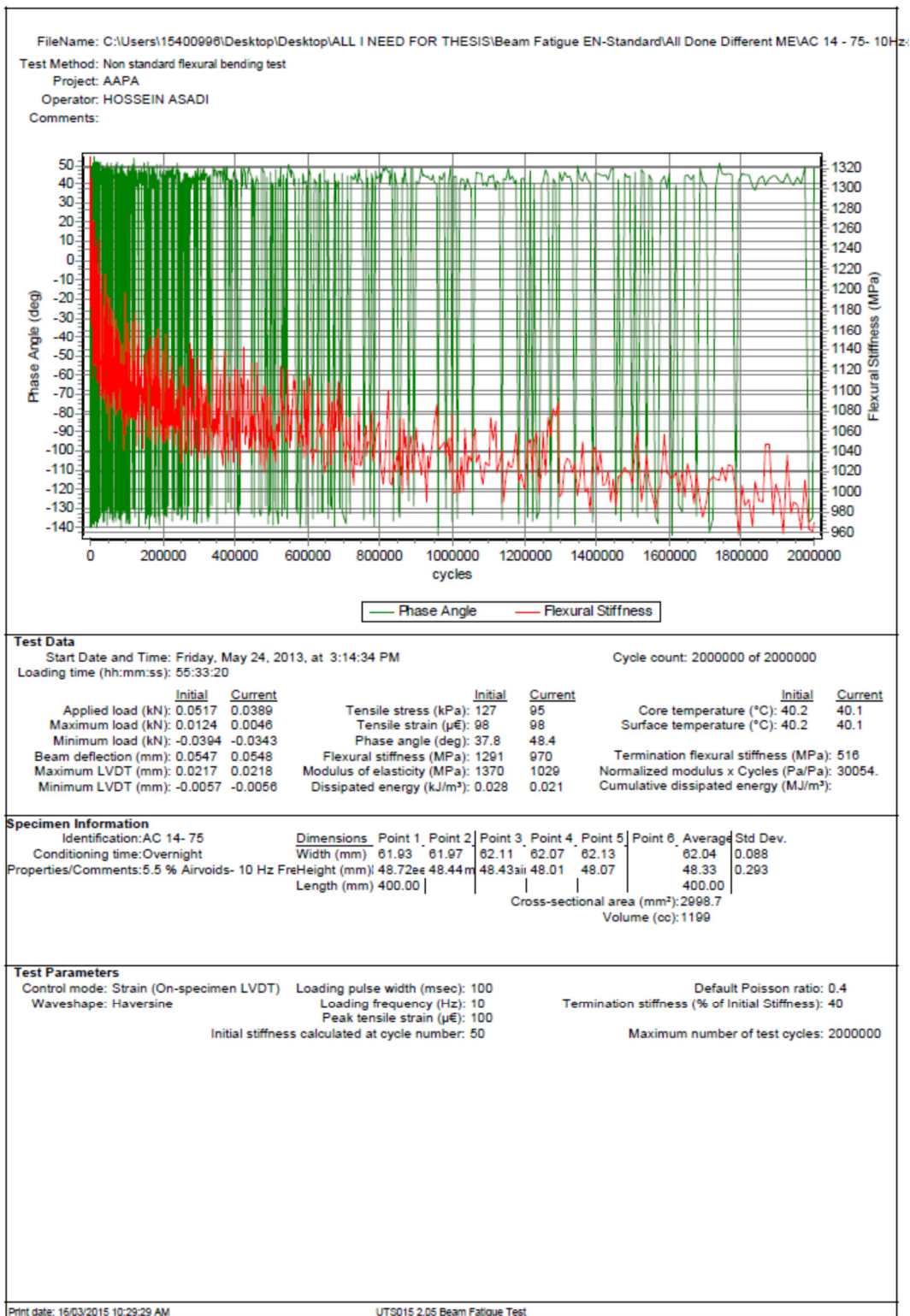


Figure A - 9. UTS 15 output for beam number 35

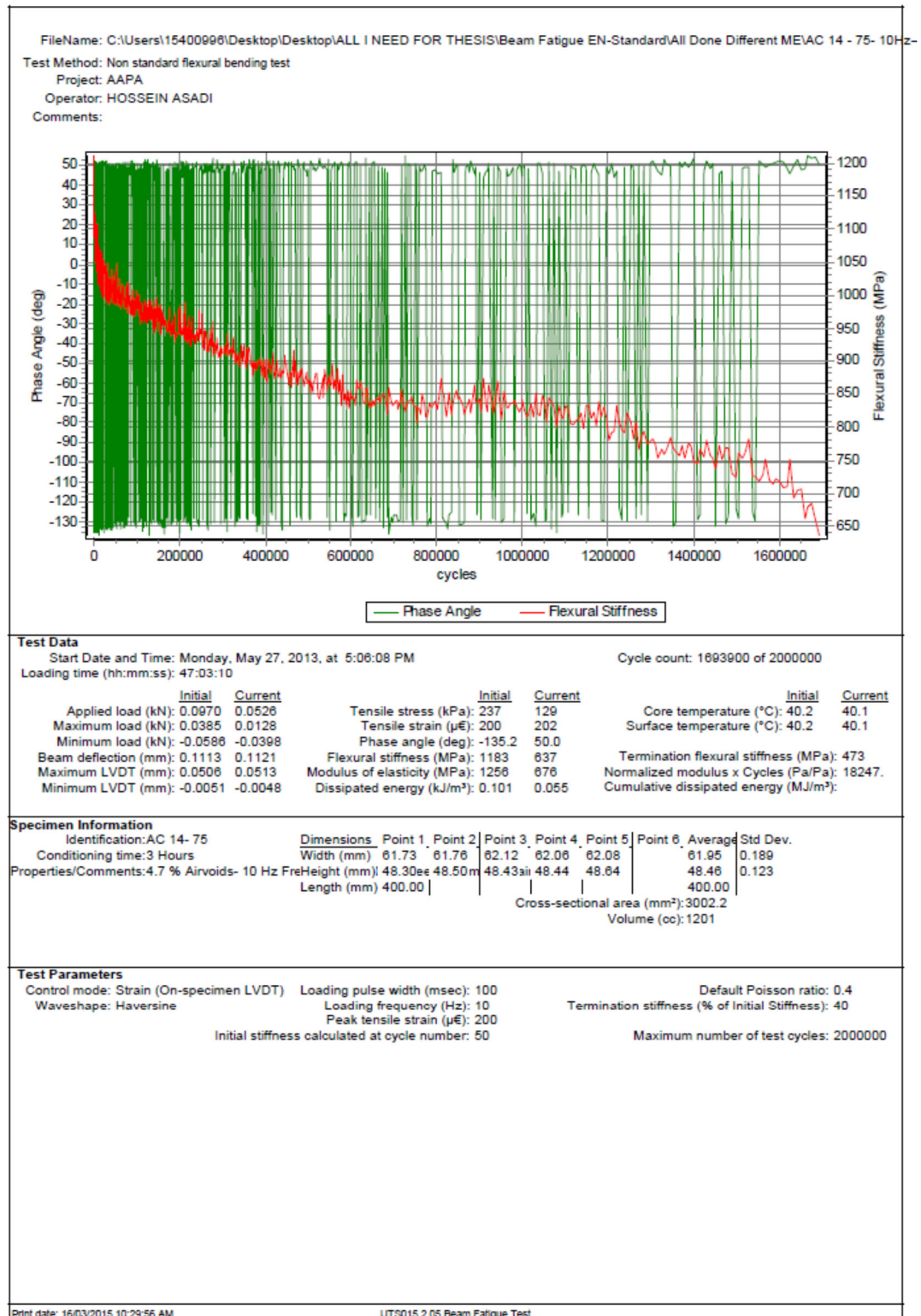


Figure A - 10. UTS 15 output for beam number 36

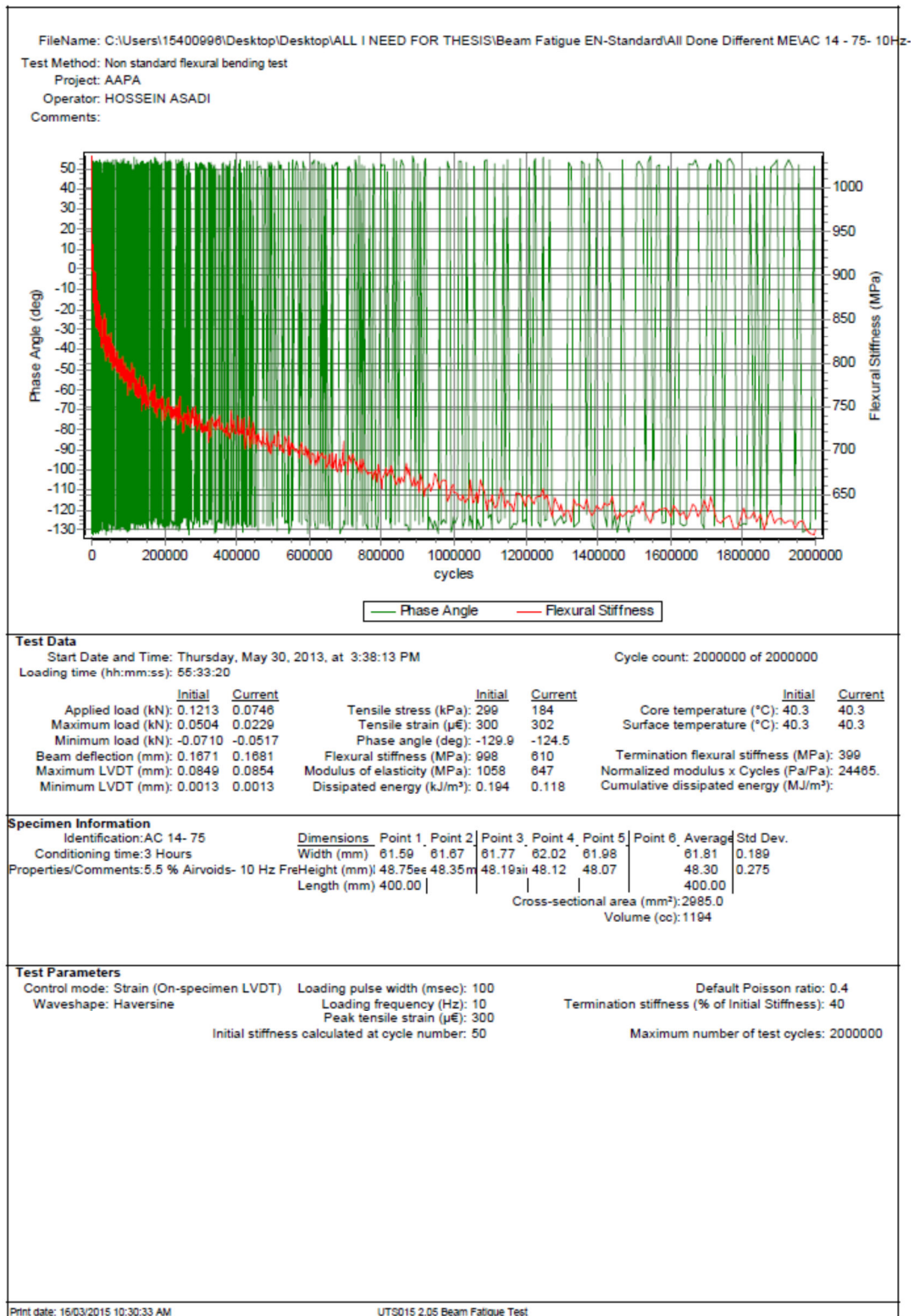


Figure A - 11. UTS 15 output for beam number 37

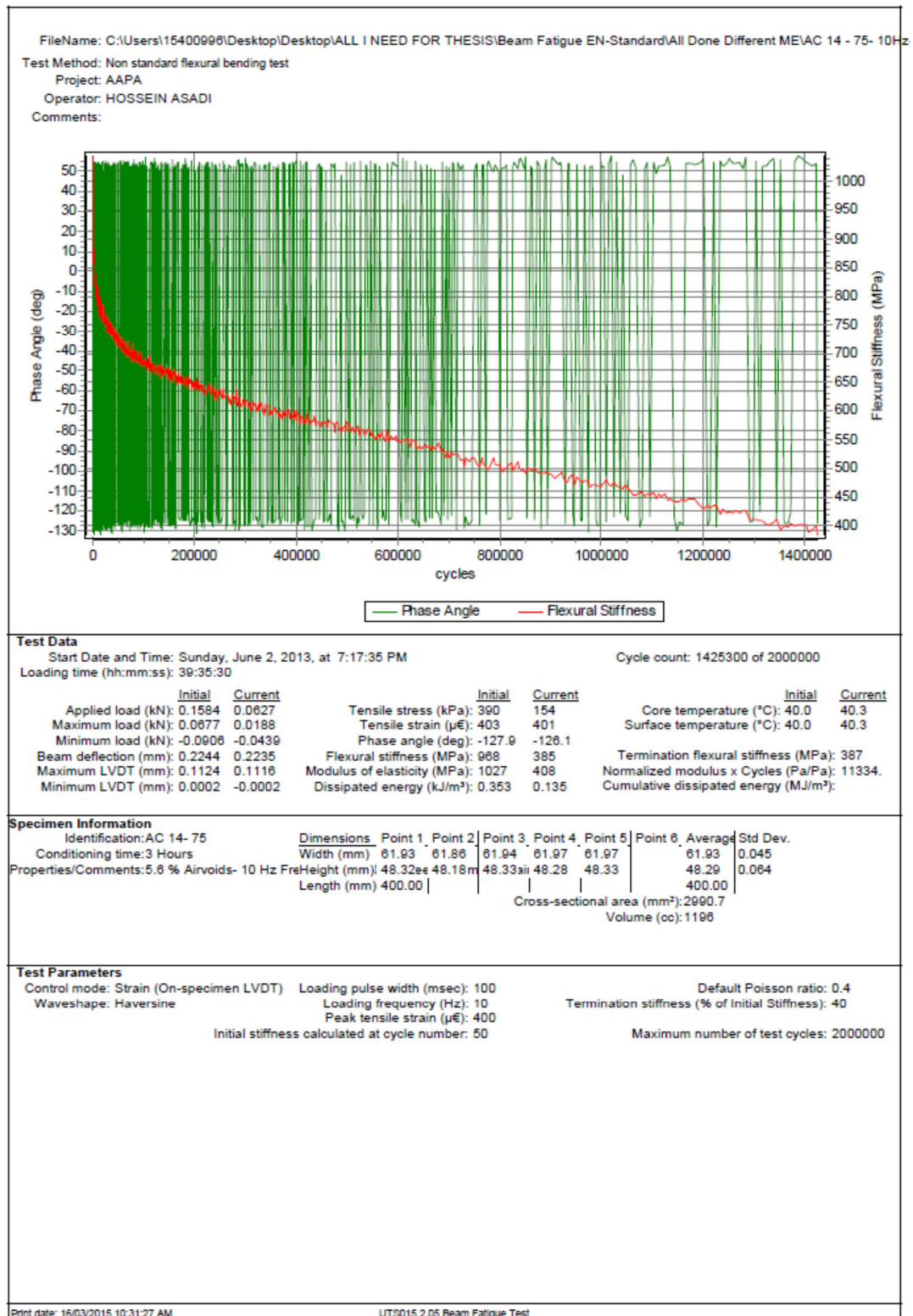


Figure A - 12. UTS 15 output for beam number 38

Appendix B

UTS18 OUTPUT IN APPROACH 3 FOR SINUSOIDAL LOADING

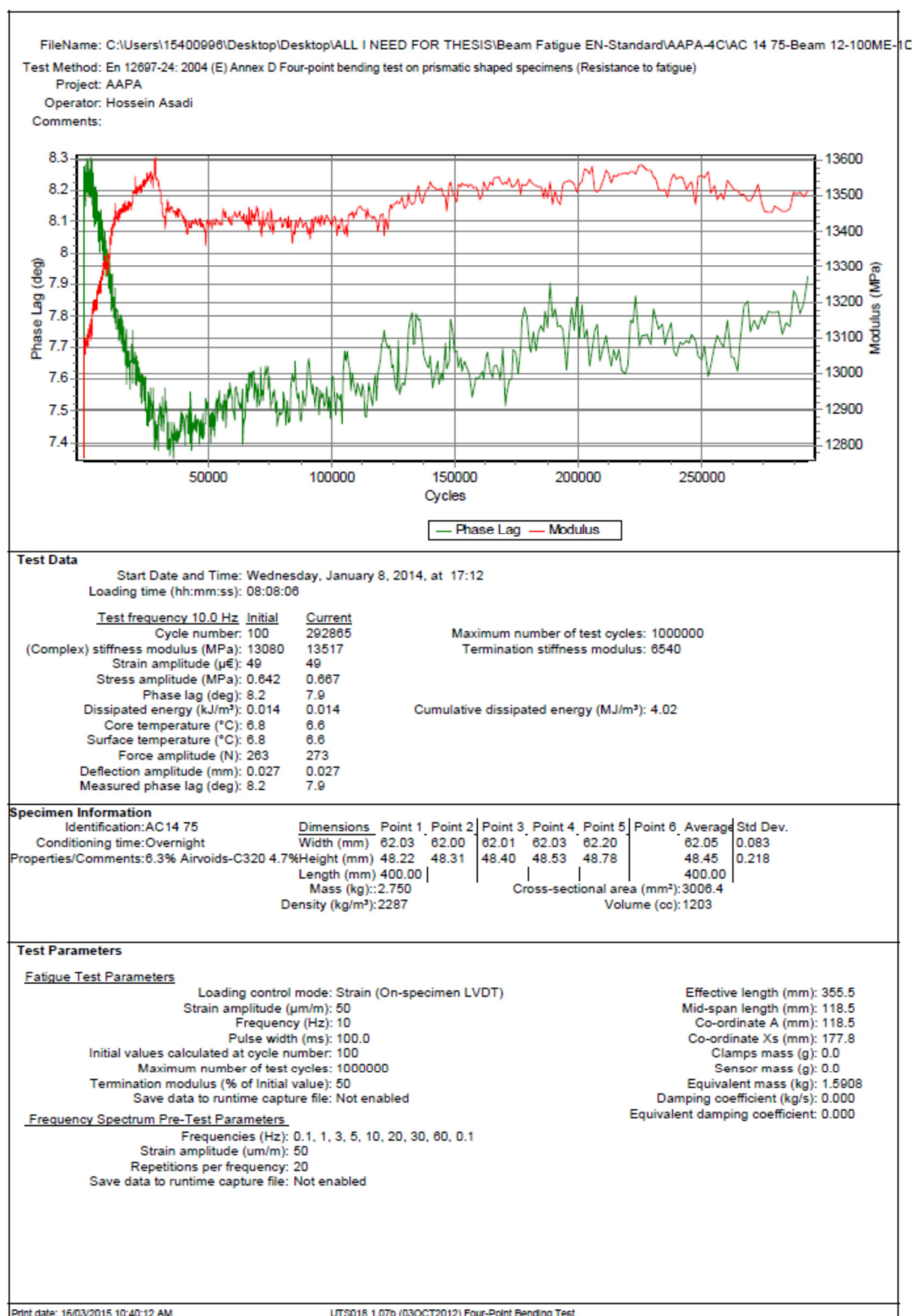


Figure B - 1. UTS 18 output for beam number 39

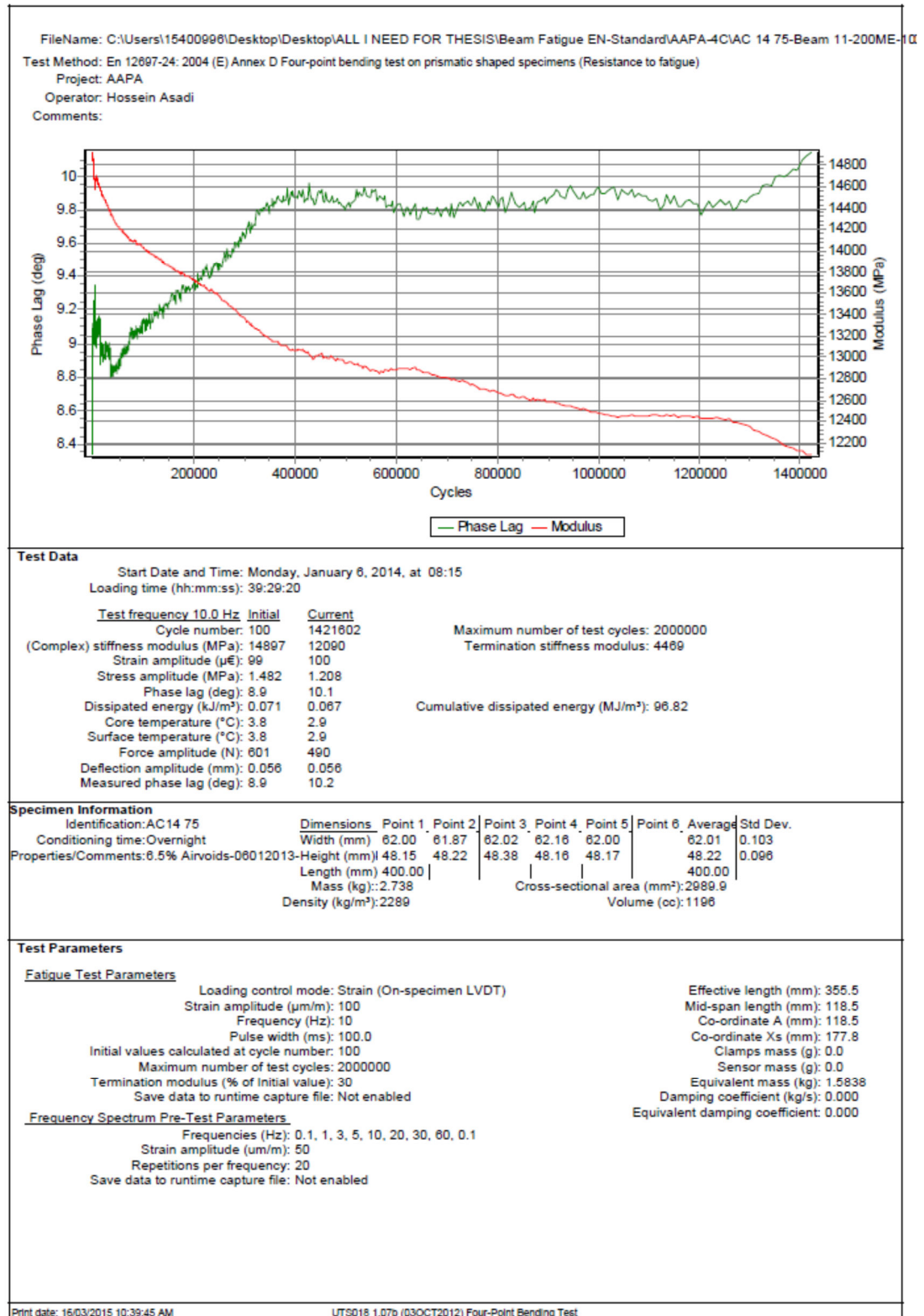


Figure B - 2. UTS 18 output for beam number 40

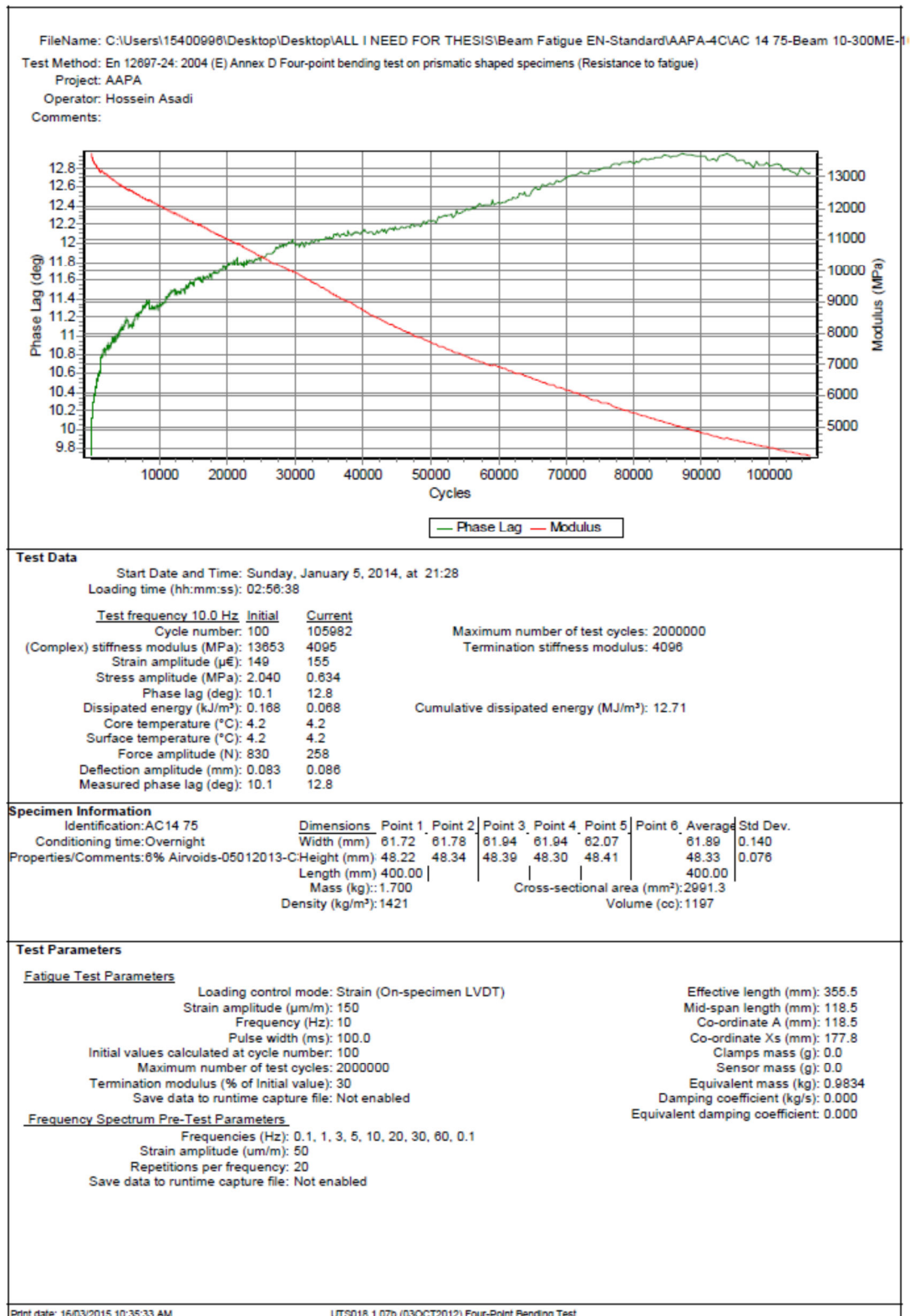


Figure B - 3. UTS 18 output for beam number 41

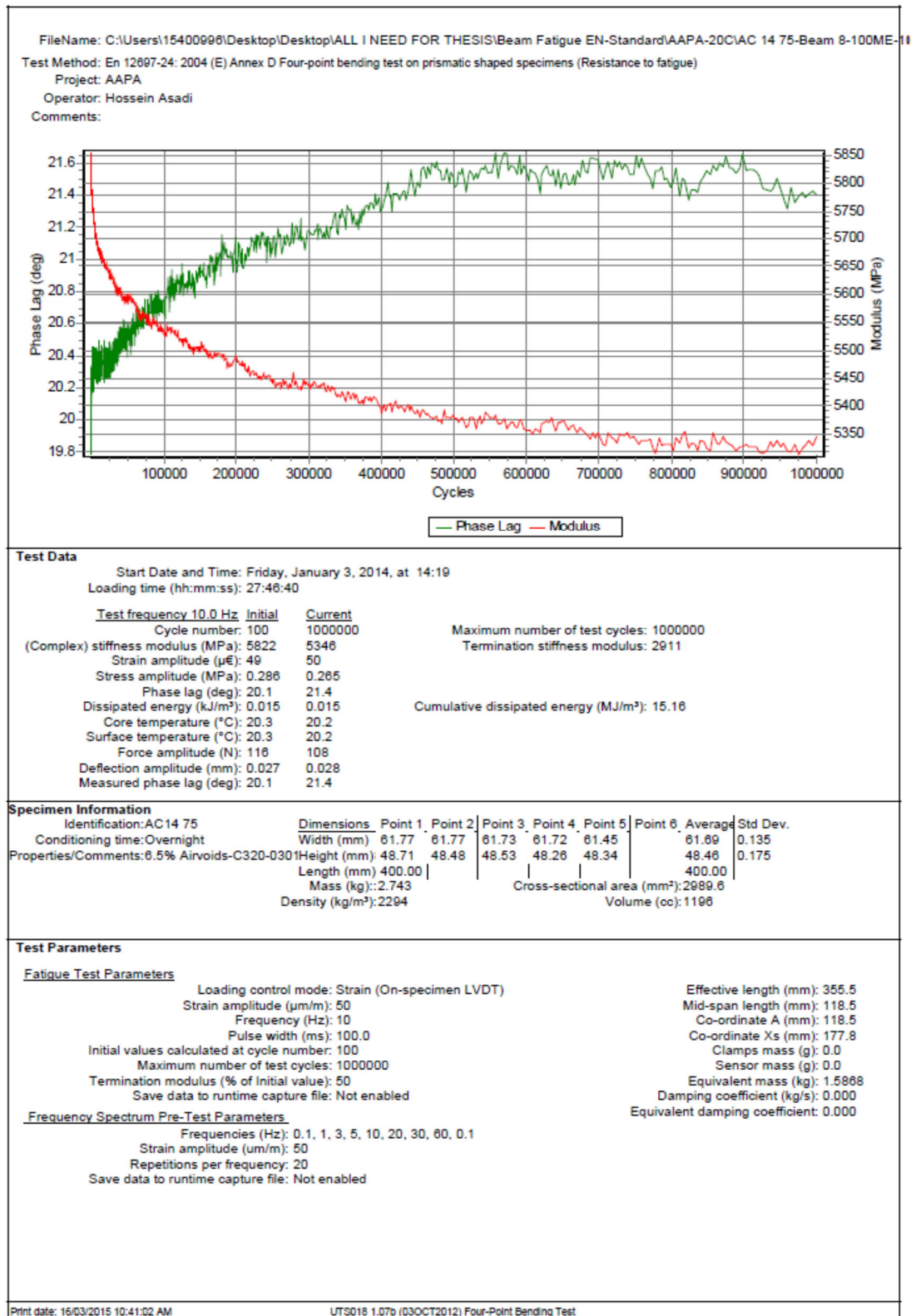


Figure B - 5. UTS 18 output for beam number 43

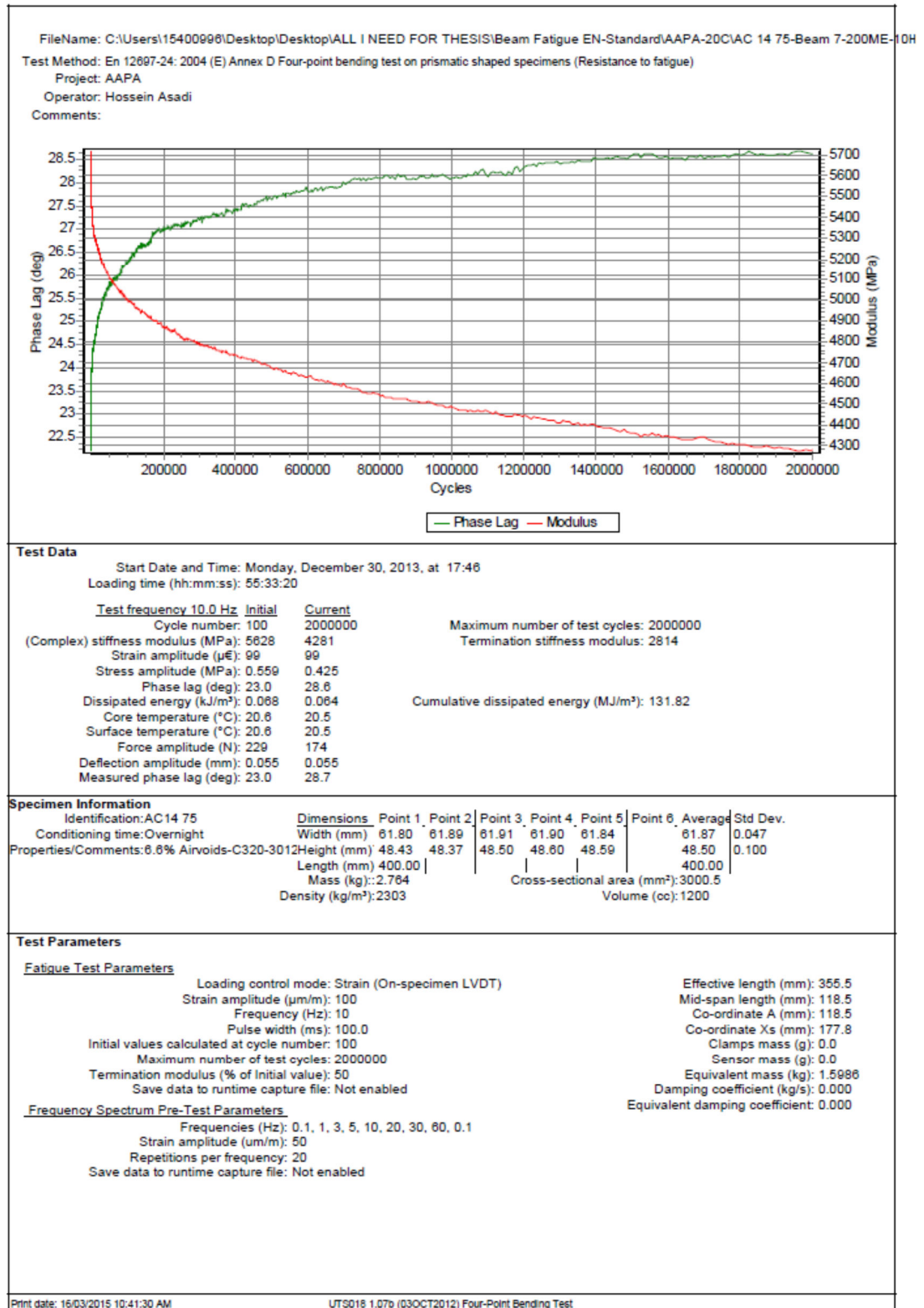


Figure B - 6. UTS 18 output for beam number 44

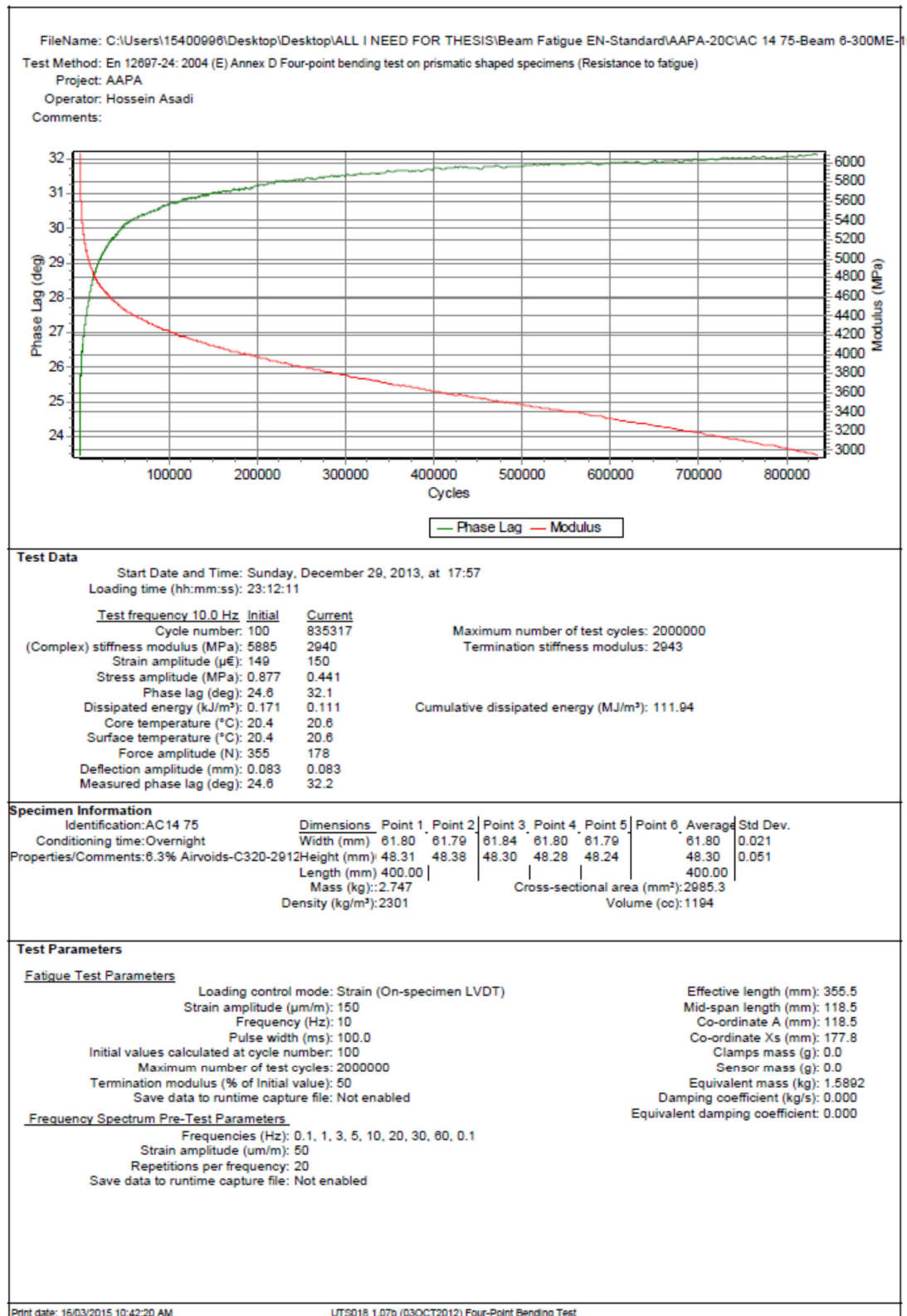


Figure B - 7. UTS 18 output for beam number 45

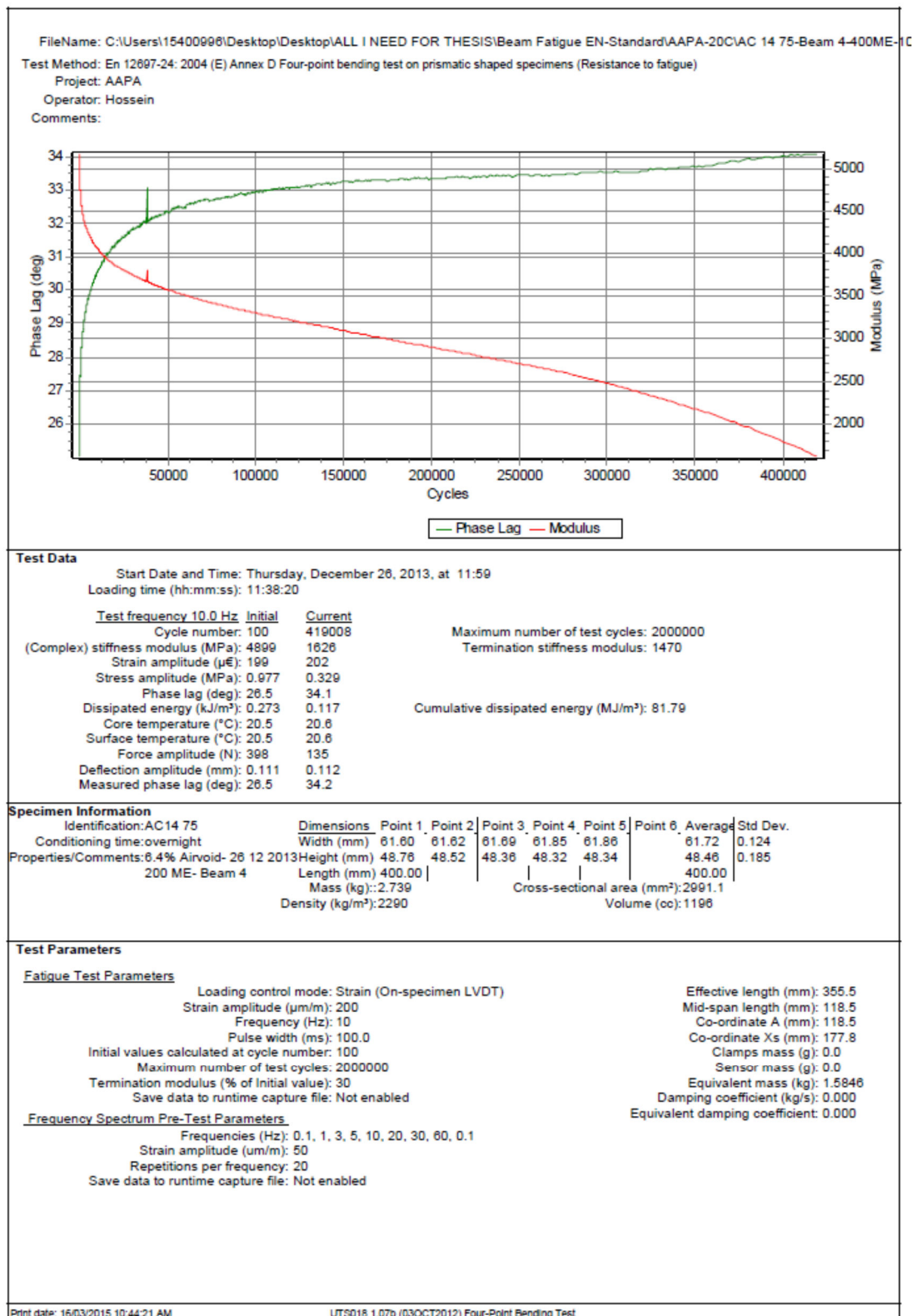


Figure B - 8. UTS 18 output for beam number 46

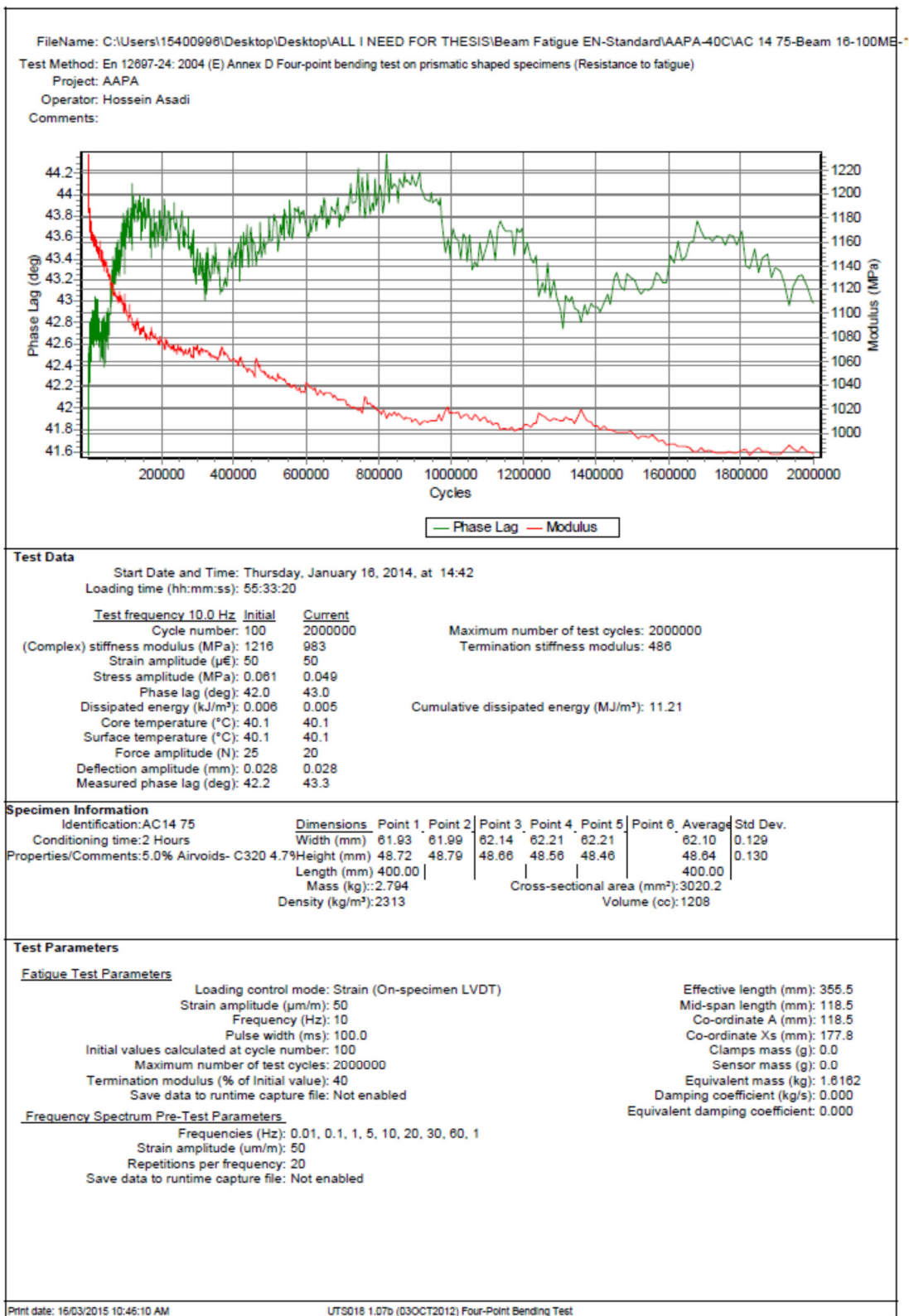


Figure B - 9. UTS 18 output for beam number47

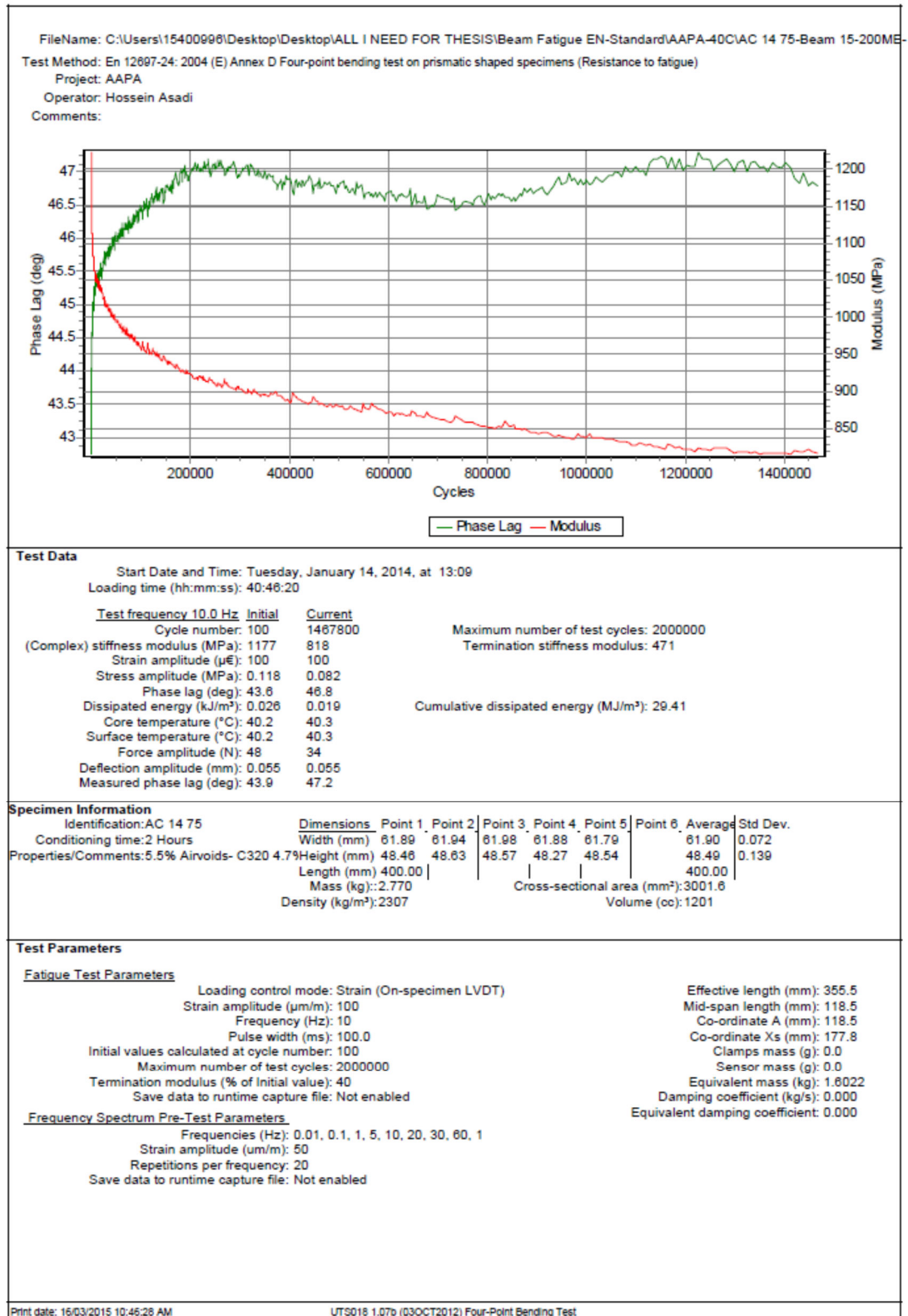


Figure B - 10. UTS 18 output for beam number 48

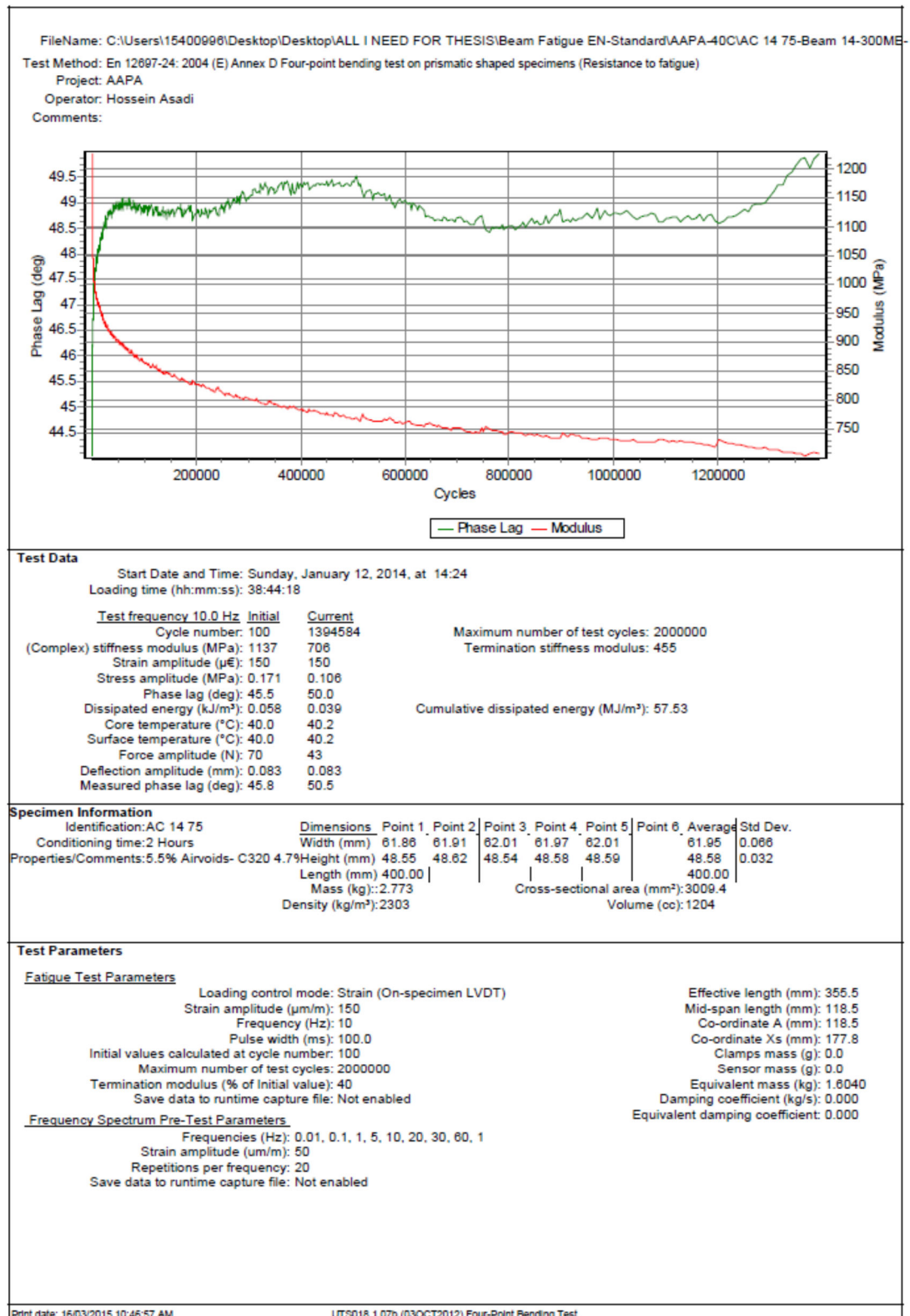


Figure B - 11. UTS 18 output for beam number 49

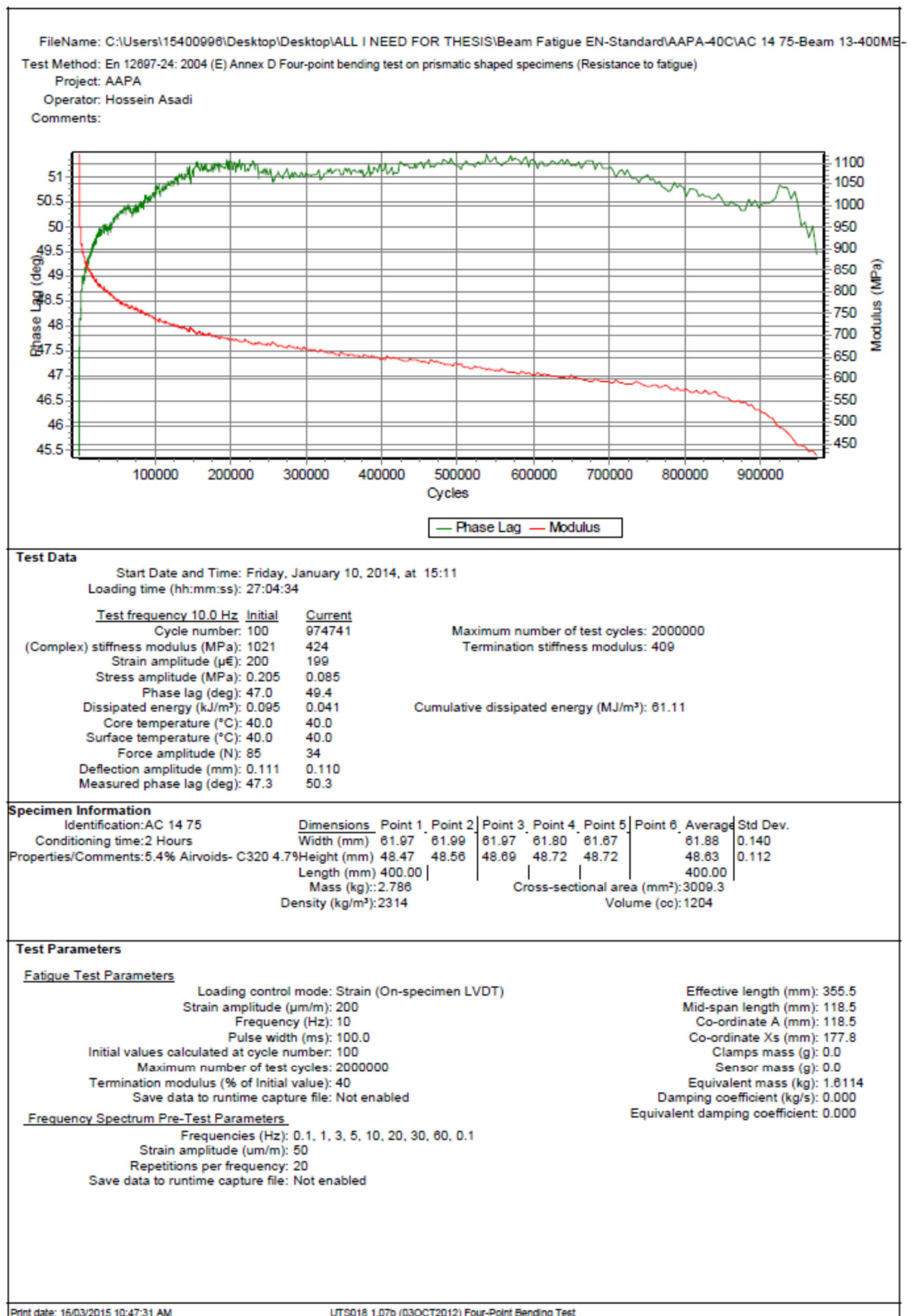


Figure B - 12. UTS 18 output for beam number 50

CURVE FITTING IN APPROACH 3
FOR SCENARIO1 AND SCENARIO2

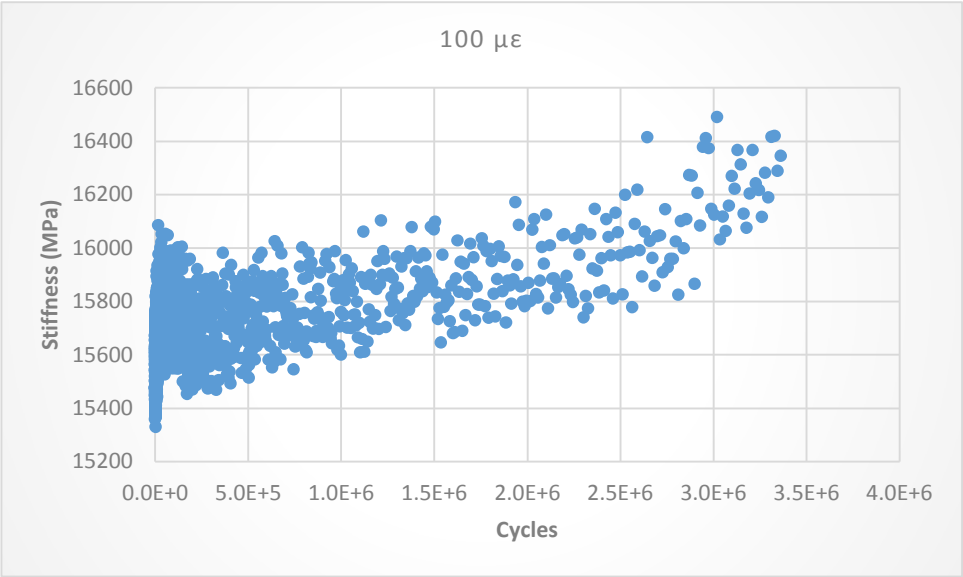


Figure C - 1. Haversine loading, Beam 39, 4°C

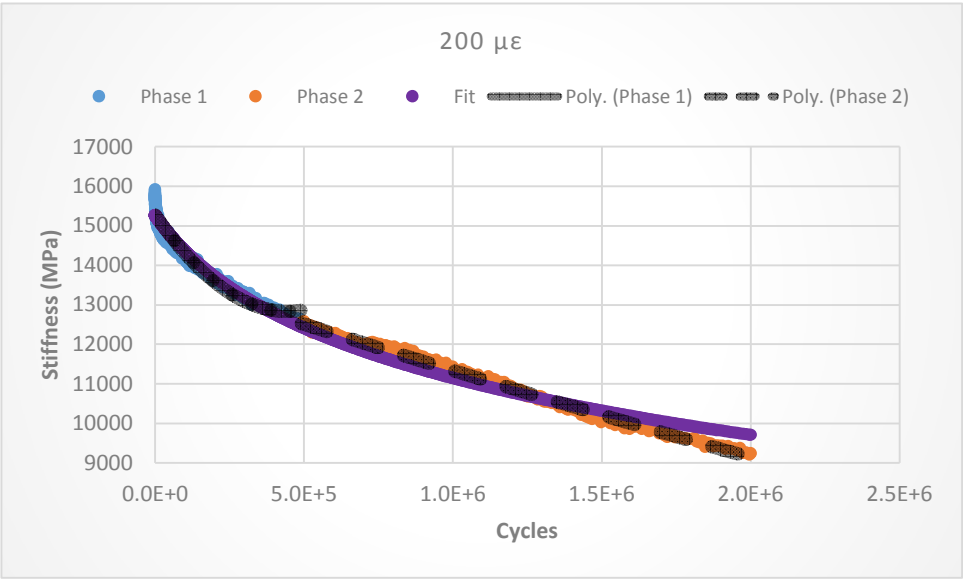


Figure C - 2. Haversine loading, Beam 40, 4°C

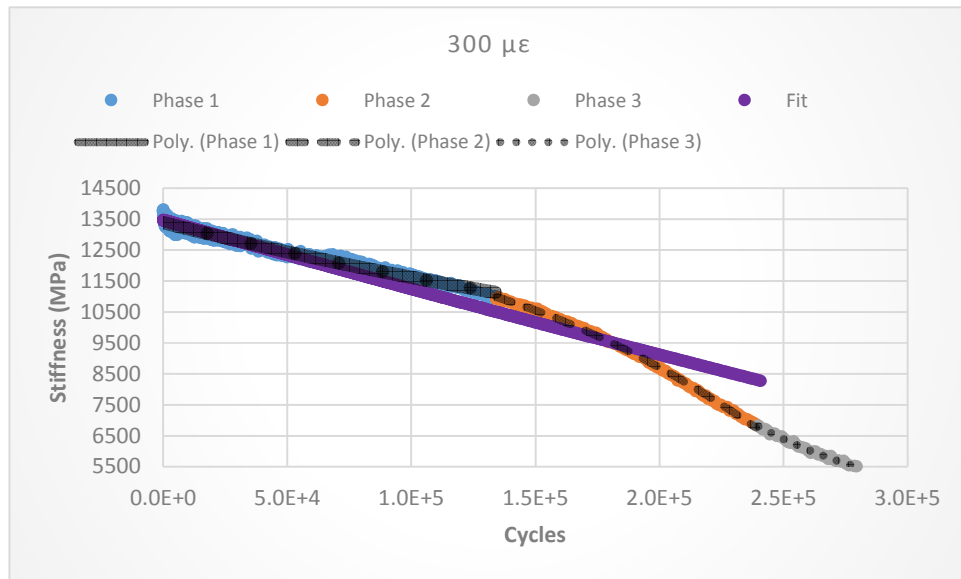


Figure C - 3. Haversine loading, Beam 41, 4°C

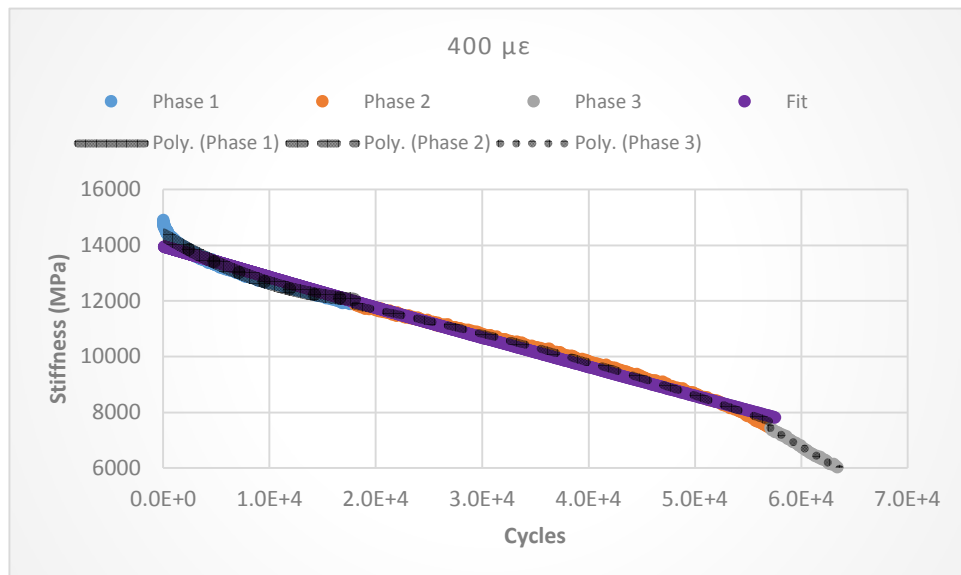


Figure C - 4. Haversine loading, Beam 42, 4°C

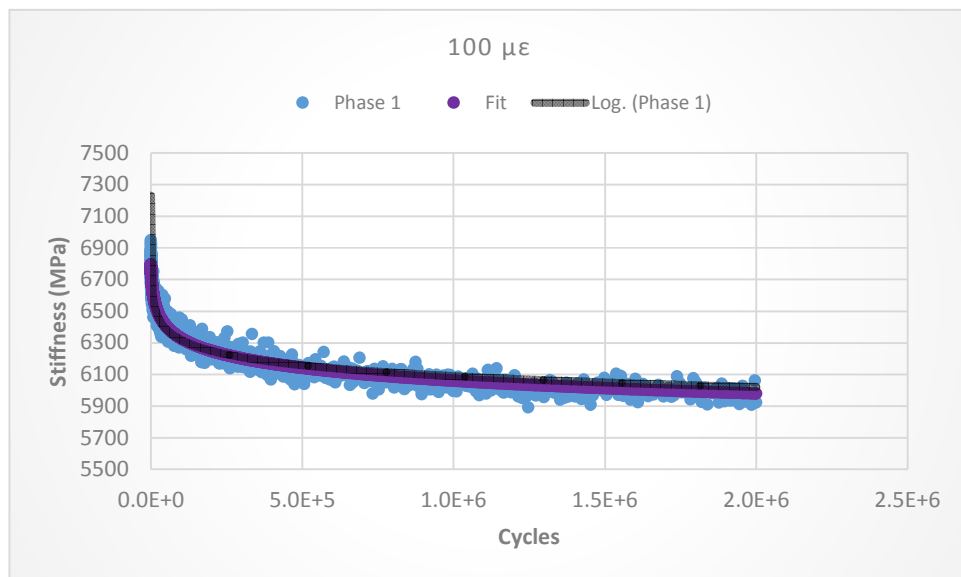


Figure C - 5. Haversine loading, Beam 43, 20°C

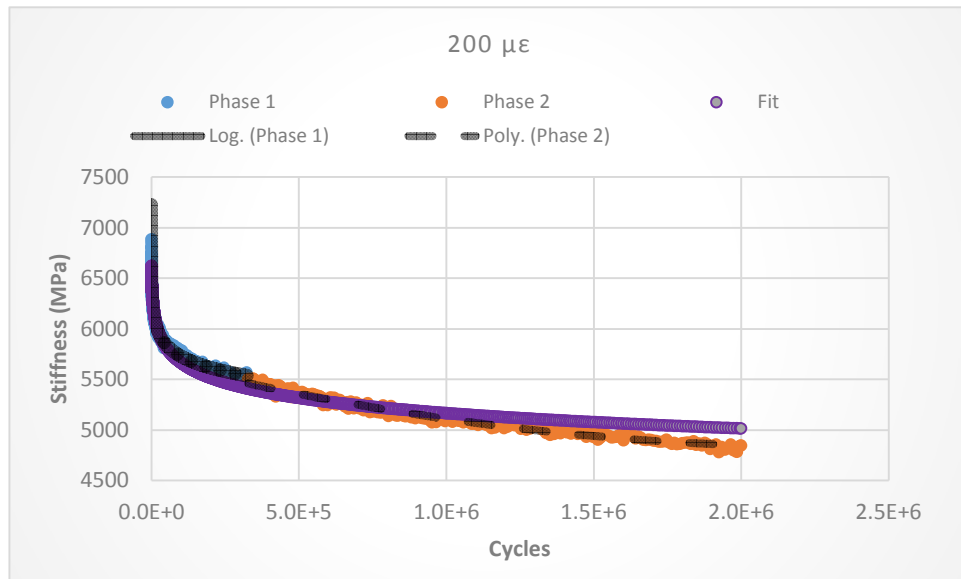


Figure C - 6. Haversine loading, Beam 44, 20°C

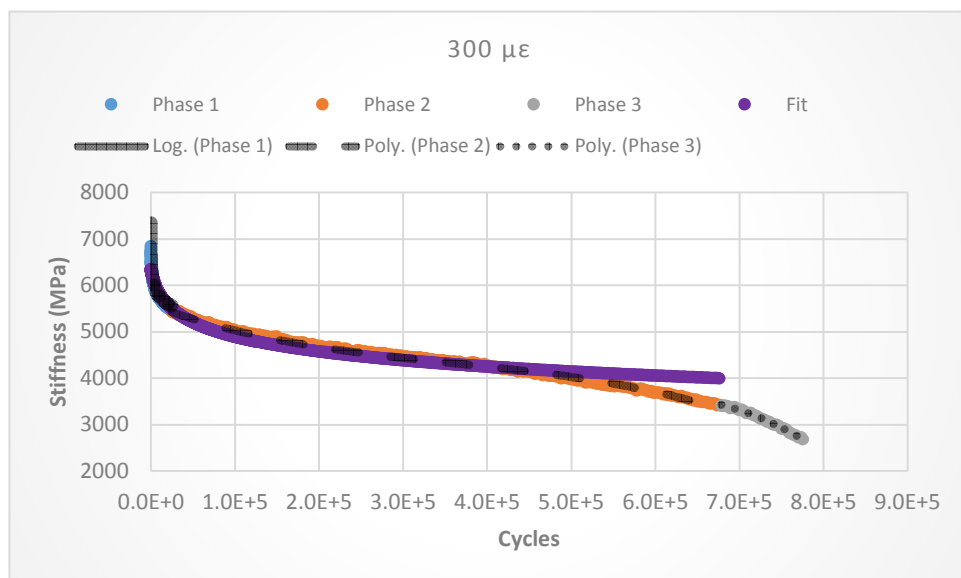


Figure C - 7. Haversine loading, Beam 45, 20°C

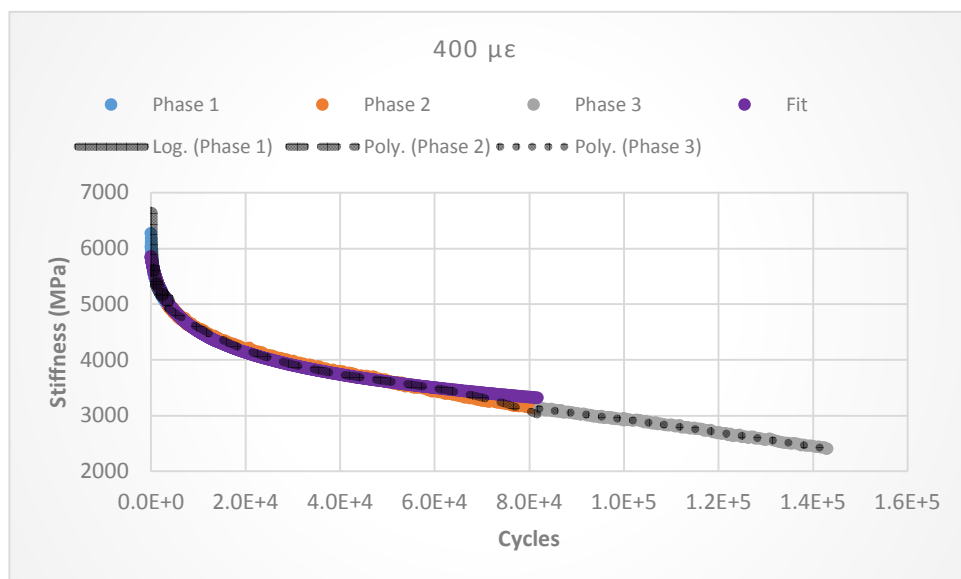


Figure C - 8. Haversine loading, Beam 46, 20°C

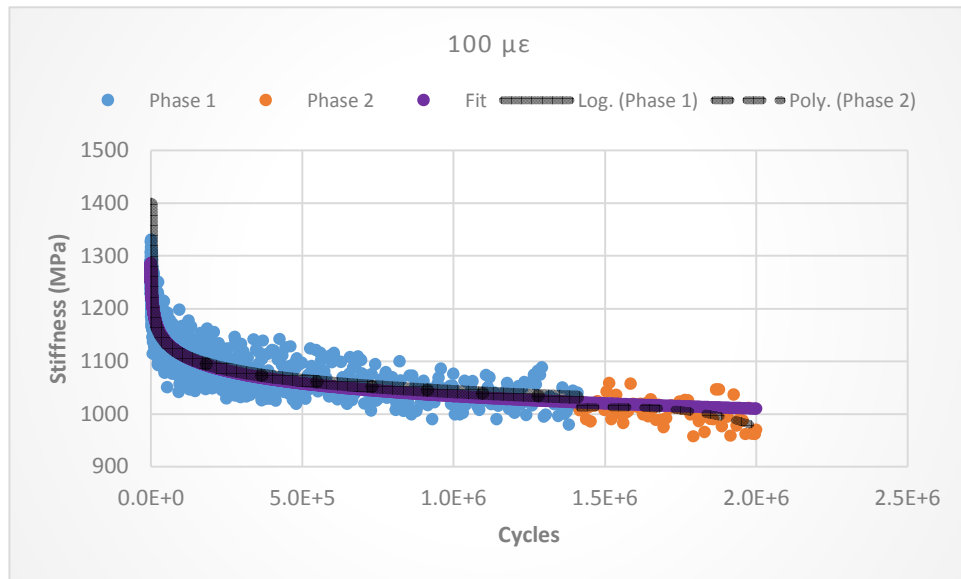


Figure C - 9. Haversine loading, Beam 47, 40°C

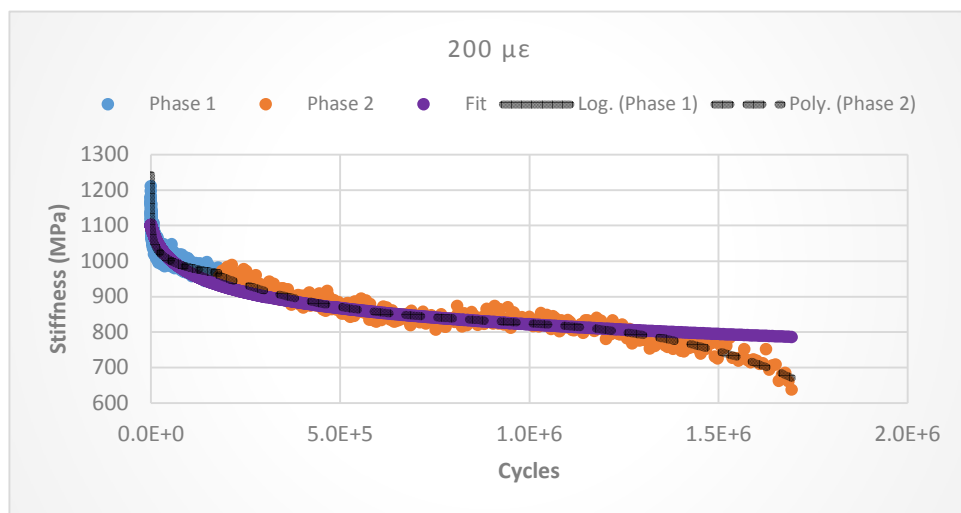


Figure C - 10. Haversine loading, Beam 48, 40°C

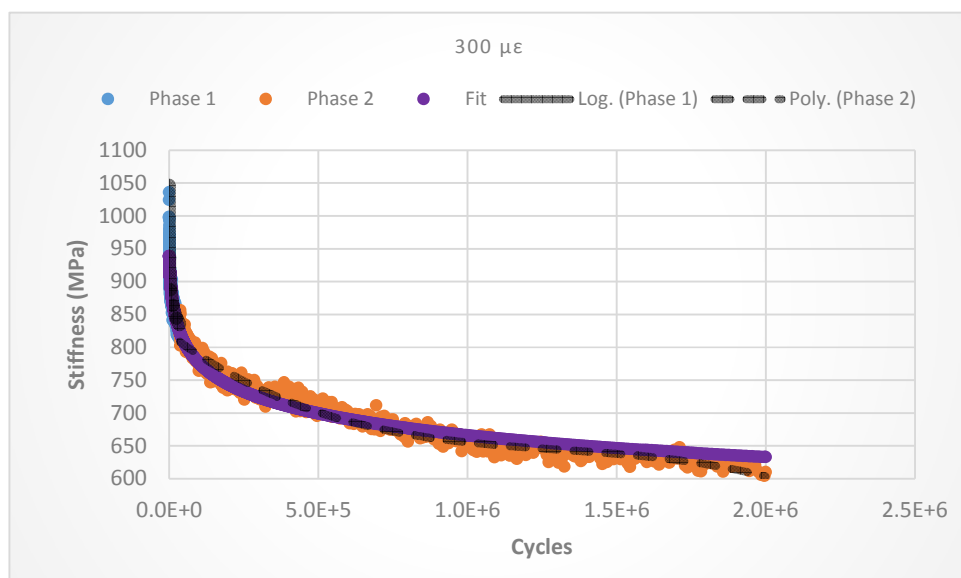


Figure C - 11. Haversine loading, Beam 49, 40°C

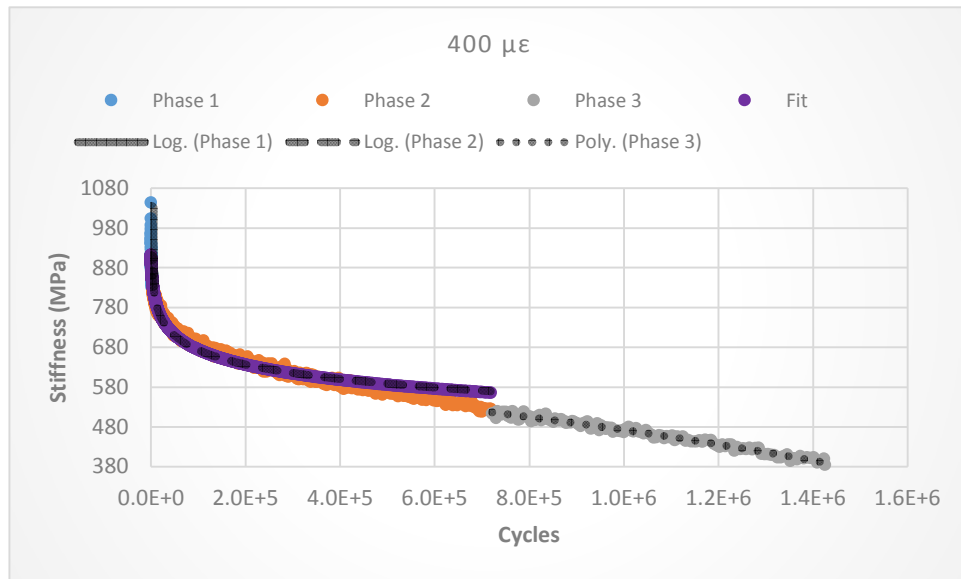


Figure C - 12. Haversine loading, Beam 50, 40°C

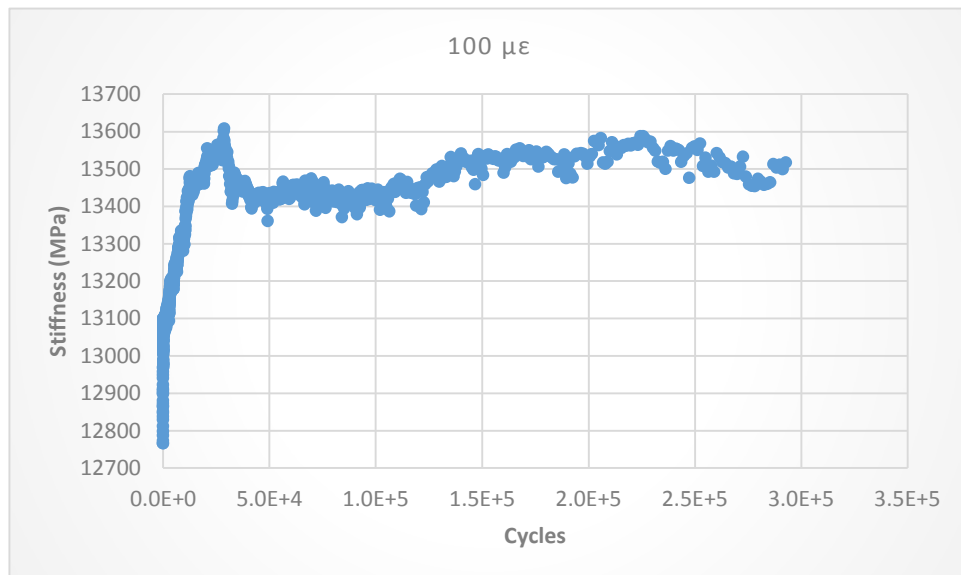


Figure C - 13. Sinusoidal loading, Beam 51, 4°C

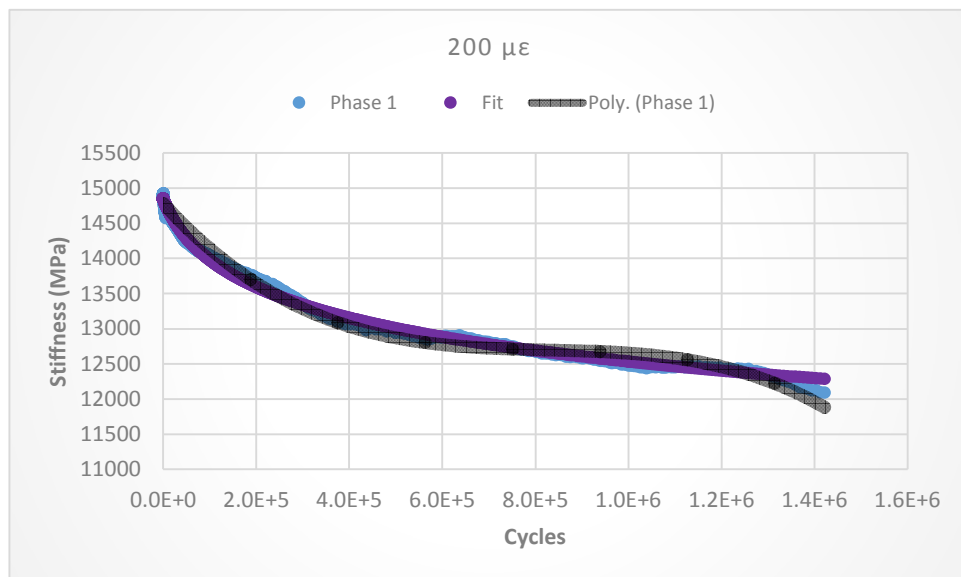


Figure C - 14. Sinusoidal loading, Beam 52, 4°C

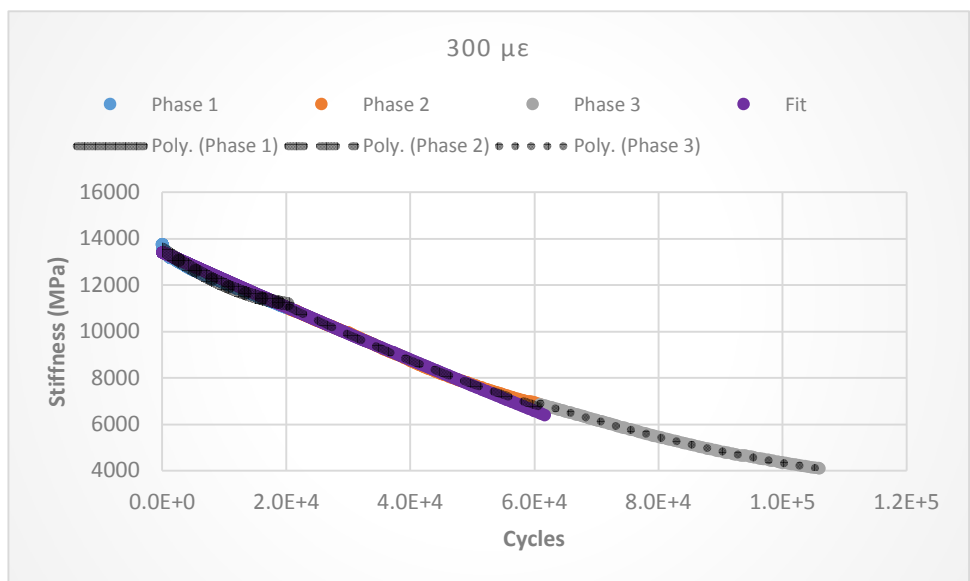


Figure C - 15. Sinusoidal loading, Beam 53, 4°C

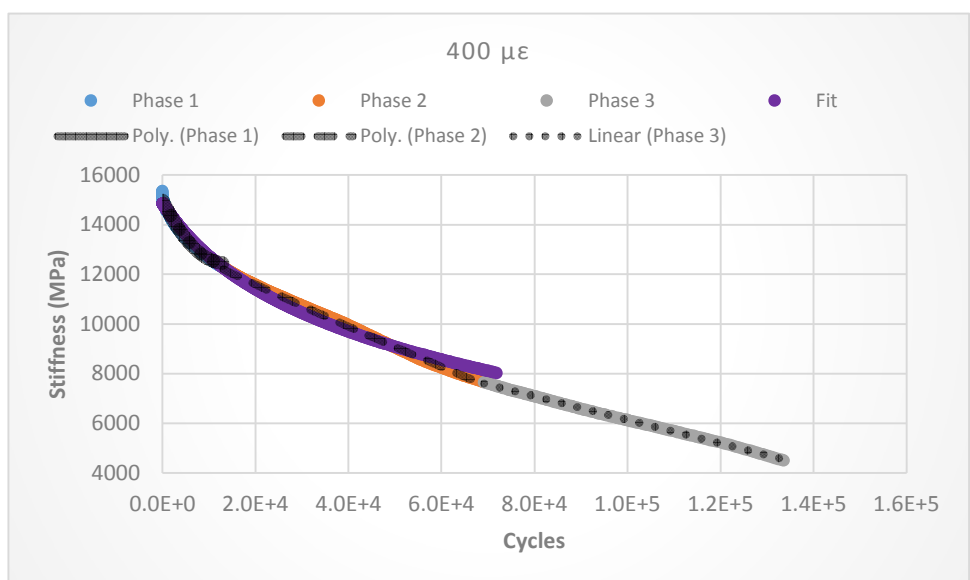


Figure C - 16. Sinusoidal loading, Beam 54, 4°C

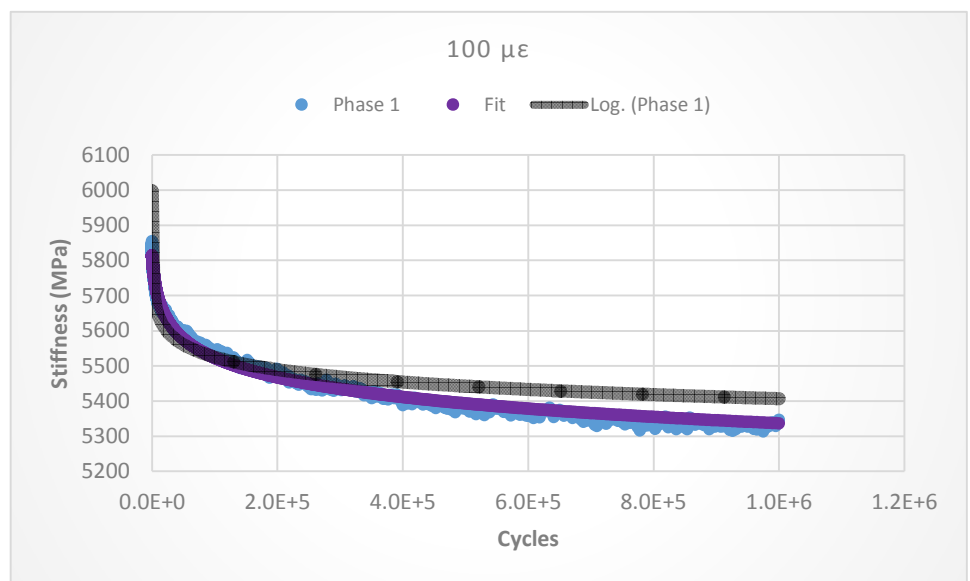


Figure C - 17. Sinusoidal loading, Beam 55, 20°C

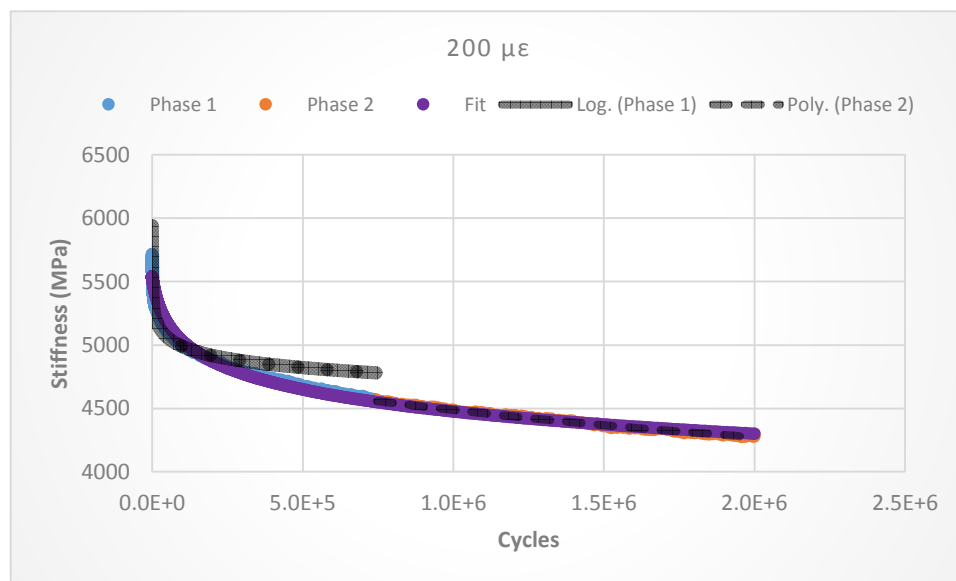


Figure C - 18. Sinusoidal loading, Beam 56, 20°C

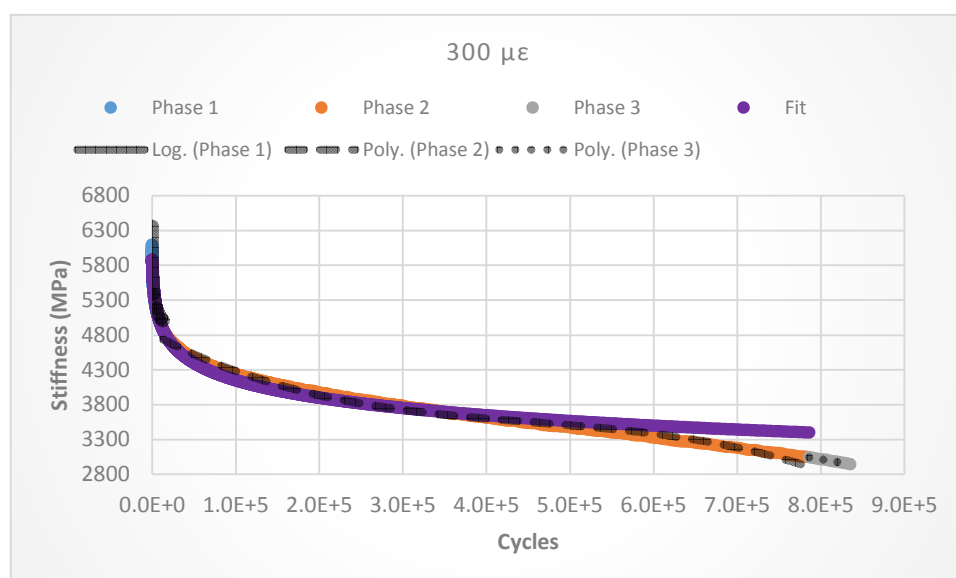


Figure C - 19. Sinusoidal loading, Beam 57, 20°C

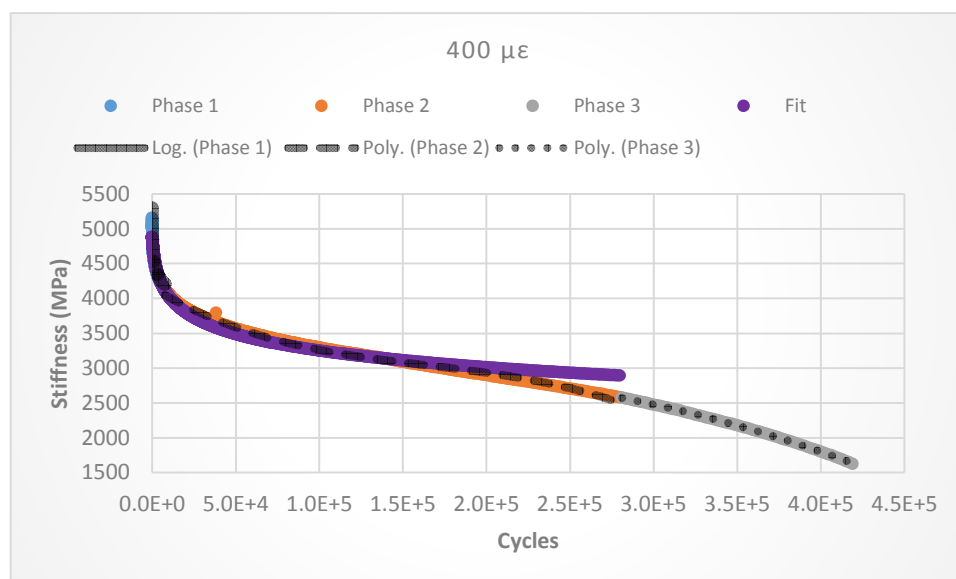


Figure C - 20. Sinusoidal loading, Beam 58, 20°C

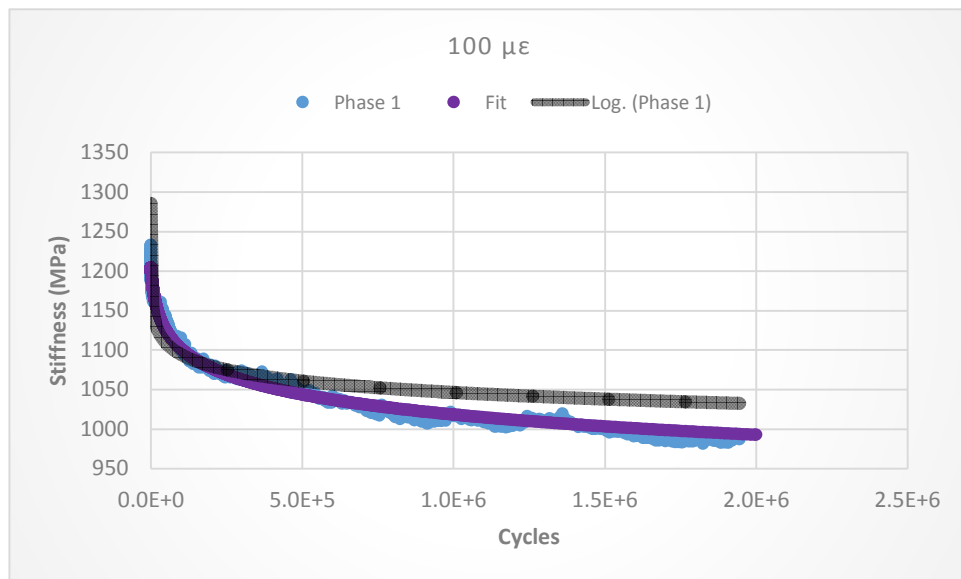


Figure C - 21. Sinusoidal loading, Beam 59, 40°C

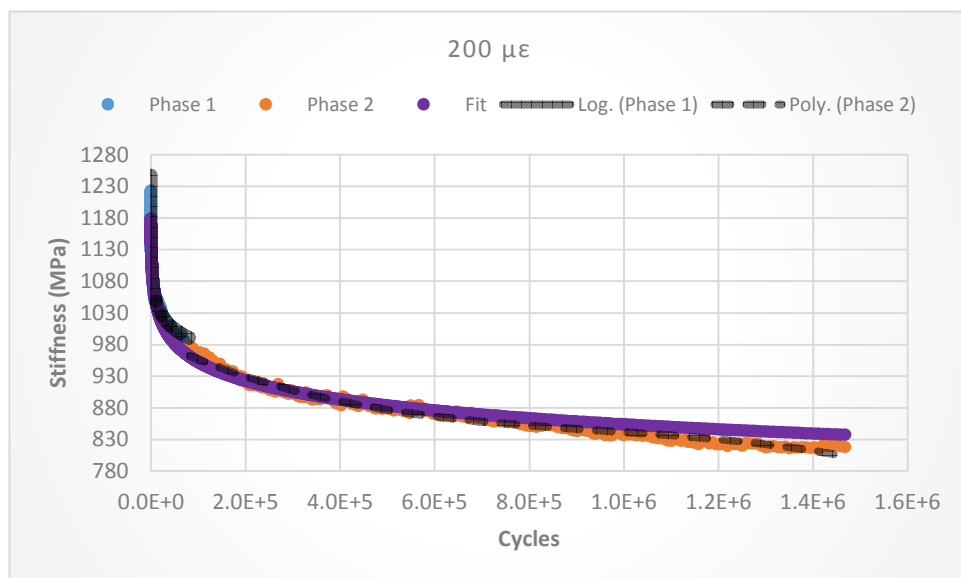


Figure C - 22. Sinusoidal loading, Beam 60, 40°C

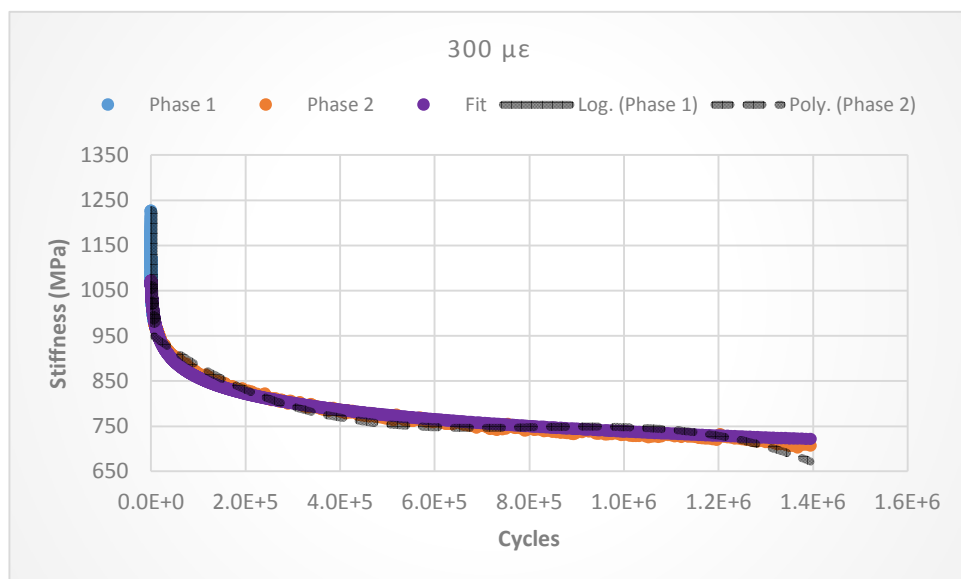


Figure C - 23. Sinusoidal loading, Beam 61, 40°C

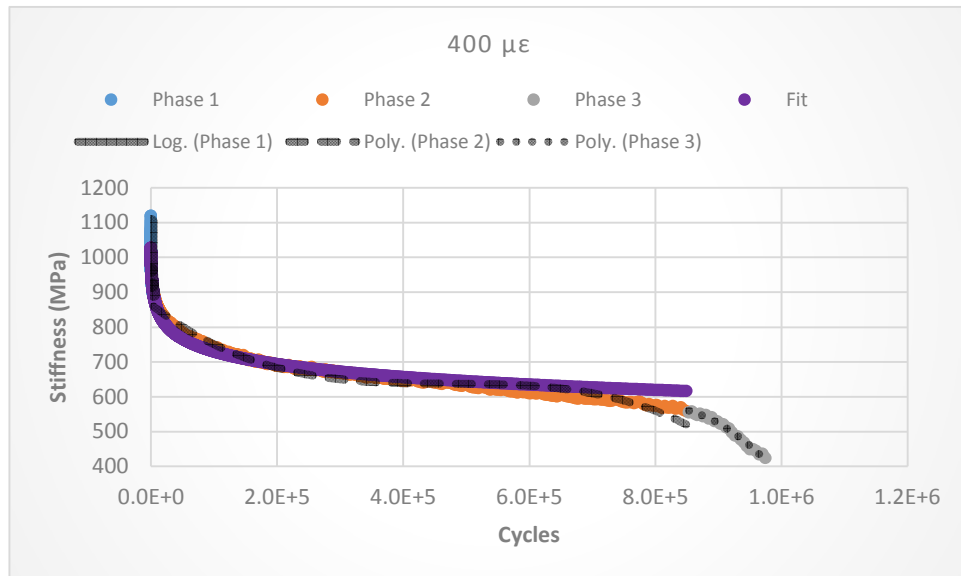


Figure C - 24. Sinusoidal loading, Beam 62, 40°C



Figure D - 1. Three steps in Approach 4, 25Hz, 4°C, Beam number 51

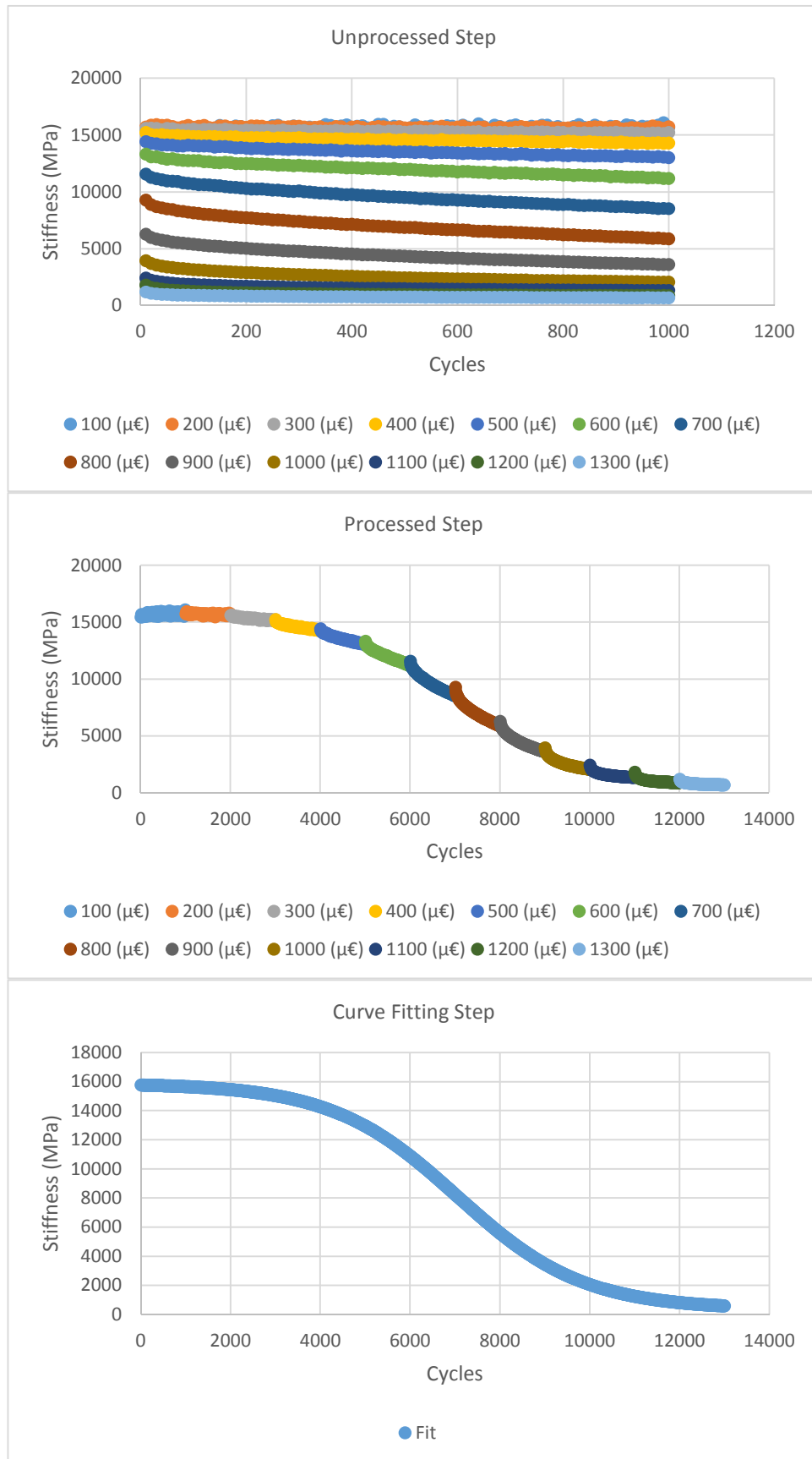


Figure D - 2. Three steps in Approach 4, 10Hz, 4°C, Beam number 52

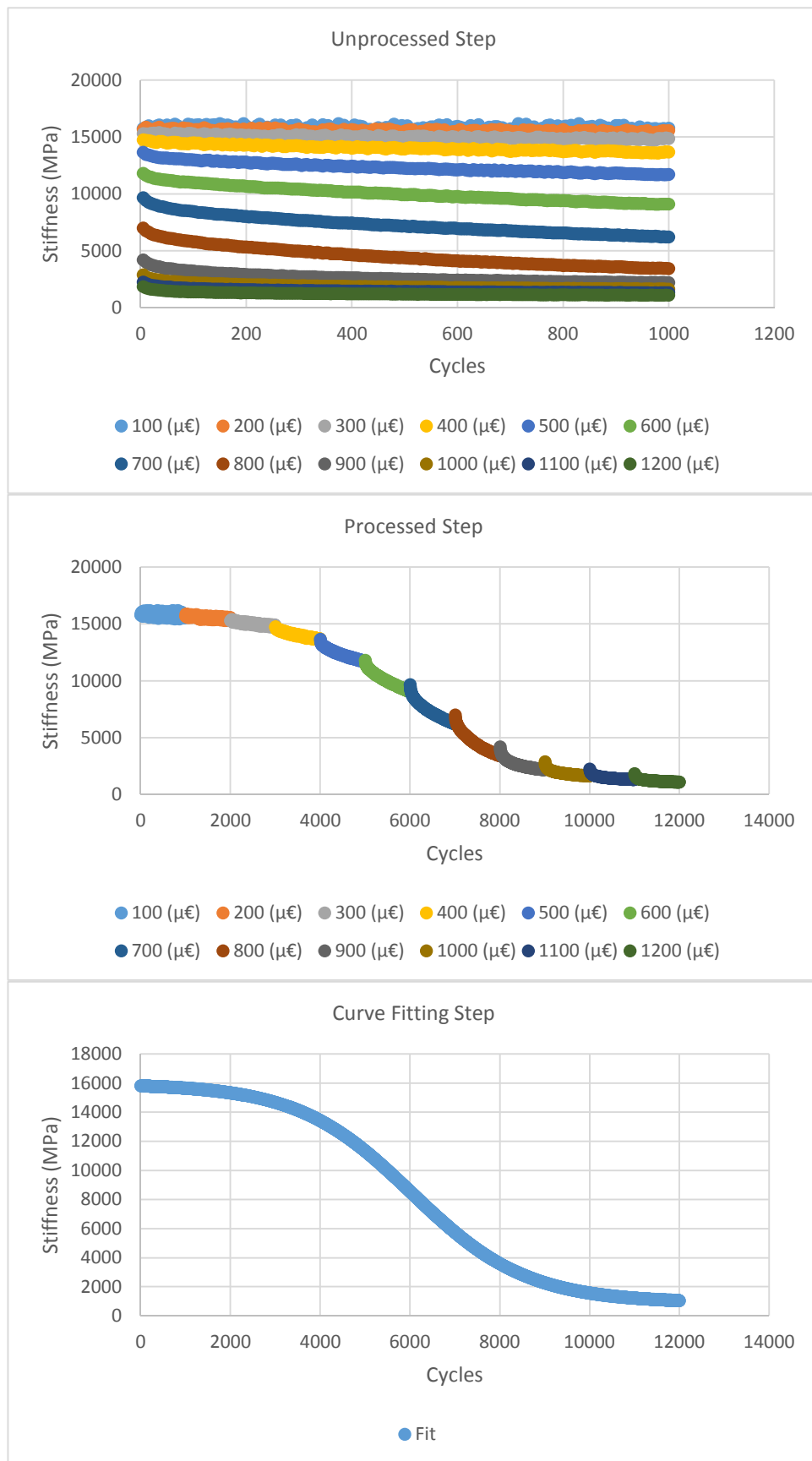


Figure D - 3. Three steps in Approach 4, 5Hz, 4°C, Beam number 52

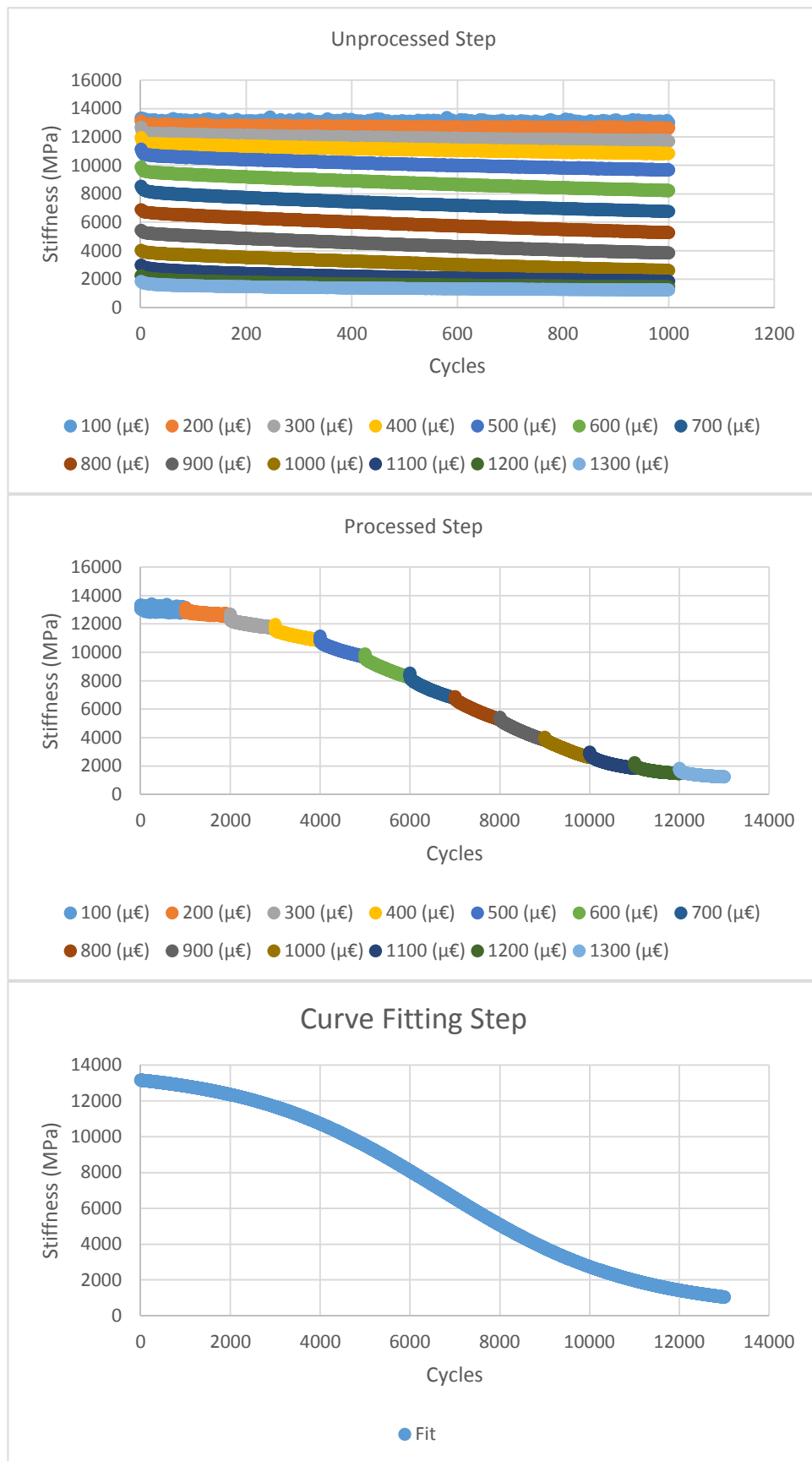


Figure D - 4. Three steps in Approach 4, 1Hz, 4°C, Beam number 53

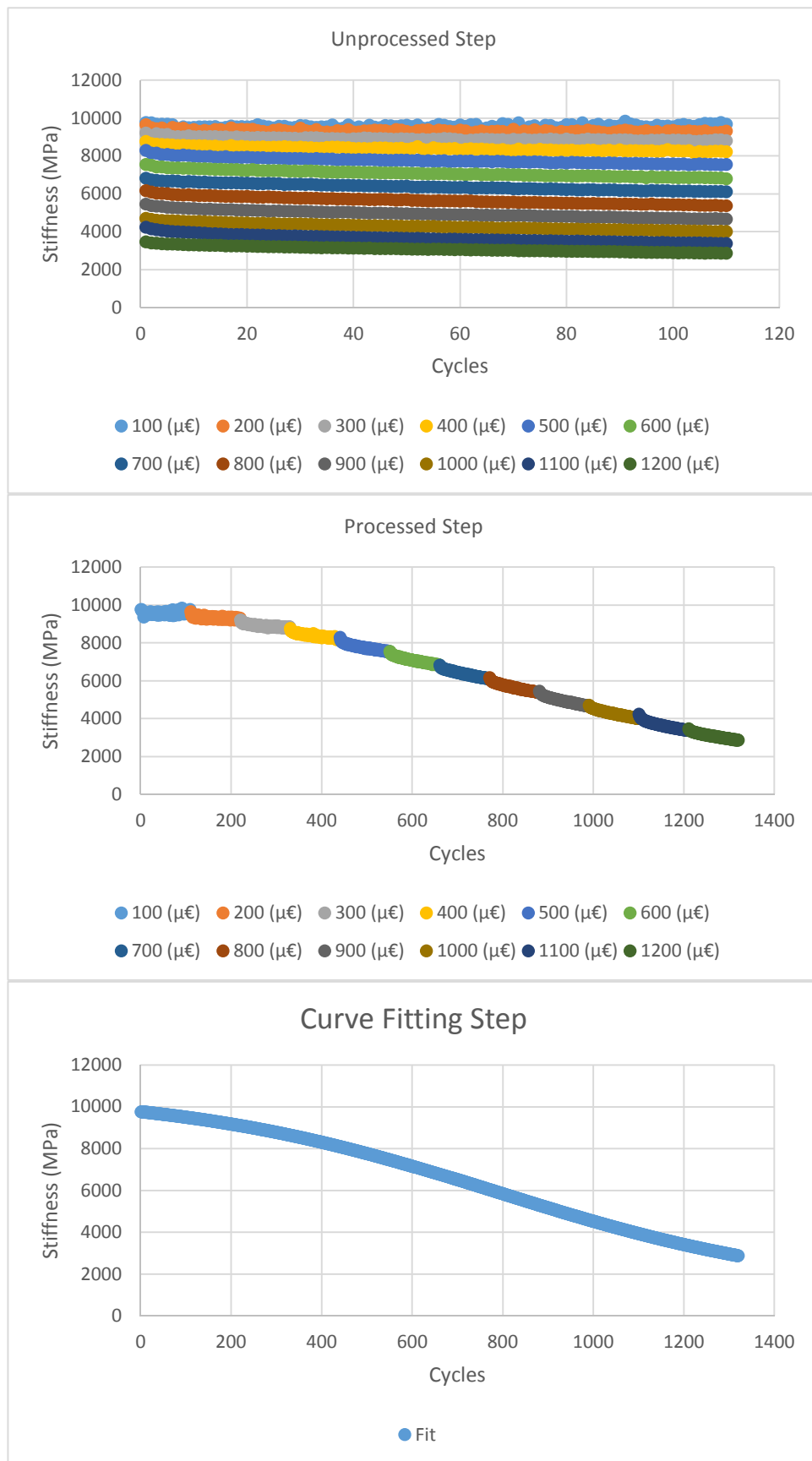


Figure D - 5. Three steps in Approach 4, 0.1Hz, 4°C, Beam number 54

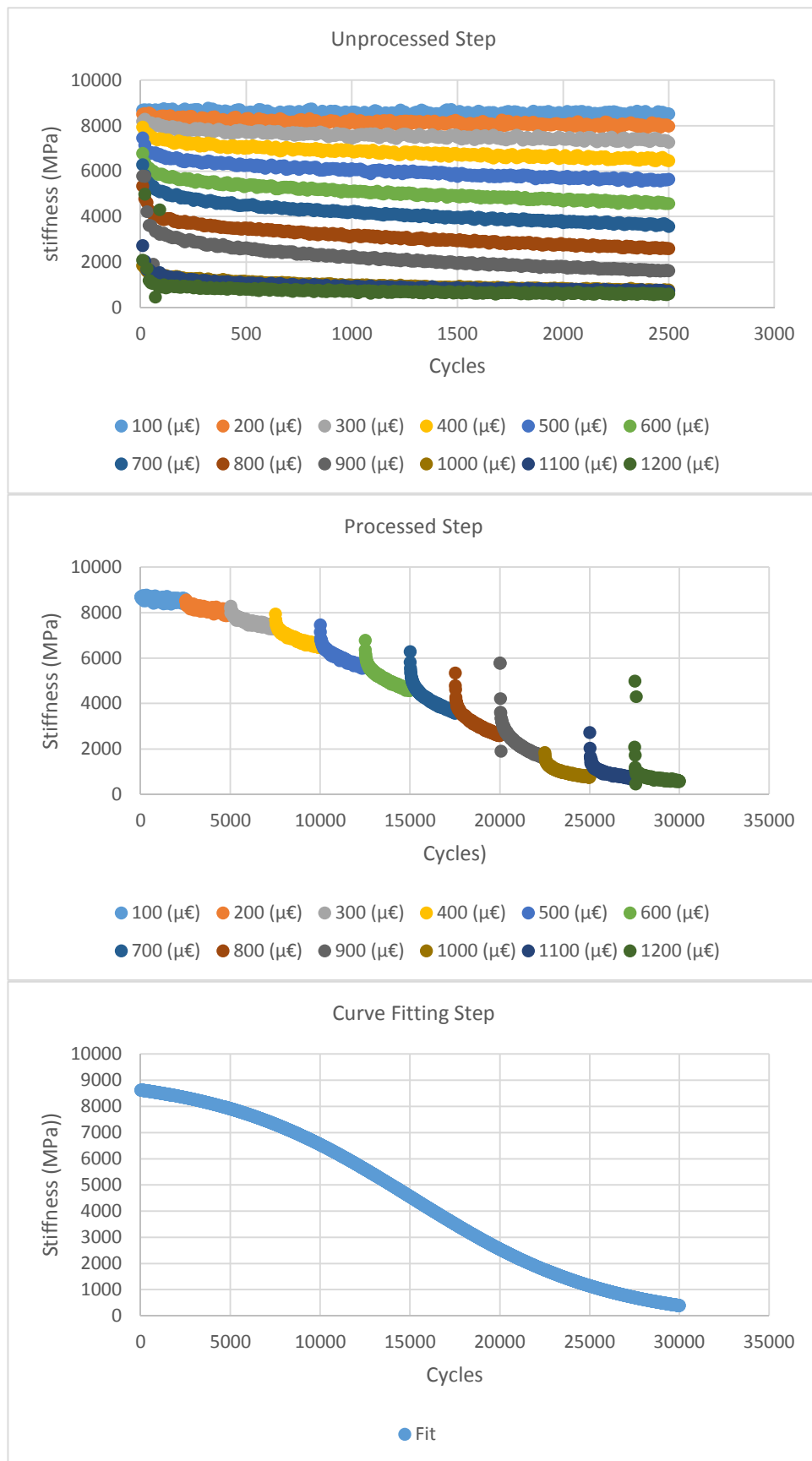


Figure D - 6. Three steps in Approach 4, 25Hz, 20°C, Beam number 55

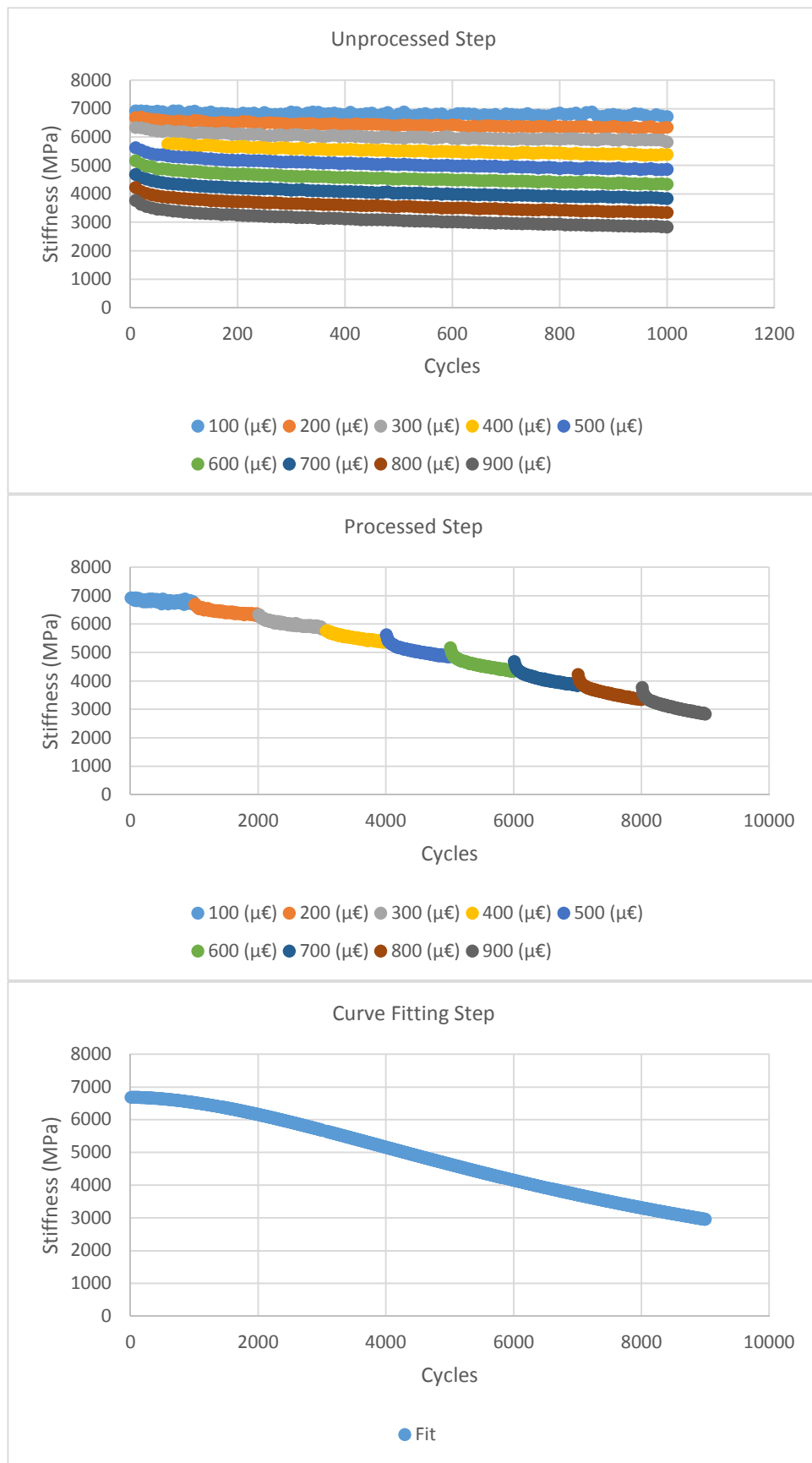


Figure D - 7. Three steps in Approach 4, 10Hz, 20°C, Beam number 56

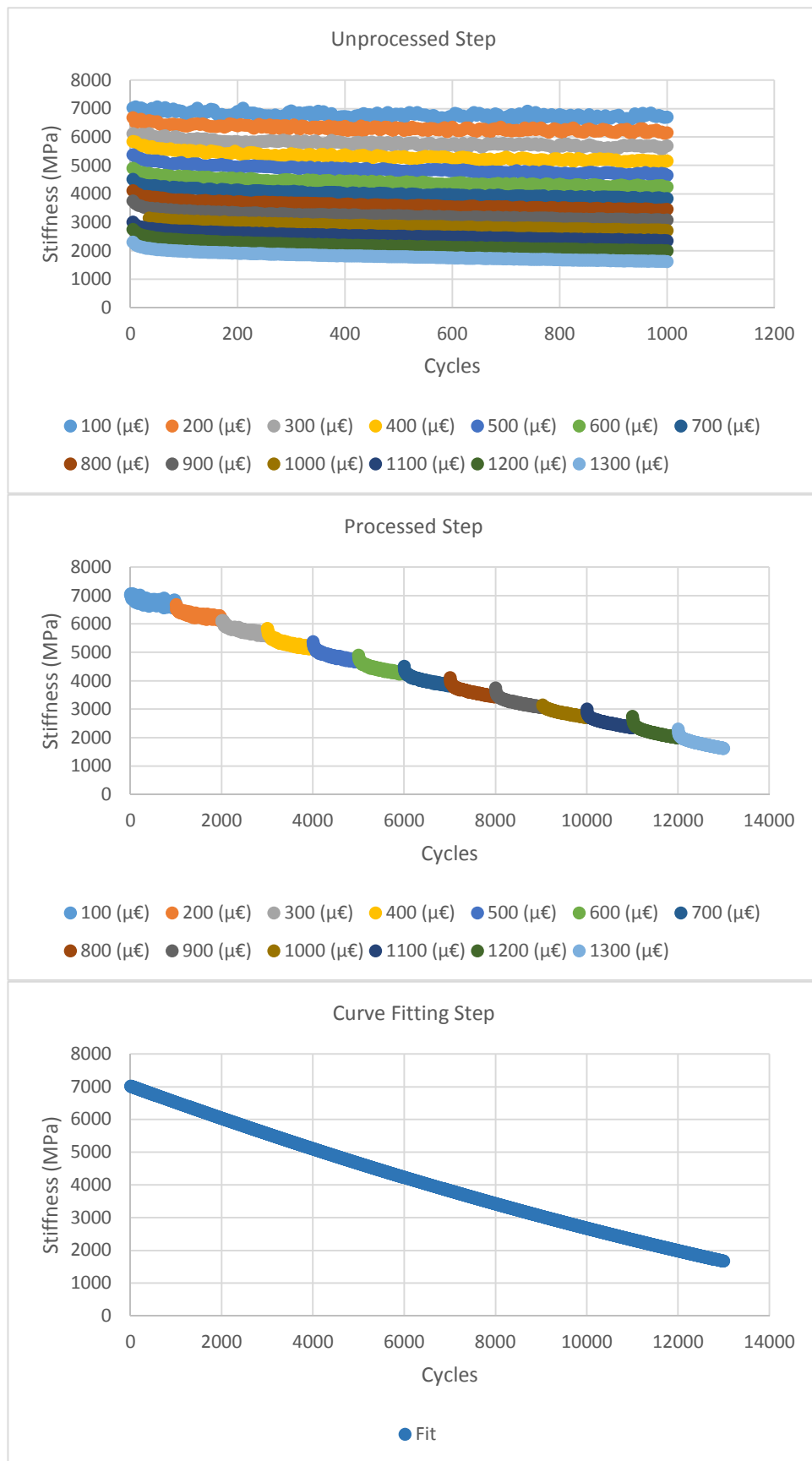


Figure D - 8. Three steps in Approach 4, 5Hz, 20°C, Beam number 57

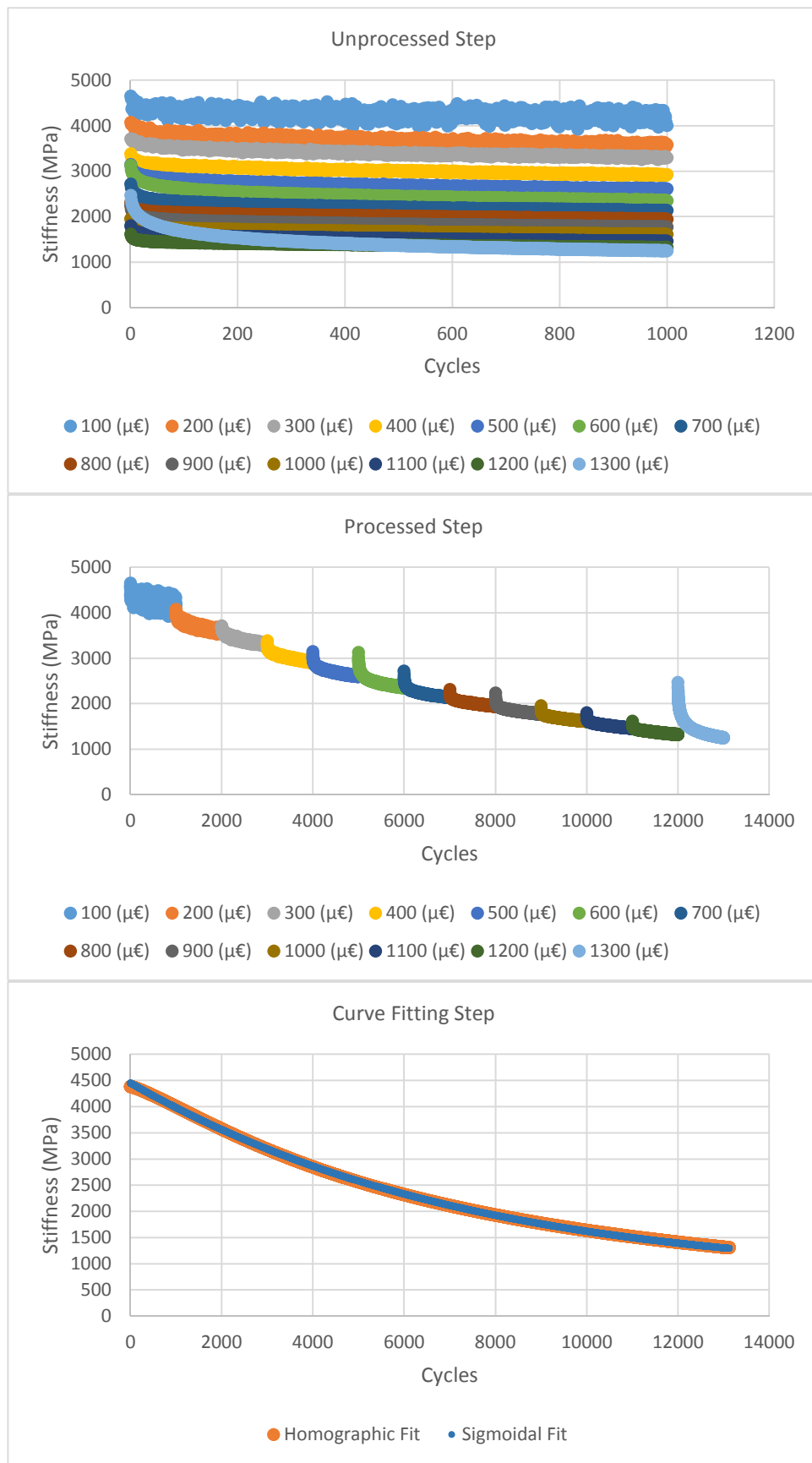


Figure D - 9. Three steps in Approach 4, 1Hz, 20°C, Beam number 58

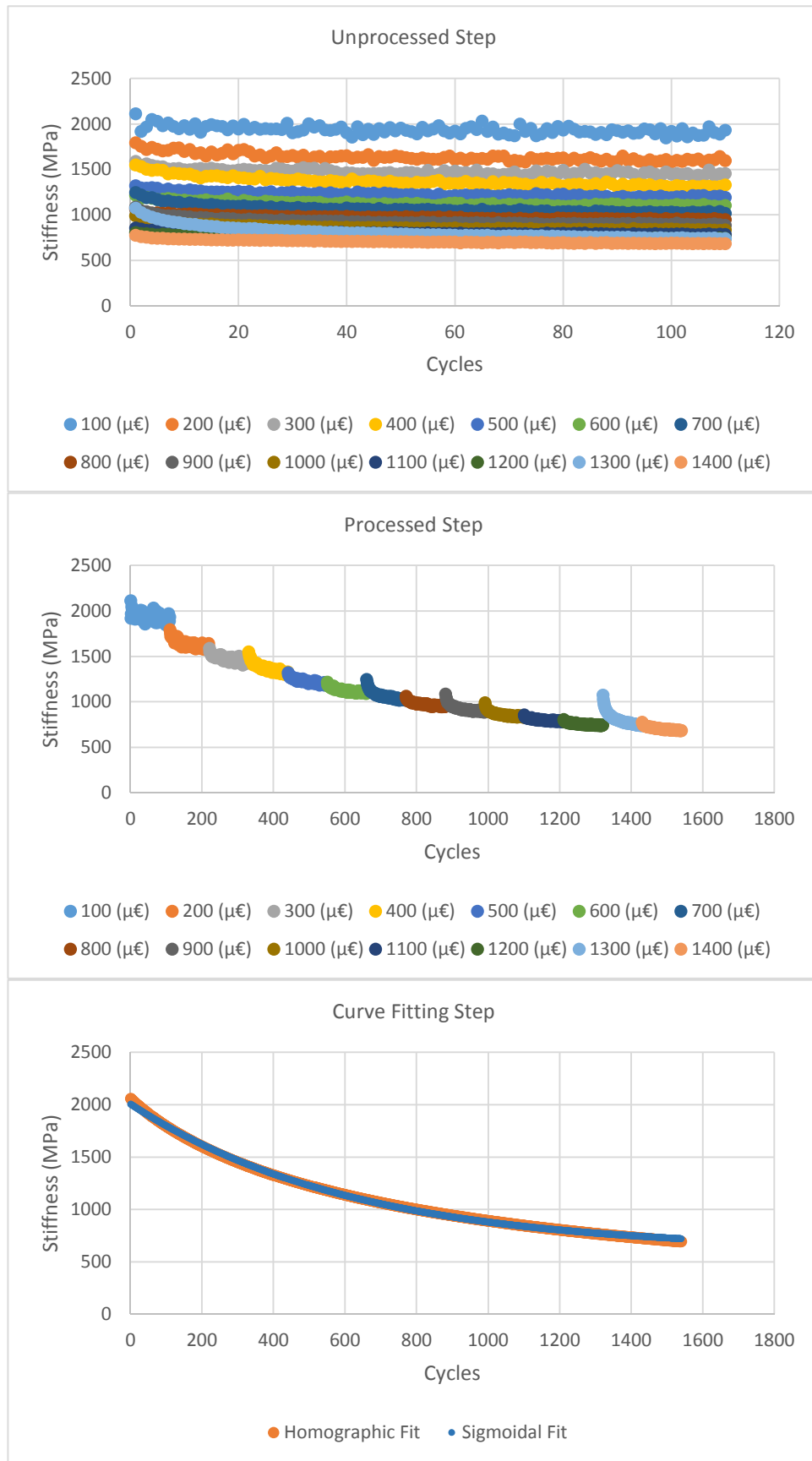


Figure D - 10. Three steps in Approach 4, 0.1Hz, 20°C, Beam number 59

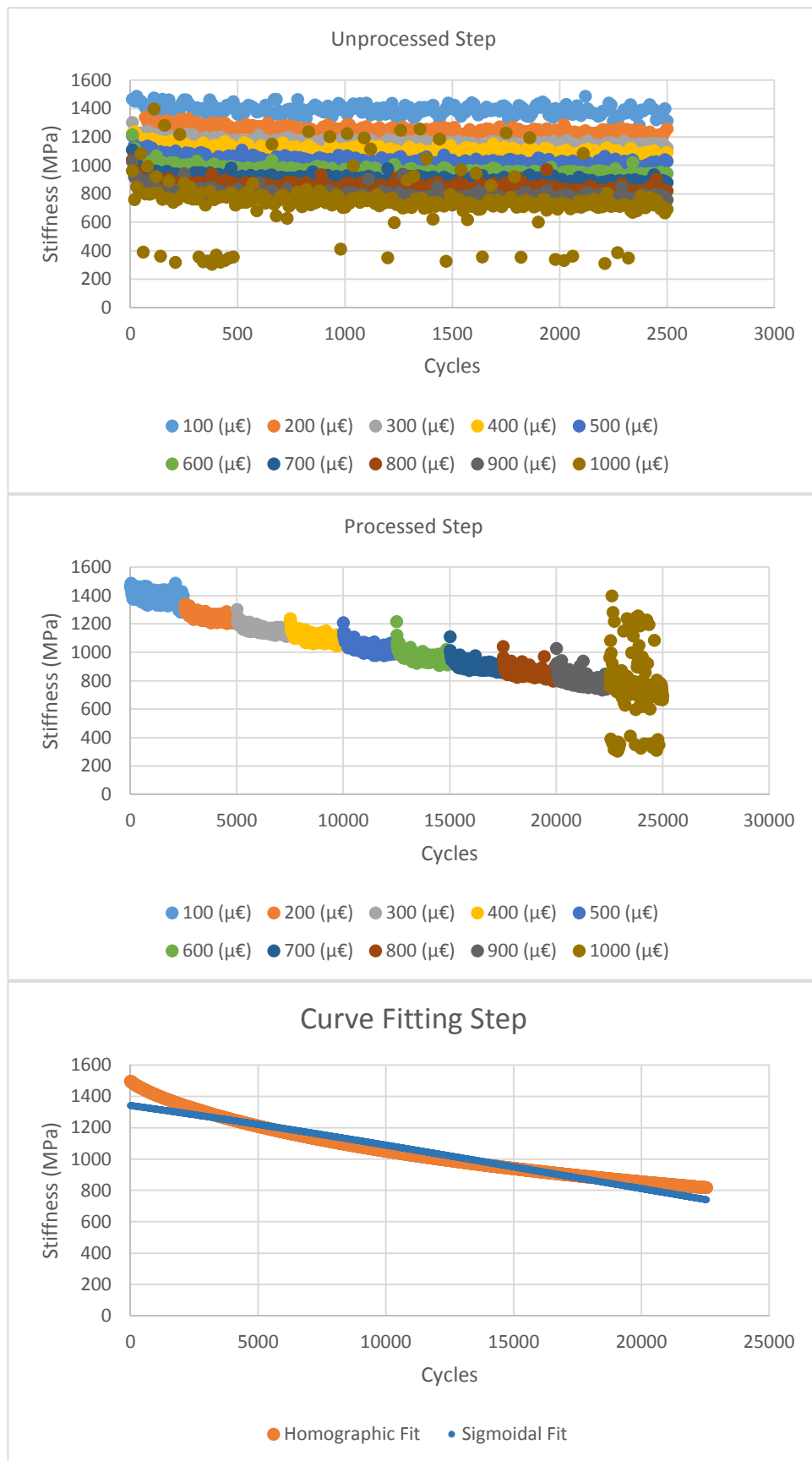


Figure D - 11. Three steps in Approach 4, 25Hz, 40°C, Beam number 60

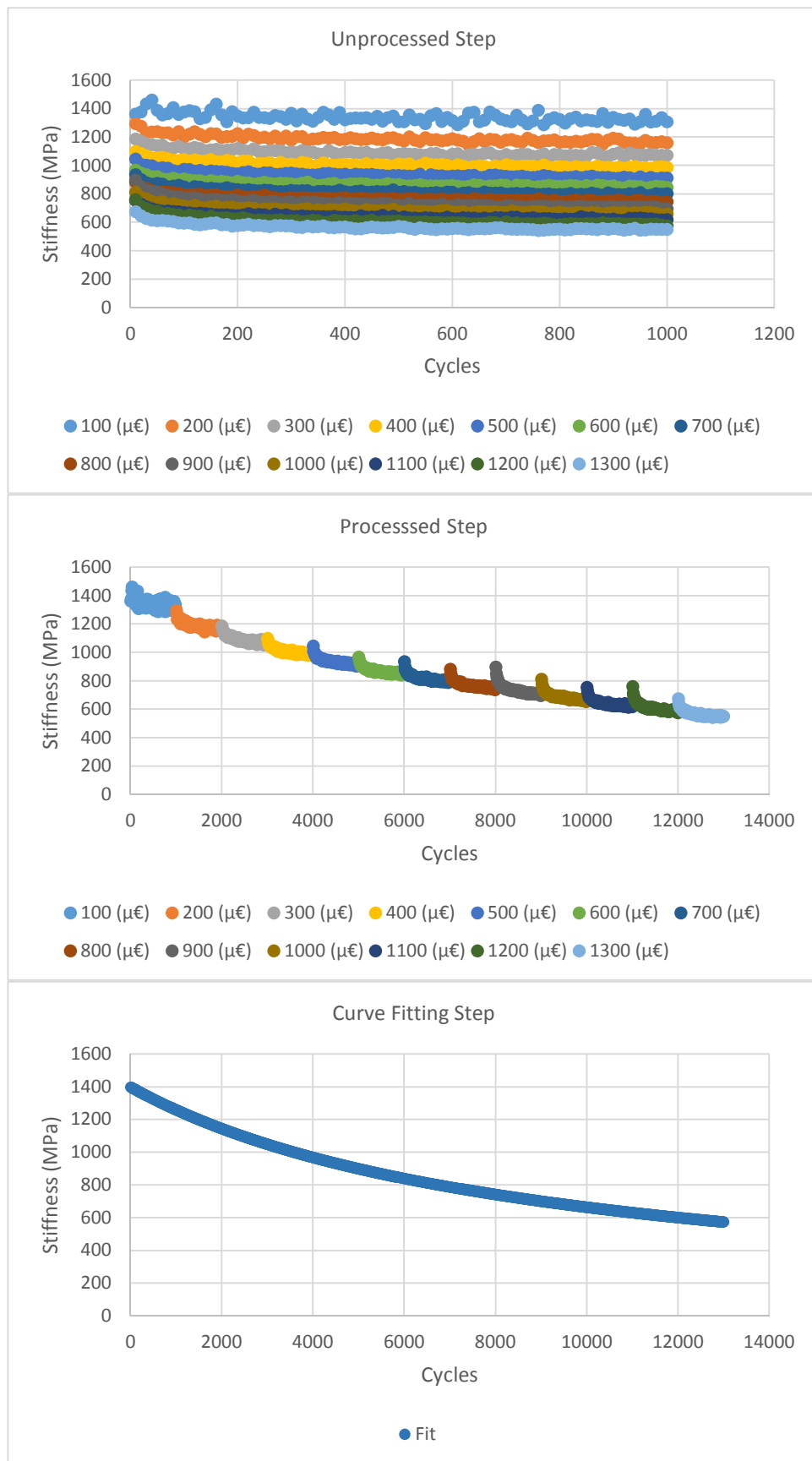


Figure D - 12. Three steps in Approach 4, 10Hz, 40°C, Beam number 61

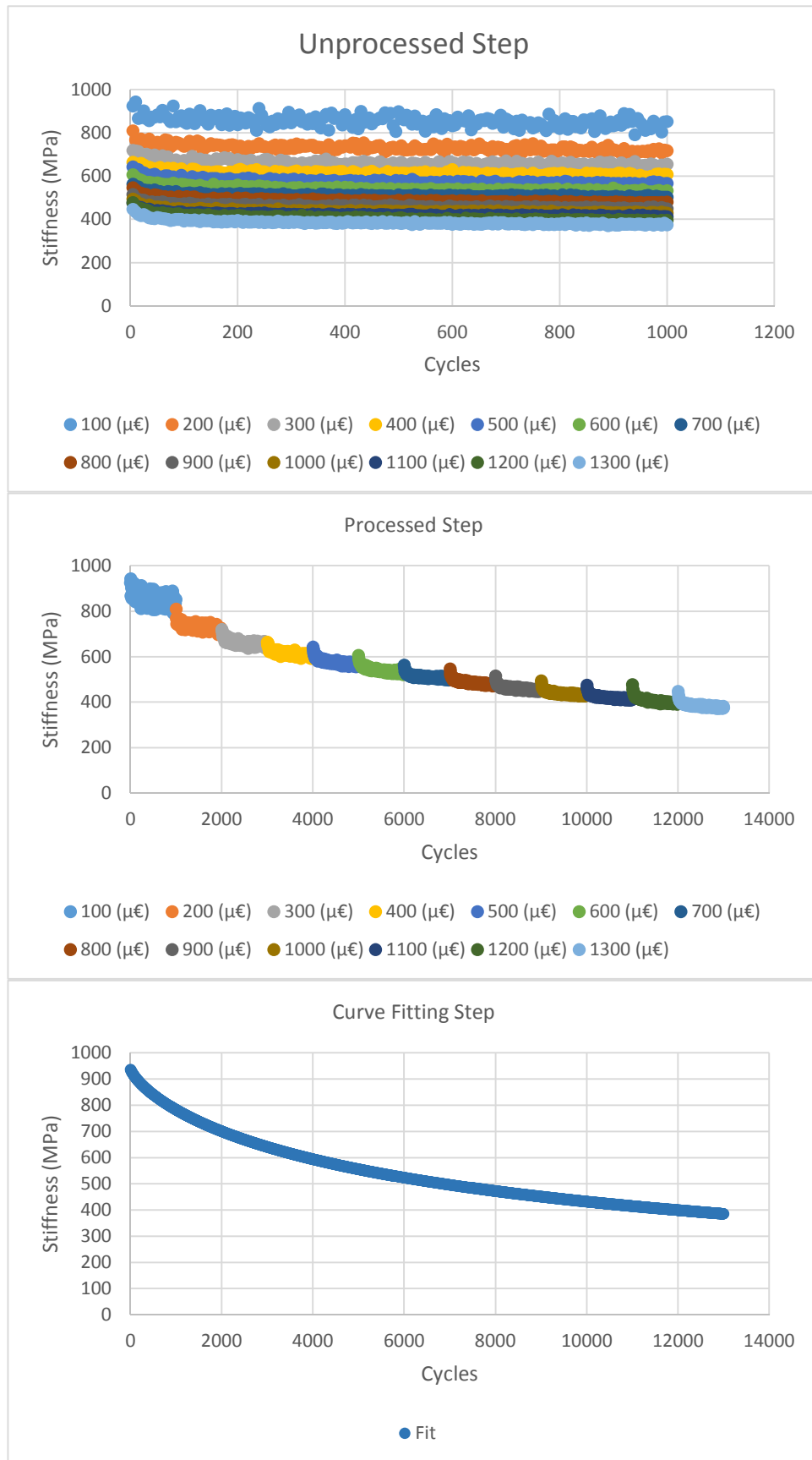


Figure D - 13. Three steps in Approach 4, 5Hz, 40°C, Beam number 62

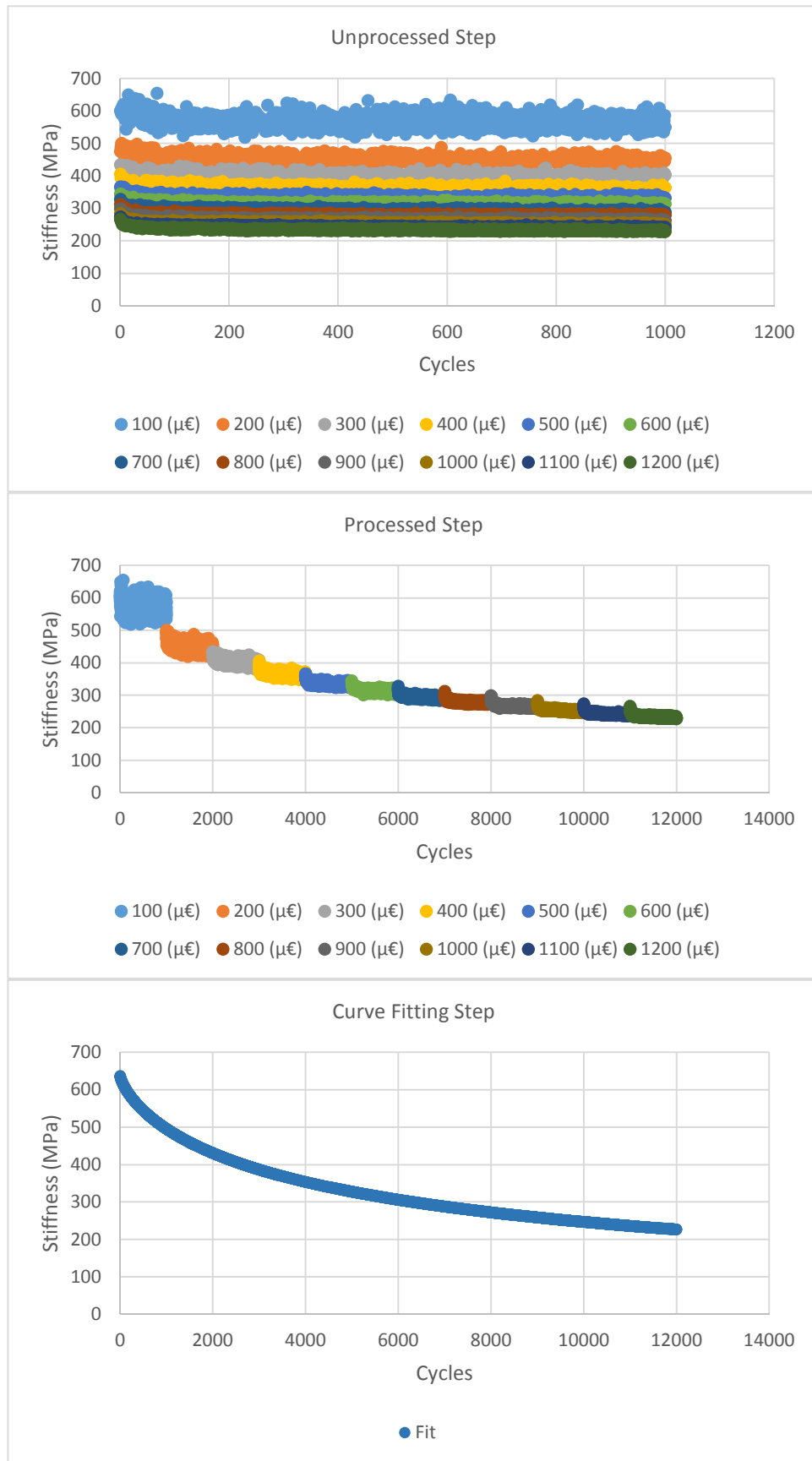


Figure D - 14. Three steps in Approach 4, 1Hz, 40°C, Beam number 63

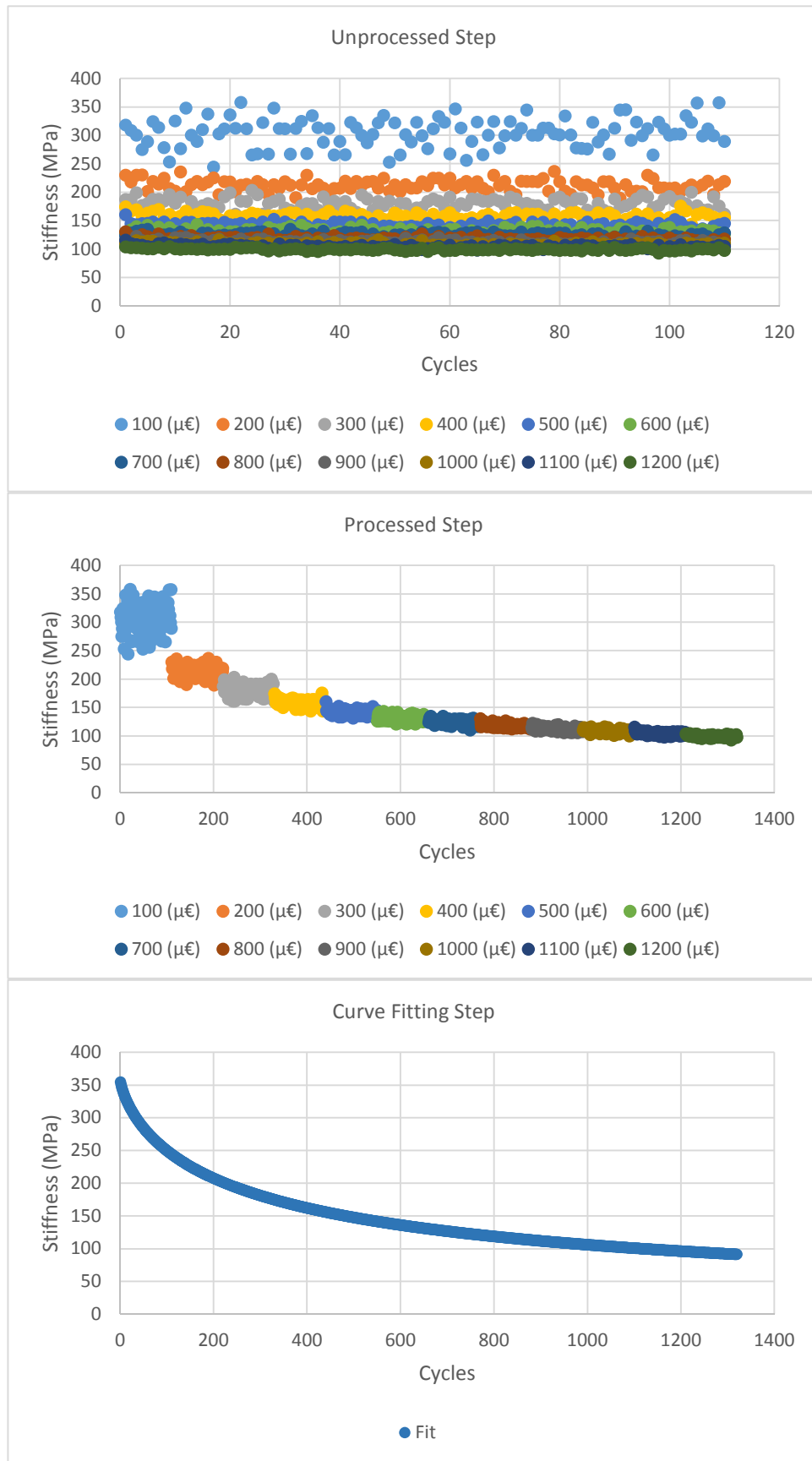


Figure D - 15. Three steps in Approach 4, 0.1Hz, 40°C, Beam number 64

Appendix E

UTS 6 OUTPUTS (AMPT – DYNAMIC MODULUS TEST)

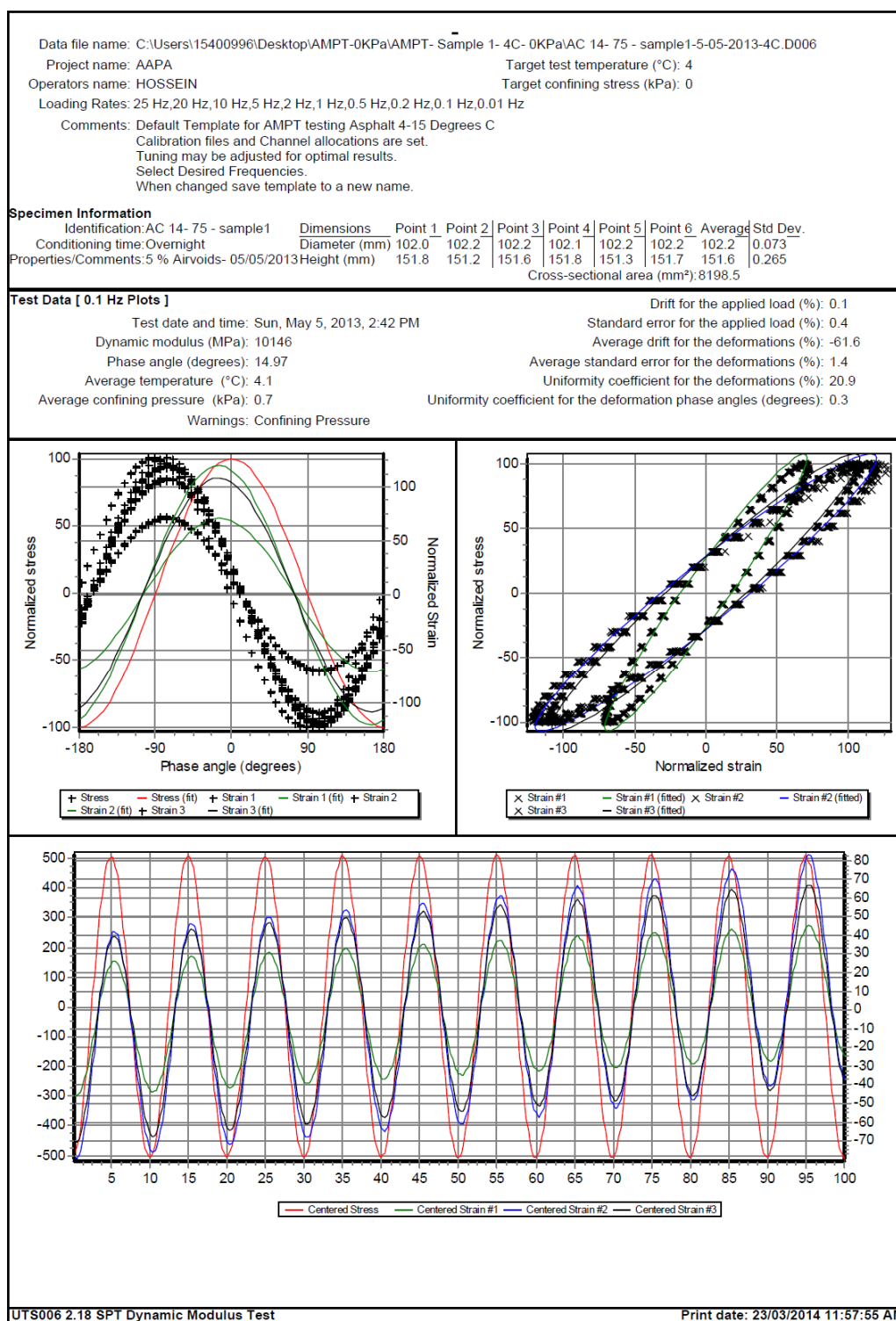


Figure E - 1. UTS6 output for sample1, 0.1 Hz and 4°C

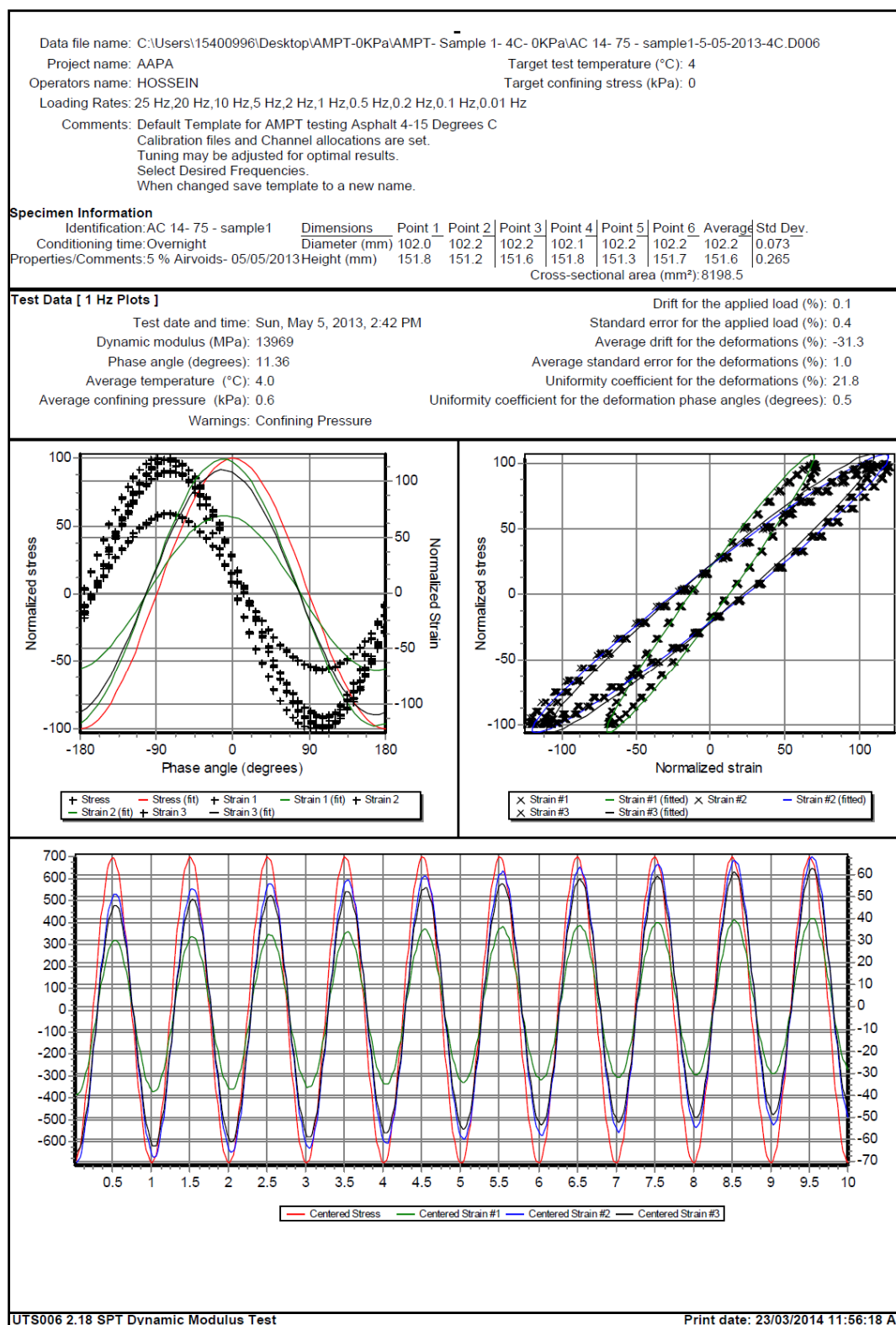
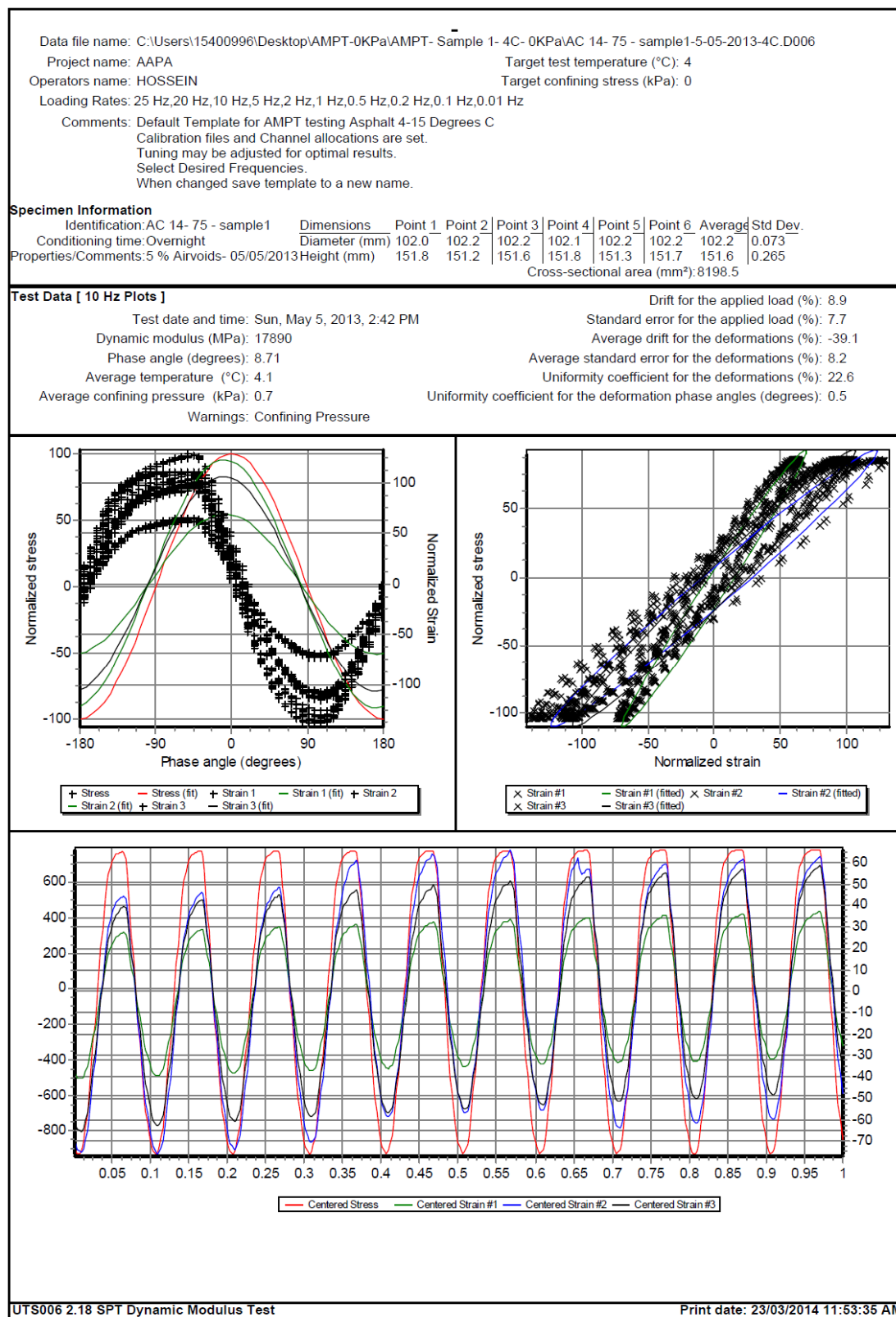
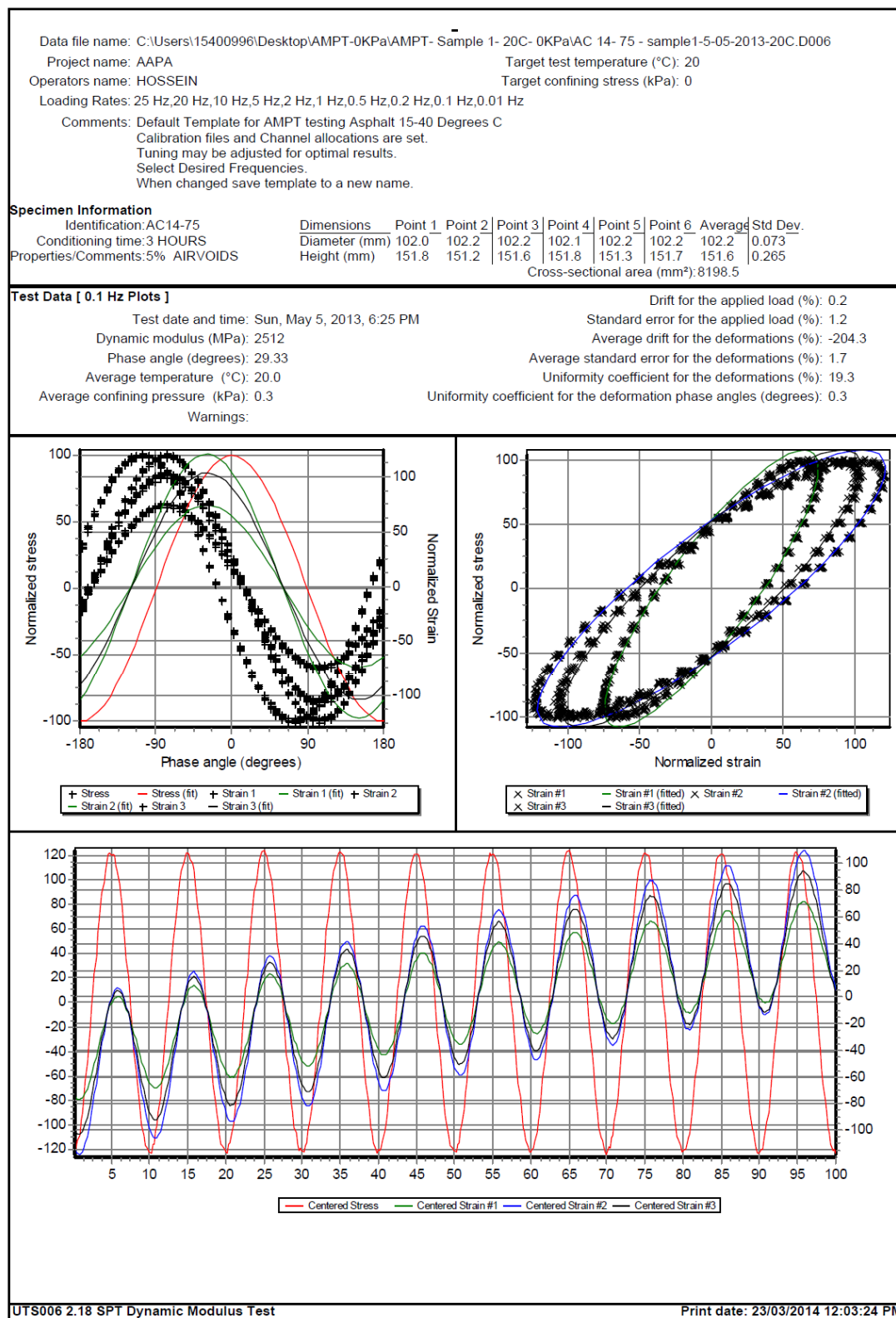


Figure E - 2. UTS6 output for sample1, 1 Hz and 4°C



Data file name: C:\Users\15400996\Desktop\AMPT-0KPa\AMPT- Sample 1- 4C- 0KPa\AC 14- 75 - sample1-5-05-2013-4C.D006											
Project name: AAPA						Target test temperature (°C): 4					
Operators name: HOSSEIN						Target confining stress (kPa): 0					
Loading Rates: 25 Hz,20 Hz,10 Hz,5 Hz,2 Hz,1 Hz,0.5 Hz,0.2 Hz,0.1 Hz,0.01 Hz											
Comments: Default Template for AMPT testing Asphalt 4-15 Degrees C											
Calibration files and Channel allocations are set.											
Tuning may be adjusted for optimal results.											
Select Desired Frequencies.											
When changed save template to a new name.											
Specimen Information											
Identification:AC 14- 75 - sample1		<u>Dimensions</u>		Point 1	Point 2	Point 3	Point 4	Point 5	Point 6	Average	Std Dev.
Conditioning time:Overnight		Diameter (mm)		102.0	102.2	102.2	102.1	102.2	102.2	102.2	0.073
Properties/Comments:5 % Airvoids- 05/05/2013		Height (mm)		151.8	151.2	151.6	151.8	151.3	151.7	151.6	0.265
Cross-sectional area (mm²):8198.5											
Tabulated Results Summary											
	25 Hz	20 Hz	10 Hz	5 Hz	2 Hz	1 Hz	0.5 Hz	0.2 Hz	0.1 Hz	0.01 Hz	
Dynamic modulus (MPa)	19402	19015	17890	16683	15130	13969	12793	11288	10146	6764	
Phase angle (Degrees)	7.80	8.17	8.71	9.30	10.54	11.36	12.31	13.72	14.97	19.85	
Average temperature (°C)	4.1	4.1	4.1	4.1	4.1	4.0	4.0	4.1	4.1	4.1	
Average confining pressure (kPa)	0.6	0.6	0.7	0.7	0.7	0.6	0.6	0.7	0.7	0.7	
Average micro-strain	89	92	100	101	101	100	100	100	100	100	
Load drift (%)	11.7	10.1	8.9	0.0	-0.1	0.1	-0.5	0.1	0.1	0.1	
Load standard error (%)	14.0	11.0	7.7	1.1	0.6	0.4	0.3	0.3	0.4	0.8	
Average deformation drift (%)	-44.8	-34.5	-39.1	-24.4	-35.8	-31.3	-35.3	-48.2	-61.6	-137.9	
Average deformation standard error (%)	13.4	10.5	8.2	2.5	1.7	1.0	3.0	1.0	1.4	1.7	
Deformation uniformity (%)	21.1	22.3	22.6	22.9	22.5	21.8	21.4	21.0	20.9	21.0	
Phase uniformity (Degrees)	0.5	0.5	0.5	0.5	0.6	0.5	0.4	0.4	0.3	0.3	



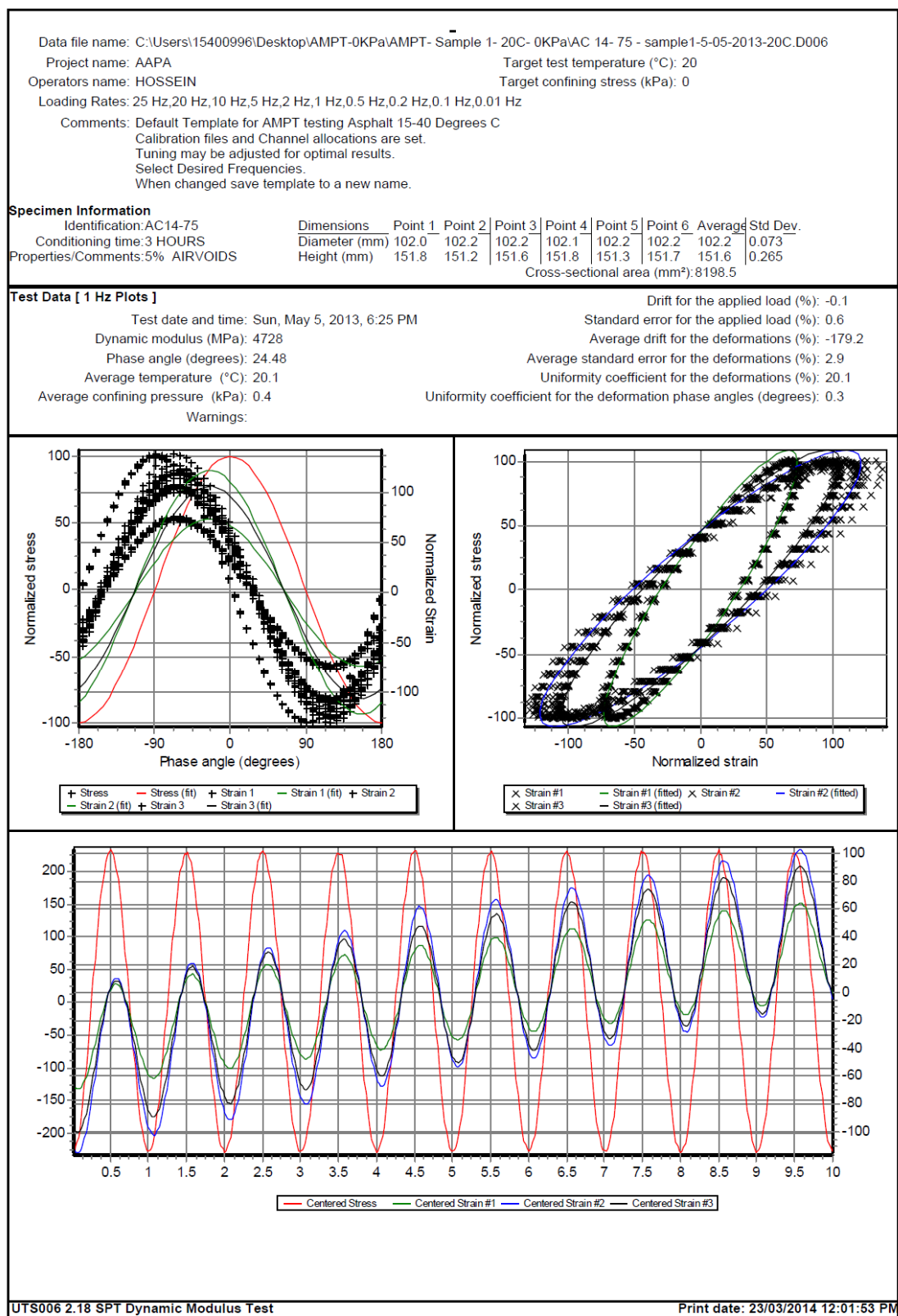


Figure E - 6. UTS6 output for sample1, 1 Hz and 20°C

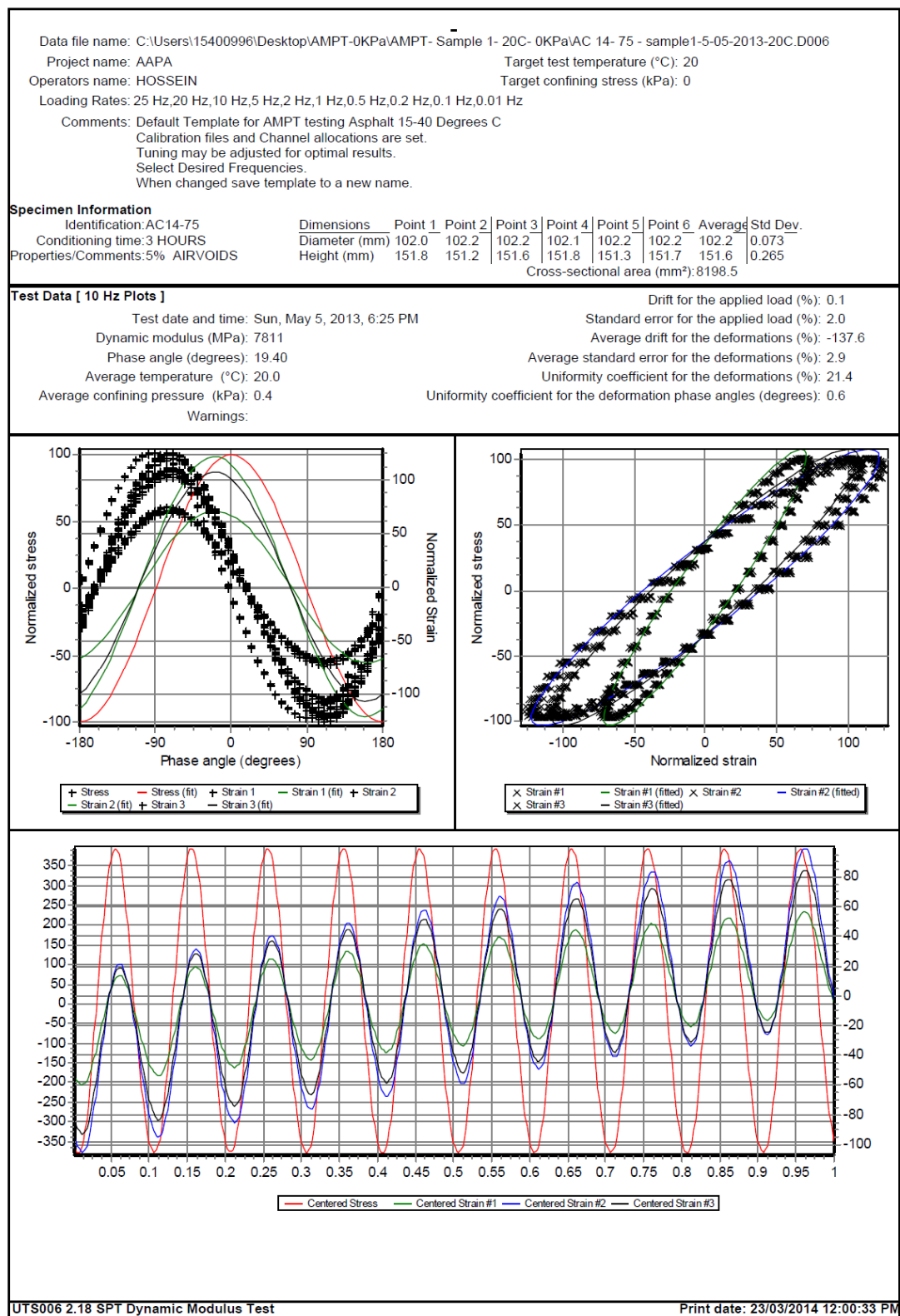


Figure E - 7. UTS6 output for sample1, 10 Hz and 20°C

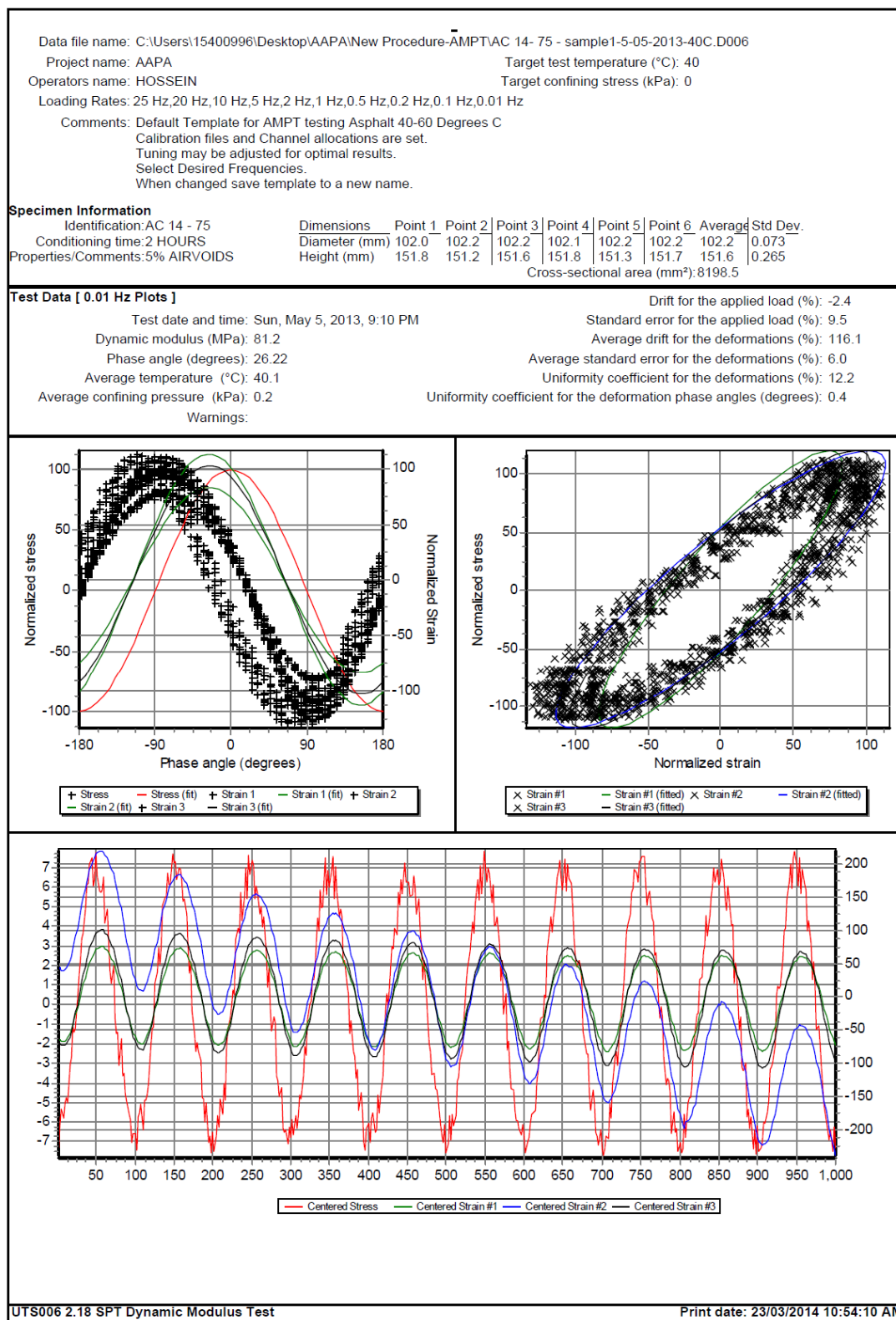


Figure E - 9. UTS6 output for sample1, 0.01 Hz and 40°C

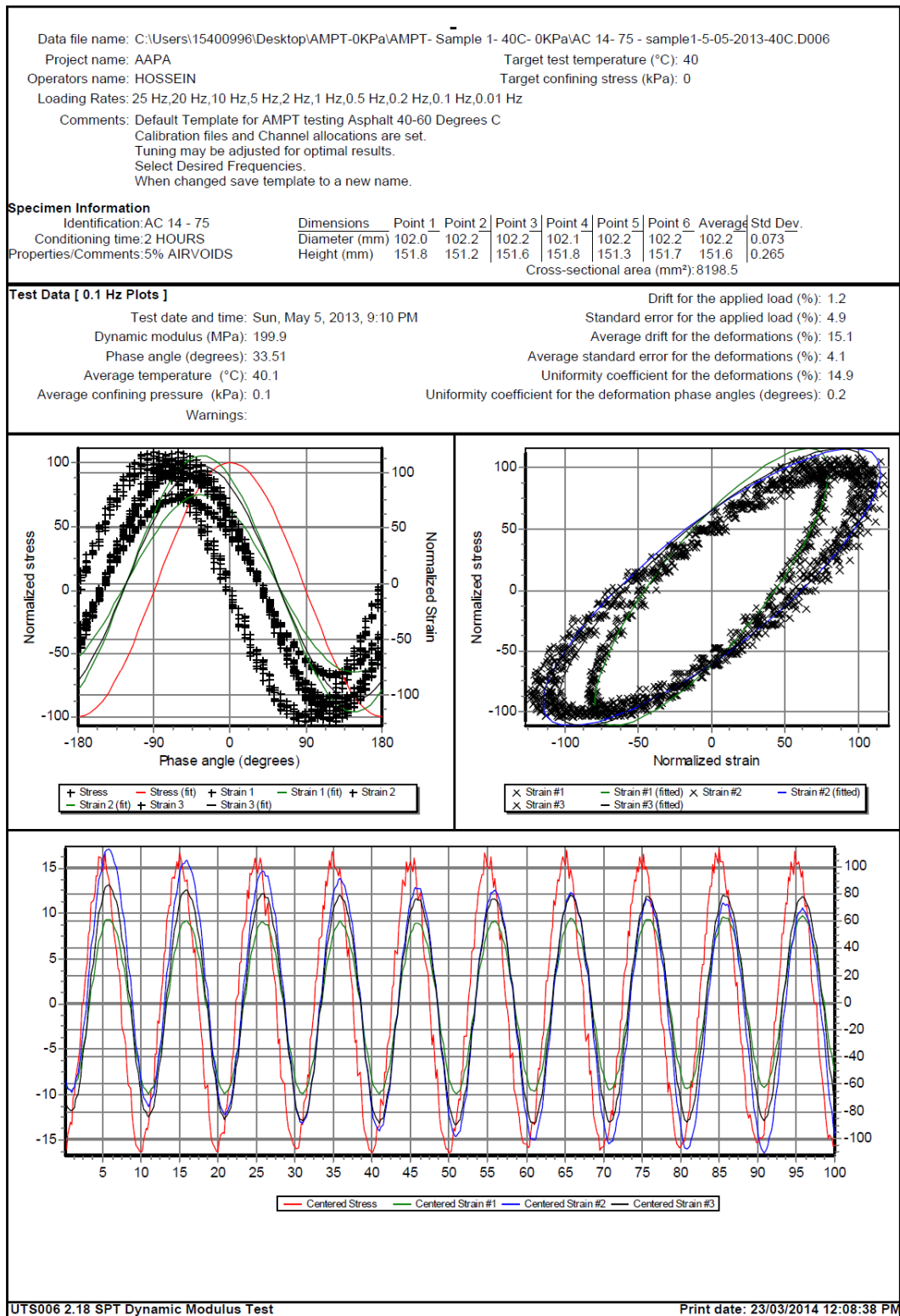


Figure E - 10. UTS6 output for sample1, 0.1 Hz and 40°C

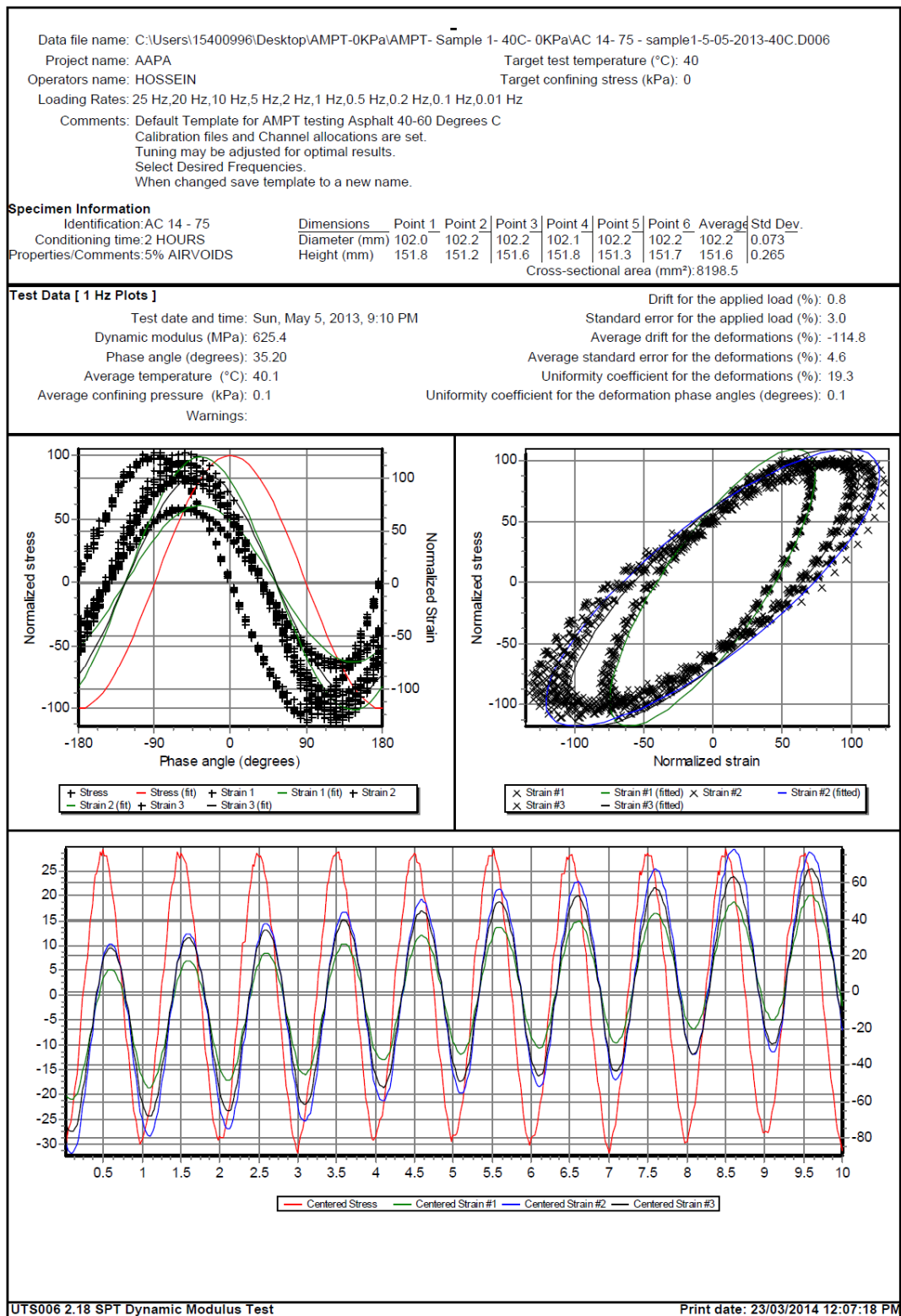


Figure E - 11. UTS6 output for sample1, 1 Hz and 40°C

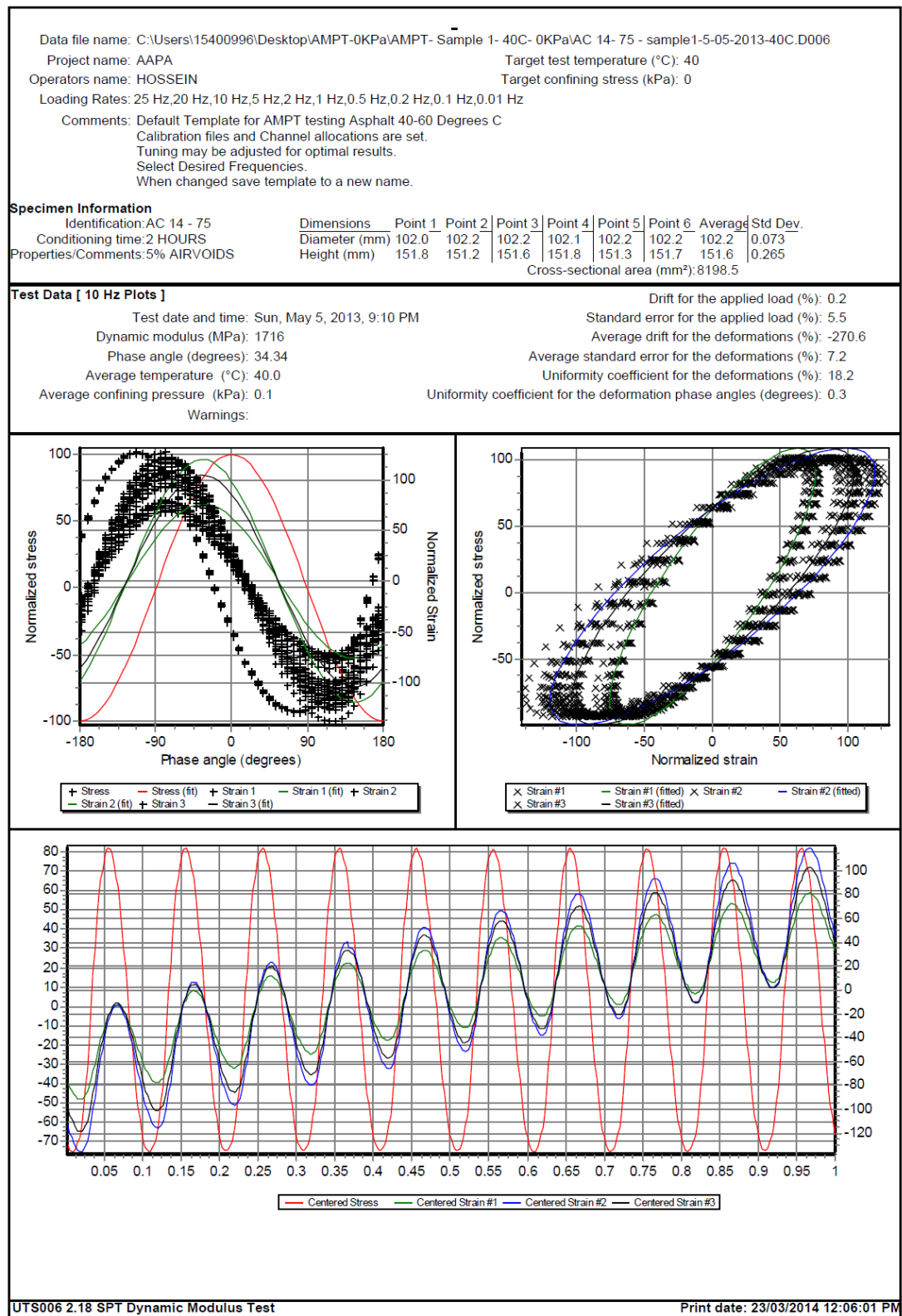


Figure E - 12. UTS6 output for sample1, 10 Hz and 40°C

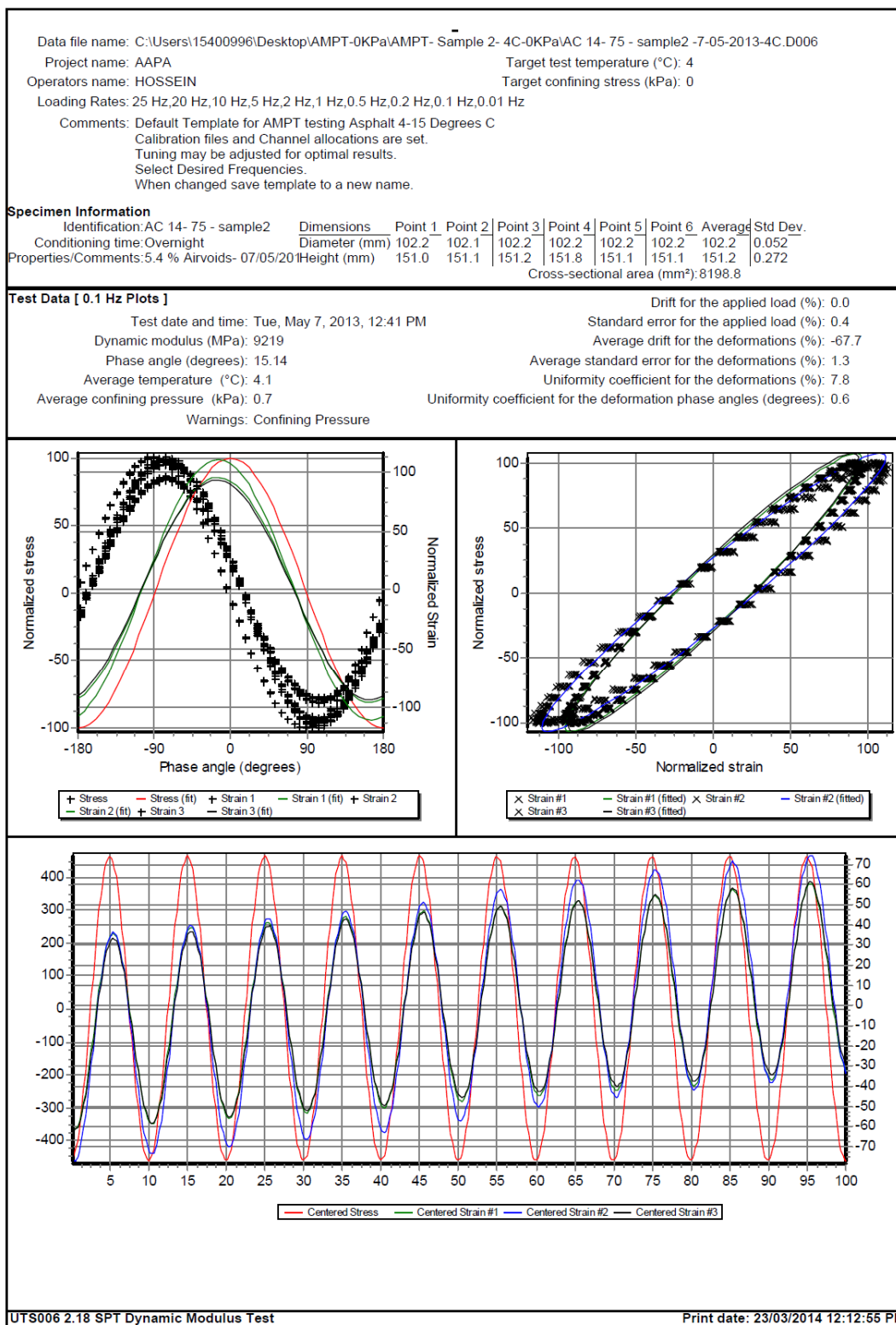


Figure E - 14. UTS6 output for sample2, 0.1 Hz and 4°C

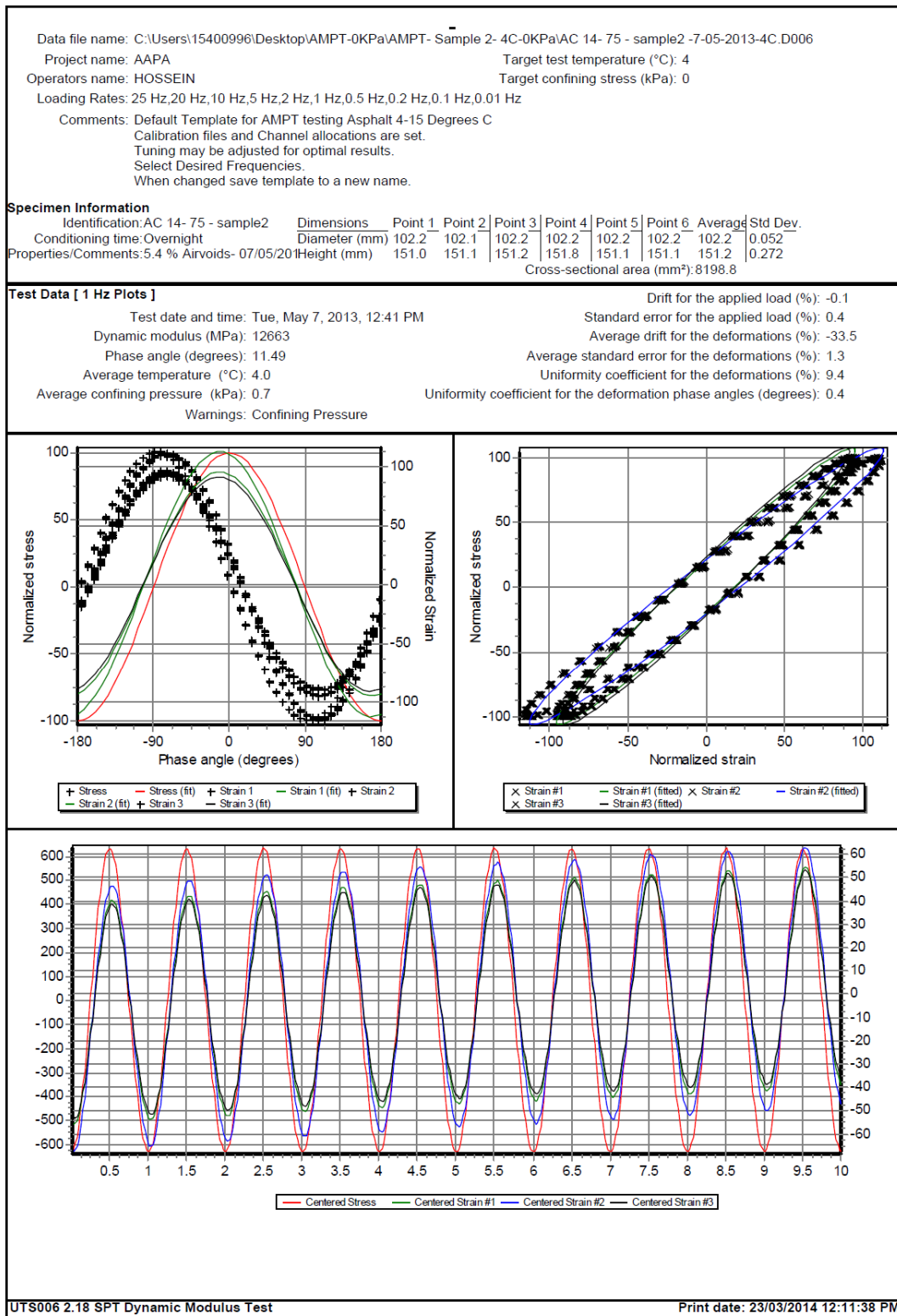


Figure E - 15. UTS6 output for sample2, 1 Hz and 4°C

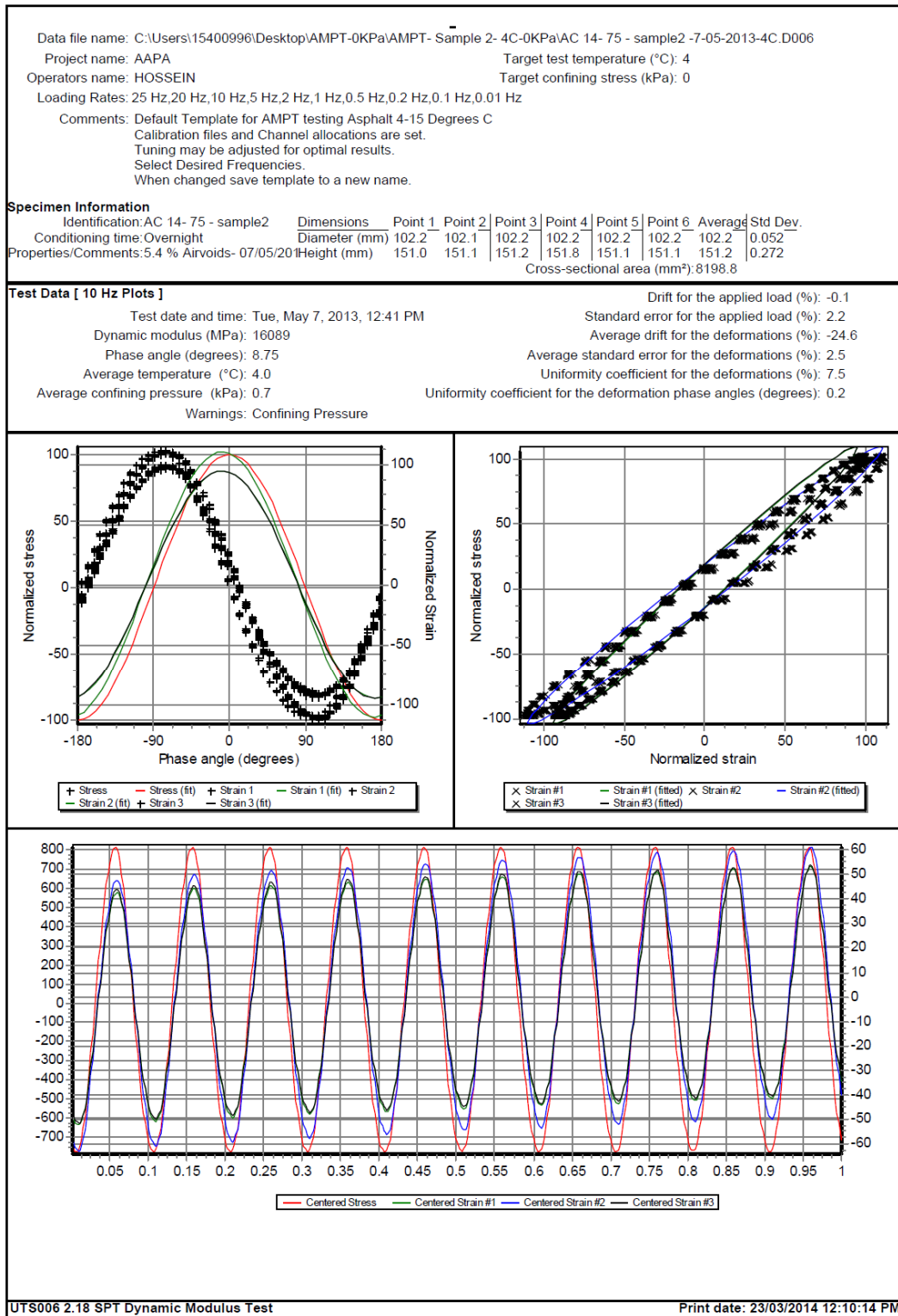


Figure E - 16. UTS6 output for sample2, 10 Hz and 4°C

Data file name: C:\Users\15400996\Desktop\AMPT-0KPa\AMPT- Sample 2- 4C-0KPa\AC 14- 75 - sample2 -7-05-2013-4C.D006											
Project name: AAPA						Target test temperature (°C): 4					
Operators name: HOSSEIN						Target confining stress (kPa): 0					
Loading Rates: 25 Hz,20 Hz,10 Hz,5 Hz,2 Hz,1 Hz,0.5 Hz,0.2 Hz,0.1 Hz,0.01 Hz											
Comments: Default Template for AMPT testing Asphalt 4-15 Degrees C											
Calibration files and Channel allocations are set.											
Tuning may be adjusted for optimal results.											
Select Desired Frequencies.											
When changed save template to a new name.											
Specimen Information											
Identification:AC 14- 75 - sample2		Dimensions	Point 1	Point 2	Point 3	Point 4	Point 5	Point 6	Average	Std Dev.	
Conditioning time:Overnight		Diameter (mm)	102.2	102.1	102.2	102.2	102.2	102.2	102.2	0.052	
Properties/Comments:5.4 % Airvoids- 07/05/2011		Height (mm)	151.0	151.1	151.2	151.8	151.1	151.1	151.2	0.272	
Cross-sectional area (mm²):8198.8											
Tabulated Results Summary											
	25 Hz	20 Hz	10 Hz	5 Hz	2 Hz	1 Hz	0.5 Hz	0.2 Hz	0.1 Hz	0.01 Hz	
Dynamic modulus (MPa)	17237	17075	16089	15085	13722	12663	11622	10238	9219	6093	
Phase angle (Degrees)	8.62	8.11	8.75	9.51	10.57	11.49	12.48	13.89	15.14	20.30	
Average temperature (°C)	4.0	4.0	4.0	4.0	4.0	4.0	4.0	4.1	4.1	4.1	
Average confining pressure (kPa)	0.7	0.7	0.7	0.7	0.7	0.7	0.7	0.7	0.7	0.7	
Average micro-strain	97	100	99	99	100	100	100	100	100	99	
Load drift (%)	5.6	5.2	-0.1	0.0	-0.1	-0.1	-0.5	0.0	0.0	0.0	
Load standard error (%)	7.6	6.9	2.2	1.2	0.6	0.4	0.3	0.4	0.4	0.7	
Average deformation drift (%)	-34.3	-32.5	-24.6	-26.2	-29.9	-33.5	-37.4	-58.6	-67.7	-146.7	
Average deformation standard error (%)	7.9	6.6	2.5	1.9	1.5	1.3	1.0	1.0	1.3	2.2	
Deformation uniformity (%)	5.1	5.9	7.5	8.4	9.2	9.4	9.3	8.7	7.8	5.4	
Phase uniformity (Degrees)	1.0	0.2	0.2	0.3	0.4	0.4	0.4	0.5	0.6	0.7	

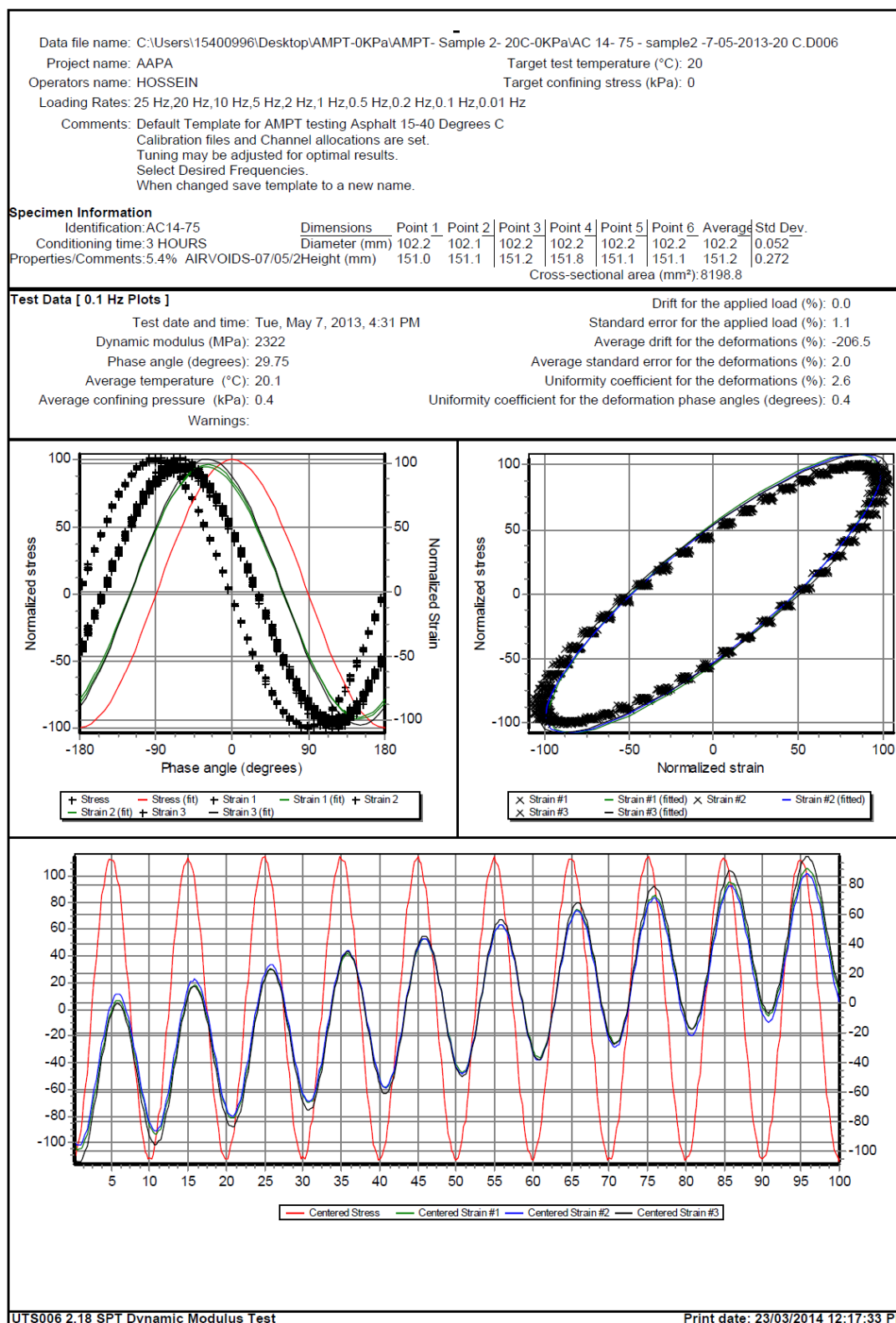


Figure E - 18. UTS6 output for sample2, 0.1 Hz and 20°C

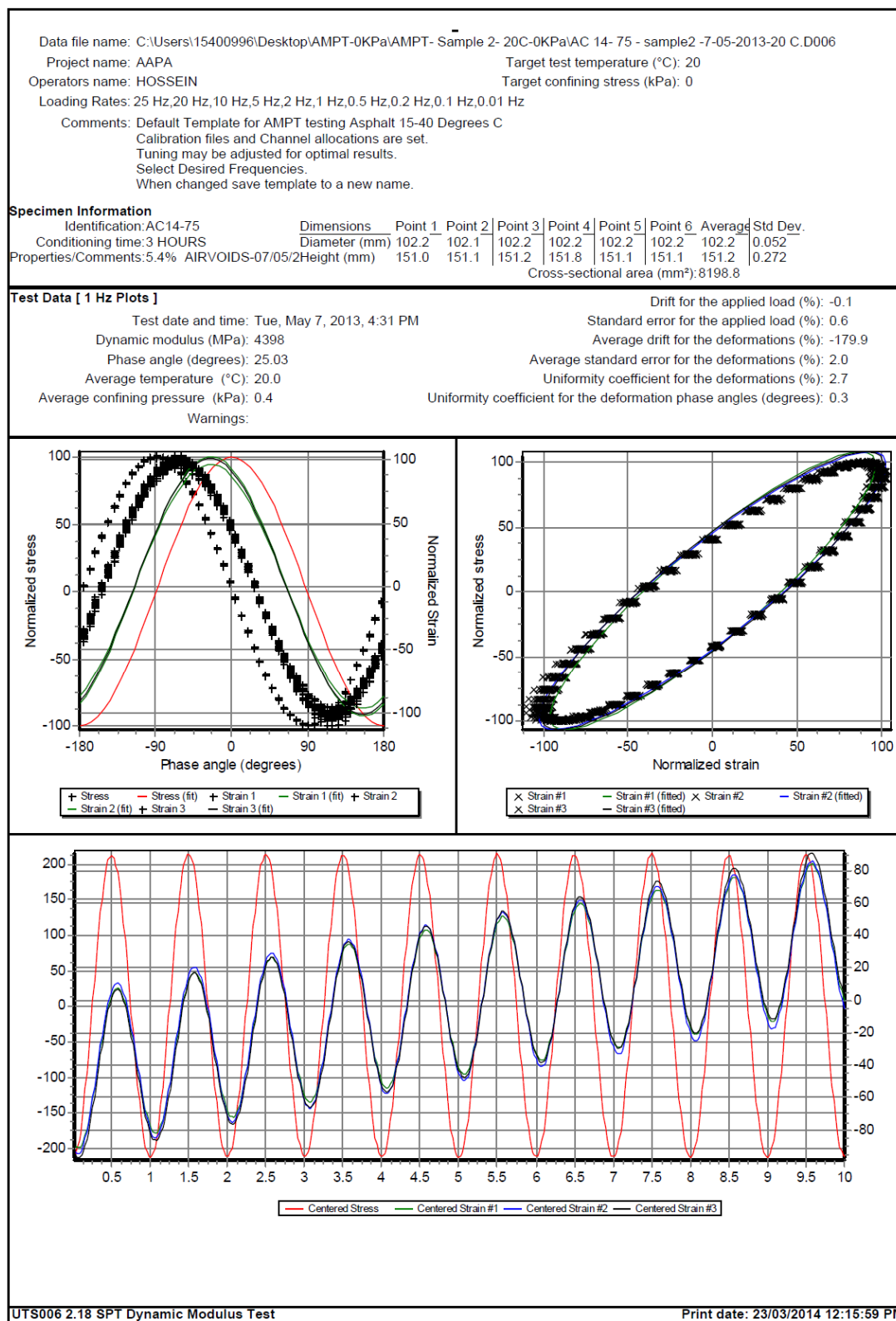


Figure E - 19. UTS6 output for sample2, 1 Hz and 20°C

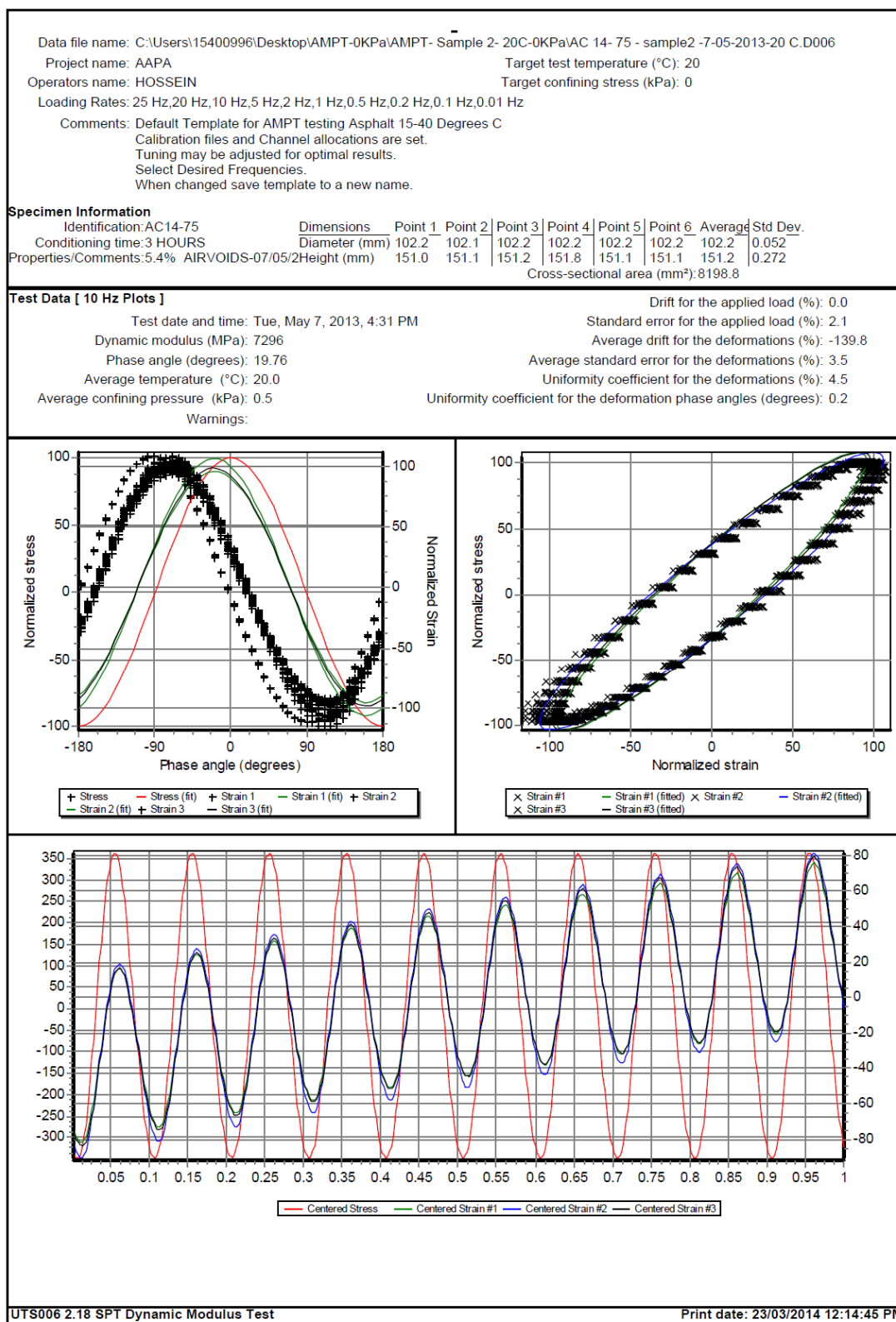


Figure E - 20. UTS6 output for sample2, 10 Hz and 20°C

Data file name: C:\Users\15400996\Desktop\AMPT-0KPa\AMPT- Sample 2- 20C-0KPa\AC 14- 75 - sample2 -7-05-2013-20 C.D006											
Project name: AAPA					Target test temperature (°C): 20						
Operators name: HOSSEIN					Target confining stress (kPa): 0						
Loading Rates: 25 Hz,20 Hz,10 Hz,5 Hz,2 Hz,1 Hz,0.5 Hz,0.2 Hz,0.1 Hz,0.01 Hz											
Comments: Default Template for AMPT testing Asphalt 15-40 Degrees C											
Calibration files and Channel allocations are set.											
Tuning may be adjusted for optimal results.											
Select Desired Frequencies.											
When changed save template to a new name.											
Specimen Information											
Identification:AC14-75		Dimensions		Point 1	Point 2	Point 3	Point 4	Point 5	Point 6	Average	Std Dev.
Conditioning time:3 HOURS		Diameter (mm)		102.2	102.1	102.2	102.2	102.2	102.2	102.2	0.052
Properties/Comments:5.4% AIRVOIDS-07/05/2		Height (mm)		151.0	151.1	151.2	151.8	151.1	151.1	151.2	0.272
Cross-sectional area (mm²): 8198.8											
Tabulated Results Summary											
	25 Hz	20 Hz	10 Hz	5 Hz	2 Hz	1 Hz	0.5 Hz	0.2 Hz	0.1 Hz	0.01 Hz	
Dynamic modulus (MPa)	8614	8313	7296	6337	5176	4398	3688	2853	2322	1014	
Phase angle (Degrees)	17.85	18.26	19.76	21.31	23.47	25.03	26.47	28.53	29.75	33.29	
Average temperature (°C)	20.0	20.0	20.0	20.0	20.0	20.0	20.1	20.1	20.1	20.0	
Average confining pressure (kPa)	0.4	0.4	0.5	0.4	0.4	0.4	0.4	0.4	0.4	0.5	
Average micro-strain	95	97	98	98	97	97	97	97	97	100	
Load drift (%)	-0.8	-0.6	0.0	0.1	0.1	-0.1	0.3	-0.2	0.0	-0.3	
Load standard error (%)	5.1	4.3	2.1	1.1	0.8	0.6	0.7	0.9	1.1	2.3	
Average deformation drift (%)	-134.3	-122.6	-139.8	-152.1	-170.7	-179.9	-189.6	-205.5	-206.5	-197.7	
Average deformation standard error (%)	5.5	4.6	3.5	3.0	2.4	2.0	1.6	1.5	2.0	2.3	
Deformation uniformity (%)	7.2	5.5	4.5	3.7	3.1	2.7	2.4	2.4	2.6	3.0	
Phase uniformity (Degrees)	0.2	0.2	0.2	0.3	0.4	0.3	0.3	0.4	0.4	0.5	

Figure E - 21. UTS6 summary output for sample2, 20°C

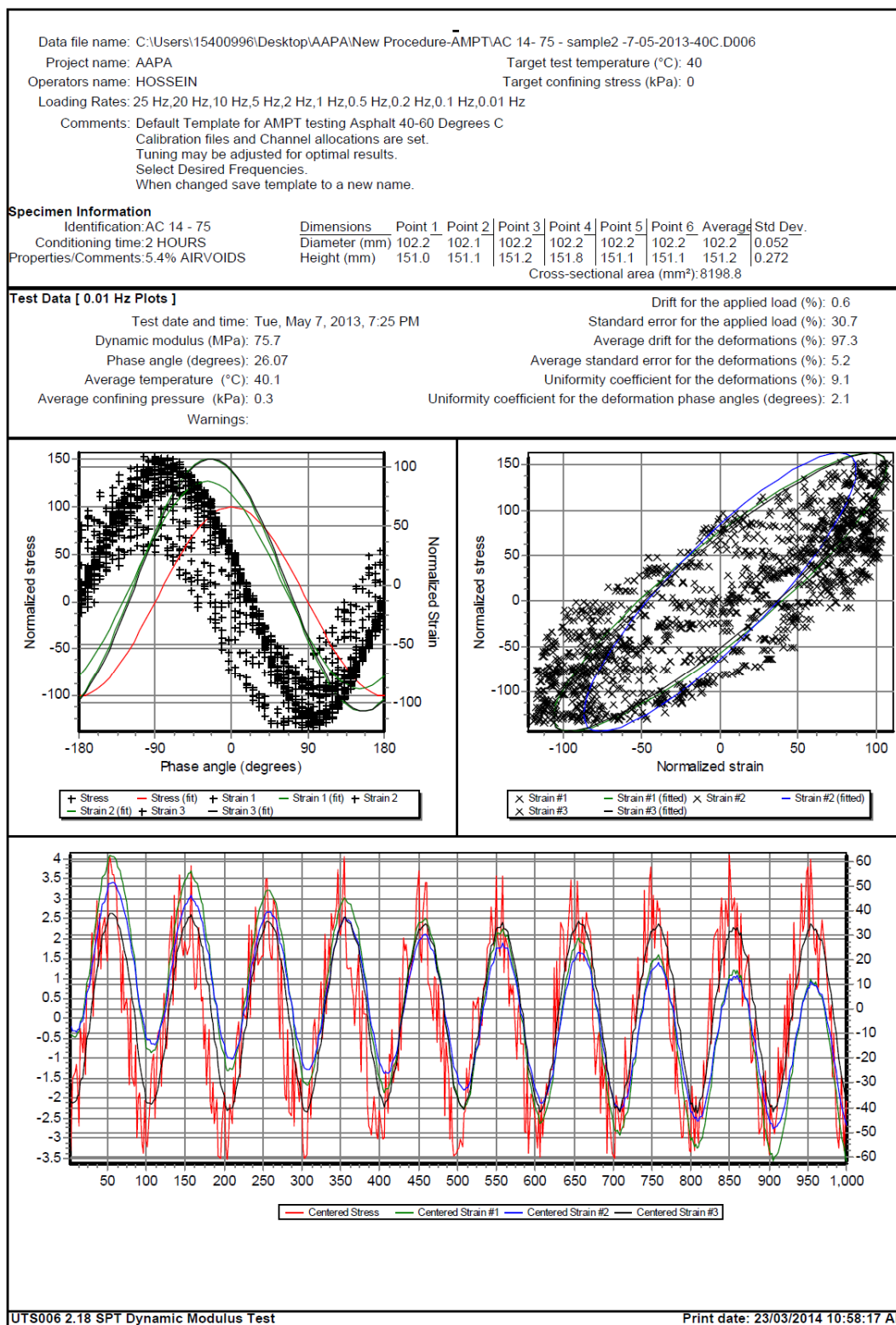


Figure E - 22. UTS6 output for sample2, 0.01 Hz and 40°C

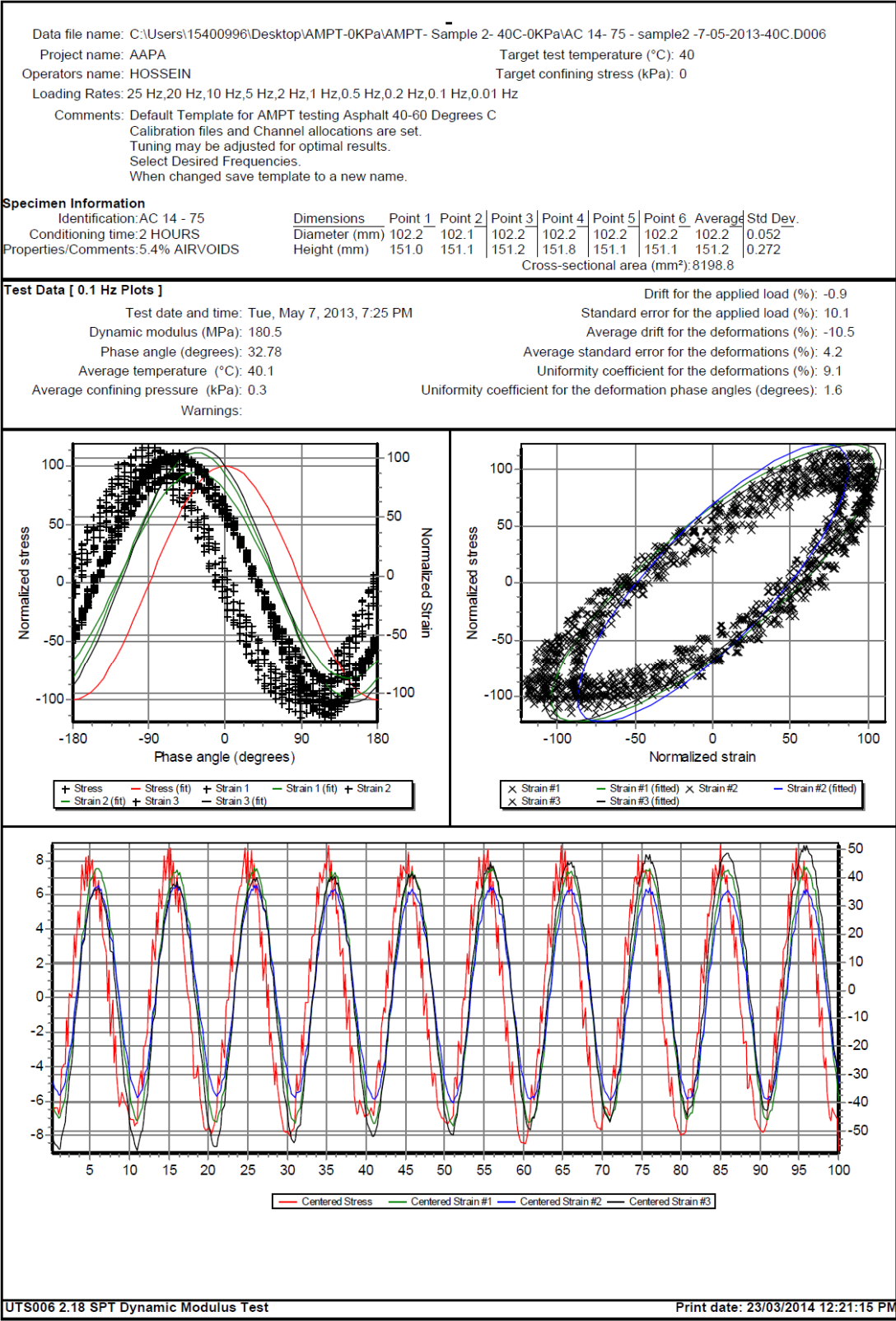


Figure E - 23. UTS6 output for sample2, 0.1 Hz and 40°C

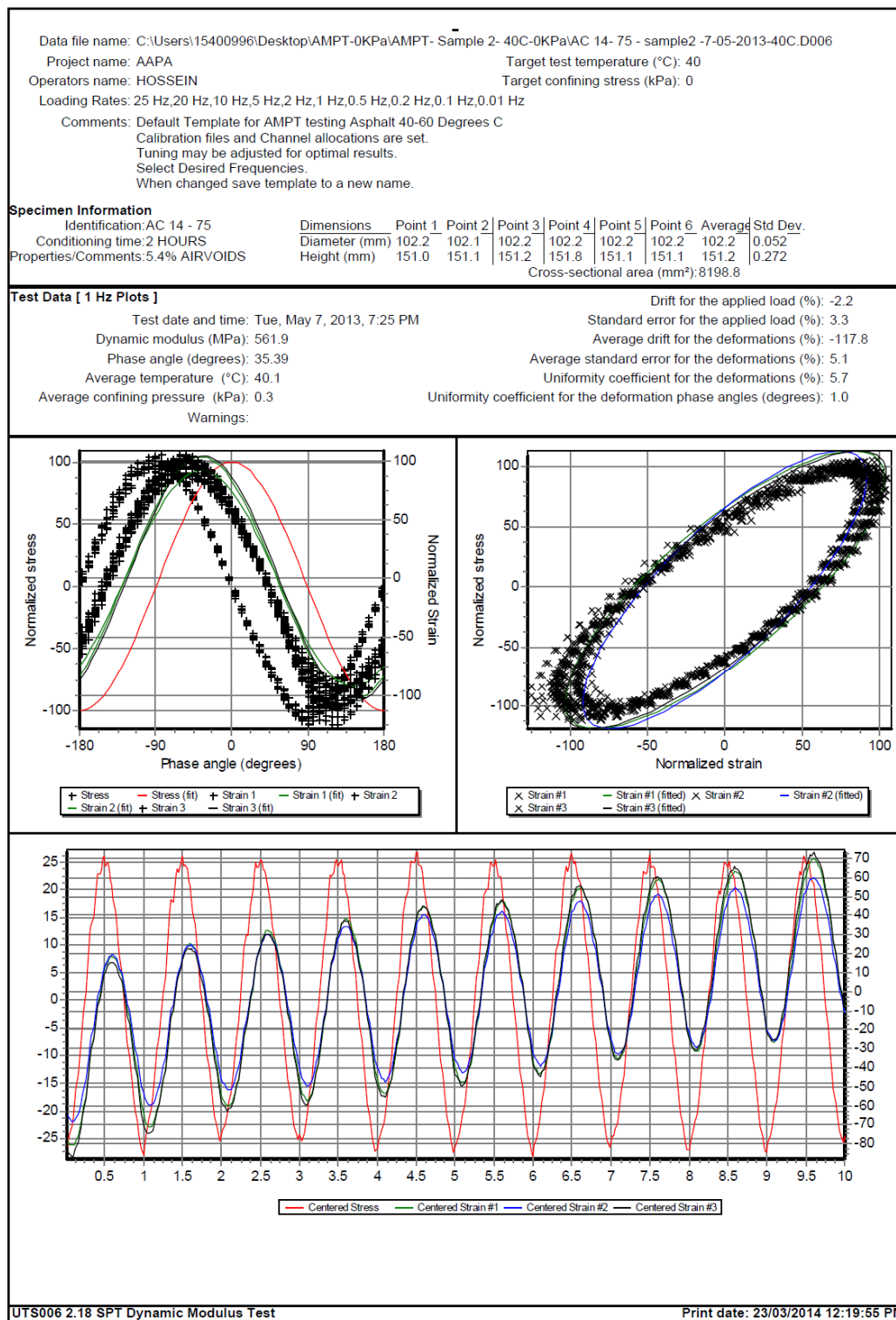


Figure E - 24. UTS6 output for sample2, 1 Hz and 40°C

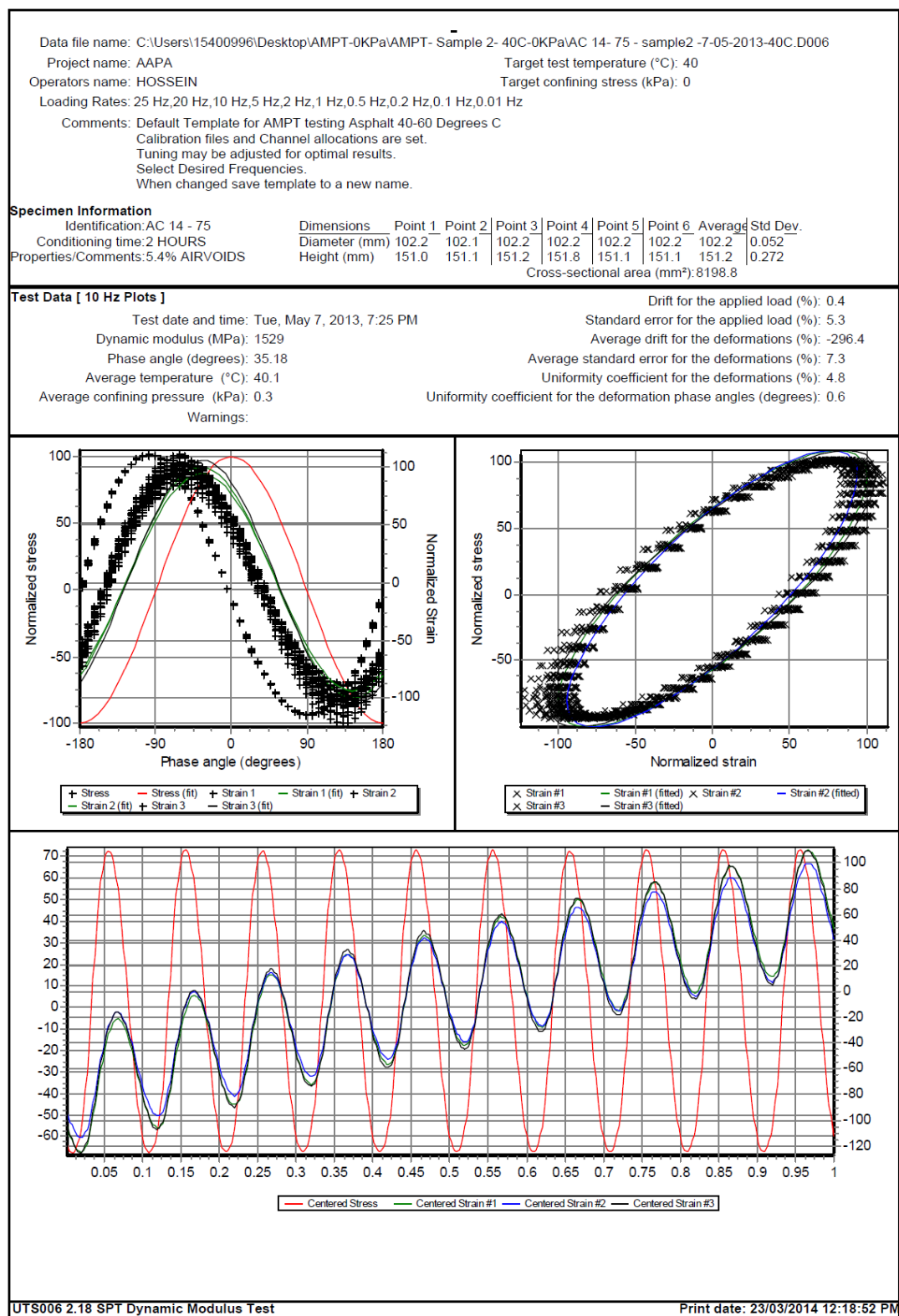


Figure E - 25. UTS6 output for sample2, 10 Hz and 40°C

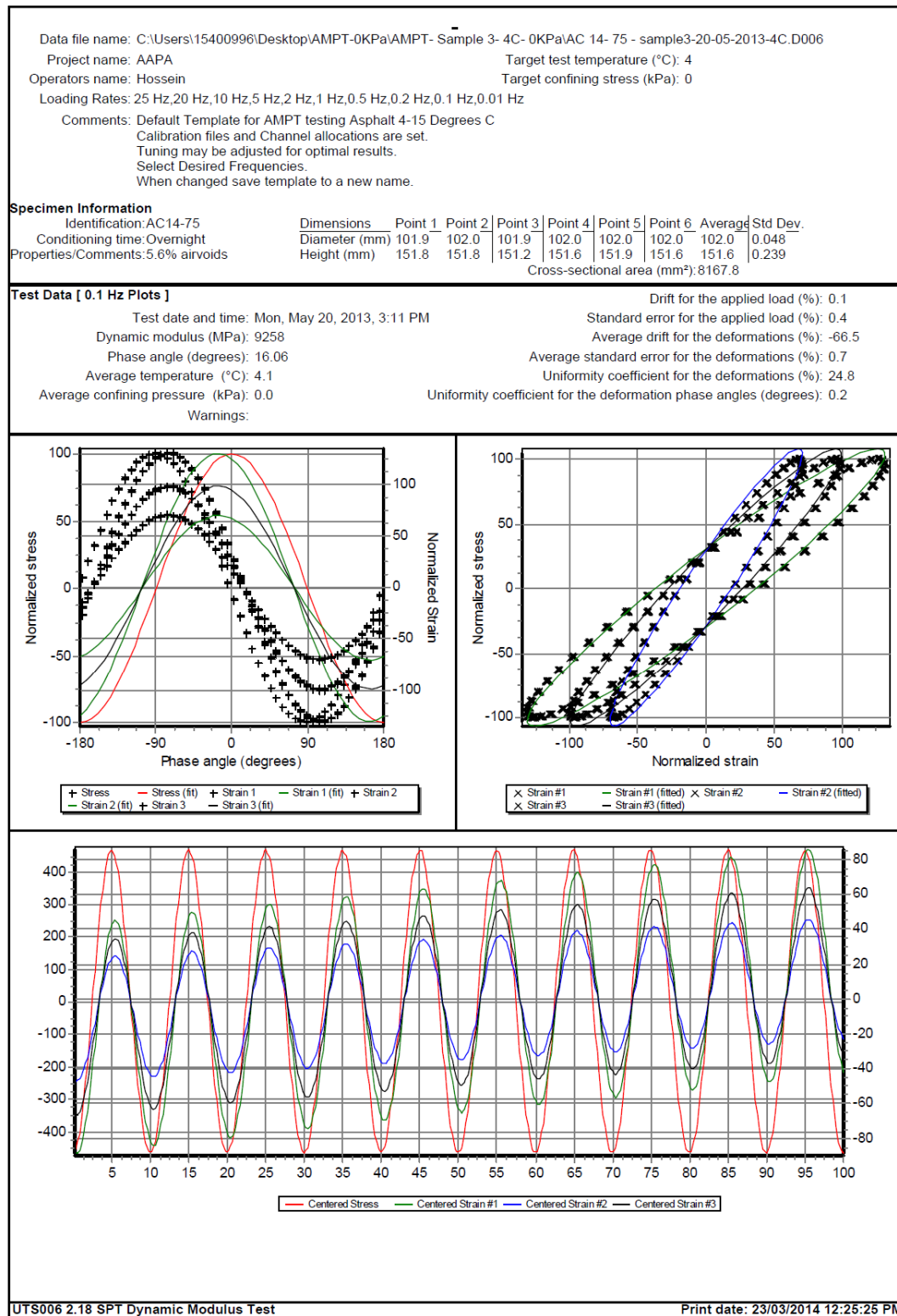


Figure E - 27. UTS6 output for sample3, 0.1 Hz and 4°C

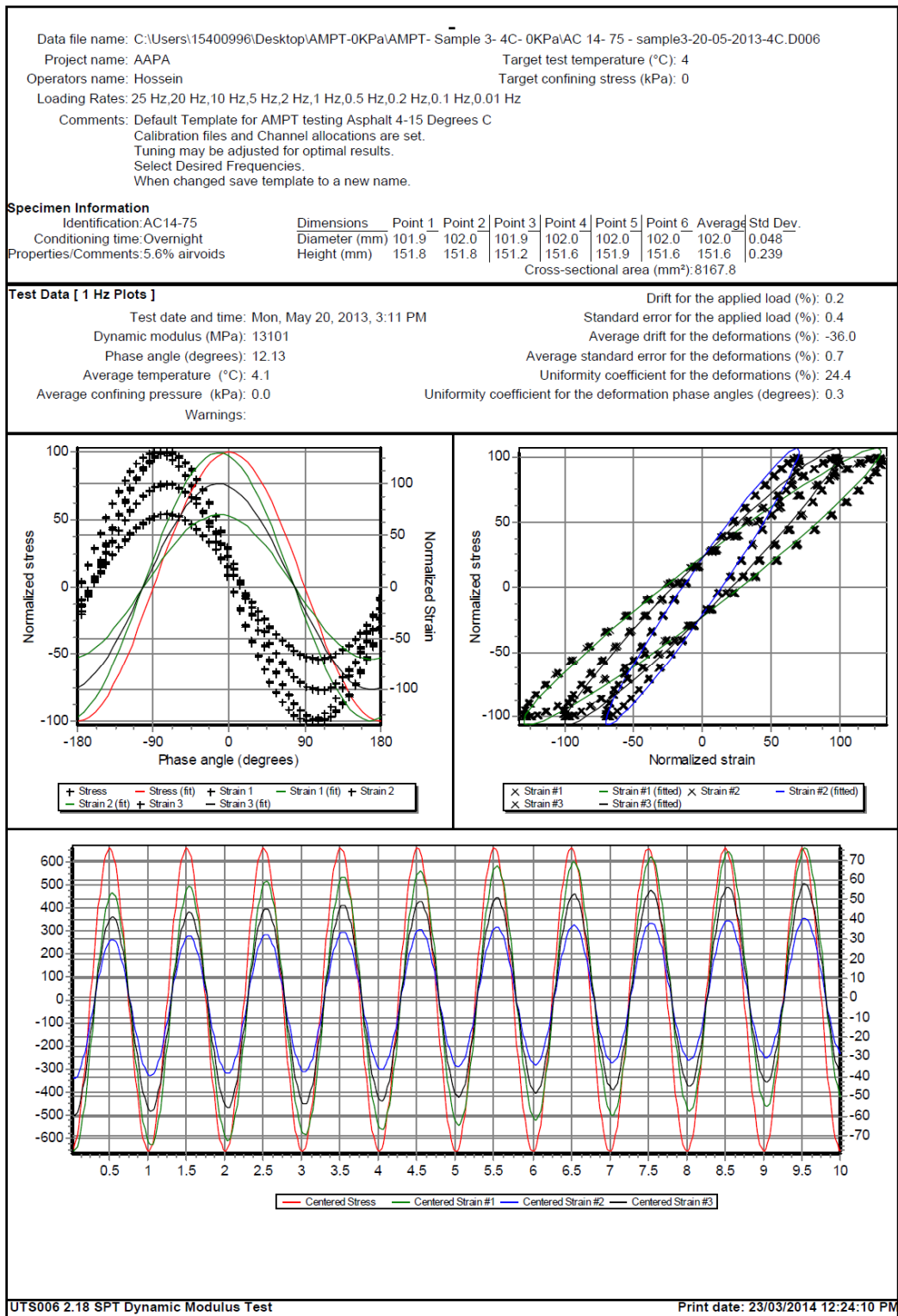


Figure E - 28. UTS6 output for sample3, 1 Hz and 4°C

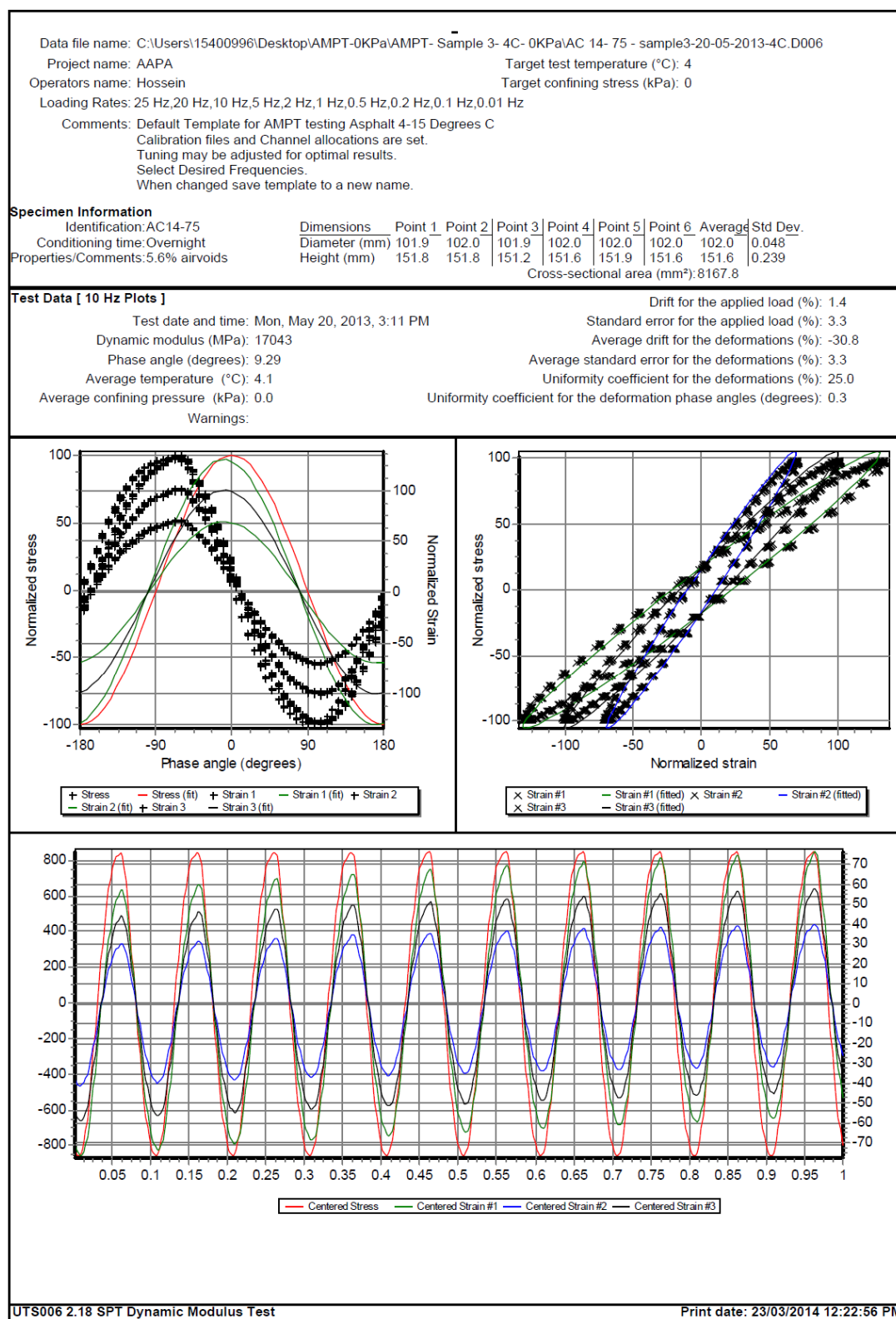


Figure E - 29. UTS6 output for sample3, 10 Hz and 4°C

Data file name: C:\Users\15400996\Desktop\AMPT-0KPa\AMPT- Sample 3- 4C- 0KPa\AC 14- 75 - sample3-20-05-2013-4C.D006													
Project name: AAPA						Target test temperature (°C): 4							
Operators name: Hossein						Target confining stress (kPa): 0							
Loading Rates: 25 Hz,20 Hz,10 Hz,5 Hz,2 Hz,1 Hz,0.5 Hz,0.2 Hz,0.1 Hz,0.01 Hz													
Comments: Default Template for AMPT testing Asphalt 4-15 Degrees C													
Calibration files and Channel allocations are set.													
Tuning may be adjusted for optimal results.													
Select Desired Frequencies.													
When changed save template to a new name.													
Specimen Information													
Identification:AC14-75				Dimensions		Point 1	Point 2	Point 3	Point 4	Point 5	Point 6	Average	Std Dev.
Conditioning time:Overnight				Diameter (mm)		101.9	102.0	101.9	102.0	102.0	102.0	102.0	0.048
Properties/Comments:5.6% airvoids				Height (mm)		151.8	151.8	151.2	151.6	151.9	151.6	151.6	0.239
Cross-sectional area (mm²): 8167.8													
Tabulated Results Summary													
	25 Hz	20 Hz	10 Hz	5 Hz	2 Hz	1 Hz	0.5 Hz	0.2 Hz	0.1 Hz	0.01 Hz			
Dynamic modulus (MPa)	18574	18213	17043	15870	14316	13101	11900	10376	9258	6002			
Phase angle (Degrees)	8.52	8.57	9.29	10.07	11.18	12.13	13.19	14.73	16.06	21.09			
Average temperature (°C)	4.1	4.1	4.1	4.1	4.1	4.1	4.1	4.0	4.1	4.1			
Average confining pressure (kPa)	0.0	0.0	0.0	0.0	0.0	0.0	0.0	0.0	0.0	0.0			
Average micro-strain	92	96	101	100	100	100	100	100	100	99			
Load drift (%)	11.8	10.7	1.4	0.1	-0.2	0.2	0.1	-0.1	0.1	0.0			
Load standard error (%)	14.4	11.6	3.3	1.2	0.6	0.4	0.3	0.3	0.4	0.6			
Average deformation drift (%)	-45.0	-42.9	-30.8	-32.0	-32.4	-36.0	-42.4	-54.8	-66.5	-153.5			
Average deformation standard error (%)	13.9	10.8	3.3	1.6	0.9	0.7	0.7	0.7	0.7	1.6			
Deformation uniformity (%)	26.3	25.8	25.0	24.6	24.3	24.4	24.6	24.7	24.8	24.9			
Phase uniformity (Degrees)	0.3	0.4	0.3	0.3	0.3	0.3	0.3	0.3	0.2	0.3			

Figure E - 30. UTS6 summary output for sample3, 4°C

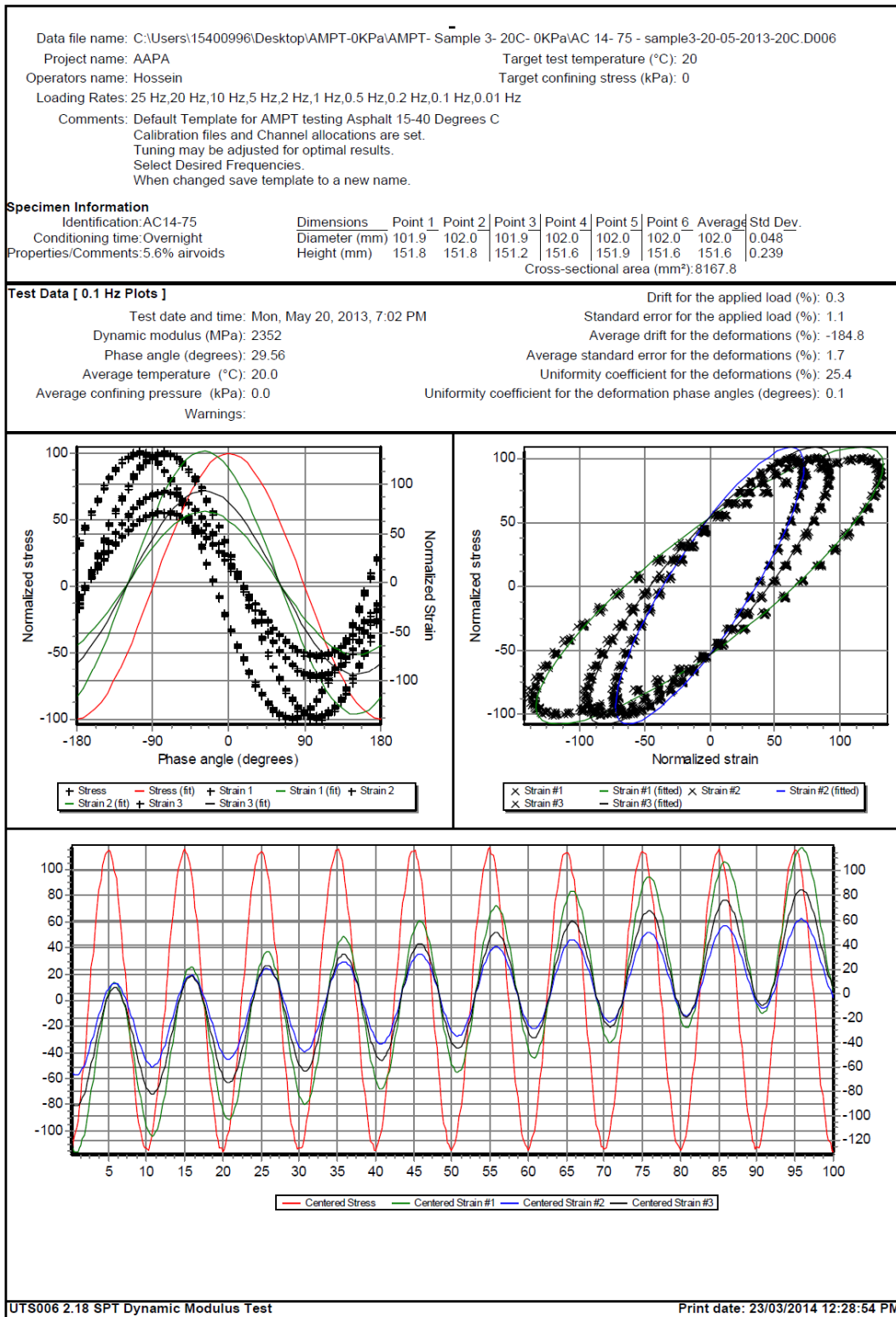


Figure E - 31. UTS6 output for sample3, 0.1 Hz and 20°C

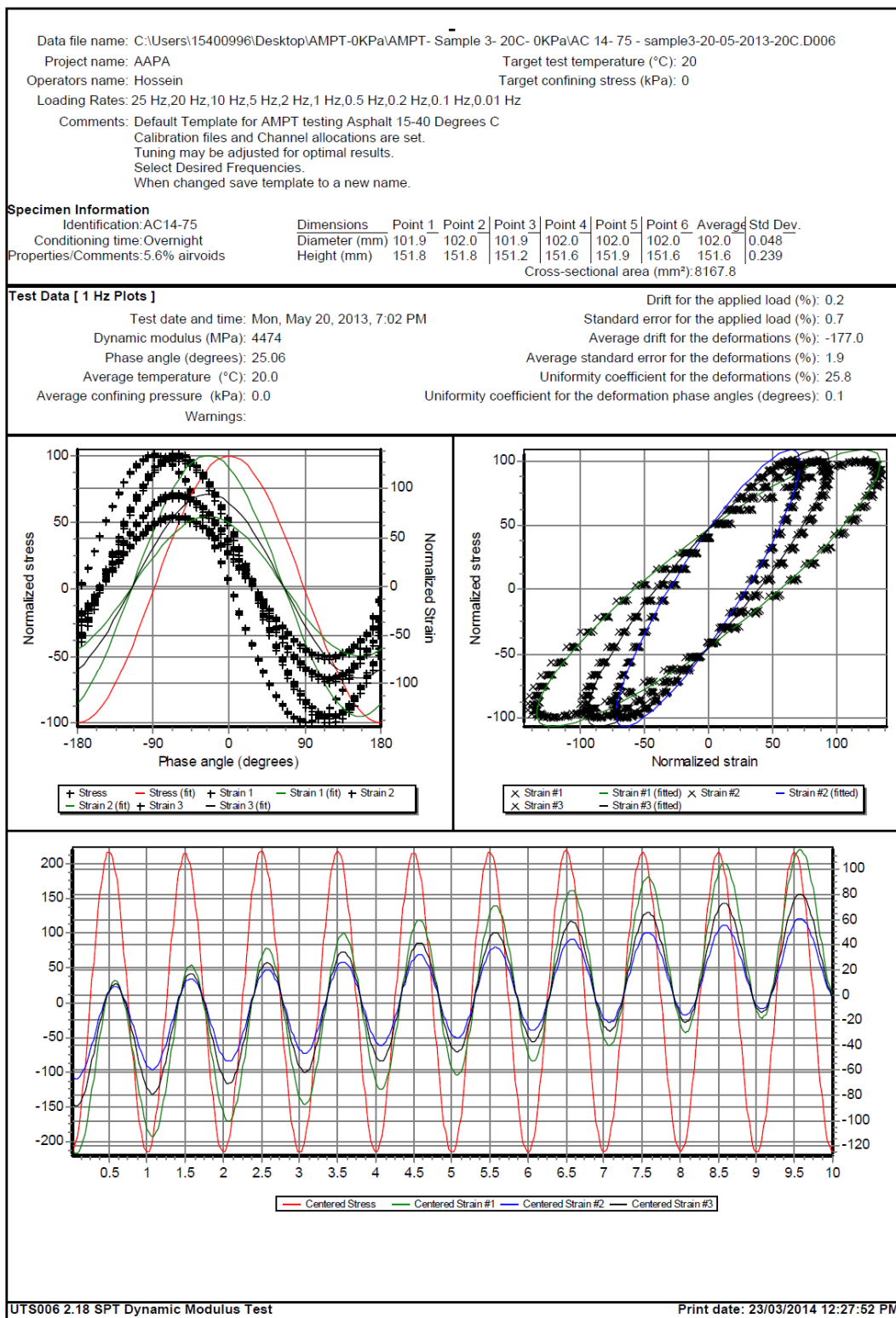


Figure E - 32. UTS6 output for sample3, 1 Hz and 20°C

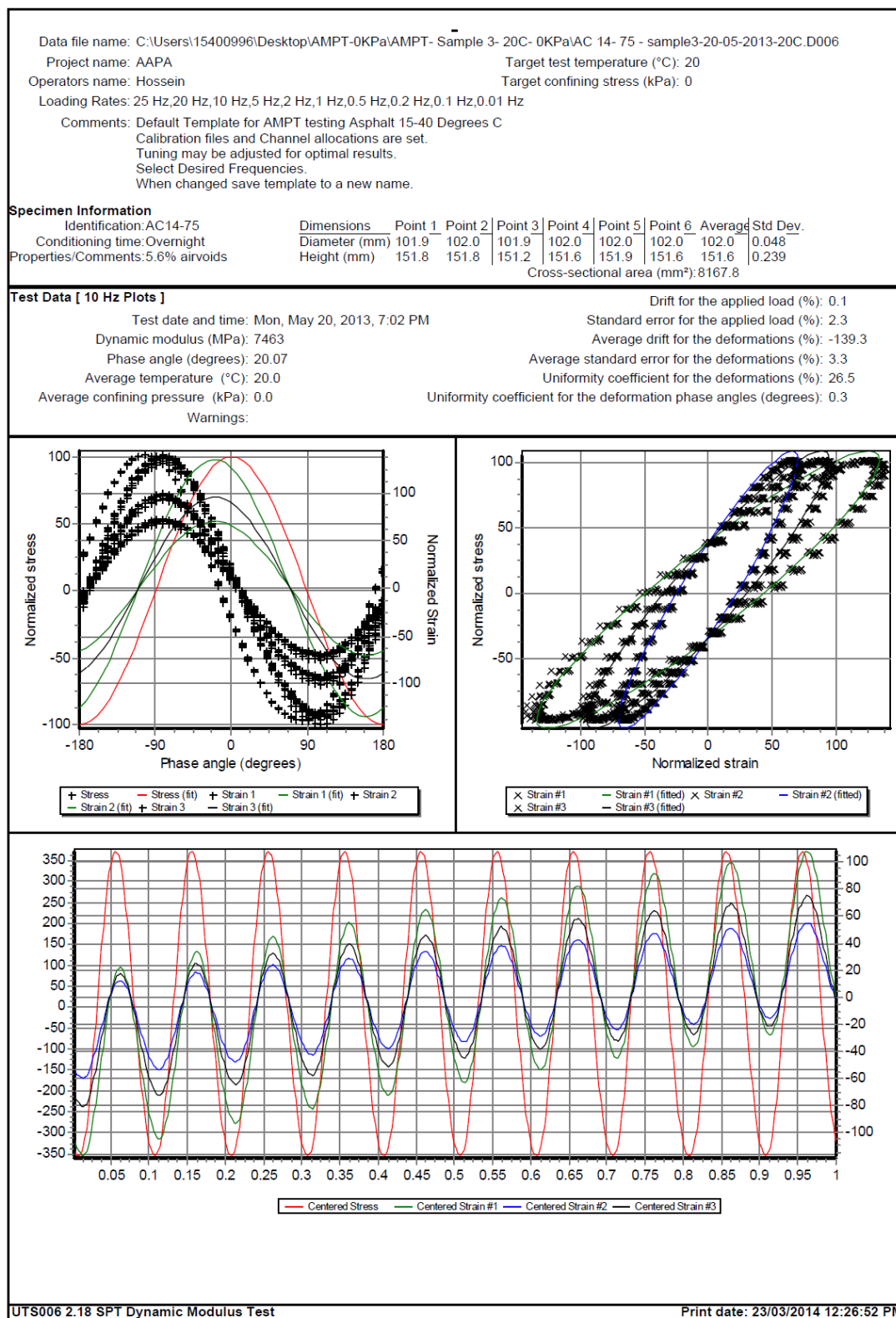


Figure E - 33. UTS6 output for sample3, 10 Hz and 20°C

Data file name: C:\Users\15400996\Desktop\AMPT-0KPa\AMPT- Sample 3- 20C- 0KPa\AC 14- 75 - sample3-20-05-2013-20C.D006											
Project name: AAPA					Target test temperature (°C): 20						
Operators name: Hossein					Target confining stress (kPa): 0						
Loading Rates: 25 Hz,20 Hz,10 Hz,5 Hz,2 Hz,1 Hz,0.5 Hz,0.2 Hz,0.1 Hz,0.01 Hz											
Comments: Default Template for AMPT testing Asphalt 15-40 Degrees C											
Calibration files and Channel allocations are set.											
Tuning may be adjusted for optimal results.											
Select Desired Frequencies.											
When changed save template to a new name.											
Specimen Information											
Identification:AC14-75		Dimensions		Point 1	Point 2	Point 3	Point 4	Point 5	Point 6	Average	Std Dev.
Conditioning time:Overnight		Diameter (mm)		101.9	102.0	101.9	102.0	102.0	102.0	102.0	0.048
Properties/Comments:5.6% airvoids		Height (mm)		151.8	151.8	151.2	151.6	151.9	151.6	151.6	0.239
Cross-sectional area (mm²): 8167.8											
Tabulated Results Summary											
	25 Hz	20 Hz	10 Hz	5 Hz	2 Hz	1 Hz	0.5 Hz	0.2 Hz	0.1 Hz	0.01 Hz	
Dynamic modulus (MPa)	8857	8534	7463	6480	5273	4474	3755	2905	2352	1019	
Phase angle (Degrees)	18.16	18.53	20.07	21.51	23.63	25.06	26.51	28.41	29.56	32.77	
Average temperature (°C)	20.0	20.0	20.0	20.0	20.1	20.0	20.0	20.0	20.0	20.1	
Average confining pressure (kPa)	0.1	0.1	0.0	0.0	0.0	0.0	0.0	0.0	0.0	0.0	
Average micro-strain	97	98	98	97	97	97	97	97	97	102	
Load drift (%)	-0.8	-0.4	0.1	-0.1	0.1	0.2	-0.3	0.2	0.3	-0.4	
Load standard error (%)	5.4	3.9	2.3	1.4	1.0	0.7	0.7	0.9	1.1	2.4	
Average deformation drift (%)	-134.1	-123.0	-139.3	-151.1	-167.9	-177.0	-180.4	-192.0	-184.8	-150.0	
Average deformation standard error (%)	5.3	4.1	3.3	2.8	2.2	1.9	1.6	1.4	1.7	2.6	
Deformation uniformity (%)	27.6	27.1	26.5	26.3	26.0	25.8	25.7	25.6	25.4	25.3	
Phase uniformity (Degrees)	0.5	0.5	0.3	0.3	0.2	0.1	0.0	0.1	0.1	0.5	

Figure E - 34. UTS6 summary output for sample3, 20°C

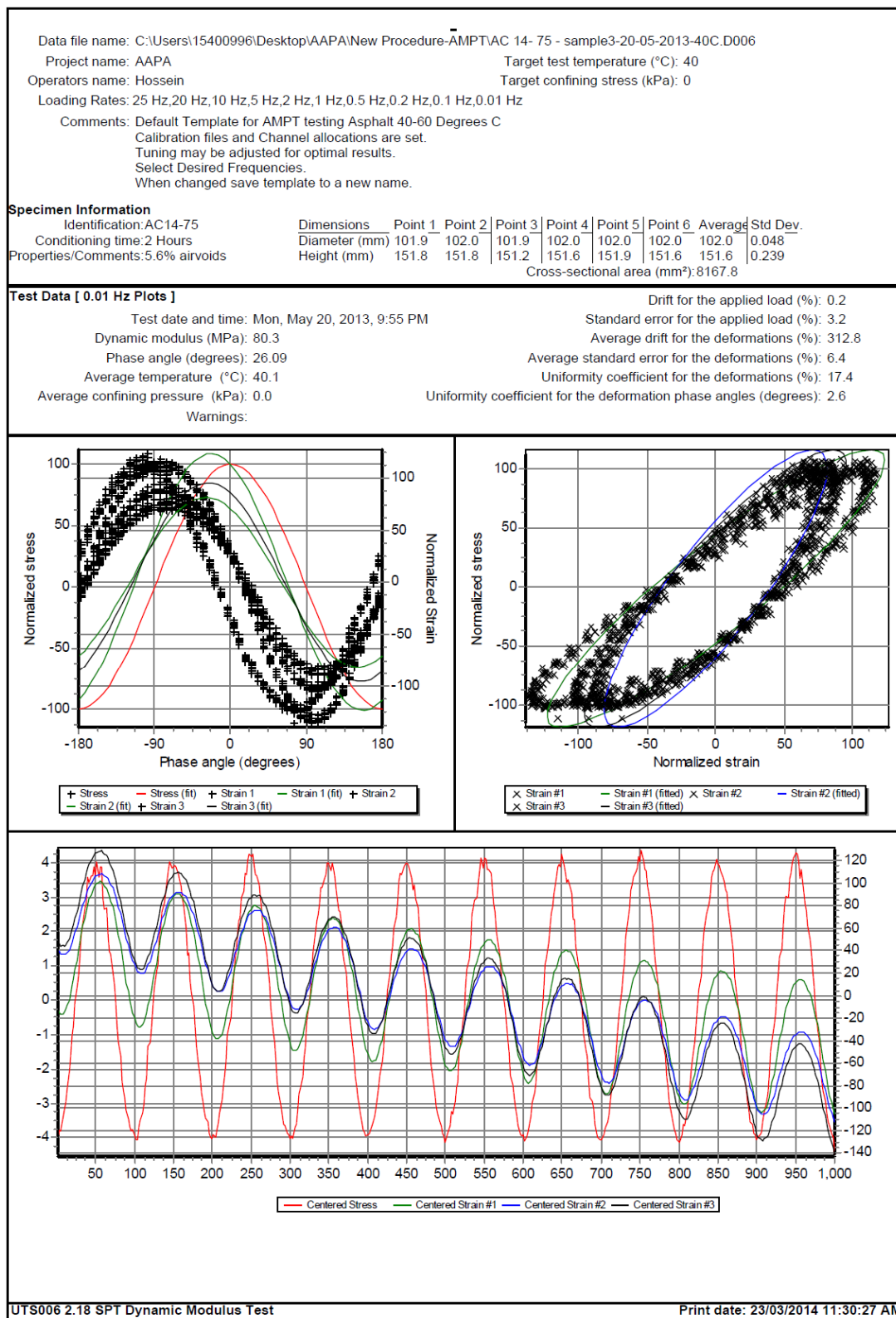
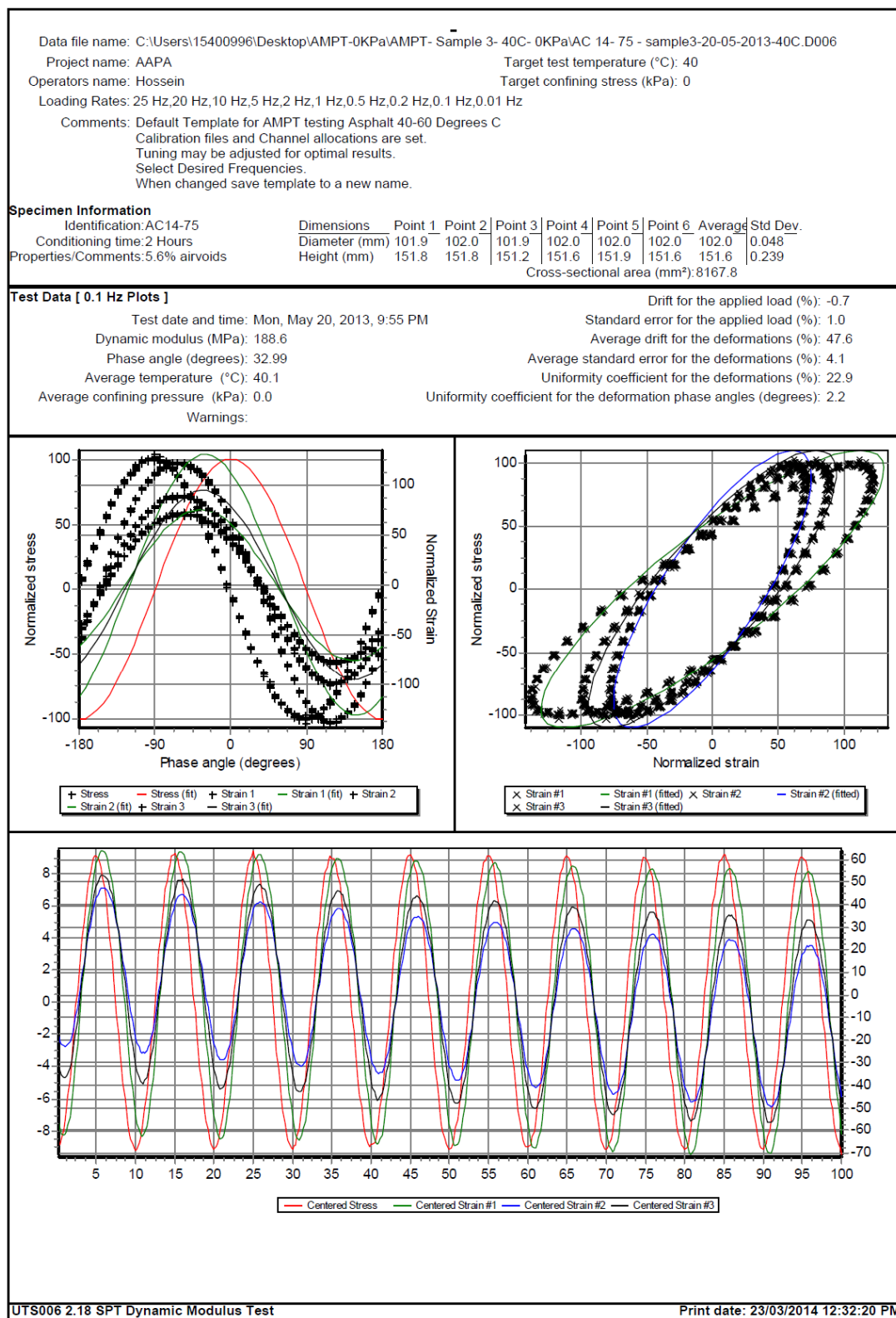


Figure E - 35. UTS6 output for sample3, 0.01 Hz and 40°C



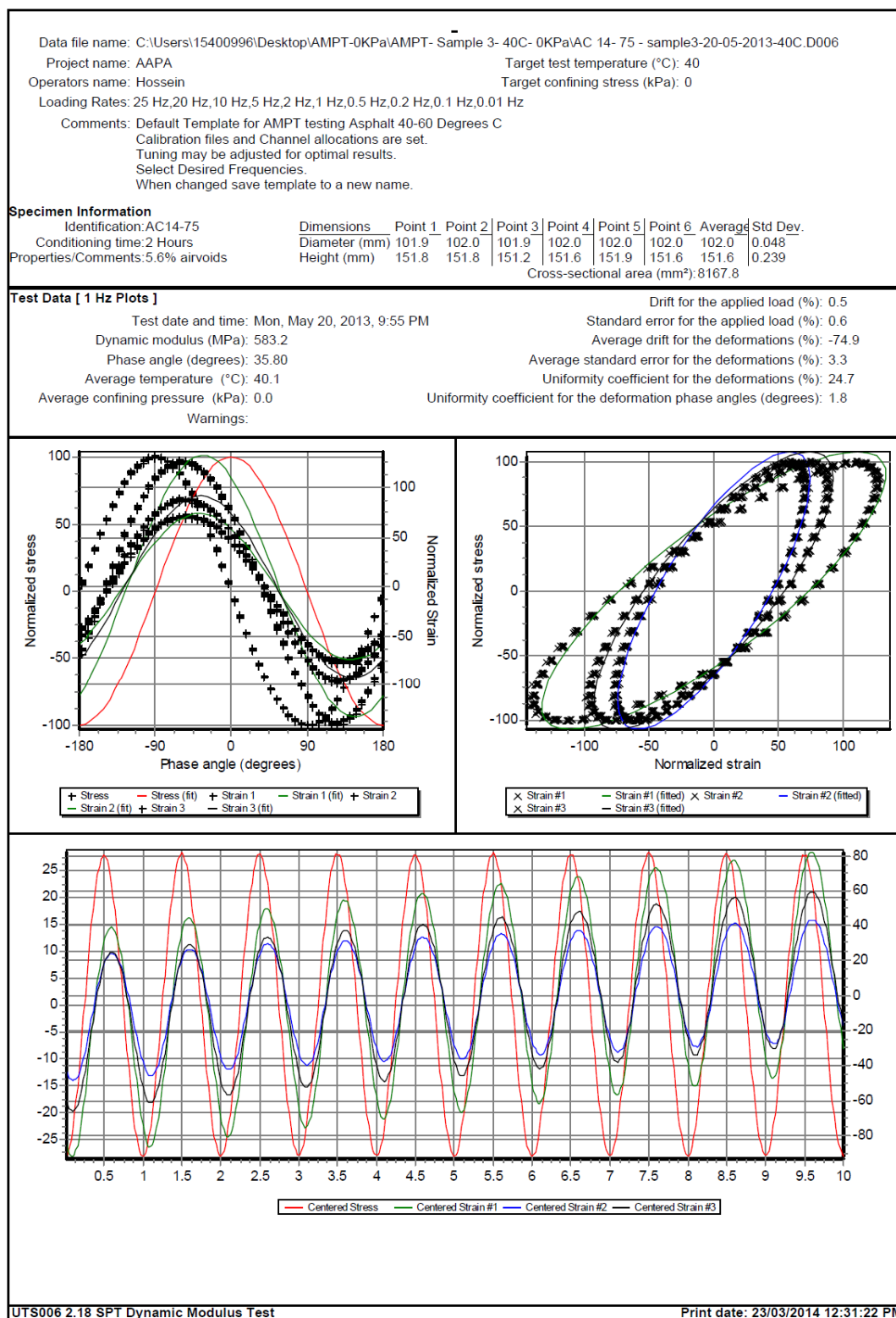


Figure E - 37. UTS6 output for sample3, 1 Hz and 40°C

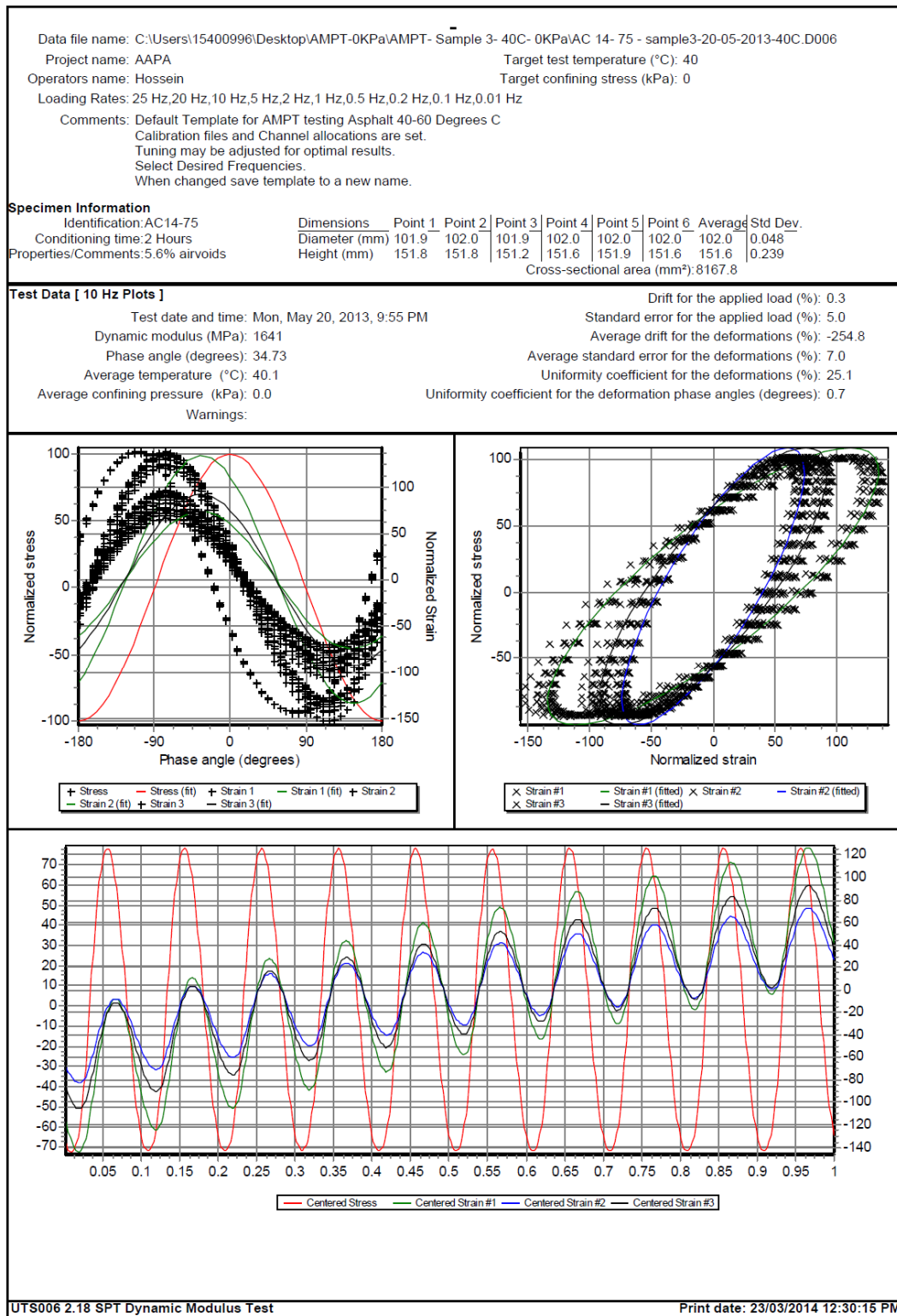


Figure E - 38. UTS6 output for sample3, 10 Hz and 40°C

Data file name: C:\Users\15400996\Desktop\AMPT-0KPa\AMPT- Sample 3- 40C- 0KPa\AC 14- 75 - sample3-20-05-2013-40C.D006										
Project name: AAPA					Target test temperature (°C): 40					
Operators name: Hossein					Target confining stress (kPa): 0					
Loading Rates: 25 Hz,20 Hz,10 Hz,5 Hz,2 Hz,1 Hz,0.5 Hz,0.2 Hz,0.1 Hz,0.01 Hz										
Comments: Default Template for AMPT testing Asphalt 40-60 Degrees C										
Calibration files and Channel allocations are set.										
Tuning may be adjusted for optimal results.										
Select Desired Frequencies.										
When changed save template to a new name.										
Specimen Information										
Identification:AC14-75		Dimensions		Point 1	Point 2	Point 3	Point 4	Point 5	Point 6	Average Std Dev.
Conditioning time:2 Hours		Diameter (mm)		101.9	102.0	101.9	102.0	102.0	102.0	0.048
Properties/Comments:5.6% airvoids		Height (mm)		151.8	151.8	151.2	151.6	151.9	151.6	0.239
Cross-sectional area (mm²):8167.8										
Tabulated Results Summary										
	25 Hz	20 Hz	10 Hz	5 Hz	2 Hz	1 Hz	0.5 Hz	0.2 Hz	0.1 Hz	0.01 Hz
Dynamic modulus (MPa)	2267	2135	1641	1230	812.0	583.2	412.9	264.6	188.6	80.3
Phase angle (Degrees)	34.41	34.03	34.73	35.39	35.91	35.80	35.35	34.19	32.99	26.09
Average temperature (°C)	40.1	40.1	40.1	40.1	40.1	40.1	40.1	40.1	40.1	40.1
Average confining pressure (kPa)	-0.1	0.0	0.0	0.0	0.0	0.0	0.0	0.0	0.0	0.0
Average micro-strain	92	93	94	94	95	96	97	101	97	100
Load drift (%)	-0.7	-0.3	0.3	0.0	0.0	0.5	-0.5	-0.6	-0.7	0.2
Load standard error (%)	7.1	6.5	5.0	3.3	2.0	0.6	0.5	0.7	1.0	3.2
Average deformation drift (%)	-413.3	-326.2	-254.8	-188.1	-116.9	-74.9	-37.4	6.4	47.6	312.8
Average deformation standard error (%)	10.2	8.8	7.0	5.1	3.7	3.3	3.3	4.0	4.1	6.4
Deformation uniformity (%)	26.7	25.7	25.1	25.0	24.8	24.7	24.3	23.6	22.9	17.4
Phase uniformity (Degrees)	0.5	0.7	0.7	0.9	1.4	1.8	1.9	2.1	2.2	2.6

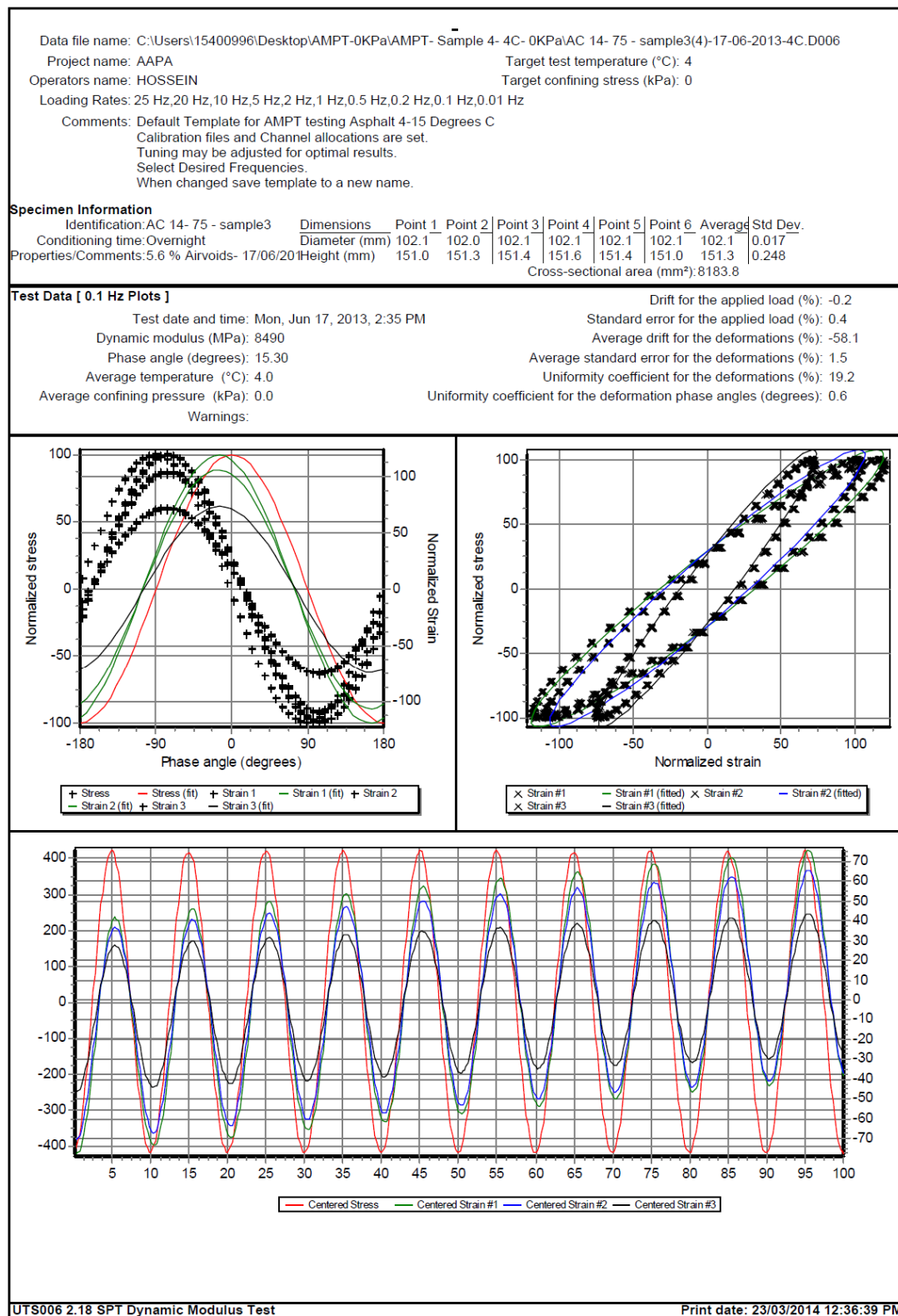


Figure E - 40. UTS6 output for sample5, 0.1 Hz and 4°C

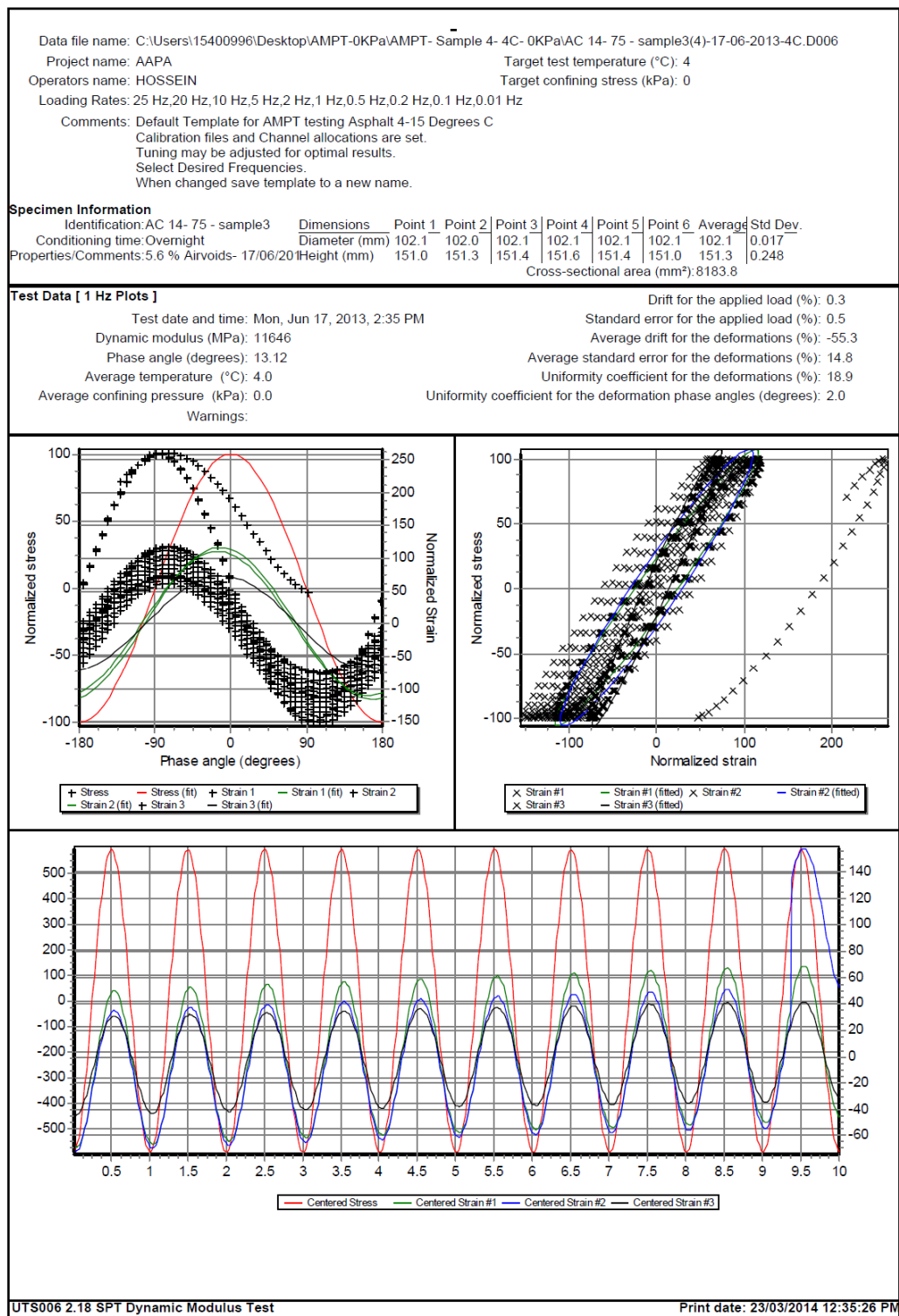


Figure E - 41. UTS6 output for sample5, 1 Hz and 4°C

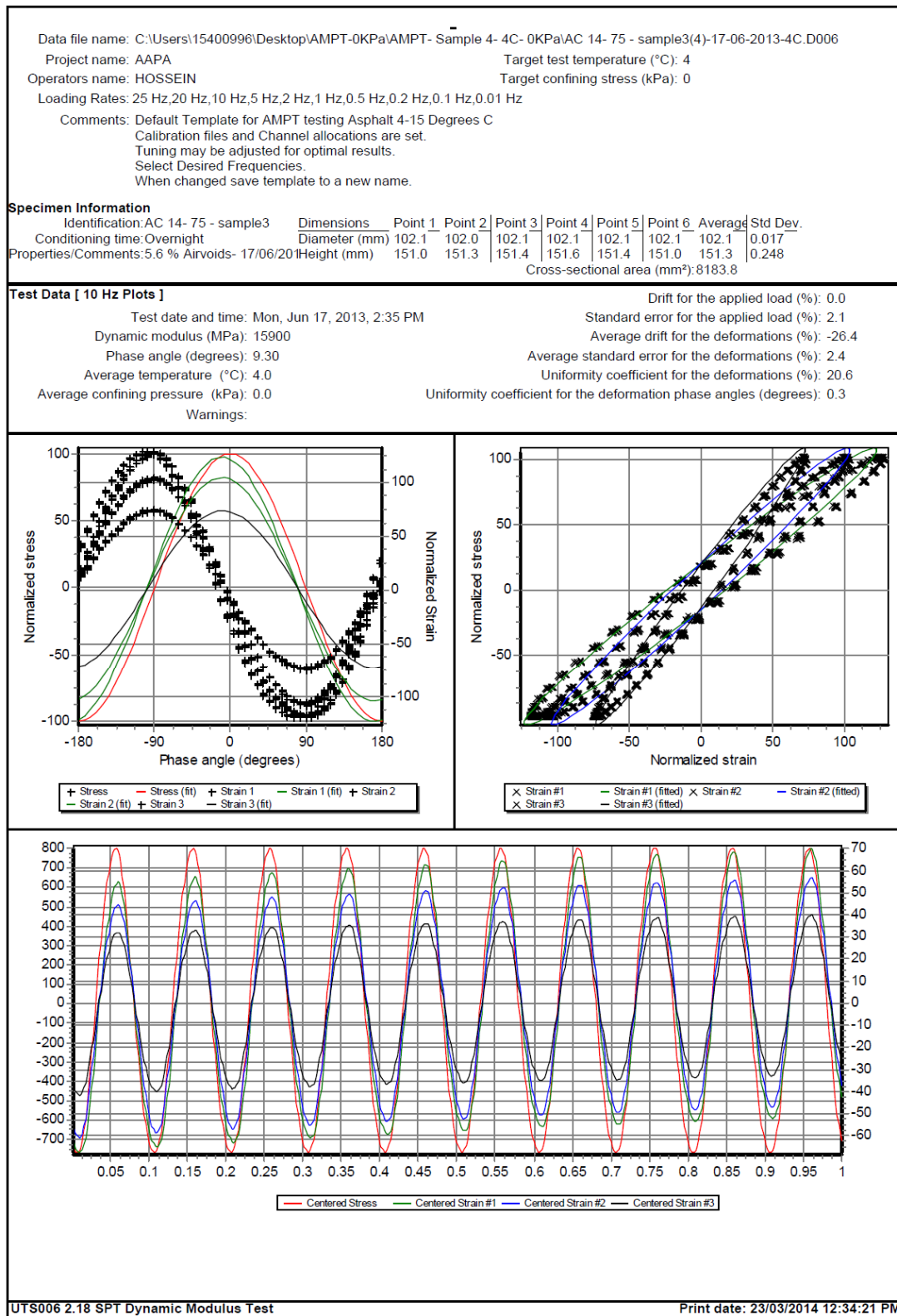


Figure E - 42. UTS6 output for sample5, 10 Hz and 4°C

Data file name: C:\Users\15400996\Desktop\AMPT-0KPa\AMPT- Sample 4- 4C- 0KPa\AC 14- 75 - sample3(4)-17-06-2013-4C.D006										
Project name: AAPA					Target test temperature (°C): 4					
Operators name: HOSSEIN					Target confining stress (kPa): 0					
Loading Rates: 25 Hz,20 Hz,10 Hz,5 Hz,2 Hz,1 Hz,0.5 Hz,0.2 Hz,0.1 Hz,0.01 Hz										
Comments: Default Template for AMPT testing Asphalt 4-15 Degrees C										
Calibration files and Channel allocations are set.										
Tuning may be adjusted for optimal results.										
Select Desired Frequencies.										
When changed save template to a new name.										
Specimen Information										
Identification:AC 14- 75 - sample3		Dimensions	Point 1	Point 2	Point 3	Point 4	Point 5	Point 6	Average	Std Dev.
Conditioning time:Overnight		Diameter (mm)	102.1	102.0	102.1	102.1	102.1	102.1	102.1	0.017
Properties/Comments:5.6 % Airvoids- 17/06/2011		Height (mm)	151.0	151.3	151.4	151.6	151.4	151.0	151.3	0.248
Cross-sectional area (mm²):8183.8										
Tabulated Results Summary										
	25 Hz	20 Hz	10 Hz	5 Hz	2 Hz	1 Hz	0.5 Hz	0.2 Hz	0.1 Hz	0.01 Hz
Dynamic modulus (MPa)	17142	16960	15900	14738	13130	11646	10745	9414	8490	5612
Phase angle (Degrees)	9.34	8.59	9.30	10.00	11.03	13.12	12.76	14.17	15.30	20.17
Average temperature (°C)	4.0	4.0	4.0	4.0	4.0	4.0	4.0	4.1	4.0	4.1
Average confining pressure (kPa)	0.0	0.0	0.0	0.0	0.0	0.0	0.0	0.0	0.0	0.0
Average micro-strain	100	100	99	100	100	102	99	99	99	99
Load drift (%)	10.6	2.9	0.0	0.1	-0.1	0.3	0.0	0.1	-0.2	-0.1
Load standard error (%)	10.6	5.4	2.1	1.2	0.7	0.5	0.3	0.4	0.4	0.7
Average deformation drift (%)	41.0	-30.0	-26.4	-28.6	-35.2	-55.3	-37.1	-49.4	-58.1	-134.7
Average deformation standard error (%)	24.3	5.2	2.4	2.4	2.4	14.8	2.0	1.7	1.5	2.0
Deformation uniformity (%)	18.3	20.1	20.6	20.2	19.2	18.9	18.2	18.5	19.2	20.8
Phase uniformity (Degrees)	1.9	0.3	0.3	0.4	0.4	2.0	0.4	0.5	0.6	0.8

Figure E - 43. UTS6 summary output for sample4, 4°C

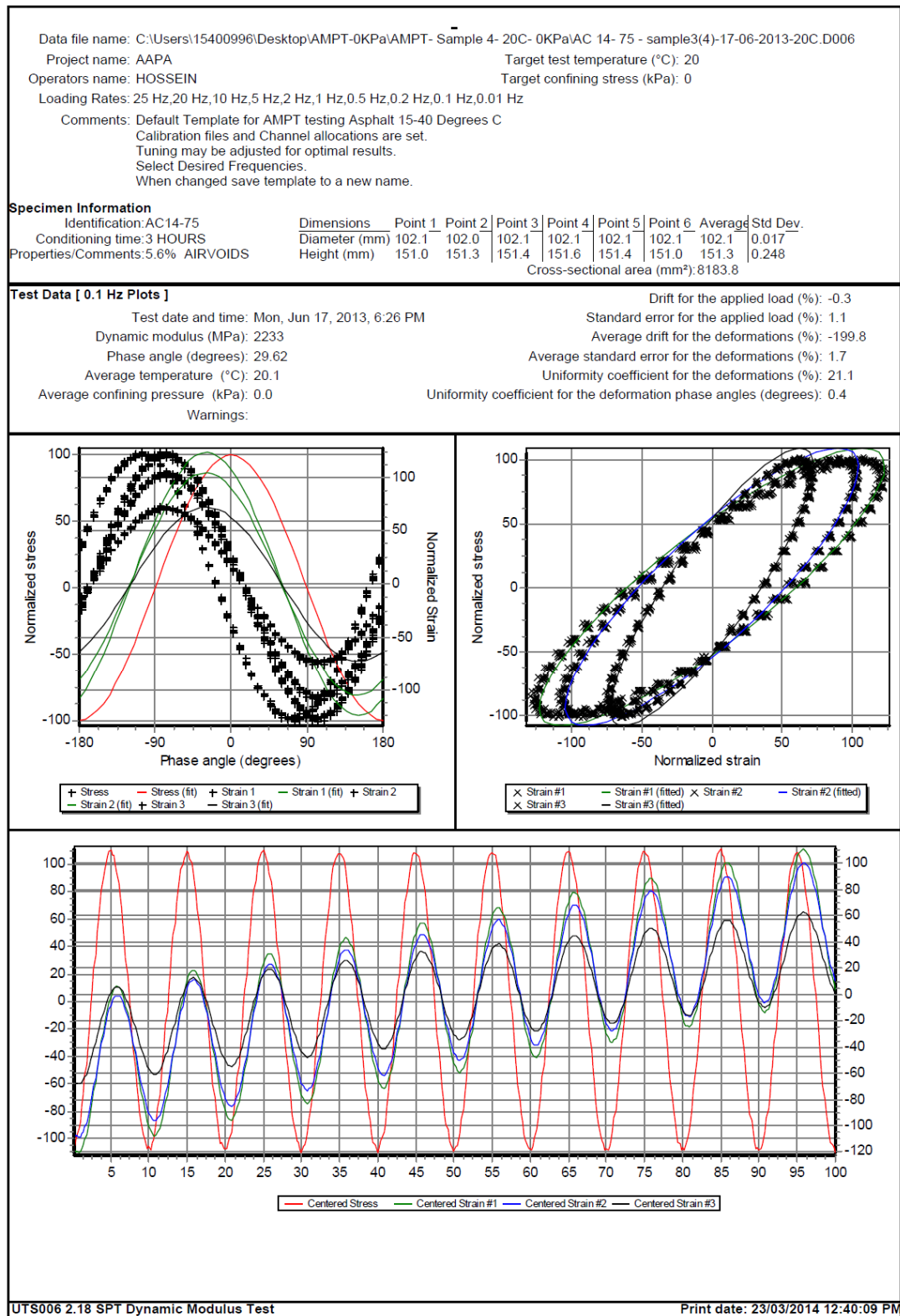


Figure E - 44. UTS6 output for sample4, 0.1 Hz and 20°C

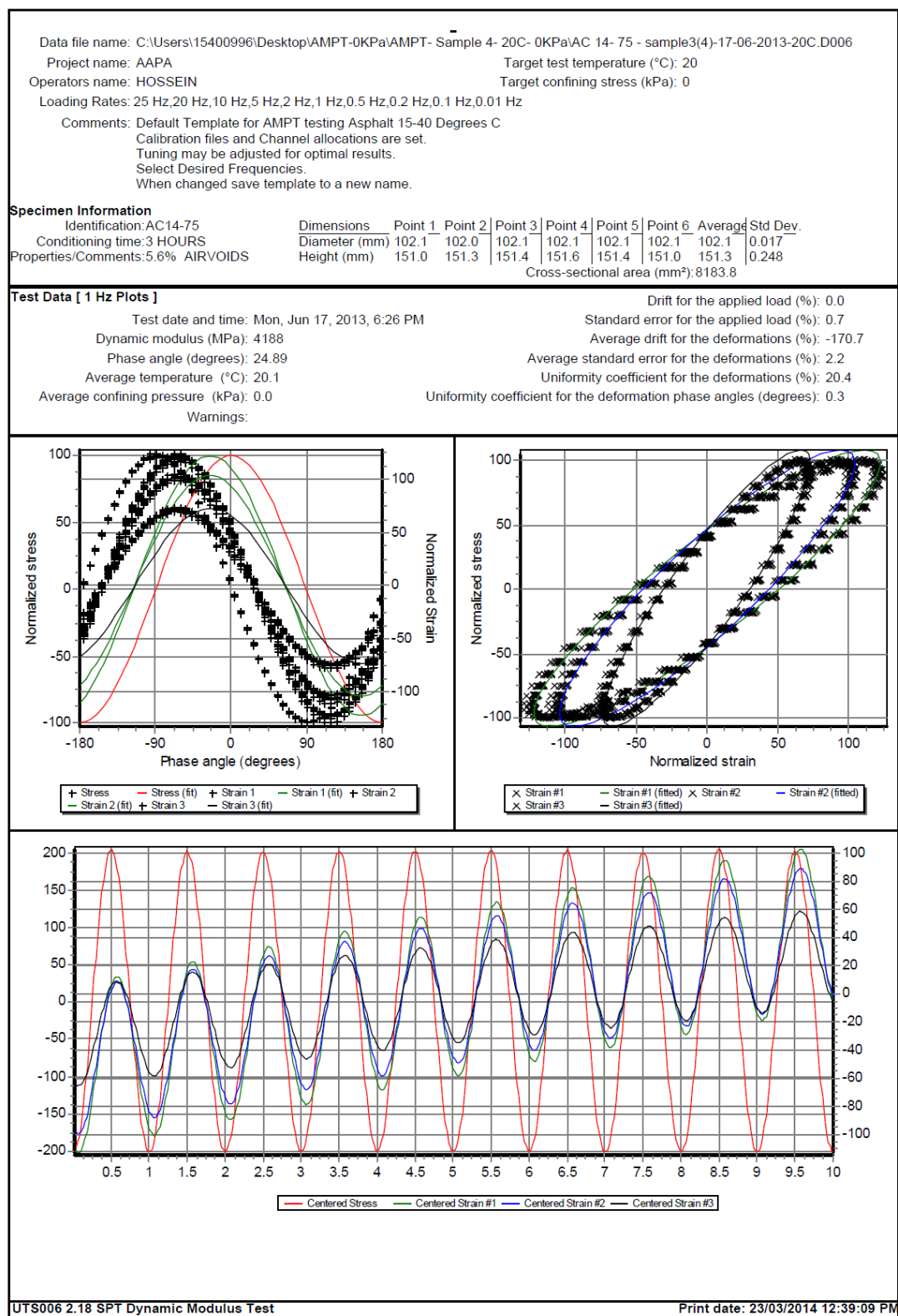


Figure E - 45. UTS6 output for sample4, 1 Hz and 20°C

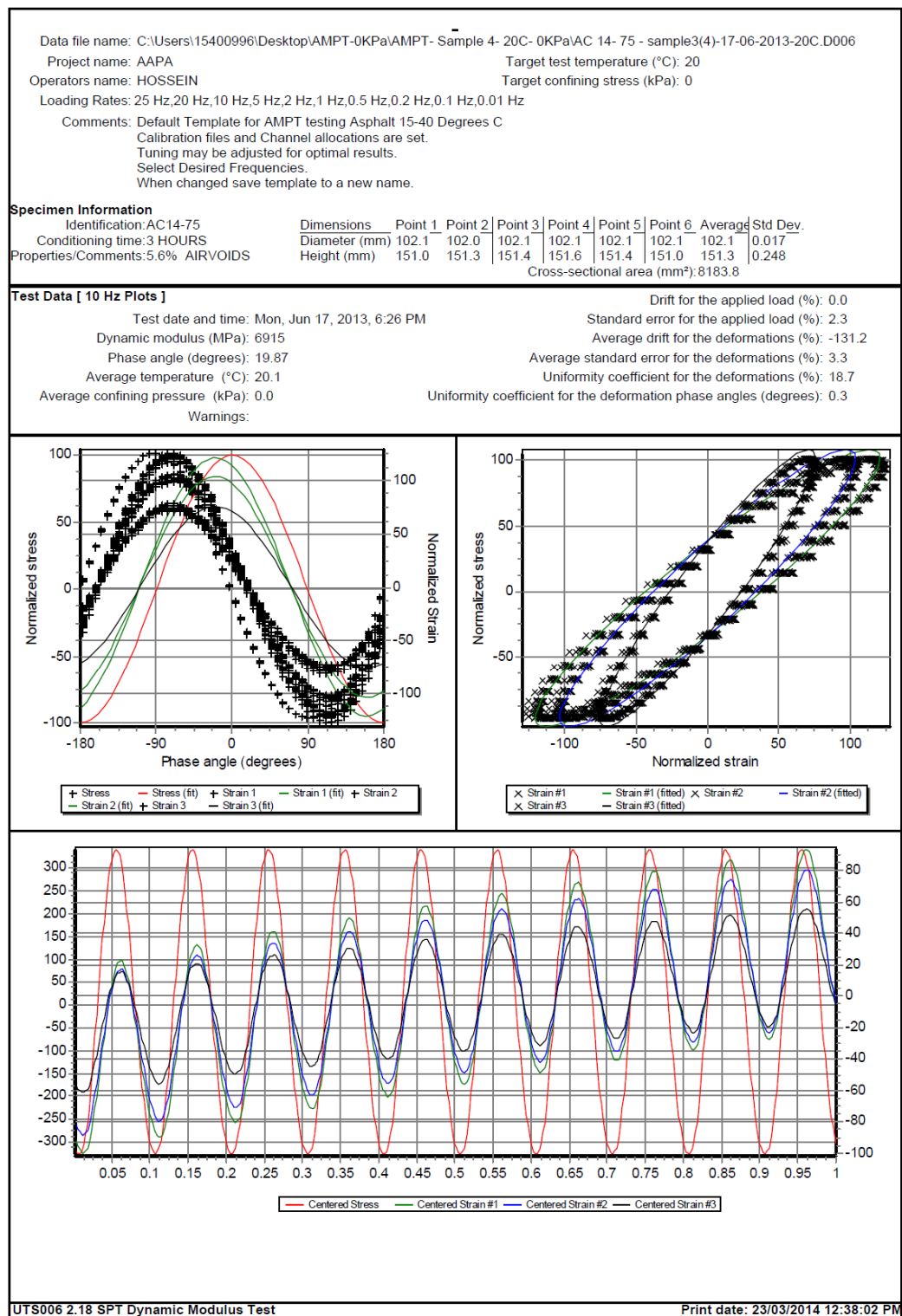


Figure E - 46. UTS6 output for sample4, 10 Hz and 20°C

Data file name: C:\Users\15400996\Desktop\AMPT-0KPa\AMPT- Sample 4- 20C- 0KPa\AC 14- 75 - sample3(4)-17-06-2013-20C.D006											
Project name: AAPA					Target test temperature (°C): 20						
Operators name: HOSSEIN					Target confining stress (kPa): 0						
Loading Rates: 25 Hz,20 Hz,10 Hz,5 Hz,2 Hz,1 Hz,0.5 Hz,0.2 Hz,0.1 Hz,0.01 Hz											
Comments: Default Template for AMPT testing Asphalt 15-40 Degrees C											
Calibration files and Channel allocations are set.											
Tuning may be adjusted for optimal results.											
Select Desired Frequencies.											
When changed save template to a new name.											
Specimen Information											
Identification:AC14-75		Dimensions		Point 1	Point 2	Point 3	Point 4	Point 5	Point 6	Average	Std Dev.
Conditioning time:3 HOURS		Diameter (mm)		102.1	102.0	102.1	102.1	102.1	102.1	102.1	0.017
Properties/Comments:5.6% AIRVOIDS		Height (mm)		151.0	151.3	151.4	151.6	151.4	151.0	151.3	0.248
Cross-sectional area (mm²):8183.8											
Tabulated Results Summary											
	25 Hz	20 Hz	10 Hz	5 Hz	2 Hz	1 Hz	0.5 Hz	0.2 Hz	0.1 Hz	0.01 Hz	
Dynamic modulus (MPa)	8093	7857	6915	6020	4919	4188	3524	2732	2233	982.9	
Phase angle (Degrees)	18.39	18.39	19.87	21.39	23.45	24.89	26.34	28.31	29.62	32.94	
Average temperature (°C)	20.1	20.1	20.1	20.1	20.1	20.1	20.0	20.1	20.1	20.1	
Average confining pressure (kPa)	0.0	-0.1	0.0	0.0	0.0	0.0	0.0	0.0	0.0	0.0	
Average micro-strain	98	96	97	97	97	97	96	97	97	101	
Load drift (%)	-1.0	-0.5	0.0	0.0	0.1	0.0	-0.2	-0.5	-0.3	0.5	
Load standard error (%)	5.5	3.8	2.3	1.4	1.0	0.7	0.8	1.0	1.1	1.7	
Average deformation drift (%)	-123.1	-115.2	-131.2	-142.2	-161.2	-170.7	-180.8	-198.0	-199.8	-192.5	
Average deformation standard error (%)	6.9	3.8	3.3	2.8	2.4	2.2	2.0	1.5	1.7	2.3	
Deformation uniformity (%)	16.6	17.8	18.7	19.4	20.0	20.4	20.8	21.1	21.1	21.2	
Phase uniformity (Degrees)	0.8	0.3	0.3	0.3	0.3	0.3	0.3	0.4	0.4	0.7	

Figure E - 47. UTS6 summary output for sample4, 20°C

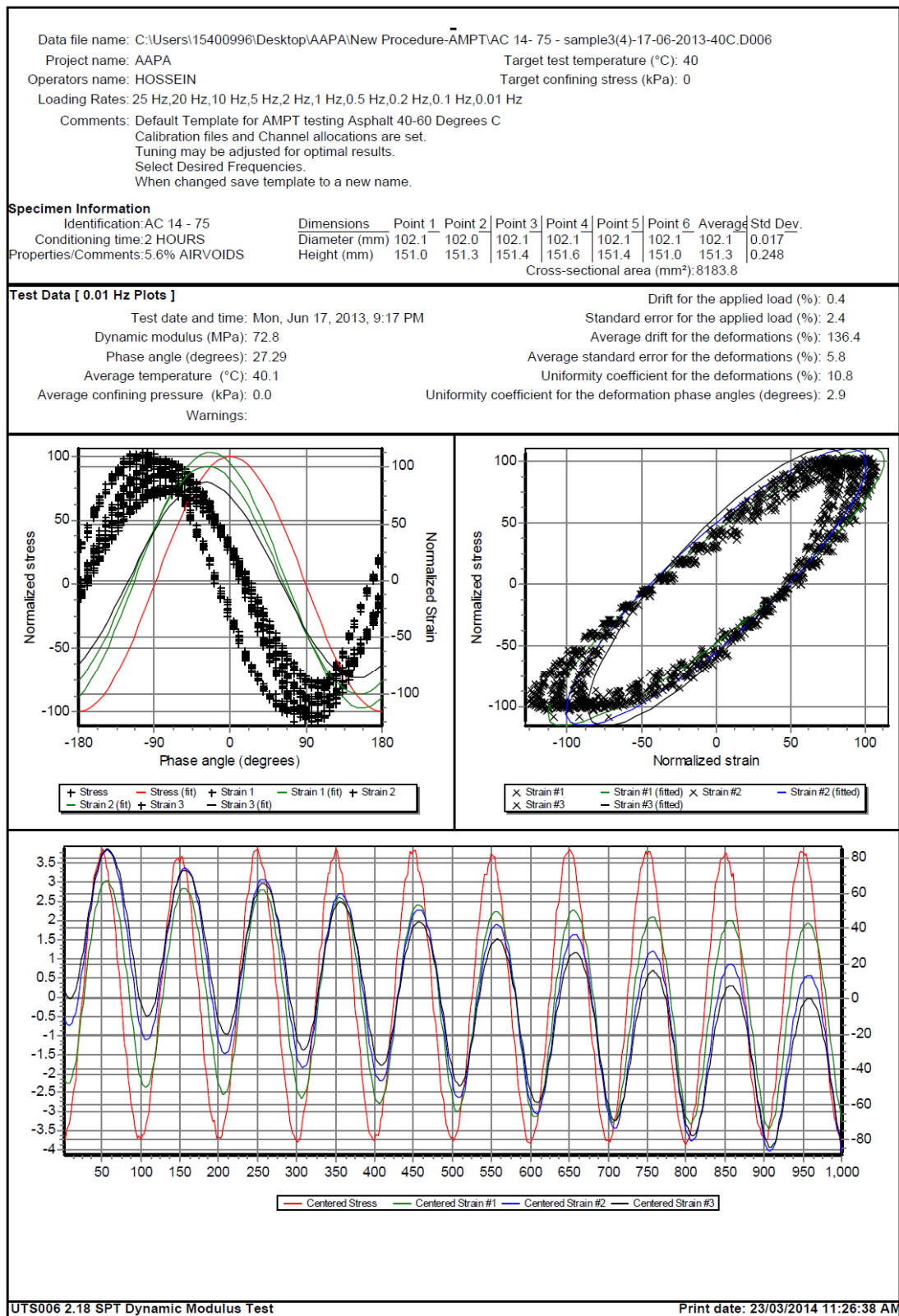


Figure E - 48. UTS6 output for sample4, 0.01 Hz and 40°C

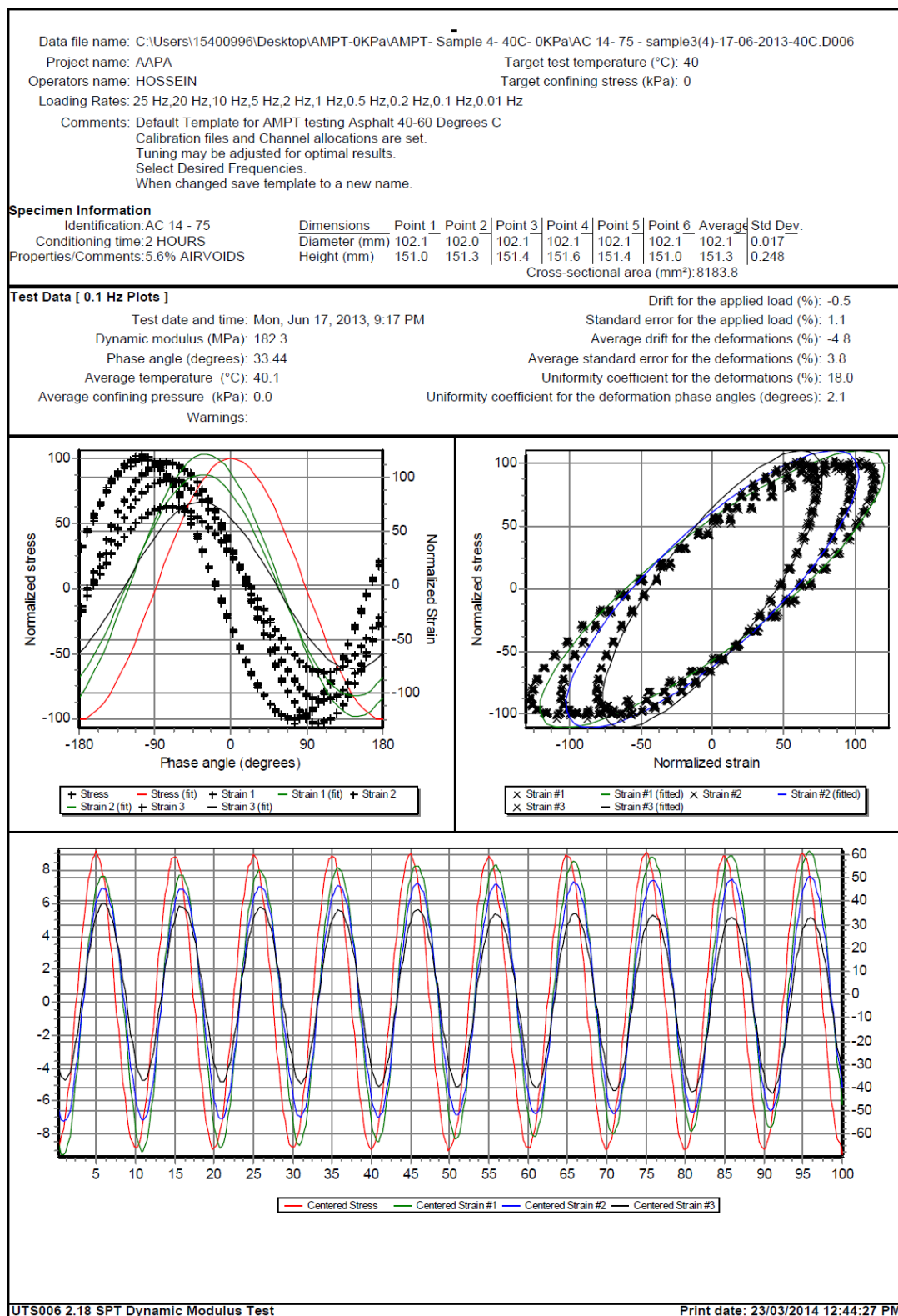


Figure E - 49. UTS6 output for sample4, 0.1 Hz and 40°C

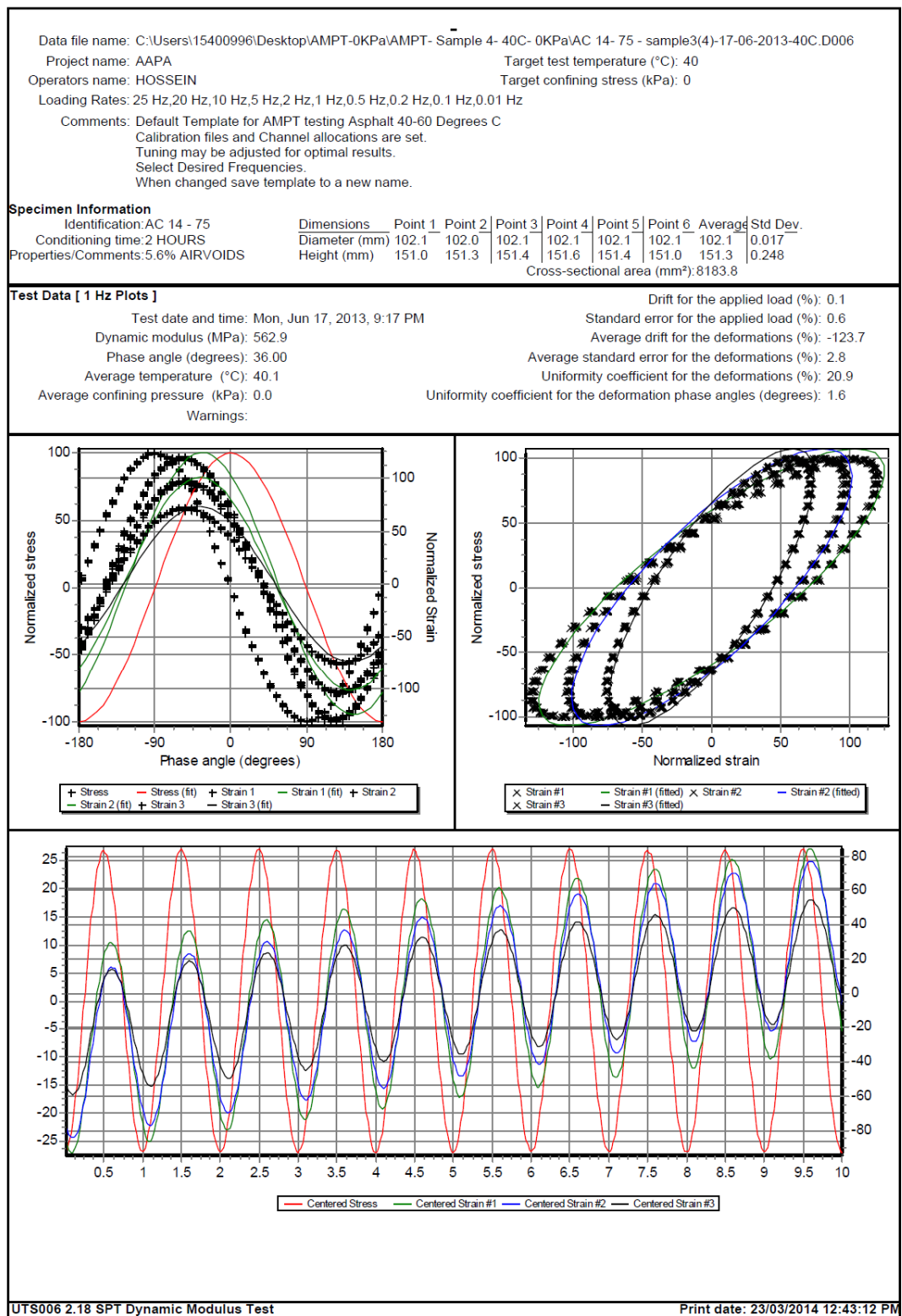


Figure E - 50. UTS6 output for sample4, 1 Hz and 40°C

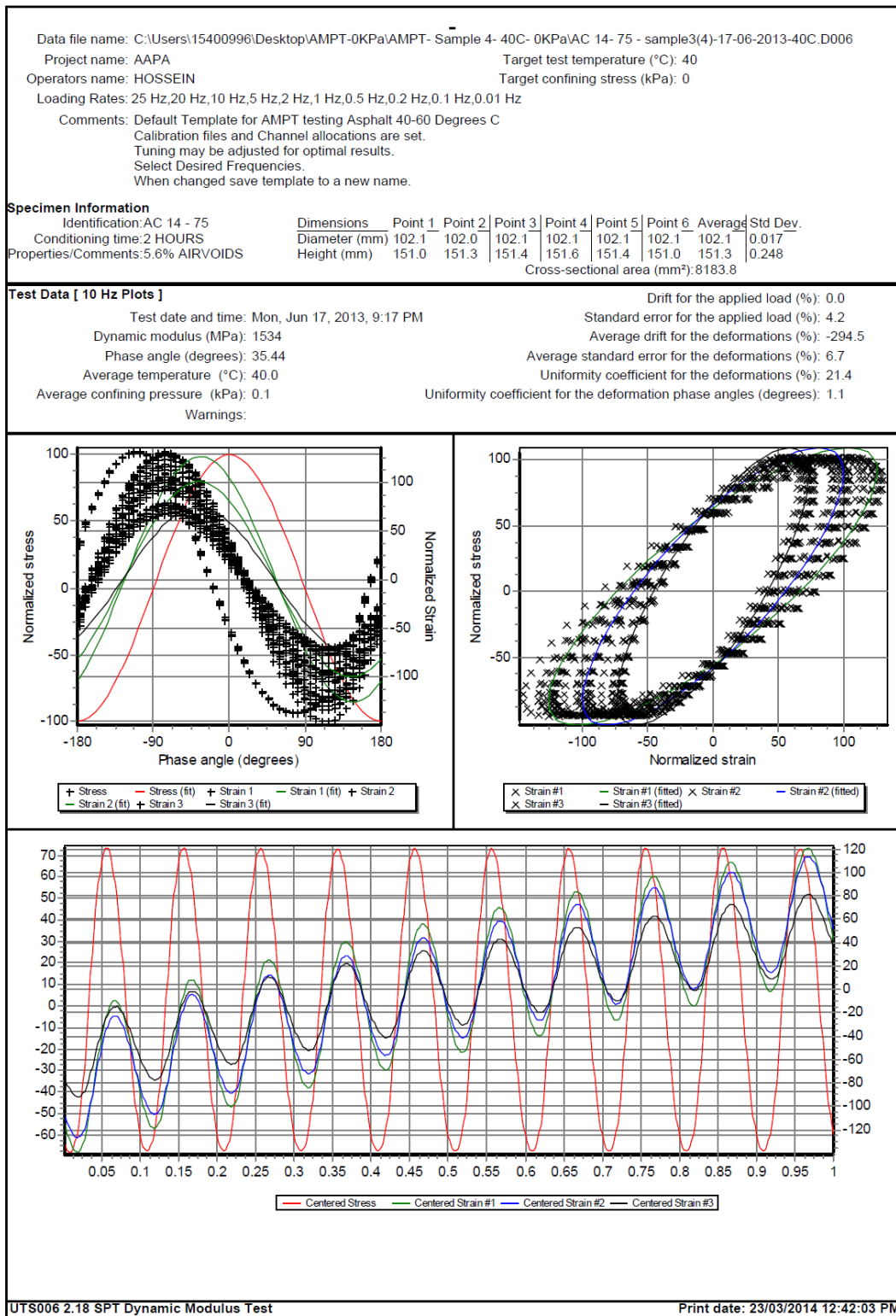


Figure E - 51. UTS6 output for sample4, 10 Hz and 40°C

Data file name: C:\Users\15400996\Desktop\AMPT-0KPa\AMPT- Sample 4- 40C- 0KPa\AC 14- 75 - sample3(4)-17-06-2013-40C.D006													
Project name: AAPA						Target test temperature (°C): 40							
Operators name: HOSSEIN						Target confining stress (kPa): 0							
Loading Rates: 25 Hz,20 Hz,10 Hz,5 Hz,2 Hz,1 Hz,0.5 Hz,0.2 Hz,0.1 Hz,0.01 Hz													
Comments: Default Template for AMPT testing Asphalt 40-60 Degrees C													
Calibration files and Channel allocations are set.													
Tuning may be adjusted for optimal results.													
Select Desired Frequencies.													
When changed save template to a new name.													
Specimen Information													
Identification:AC 14 - 75				Dimensions		Point 1	Point 2	Point 3	Point 4	Point 5	Point 6	Average	Std Dev.
Conditioning time:2 HOURS				Diameter (mm)		102.1	102.0	102.1	102.1	102.1	102.1	102.1	0.017
Properties/Comments:5.6% AIRVOIDS				Height (mm)		151.0	151.3	151.4	151.6	151.4	151.0	151.3	0.248
Cross-sectional area (mm²): 8183.8													
Tabulated Results Summary													
	25 Hz	20 Hz	10 Hz	5 Hz	2 Hz	1 Hz	0.5 Hz	0.2 Hz	0.1 Hz	0.01 Hz			
Dynamic modulus (MPa)	2120	1992	1534	1159	776.6	562.9	400.5	256.4	182.3	72.8			
Phase angle (Degrees)	35.18	34.85	35.44	35.99	36.28	36.00	35.64	34.57	33.44	27.29			
Average temperature (°C)	40.0	40.0	40.0	40.1	40.1	40.1	40.1	40.0	40.1	40.1			
Average confining pressure (kPa)	-0.1	0.0	0.1	0.0	0.0	0.0	0.0	0.0	0.0	0.0			
Average micro-strain	94	94	94	93	95	96	98	101	98	103			
Load drift (%)	-1.2	-0.5	0.0	0.4	0.4	0.1	-0.4	0.7	-0.5	0.4			
Load standard error (%)	6.0	5.8	4.2	2.9	1.7	0.6	0.6	0.7	1.1	2.4			
Average deformation drift (%)	-456.7	-363.5	-294.5	-236.6	-164.8	-123.7	-80.0	-41.3	-4.8	136.4			
Average deformation standard error (%)	10.4	9.2	6.7	5.1	3.2	2.8	3.0	3.5	3.8	5.8			
Deformation uniformity (%)	21.5	21.3	21.4	21.6	21.5	20.9	19.9	18.7	18.0	10.8			
Phase uniformity (Degrees)	1.0	1.1	1.1	1.2	1.5	1.6	1.8	1.9	2.1	2.9			

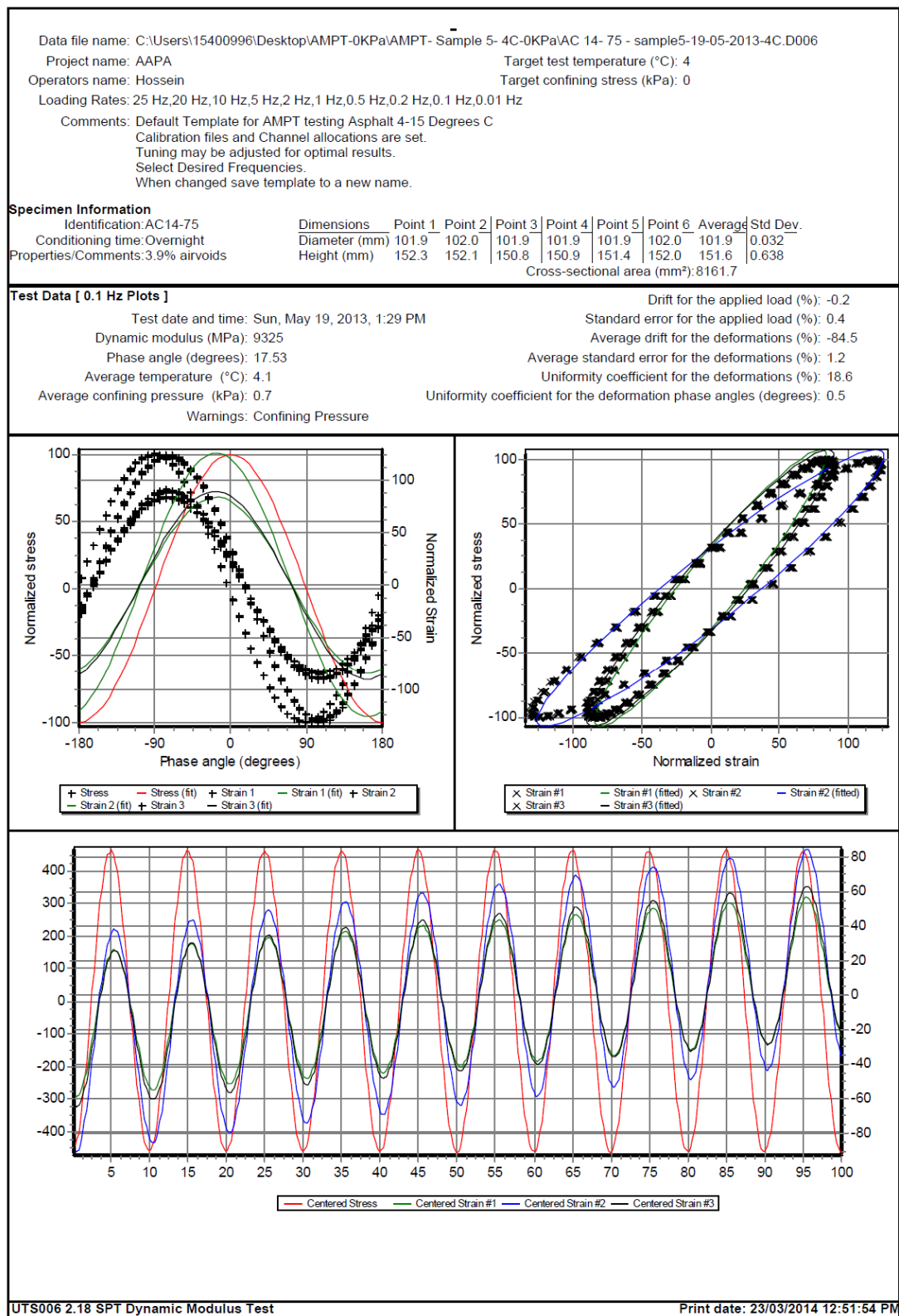


Figure E - 53. UTS6 output for sample5, 0.1 Hz and 4°C

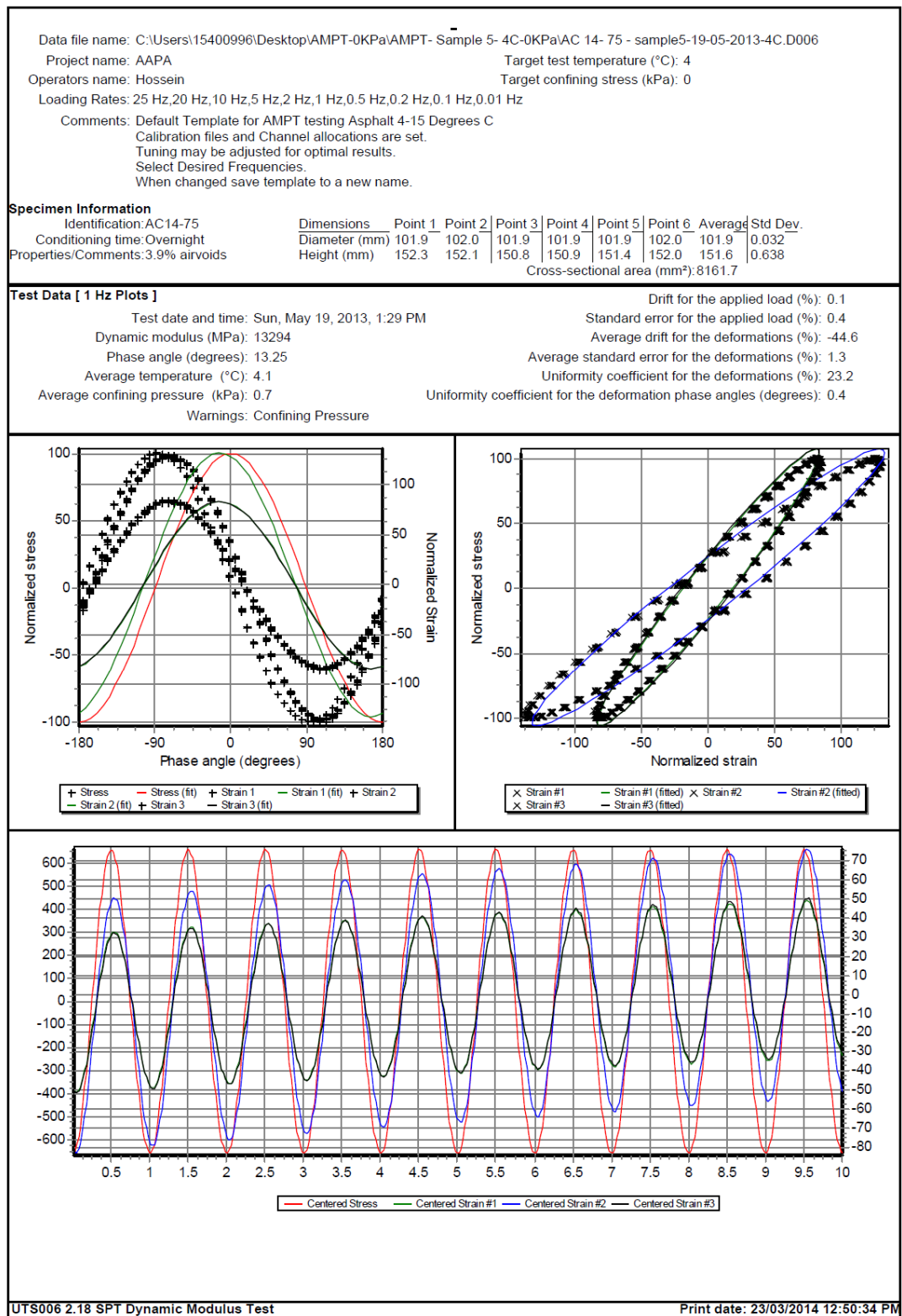
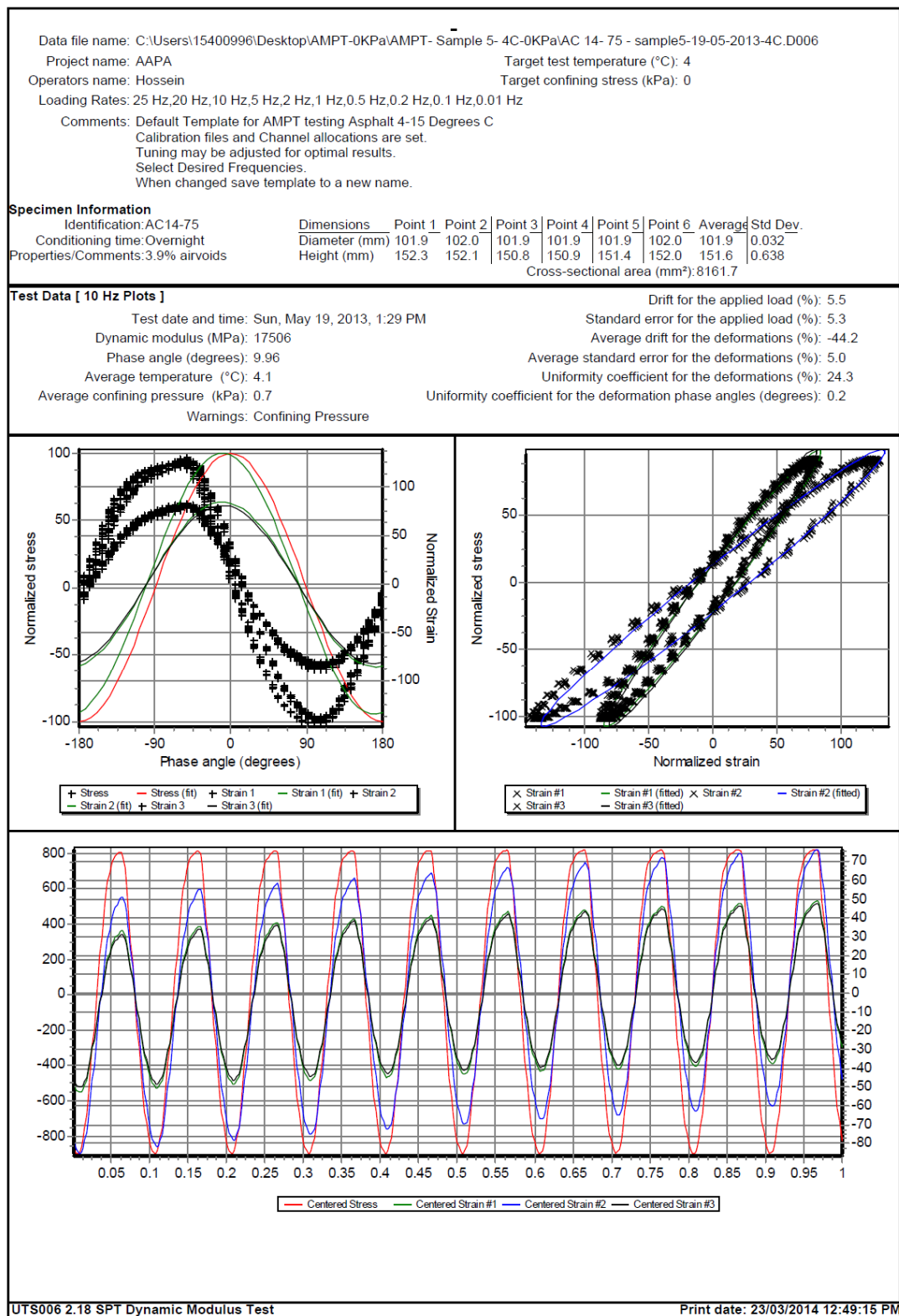


Figure E - 54. UTS6 output for sample5, 1 Hz and 4°C



Data file name: C:\Users\15400996\Desktop\AMPT-0KPa\AMPT- Sample 5- 4C-0KPa\AC 14- 75 - sample5-19-05-2013-4C.D006										
Project name: AAPA					Target test temperature (°C): 4					
Operators name: Hossein					Target confining stress (kPa): 0					
Loading Rates: 25 Hz,20 Hz,10 Hz,5 Hz,2 Hz,1 Hz,0.5 Hz,0.2 Hz,0.1 Hz,0.01 Hz										
Comments: Default Template for AMPT testing Asphalt 4-15 Degrees C										
Calibration files and Channel allocations are set.										
Tuning may be adjusted for optimal results.										
Select Desired Frequencies.										
When changed save template to a new name.										
Specimen Information										
Identification:AC14-75		Dimensions		Point 1	Point 2	Point 3	Point 4	Point 5	Point 6	Average Std Dev.
Conditioning time: Overnight		Diameter (mm)		101.9	102.0	101.9	101.9	101.9	102.0	101.9 0.032
Properties/Comments:3.9% airvoids		Height (mm)		152.3	152.1	150.8	150.9	151.4	152.0	151.6 0.638
Cross-sectional area (mm²):8161.7										
Tabulated Results Summary										
	25 Hz	20 Hz	10 Hz	5 Hz	2 Hz	1 Hz	0.5 Hz	0.2 Hz	0.1 Hz	0.01 Hz
Dynamic modulus (MPa)	19128	18756	17506	16225	14554	13294	12056	10471	9325	5869
Phase angle (Degrees)	8.92	9.10	9.96	10.88	12.17	13.25	14.43	16.10	17.53	23.11
Average temperature (°C)	4.1	4.1	4.1	4.1	4.1	4.1	4.0	4.1	4.1	4.1
Average confining pressure (kPa)	0.7	0.7	0.7	0.7	0.7	0.7	0.7	0.7	0.7	0.7
Average micro-strain	89	92	101	99	99	99	99	99	99	99
Load drift (%)	12.2	11.5	5.5	0.0	-0.1	0.1	0.1	0.0	-0.2	0.1
Load standard error (%)	14.4	11.2	5.3	1.1	0.6	0.4	0.2	0.4	0.4	0.6
Average deformation drift (%)	-56.7	-50.7	-44.2	-35.1	-40.8	-44.6	-51.4	-69.5	-84.5	-183.3
Average deformation standard error (%)	13.7	10.5	5.0	1.6	1.3	1.3	1.2	1.2	1.2	1.6
Deformation uniformity (%)	25.4	25.2	24.3	24.3	23.9	23.2	22.1	20.4	18.6	16.3
Phase uniformity (Degrees)	0.3	0.3	0.2	0.2	0.3	0.4	0.4	0.5	0.5	0.5

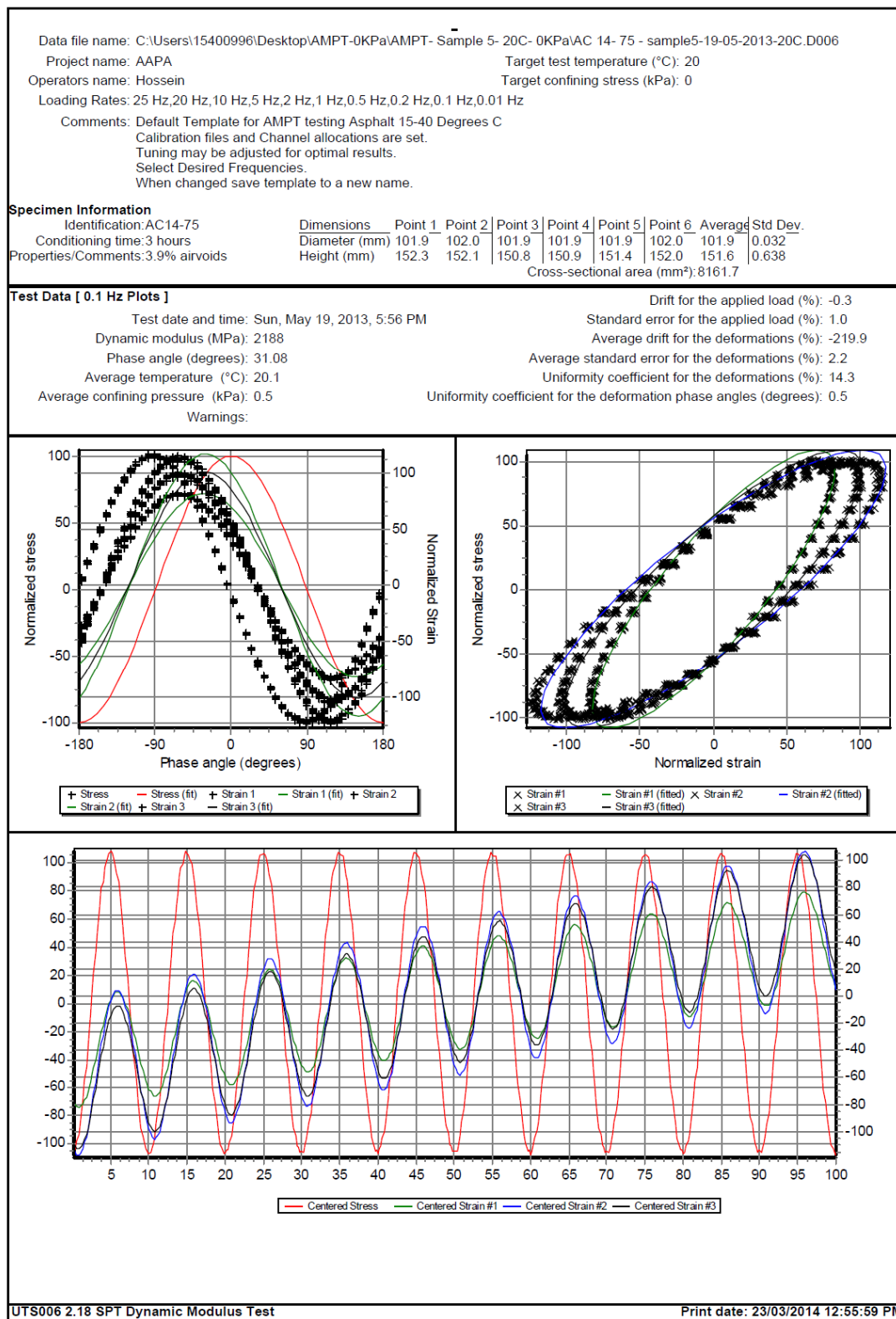
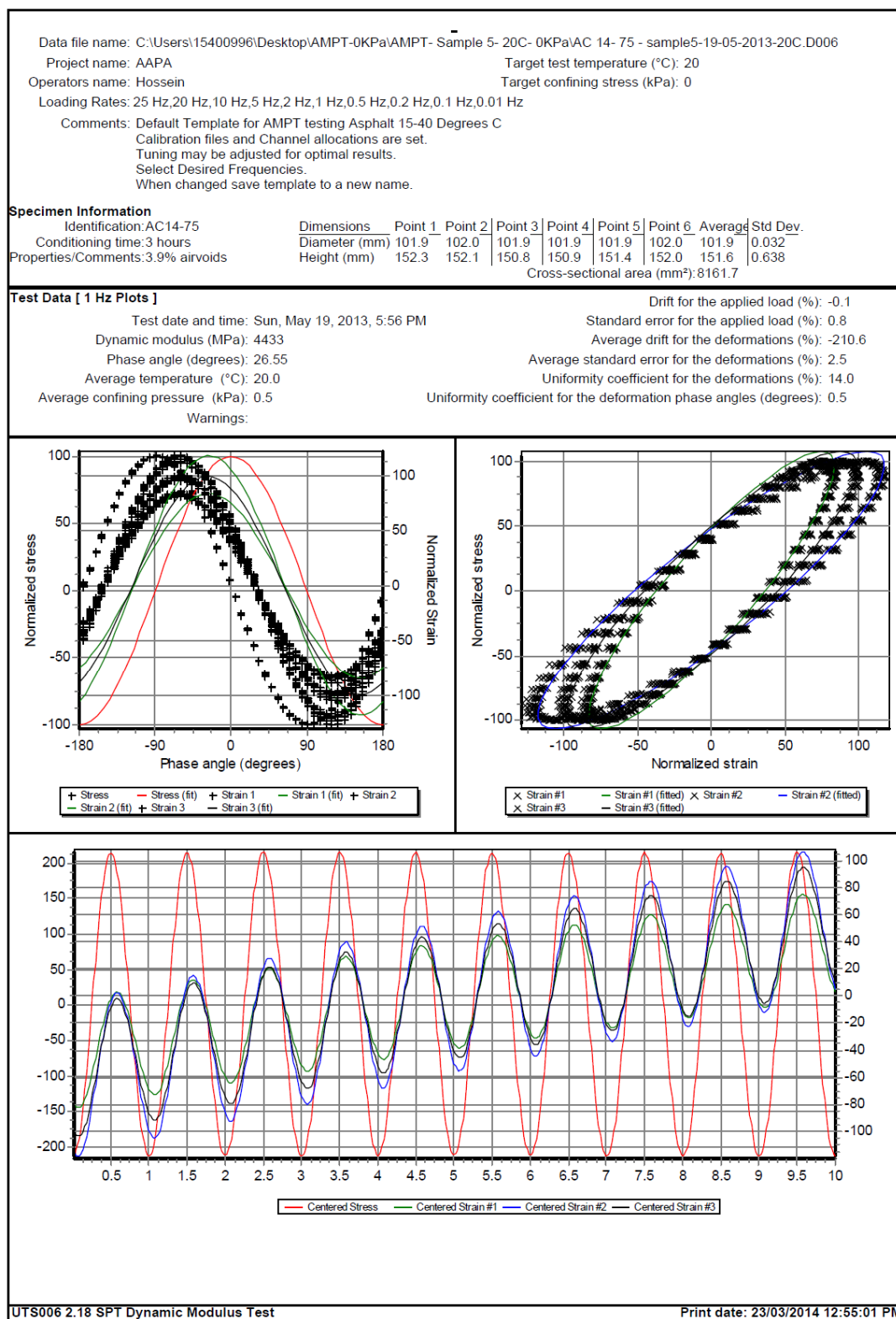
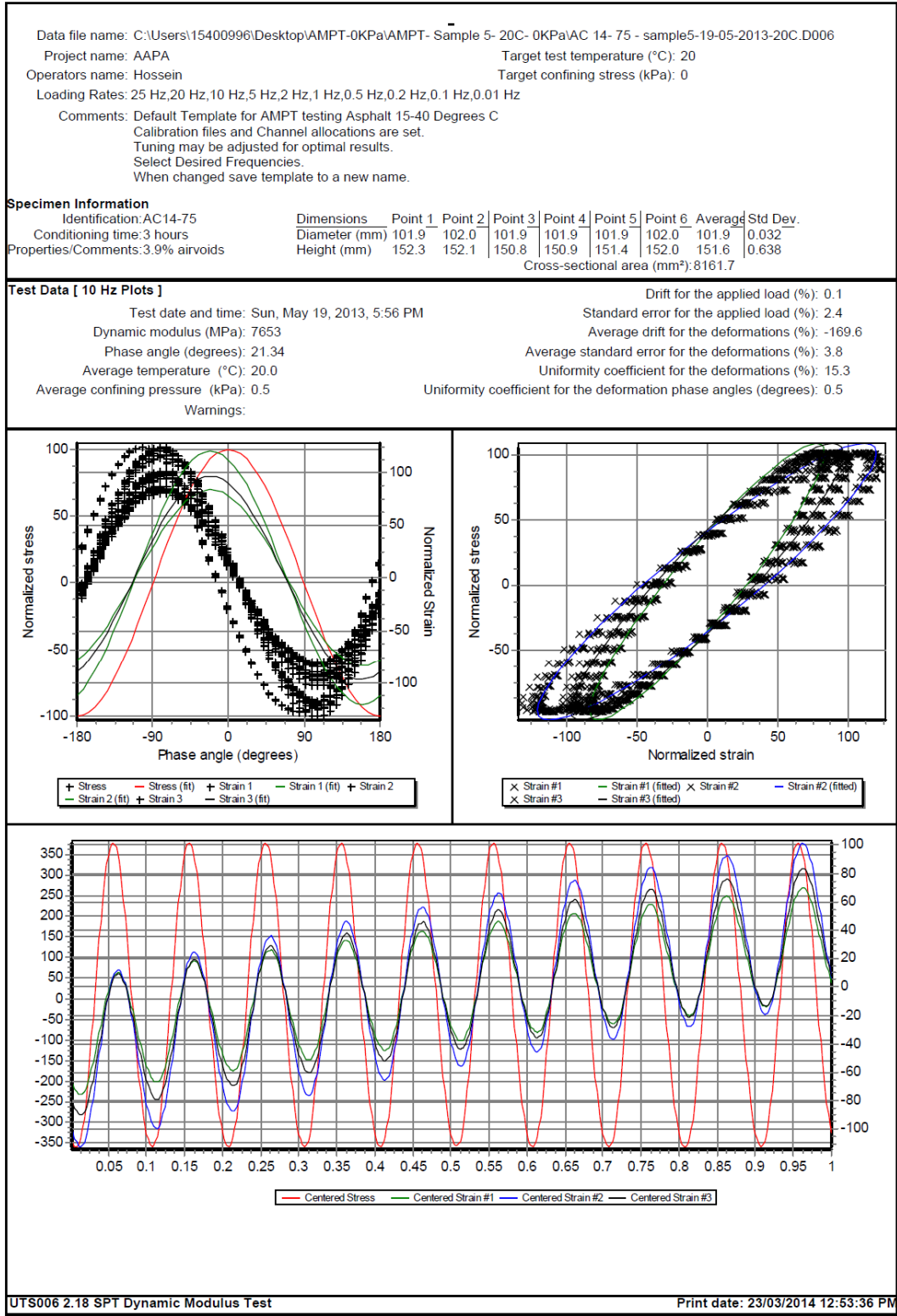


Figure E - 57. UTS6 output for sample5, 0.1 Hz and 20°C





Data file name: C:\Users\15400996\Desktop\AMPT-0KPa\AMPT- Sample 5- 20C- 0KPa\AC 14- 75 - sample5-19-05-2013-20C.D006										
Project name: AAPA					Target test temperature (°C): 20					
Operators name: Hossein					Target confining stress (kPa): 0					
Loading Rates: 25 Hz,20 Hz,10 Hz,5 Hz,2 Hz,1 Hz,0.5 Hz,0.2 Hz,0.1 Hz,0.01 Hz										
Comments: Default Template for AMPT testing Asphalt 15-40 Degrees C										
Calibration files and Channel allocations are set.										
Tuning may be adjusted for optimal results.										
Select Desired Frequencies.										
When changed save template to a new name.										
Specimen Information										
Identification:AC14-75		Dimensions		Point 1	Point 2	Point 3	Point 4	Point 5	Point 6	Average Std Dev.
Conditioning time:3 hours		Diameter (mm)		101.9	102.0	101.9	101.9	101.9	102.0	101.9 0.032
Properties/Comments:3.9% airvoids		Height (mm)		152.3	152.1	150.8	150.9	151.4	152.0	151.6 0.638
Cross-sectional area (mm²):8161.7										
Tabulated Results Summary										
	25 Hz	20 Hz	10 Hz	5 Hz	2 Hz	1 Hz	0.5 Hz	0.2 Hz	0.1 Hz	0.01 Hz
Dynamic modulus (MPa)	9145	8810	7653	6585	5293	4433	3662	2759	2188	876.9
Phase angle (Degrees)	19.63	19.84	21.34	22.90	25.07	26.55	28.01	29.94	31.08	33.39
Average temperature (°C)	20.0	20.0	20.0	20.0	20.0	20.0	20.1	20.1	20.1	20.1
Average confining pressure (kPa)	0.5	0.5	0.5	0.5	0.5	0.5	0.5	0.5	0.5	0.5
Average micro-strain	100	96	97	97	96	97	97	98	98	105
Load drift (%)	0.2	-0.6	0.1	0.0	-0.1	-0.1	-0.1	0.2	-0.3	0.6
Load standard error (%)	5.3	4.3	2.4	1.4	1.0	0.8	0.8	0.9	1.0	2.8
Average deformation drift (%)	-179.8	-153.5	-169.6	-182.5	-201.6	-210.6	-215.2	-230.5	-219.9	-200.5
Average deformation standard error (%)	5.9	4.8	3.8	3.1	2.6	2.5	1.6	1.9	2.2	3.6
Deformation uniformity (%)	18.1	16.4	15.3	14.6	14.3	14.0	13.9	14.1	14.3	15.5
Phase uniformity (Degrees)	0.5	0.5	0.5	0.5	0.5	0.5	0.5	0.5	0.5	0.6

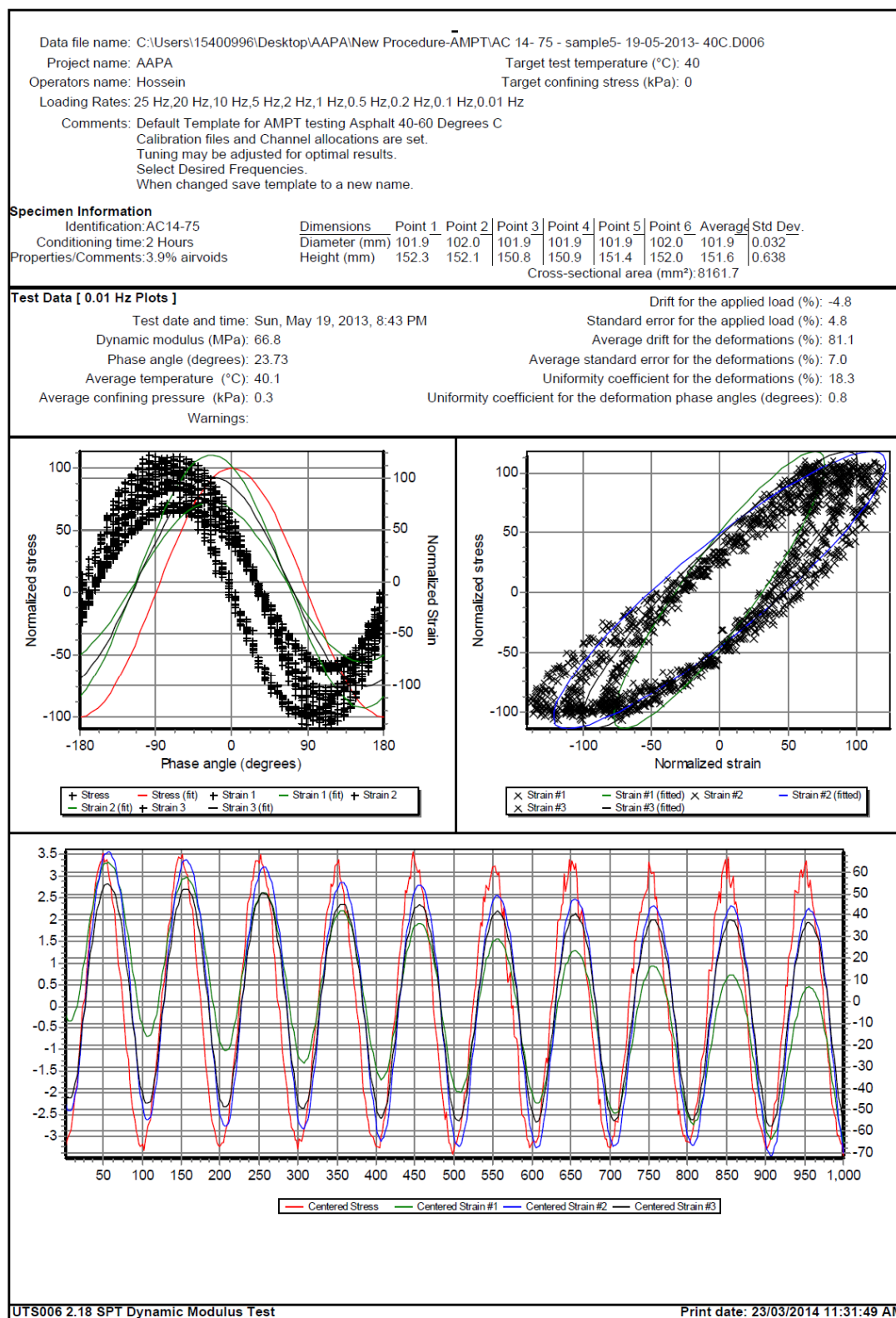


Figure E - 61. UTS6 output for sample5, 0.01 Hz and 40°C

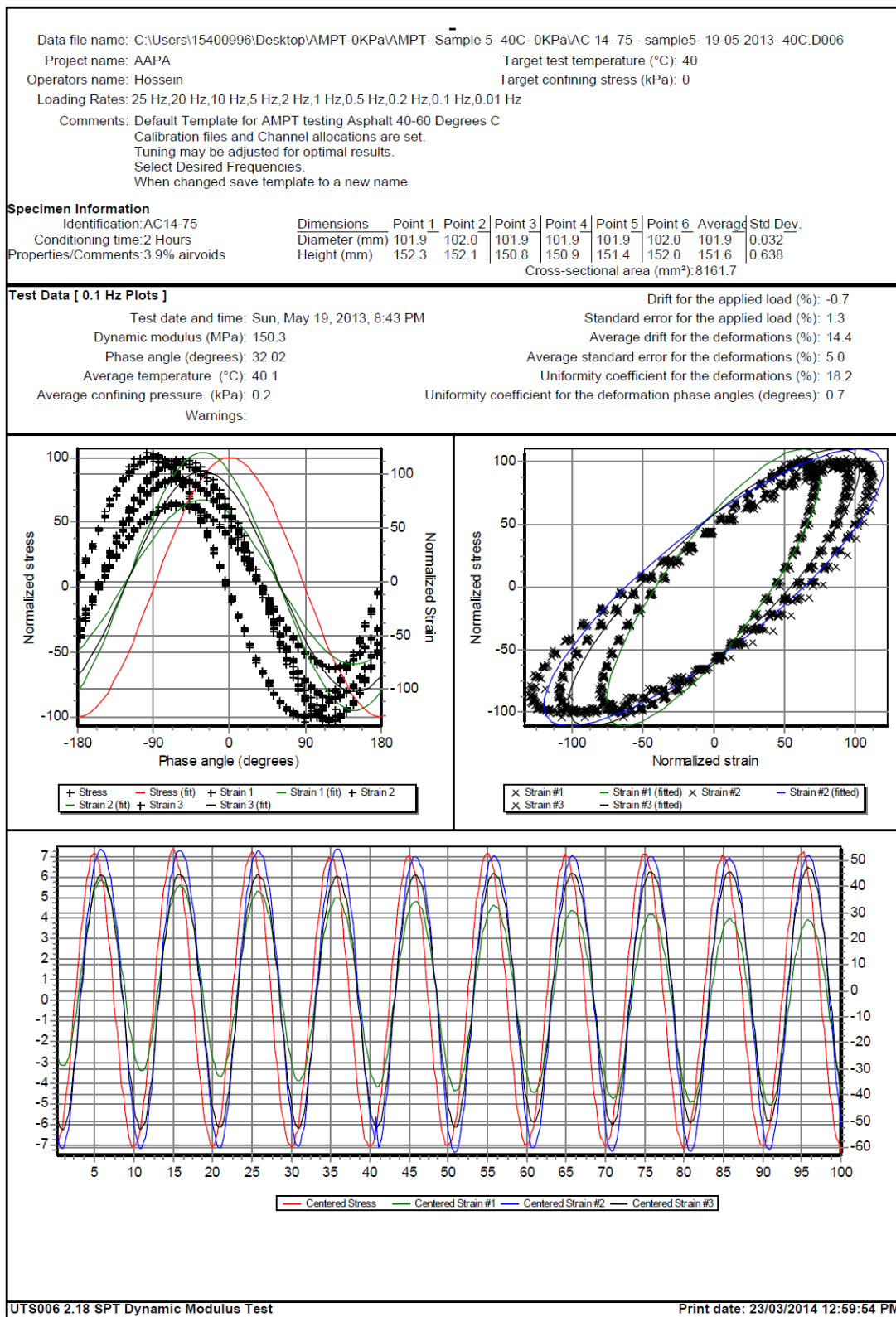


Figure E - 62. UTS6 output for sample5, 0.1 Hz and 40°C

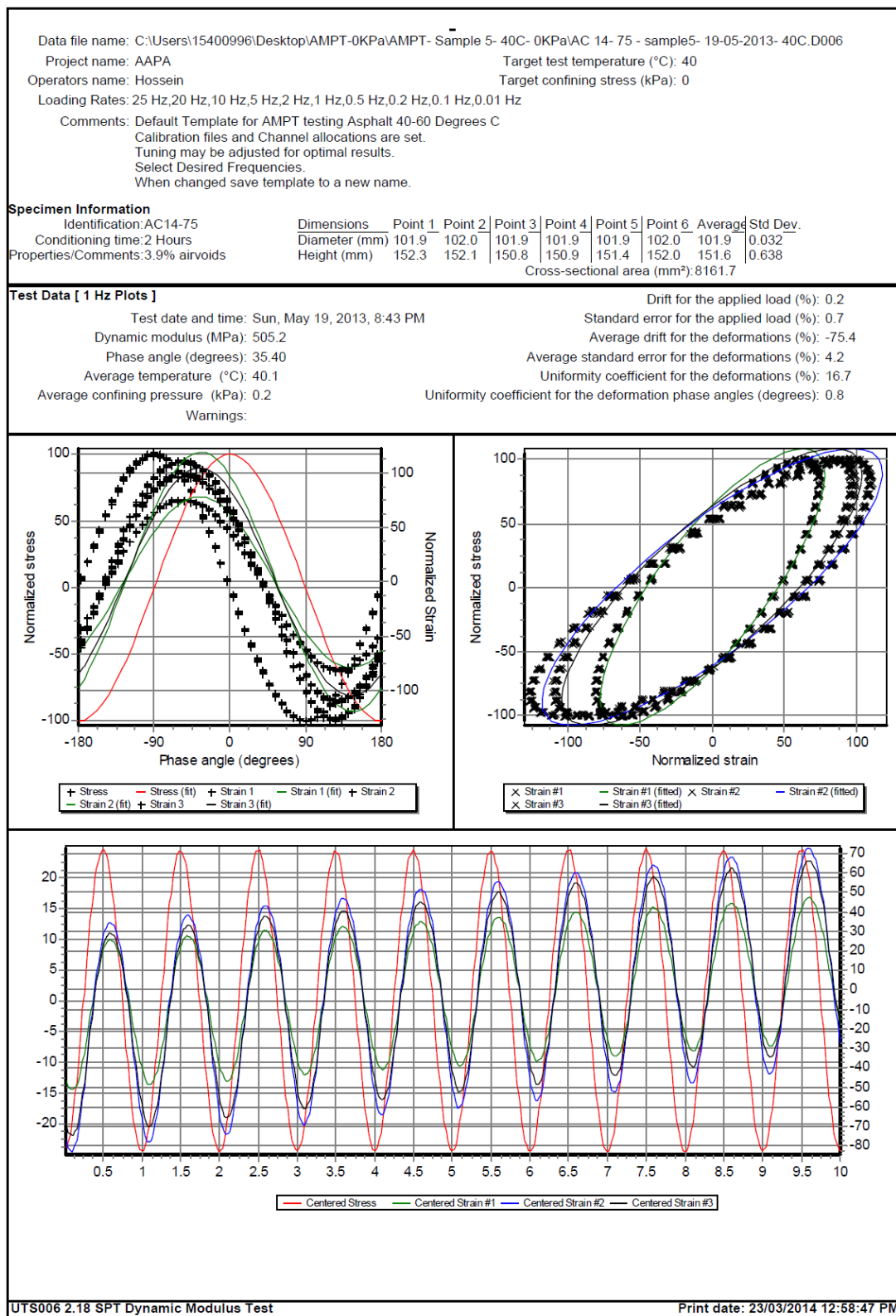


Figure E - 63. UTS6 output for sample5, 1 Hz and 40°C

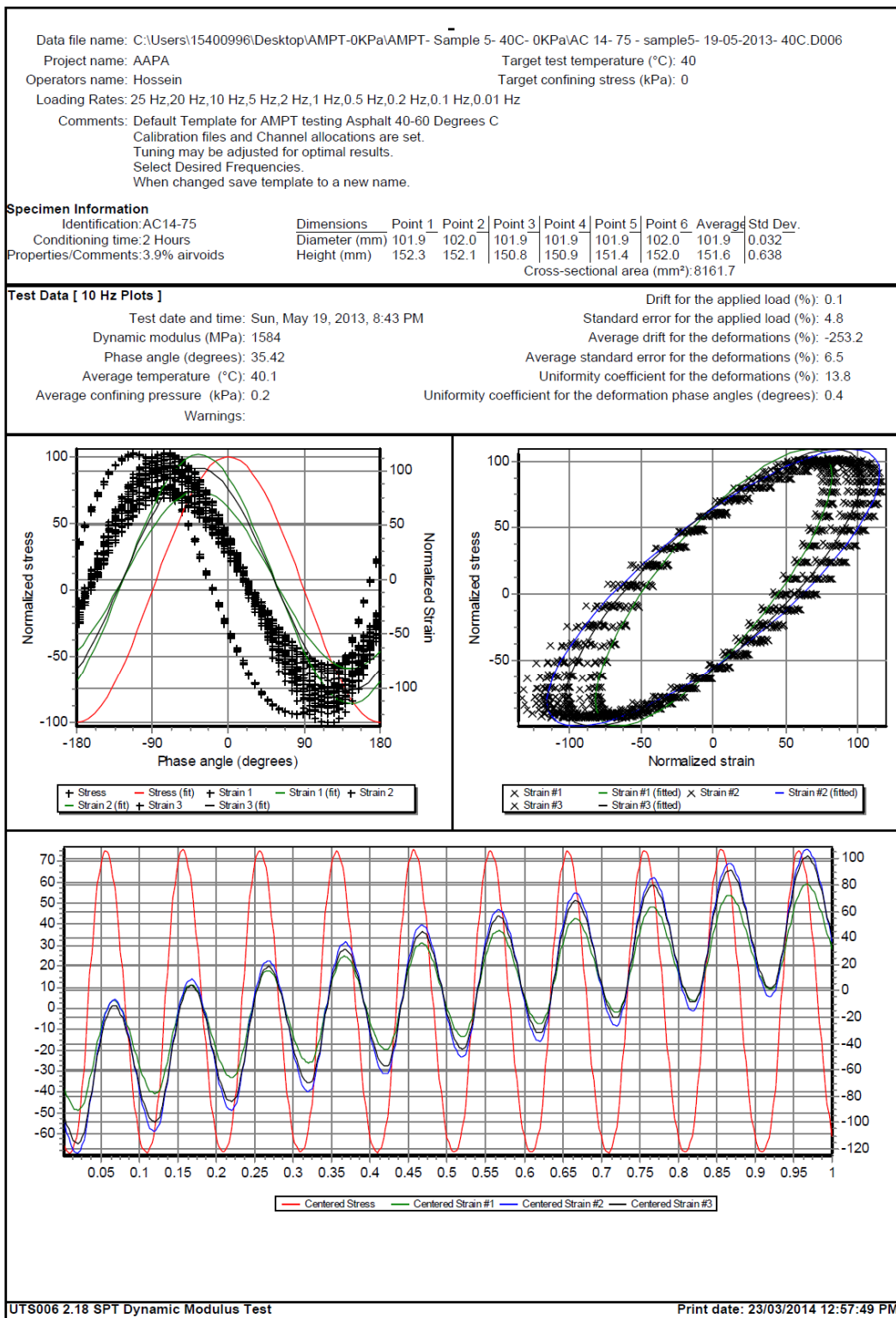


Figure E - 64. UTS6 output for sample5, 10 Hz and 40°C

Data file name: C:\Users\15400996\Desktop\AMPT-0KPa\AMPT- Sample 5- 40C- 0KPa\AC 14- 75 - sample5- 19-05-2013- 40C.D006											
Project name: AAPA					Target test temperature (°C): 40						
Operators name: Hossein					Target confining stress (kPa): 0						
Loading Rates: 25 Hz,20 Hz,10 Hz,5 Hz,2 Hz,1 Hz,0.5 Hz,0.2 Hz,0.1 Hz,0.01 Hz											
Comments: Default Template for AMPT testing Asphalt 40-60 Degrees C											
Calibration files and Channel allocations are set.											
Tuning may be adjusted for optimal results.											
Select Desired Frequencies.											
When changed save template to a new name.											
Specimen Information											
Identification:AC14-75		<u>Dimensions</u>		Point 1	Point 2	Point 3	Point 4	Point 5	Point 6	Average	Std Dev.
Conditioning time:2 Hours		Diameter (mm)		101.9	102.0	101.9	101.9	101.9	102.0	101.9	0.032
Properties/Comments:3.9% airvoids		Height (mm)		152.3	152.1	150.8	150.9	151.4	152.0	151.6	0.638
				Cross-sectional area (mm²):8161.7							
Tabulated Results Summary											
	25 Hz	20 Hz	10 Hz	5 Hz	2 Hz	1 Hz	0.5 Hz	0.2 Hz	0.1 Hz	0.01 Hz	
Dynamic modulus (MPa)	2297	2119	1584	1150	743.4	505.2	347.5	218.1	150.3	66.8	
Phase angle (Degrees)	35.10	34.74	35.42	35.85	35.51	35.40	34.78	33.13	32.02	23.73	
Average temperature (°C)	40.1	40.1	40.1	40.1	40.1	40.1	40.1	40.0	40.1	40.1	
Average confining pressure (kPa)	0.3	0.3	0.2	0.2	0.2	0.2	0.2	0.2	0.2	0.3	
Average micro-strain	97	93	93	94	101	97	97	101	94	97	
Load drift (%)	-0.7	-0.5	0.1	0.0	0.4	0.2	0.3	-0.1	-0.7	-4.8	
Load standard error (%)	6.5	6.2	4.8	3.3	2.0	0.7	0.9	1.2	1.3	4.8	
Average deformation drift (%)	-435.7	-321.0	-253.2	-186.6	-133.5	-75.4	-42.0	-14.4	14.4	81.1	
Average deformation standard error (%)	10.0	8.0	6.5	5.3	4.3	4.2	4.3	4.8	5.0	7.0	
Deformation uniformity (%)	13.2	13.0	13.8	14.6	15.6	16.7	17.2	17.6	18.2	18.3	
Phase uniformity (Degrees)	0.2	0.3	0.4	0.6	0.6	0.8	0.8	0.7	0.7	0.8	

Figure E - 65. UTS6 summary output for sample5, 40°C

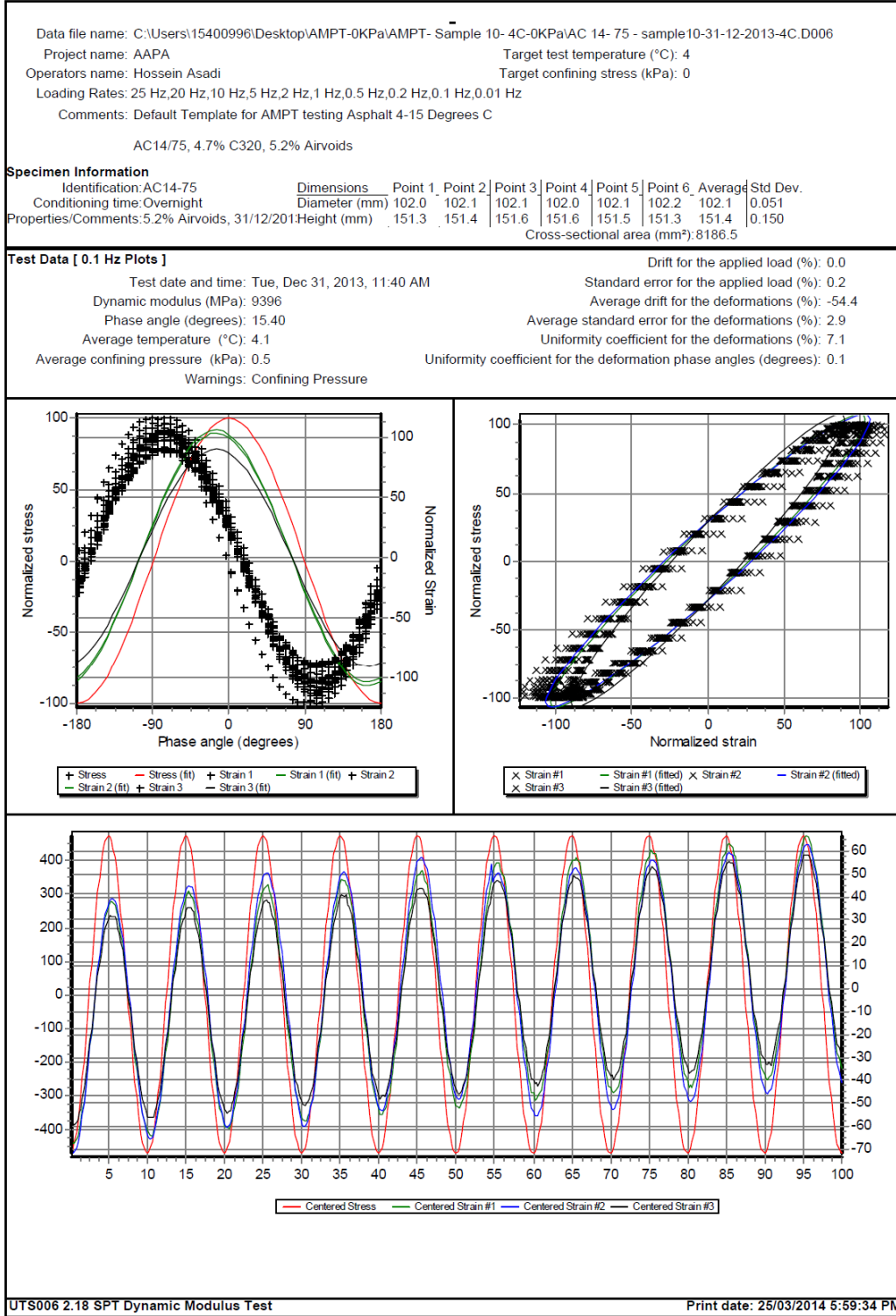


Figure E - 66. UTS6 output for sample6, 0.1 Hz and 4°C

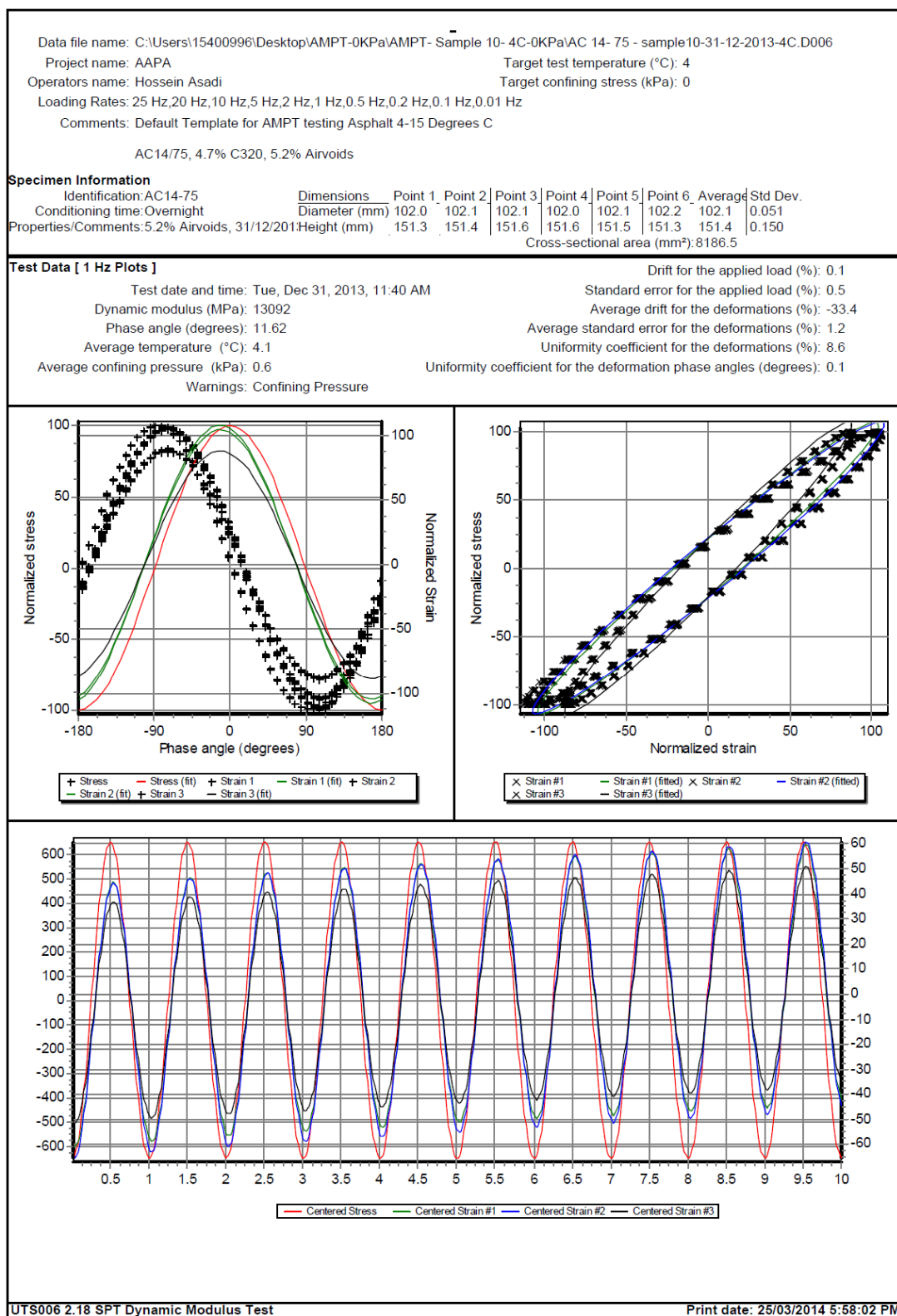


Figure E - 67. UTS6 output for sample6, 1 Hz and 4°C

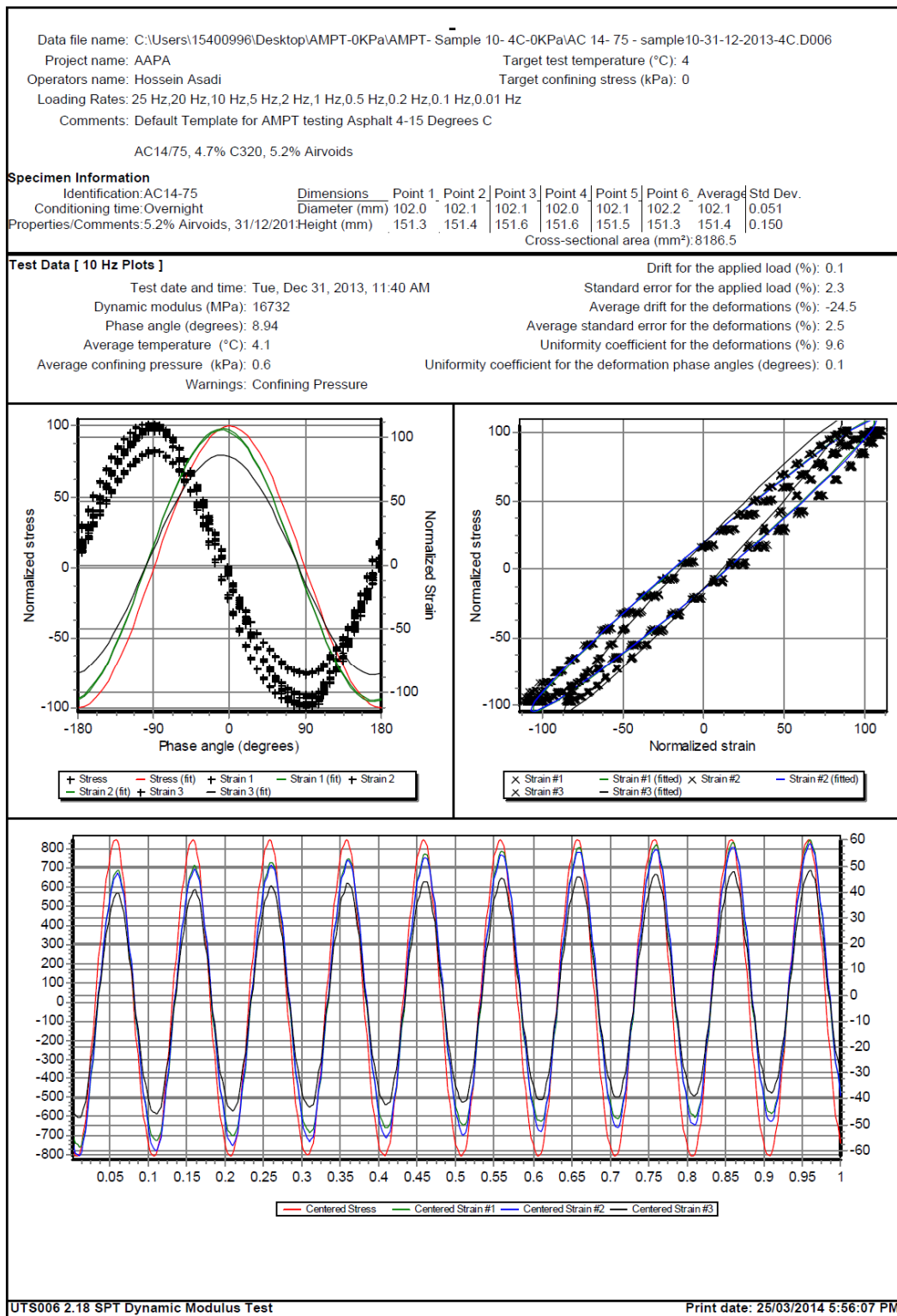


Figure E - 68. UTS6 output for sample6, 10 Hz and 4°C

Data file name: C:\Users\15400996\Desktop\AMPT-0KPa\AMPT- Sample 10- 4C-0KPa\AC 14- 75 - sample10-31-12-2013-4C.D006											
Project name: AAPA					Target test temperature (°C): 4						
Operators name: Hossein Asadi					Target confining stress (kPa): 0						
Loading Rates: 25 Hz,20 Hz,10 Hz,5 Hz,2 Hz,1 Hz,0.5 Hz,0.2 Hz,0.1 Hz,0.01 Hz											
Comments: Default Template for AMPT testing Asphalt 4-15 Degrees C											
AC14/75, 4.7% C320, 5.2% Airvoids											
Specimen Information											
Identification:AC14-75		Dimensions		Point 1	Point 2	Point 3	Point 4	Point 5	Point 6	Average	Std Dev.
Conditioning time: Overnight		Diameter (mm)		102.0	102.1	102.1	102.0	102.1	102.2	102.1	0.051
Properties/Comments:5.2% Airvoids, 31/12/201		Height (mm)		151.3	151.4	151.6	151.6	151.5	151.3	151.4	0.150
Cross-sectional area (mm²): 8186.5											
Tabulated Results Summary											
	25 Hz	20 Hz	10 Hz	5 Hz	2 Hz	1 Hz	0.5 Hz	0.2 Hz	0.1 Hz	0.01 Hz	
Dynamic modulus (MPa)	18108	17765	16732	15673	14207	13092	11977	10505	9396	6143	
Phase angle (Degrees)	8.07	8.28	8.94	9.66	10.70	11.62	12.62	14.17	15.40	20.53	
Average temperature (°C)	4.1	4.1	4.1	4.1	4.1	4.1	4.1	4.1	4.1	4.1	
Average confining pressure (kPa)	0.6	0.6	0.6	0.6	0.6	0.6	0.6	0.5	0.5	0.6	
Average micro-strain	95	99	99	99	99	100	100	101	101	101	
Load drift (%)	13.2	9.5	0.1	0.1	-0.1	0.1	0.1	0.0	0.0	0.0	
Load standard error (%)	14.1	10.4	2.3	1.1	0.6	0.5	0.2	0.2	0.2	0.5	
Average deformation drift (%)	-45.8	-39.8	-24.5	-26.3	-29.5	-33.4	-38.7	-51.5	-54.4	-142.3	
Average deformation standard error (%)	13.4	9.9	2.5	1.8	1.4	1.2	1.0	1.1	2.9	1.4	
Deformation uniformity (%)	9.7	9.8	9.6	9.3	9.0	8.6	8.1	7.6	7.1	6.8	
Phase uniformity (Degrees)	0.3	0.2	0.1	0.1	0.2	0.1	0.1	0.1	0.1	0.1	
</											

Figure E - 69. UTS6 summary output for sample6, 4°C

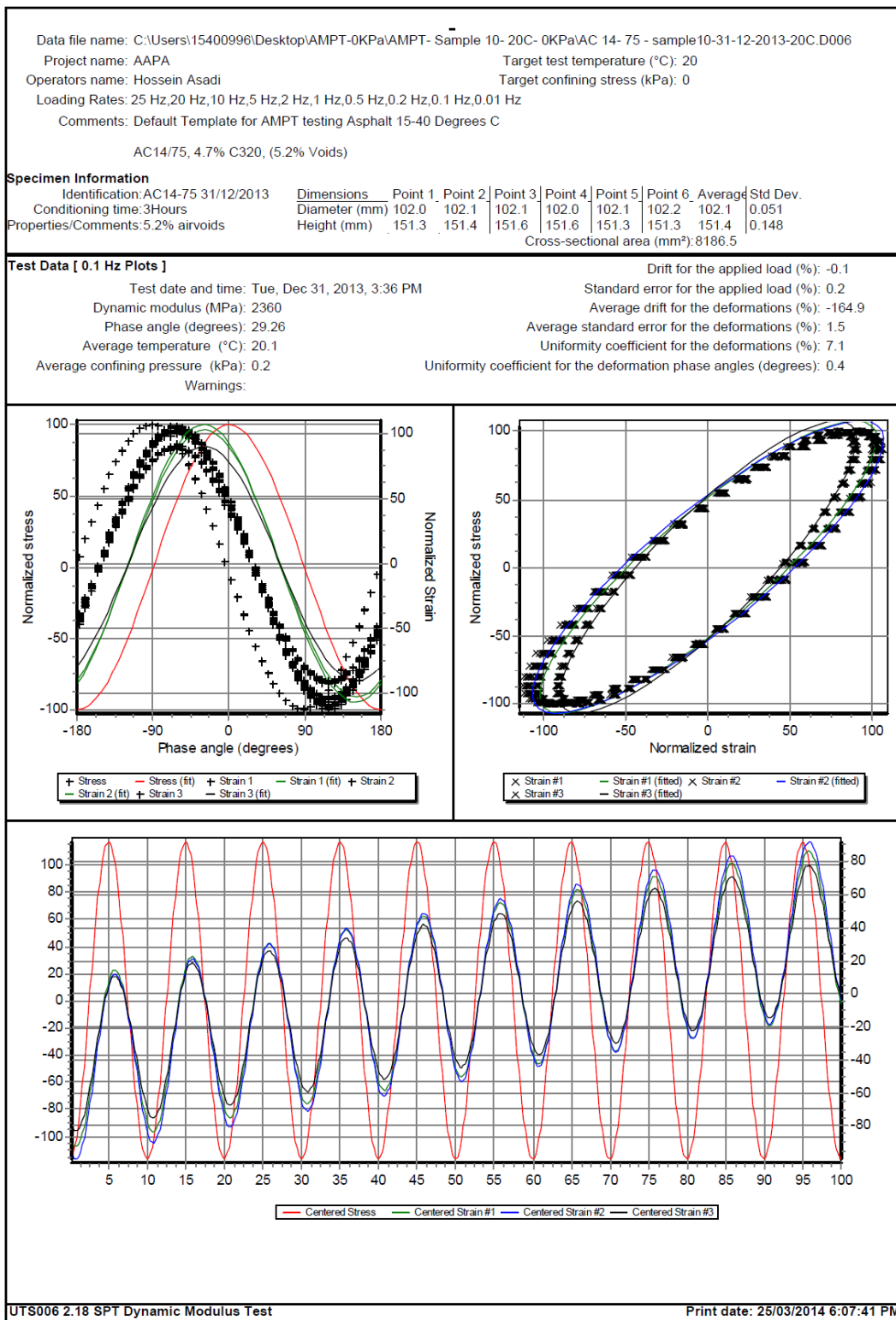


Figure E - 70. UTS6 output for sample6, 0.1 Hz and 20°C

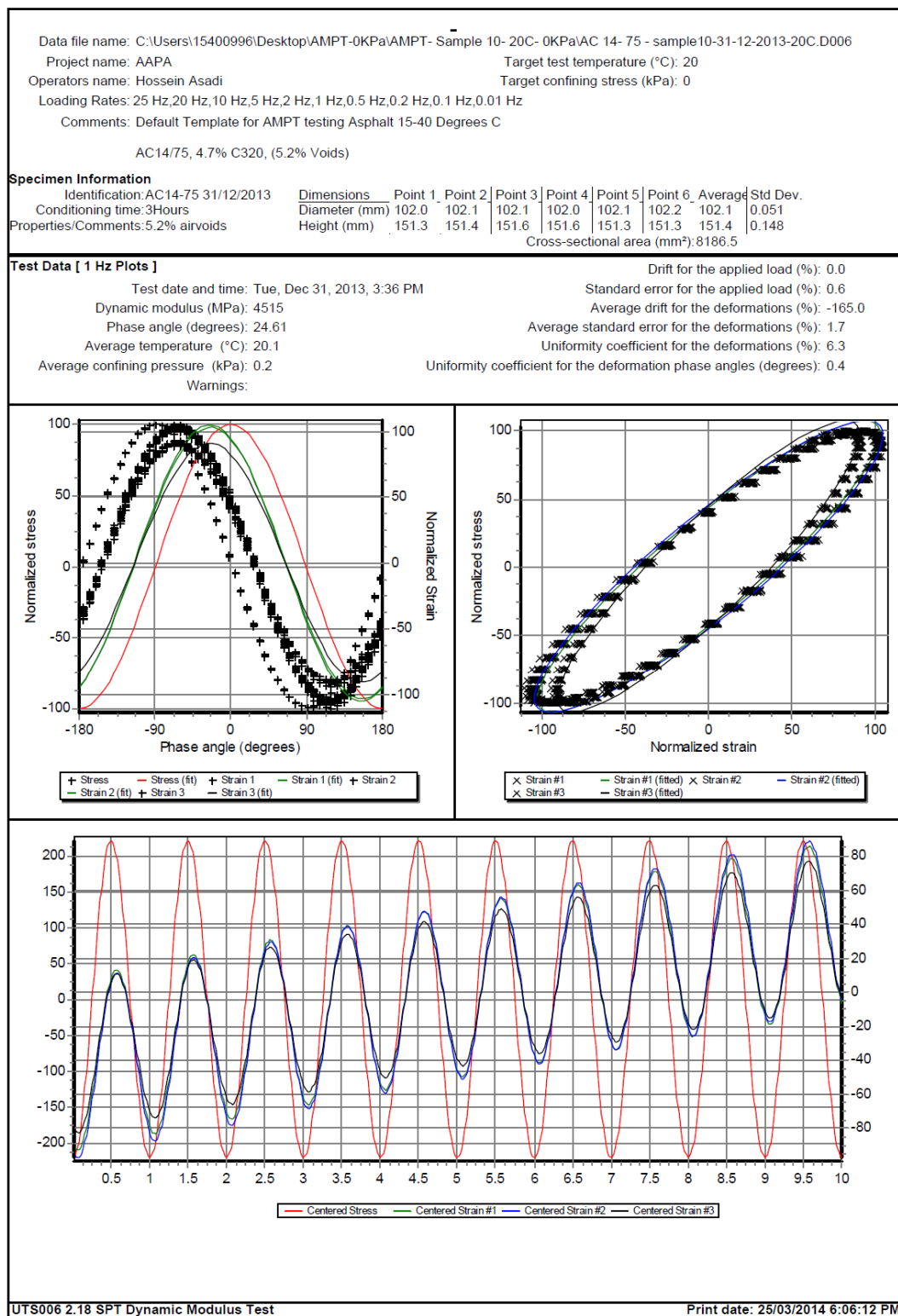


Figure E - 71. UTS6 output for sample6, 1 Hz and 20°C

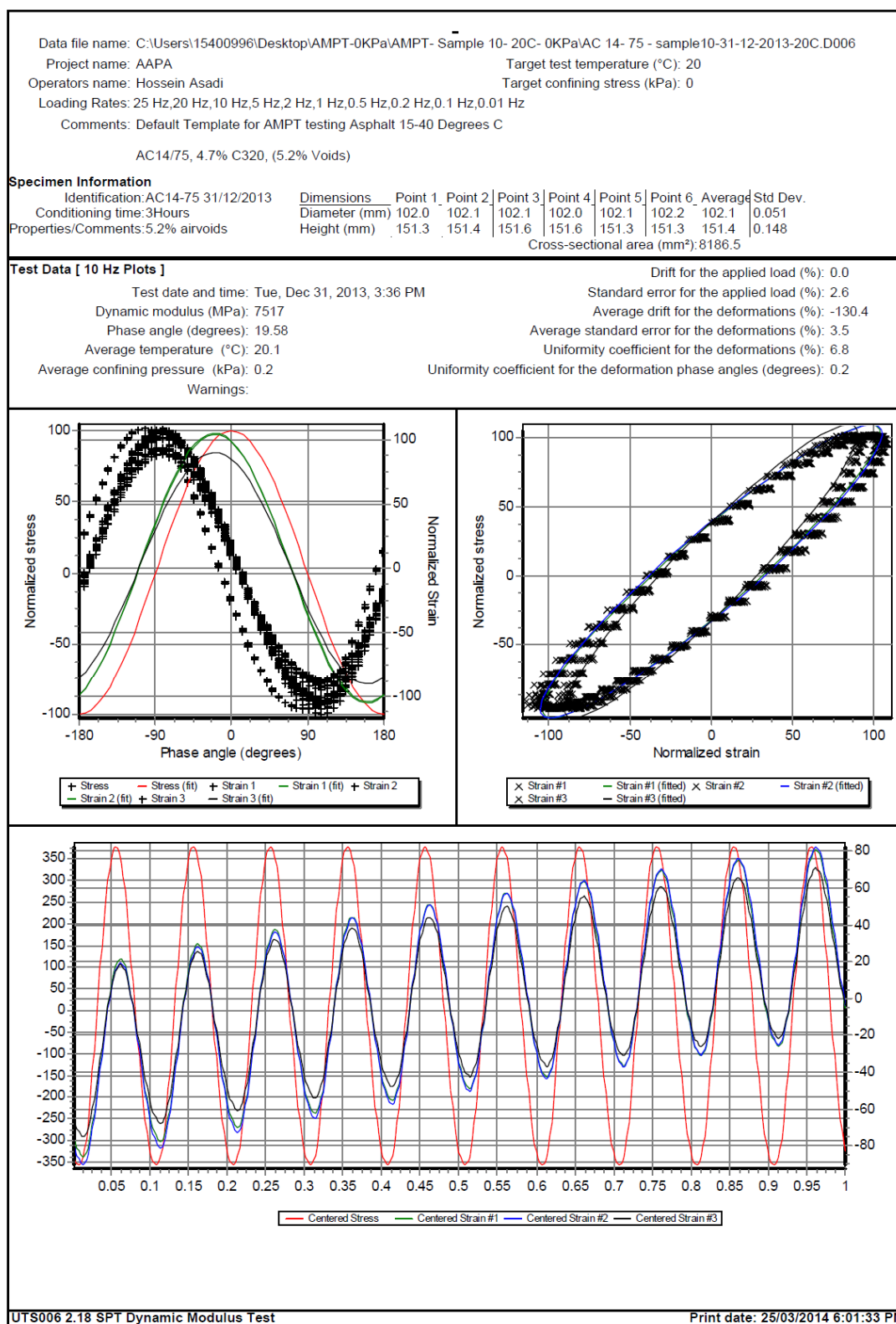


Figure E - 72. UTS6 output for sample6, 10 Hz and 20°C

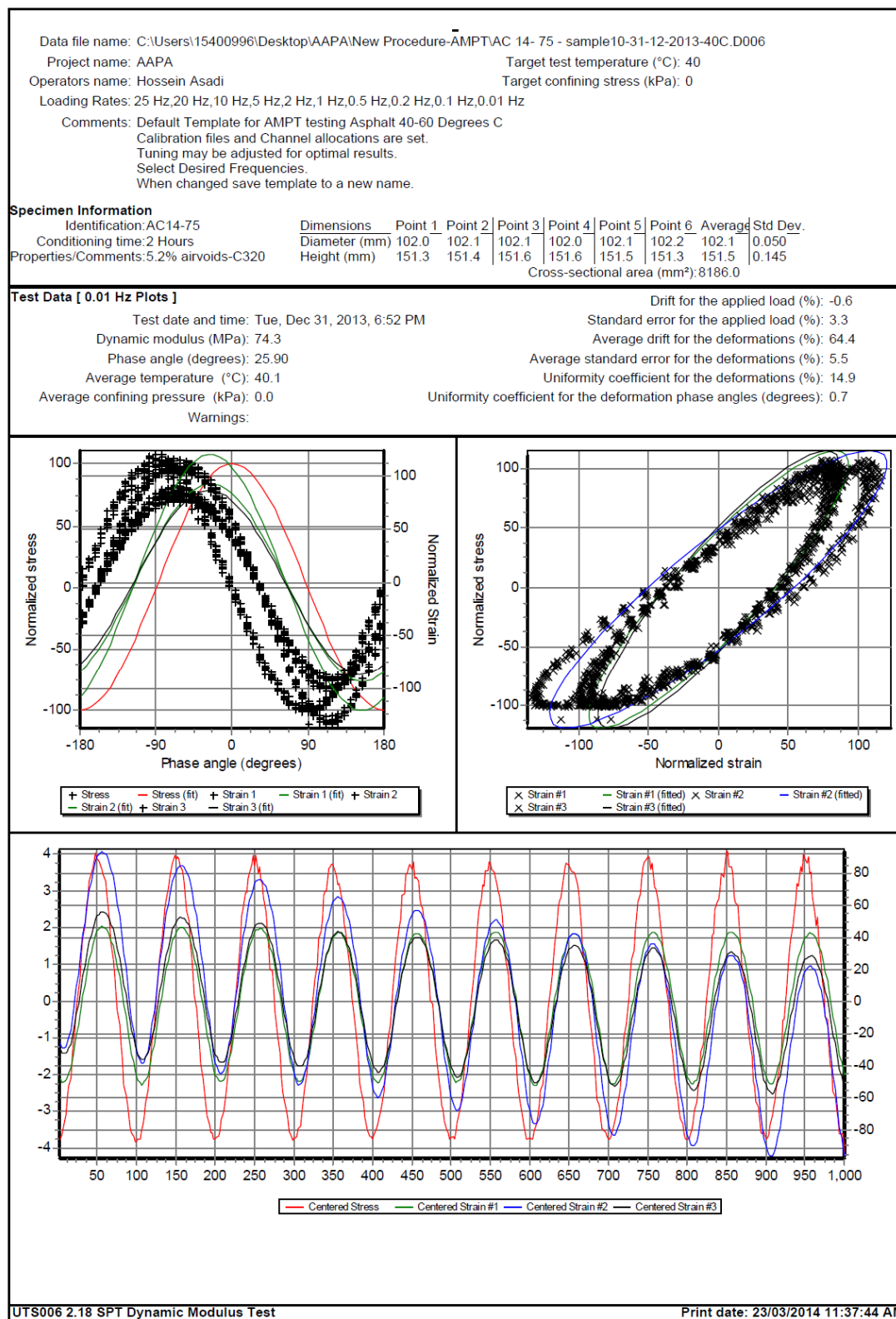


Figure E - 74. UTS6 output for sample6, 0.01 Hz and 40°C

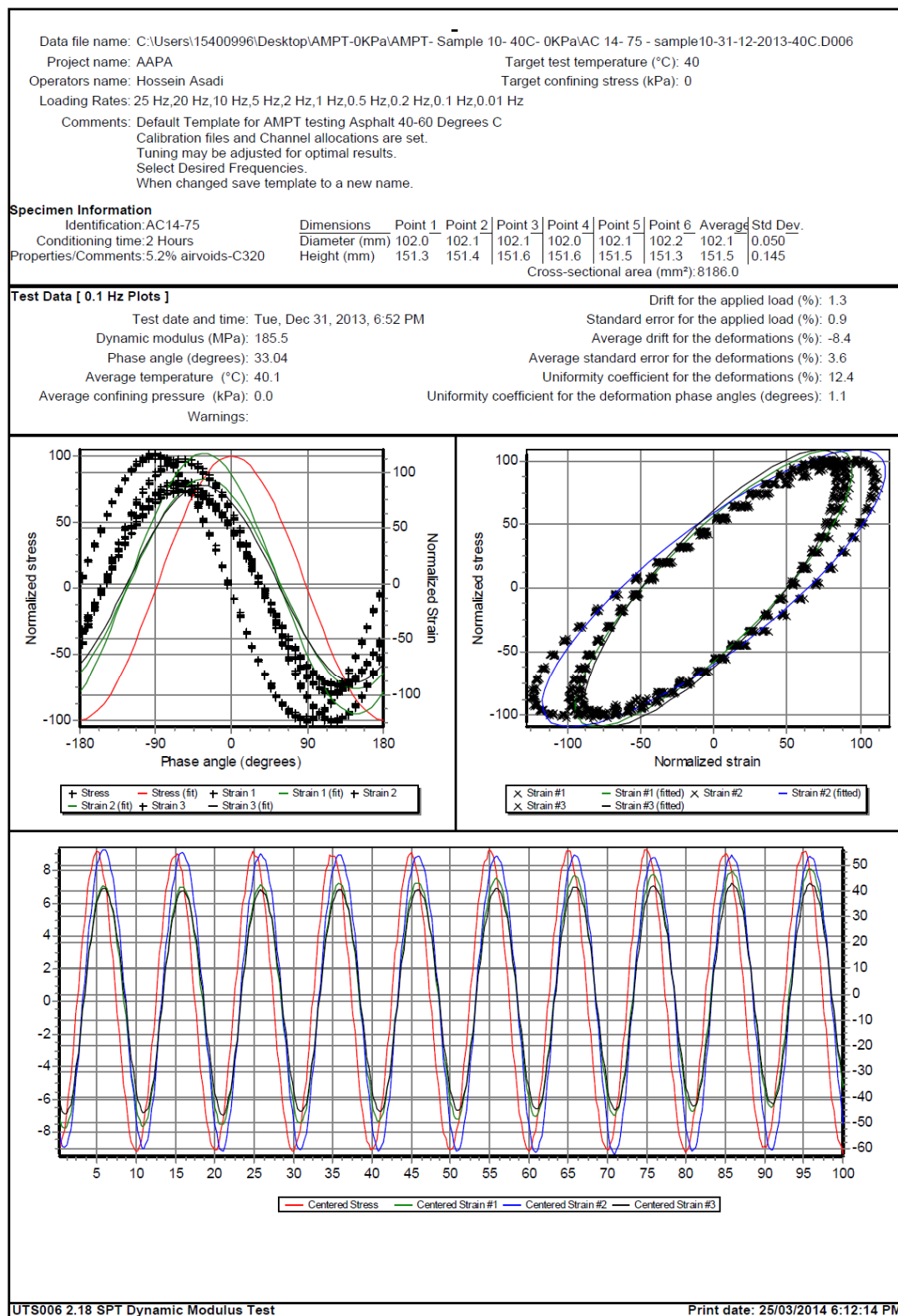


Figure E - 75. UTS6 output for sample6, 0.1 Hz and 40°C

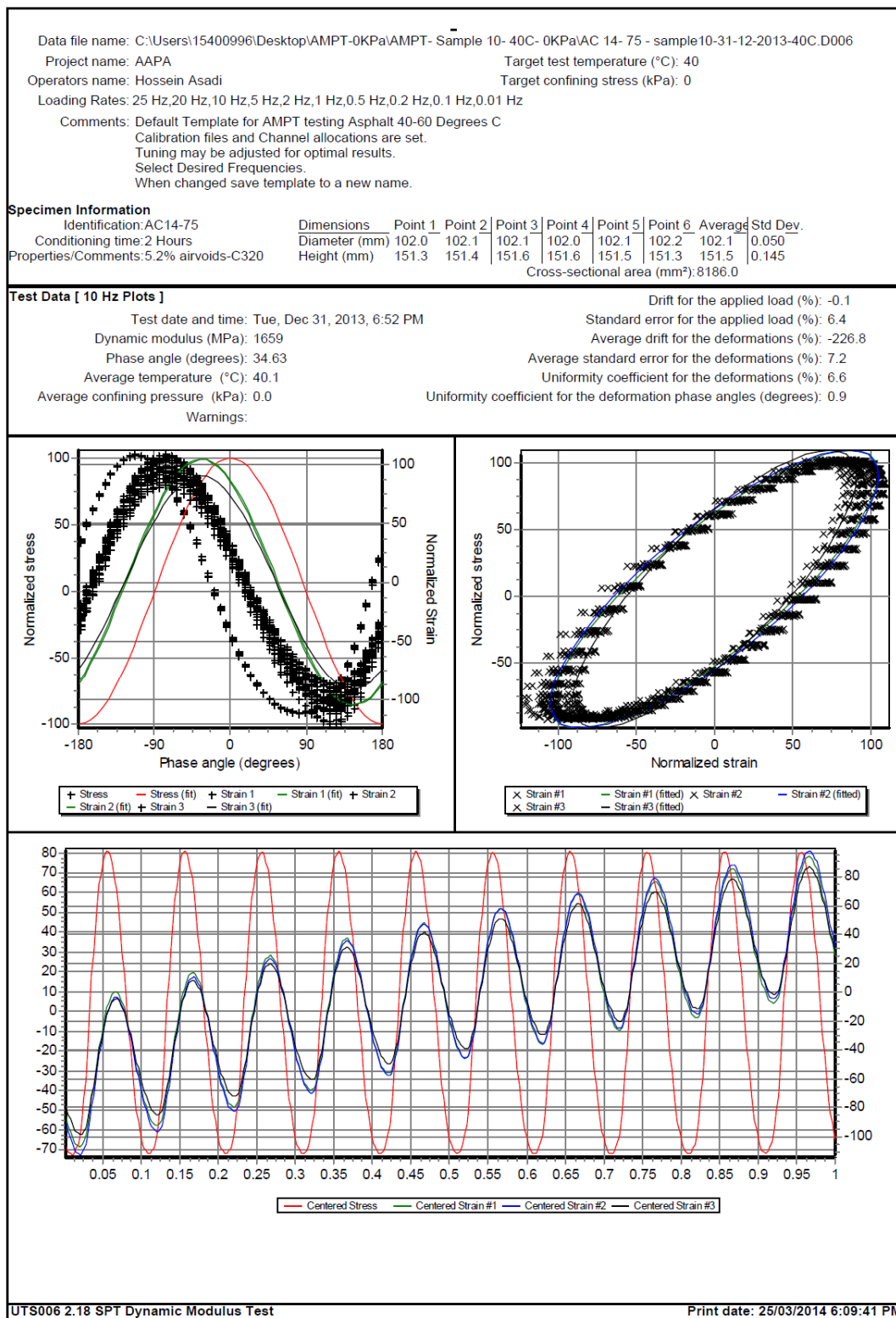


Figure E - 77. UTS6 output for sample6, 10 Hz and 40°C

Data file name: C:\Users\15400996\Desktop\AMPT-0KPa\AMPT- Sample 10- 40C- 0KPa\AC 14- 75 - sample10-31-12-2013-40C.D006											
Project name: AAPA					Target test temperature (°C): 40						
Operators name: Hossein Asadi					Target confining stress (kPa): 0						
Loading Rates: 25 Hz,20 Hz,10 Hz,5 Hz,2 Hz,1 Hz,0.5 Hz,0.2 Hz,0.1 Hz,0.01 Hz											
Comments: Default Template for AMPT testing Asphalt 40-60 Degrees C											
Calibration files and Channel allocations are set.											
Tuning may be adjusted for optimal results.											
Select Desired Frequencies.											
When changed save template to a new name.											
Specimen Information											
Identification:AC14-75		<u>Dimensions</u>		Point 1	Point 2	Point 3	Point 4	Point 5	Point 6	Average	Std Dev.
Conditioning time:2 Hours		Diameter (mm)		102.0	102.1	102.1	102.0	102.1	102.2	102.1	0.050
Properties/Comments:5.2% airvoids-C320		Height (mm)		151.3	151.4	151.6	151.6	151.5	151.3	151.5	0.145
				Cross-sectional area (mm²):8186.0							
Tabulated Results Summary											
	25 Hz	20 Hz	10 Hz	5 Hz	2 Hz	1 Hz	0.5 Hz	0.2 Hz	0.1 Hz	0.01 Hz	
Dynamic modulus (MPa)	2305	2160	1659	1239	817.7	585.0	413.4	262.7	185.5	74.3	
Phase angle (Degrees)	34.08	33.81	34.63	35.27	35.72	35.58	35.16	34.13	33.04	25.90	
Average temperature (°C)	40.1	40.1	40.1	40.1	40.1	40.1	40.0	40.1	40.1	40.1	
Average confining pressure (kPa)	0.1	0.1	0.0	0.0	0.0	0.0	0.0	0.0	0.0	0.0	
Average micro-strain	94	95	95	95	96	97	98	101	98	102	
Load drift (%)	-1.9	-0.7	-0.1	0.3	1.2	0.4	-0.1	0.5	1.3	-0.6	
Load standard error (%)	8.7	7.9	6.4	4.7	2.9	1.2	0.6	0.7	0.9	3.3	
Average deformation drift (%)	-369.6	-291.6	-226.8	-167.4	-111.1	-78.3	-49.4	-23.4	-8.4	64.4	
Average deformation standard error (%)	10.6	8.9	7.2	5.4	3.7	3.2	2.9	3.3	3.6	5.5	
Deformation uniformity (%)	6.8	6.7	6.6	6.9	7.4	8.2	9.4	11.1	12.4	14.9	
Phase uniformity (Degrees)	0.8	0.8	0.9	1.2	1.3	1.2	1.2	1.2	1.1	0.7	

Figure E - 78. UTS6 summary output for sample6, 40°C

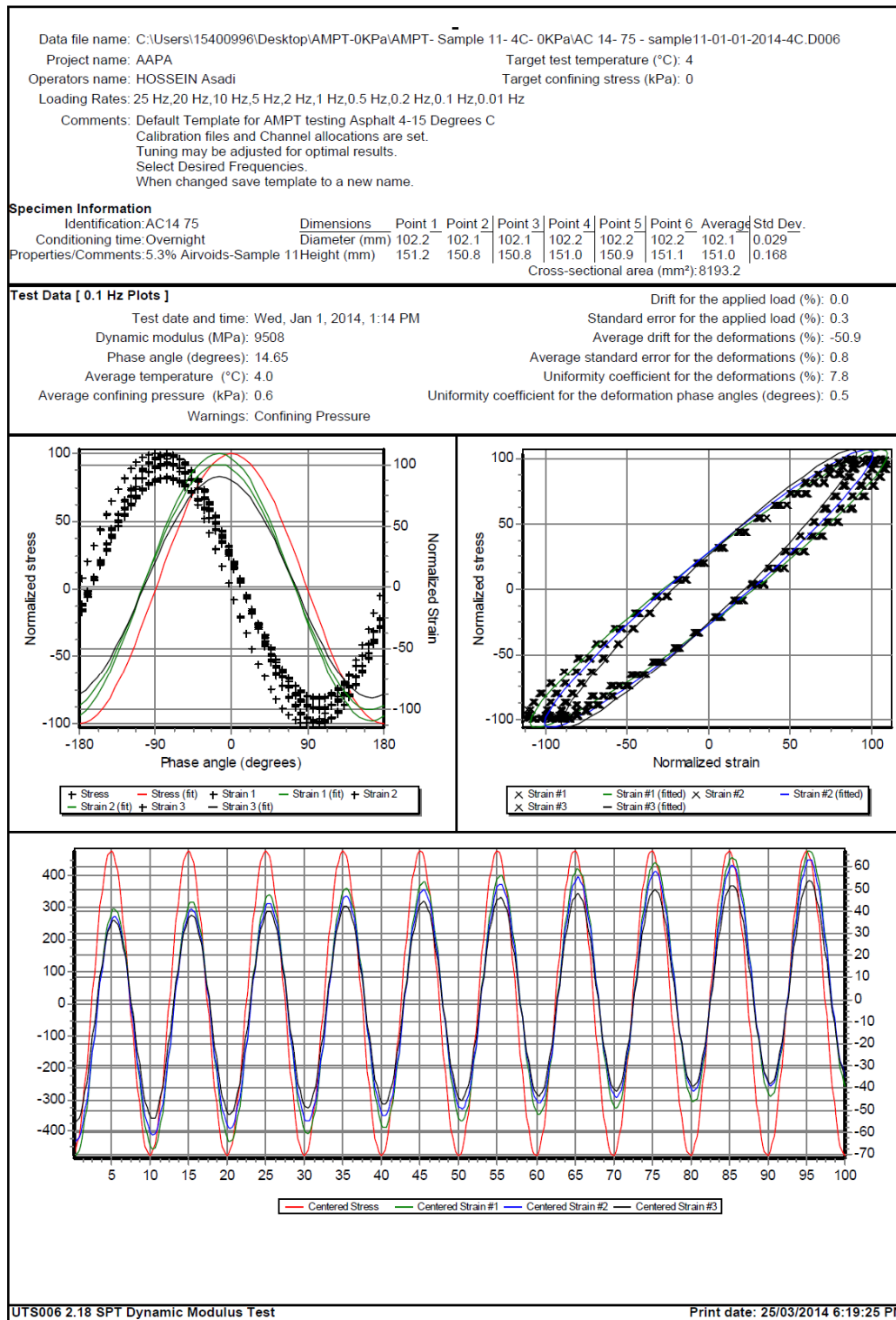


Figure E - 79. UTS6 output for sample7, 0.1 Hz and 4°C

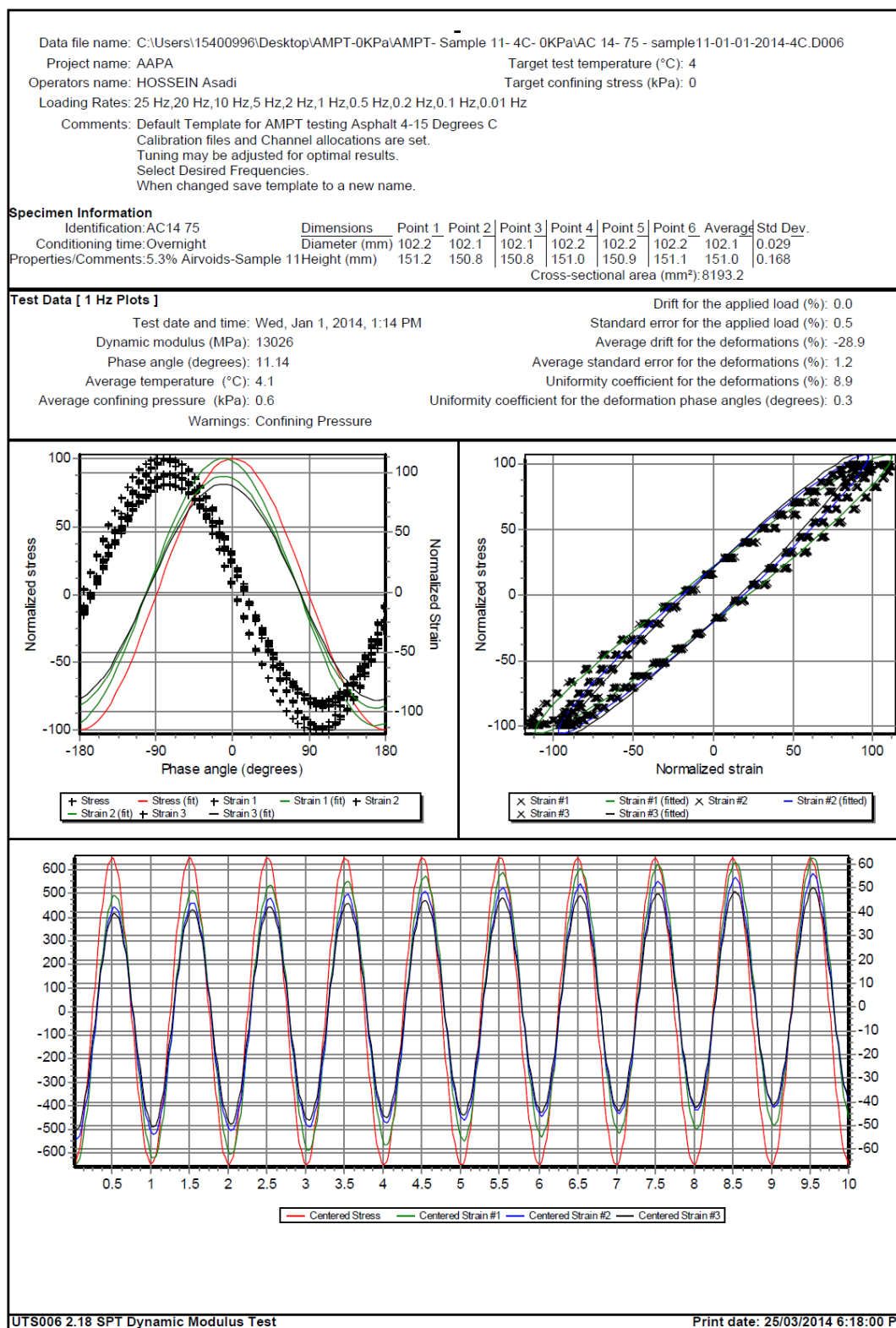


Figure E - 80. UTS6 output for sample7, 1 Hz and 4°C

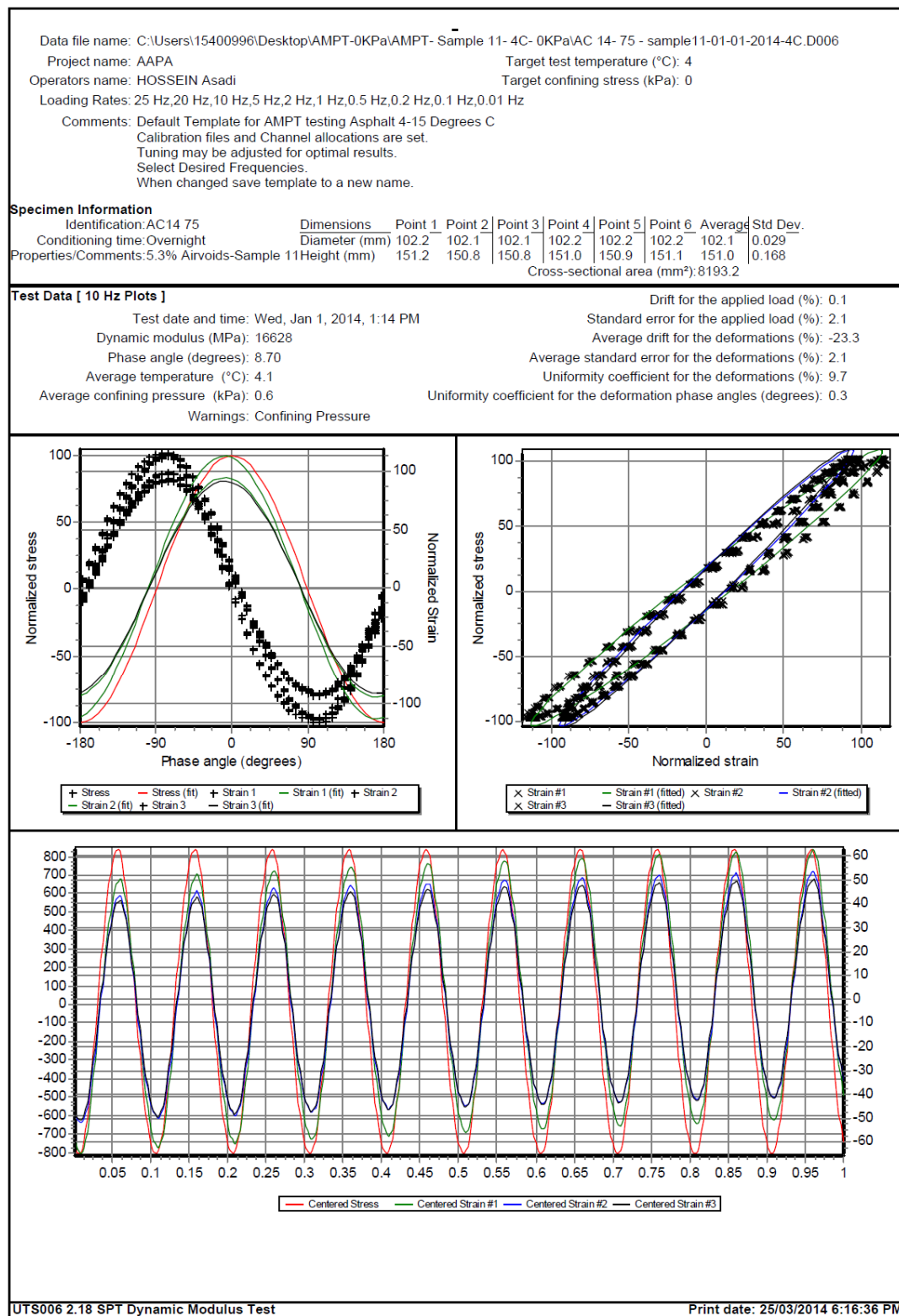


Figure E - 81. UTS6 output for sample7, 10 Hz and 4°C

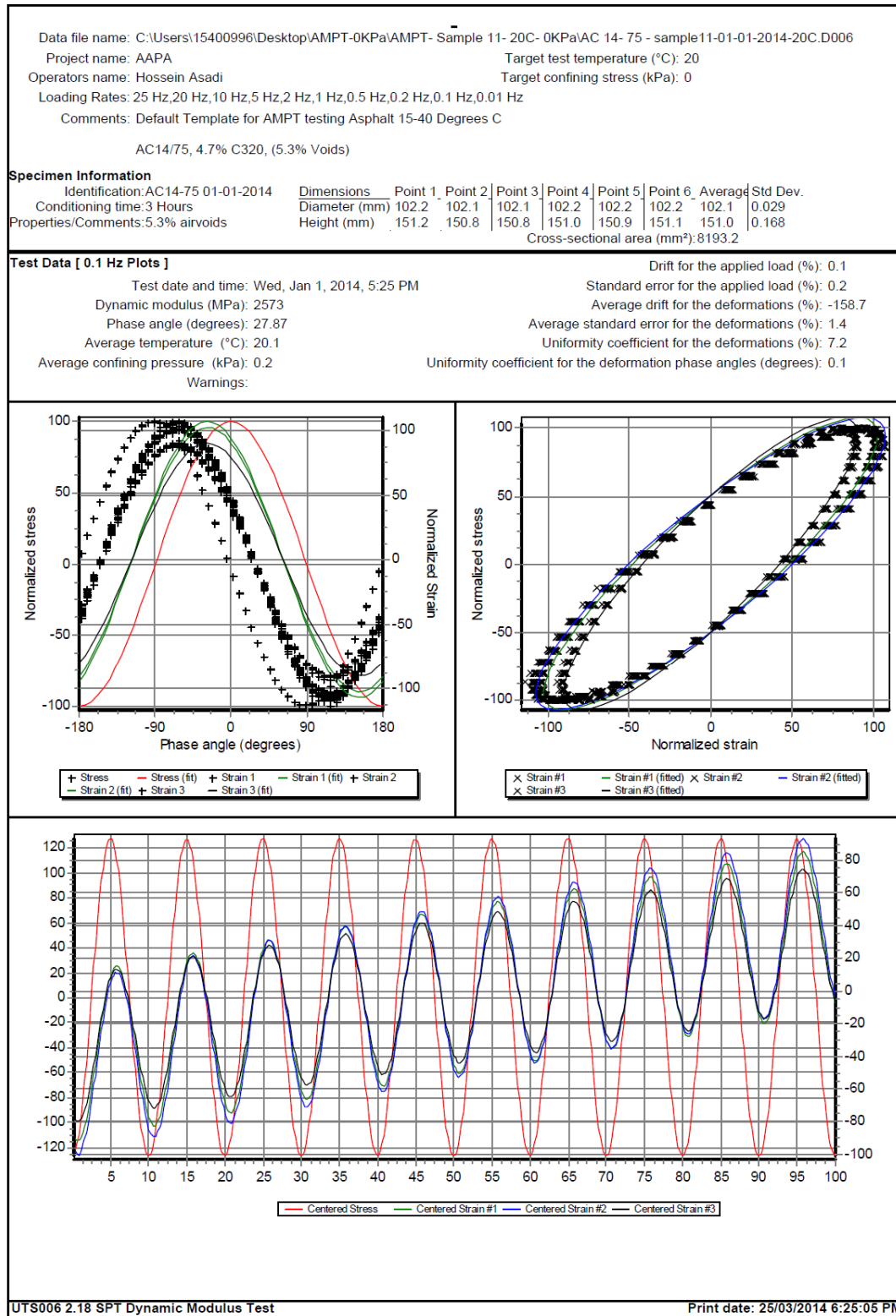


Figure E - 83. UTS6 output for sample7, 0.1 Hz and 20°C

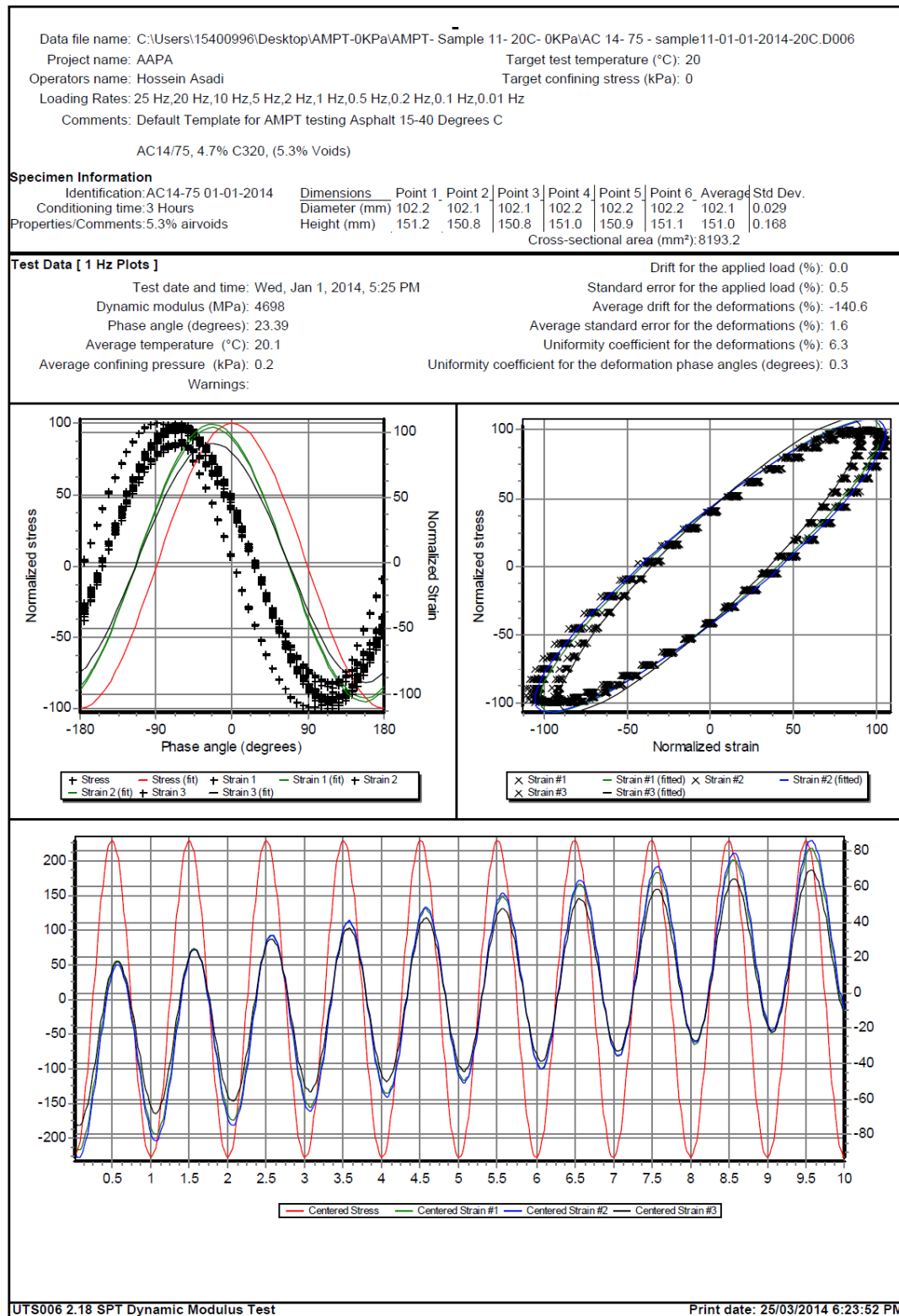


Figure E - 84. UTS6 output for sample7, 1 Hz and 20°C

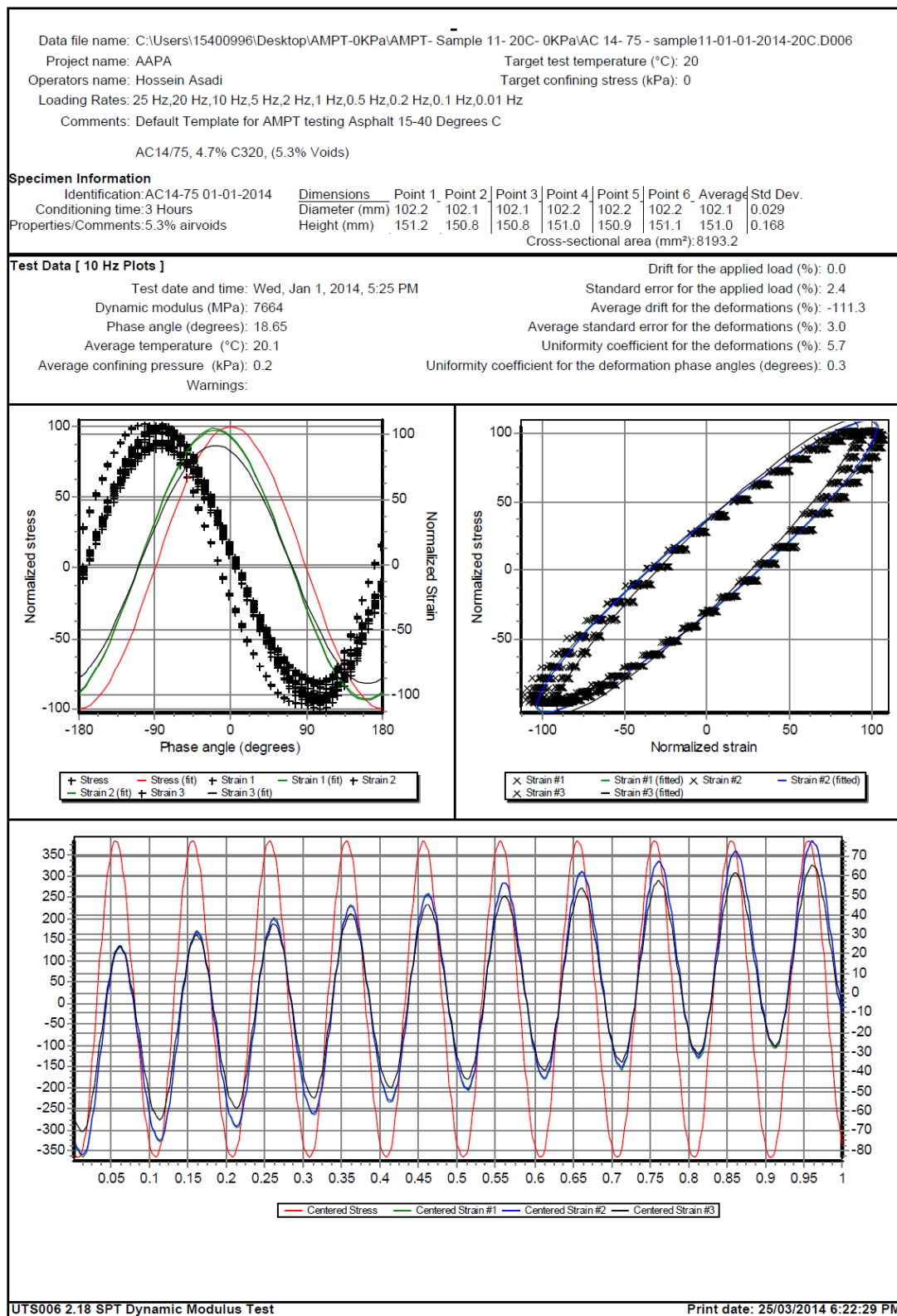


Figure E - 85. UTS6 output for sample7, 10 Hz and 20°C

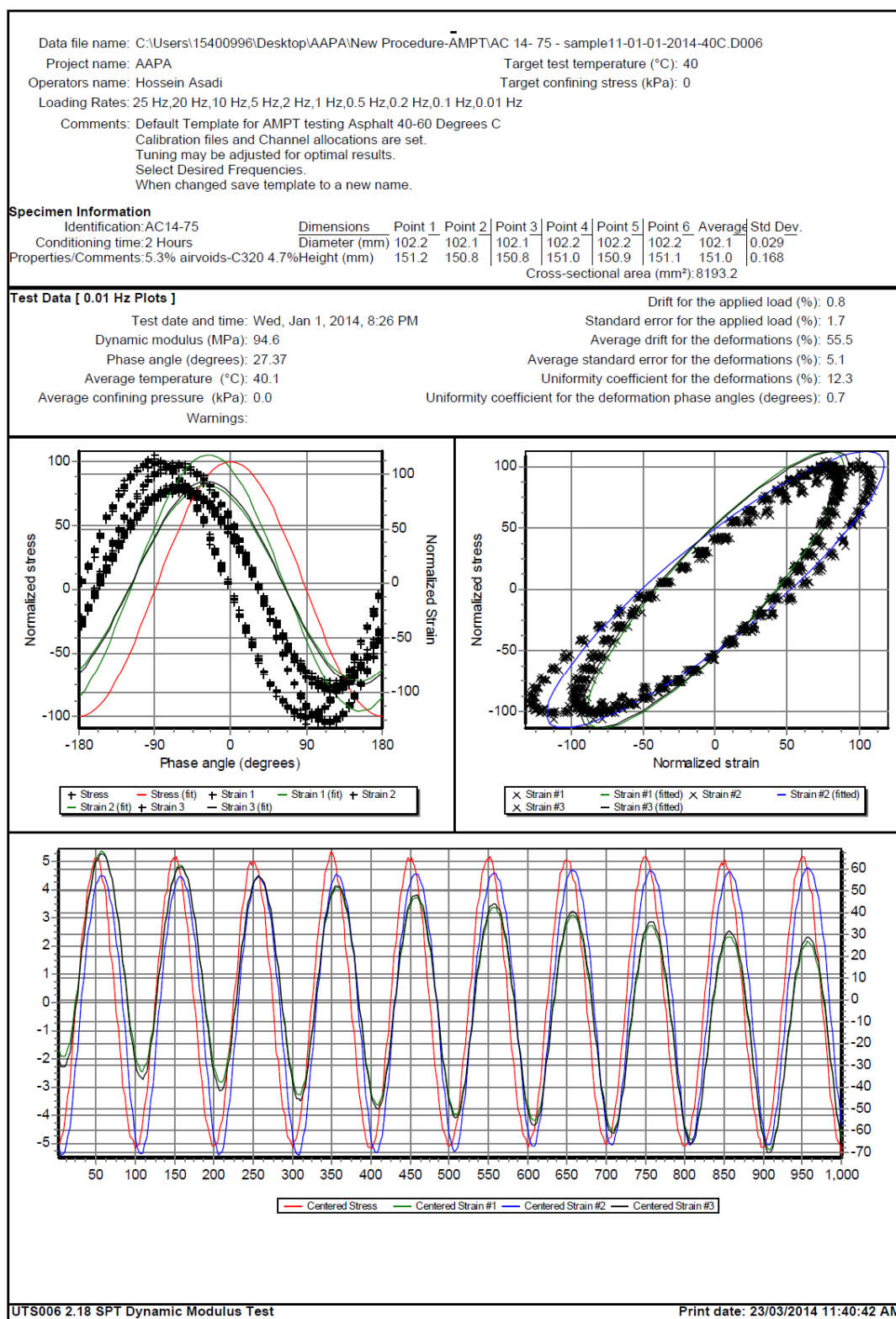


Figure E - 87. UTS6 output for sample7, 0.01 Hz and 40°C

Data file name: C:\Users\15400996\Desktop\AMPT-0KPa\AMPT- Sample 11- 40C- 0KPa\AC 14- 75 - sample11-01-01-2014-40C.D006
 Project name: AAPA Target test temperature (°C): 40
 Operators name: Hossein Asadi Target confining stress (kPa): 0
 Loading Rates: 25 Hz,20 Hz,10 Hz,5 Hz,2 Hz,1 Hz,0.5 Hz,0.2 Hz,0.1 Hz,0.01 Hz
 Comments: Default Template for AMPT testing Asphalt 40-60 Degrees C
 Calibration files and Channel allocations are set.
 Tuning may be adjusted for optimal results.
 Select Desired Frequencies.
 When changed save template to a new name.

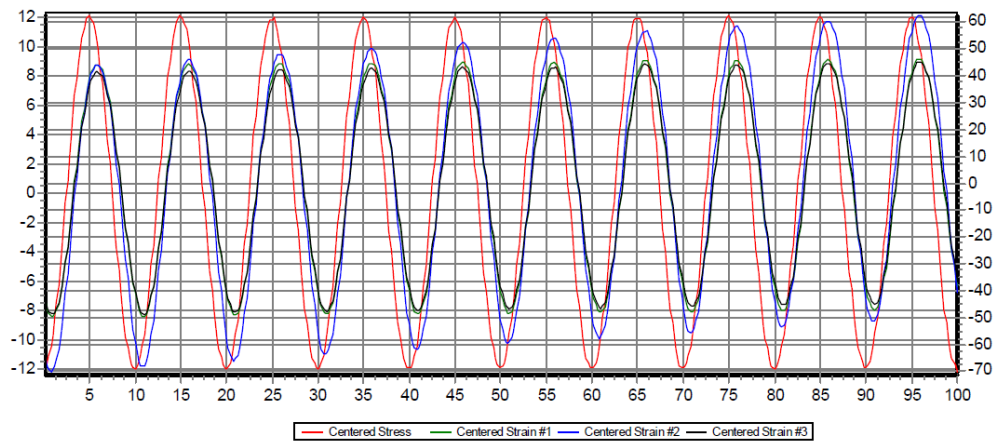
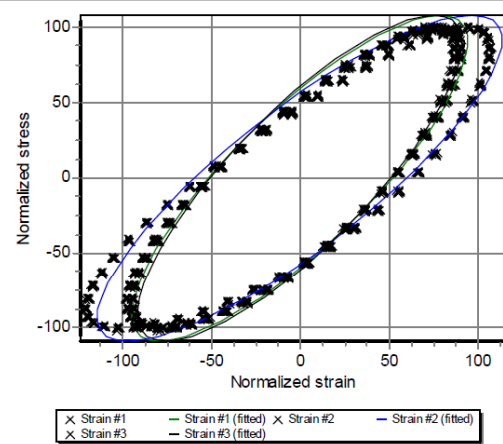
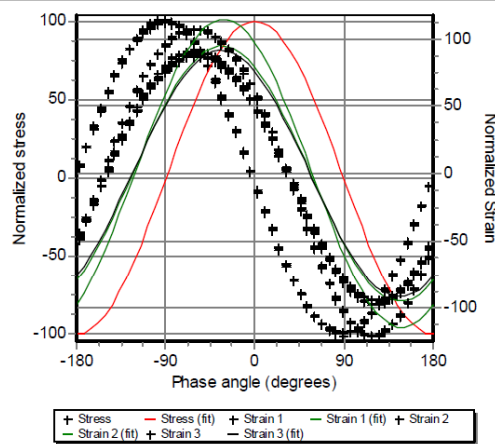
Specimen Information

Identification: AC14-75	Dimensions	Point 1	Point 2	Point 3	Point 4	Point 5	Point 6	Average	Std Dev.
Conditioning time: 2 Hours	Diameter (mm)	102.2	102.1	102.1	102.2	102.2	102.2	102.1	0.029
Properties/Comments: 5.3% airvoids-C320 4.7%	Height (mm)	151.2	150.8	150.8	151.0	150.9	151.1	151.0	0.168
	Cross-sectional area (mm²):	8193.2							

Test Data [0.1 Hz Plots]

Test date and time: Wed, Jan 1, 2014, 8:26 PM
 Dynamic modulus (MPa): 241.6
 Phase angle (degrees): 32.98
 Average temperature (°C): 40.1
 Average confining pressure (kPa): 0.0
 Warnings:

Drift for the applied load (%): -0.2
 Standard error for the applied load (%): 0.7
 Average drift for the deformations (%): -17.8
 Average standard error for the deformations (%): 3.3
 Uniformity coefficient for the deformations (%): 10.1
 Uniformity coefficient for the deformation phase angles (degrees): 1.0



UTS006 2.18 SPT Dynamic Modulus Test

Print date: 25/03/2014 6:29:39 PM

Figure E - 88. UTS6 output for sample7, 0.1 Hz and 40°C

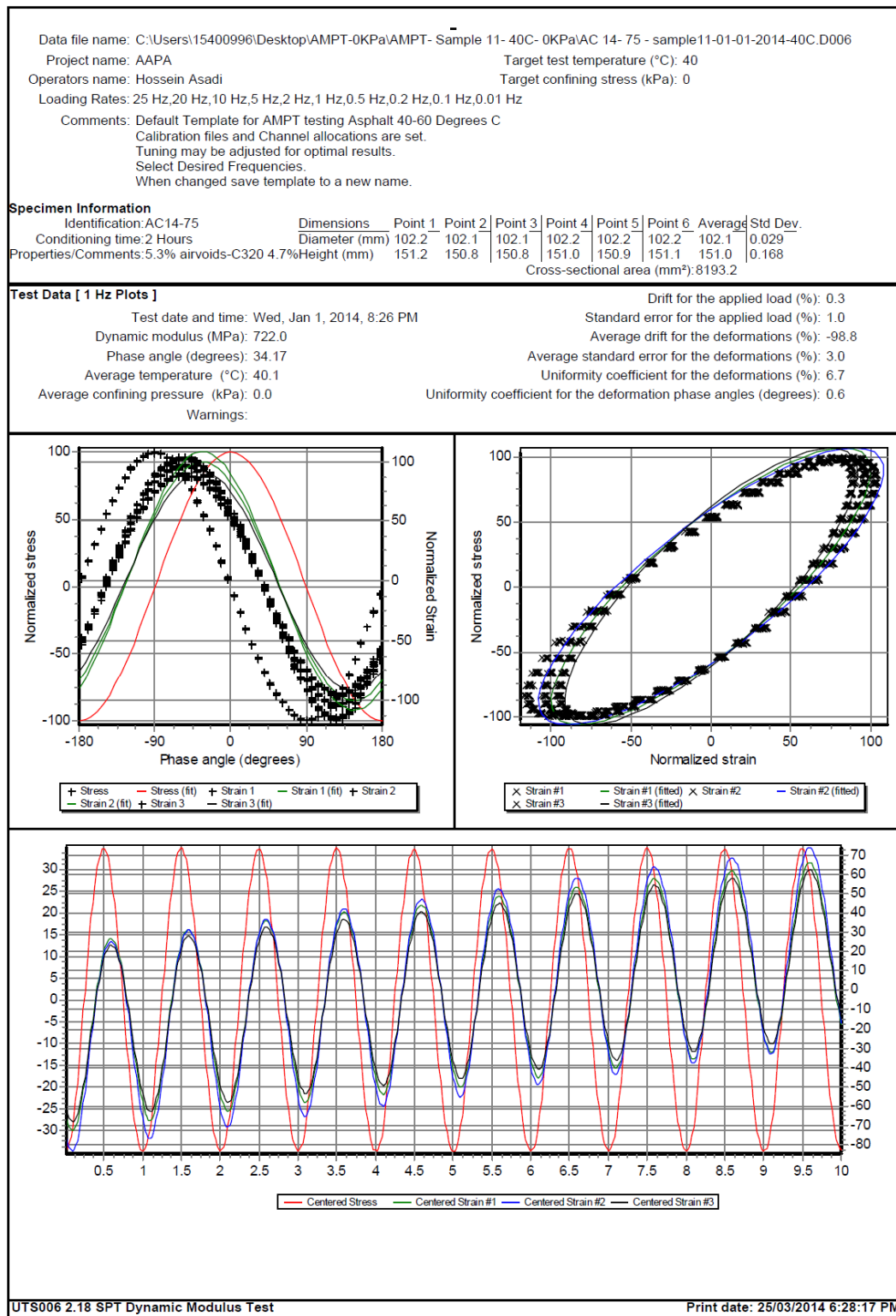
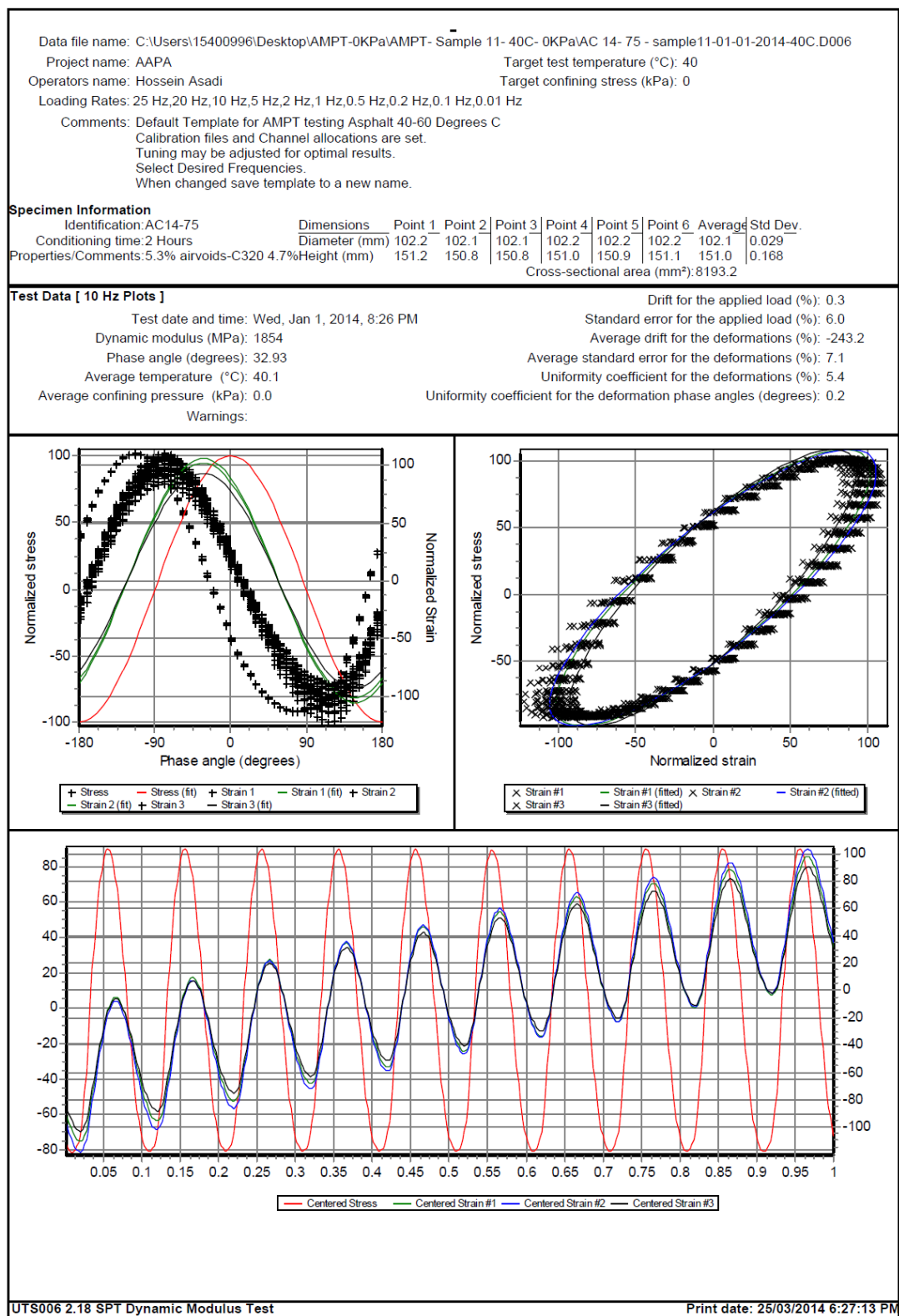


Figure E - 89. UTS6 output for sample7, 1 Hz and 40°C



Data file name: C:\Users\15400996\Desktop\AMPT-0KPa\AMPT- Sample 11- 40C- 0KPa\AC 14- 75 - sample11-01-01-2014-40C.D006											
Project name: AAPA					Target test temperature (°C): 40						
Operators name: Hossein Asadi					Target confining stress (kPa): 0						
Loading Rates: 25 Hz,20 Hz,10 Hz,5 Hz,2 Hz,1 Hz,0.5 Hz,0.2 Hz,0.1 Hz,0.01 Hz											
Comments: Default Template for AMPT testing Asphalt 40-60 Degrees C											
Calibration files and Channel allocations are set.											
Tuning may be adjusted for optimal results.											
Select Desired Frequencies.											
When changed save template to a new name.											
Specimen Information											
Identification:AC14-75		Dimensions		Point 1	Point 2	Point 3	Point 4	Point 5	Point 6	Average	Std Dev.
Conditioning time:2 Hours		Diameter (mm)		102.2	102.1	102.1	102.2	102.2	102.2	102.1	0.029
Properties/Comments:5.3% airvoids-C320 4.7%		Height (mm)		151.2	150.8	150.8	151.0	150.9	151.1	151.0	0.168
Cross-sectional area (mm²):8193.2											
Tabulated Results Summary											
	25 Hz	20 Hz	10 Hz	5 Hz	2 Hz	1 Hz	0.5 Hz	0.2 Hz	0.1 Hz	0.01 Hz	
Dynamic modulus (MPa)	2478	2348	1854	1429	979.1	722.0	521.5	337.5	241.6	94.6	
Phase angle (Degrees)	32.57	32.16	32.93	33.57	34.17	34.17	33.98	33.50	32.98	27.37	
Average temperature (°C)	40.1	40.1	40.1	40.1	40.1	40.1	40.1	40.0	40.1	40.1	
Average confining pressure (kPa)	0.0	-0.1	0.0	0.0	0.0	0.0	0.0	0.0	0.0	0.0	
Average micro-strain	94	96	95	95	96	96	100	101	99	108	
Load drift (%)	-2.0	-1.1	0.3	0.4	0.2	0.3	-0.2	0.2	-0.2	0.8	
Load standard error (%)	9.1	8.1	6.0	4.3	2.6	1.0	0.3	0.6	0.7	1.7	
Average deformation drift (%)	-359.8	-284.1	-243.2	-189.9	-134.0	-98.8	-70.9	-40.6	-17.8	55.5	
Average deformation standard error (%)	10.2	8.5	7.1	5.2	3.4	3.0	2.7	3.0	3.3	5.1	
Deformation uniformity (%)	4.4	5.0	5.4	5.9	6.4	6.7	8.3	9.3	10.1	12.3	
Phase uniformity (Degrees)	0.1	0.0	0.2	0.3	0.5	0.6	0.8	0.9	1.0	0.7	

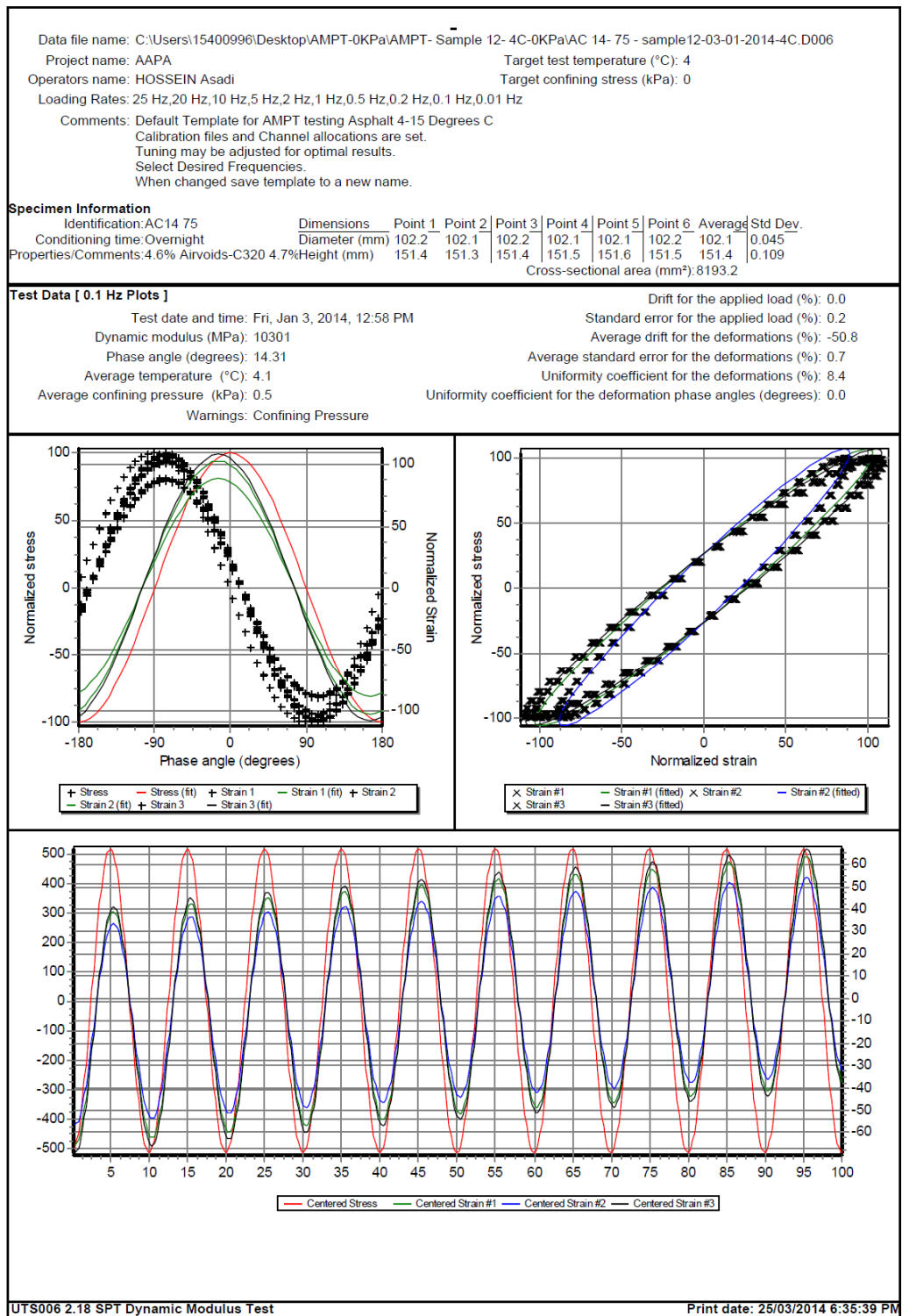


Figure E - 92. UTS6 output for sample8, 0.1 Hz and 4°C

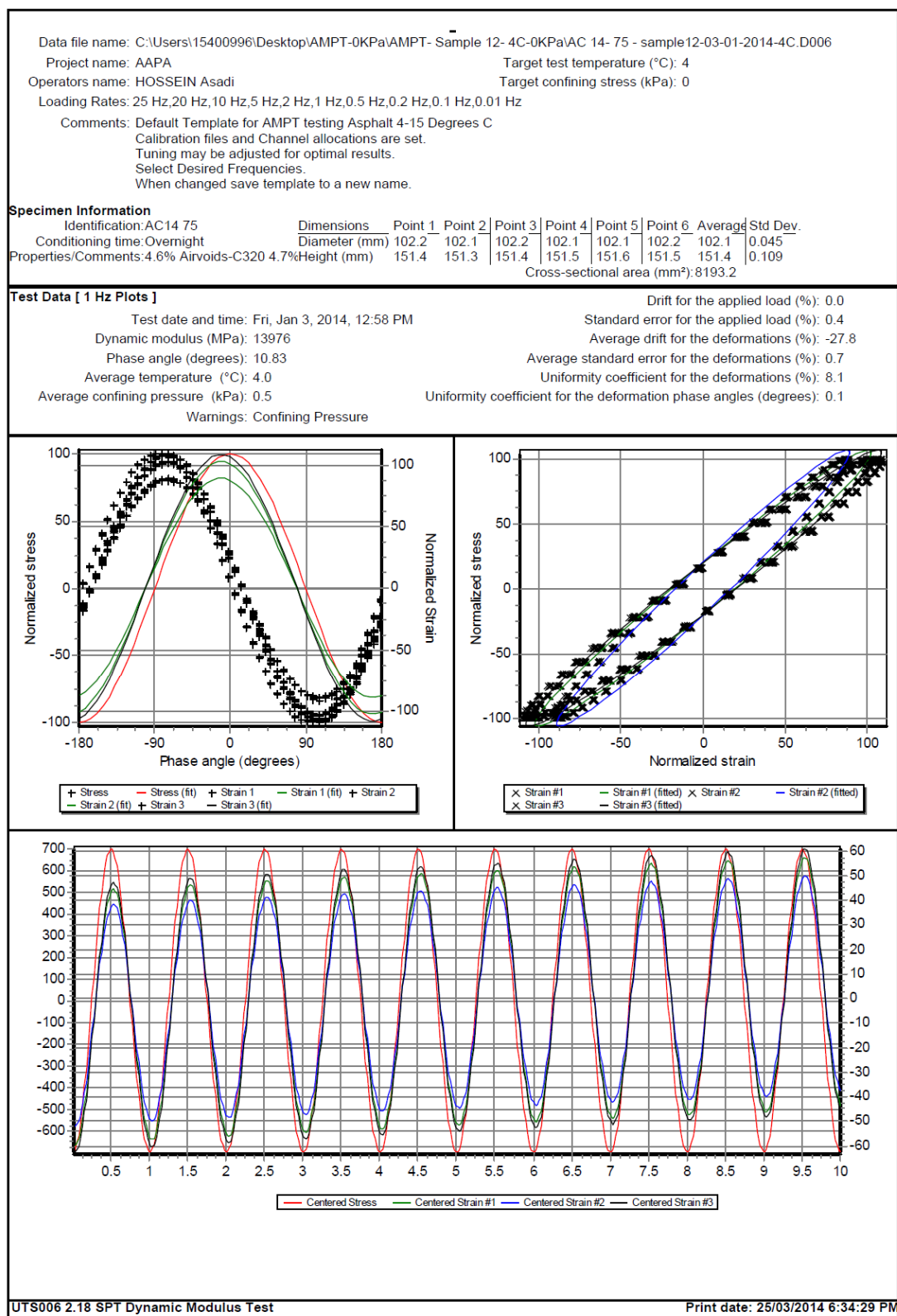


Figure E - 93. UTS6 output for sample8, 1 Hz and 4°C

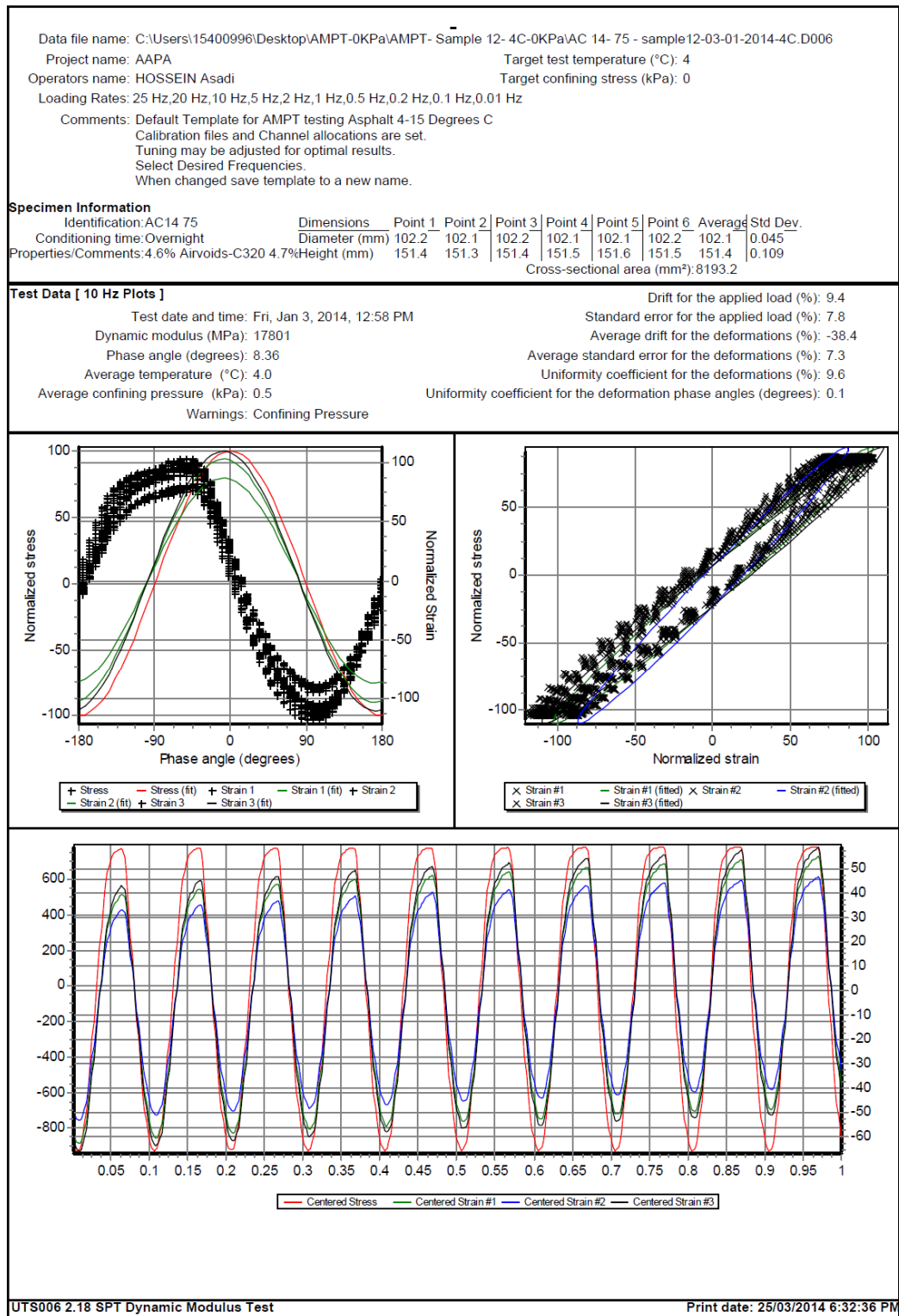


Figure E - 94. UTS6 output for sample8, 10 Hz and 4°C

Data file name: C:\Users\15400996\Desktop\AMPT-0KPa\AMPT- Sample 12- 4C-0KPa\AC 14- 75 - sample12-03-01-2014-4C.D006											
Project name: AAPA					Target test temperature (°C): 4						
Operators name: HOSSEIN Asadi					Target confining stress (kPa): 0						
Loading Rates: 25 Hz,20 Hz,10 Hz,5 Hz,2 Hz,1 Hz,0.5 Hz,0.2 Hz,0.1 Hz,0.01 Hz											
Comments: Default Template for AMPT testing Asphalt 4-15 Degrees C											
Calibration files and Channel allocations are set.											
Tuning may be adjusted for optimal results.											
Select Desired Frequencies.											
When changed save template to a new name.											
Specimen Information											
Identification:AC14 75		Dimensions		Point 1	Point 2	Point 3	Point 4	Point 5	Point 6	Average	Std Dev.
Conditioning time:Overnight		Diameter (mm)		102.2	102.1	102.2	102.1	102.1	102.2	102.1	0.045
Properties/Comments:4.6% Airvoids-C320 4.7%		Height (mm)		151.4	151.3	151.4	151.5	151.6	151.5	151.4	0.109
Cross-sectional area (mm²):8193.2											
Tabulated Results Summary											
	25 Hz	20 Hz	10 Hz	5 Hz	2 Hz	1 Hz	0.5 Hz	0.2 Hz	0.1 Hz	0.01 Hz	
Dynamic modulus (MPa)	19317	19198	17801	16646	15121	13976	12845	11378	10301	6988	
Phase angle (Degrees)	7.62	8.89	8.36	9.03	10.00	10.83	11.74	13.13	14.31	18.96	
Average temperature (°C)	4.0	4.0	4.0	4.0	4.0	4.0	4.1	4.1	4.1	4.1	
Average confining pressure (kPa)	0.5	0.5	0.5	0.5	0.5	0.5	0.5	0.5	0.5	0.6	
Average micro-strain	89	91	101	100	100	100	100	100	100	100	
Load drift (%)	12.1	10.5	9.4	-0.1	-0.1	0.0	0.0	0.1	0.0	0.0	
Load standard error (%)	14.4	10.3	7.8	1.2	0.6	0.4	0.2	0.2	0.2	0.5	
Average deformation drift (%)	-43.4	-172.2	-38.4	-23.0	-25.9	-27.8	-32.4	-41.5	-50.8	-115.7	
Average deformation standard error (%)	13.6	29.1	7.3	1.3	0.8	0.7	0.6	0.8	0.7	1.2	
Deformation uniformity (%)	11.2	12.2	9.6	9.0	8.5	8.1	8.0	8.2	8.4	8.5	
Phase uniformity (Degrees)	0.1	1.6	0.1	0.1	0.1	0.1	0.1	0.1	0.0	0.1	

Figure E - 95. UTS6 output summary for sample8, 4°C

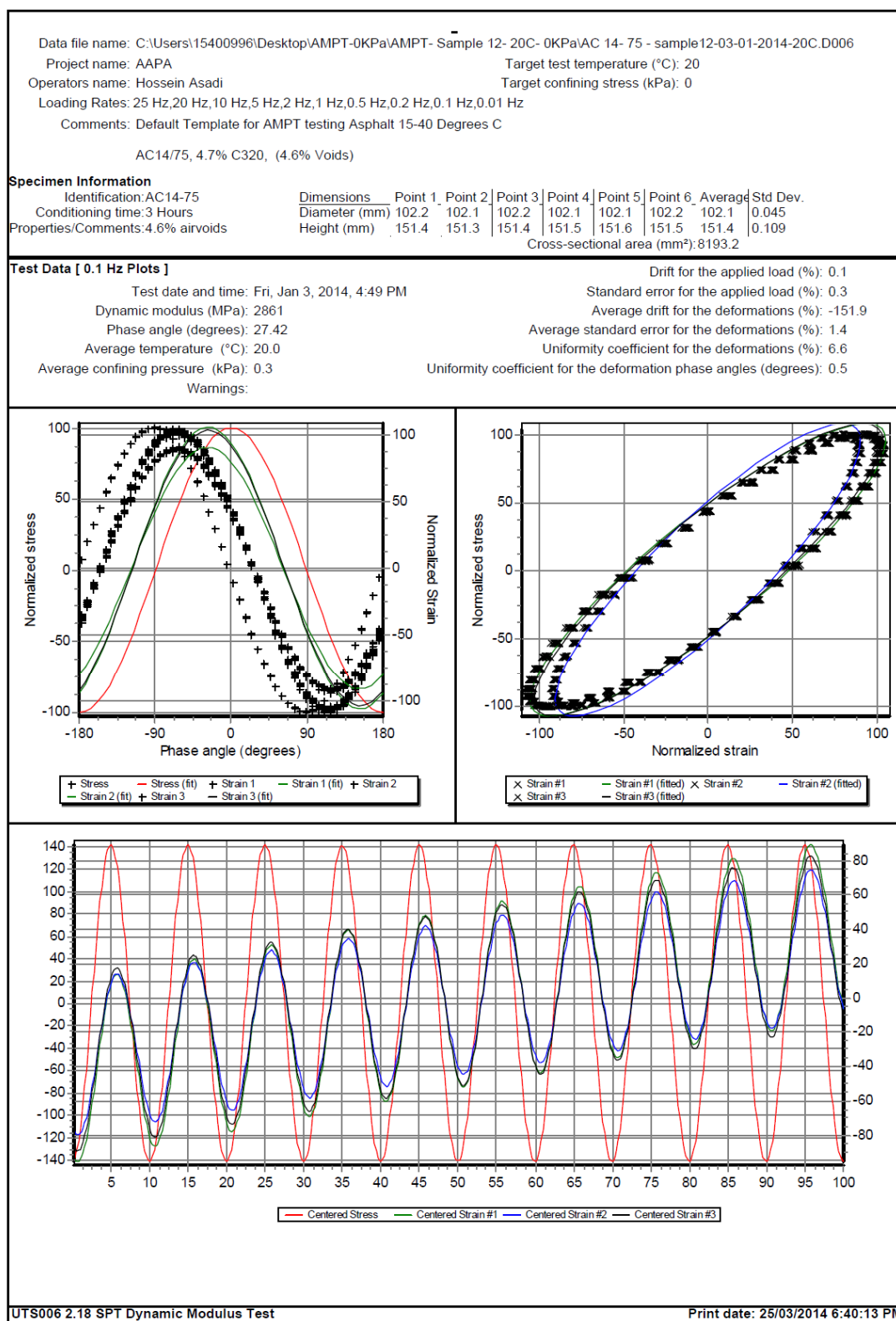


Figure E - 96. UTS6 output for sample8, 0.1 Hz and 20°C

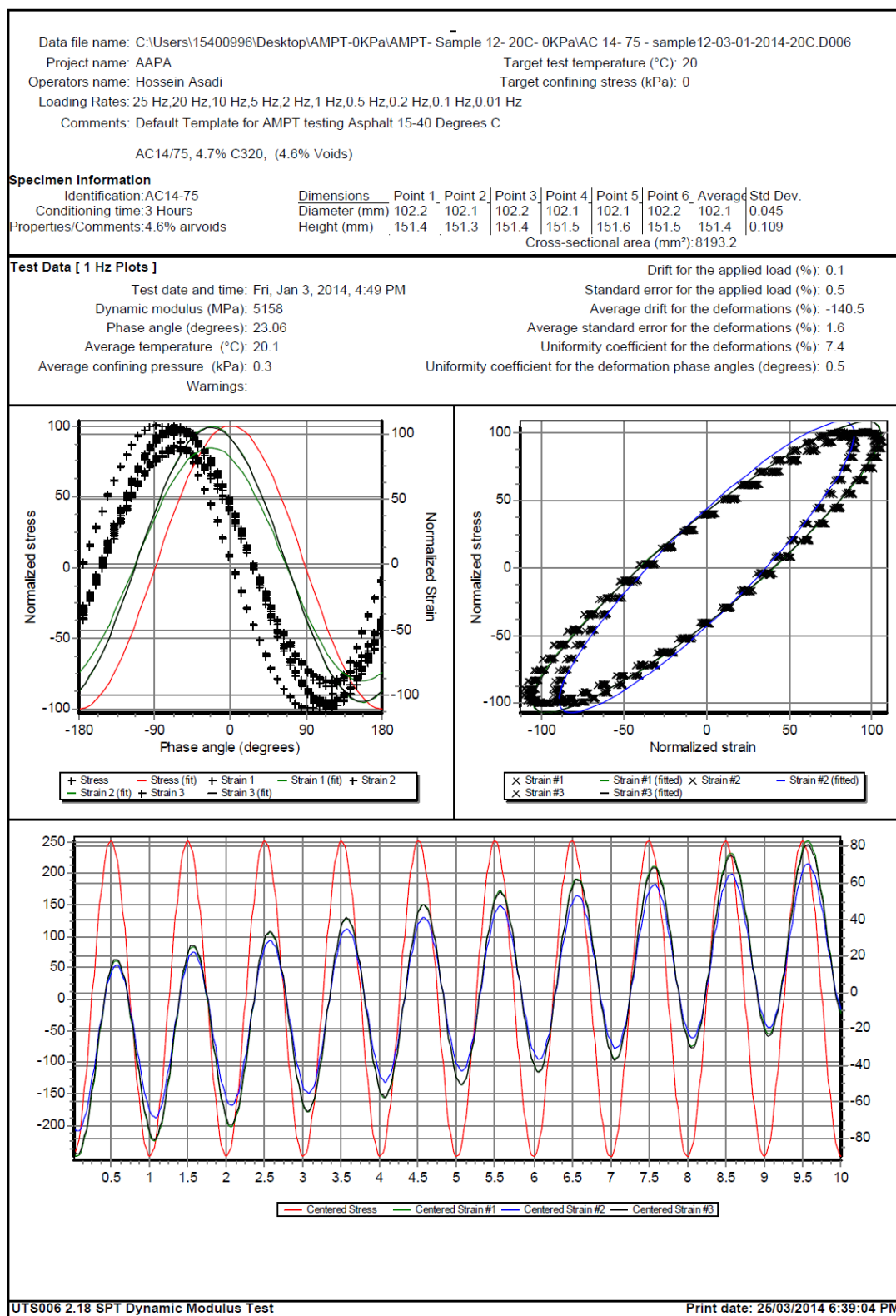


Figure E - 97. UTS6 output for sample8, 1 Hz and 20°C

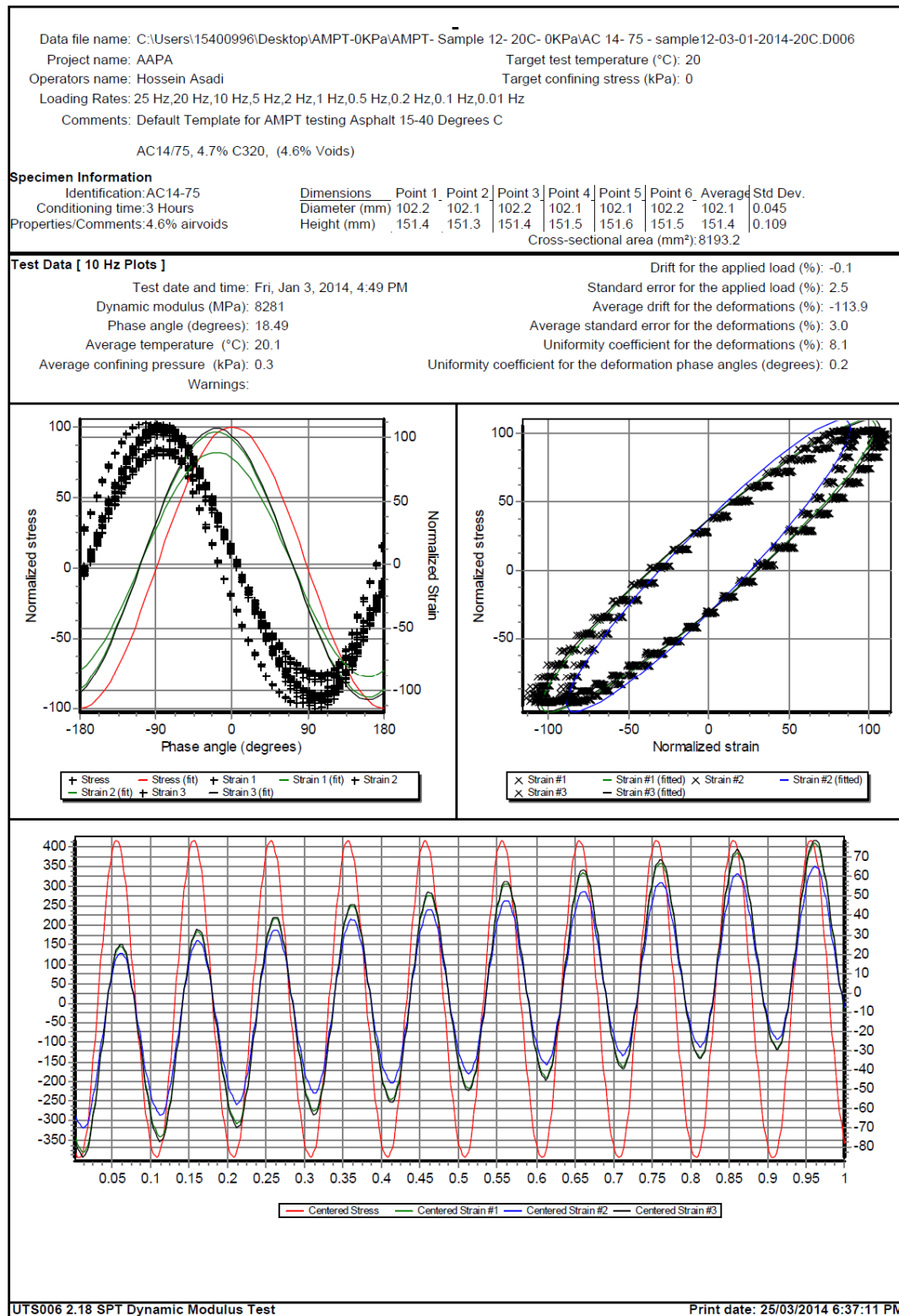


Figure E - 98. UTS6 output for sample8, 10 Hz and 20°C

Data file name: C:\Users\15400996\Desktop\AMPT-0KPa\AMPT- Sample 12- 20C- 0KPa\AC 14- 75 - sample12-03-01-2014-20C.D006											
Project name: AAPA					Target test temperature (°C): 20						
Operators name: Hossein Asadi					Target confining stress (kPa): 0						
Loading Rates: 25 Hz,20 Hz,10 Hz,5 Hz,2 Hz,1 Hz,0.5 Hz,0.2 Hz,0.1 Hz,0.01 Hz											
Comments: Default Template for AMPT testing Asphalt 15-40 Degrees C											
AC14/75, 4.7% C320, (4.6% Voids)											
Specimen Information											
Identification:AC14-75		Dimensions		Point 1	Point 2	Point 3	Point 4	Point 5	Point 6	Average	Std Dev.
Conditioning time:3 Hours		Diameter (mm)	102.2	102.1	102.2	102.1	102.1	102.2	102.1	102.1	0.045
Properties/Comments:4.6% airvoids		Height (mm)	151.4	151.3	151.4	151.5	151.6	151.5	151.4	151.4	0.109
Cross-sectional area (mm²):8193.2											
Tabulated Results Summary											
	25 Hz	20 Hz	10 Hz	5 Hz	2 Hz	1 Hz	0.5 Hz	0.2 Hz	0.1 Hz	0.01 Hz	
Dynamic modulus (MPa)	9758	9405	8281	7251	5996	5158	4390	3468	2861	1312	
Phase angle (Degrees)	16.79	17.14	18.49	19.84	21.75	23.06	24.41	26.27	27.42	31.18	
Average temperature (°C)	20.1	20.1	20.1	20.1	20.1	20.1	20.1	20.0	20.0	20.1	
Average confining pressure (kPa)	0.3	0.3	0.3	0.3	0.3	0.3	0.3	0.3	0.3	0.3	
Average micro-strain	98	96	98	98	97	97	98	98	99	104	
Load drift (%)	-0.3	-0.7	-0.1	-0.1	-0.1	0.1	0.0	0.1	0.1	0.0	
Load standard error (%)	5.5	5.3	2.5	1.3	0.7	0.5	0.2	0.2	0.3	0.6	
Average deformation drift (%)	-115.7	-102.3	-113.9	-121.6	-134.2	-140.5	-145.2	-156.5	-151.9	-142.4	
Average deformation standard error (%)	5.2	4.9	3.0	2.4	1.7	1.6	1.5	1.3	1.4	2.5	
Deformation uniformity (%)	7.9	8.3	8.1	8.0	7.6	7.4	7.2	6.8	6.6	5.4	
Phase uniformity (Degrees)	0.1	0.1	0.2	0.3	0.5	0.5	0.6	0.6	0.5	0.4	

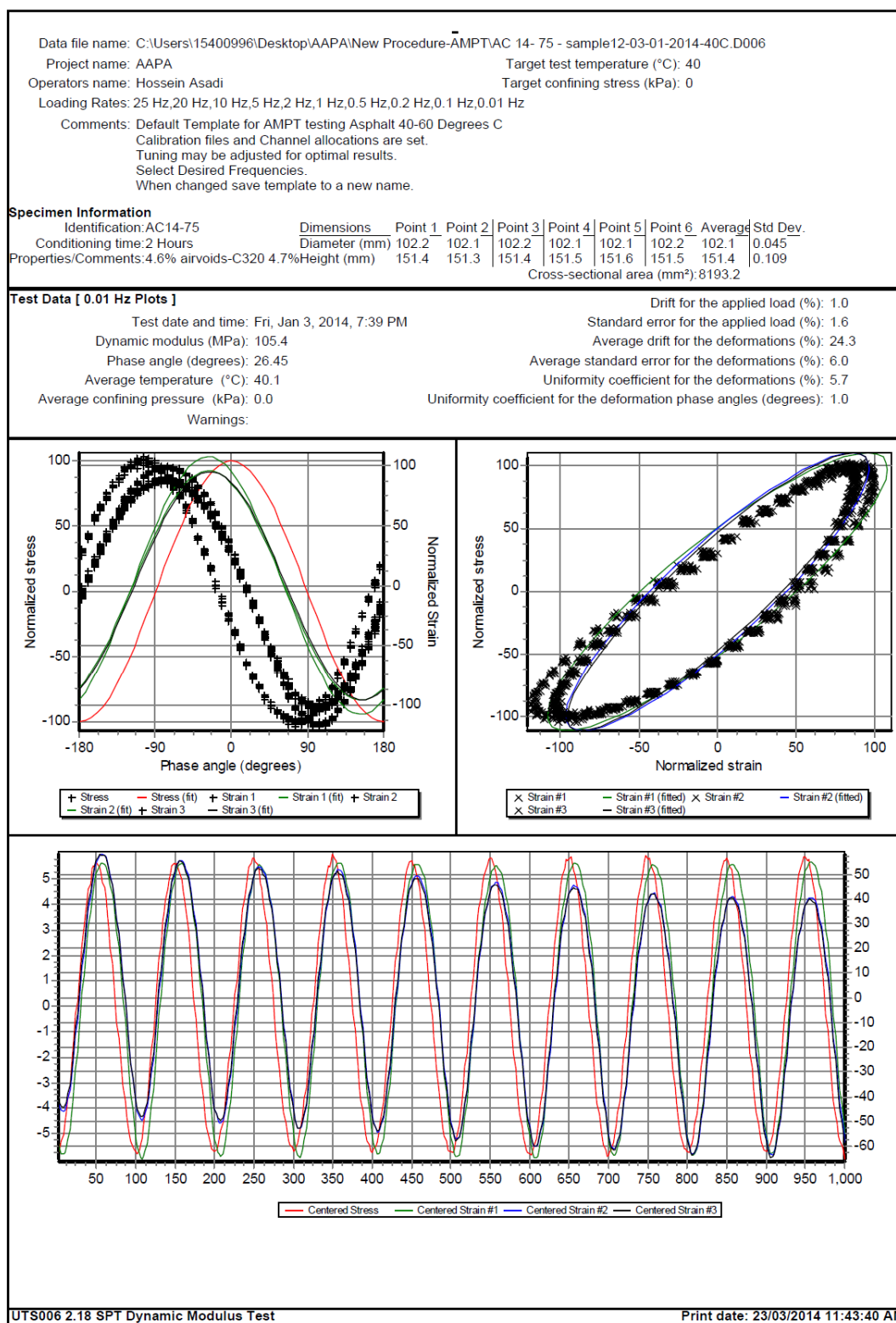
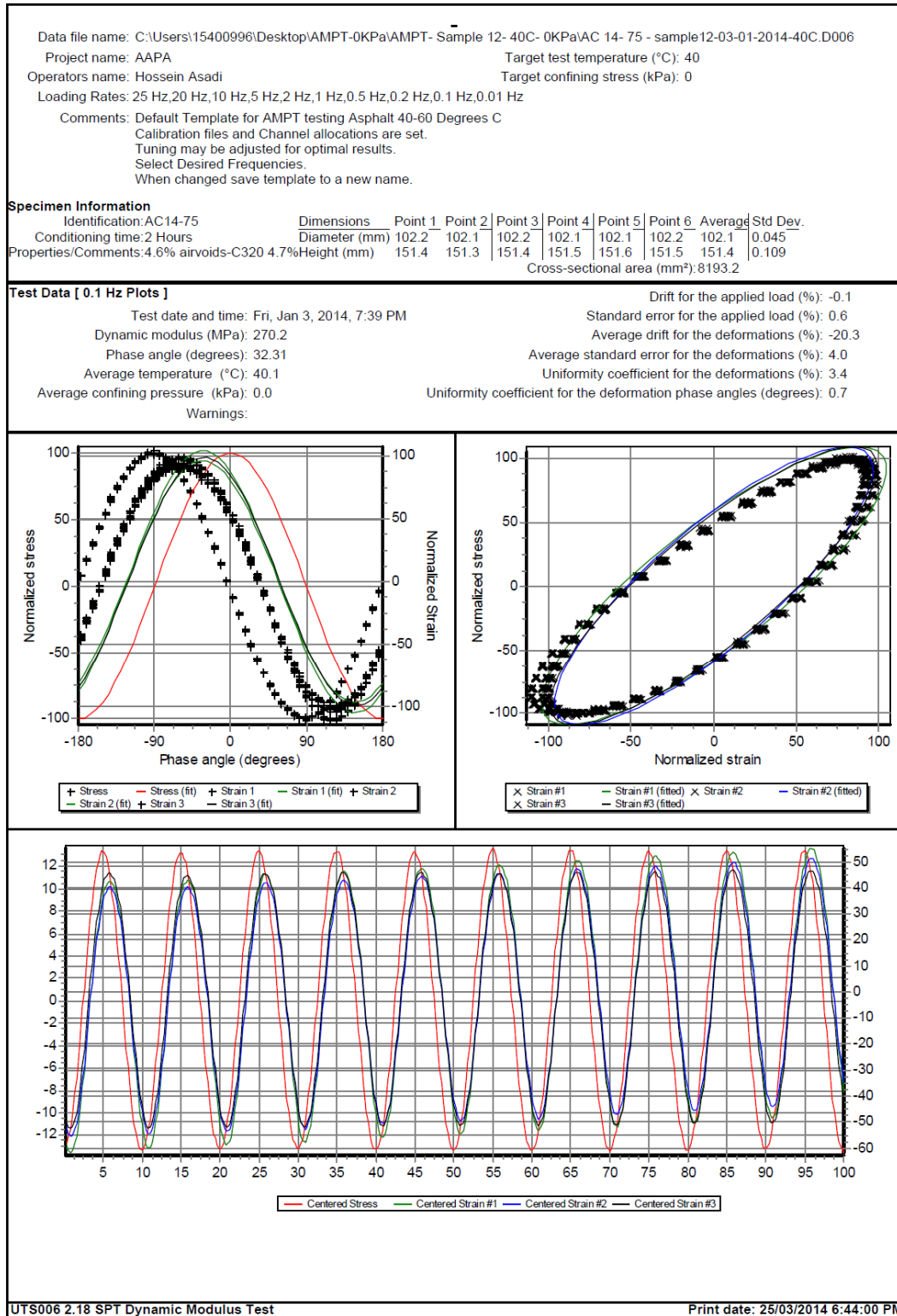


Figure E - 100. UTS6 output for sample8, 0.01 Hz and 40°C



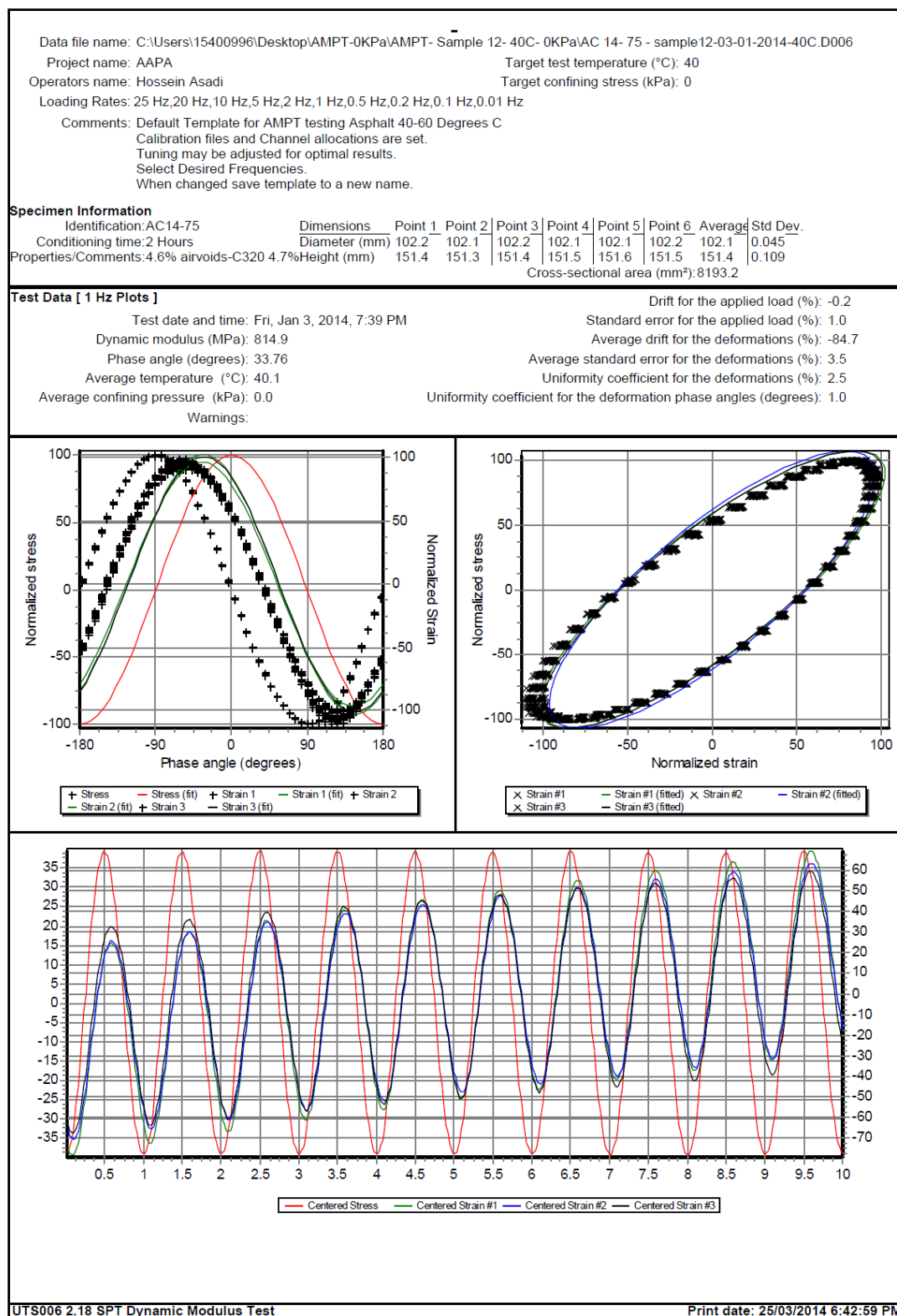


Figure E - 102. UTS6 output for sample8, 1 Hz and 40°C

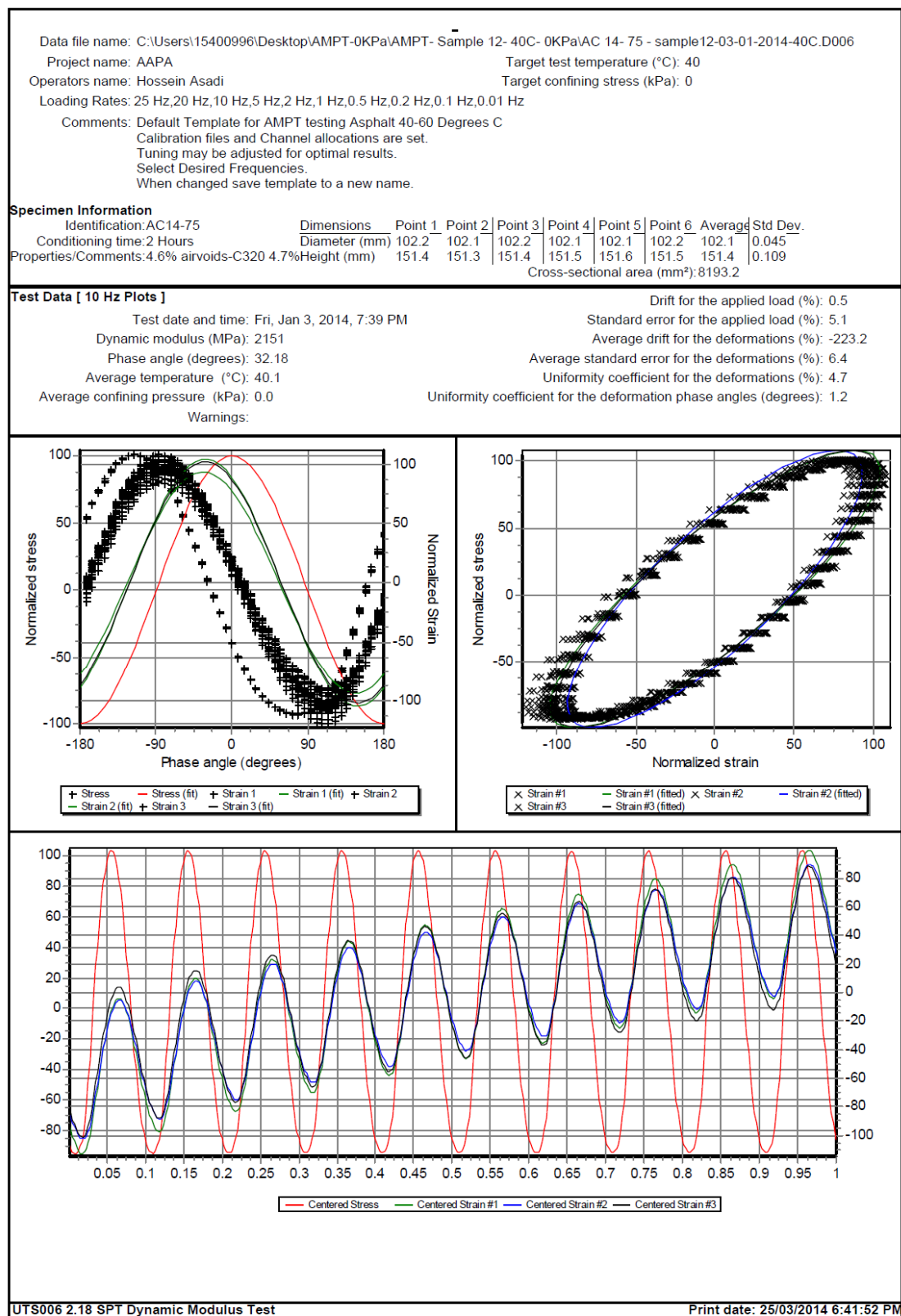
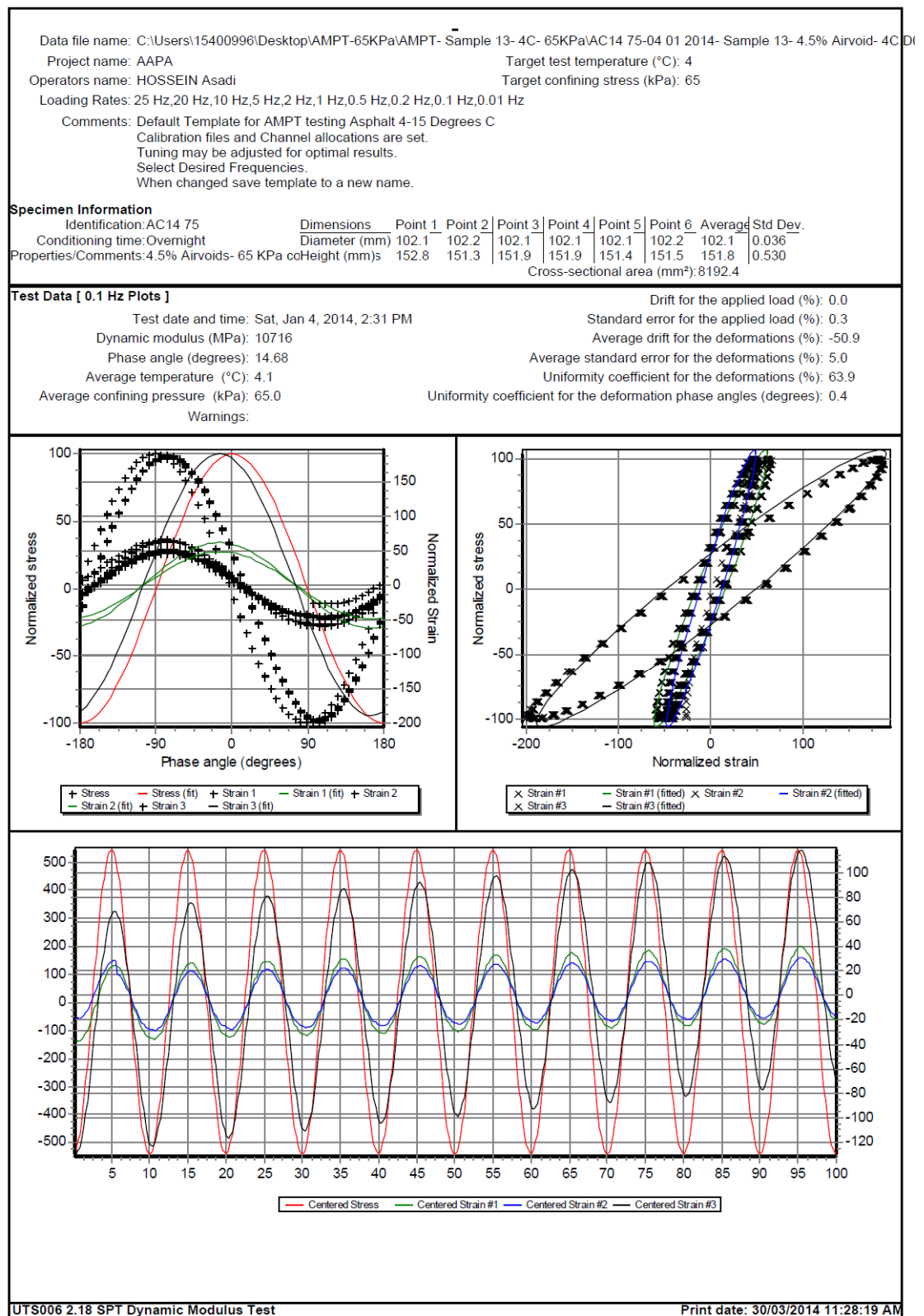


Figure E - 103. UTS6 output for sample8, 10 Hz and 40°C



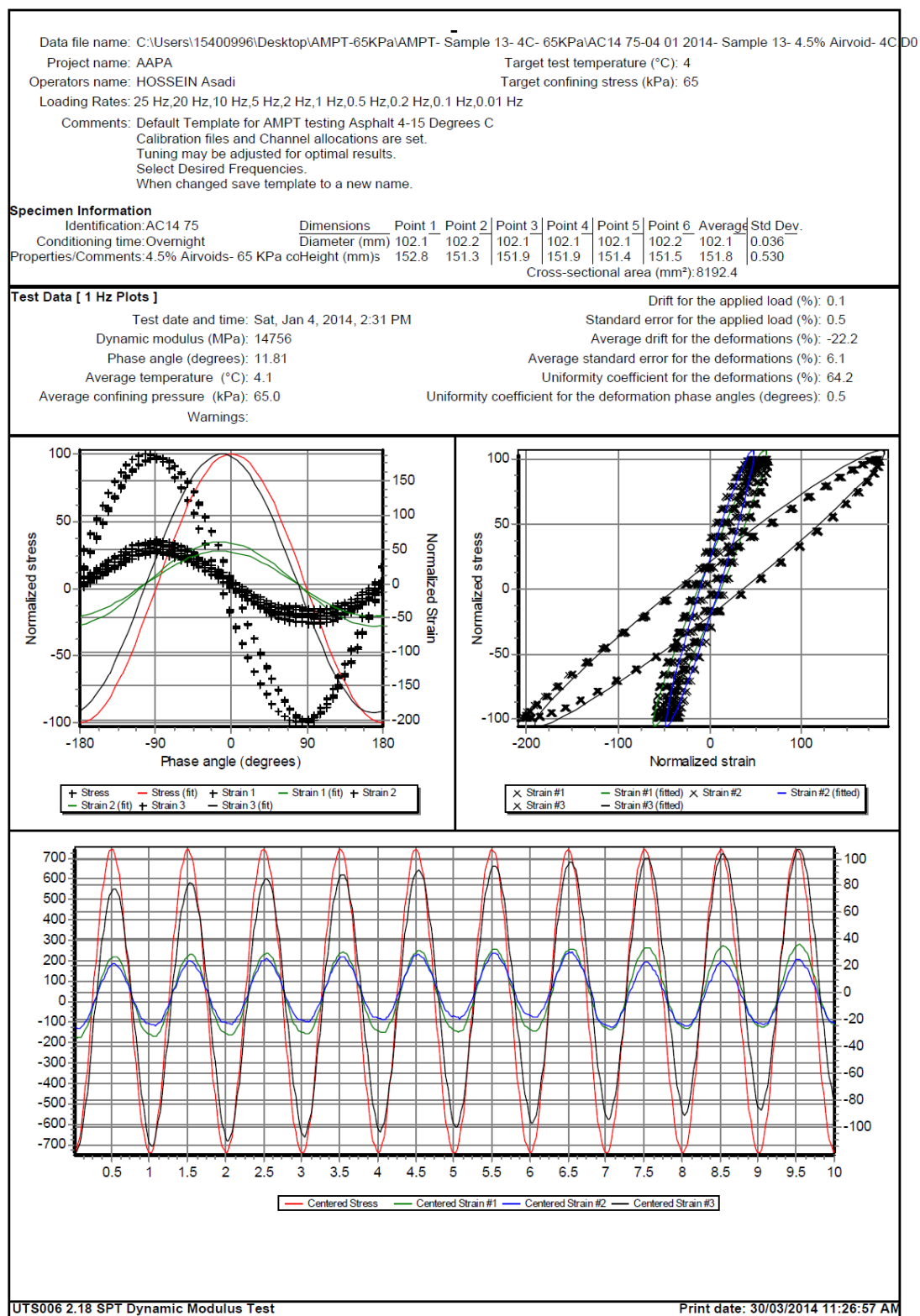


Figure E - 106. UTS6 output for sample9, 1 Hz and 4°C

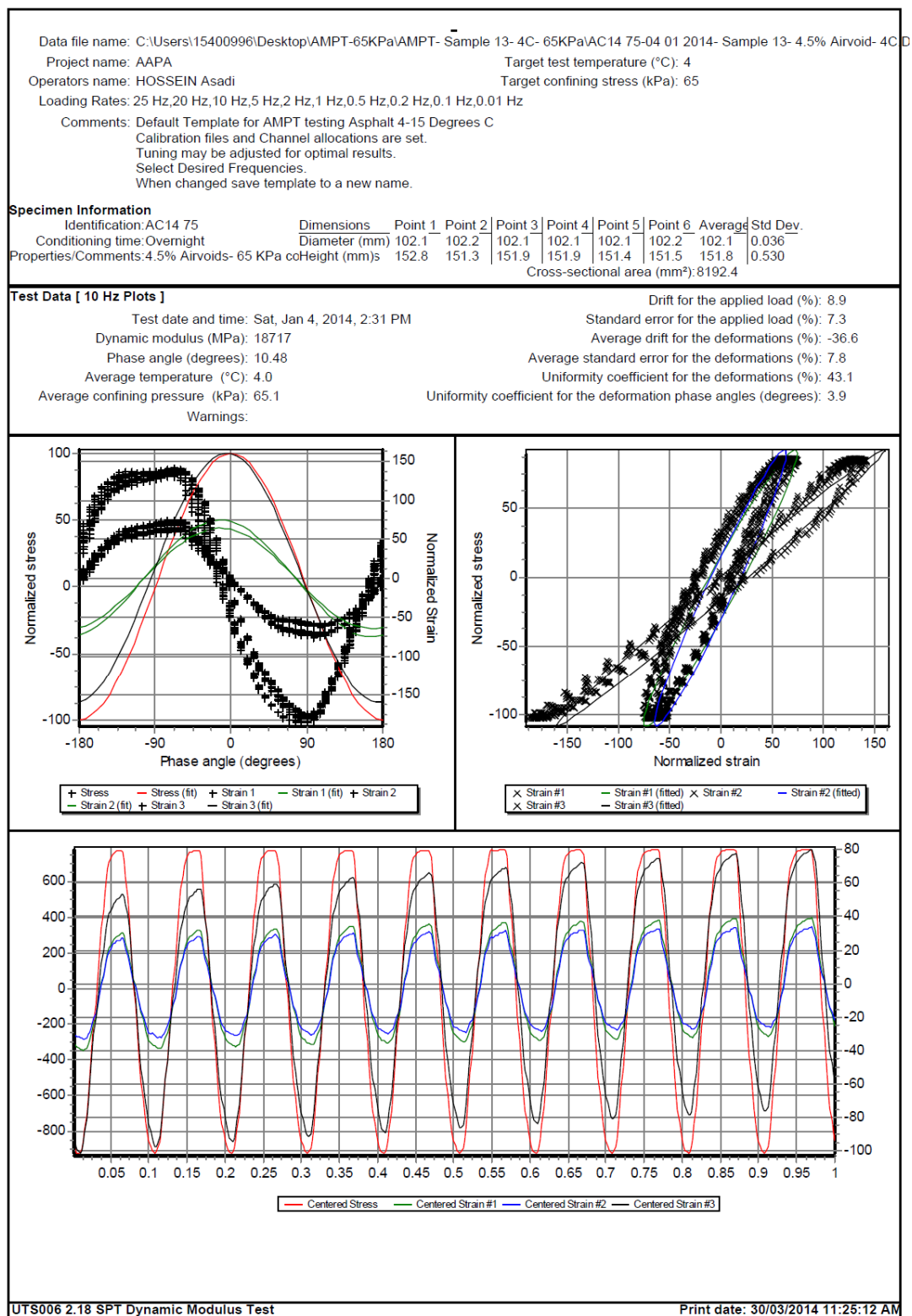


Figure E - 107. UTS6 output for sample9, 10 Hz and 4°C

Data file name: C:\Users\15400996\Desktop\AMPT-65KPa\AMPT- Sample 13- 4C- 65KPa\AC14 75-04 01 2014- Sample 13- 4.5% Airvoid- 4C											
Project name: AAPA				Target test temperature (°C): 4							
Operators name: HOSSEIN Asadi				Target confining stress (kPa): 65							
Loading Rates: 25 Hz,20 Hz,10 Hz,5 Hz,2 Hz,1 Hz,0.5 Hz,0.2 Hz,0.1 Hz,0.01 Hz											
Comments: Default Template for AMPT testing Asphalt 4-15 Degrees C											
Calibration files and Channel allocations are set.											
Tuning may be adjusted for optimal results.											
Select Desired Frequencies.											
When changed save template to a new name.											
Specimen Information											
Identification:AC14 75		Dimensions		Point 1	Point 2	Point 3	Point 4	Point 5	Point 6	Average	Std Dev.
Conditioning time:Overnight		Diameter (mm)		102.1	102.2	102.1	102.1	102.1	102.2	102.1	0.036
Properties/Comments:4.5% Airvoids- 65 KPa co		Height (mm)s		152.8	151.3	151.9	151.9	151.4	151.5	151.8	0.530
				Cross-sectional area (mm²):8192.4							
Tabulated Results Summary											
	25 Hz	20 Hz	10 Hz	5 Hz	2 Hz	1 Hz	0.5 Hz	0.2 Hz	0.1 Hz	0.01 Hz	
Dynamic modulus (MPa)	20685	19903	18717	17505	16034	14756	13543	11920	10716	7134	
Phase angle (Degrees)	10.47	10.56	10.48	11.01	10.90	11.81	12.63	14.03	14.68	20.10	
Average temperature (°C)	4.0	4.0	4.0	4.0	4.1	4.1	4.2	4.1	4.1	4.1	
Average confining pressure (kPa)	64.9	64.9	65.1	65.1	65.0	65.0	65.0	65.0	65.0	65.0	
Average micro-strain	85	90	97	104	100	101	101	101	101	101	
Load drift (%)	9.3	9.2	8.9	9.6	-0.1	0.1	0.0	0.0	0.0	0.0	
Load standard error (%)	10.6	8.4	7.3	9.7	0.7	0.5	0.1	0.2	0.3	0.5	
Average deformation drift (%)	-45.1	-35.6	-36.6	-41.8	-26.8	-22.2	-36.4	-46.4	-50.9	-115.5	
Average deformation standard error (%)	12.0	8.9	7.8	9.3	4.6	6.1	3.5	3.1	5.0	2.8	
Deformation uniformity (%)	42.7	42.2	43.1	45.8	64.3	64.2	65.3	64.0	63.9	62.3	
Phase uniformity (Degrees)	4.7	4.7	3.9	3.3	0.6	0.5	0.3	0.3	0.4	0.8	
</											

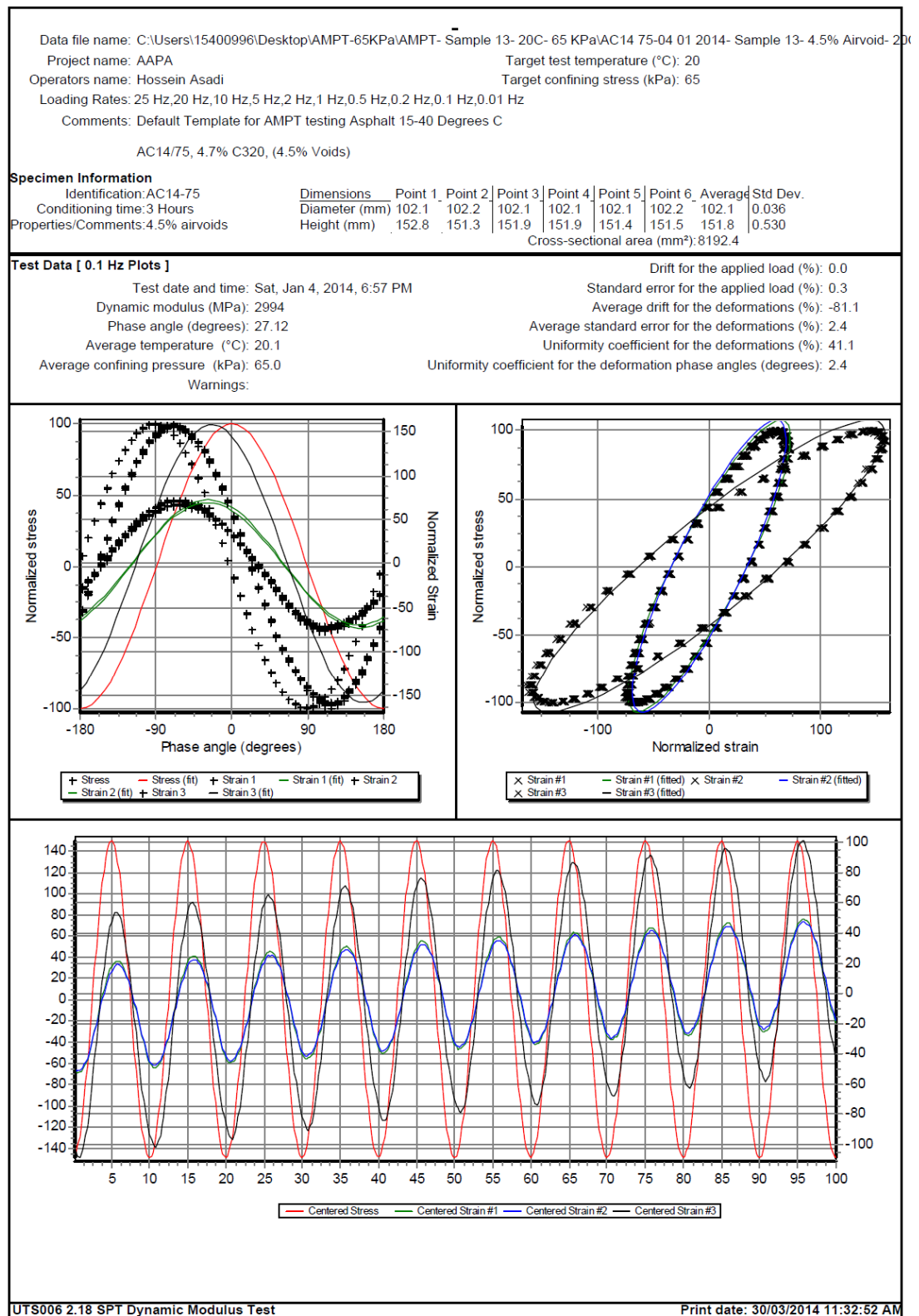


Figure E - 109. UTS6 output for sample9, 0.1 Hz and 20°C

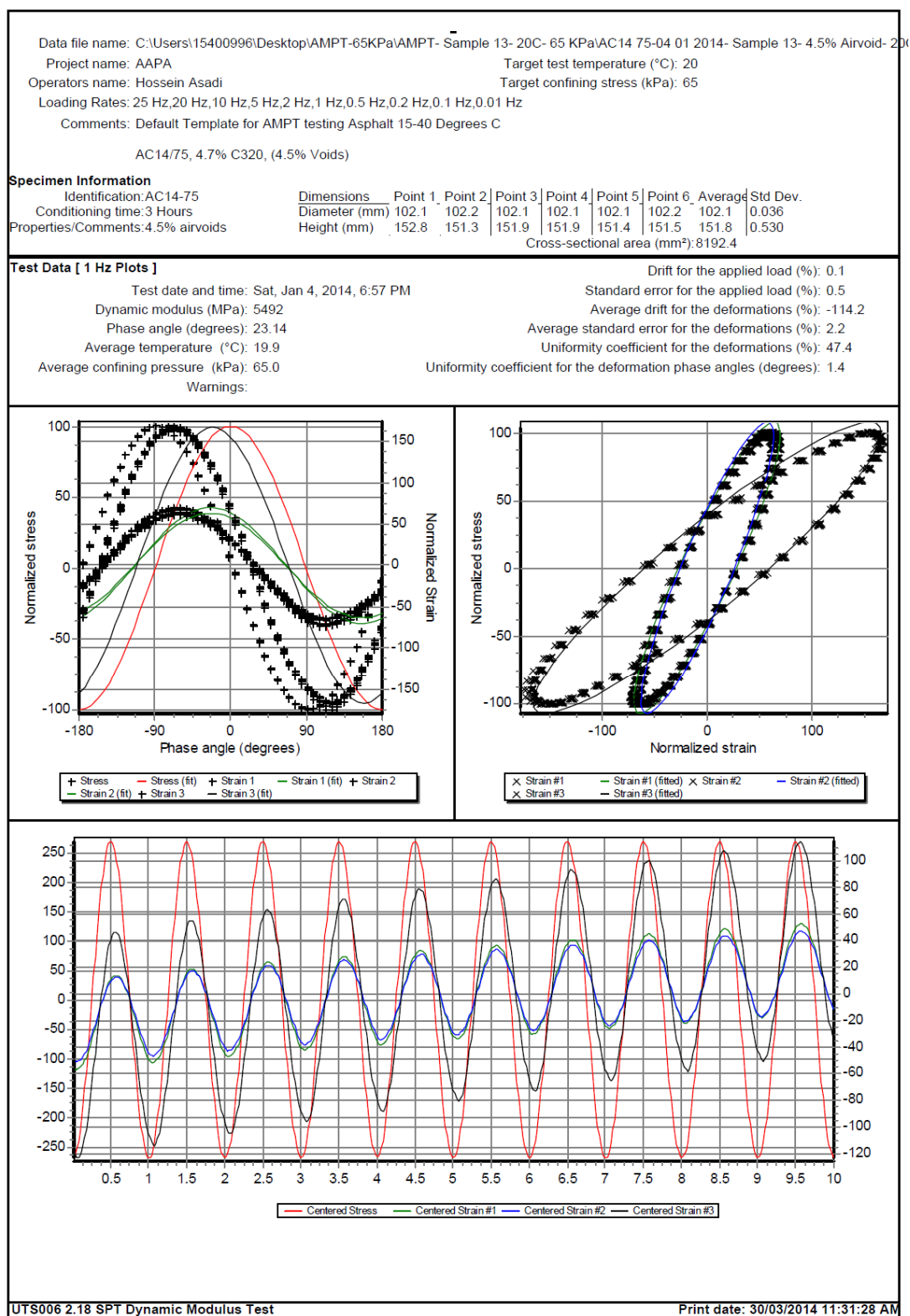


Figure E - 110. UTS6 output for sample9, 1 Hz and 20°C

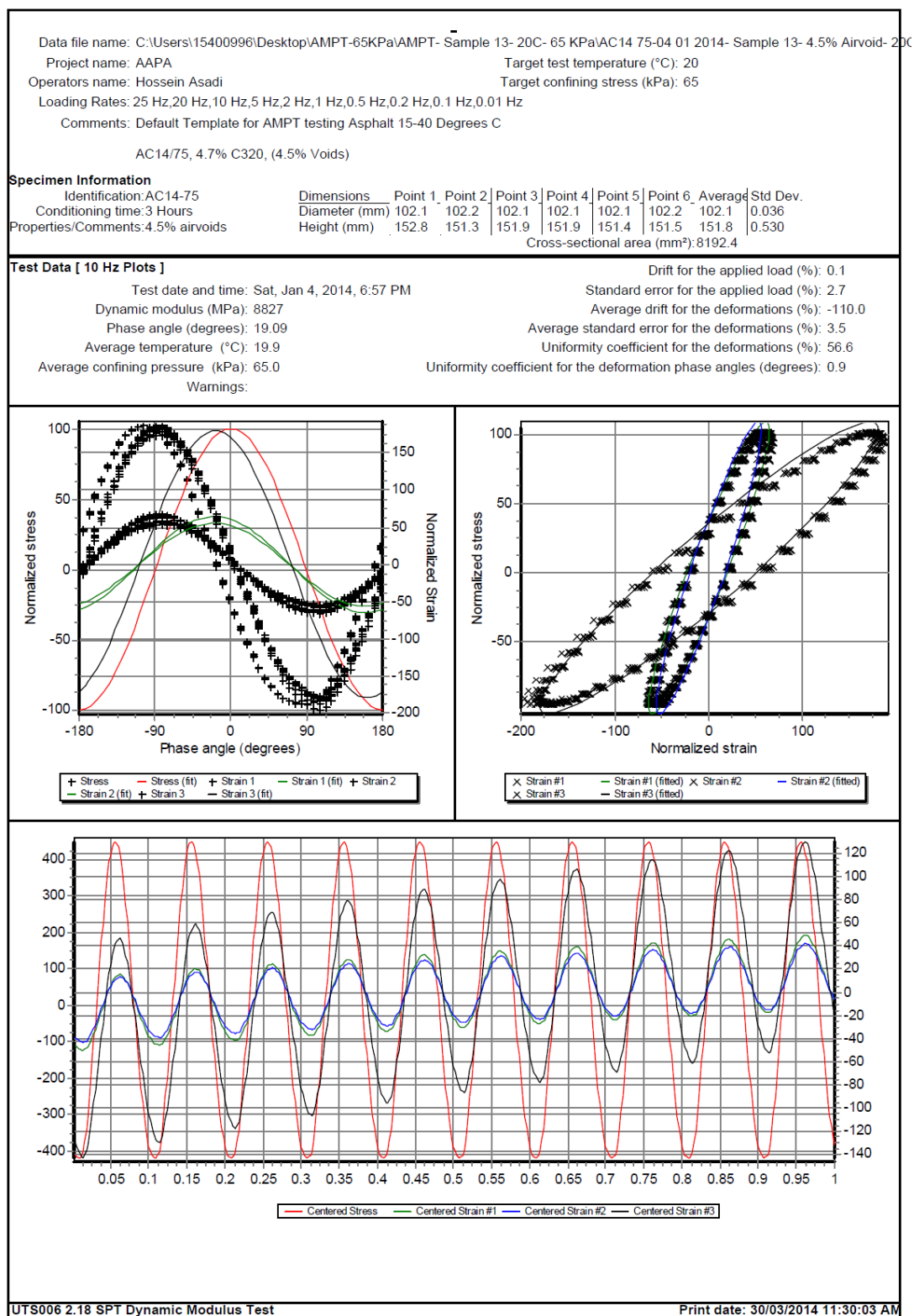


Figure E - 111. UTS6 output for sample9, 10 Hz and 20°C

Data file name: C:\Users\15400996\Desktop\AMPT-65KPa\AMPT- Sample 13- 20C- 65 KPa\AC14 75-04 01 2014- Sample 13- 4.5% Airvoid- 20											
Project name: AAPA						Target test temperature (°C): 20					
Operators name: Hossein Asadi						Target confining stress (kPa): 65					
Loading Rates: 25 Hz,20 Hz,10 Hz,5 Hz,2 Hz,1 Hz,0.5 Hz,0.2 Hz,0.1 Hz,0.01 Hz											
Comments: Default Template for AMPT testing Asphalt 15-40 Degrees C											
AC14/75, 4.7% C320, (4.5% Voids)											
Specimen Information											
Identification:AC14-75			Dimensions	Point 1	Point 2	Point 3	Point 4	Point 5	Point 6	Average	Std Dev.
Conditioning time:3 Hours			Diameter (mm)	102.1	102.2	102.1	102.1	102.1	102.2	102.1	0.036
Properties/Comments:4.5% airvoids			Height (mm)	152.8	151.3	151.9	151.9	151.4	151.5	151.8	0.530
Cross-sectional area (mm²):8192.4											
Tabulated Results Summary											
	25 Hz	20 Hz	10 Hz	5 Hz	2 Hz	1 Hz	0.5 Hz	0.2 Hz	0.1 Hz	0.01 Hz	
Dynamic modulus (MPa)	10351	9997	8827	7723	6399	5492	4664	3663	2994	1368	
Phase angle (Degrees)	18.78	18.99	19.09	20.27	21.98	23.14	24.32	26.01	27.12	30.31	
Average temperature (°C)	19.9	19.9	19.9	19.8	19.8	19.9	20.0	20.2	20.1	20.1	
Average confining pressure (kPa)	65.0	65.1	65.0	65.0	65.0	65.0	65.0	65.0	65.0	65.0	
Average micro-strain	100	97	99	99	98	98	98	99	100	108	
Load drift (%)	0.3	-0.6	0.1	0.1	0.2	0.1	-0.1	0.0	0.0	0.0	
Load standard error (%)	6.2	5.5	2.7	1.4	0.7	0.5	0.2	0.3	0.3	0.6	
Average deformation drift (%)	-111.0	-99.6	-110.0	-115.4	-120.4	-114.2	-106.2	-95.8	-81.1	-54.6	
Average deformation standard error (%)	7.4	6.2	3.5	2.5	2.2	2.2	2.2	2.6	2.4	2.5	
Deformation uniformity (%)	59.2	58.5	56.6	54.6	50.9	47.4	46.1	43.9	41.1	39.3	
Phase uniformity (Degrees)	2.7	2.6	0.9	0.9	1.2	1.4	1.7	2.1	2.4	3.8	

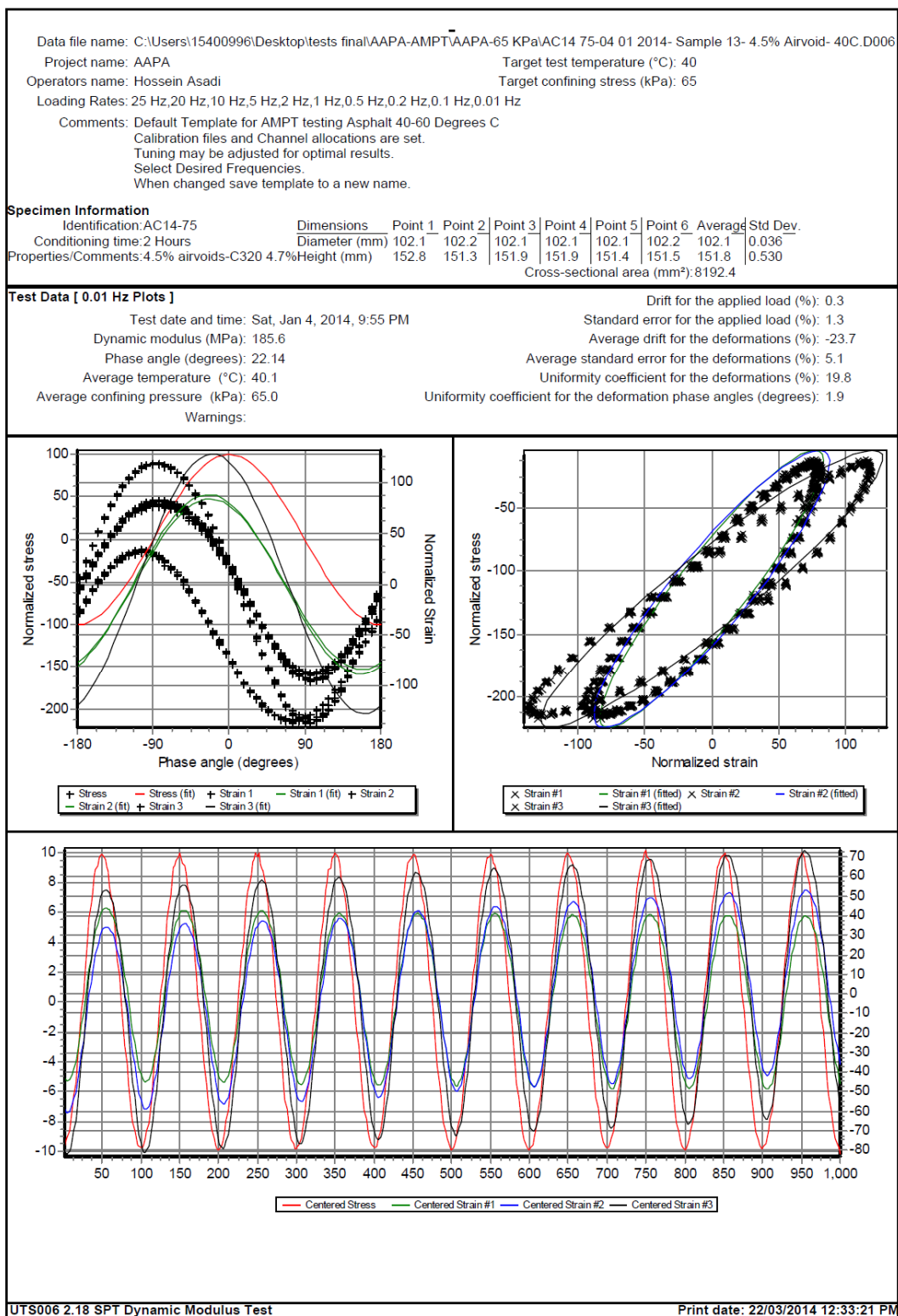


Figure E - 113. UTS6 output for sample9, 0.01 Hz and 40°C

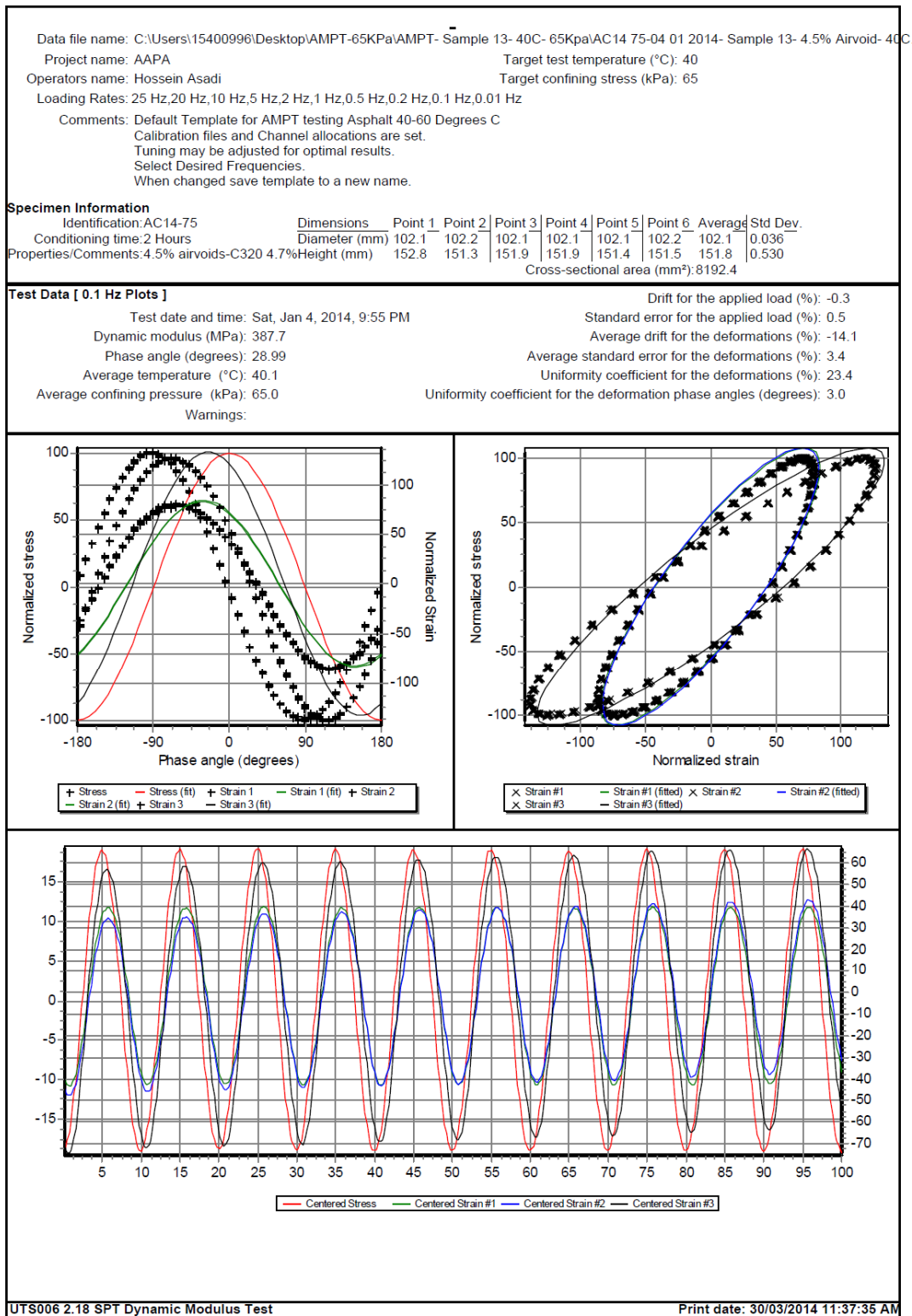


Figure E - 114. UTS6 output for sample9, 0.1 Hz and 40°C

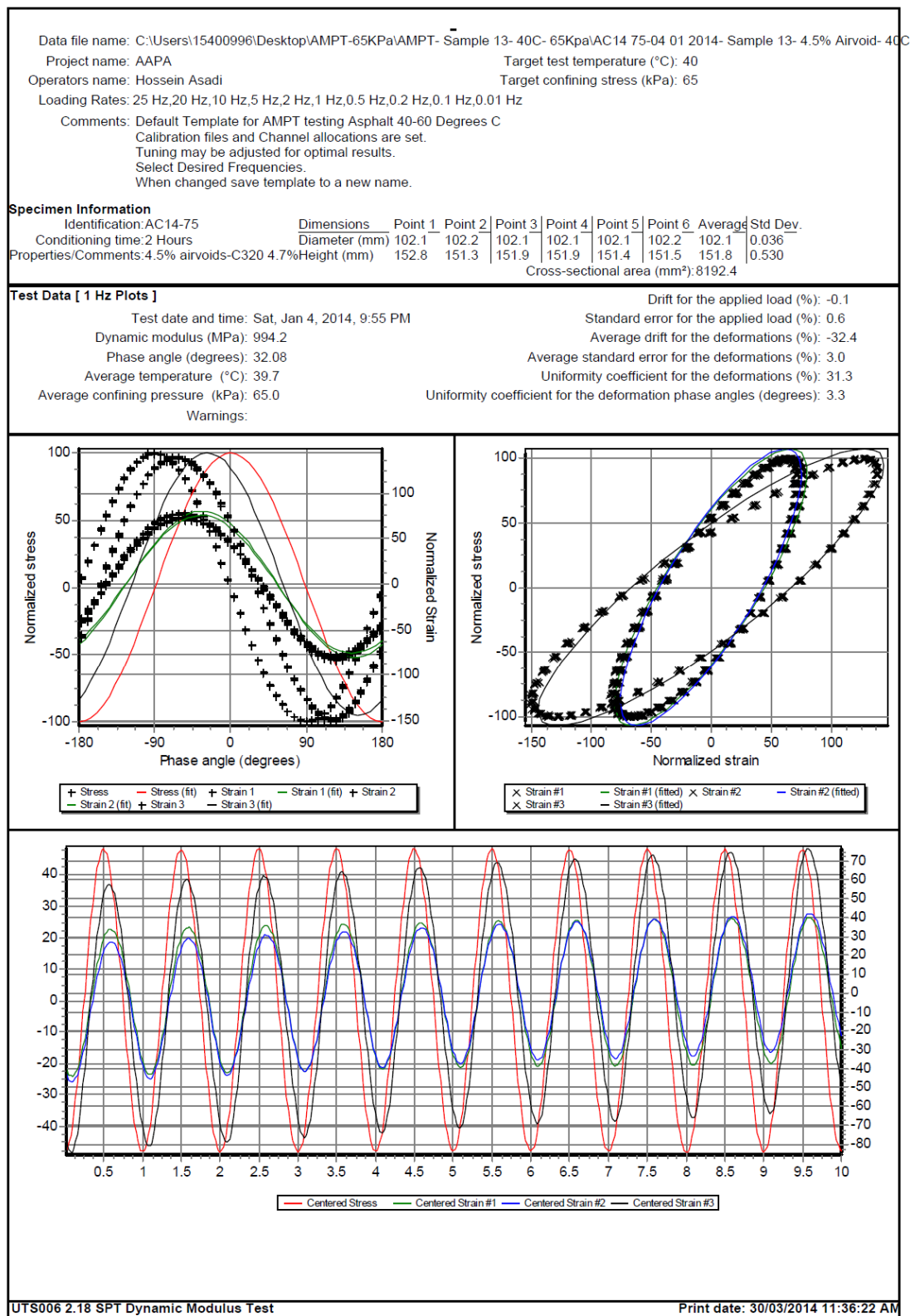


Figure E - 115. UTS6 output for sample9, 1 Hz and 40°C

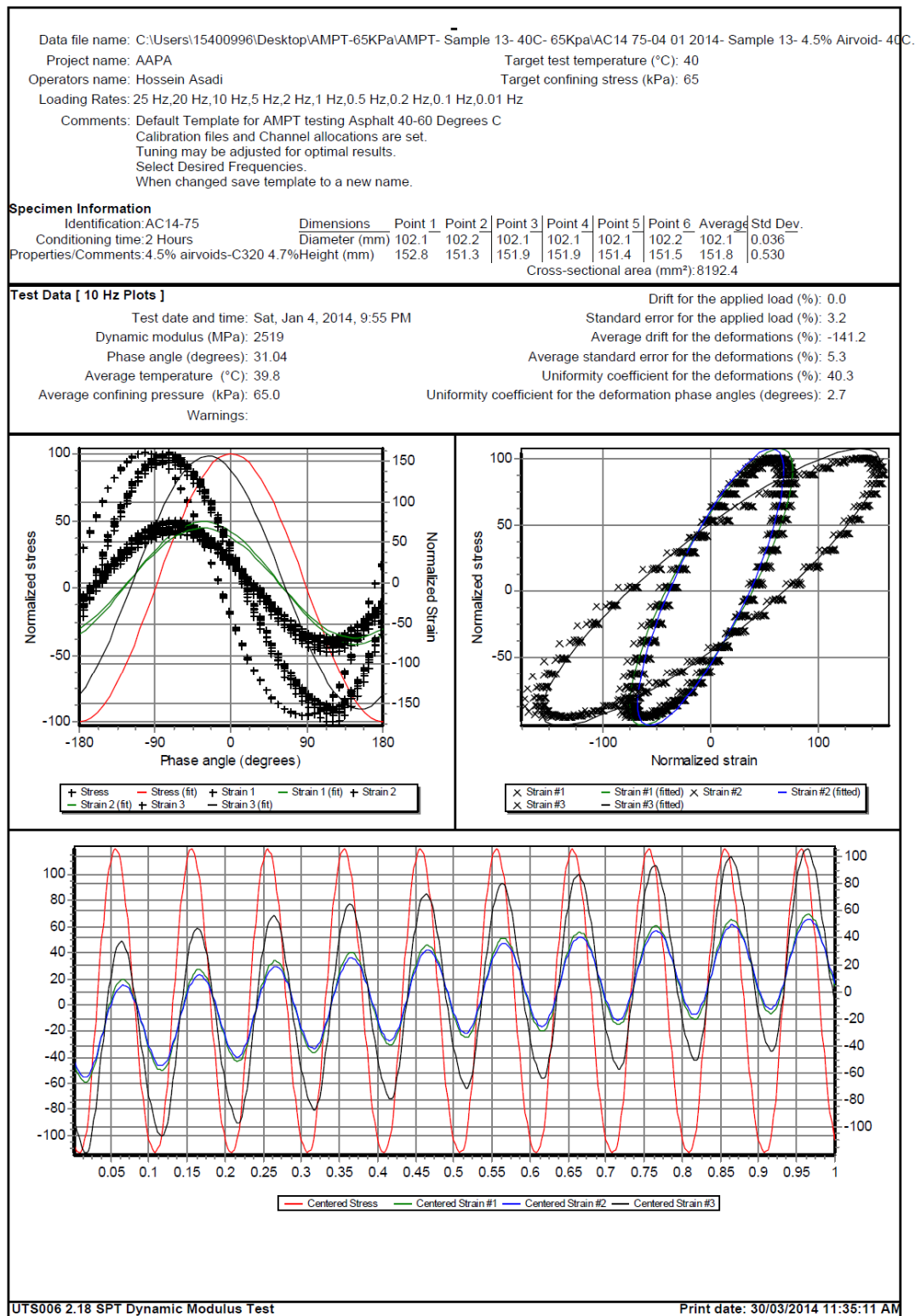


Figure E - 116. UTS6 output for sample9, 10 Hz and 40°C

Data file name: C:\Users\15400996\Desktop\AMPT-65KPa\AMPT- Sample 13- 40C- 65Kpa\AC14 75-04 01 2014- Sample 13- 4.5% Airvoid- 40C											
Project name: AAPA					Target test temperature (°C): 40						
Operators name: Hossein Asadi					Target confining stress (kPa): 65						
Loading Rates: 25 Hz,20 Hz,10 Hz,5 Hz,2 Hz,1 Hz,0.5 Hz,0.2 Hz,0.1 Hz,0.01 Hz											
Comments: Default Template for AMPT testing Asphalt 40-60 Degrees C											
Calibration files and Channel allocations are set.											
Tuning may be adjusted for optimal results.											
Select Desired Frequencies.											
When changed save template to a new name.											
Specimen Information											
Identification:AC14-75		Dimensions		Point 1	Point 2	Point 3	Point 4	Point 5	Point 6	Average	Std Dev.
Conditioning time:2 Hours		Diameter (mm)		102.1	102.2	102.1	102.1	102.1	102.2	102.1	0.036
Properties/Comments:4.5% airvoids-C320 4.7%		Height (mm)		152.8	151.3	151.9	151.9	151.4	151.5	151.8	0.530
Cross-sectional area (mm²): 8192.4											
Tabulated Results Summary											
	25 Hz	20 Hz	10 Hz	5 Hz	2 Hz	1 Hz	0.5 Hz	0.2 Hz	0.1 Hz	0.01 Hz	
Dynamic modulus (MPa)	3358	3175	2519	1944	1340	994.2	739.2	509.9	387.7	185.6	
Phase angle (Degrees)	31.52	30.55	31.04	31.61	32.12	32.08	31.61	30.33	28.99	22.14	
Average temperature (°C)	39.8	39.8	39.8	39.7	39.7	39.7	39.8	40.2	40.1	40.1	
Average confining pressure (kPa)	65.0	65.0	65.0	65.0	65.0	65.0	65.0	65.0	65.0	65.0	
Average micro-strain	94	94	94	94	96	97	98	101	99	106	
Load drift (%)	-1.2	-1.2	0.0	0.1	-0.2	-0.1	0.0	0.0	-0.3	0.3	
Load standard error (%)	5.0	4.7	3.2	2.1	1.3	0.6	0.4	0.4	0.5	1.3	
Average deformation drift (%)	-318.7	-203.1	-141.2	-91.4	-48.3	-32.4	-23.5	-18.5	-14.1	-23.7	
Average deformation standard error (%)	10.3	7.1	5.3	3.9	3.1	3.0	2.9	3.1	3.4	5.1	
Deformation uniformity (%)	49.7	43.6	40.3	37.6	34.5	31.3	28.5	25.4	23.4	19.8	
Phase uniformity (Degrees)	3.0	2.7	2.7	2.7	2.9	3.3	3.3	3.3	3.0	1.9	

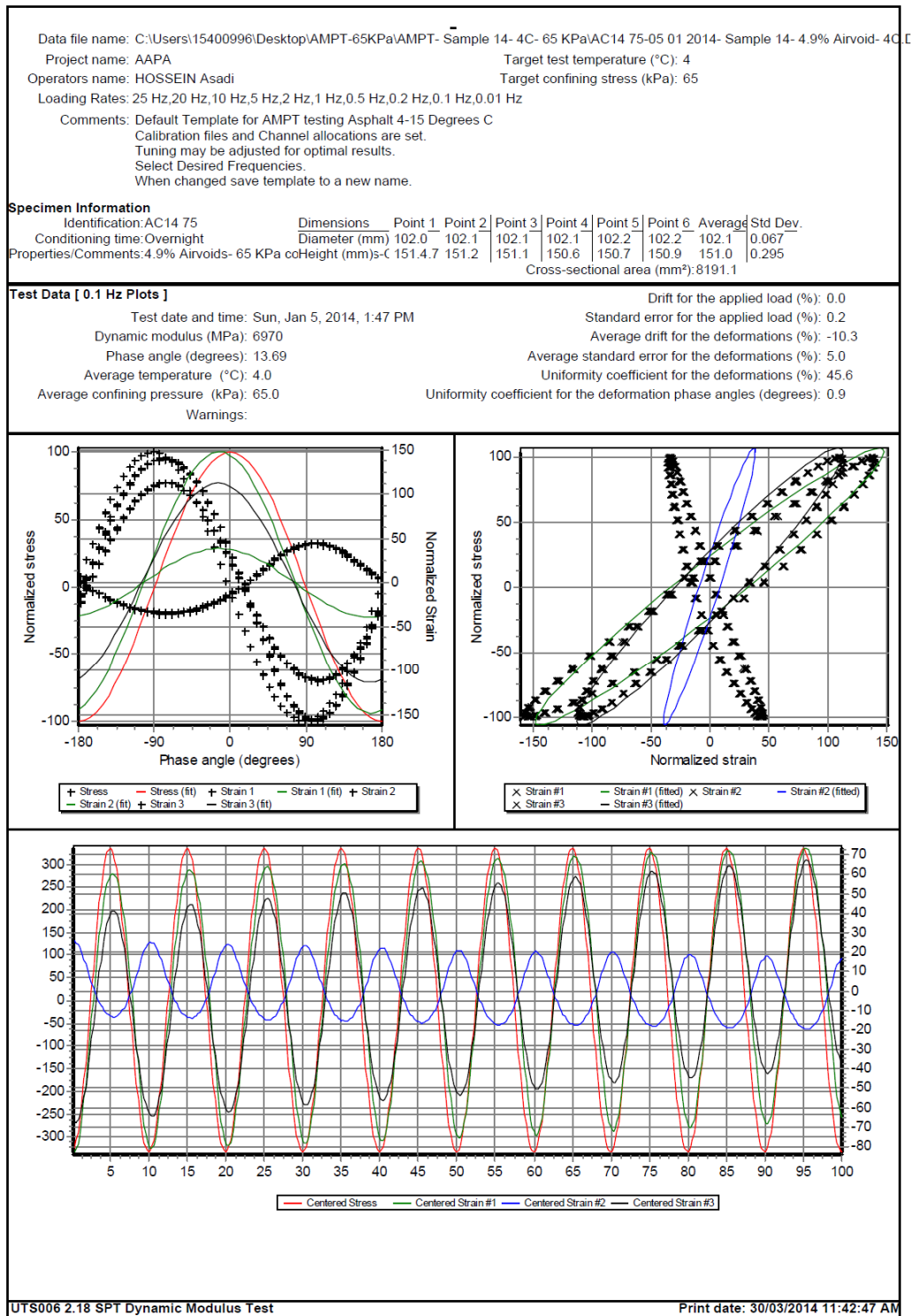


Figure E - 118. UTS6 output for sample10, 0.1 Hz and 4°C

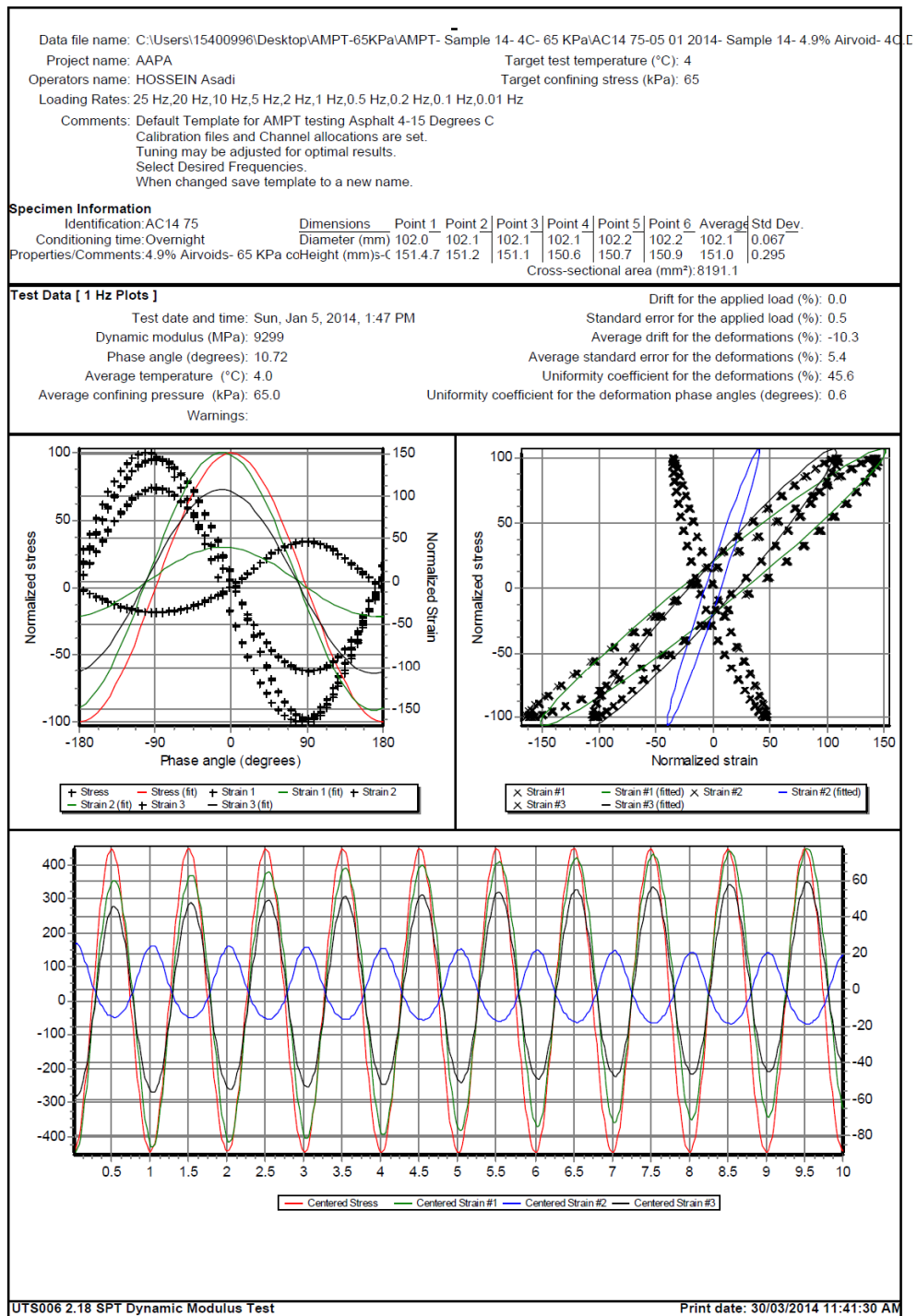


Figure E - 119. UTS6 output for sample10, 1 Hz and 4°C

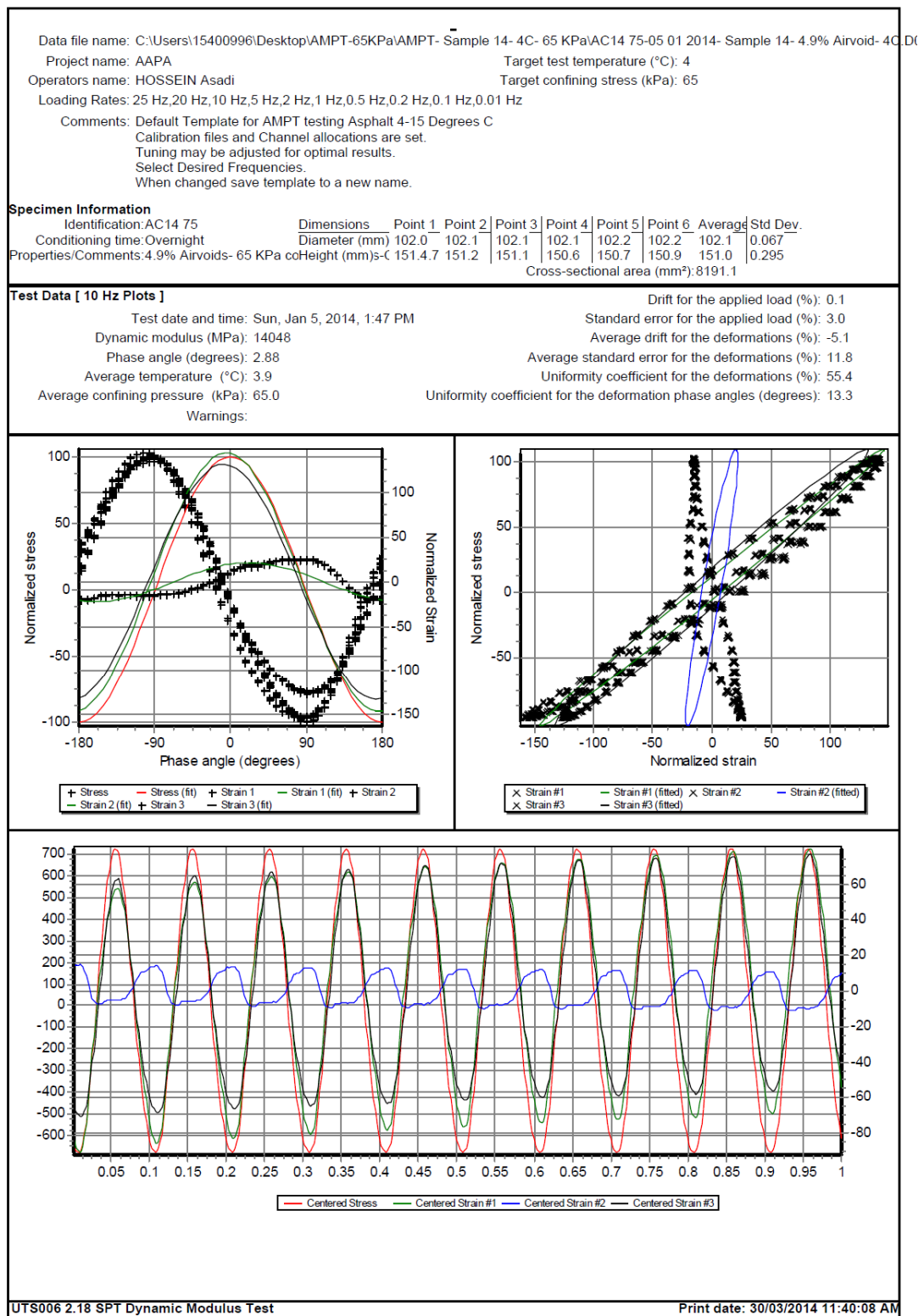


Figure E - 120. UTS6 output for sample10, 10 Hz and 4°C

Project name: AAPA Target test temperature (°C): 4
Operators name: HOSSEIN Asadi Target confining stress (kPa): 65
Loading Rates: 25 Hz, 20 Hz, 10 Hz, 5 Hz, 2 Hz, 1 Hz, 0.5 Hz, 0.2 Hz, 0.1 Hz, 0.01 Hz

Comments: Default Template for AMPT testing Asphalt 4-15 Degrees C
Calibration files and Channel allocations are set.
Tuning may be adjusted for optimal results.
Select Desired Frequencies.
When changed save template to a new name.

Identification: AC14 75	Dimensions	Point 1	Point 2	Point 3	Point 4	Point 5	Point 6	Average	Std Dev.
Conditioning time: Overnight	Diameter (mm)	102.0	102.1	102.1	102.1	102.2	102.2	102.1	0.067
Properties/Comments: 4.9% Airvoids- 65 KPa coHeight (mm)-c		151.4	151.2	151.1	150.6	150.7	150.9	151.0	0.295
Cross-sectional area (mm²): 8191.1									

	25 Hz	20 Hz	10 Hz	5 Hz	2 Hz	1 Hz	0.5 Hz	0.2 Hz	0.1 Hz	0.01 Hz
Dynamic modulus (MPa)	16498	17119	14048	12464	10127	9299	8569	7692	6970	4807
Phase angle (Degrees)	2.08	9.39	2.88	1.46	9.67	10.72	11.66	12.28	13.69	18.06
Average temperature (°C)	3.9	3.9	3.9	3.9	4.0	4.0	4.1	4.1	4.0	4.1
Average confining pressure (kPa)	65.0	65.0	65.0	65.0	65.0	65.0	65.0	65.0	65.0	65.0
Average micro-strain	66	91	100	98	100	96	96	96	96	98
Load drift (%)	-1.6	-0.2	0.1	0.2	0.0	0.0	0.0	0.0	0.0	0.0
Load standard error (%)	6.6	5.4	3.0	1.7	0.8	0.5	0.2	0.2	0.2	0.5
Average deformation drift (%)	-34.7	-19.8	-5.1	-4.3	-6.2	-10.3	-13.2	2.5	-10.3	-42.9
Average deformation standard error (%)	10.6	14.3	11.8	9.5	5.9	5.4	5.2	5.5	5.0	5.7
Deformation uniformity (%)	51.4	57.7	55.4	51.9	45.9	45.6	45.6	44.9	45.6	47.0
Phase uniformity (Degrees)	9.7	18.4	13.3	8.8	0.9	0.6	0.6	1.3	0.9	1.0

Print date: 30/03/2014 11:40:08 AM

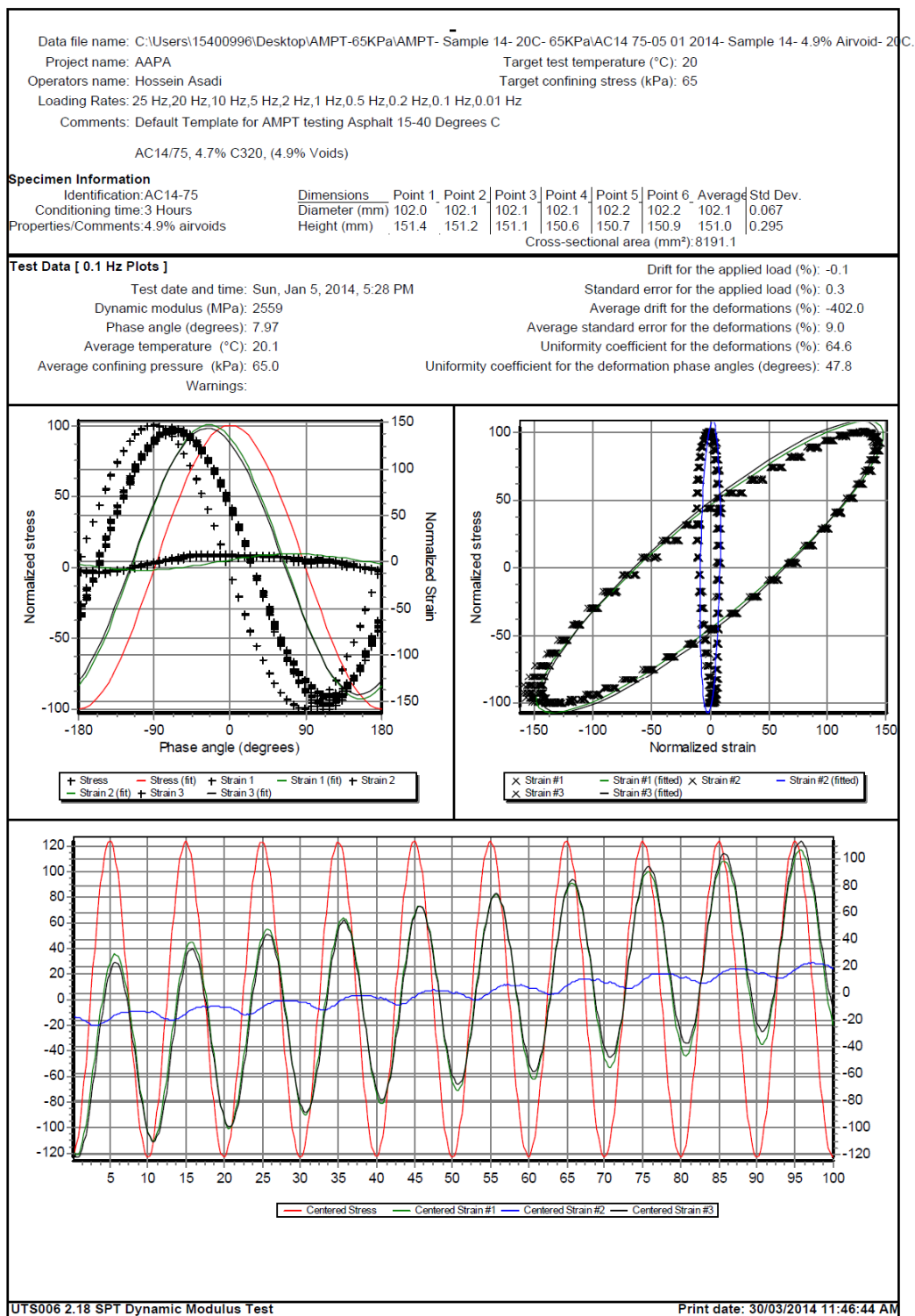


Figure E - 122. UTS6 output for sample10, 0.1 Hz and 20°C

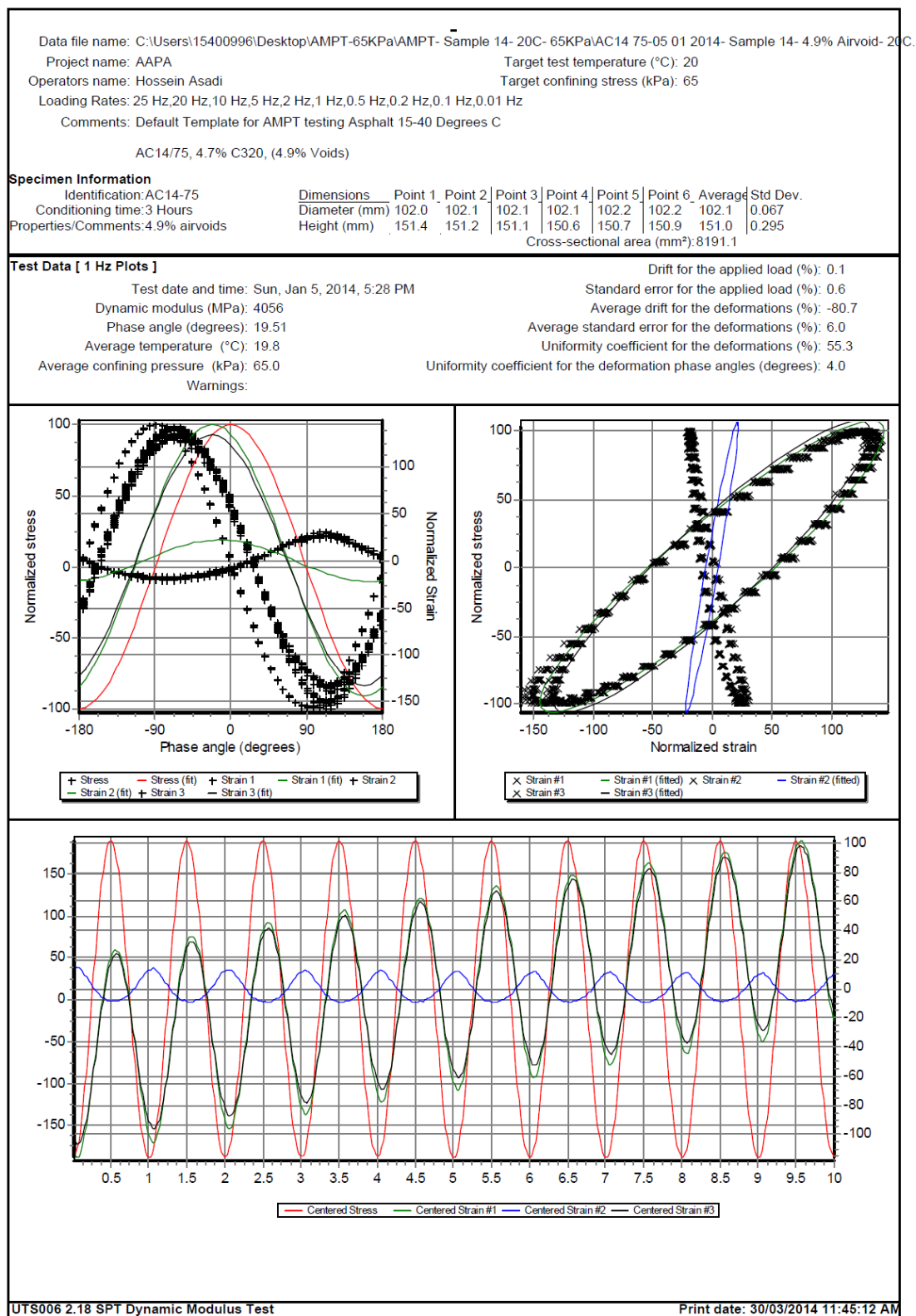


Figure E - 123. UTS6 output for sample10, 1 Hz and 20°C

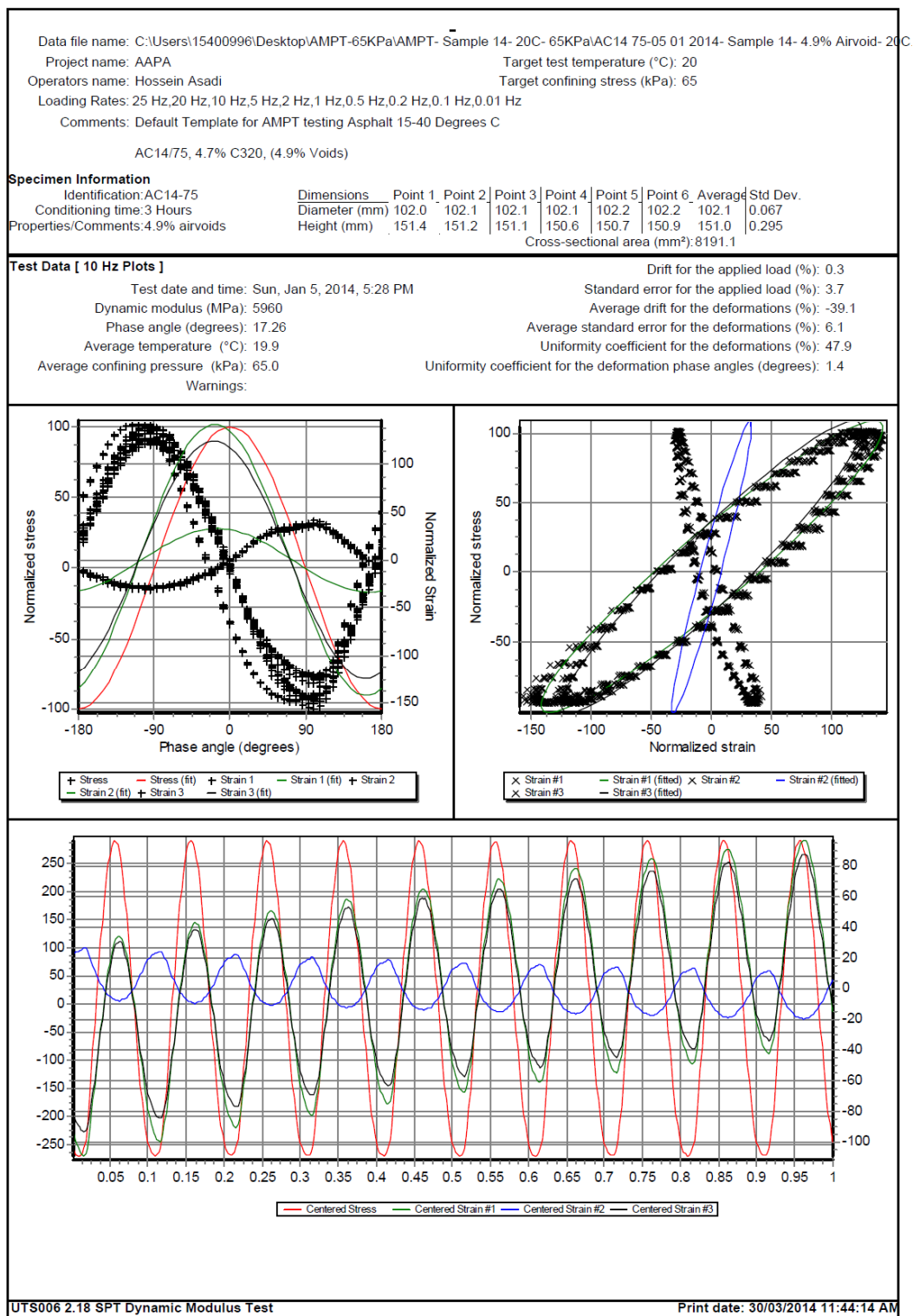


Figure E - 124. UTS6 output for sample10, 10 Hz and 20°C

Data file name: C:\Users\15400996\Desktop\AMPT-65KPa\AMPT- Sample 14- 20C- 65KPa\AC14 75-05 01 2014- Sample 14- 4.9% Airvoid- 20C											
Project name: AAPA					Target test temperature (°C): 20						
Operators name: Hossein Asadi					Target confining stress (kPa): 65						
Loading Rates: 25 Hz,20 Hz,10 Hz,5 Hz,2 Hz,1 Hz,0.5 Hz,0.2 Hz,0.1 Hz,0.01 Hz											
Comments: Default Template for AMPT testing Asphalt 15-40 Degrees C											
AC14/75, 4.7% C320, (4.9% Voids)											
Specimen Information											
Identification:AC14-75		Dimensions		Point 1	Point 2	Point 3	Point 4	Point 5	Point 6	Average	Std Dev.
Conditioning time:3 Hours		Diameter (mm)		102.0	102.1	102.1	102.1	102.2	102.2	102.1	0.067
Properties/Comments:4.9% airvoids		Height (mm)		151.4	151.2	151.1	150.6	150.7	150.9	151.0	0.295
Cross-sectional area (mm²): 8191.1											
Tabulated Results Summary											
	25 Hz	20 Hz	10 Hz	5 Hz	2 Hz	1 Hz	0.5 Hz	0.2 Hz	0.1 Hz	0.01 Hz	
Dynamic modulus (MPa)	6895	6771	5960	5336	4551	4056	3617	3003	2559	1207	
Phase angle (Degrees)	11.84	13.63	17.26	18.37	19.41	19.51	17.92	9.95	7.97	43.18	
Average temperature (°C)	19.9	19.9	19.9	19.9	19.8	19.8	19.9	20.2	20.1	20.1	
Average confining pressure (kPa)	65.0	65.0	65.0	65.0	65.0	65.0	65.0	65.0	65.0	65.0	
Average micro-strain	82	94	96	94	94	93	93	94	96	102	
Load drift (%)	-0.2	-0.9	0.3	0.2	0.1	0.1	-0.1	0.0	-0.1	-0.1	
Load standard error (%)	6.5	5.5	3.7	2.0	1.0	0.6	0.2	0.2	0.3	0.6	
Average deformation drift (%)	-34.3	-32.8	-39.1	-46.4	-57.9	-80.7	-129.7	-280.2	-402.0	-278.6	
Average deformation standard error (%)	6.9	6.5	6.1	5.9	5.8	6.0	11.5	9.6	9.0	7.3	
Deformation uniformity (%)	45.3	47.9	47.9	49.6	52.1	55.3	59.8	64.0	64.6	58.6	
Phase uniformity (Degrees)	4.1	3.7	1.4	1.6	2.5	4.0	7.8	21.2	47.8	21.2	

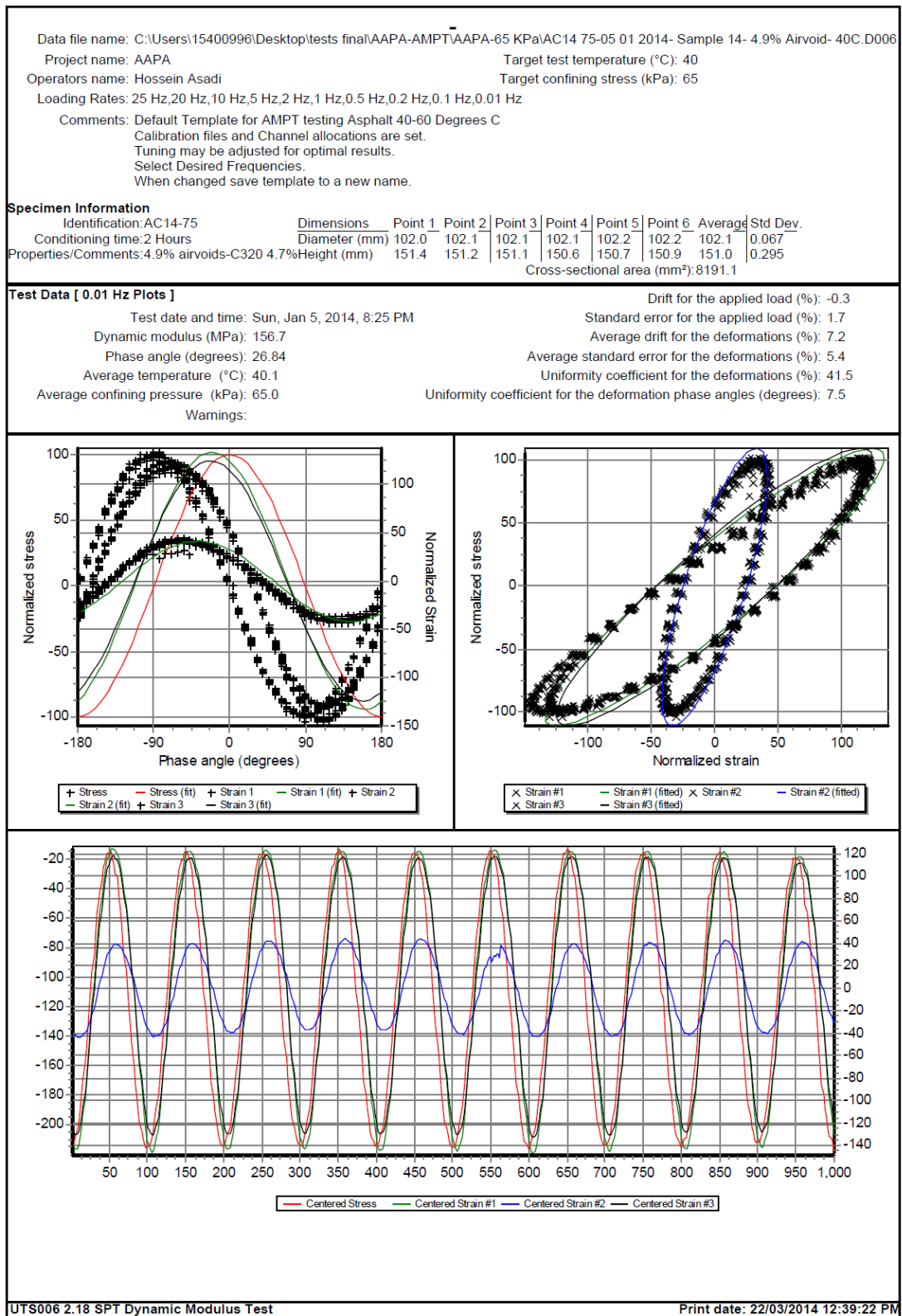


Figure E - 126. UTS6 output for sample10, 0.01 Hz and 40°C

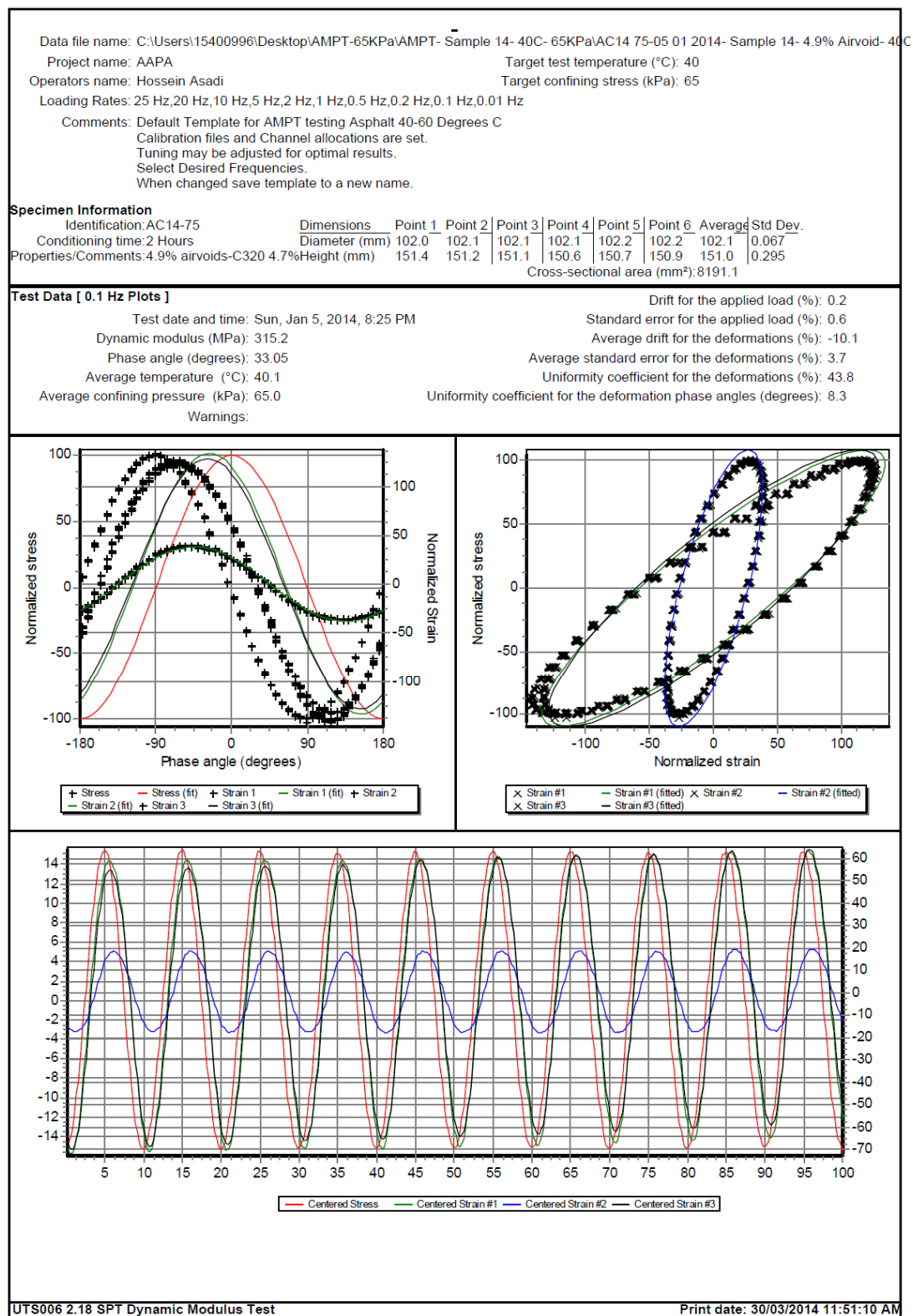


Figure E - 127. UTS6 output for sample10, 0.1 Hz and 40°C

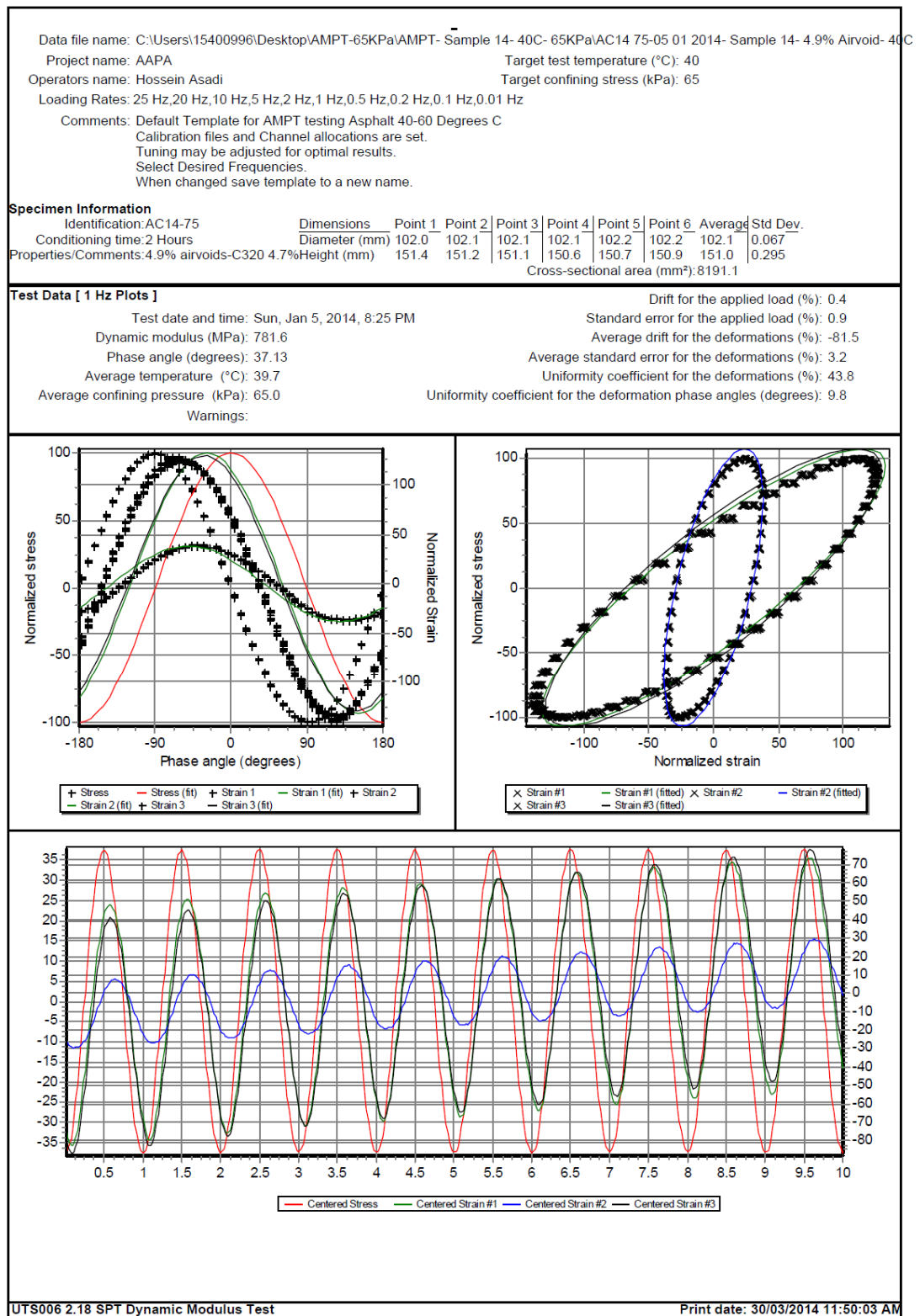
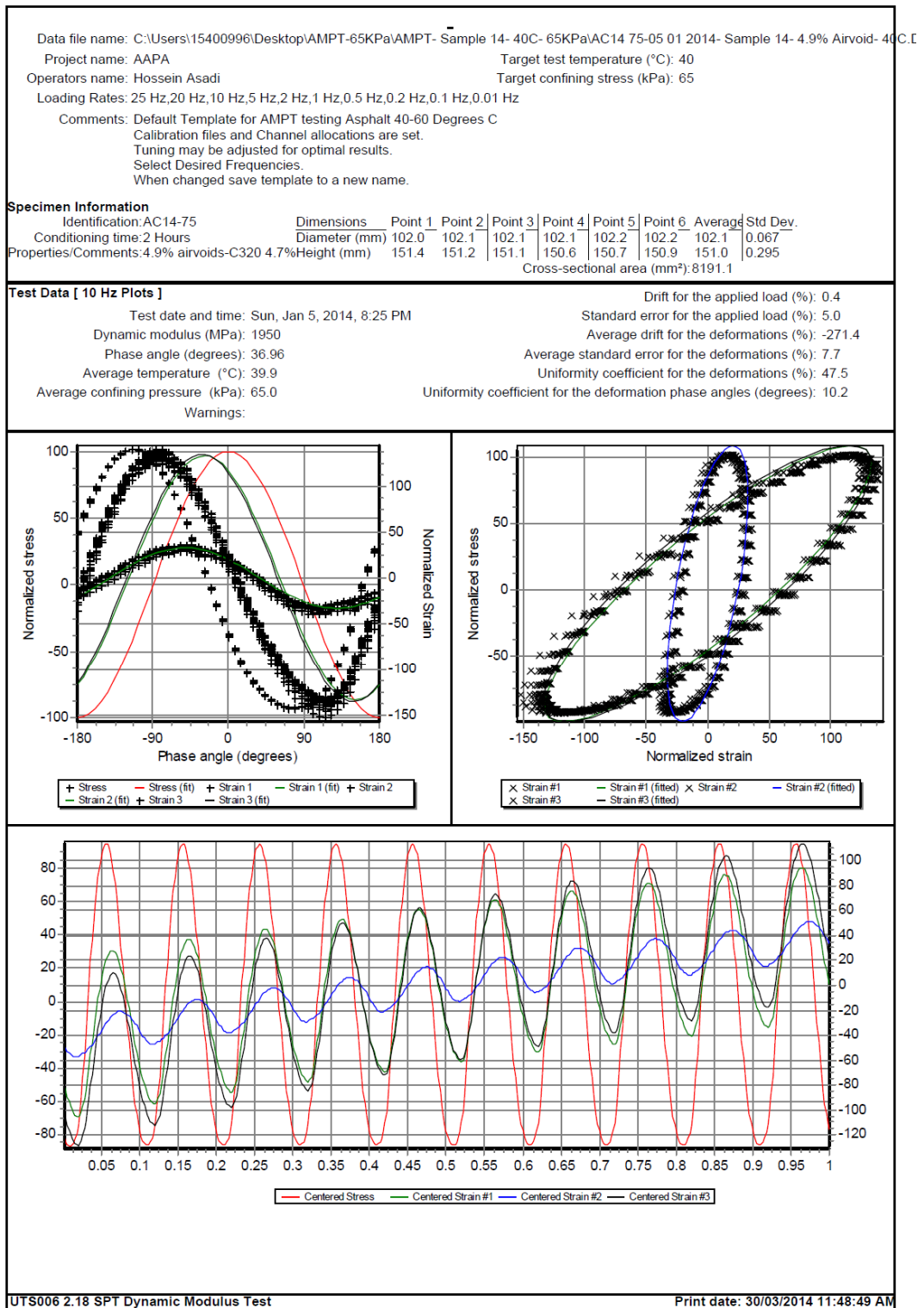


Figure E - 128. UTS6 output for sample10, 1 Hz and 40°C



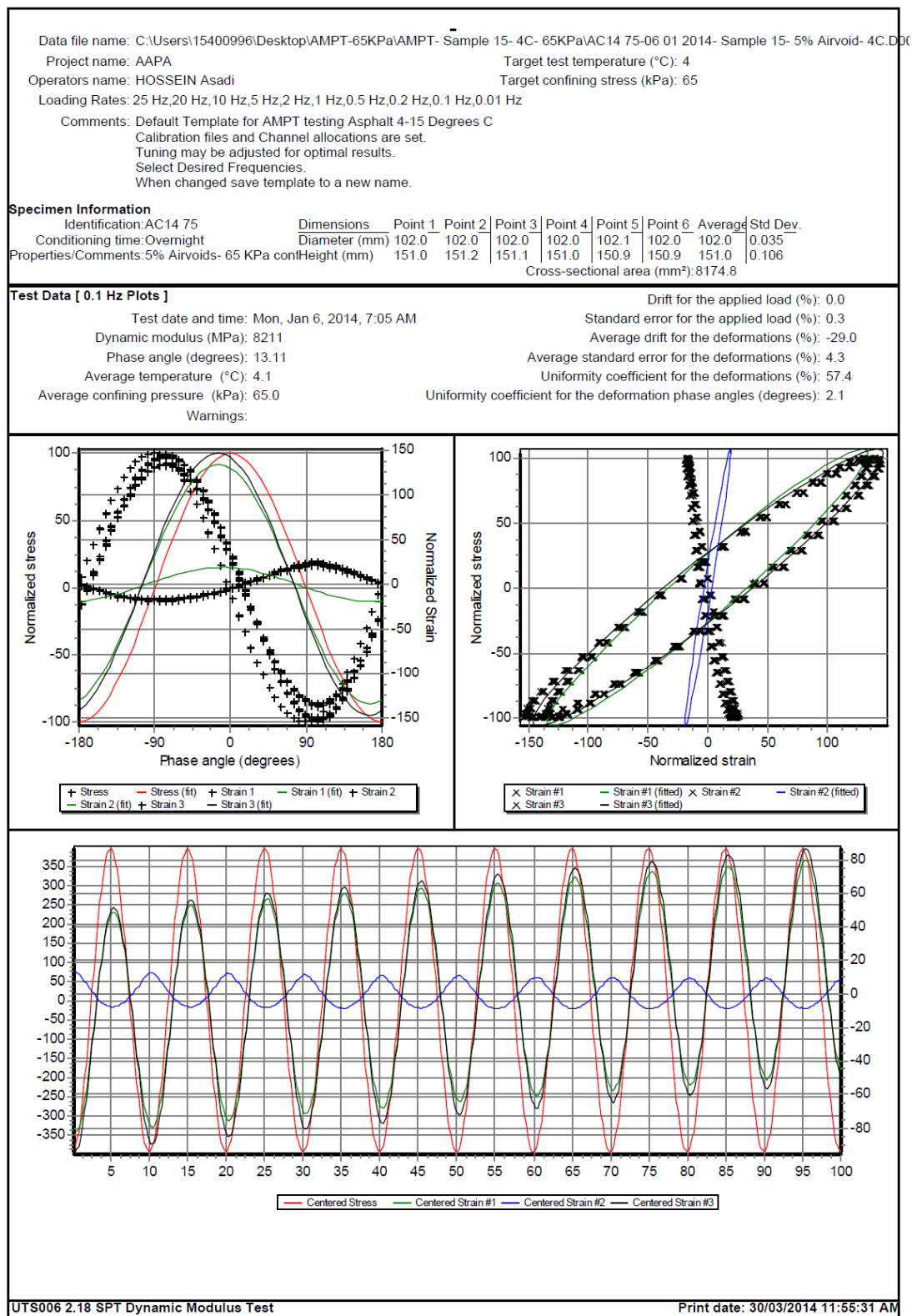


Figure E - 131. UTS6 output for sample11, 0.1 Hz and 4°C

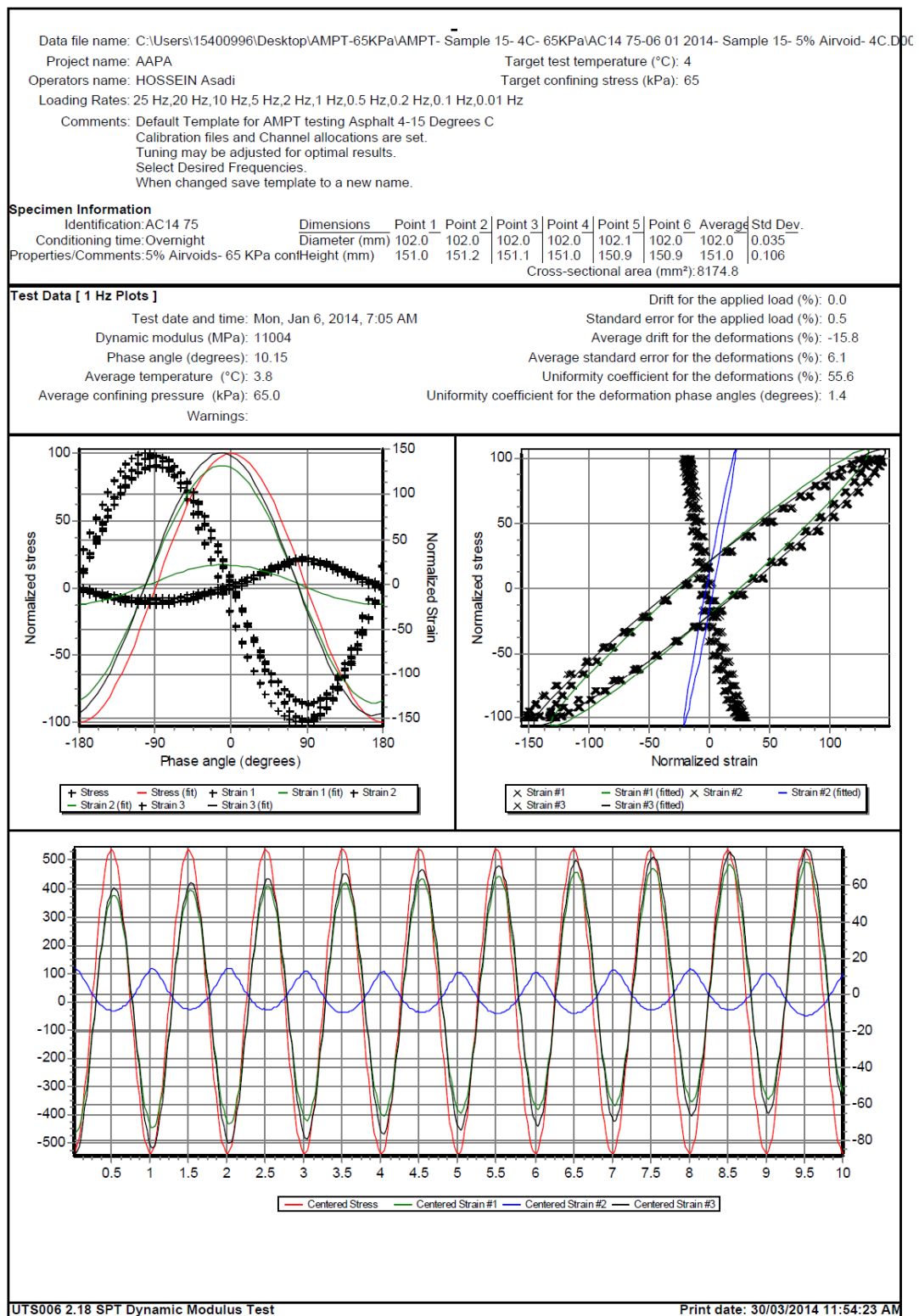


Figure E - 132. UTS6 output for sample11, 1 Hz and 4°C

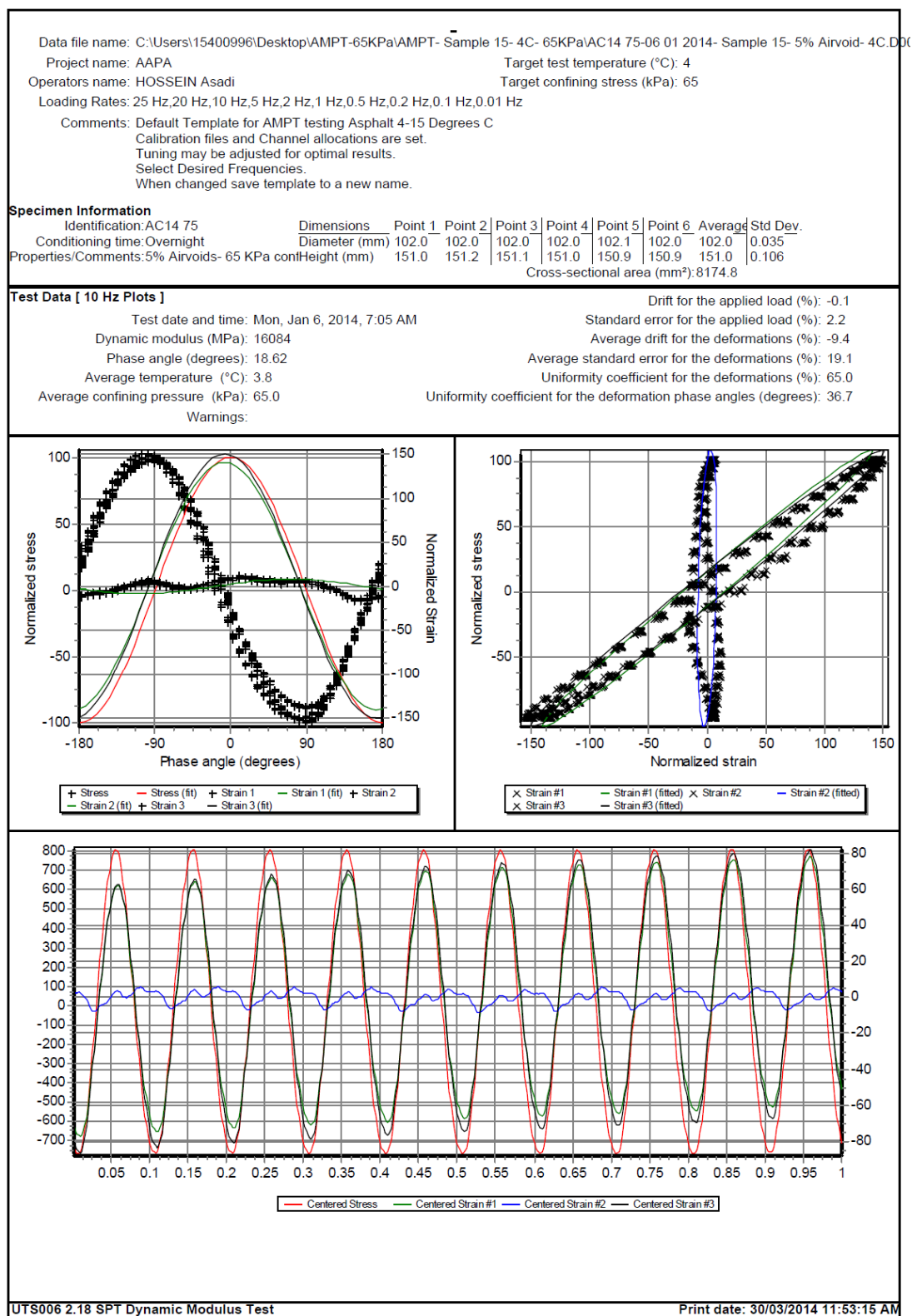


Figure E - 133. UTS6 output for sample11, 10 Hz and 4°C

AC14/75, 4.7% C320, (5.0% Voids)

Specimen Information

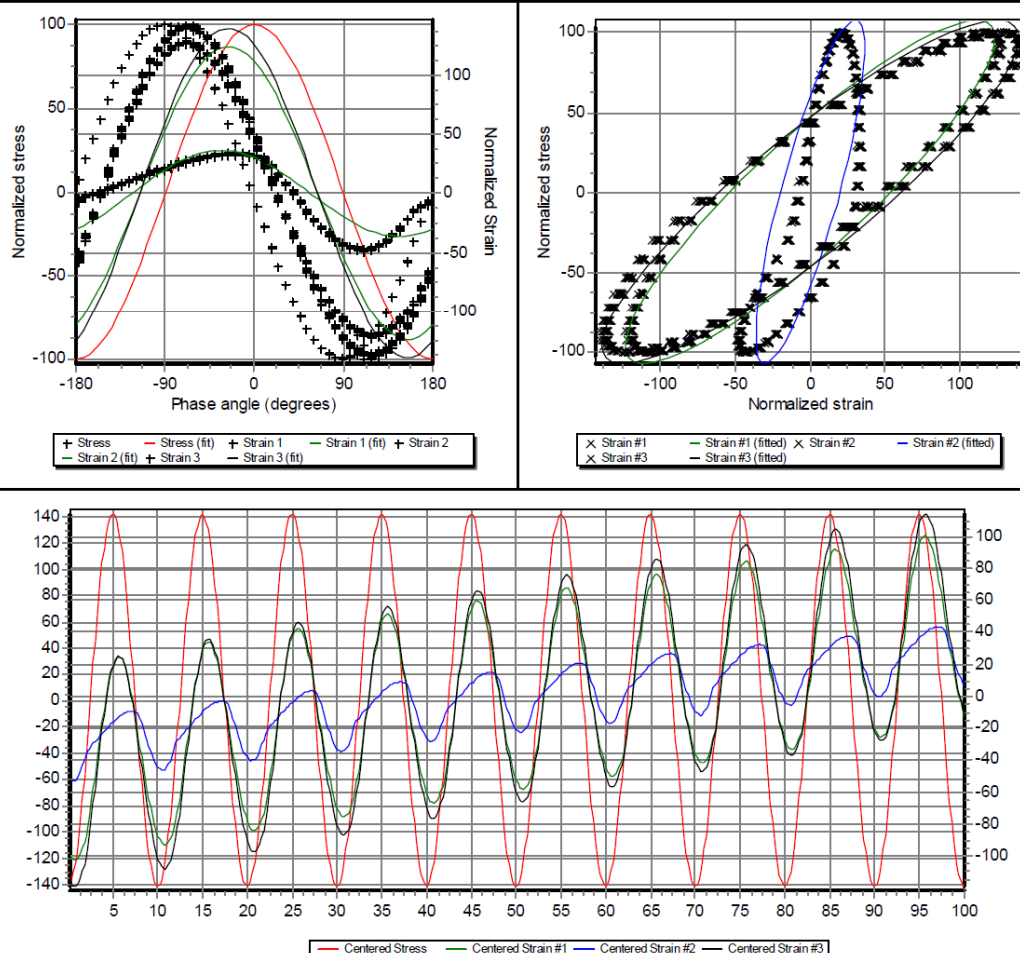
Dimensions	Point 1	Point 2	Point 3	Point 4	Point 5	Point 6	Average	Std Dev.
Diameter (mm)	102.0	102.0	102.0	102.0	102.1	102.0	102.0	0.035
Height (mm)	151.0	151.2	151.1	151.0	150.9	150.9	151.0	0.106

Cross-sectional area (mm²): 8174.8

Test Data [0.1 Hz Plots]

Drift for the applied load (%)	0.0
Standard error for the applied load (%)	0.2
Average drift for the deformations (%)	-200.7
Average standard error for the deformations (%)	10.1
Uniformity coefficient for the deformations (%)	45.4
Uniformity coefficient for the deformation phase angles (degrees)	3.6

Warnings:



Print date: 30/03/2014 12:00:15 PM

Figure E - 135. UTS6 output for sample11, 0.1 Hz and 20°C

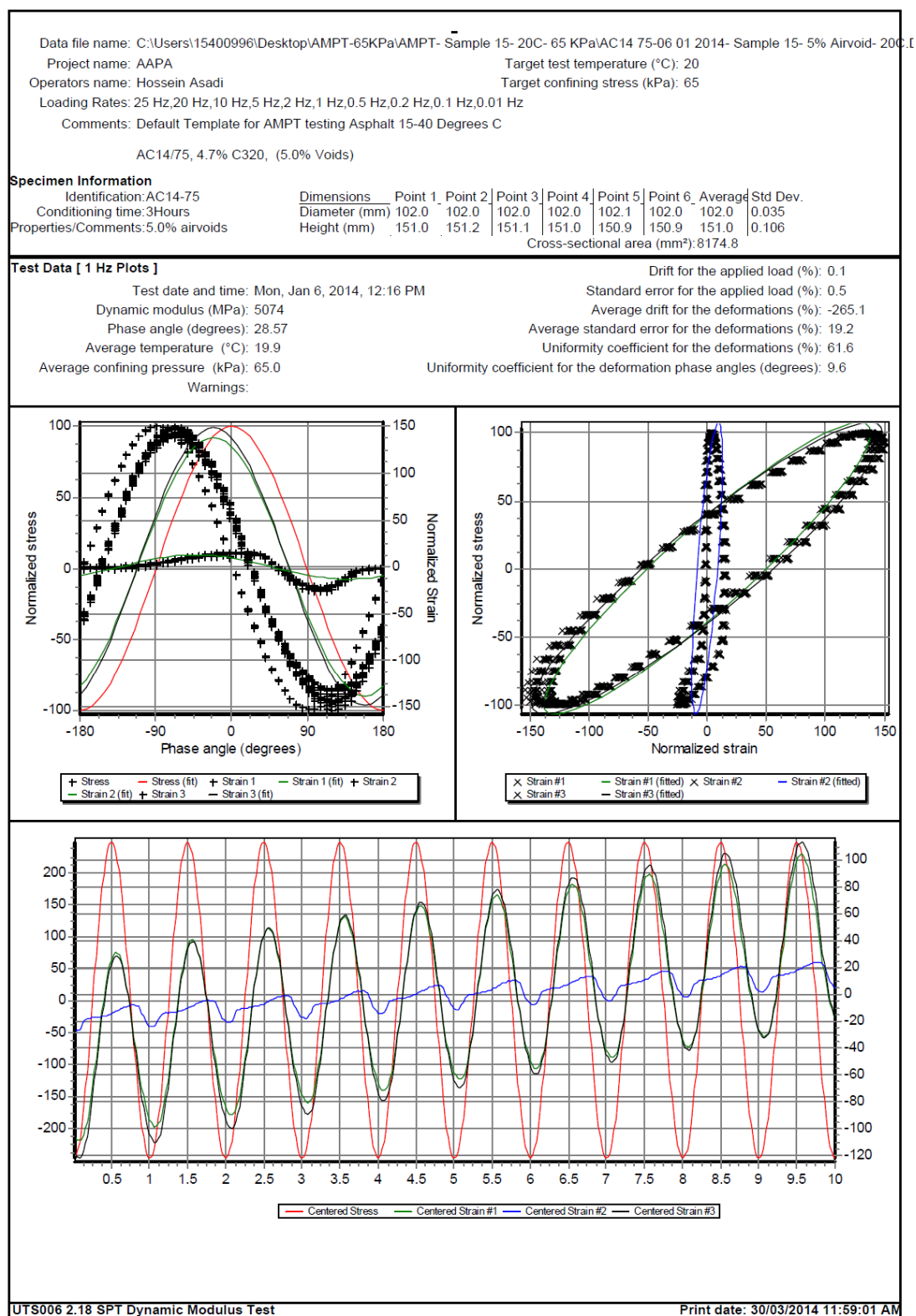


Figure E - 136. UTS6 output for sample11, 1 Hz and 20°C

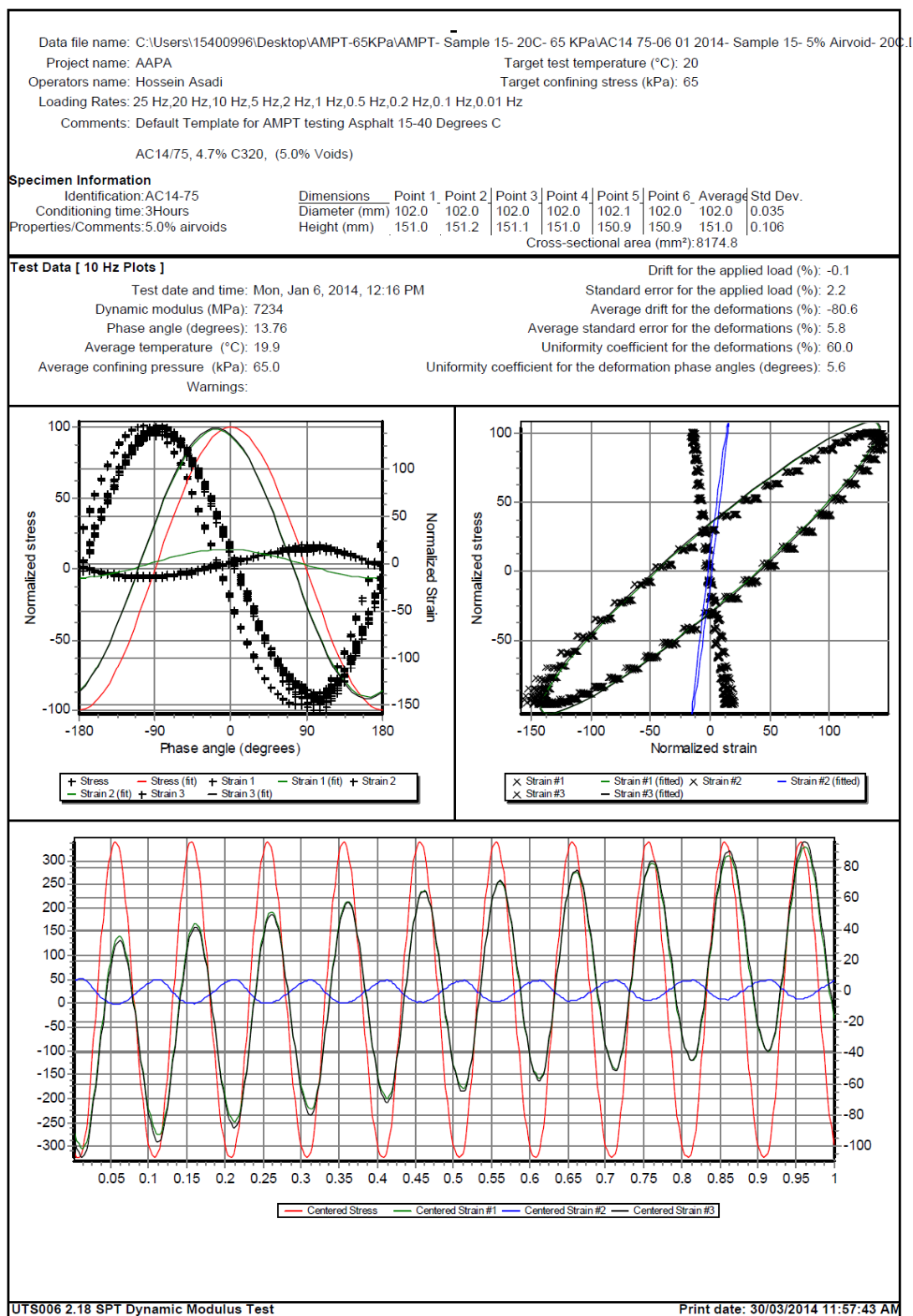


Figure E - 137. UTS6 output for sample11, 10 Hz and 20°C

Target test temperature (°C): 20

Target confining stress (kPa): 65

Loading Rates: 25 Hz, 20 Hz, 10 Hz, 5 Hz, 2 Hz, 1 Hz, 0.5 Hz, 0.2 Hz, 0.1 Hz, 0.01 Hz

Comments: Default Template for AMPT testing Asphalt 15-40 Degrees C

AC14/75, 4.7% C320, (5.0% Voids)

Specimen Information

Identification: AC14-75

Conditioning time:3Hours

Properties/Comments: 5.0% airvoids

Dimensions

Point 1 Poir

2 | Point 3 | Po

Point 4 | Point 5 | Point 6

int 6 Average

Std Dev.

1

Diameter (m)

102.0 102.0

2	Point 5	10
	102.0	10

10	102.1	1
----	-------	---

2.0 - 102.0

.035

111

Diameter (mm)
Height (mm)

102.0	102
151.0	151

102.0	10
151.1	15

0	102.1	1
0	150.9	1

2.0	102.0
0.9	151.0

.106

[illegible]

Cross-sectional area (mm²): 8174.8

Tabulated Results Summary

	25 Hz	20 Hz	10 Hz	5 Hz	2 Hz	1 Hz	0.5 Hz	0.2 Hz	0.1 Hz	0.01 Hz
Dynamic modulus (MPa)	7408	7670	7234	6712	5844	5074	4336	3451	2864	1370
Phase angle (Degrees)	15.18	11.45	13.76	9.97	40.16	28.57	27.15	27.83	28.37	31.11
Average temperature (°C)	19.9	19.9	19.9	19.8	19.9	19.9	20.0	20.1	20.1	20.0
Average confining pressure (kPa)	65.0	65.0	65.0	65.0	65.0	65.0	65.0	65.0	65.0	65.0
Average micro-strain	81	92	93	93	94	97	98	98	99	103
Load drift (%)	0.2	-0.1	-0.1	0.1	0.2	0.1	0.0	0.0	0.0	-0.3
Load standard error (%)	4.4	3.8	2.2	1.4	0.8	0.5	0.2	0.3	0.2	0.6
Average deformation drift (%)	-37.6	-24.9	-80.6	-169.7	-403.0	-265.1	-224.2	-213.8	-200.7	-225.4
Average deformation standard error (%)	6.0	19.4	5.8	11.1	33.0	19.2	14.5	11.7	10.1	6.9
Deformation uniformity (%)	48.1	53.4	60.0	65.0	67.2	61.6	55.6	49.6	45.4	37.5
Phase uniformity (Degrees)	1.7	7.1	5.6	12.6	27.7	9.6	5.8	4.4	3.6	3.5

UTS006 2.18 SPT Dynamic Modulus Test

Print date: 30/03/2014 11:57:43 AM

Figure E - 138. UTS6 summary output for sample11, 20°C

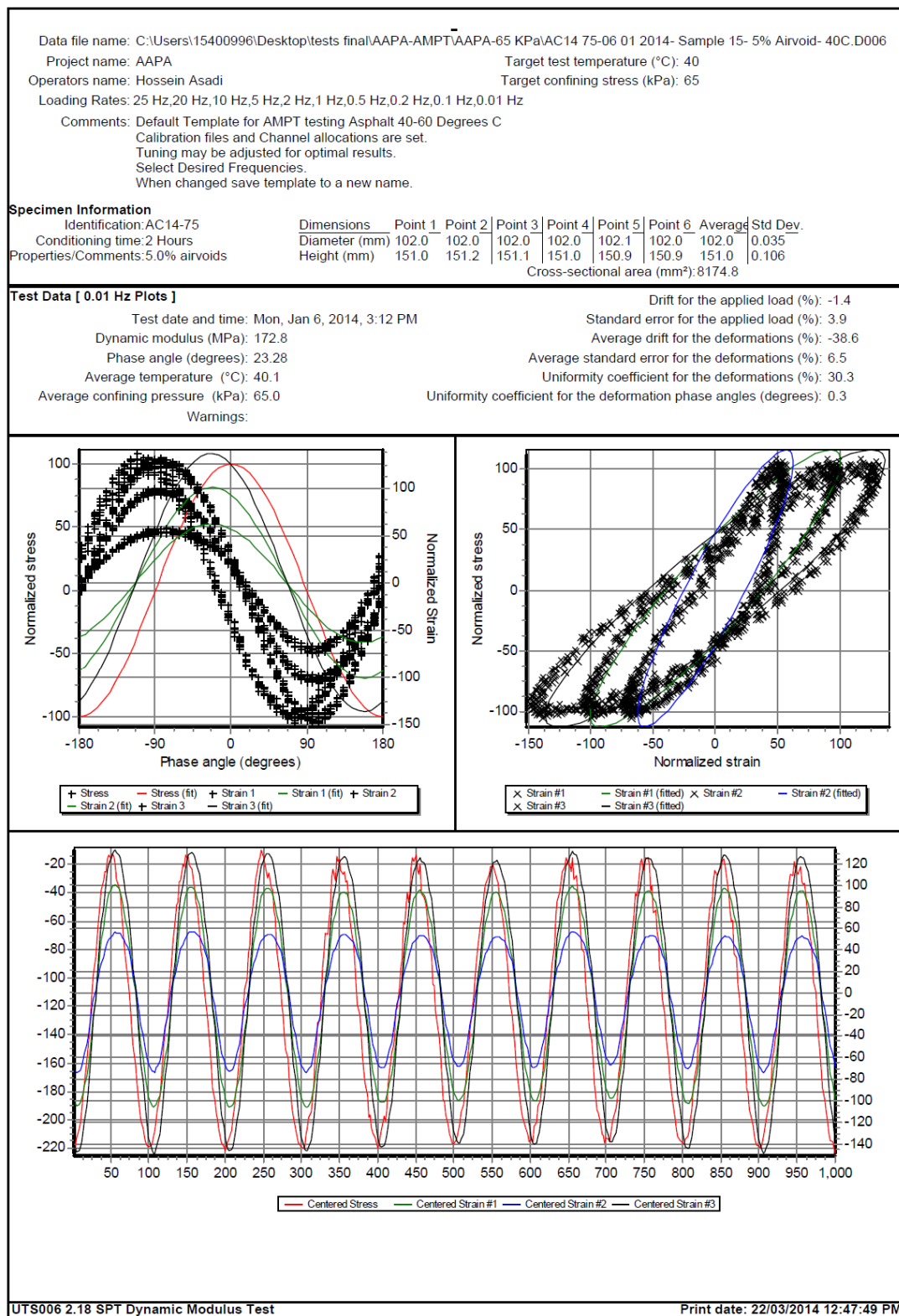


Figure E - 139. UTS6 output for sample11, 0.01 Hz and 40°C

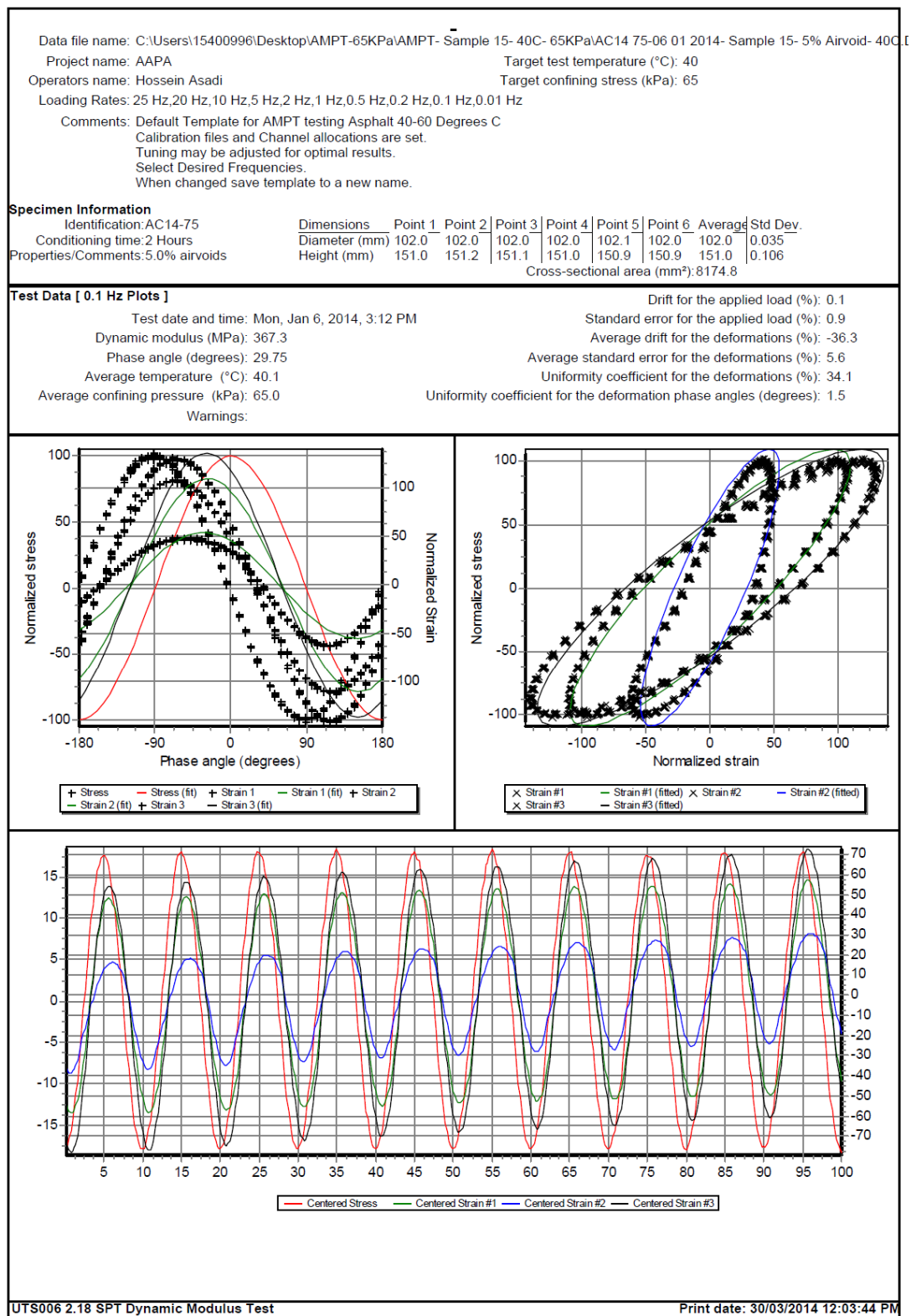


Figure E - 140. UTS6 output for sample11, 0.1 Hz and 40°C

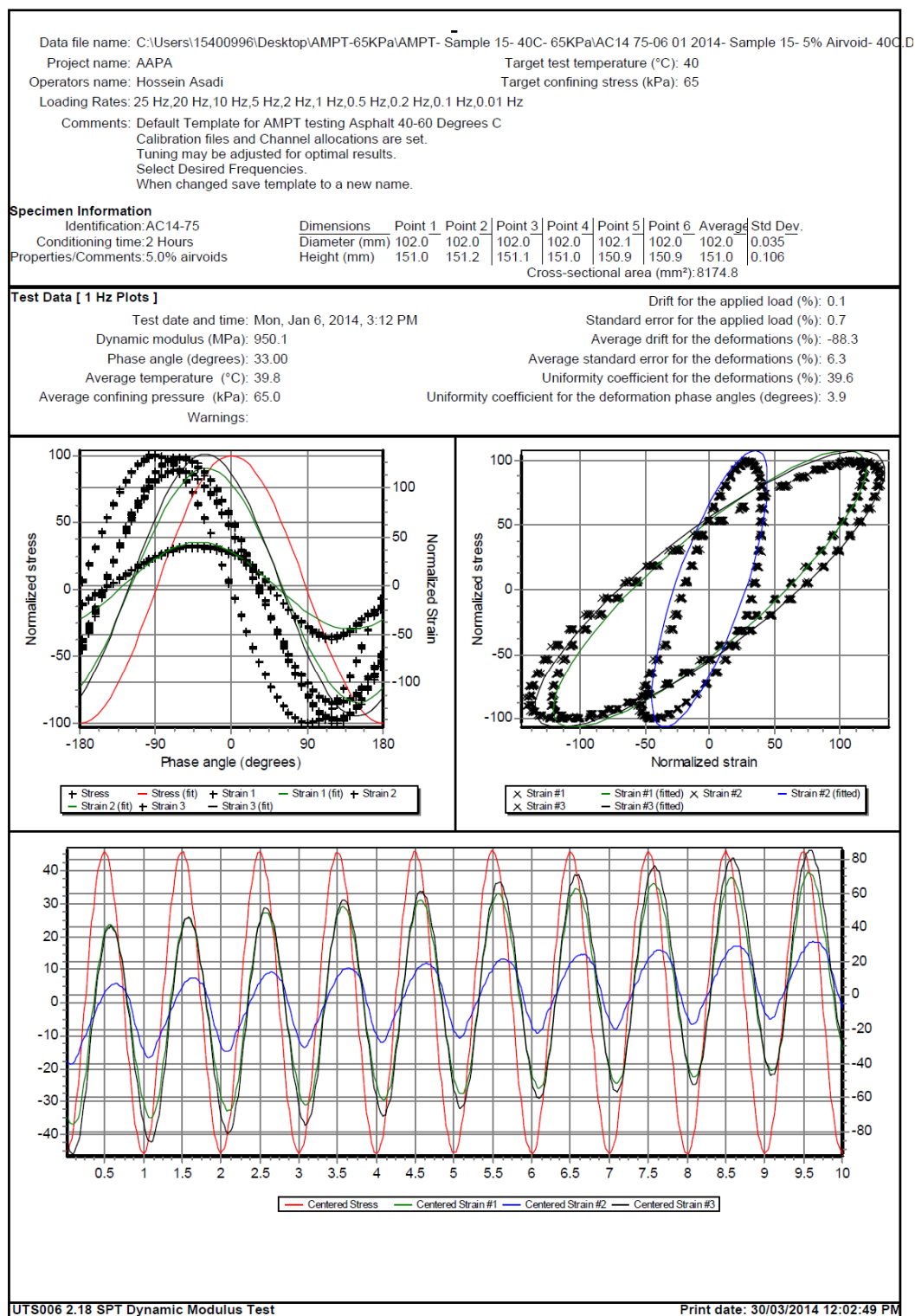


Figure E - 141. UTS6 output for sample11, 1 Hz and 40°C

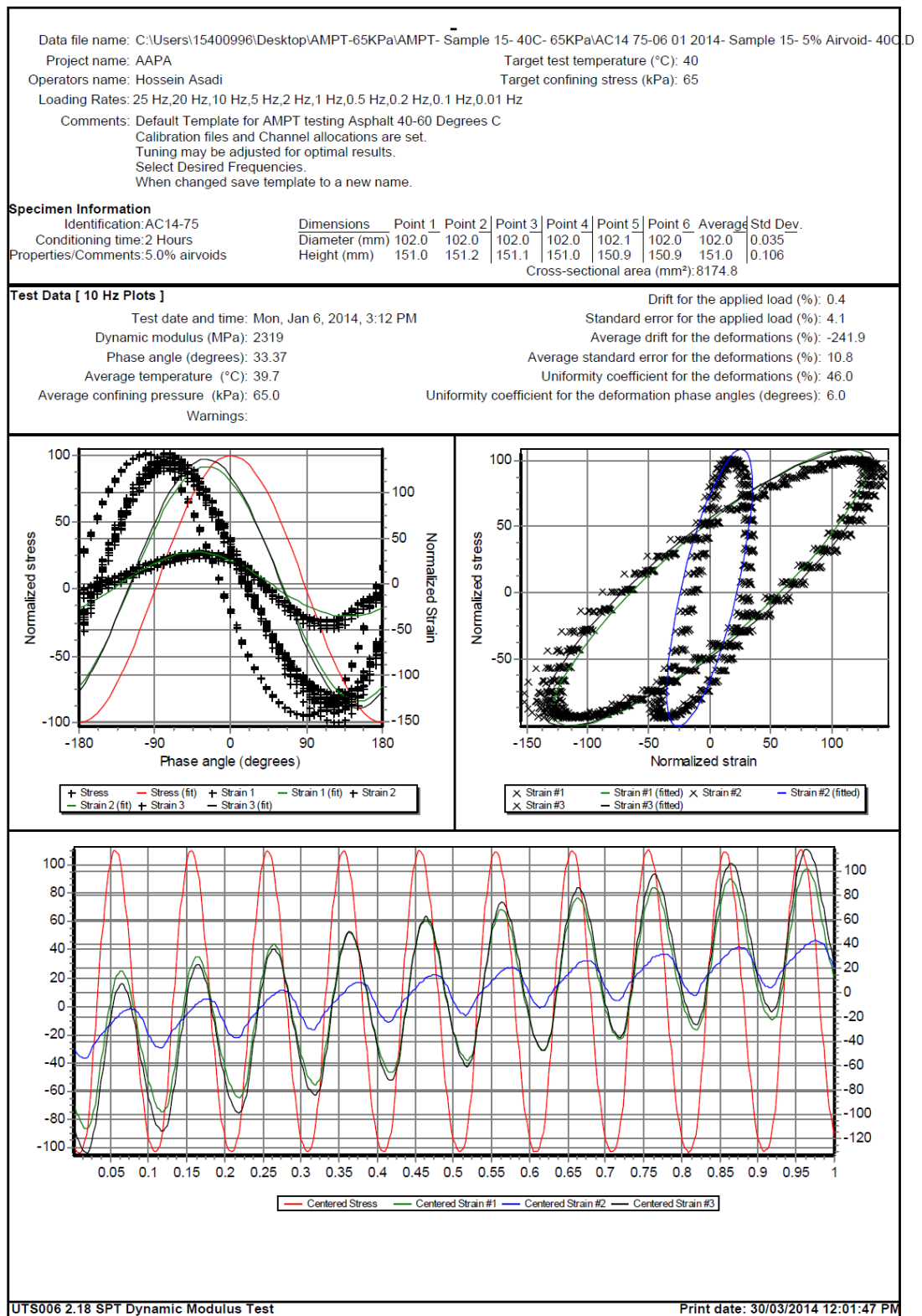


Figure E - 142. UTS6 output for sample11, 10 Hz and 40°C

Data file name: C:\Users\15400996\Desktop\AMPT-65KPa\AMPT- Sample 15- 40C- 65KPa\AC14 75-06 01 2014- Sample 15- 5% Airvoid- 40C.I											
Project name: AAPA					Target test temperature (°C): 40						
Operators name: Hossein Asadi					Target confining stress (kPa): 65						
Loading Rates: 25 Hz,20 Hz,10 Hz,5 Hz,2 Hz,1 Hz,0.5 Hz,0.2 Hz,0.1 Hz,0.01 Hz											
Comments: Default Template for AMPT testing Asphalt 40-60 Degrees C											
Calibration files and Channel allocations are set.											
Tuning may be adjusted for optimal results.											
Select Desired Frequencies.											
When changed save template to a new name.											
Specimen Information											
Identification: AC14-75		Dimensions		Point 1	Point 2	Point 3	Point 4	Point 5	Point 6	Average	Std Dev.
Conditioning time: 2 Hours		Diameter (mm)		102.0	102.0	102.0	102.0	102.1	102.0	102.0	0.035
Properties/Comments: 5.0% airvoids		Height (mm)		151.0	151.2	151.1	151.0	150.9	150.9	151.0	0.106
Cross-sectional area (mm²): 8174.8											
Tabulated Results Summary											
	25 Hz	20 Hz	10 Hz	5 Hz	2 Hz	1 Hz	0.5 Hz	0.2 Hz	0.1 Hz	0.01 Hz	
Dynamic modulus (MPa)	3051	2894	2319	1815	1270	950.1	708.5	486.3	367.3	172.8	
Phase angle (Degrees)	37.37	34.05	33.37	33.15	33.29	33.00	32.45	31.21	29.75	23.28	
Average temperature (°C)	39.7	39.7	39.7	39.7	39.7	39.8	40.0	40.2	40.1	40.1	
Average confining pressure (kPa)	65.0	65.0	65.0	65.0	65.0	65.0	65.0	65.0	65.0	65.0	
Average micro-strain	90	95	94	94	95	97	97	100	98	101	
Load drift (%)	-0.8	-1.0	0.4	0.4	0.7	0.1	0.2	0.5	0.1	-1.4	
Load standard error (%)	6.3	5.8	4.1	2.7	1.6	0.7	0.6	0.8	0.9	3.9	
Average deformation drift (%)	-492.2	-326.1	-241.9	-173.6	-127.5	-88.3	-66.0	-45.6	-36.3	-38.6	
Average deformation standard error (%)	14.7	12.8	10.8	9.8	7.2	6.3	5.8	5.5	5.6	6.5	
Deformation uniformity (%)	56.3	50.3	46.0	43.7	41.6	39.6	38.2	36.1	34.1	30.3	
Phase uniformity (Degrees)	12.0	8.1	6.0	4.7	4.2	3.9	3.5	2.9	1.5	0.3	

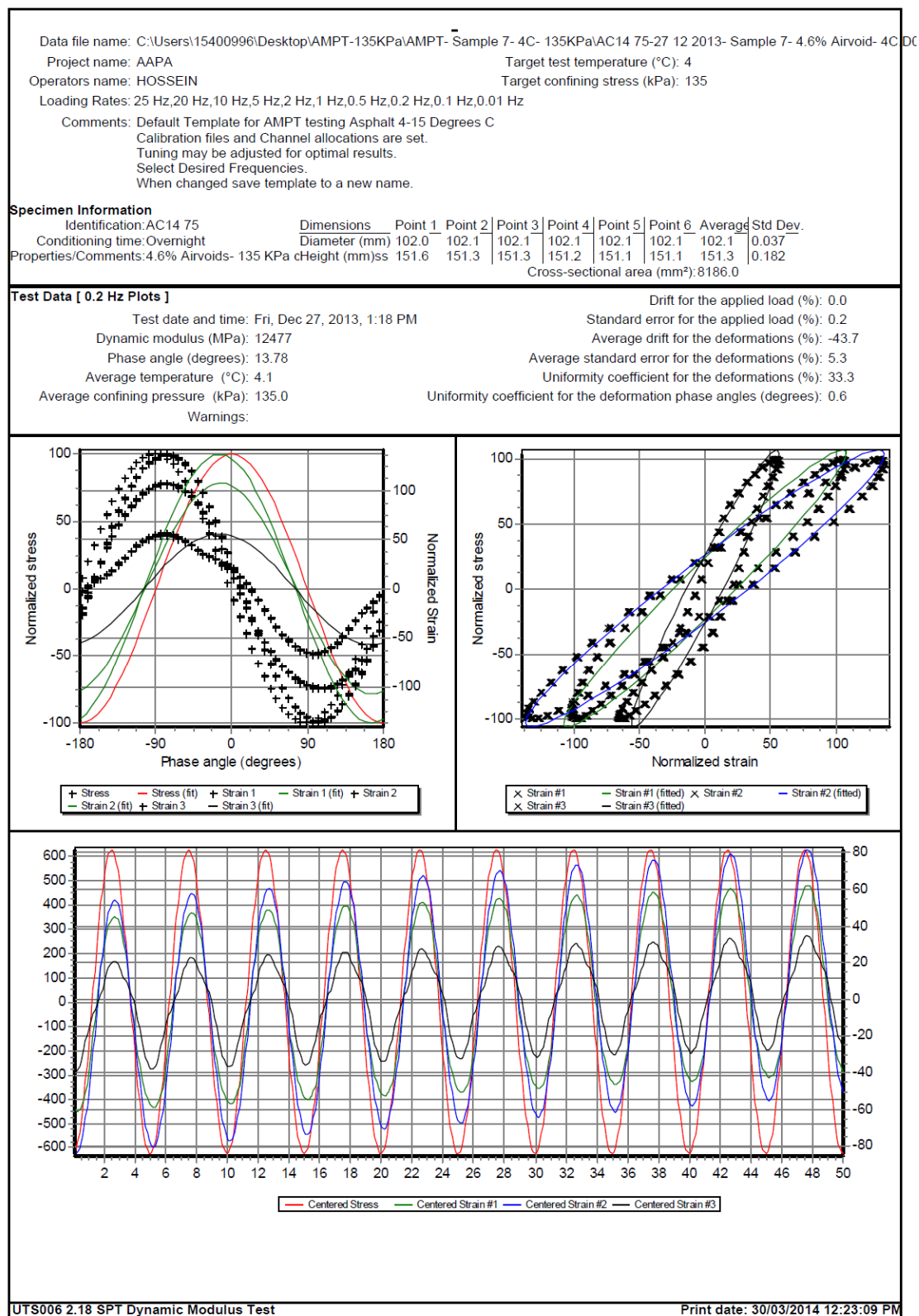


Figure E - 144. UTS6 output for sample12, 0.1 Hz and 4°C

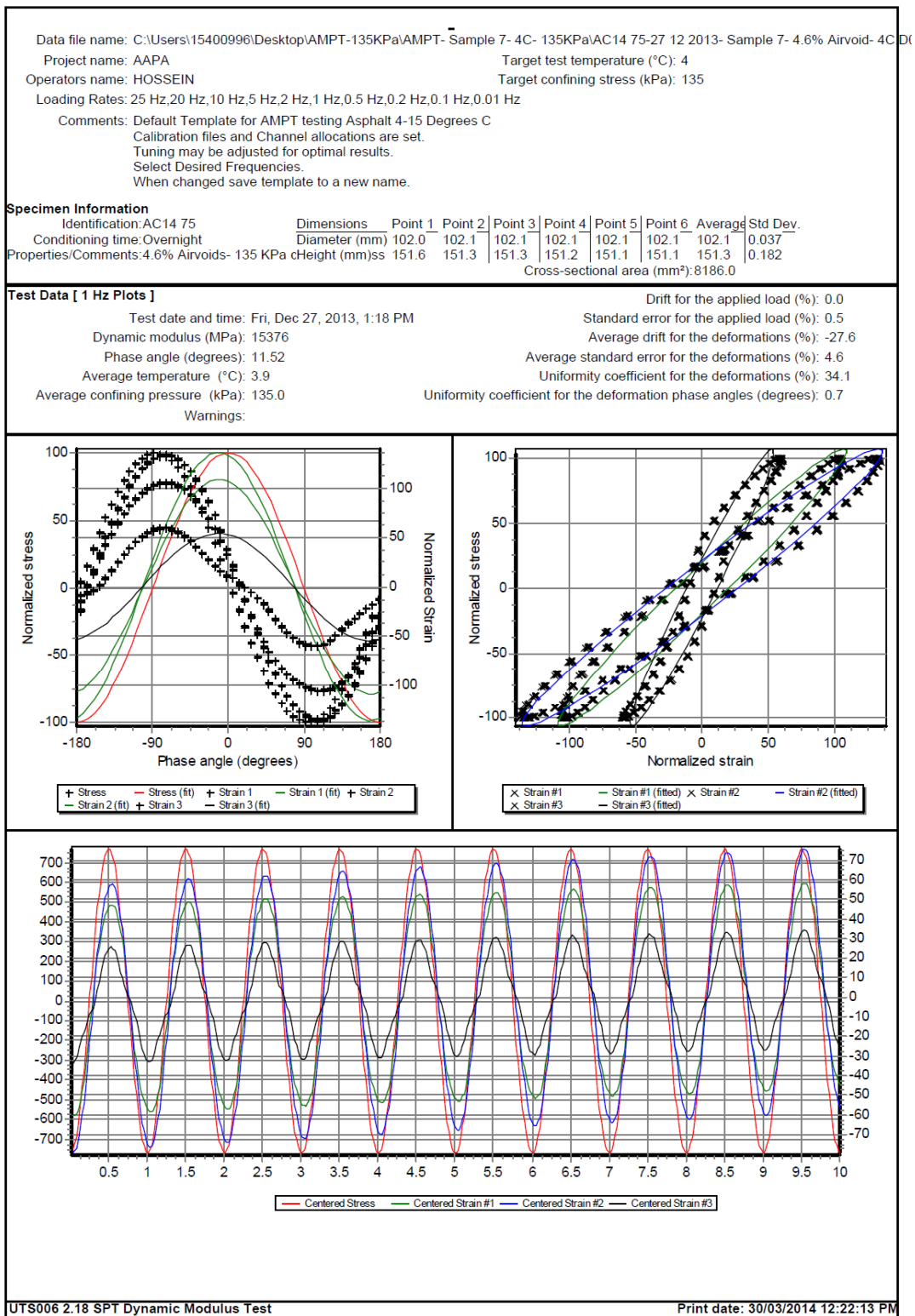


Figure E - 145. UTS6 output for sample12, 1 Hz and 4°C

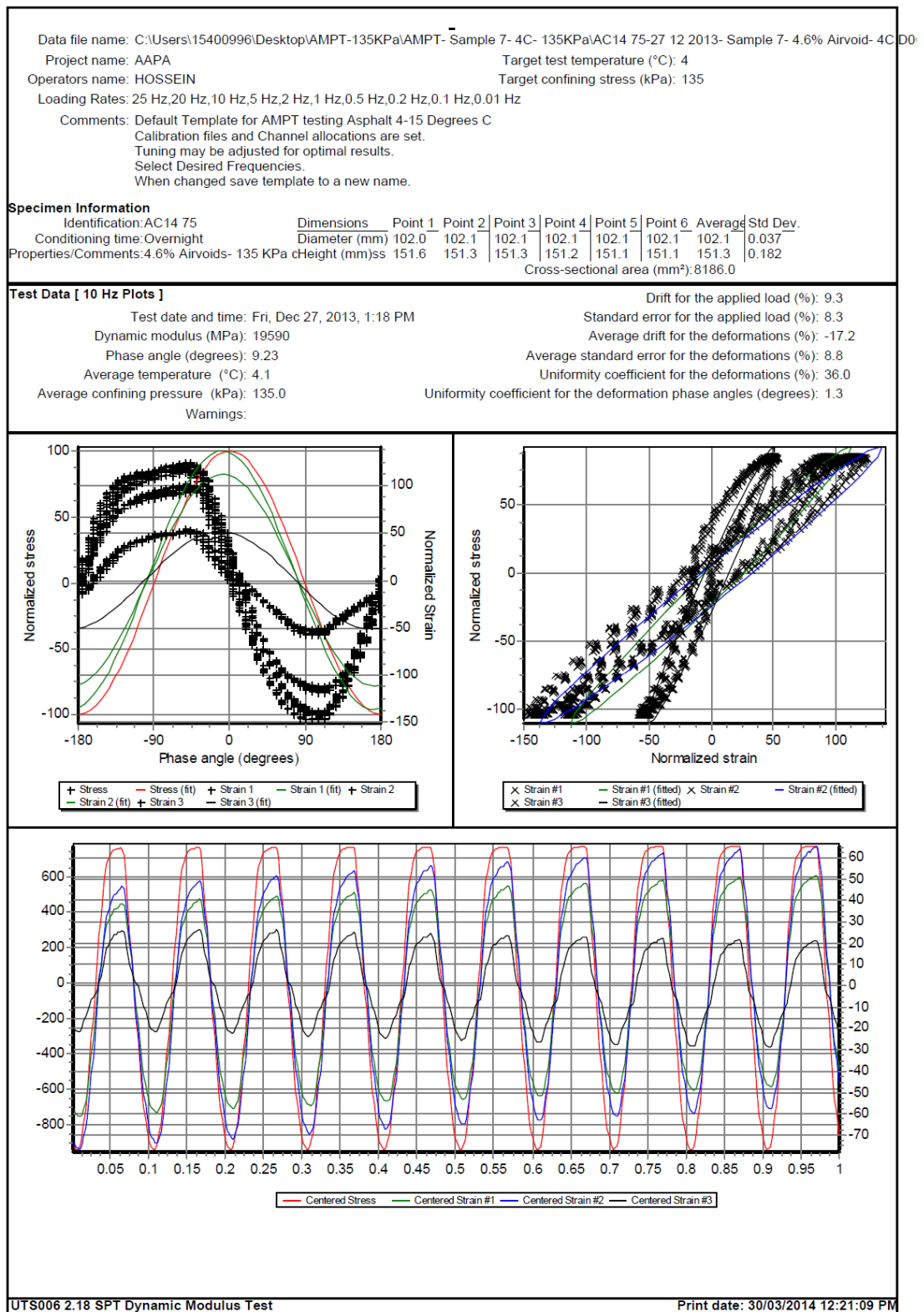


Figure E - 146. UTS6 output for sample12, 10 Hz and 4°C

Data file name: C:\Users\15400996\Desktop\AMPT-135KPa\AMPT- Sample 7- 4C- 135KPa\AC14 75-27 12 2013- Sample 7- 4.6% Airvoid- 4C.D											
Project name: AAPA				Target test temperature (°C): 4							
Operators name: HOSSEIN				Target confining stress (kPa): 135							
Loading Rates: 25 Hz,20 Hz,10 Hz,5 Hz,2 Hz,1 Hz,0.5 Hz,0.2 Hz,0.1 Hz,0.01 Hz											
Comments: Default Template for AMPT testing Asphalt 4-15 Degrees C											
Calibration files and Channel allocations are set.											
Tuning may be adjusted for optimal results.											
Select Desired Frequencies.											
When changed save template to a new name.											
Specimen Information											
Identification:AC14 75		Dimensions		Point 1	Point 2	Point 3	Point 4	Point 5	Point 6	Average	Std Dev.
Conditioning time:Overnight		Diameter (mm)		102.0	102.1	102.1	102.1	102.1	102.1	102.1	0.037
Properties/Comments:4.6% Airvoids- 135 KPa		Height (mm)		151.6	151.3	151.3	151.2	151.1	151.1	151.3	0.182
Cross-sectional area (mm²):8186.0											
Tabulated Results Summary											
	25 Hz	20 Hz	10 Hz	5 Hz	2 Hz	1 Hz	0.5 Hz	0.2 Hz	0.1 Hz	0.01 Hz	
Dynamic modulus (MPa)	21609	20943	19590	18341	16648	15376	14104	12477	11260	7636	
Phase angle (Degrees)	9.05	8.68	9.23	9.66	10.68	11.52	12.41	13.78	14.87	19.46	
Average temperature (°C)	4.2	4.1	4.1	4.1	4.0	3.9	3.9	4.1	4.0	4.1	
Average confining pressure (kPa)	135.0	135.0	135.0	135.0	135.0	135.0	135.0	135.0	135.0	135.0	
Average micro-strain	81	84	92	99	101	100	100	101	101	100	
Load drift (%)	11.4	9.9	9.3	9.9	-0.2	0.0	0.0	0.0	0.0	0.0	
Load standard error (%)	11.5	8.7	8.3	9.8	0.7	0.5	0.1	0.2	0.2	0.5	
Average deformation drift (%)	-19.3	-32.7	-17.2	-41.0	-24.7	-27.6	-32.1	-43.7	-53.5	-125.4	
Average deformation standard error (%)	12.3	9.1	8.8	9.8	4.9	4.6	4.6	5.3	6.1	6.4	
Deformation uniformity (%)	41.7	38.9	36.0	33.9	34.2	34.1	34.0	33.3	31.3	21.6	
Phase uniformity (Degrees)	3.4	1.5	1.3	0.9	0.7	0.7	0.6	0.6	0.6	0.6	

Figure E - 147. UTS6 output summary for sample12, 4°C

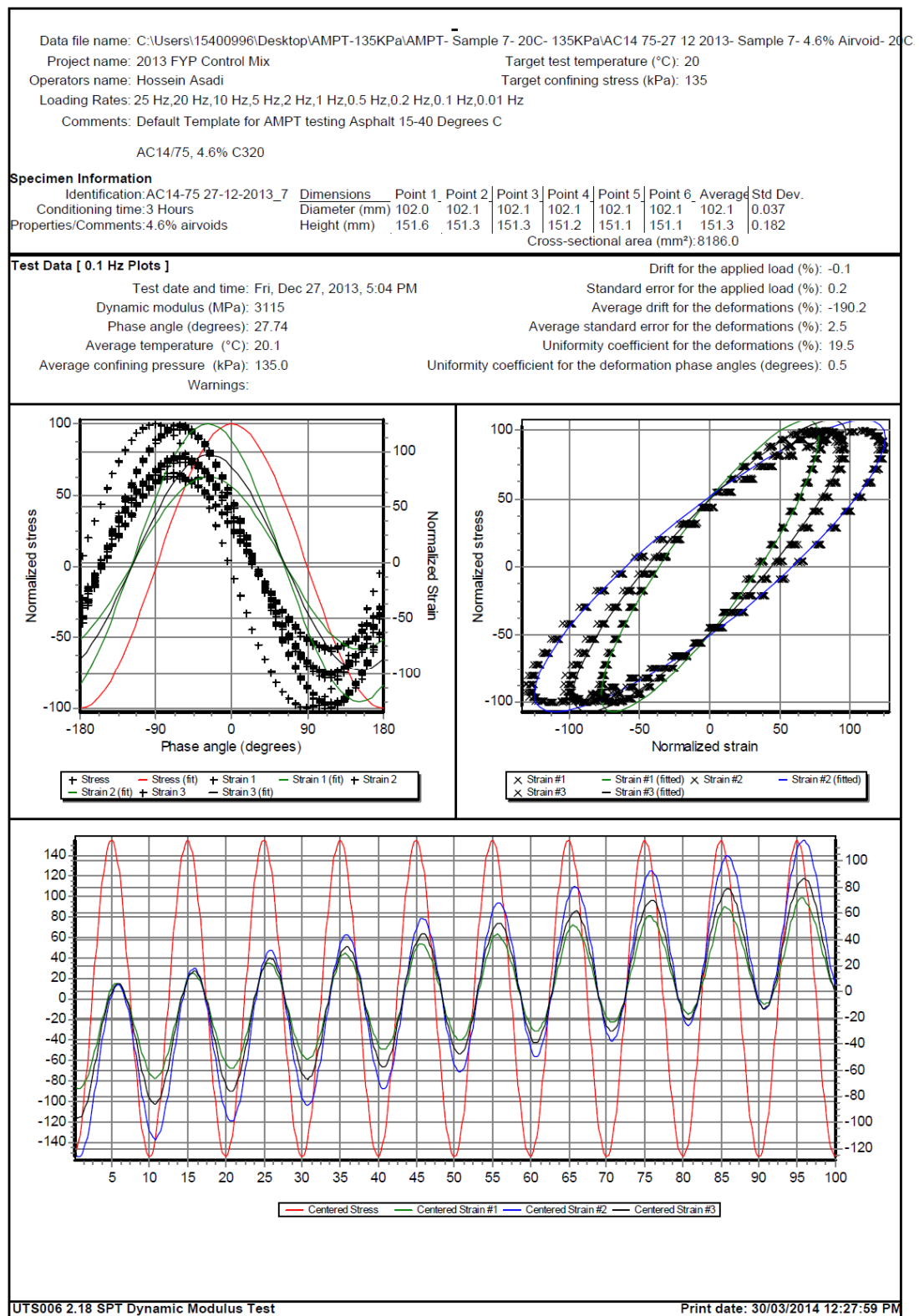


Figure E - 148. UTS6 output for sample12, 0.1 Hz and 20°C

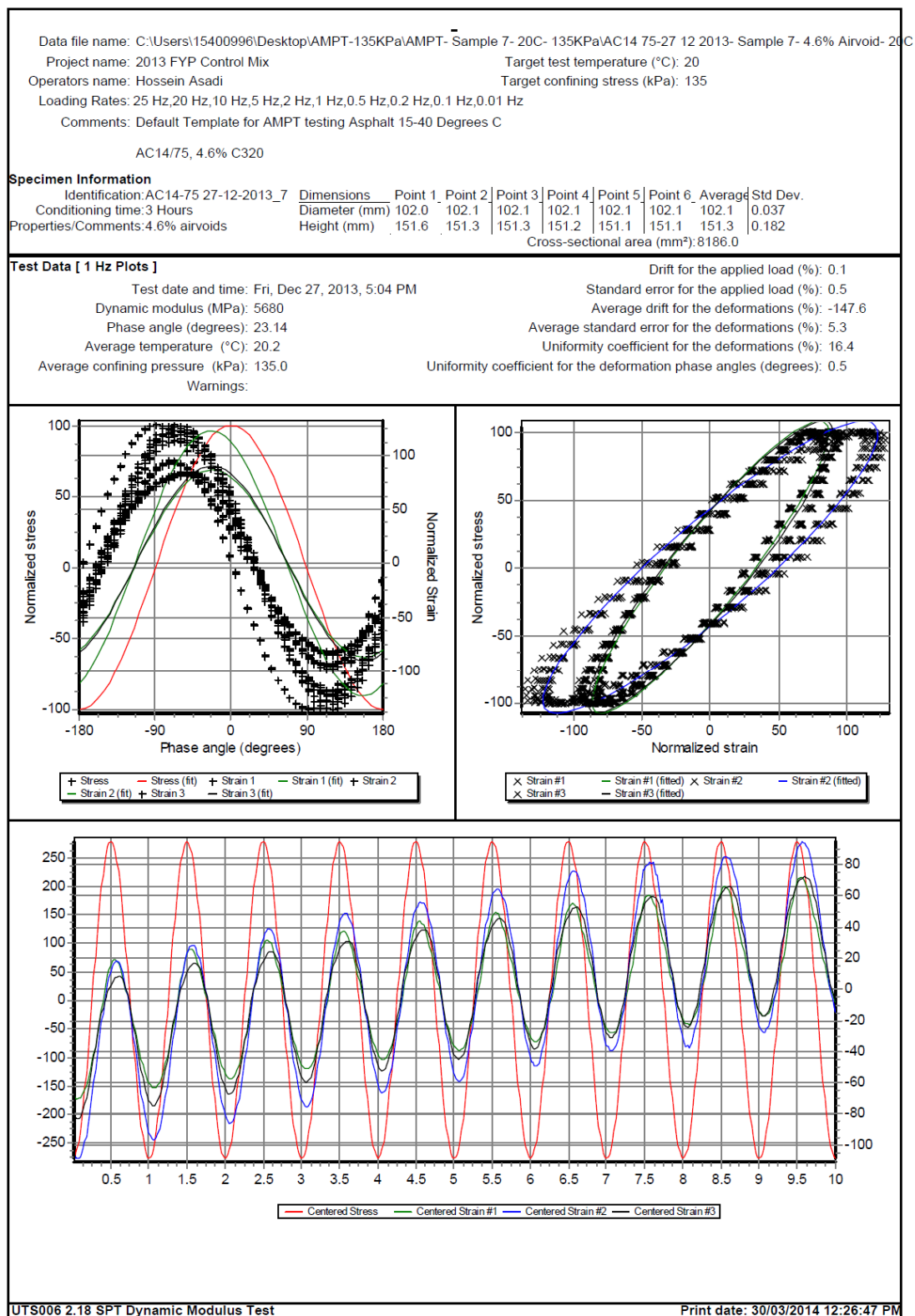


Figure E - 149. UTS6 output for sample12, 1 Hz and 20°C

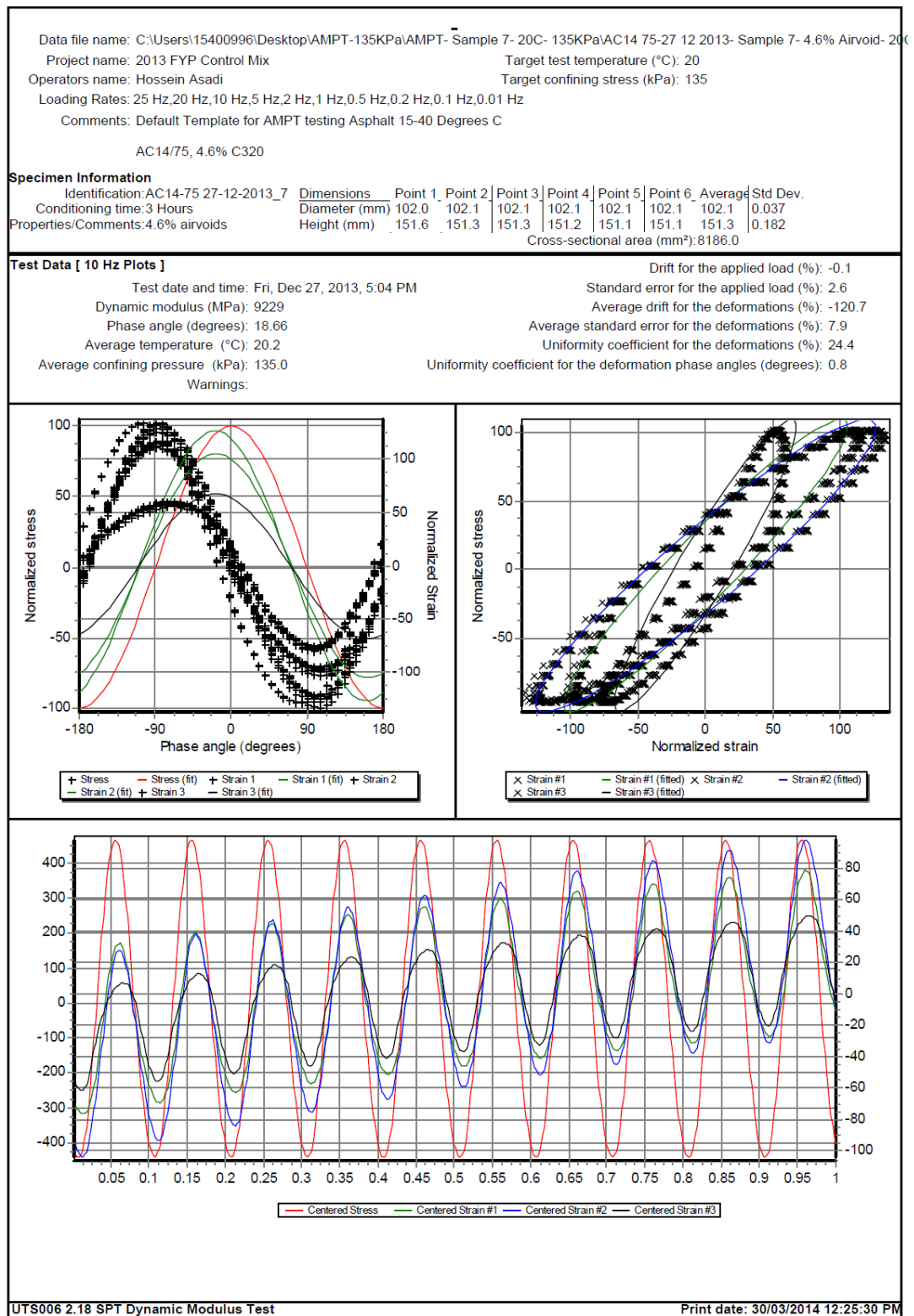


Figure E - 150. UTS6 output for sample12, 10 Hz and 20°C

Data file name: C:\Users\15400996\Desktop\AMPT-135KPa\AMPT- Sample 7- 20C- 135KPa\AC14 75-27 12 2013- Sample 7- 4.6% Airvoid- 20C										
Project name: 2013 FYP Control Mix					Target test temperature (°C): 20					
Operators name: Hossein Asadi					Target confining stress (kPa): 135					
Loading Rates: 25 Hz,20 Hz,10 Hz,5 Hz,2 Hz,1 Hz,0.5 Hz,0.2 Hz,0.1 Hz,0.01 Hz										
Comments: Default Template for AMPT testing Asphalt 15-40 Degrees C										
AC14/75, 4.6% C320										
Specimen Information										
Identification:AC14-75 27-12-2013_7		Dimensions	Point 1	Point 2	Point 3	Point 4	Point 5	Point 6	Average	Std Dev.
Conditioning time:3 Hours		Diameter (mm)	102.0	102.1	102.1	102.1	102.1	102.1	102.1	0.037
Properties/Comments:4.6% airvoids		Height (mm)	151.6	151.3	151.3	151.2	151.1	151.1	151.3	0.182
Cross-sectional area (mm²):8186.0										
Tabulated Results Summary										
	25 Hz	20 Hz	10 Hz	5 Hz	2 Hz	1 Hz	0.5 Hz	0.2 Hz	0.1 Hz	0.01 Hz
Dynamic modulus (MPa)	10892	10466	9229	8065	6642	5680	4819	3783	3115	1442
Phase angle (Degrees)	17.06	17.23	18.66	19.94	21.84	23.14	24.48	26.47	27.74	31.37
Average temperature (°C)	20.2	20.2	20.2	20.2	20.2	20.2	20.1	20.1	20.1	20.0
Average confining pressure (kPa)	135.0	135.0	135.0	135.0	135.0	135.0	135.0	135.0	135.0	135.0
Average micro-strain	102	97	99	98	98	97	98	99	99	103
Load drift (%)	-0.3	-0.5	-0.1	0.0	0.1	0.1	0.1	0.1	-0.1	0.1
Load standard error (%)	5.5	5.1	2.6	1.4	0.7	0.5	0.2	0.3	0.2	0.6
Average deformation drift (%)	-121.1	-105.9	-120.7	-130.6	-146.2	-147.6	-170.4	-187.3	-190.2	-210.5
Average deformation standard error (%)	8.5	8.7	7.9	6.8	5.3	5.3	4.3	2.9	2.5	2.2
Deformation uniformity (%)	32.9	28.4	24.4	19.7	16.6	16.4	16.8	18.7	19.5	22.0
Phase uniformity (Degrees)	0.8	0.6	0.8	0.7	0.6	0.5	0.4	0.4	0.5	0.3

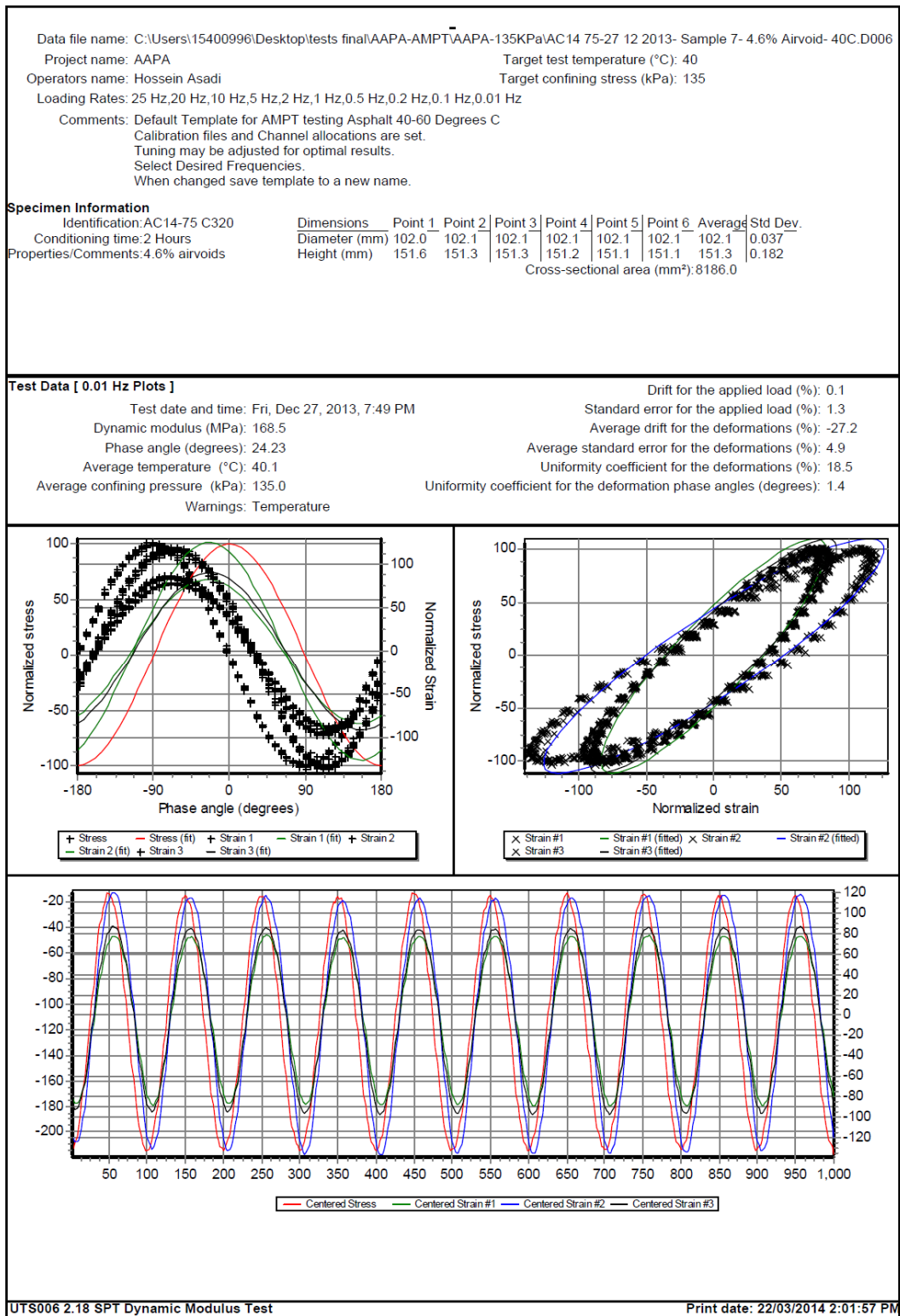


Figure E - 152. UTS6 output for sample12, 0.01 Hz and 40°C

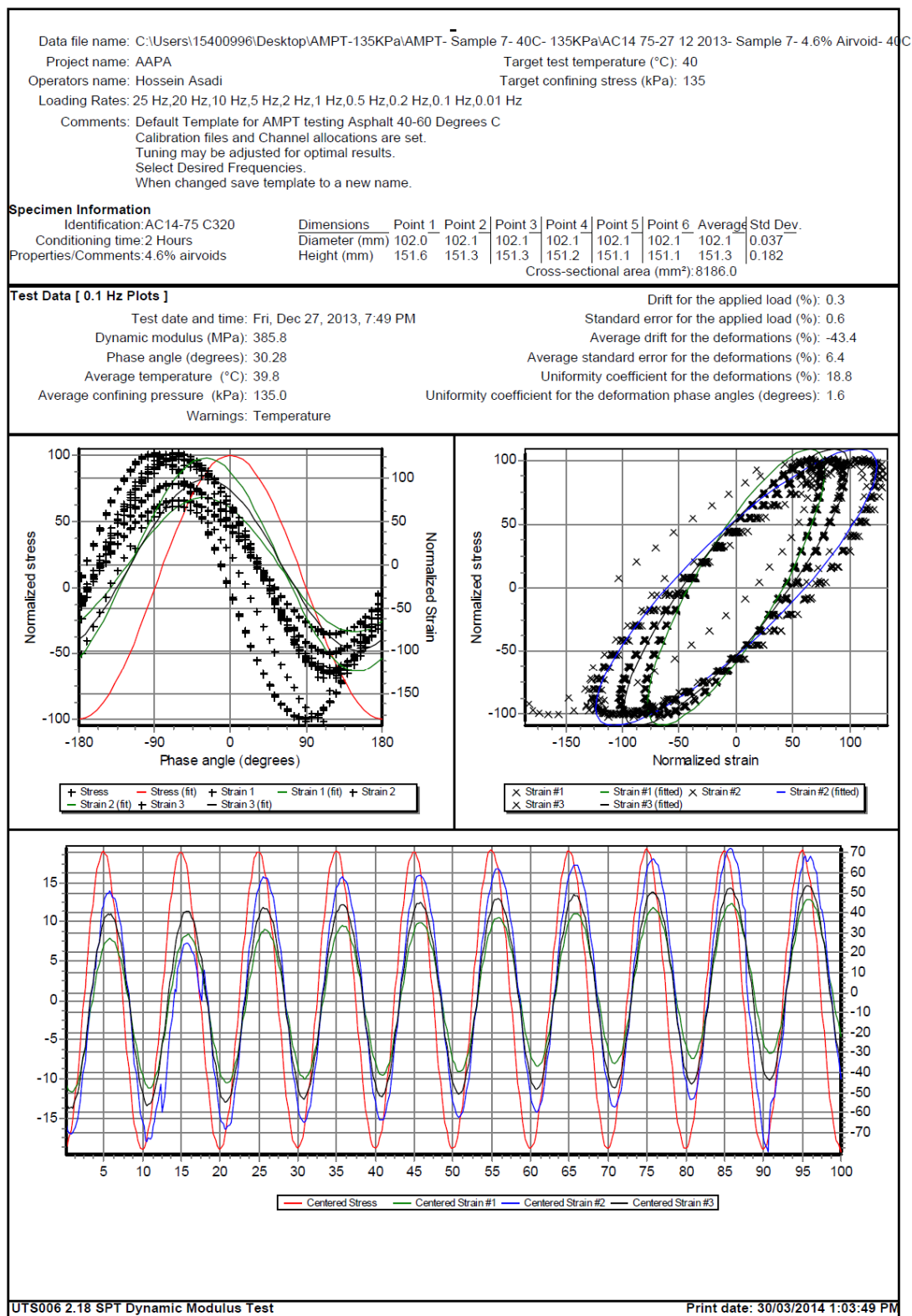


Figure E - 153. UTS6 output for sample12, 0.1 Hz and 40°C

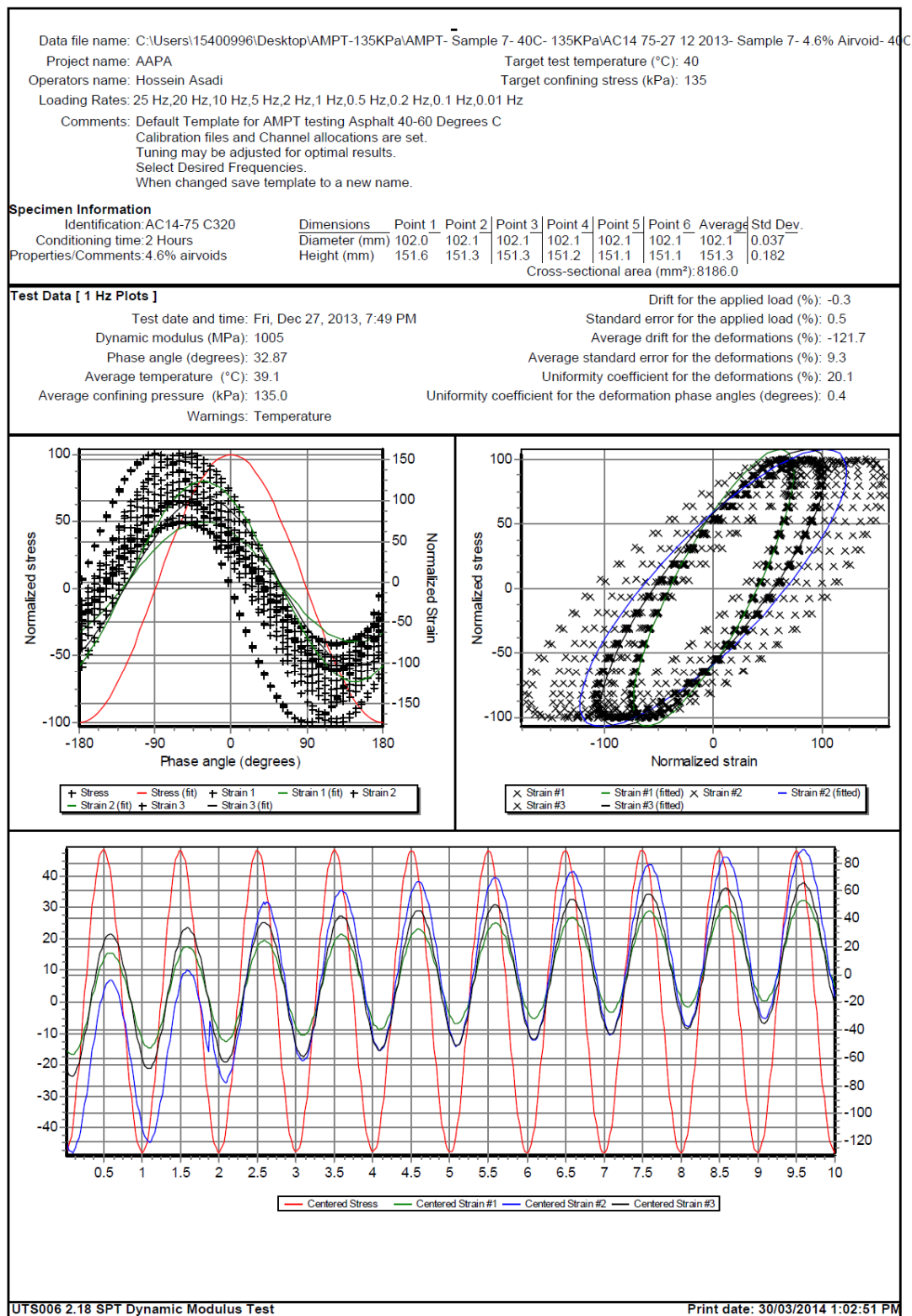


Figure E - 154. UTS6 output for sample12, 1Hz and 40°C

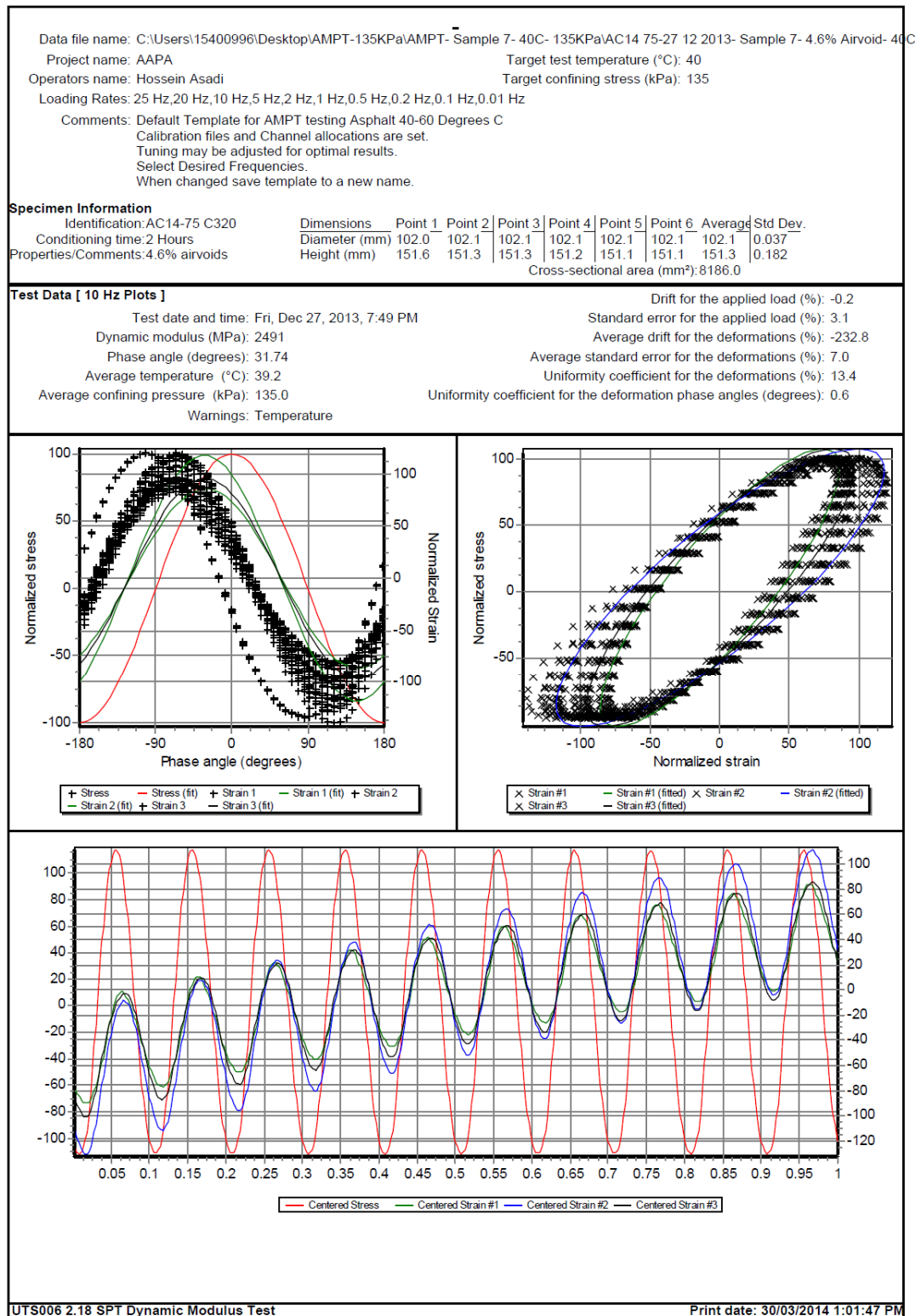


Figure E - 155. UTS6 output for sample12, 10 Hz and 40°C

Data file name: C:\Users\15400996\Desktop\AMPT-135KPa\AMPT- Sample 7- 40C- 135KPa\AC14 75-27 12 2013- Sample 7- 4.6% Airvoid- 40C.												
Project name: AAPA				Target test temperature (°C): 40								
Operators name: Hossein Asadi				Target confining stress (kPa): 135								
Loading Rates: 25 Hz,20 Hz,10 Hz,5 Hz,2 Hz,1 Hz,0.5 Hz,0.2 Hz,0.1 Hz,0.01 Hz												
Comments: Default Template for AMPT testing Asphalt 40-60 Degrees C												
Calibration files and Channel allocations are set.												
Tuning may be adjusted for optimal results.												
Select Desired Frequencies.												
When changed save template to a new name.												
Specimen Information												
Identification:AC14-75 C320				Dimensions	Point 1	Point 2	Point 3	Point 4	Point 5	Point 6	Average	Std Dev.
Conditioning time:2 Hours				Diameter (mm)	102.0	102.1	102.1	102.1	102.1	102.1	102.1	0.037
Properties/Comments:4.6% airvoids				Height (mm)	151.6	151.3	151.3	151.2	151.1	151.1	151.3	0.182
Cross-sectional area (mm²): 8186.0												
Tabulated Results Summary												
	25 Hz	20 Hz	10 Hz	5 Hz	2 Hz	1 Hz	0.5 Hz	0.2 Hz	0.1 Hz	0.01 Hz		
Dynamic modulus (MPa)	3324	3148	2491	1928	1344	1005	745.4	509.0	385.8	168.5		
Phase angle (Degrees)	31.62	30.96	31.74	32.45	32.14	32.87	32.32	31.61	30.28	24.23		
Average temperature (°C)	39.3	39.2	39.2	39.2	39.1	39.1	39.1	39.3	39.8	40.1		
Average confining pressure (kPa)	135.0	135.0	135.0	135.0	135.0	135.0	135.0	135.0	135.0	135.0		
Average micro-strain	93	94	94	94	94	96	97	100	99	109		
Load drift (%)	-0.2	-0.4	-0.2	0.1	-0.1	-0.3	0.0	-0.2	0.3	0.1		
Load standard error (%)	5.1	4.4	3.1	2.0	1.2	0.5	0.3	0.4	0.6	1.3		
Average deformation drift (%)	-390.7	-283.3	-232.8	-183.6	-122.4	-121.7	-43.4	-52.2	-43.4	-27.2		
Average deformation standard error (%)	11.3	8.3	7.0	5.0	7.8	9.3	5.0	3.4	6.4	4.9		
Deformation uniformity (%)	11.1	10.9	13.4	16.3	19.6	20.1	20.5	20.4	18.8	18.5		
Phase uniformity (Degrees)	1.3	1.1	0.6	0.5	0.8	0.4	0.8	1.2	1.6	1.4		

Figure E - 156. UTS6 summary output for sample12, 40°C

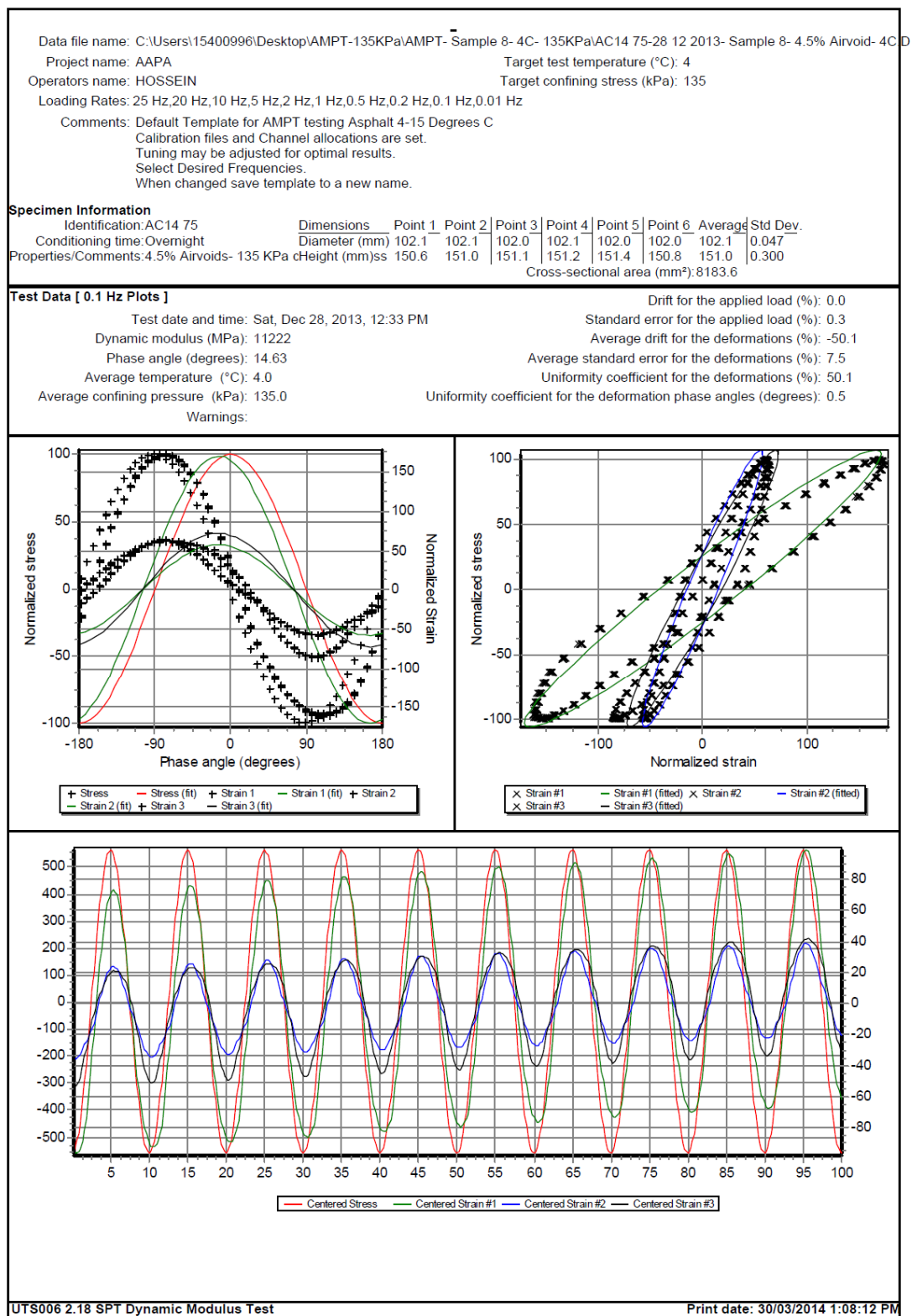


Figure E - 157. UTS6 output for sample13, 0.1 Hz and 4°C

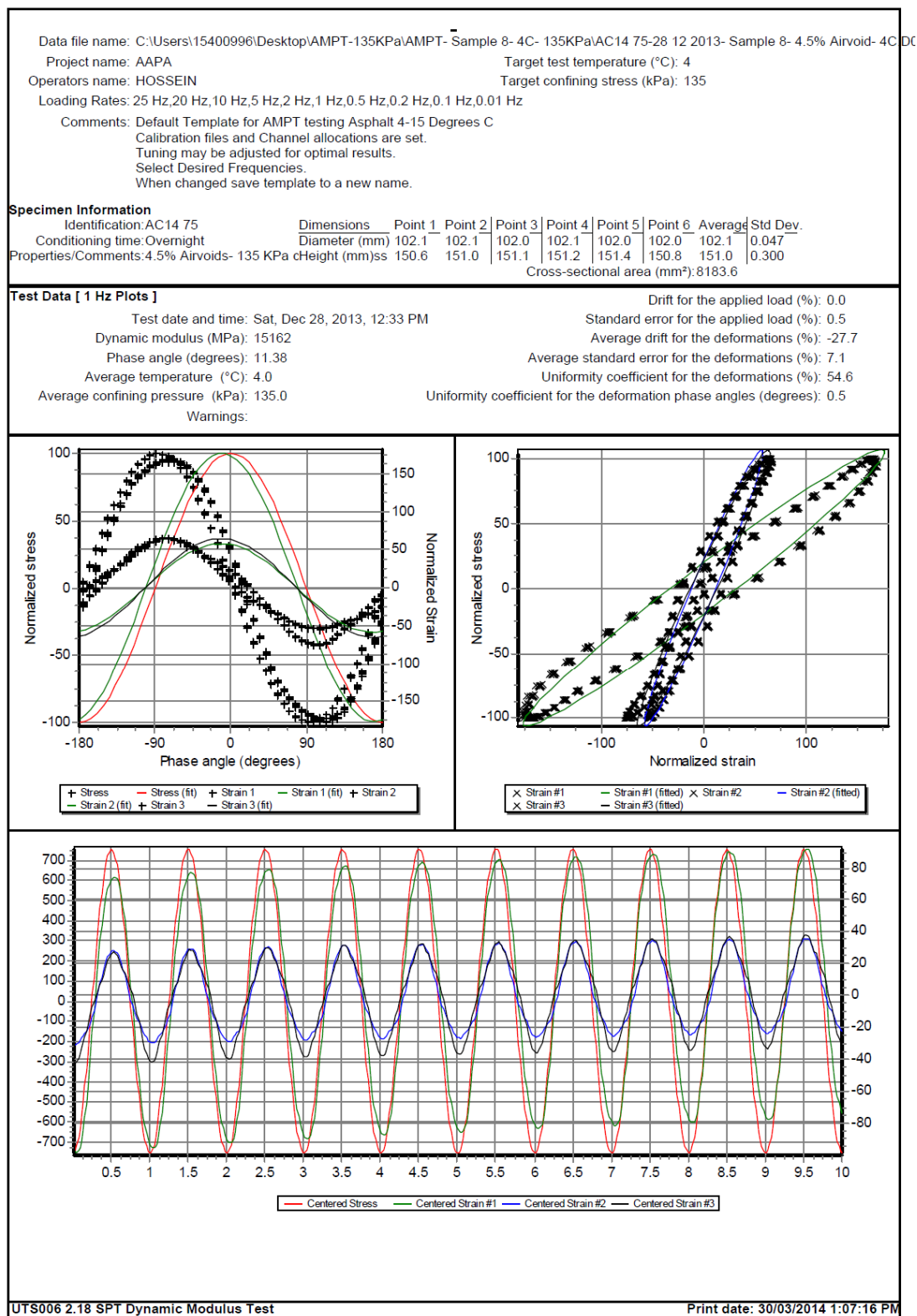


Figure E - 158. UTS6 output for sample13, 1 Hz and 4°C

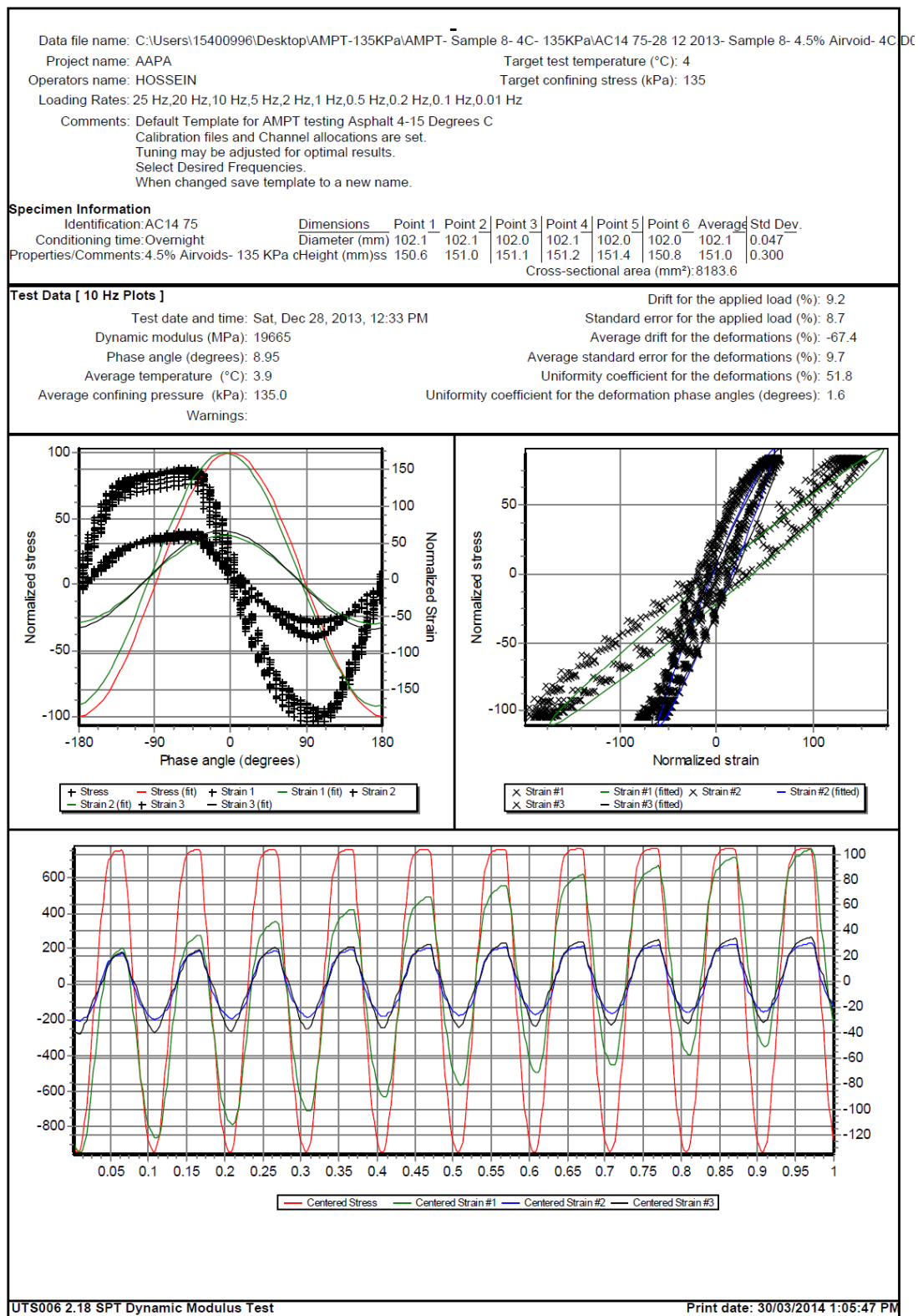


Figure E - 159. UTS6 output for sample13, 10 Hz and 4°C

Target test temperature (°C): 4

Target confining stress (kPa): 135

Loading Rates: 25 Hz, 20 Hz, 10 Hz, 5 Hz, 2 Hz, 1 Hz, 0.5 Hz, 0.2 Hz, 0.1 Hz, 0.01 Hz

Comments: Default Template for AMPT testing Asphalt 4-15 Degrees C

Calibration files and Channel allocations are set.

Tuning may be adjusted for optimal results.
Select Desired Frequency

Select Desired Frequencies.
When changed save template

When changed save template to a new name.

Specimen Information

Identification: AC14 75	Dimensions	Point 1	Point 2	Point 3	Point 4	Point 5	Point 6	Average	Std Dev.
Conditioning time: Overnight	Diameter (mm)	102.1	102.1	102.0	102.1	102.0	102.0	102.1	0.047
Properties/Comments: 4.5% Airvoids- 135 KPa c	Height (mm)ss	150.6	151.0	151.1	151.2	151.4	150.8	151.0	0.300
Cross-sectional area (mm²): 8183.6									

Tabulated Results Summary

	25 Hz	20 Hz	10 Hz	5 Hz	2 Hz	1 Hz	0.5 Hz	0.2 Hz	0.1 Hz	0.01 Hz
Dynamic modulus (MPa)	22523	21494	19665	18016	16374	15162	13948	12384	11222	7712
Phase angle (Degrees)	8.62	8.72	8.95	9.74	10.64	11.38	12.25	13.54	14.63	19.04
Average temperature (°C)	3.9	3.9	3.9	3.9	3.9	4.0	4.0	4.1	4.0	4.1
Average confining pressure (kPa)	135.0	135.0	135.0	135.0	135.0	135.0	135.0	135.0	135.0	135.0
Average micro-strain	77	82	92	101	100	100	100	100	100	99
Load drift (%)	10.0	10.0	9.2	9.6	-0.1	0.0	0.0	0.0	0.0	0.0
Load standard error (%)	12.1	9.9	8.7	10.0	0.6	0.5	0.1	0.2	0.3	0.5
Average deformation drift (%)	-142.5	-73.3	-67.4	-43.5	-24.9	-27.7	-29.8	-39.4	-50.1	-129.8
Average deformation standard error (%)	14.6	10.9	9.7	10.2	7.0	7.1	7.3	7.5	7.5	6.7
Deformation uniformity (%)	52.8	52.6	51.8	50.7	53.9	54.6	54.6	53.2	50.1	39.5
Phase uniformity (Degrees)	2.5	1.9	1.6	1.0	0.6	0.5	0.5	0.5	0.5	0.7

Figure E - 160. UTS6 summary output for sample13, 4°C

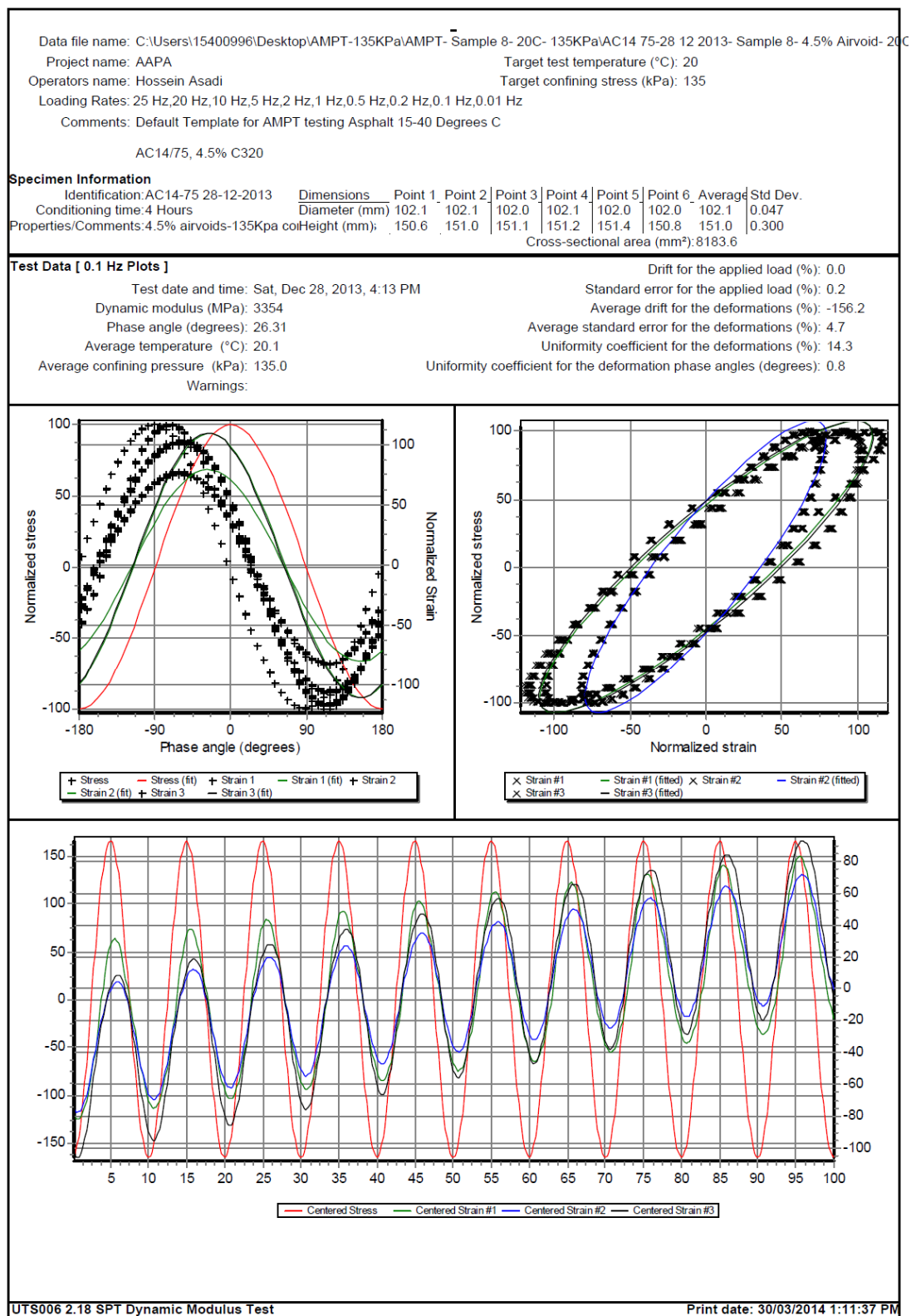


Figure E - 161. UTS6 output for sample13, 0.1 Hz and 20°C

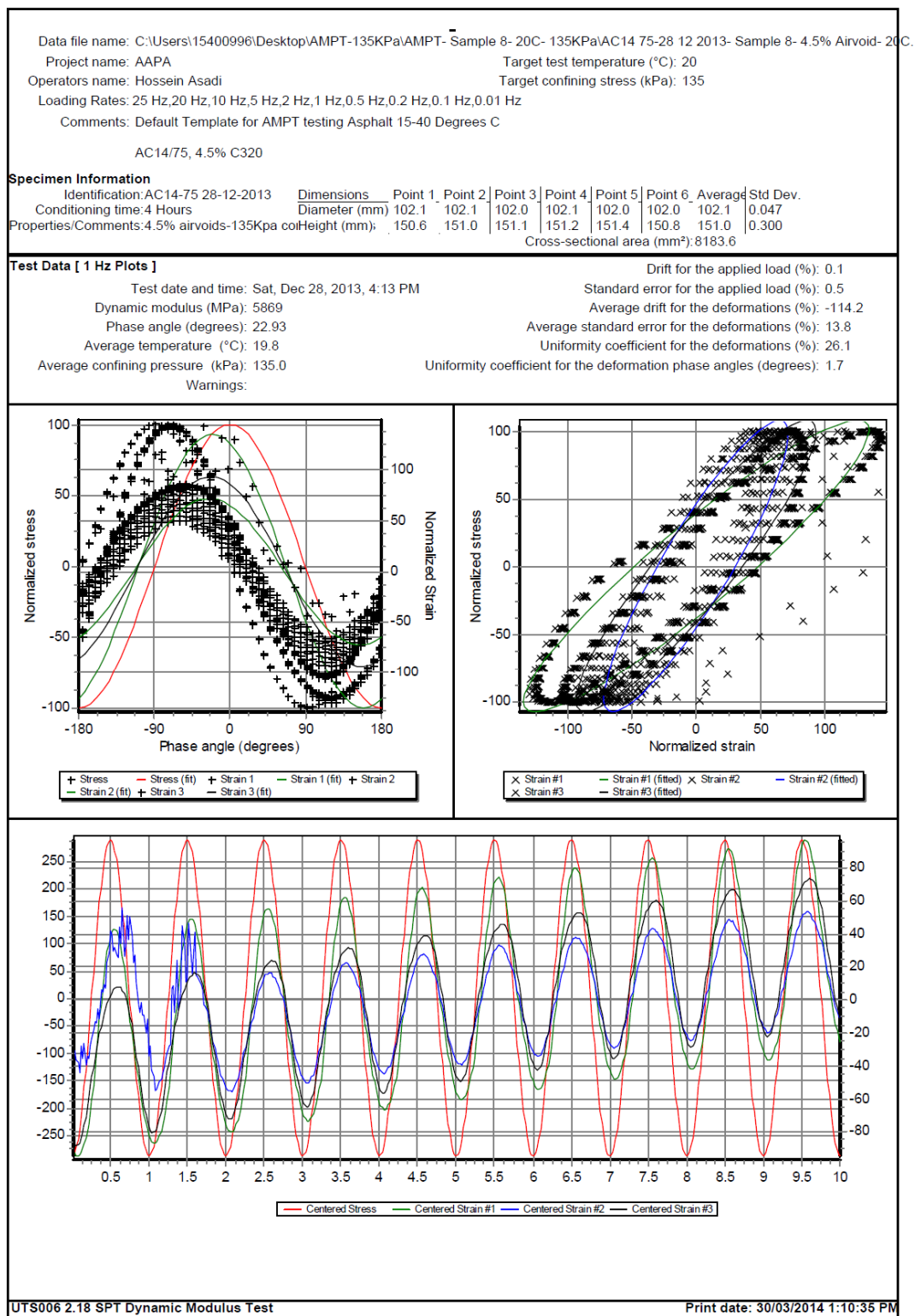


Figure E - 162. UTS6 output for sample13, 1 Hz and 20°C

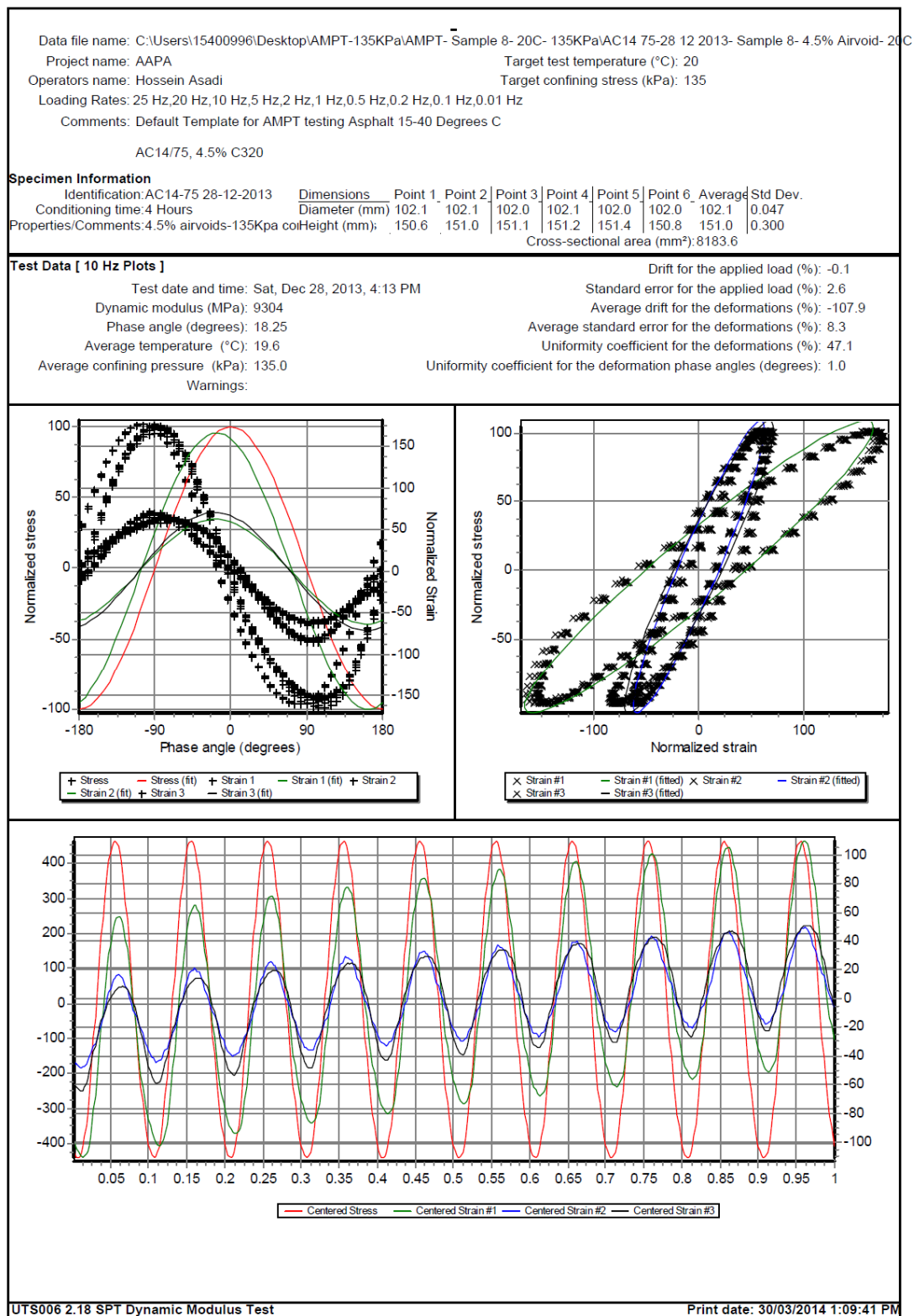


Figure E - 163. UTS6 output for sample13, 10 Hz and 20°C

Project name: AAPA Target test temperature (°C): 20
Operators name: Hossein Asadi Target confining stress (kPa): 135
Loading rates: 25 Hz, 20 Hz, 10 Hz, 5 Hz, 2 Hz, 1 Hz, 0.5 Hz, 0.2 Hz, 0.1 Hz, 0.01 Hz
Comments: Default Template for AMPT testing Asphalt 15-40 Degrees C

AC14/75, 4.5% C320

Specimen Information

Identification: AC14-75 28-12-2013	Dimensions	Point 1	Point 2	Point 3	Point 4	Point 5	Point 6	Average	Std Dev.
Conditioning time: 4 Hours	Diameter (mm)	102.1	102.1	102.0	102.1	102.0	102.0	102.1	0.047
Properties/Comments: 4.5% airvoids-135Kpa co	Height (mm);	150.6	151.0	151.1	151.2	151.4	150.8	151.0	0.300
Cross-sectional area (mm²): 8183.6									

Tabulated Results Summary

	25 Hz	20 Hz	10 Hz	5 Hz	2 Hz	1 Hz	0.5 Hz	0.2 Hz	0.1 Hz	0.01 Hz
Dynamic modulus (MPa)	11669	10758	9304	8177	6828	5869	5054	4031	3354	1644
Phase angle (Degrees)	16.05	16.24	18.25	19.68	21.09	22.93	23.43	25.06	26.31	29.04
Average temperature (°C)	19.6	19.6	19.6	19.6	19.6	19.8	20.1	20.2	20.1	20.0
Average confining pressure (kPa)	135.0	135.0	135.0	135.0	135.0	135.0	135.0	135.0	135.0	135.0
Average micro-strain	89	95	98	98	97	98	98	99	99	101
Load drift (%)	-0.6	-0.4	-0.1	0.1	0.0	0.1	0.1	0.1	0.0	0.0
Load standard error (%)	5.3	4.8	2.6	1.5	0.7	0.5	0.2	0.3	0.2	0.6
Average deformation drift (%)	-149.1	-106.9	-107.9	-122.0	-128.6	-114.2	-132.8	-140.5	-156.2	-208.7
Average deformation standard error (%)	9.5	9.4	8.3	8.7	6.9	13.8	6.1	6.6	4.7	14.5
Deformation uniformity (%)	55.5	51.0	47.1	40.4	33.0	26.1	21.7	16.9	14.3	19.5
Phase uniformity (Degrees)	2.3	2.1	1.0	1.1	0.9	1.7	0.9	0.8	0.8	0.8

UTS006 2.18 SPT Dynamic Modulus Test

Print date: 30/03/2014 1:09:41 PM

Figure E - 164. UTS6 summary output for sample13, 20°C

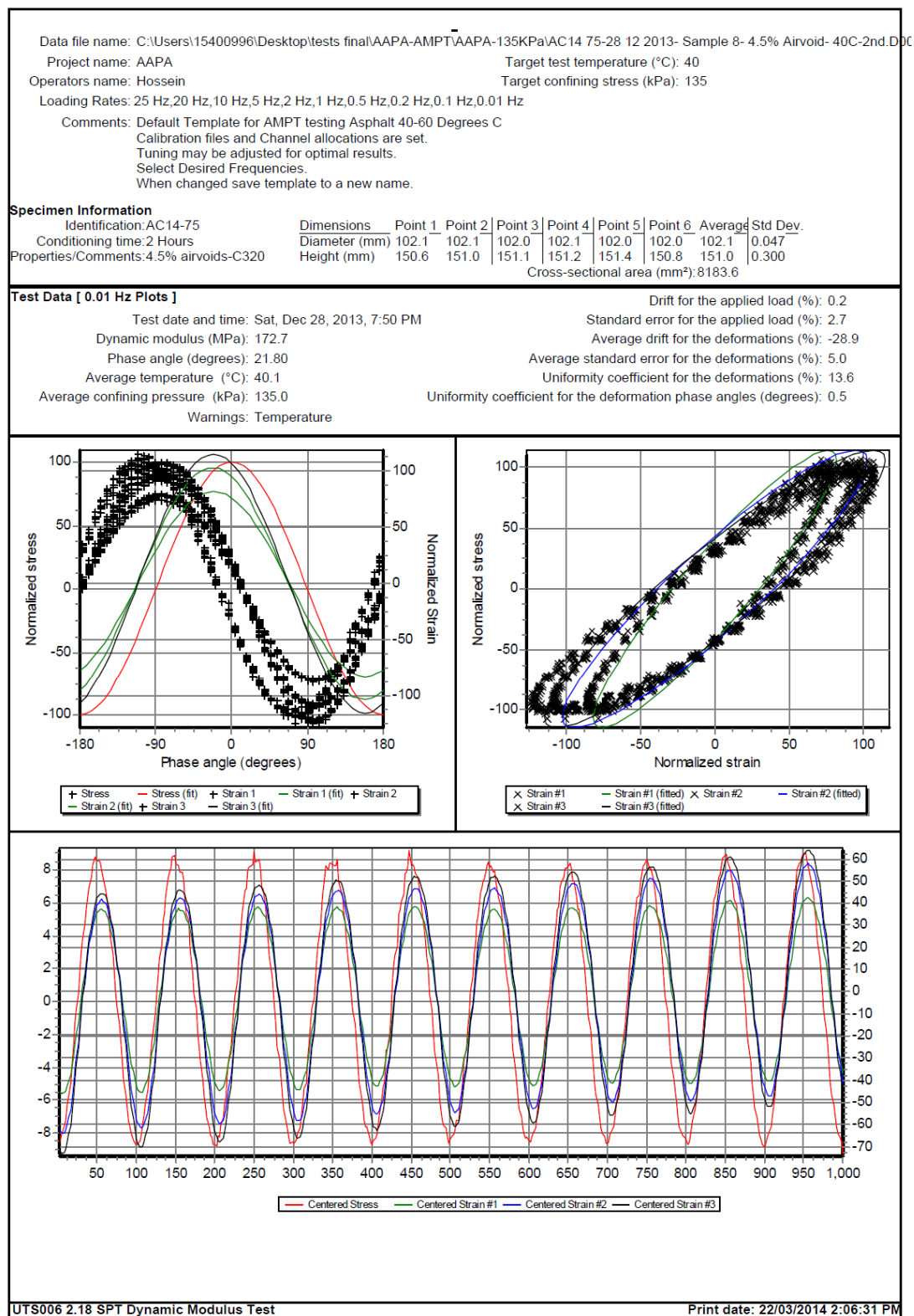


Figure E - 165. UTS6 output for sample13, 0.01 Hz and 40°C

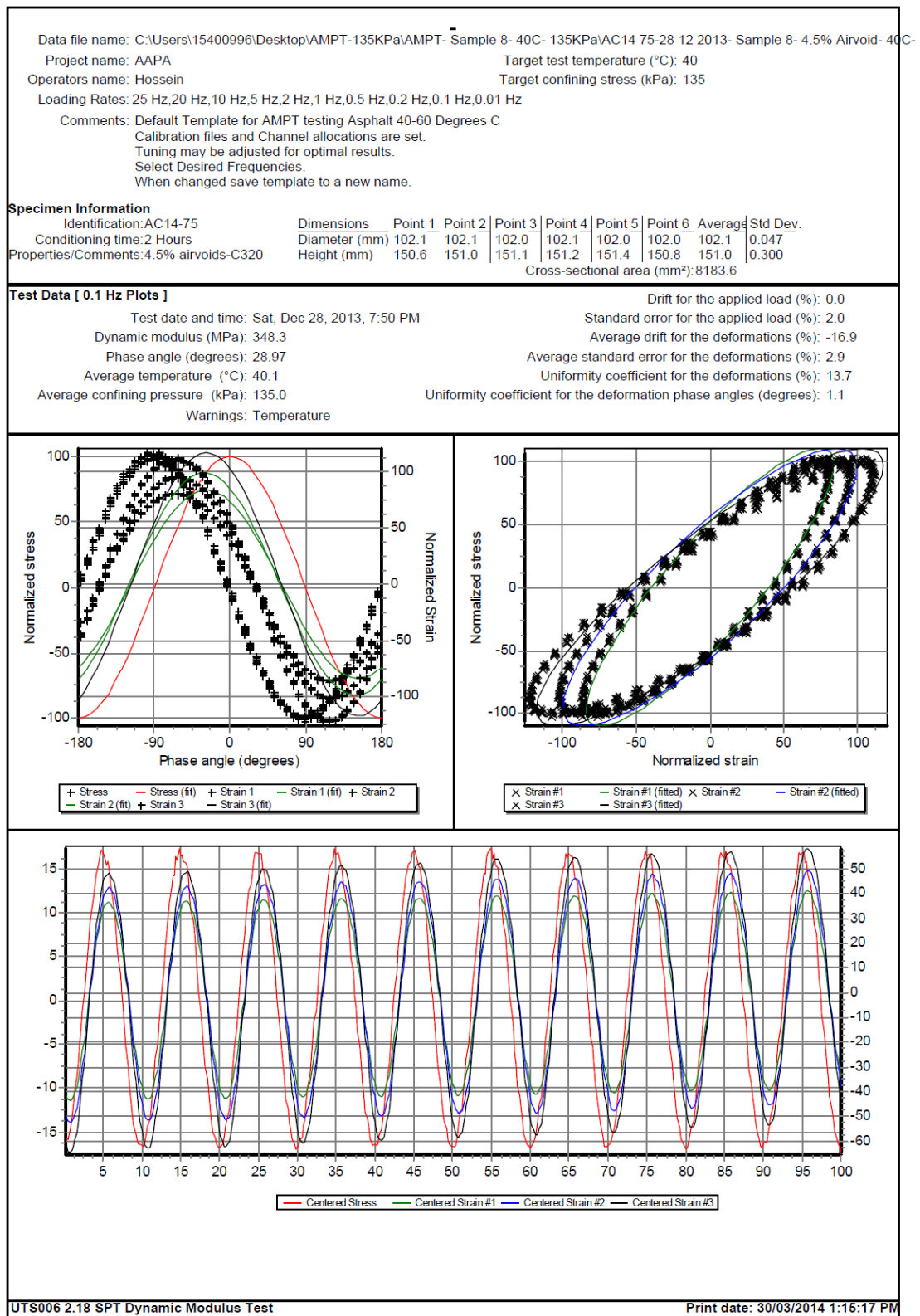


Figure E - 166. UTS6 output for sample13, 0.1 Hz and 40°C

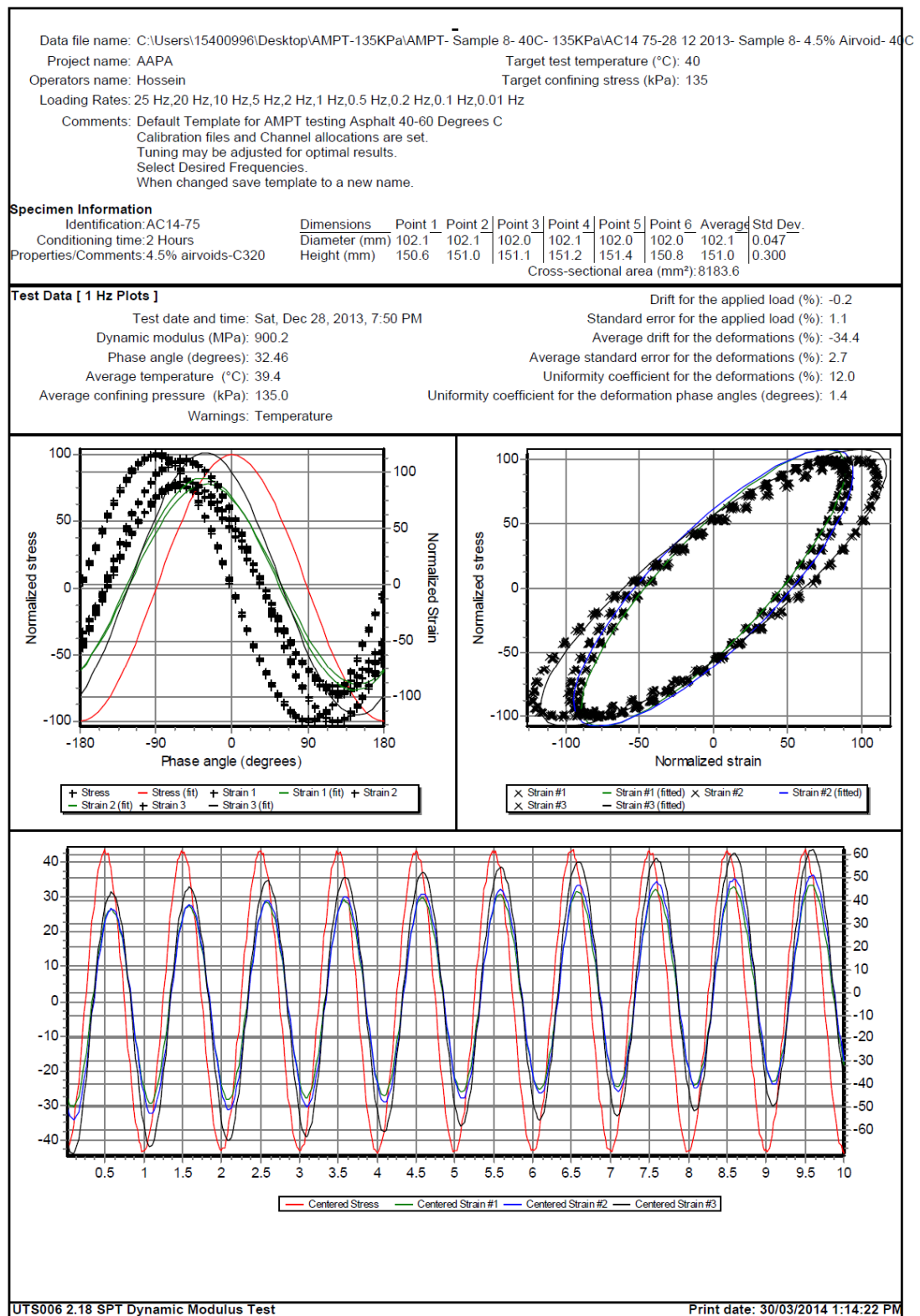


Figure E - 167. UTS6 output for sample13, 1 Hz and 40°C

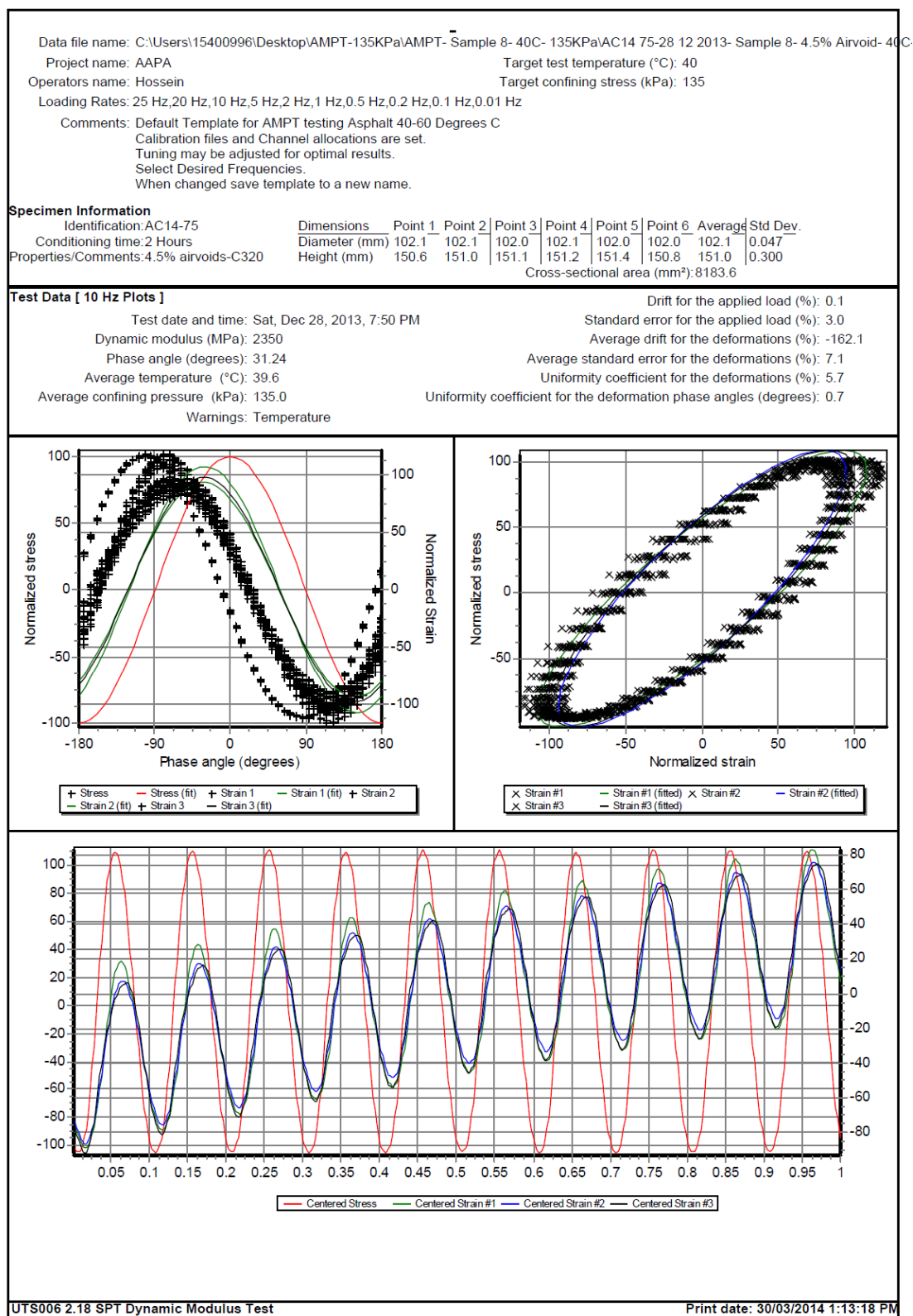


Figure E - 168. UTS6 output for sample13, 10 Hz and 40°C

Project name: AAPA	Target test temperature (°C): 40
Operators name: Hossein	Target confining stress (kPa): 135
Loading Rates: 25 Hz,20 Hz,10 Hz,5 Hz,2 Hz,1 Hz,0.5 Hz,0.2 Hz,0.1 Hz,0.01 Hz	
Comments: Default Template for AMPT testing Asphalt 40-60 Degrees C Calibration files and Channel allocations are set. Tuning may be adjusted for optimal results. Select Desired Frequencies. When changed save template to a new name.	

Specimen Information		Dimensions	Point 1	Point 2	Point 3	Point 4	Point 5	Point 6	Average	Std Dev.
Identification: AC14-75		Diameter (mm)	102.1	102.1	102.0	102.1	102.0	102.0	102.1	0.047
Conditioning time: 2 Hours		Height (mm)	150.6	151.0	151.1	151.2	151.4	150.8	151.0	0.300
Properties/Comments: 4.5% airvoids-C320		Cross-sectional area (mm²): 8183.6								

	25 Hz	20 Hz	10 Hz	5 Hz	2 Hz	1 Hz	0.5 Hz	0.2 Hz	0.1 Hz	0.01 Hz
Dynamic modulus (MPa)	3161	2987	2350	1797	1226	900.2	665.3	457.0	348.3	172.7
Phase angle (Degrees)	31.66	30.64	31.24	31.93	32.49	32.46	31.90	30.43	28.97	21.80
Average temperature (°C)	39.6	39.6	39.6	39.5	39.4	39.4	39.7	40.2	40.1	40.1
Average confining pressure (kPa)	135.0	135.0	135.0	135.0	135.0	135.0	135.0	135.0	135.0	135.0
Average micro-strain	93	93	93	94	95	96	96	98	96	100
Load drift (%)	-1.0	-0.2	0.1	0.3	-0.6	-0.2	0.2	0.6	0.0	0.2
Load standard error (%)	5.2	4.5	3.0	2.1	1.4	1.1	1.3	1.8	2.0	2.7
Average deformation drift (%)	-348.6	-225.8	-162.1	-108.8	-57.3	-34.4	-26.5	-20.8	-16.9	-28.9
Average deformation standard error (%)	12.7	9.1	7.1	5.1	3.5	2.7	2.7	2.9	2.9	5.0
Deformation uniformity (%)	18.0	12.0	5.7	5.1	9.3	12.0	13.2	13.5	13.7	13.6
Phase uniformity (Degrees)	1.9	1.2	0.7	0.8	1.1	1.4	1.5	1.4	1.1	0.5

Print date: 30/03/2014 1:13:18 PM

Figure E - 169. UTS6 output for sample13, 40°C

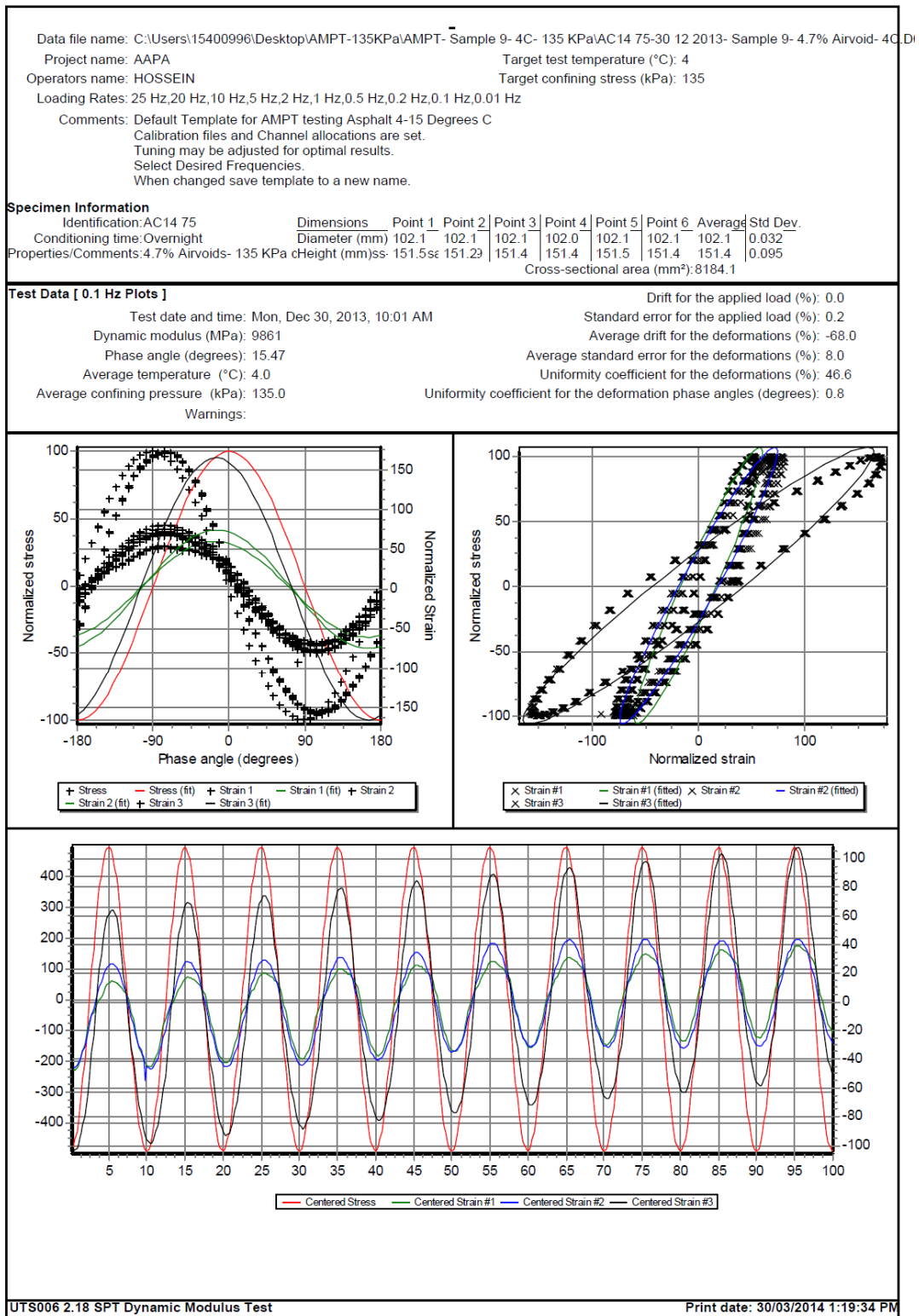


Figure E - 170. UTS6 output for sample14, 0.1 Hz and 4°C

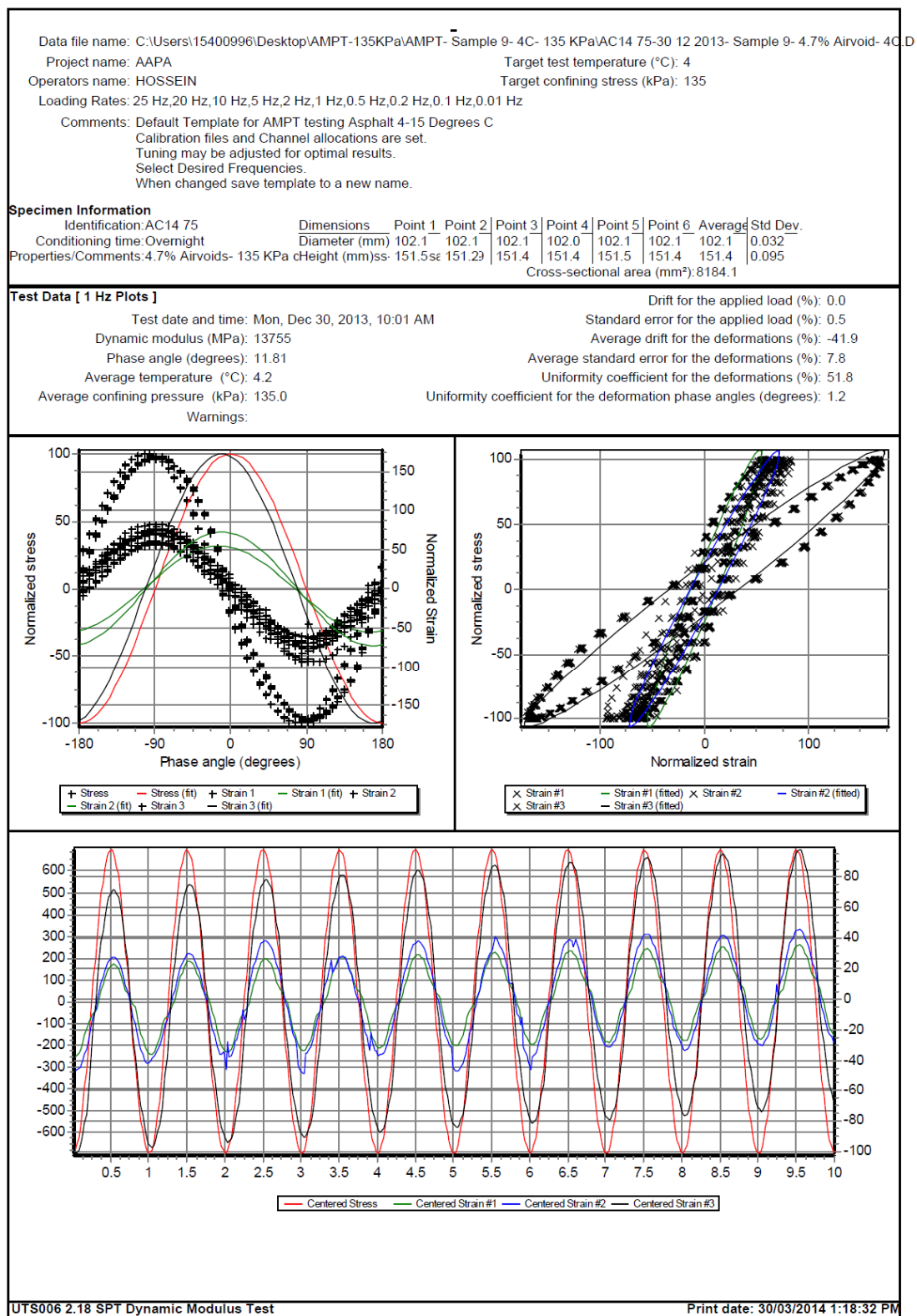


Figure E - 171. UTS6 output for sample14, 1 Hz and 4°C

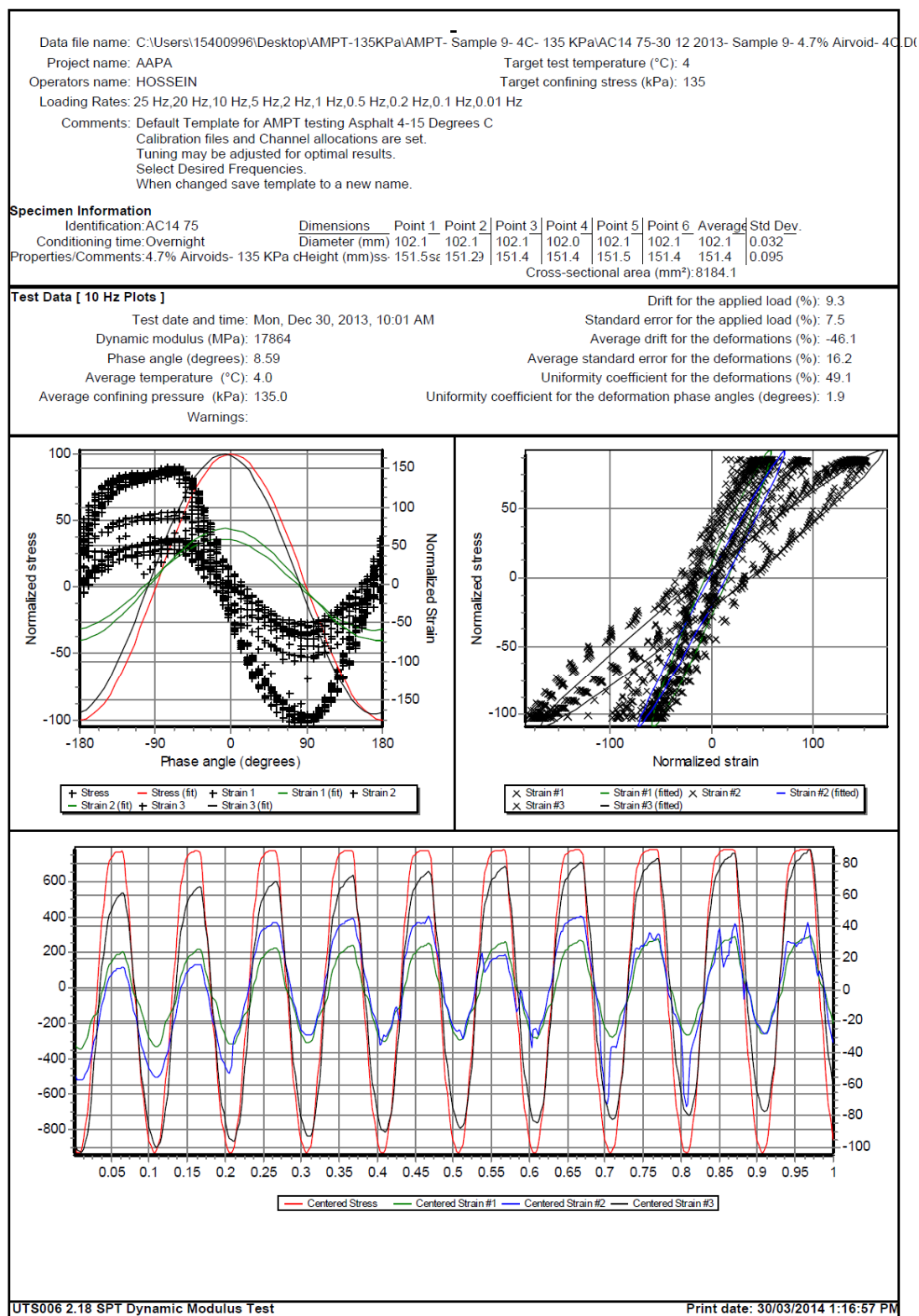


Figure E - 172. UTS6 output for sample14, 10 Hz and 4°C

Project name: AAPA	Target test temperature (°C): 4
Operators name: HOSSEIN	Target confining stress (kPa): 135
Loading Rates: 25 Hz, 20 Hz, 10 Hz, 5 Hz, 2 Hz, 1 Hz, 0.5 Hz, 0.2 Hz, 0.1 Hz, 0.01 Hz	
Comments: Default Template for AMPT testing Asphalt 4-15 Degrees C Calibration files and Channel allocations are set. Tuning may be adjusted for optimal results. Select Desired Frequencies. When changed save template to a new name.	

Identification: AC14.75	Dimensions	Point 1	Point 2	Point 3	Point 4	Point 5	Point 6	Average	Std Dev.
Conditioning time: Overnight	Diameter (mm)	102.1	102.1	102.1	102.0	102.1	102.1	102.1	0.032
Properties/Comments: 4.7% Airvoids- 135 KPa	Height (mm): ss.	151.5	151.2	151.4	151.4	151.5	151.4	151.4	0.095
Cross-sectional area (mm²): 8184.1									

	25 Hz	20 Hz	10 Hz	5 Hz	2 Hz	1 Hz	0.5 Hz	0.2 Hz	0.1 Hz	0.01 Hz
Dynamic modulus (MPa)	19431	18772	17864	16699	15106	13755	12561	10978	9861	6573
Phase angle (Degrees)	9.44	9.02	8.59	9.59	12.33	11.81	13.09	14.39	15.47	20.26
Average temperature (°C)	4.0	4.0	4.0	4.0	4.1	4.2	4.2	4.1	4.0	4.1
Average confining pressure (kPa)	135.0	135.0	135.0	135.0	135.0	135.0	135.0	135.0	135.0	135.0
Average micro-strain	90	94	102	100	99	101	100	101	100	100
Load drift (%)	12.0	10.0	9.3	0.1	-0.1	0.0	0.0	0.0	0.0	0.0
Load standard error (%)	11.1	7.7	7.5	1.2	0.7	0.5	0.2	0.3	0.2	0.5
Average deformation drift (%)	-35.4	-43.5	-46.1	-69.4	-30.0	-41.9	-38.5	-58.5	-68.0	-150.9
Average deformation standard error (%)	14.6	13.8	16.2	19.5	28.2	7.8	6.5	11.5	8.0	4.9
Deformation uniformity (%)	44.9	47.0	49.1	51.8	53.2	51.8	51.5	49.5	46.6	29.9
Phase uniformity (Degrees)	1.7	1.3	1.9	1.6	1.6	1.2	0.8	1.0	0.8	0.4

Print date: 30/03/2014 1:16:57 PM

- 338 -

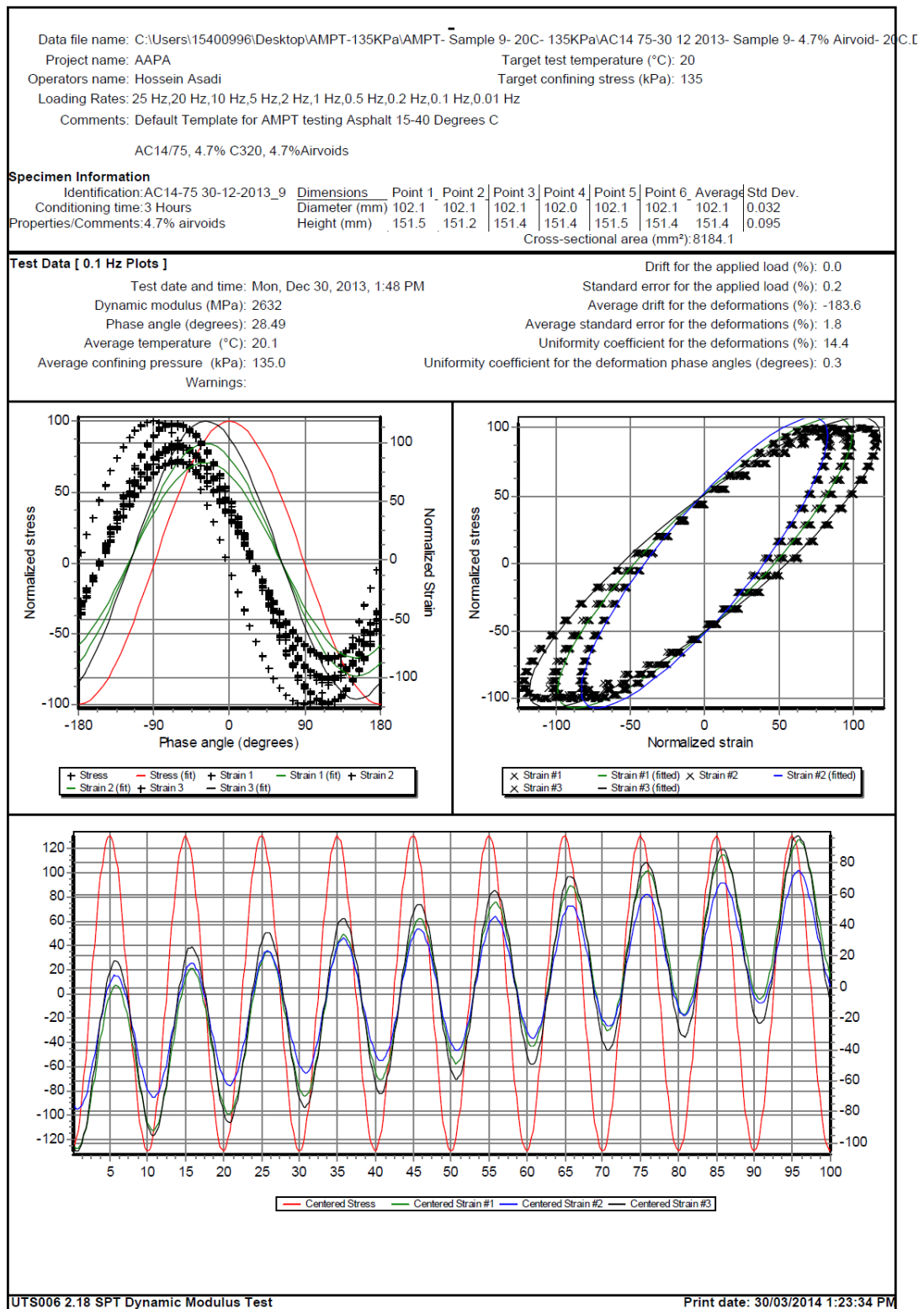


Figure E - 174. UTS6 output for sample14, 0.1 Hz and 20°C

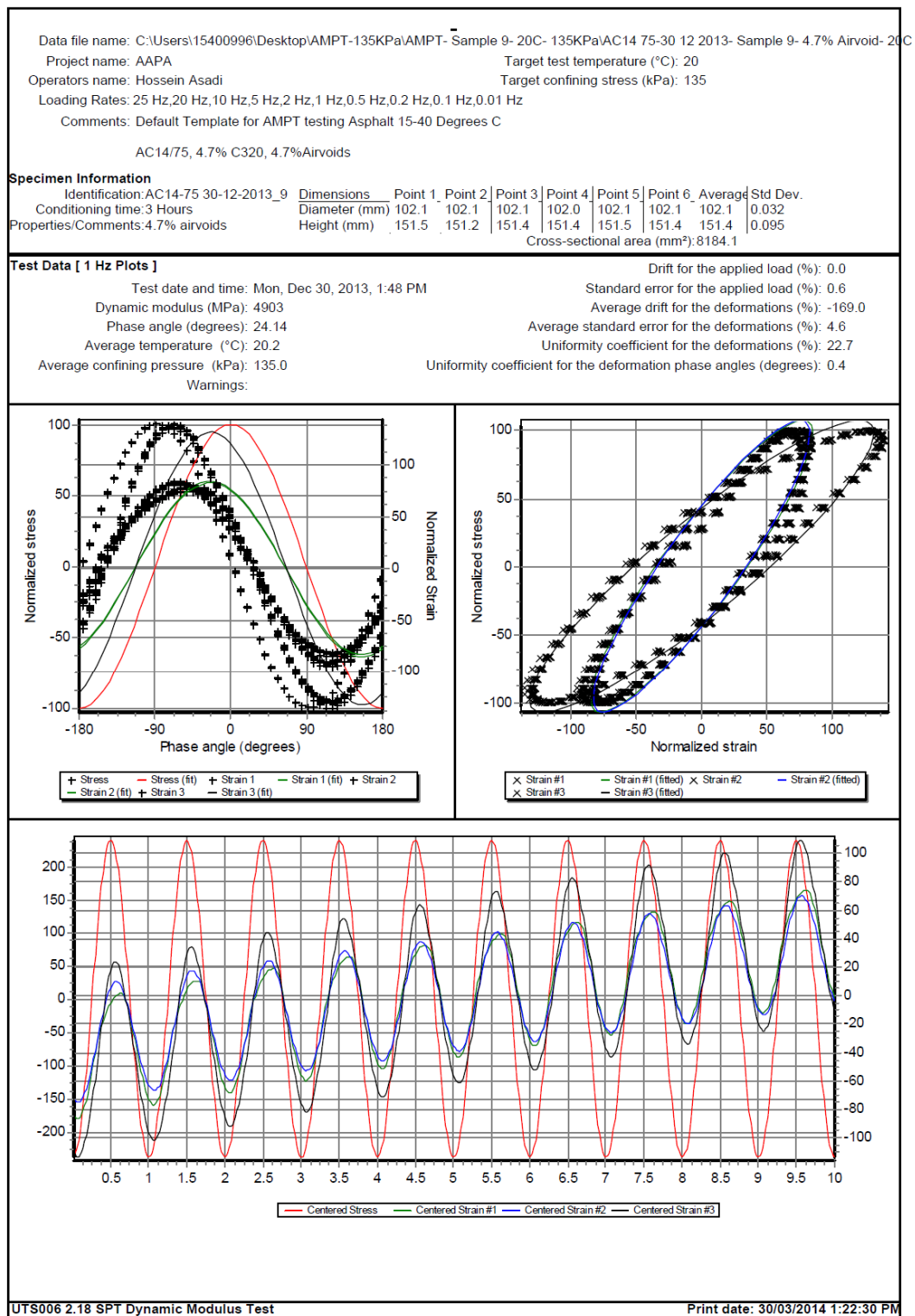
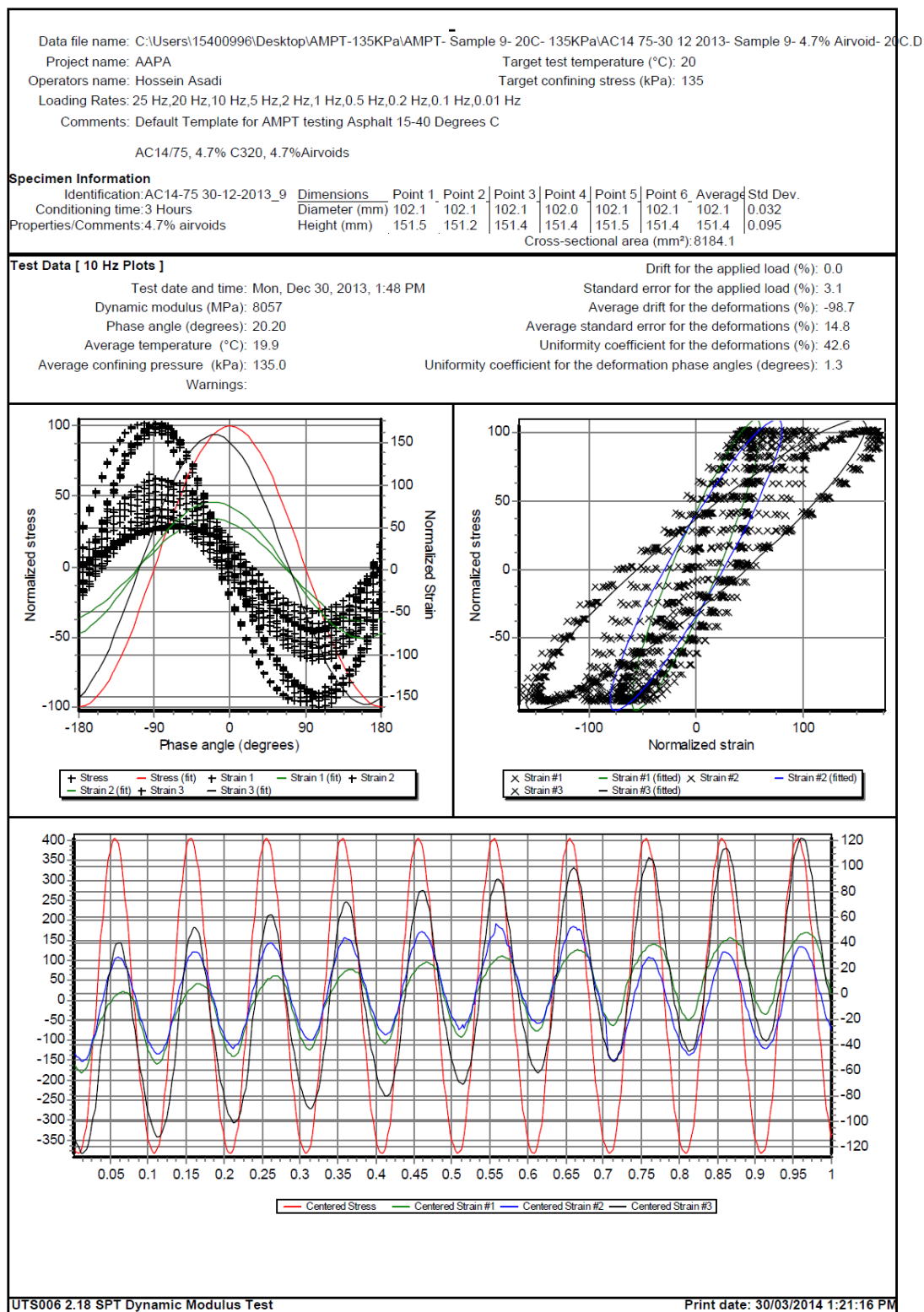


Figure E - 175. UTS6 output for sample14, 1 Hz and 20°C



Project name: AAPA	Target test temperature (°C): 20
Operators name: Hossein Asadi	Target confining stress (kPa): 135
Loading Rates: 25 Hz, 20 Hz, 10 Hz, 5 Hz, 2 Hz, 1 Hz, 0.5 Hz, 0.2 Hz, 0.1 Hz, 0.01 Hz	
Comments: Default Template for AMPT testing Asphalt 15-40 Degrees C	

Specimen Information

Tabulated Results Summary

	25 Hz	20 Hz	10 Hz	5 Hz	2 Hz	1 Hz	0.5 Hz	0.2 Hz	0.1 Hz	0.01 Hz
Dynamic modulus (MPa)	9891	9224	8057	7030	5763	4903	4140	3220	2632	1189
Phase angle (Degrees)	18.66	18.31	20.20	21.01	22.82	24.14	25.51	27.35	28.49	31.64
Average temperature (°C)	19.9	19.9	19.9	20.0	20.0	20.2	20.3	20.2	20.1	20.0
Average confining pressure (kPa)	135.0	135.1	135.0	135.0	135.0	135.0	135.0	135.0	135.0	135.0
Average micro-strain	94	96	99	98	97	98	98	99	99	103
Load drift (%)	-0.4	-0.5	0.0	0.0	0.0	0.0	0.1	0.1	0.0	0.1
Load standard error (%)	6.2	5.7	3.1	1.8	0.9	0.6	0.2	0.2	0.2	0.6
Average deformation drift (%)	-291.3	-124.0	-98.7	-146.6	-162.4	-169.0	-180.3	-186.9	-183.6	-191.9
Average deformation standard error (%)	17.9	10.0	14.8	7.2	5.6	4.6	5.1	2.1	1.8	2.5
Deformation uniformity (%)	56.5	48.8	42.6	36.0	27.9	22.7	19.1	15.6	14.4	15.2
Phase uniformity (Degrees)	1.6	1.3	1.3	0.9	0.5	0.4	0.4	0.3	0.3	0.7

Print date: 30/03/2014 1:21:16 PM

- 342 -

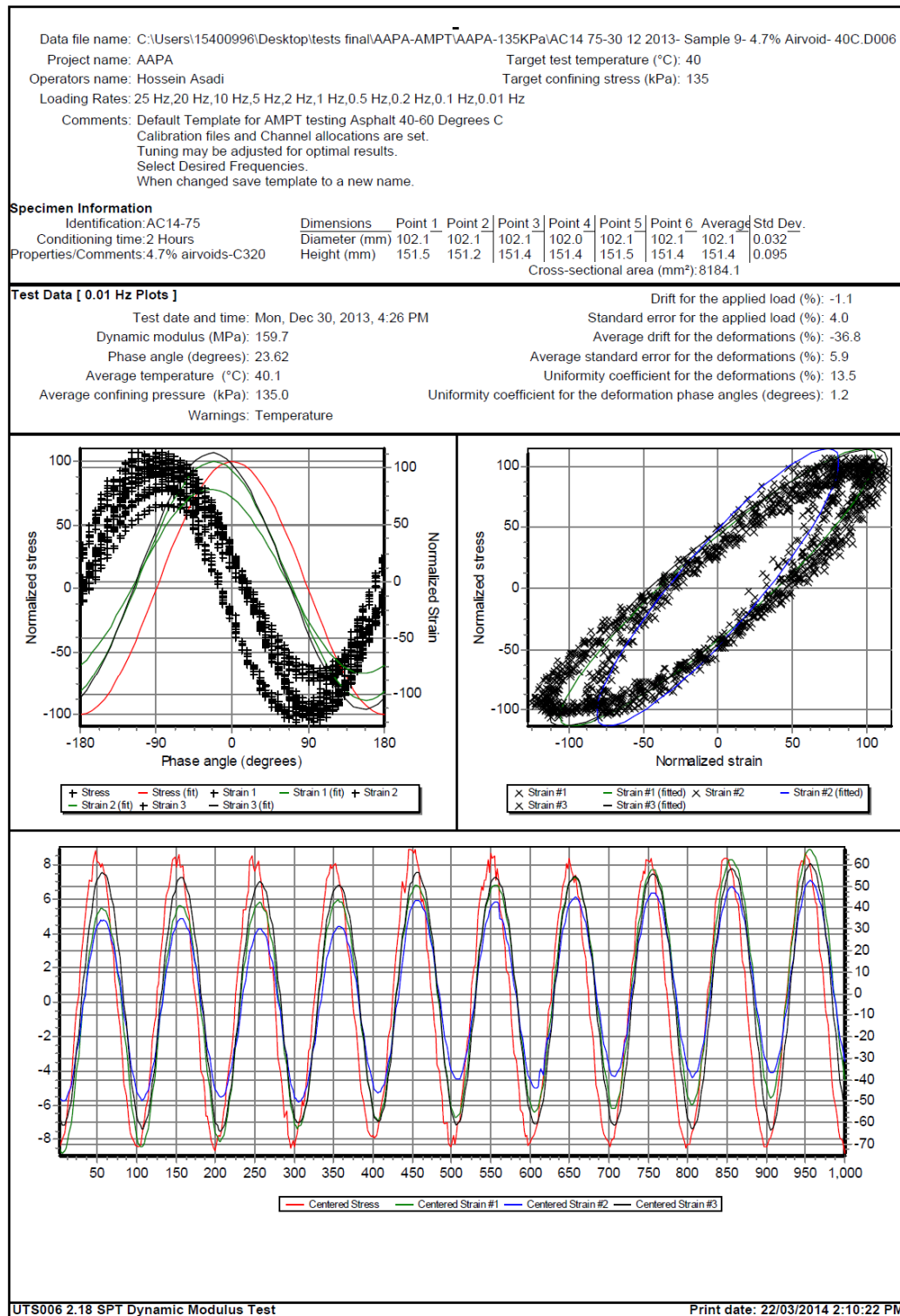


Figure E - 178. UTS6 output for sample14, 0.01 Hz and 40°C

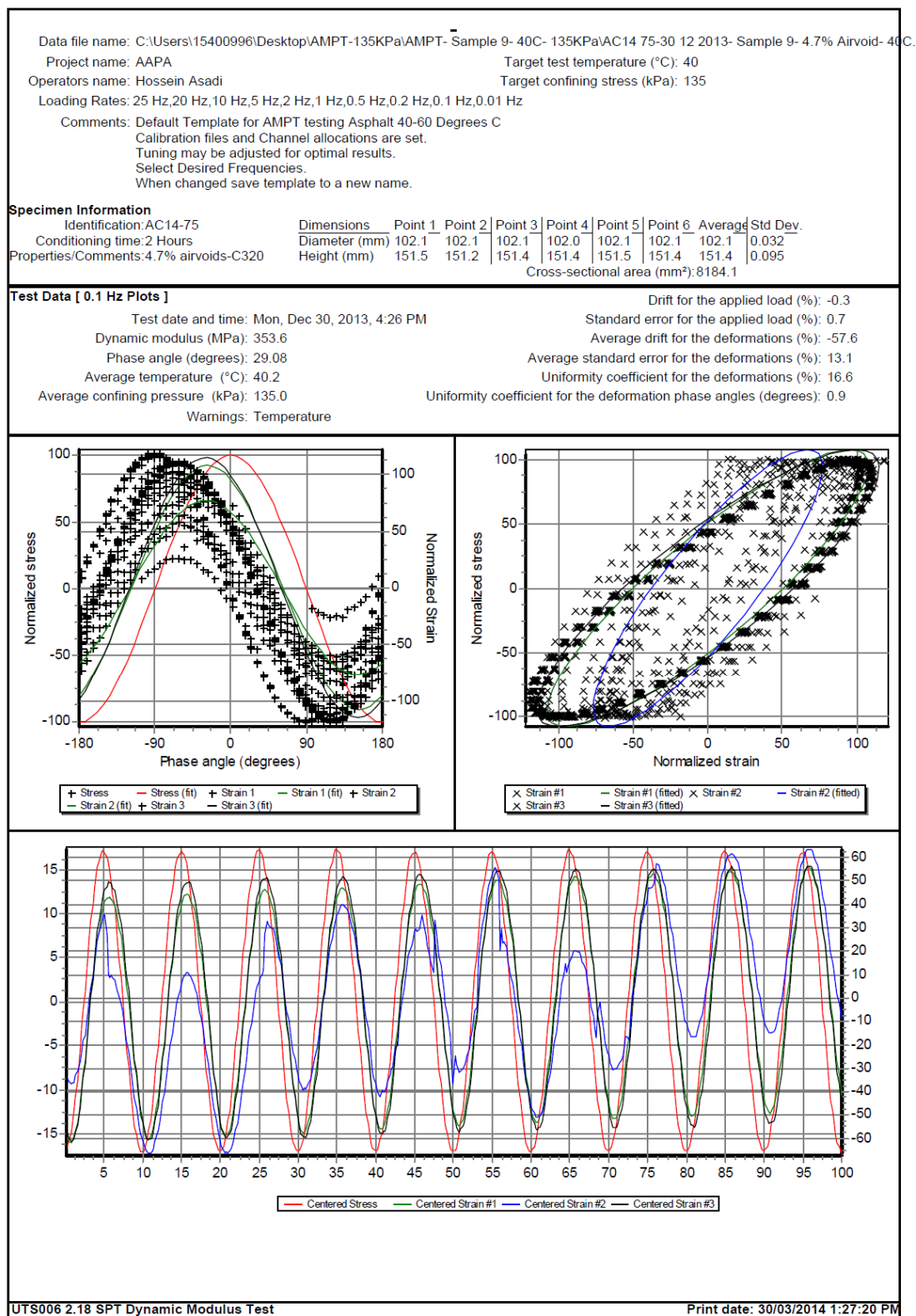


Figure E - 179. UTS6 output for sample14, 0.01 Hz and 40°C

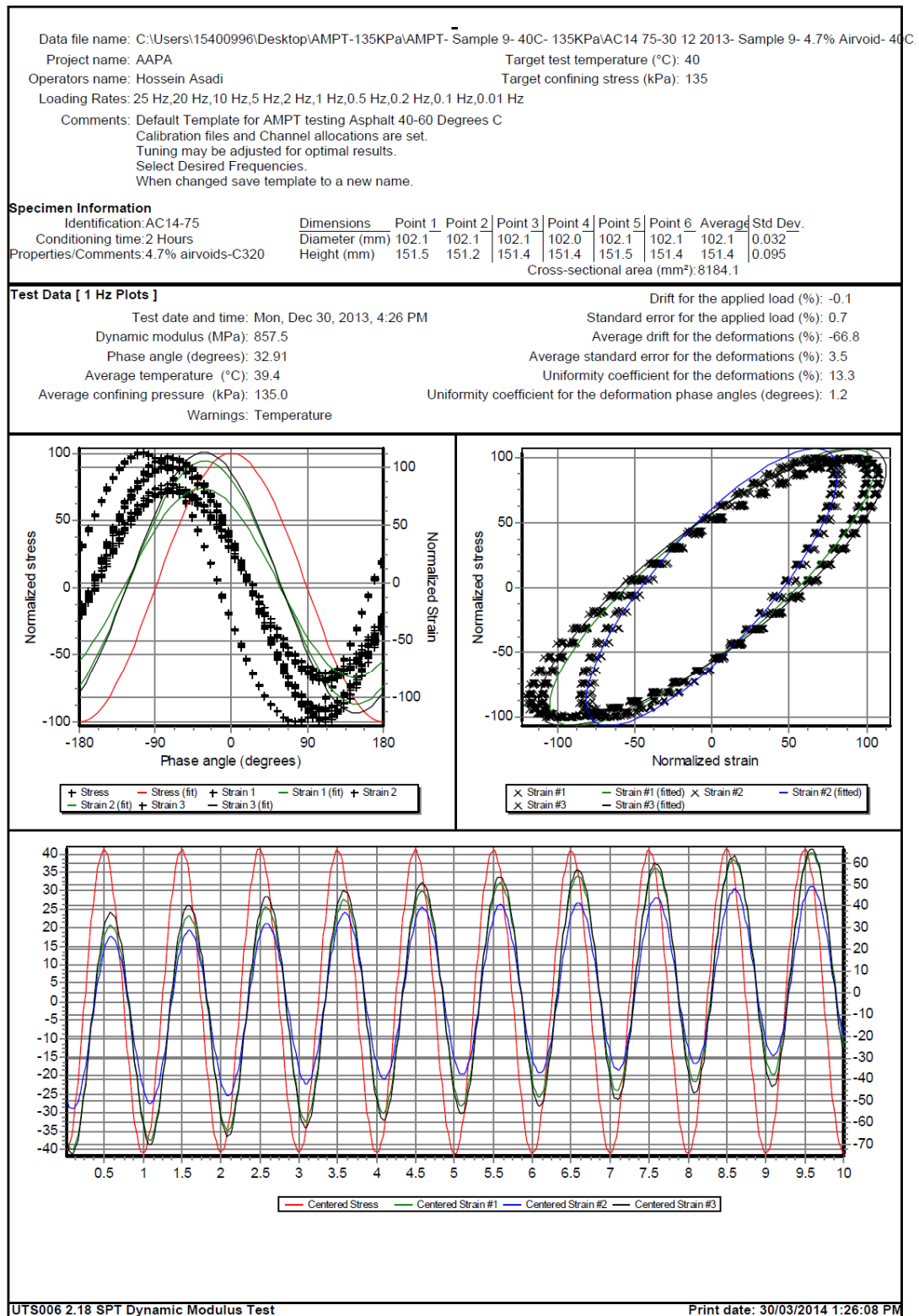


Figure E - 180. UTS6 output for sample14, 1 Hz and 40°C

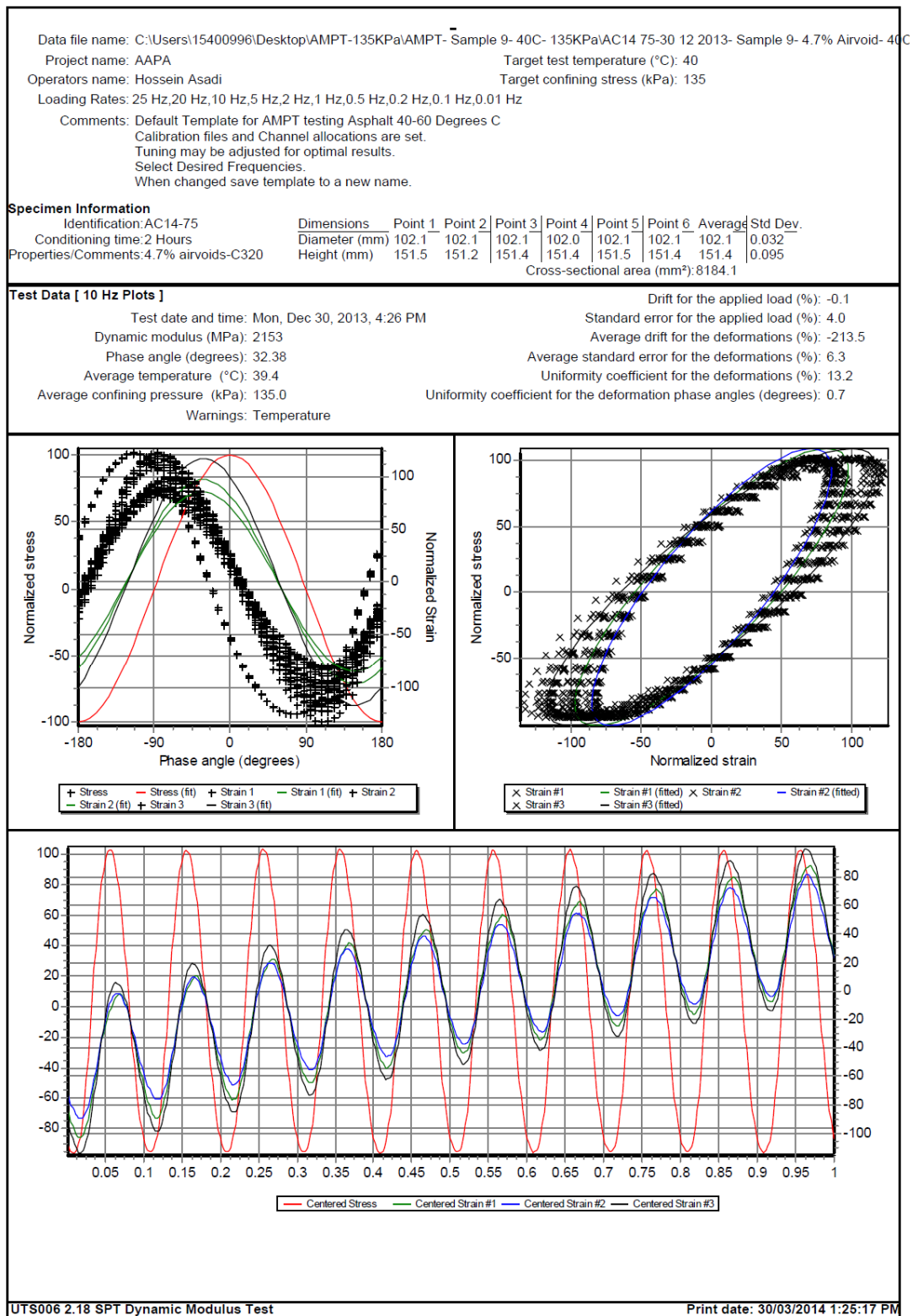


Figure E - 181. UTS6 output for sample14, 10 Hz and 40°C

Project name: AAPA	Target test temperature (°C): 40
Operators name: Hossein Asadi	Target confining stress (kPa): 135
Loading Rates: 25 Hz,20 Hz,10 Hz,5 Hz,2 Hz,1 Hz,0.5 Hz,0.2 Hz,0.1 Hz,0.01 Hz	
Comments: Default Template for AMPT testing Asphalt 40-60 Degrees C Calibration files and Channel allocations are set. Tuning may be adjusted for optimal results. Select Desired Frequencies. When changed save template to a new name.	

Specimen Information

Identification: AC14-75	Dimensions	Point 1	Point 2	Point 3	Point 4	Point 5	Point 6	Average	Std Dev.
Conditioning time: 2 Hours	Diameter (mm)	102.1	102.1	102.1	102.0	102.1	102.1	102.1	0.032
Properties/Comments: 4.7% airvoids-C320	Height (mm)	151.5	151.2	151.4	151.4	151.5	151.4	151.4	0.095
Cross-sectional area (mm²): 8184.1									

Tabulated Results Summary

	25 Hz	20 Hz	10 Hz	5 Hz	2 Hz	1 Hz	0.5 Hz	0.2 Hz	0.1 Hz	0.01 Hz
Dynamic modulus (MPa)	2916	2177	2153	1653	1142	857.5	645.6	452.2	353.6	159.7
Phase angle (Degrees)	32.52	31.78	32.38	32.95	33.21	32.91	32.30	31.19	29.08	23.62
Average temperature (°C)	39.5	39.5	39.4	39.4	39.4	39.4	39.5	39.8	40.2	40.1
Average confining pressure (kPa)	135.0	135.0	135.0	135.0	135.0	135.0	135.0	135.0	135.0	135.0
Average micro-strain	95	94	94	94	95	96	97	98	97	104
Load drift (%)	-1.8	-0.4	-0.1	-0.1	0.2	-0.1	-0.3	-0.2	-0.3	-1.1
Load standard error (%)	6.6	5.7	4.0	2.8	1.6	0.7	0.4	0.6	0.7	4.0
Average deformation drift (%)	-394.9	-279.5	-213.5	-152.8	-96.7	-66.8	-42.9	-36.8	-57.6	-36.8
Average deformation standard error (%)	11.3	8.8	6.3	4.5	3.0	3.5	2.6	7.2	13.1	5.9
Deformation uniformity (%)	18.4	15.4	13.2	12.6	13.0	13.3	13.7	14.2	16.6	13.5
Phase uniformity (Degrees)	1.1	0.8	0.7	0.9	1.1	1.2	1.3	1.5	0.9	1.2

UTS006 2.18 SPT Dynamic Modulus Test

Print date: 30/03/2014 1:25:18 PM

Figure E - 182. UTS6 summary output for sample14, 40°C